A product of skin microbiota improves hallmarks of wound healing in diabetes mellitus: an in vitro investigation

A thesis submitted in fulfilment of the requirements for the degree of Doctor of Philosophy

By

Aveen Tayeb Sabir

Supervisors: Dr Sarah B. Withers, and Dr Joe Latimer

School of Science, Engineering and Environment

I. Table of Contents

II. List of tables

III. List of figures

IV. Acknowledgements

I would like to express my sincere gratitude to Dr Joe Latimer and Dr Sarah Withers for their support, guidance, understanding, and motivation throughout my PhD journey.

I would like to acknowledge other postgraduates, postdoctoral researchers, technicians, and academics working within translational medicine and microbiology laboratories at the University of Salford. My PhD journey was enriched by their knowledge, training, ideas, and friendship during my time as a PhD candidate.

I am also thankful to my family and friends for their unwavering love and support during this time. My mother, and two sisters have provided continuous understanding and encouragement over the past four years. In addition, I would like to thank all psychologists, life coaches, and pranic healers who helped me cope with grief associated with my father's death during the PhD and encouraged me to complete the course.

V. Declaration

This thesis is a product of the candidate's own study and research. It contains work that presented in multiple conferences: University of Salford Postgraduate Annual Research Conference (SPARC) (2021, 2022, 2023), Microbiome Interactions in Health and Disease conference (2022) and the Microbiology Society Annual conference (2024).

VI. Publication in preparation

Sabir A., Withers S., Latimer, J. Latimer, **A product of skin microbiota improves hallmarks of wound healing in diabetes mellitus: an in vitro investigation**, In preparation.

VII. List of acronyms and abbreviations

DM	Diabetes mellitus
IDF	International Diabetes Federation
NICE	National institute for health and care excellence
DFU	Diabetic foot ulcer
PDGF	Platelet derived growth factor
TLR	Toll-like receptors
TGF-β	Transforming growth factor beta
TNF-α	Tumour necrosis factor alpha
IL-1	Interleukin-1
FGF	Fibroblasts growth factor
Spp.	Species
S. epidermidis	*Staphylococcus epidermidis*
S. aureus	*Staphylococcus aureus*
C. jeikeium	*Corynebacterium jeikeium*
P. acnes	*Propionibacterium acnes*
OD600	Optical Density
OD600%	Percentage of change of OD600
SCFAs	*Short chain fatty acids*
TLR	Toll-like receptor
MMP	Matrix metalloproteinase
PSMs	Phenol-soluble modulins
AMPs	Antimicrobial peptides
PCR	Polymerase chain reaction
MHA	Mueller Hinton Agar
MHB	Mueller Hinton Broth
NB	Nutrient broth
NA	Nutrient agar
CBA	Columbia blood agar
GO	Gene ontology

DEG	Differential expression genes
KEGG	Kyoto Encyclopaedia of Genes and Genomes
GSEA	Gene Set Enrichment Analysis
BP	Biological process
CC	Cellular component
MF	Molecular function
ROS	reactive oxygen species

Abstract

Diabetes mellitus is a critical global health disease characterised by persistent hyperglycaemia, which leads to various complications. Poor wound healing and diabetic foot ulcers are the two main complications of this disease. Lysates and cell-free supernatants prepared from some *Lactobacillus* spp. were found to improve the hallmarks of wound healing under healthy conditions in vitro. Dysbiosis in the skin microbiota is widely reported in the skin of diabetic patients, and the presence of some members of the skin microbiota was correlated with a positive prognosis of diabetic foot ulcers. Thus, the present study aimed to test the effects of lysates or cell-free supernatants prepared from some members of the skin microbiota on wound healing in diabetes mellitus in vitro.

Bacterial lysates and cell-free supernatants were prepared from three main commensal skin bacteria: *Staphylococcus epidermidis, Staphylococcus aureus,* and *Corynebacterium jeikeium.* Human skin cells, particularly human skin fibroblasts and keratinocytes, were co-cultured with the skin commensal lysate and cell-free supernatant in euglycemic and hyperglycaemic glucose concentrations. Various in vitro experiments were performed: proliferation assay (MTS assay), migration assay (scratch assay), and transcriptomic analysis (whole mRNA sequencing).

Only one bacterial product, *Staphylococcus epidermidis* lysate, significantly induced the proliferation and migration of human skin fibroblasts at hyperglycaemic glucose concentrations. Transcriptomic analysis revealed that the main effect of *Staphylococcus epidermidis* lysate on fibroblasts was through the significant enrichment of the IL-17 signalling pathway. Moreover, CXCL6 was the main chemokine that was significantly upregulated and secreted by fibroblasts when exposed to *Staphylococcus epidermidis* lysate at hyperglycaemic glucose concentrations.

These results indicate that *the Staphylococcus epidermidis* lysate improves the hallmarks of wound healing under hyperglycaemic conditions in vitro. Moreover, these findings encourage further ex vivo, in vivo, and clinical studies to investigate the efficacy and safety of *Staphylococcus epidermidis* lysate as a novel therapeutic for the treatment of diabetic foot ulcers.

Chapter 1: General Introduction

1.1 Diabetes mellitus

1.1.1 Prevalence and Risk Factors

Diabetes mellitus (DM) is a critical global health issue that is increasing rapidly more than scientists' prediction. The predicted number of diabetic patients was 336 million worldwide in 2030 (Wild et al., 2004). However, based on the International Diabetes Federation (IDF), 540 million individuals are diagnosed with DM worldwide in 2024 (IDF, 2024). The total prevalence of DM worldwide was estimated increase to 4.4% in 2030 (Wild et al., 2004). However, based on IDF, prevalence of DM (%) was already 9.8% in 2021, and is estimated to increase to 11.2% in 2045 worldwide (IDF, 2024).

In the UK, DM is reported to be one of the most common chronic diseases (NICE, 2024a). In 2018-2019, 3.9 million people in UK were diagnosed with DM. This number was estimated to increase to 5 million diabetic patients (NICE, 2024a).

The main risk factors for DM are obesity, sedentary lifestyle, increase stress level due to urbanisation, population growth, aging, and a strong family history (Fletcher et al., 2002; Wild et al., 2004). The prevalence of obesity worldwide has been steadily increasing, contributing to further rising the risk of DM (Boutari & Mantzoros, 2022)

1.1.2 Pathophysiology and Diagnosis

DM is a chronic disease characterised by persistent increase in blood glucose level (hyperglycaemia) as a result in disturbance in glucose uptake by some peripheral human cells (Guthrie & Guthrie, 2004; Ramakant et al., 2011). Glucose uptake is performed by two main types of glucose transporters: 1- insulin dependent transporter, such as GLUT4, mainly present in insulin dependent cells such as adipocyte, cardiac cells and skeletal muscles (Brown, 2000; Bryant & Gould, 2020) and 2- insulin independent glucose transporters (such as GLUT1, GLUT2, GLUT3) mainly present in insulin independent cells, such as erythrocyte, vascular endothelia, renal proximal tubule hepatocytes, neurons, and intestinal mucosa as reviewed (Brown, 2000; Navale & Paranjape, 2016).

Under healthy physiological conditions, high blood glucose induces beta cells, in the islets of Langerhans of the pancreas, to secrete insulin which binds to insulin receptors in insulin dependent cells (Guthrie & Guthrie, 2004). This binding initiates a signal

cascade inside the cells, which leads to activation of the insulin dependent glucose transporters (GLUT4) and subsequent entry of glucose into the cells (Cabrera et al., 2006; Guthrie & Guthrie, 2004; van Gerwen et al., 2023). The results of which utilisation of glucose by cells and reduction in blood glucose level (Cabrera et al., 2006; Guthrie & Guthrie, 2004) (Figure 1.1 B). However, in insulin independent cells, glucose transporter uptake glucose solely based on glucose concentration gradient regardless of the presence of insulin (Brown, 2000) (Figure 1.1 A).

In DM, either beta cells of islet Langerhans cells are destroyed due to autoimmune disease and as result insulin is not produced (DM type I) (Cheon, 2018) (Figure 1.1 C) or the sensitivity of peripheral cell receptors to insulin is diminished (DM type II) (Whitmore, 2010) (Figure 1.1 D). In both types, glucose uptake by cells is disturbed leading to persistent hyperglycaemia (Cheon, 2018; van Gerwen et al., 2023; Whitmore, 2010)

Based on national institute for health and care excellence (NICE) guideline, adults are diagnosed with DM if their blood lab test reports the presence of persistent hyperglycaemic level that might be accompanied by clinical features (NICE, 2022).

Persistent hyperglycaemia is defined as: a) glycated haemoglobin test HbA1c of 48 mmol/mol (6.5%) or higher, b) a fasting plasma glucose level of 7 mmol/L (mM) or higher, c) Random plasma glucose of 11.1 mmol/L (mM) or more in the presence of symptoms or signs of diabetes (NICE, 2022).

Possible clinical presentation of DM- type II include: a) Symptoms such as polyuria, polydipsia, unexplained weight loss, blurred vision, tiredness, and recurrent infections, b) The presence of risk factors, c) the presence of signs such as acanthosis nigricans (skin condition causing dark pigmentation of skin folds, typically the axillae, groin, and neck), which suggests insulin resistance (NICE, 2022).

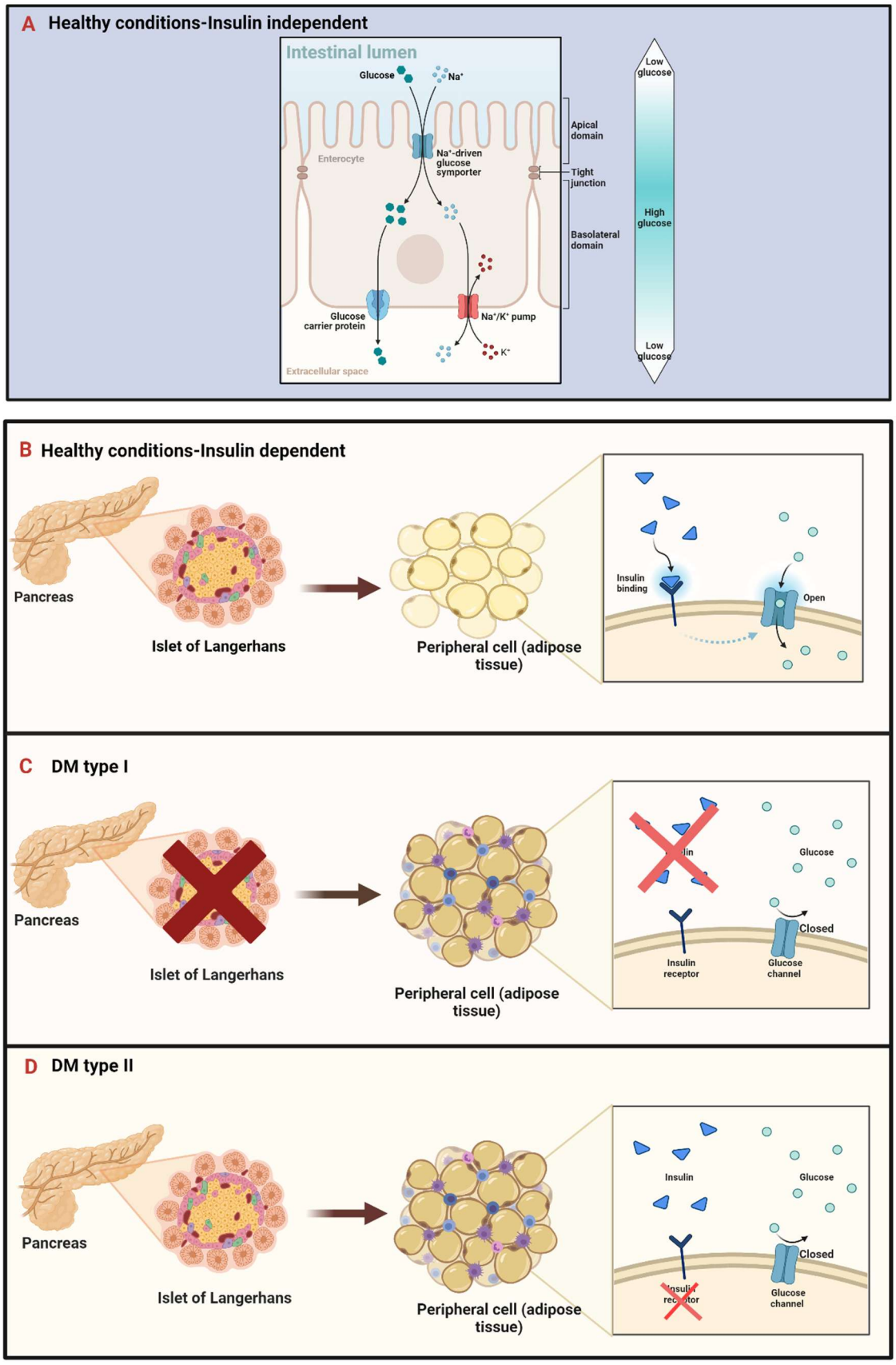

Figure 1.1: Pathophysiology of DM. A) Transcellular transport of glucose in the intestinal mucosa, exemplifying insulin-independent glucose transport into the cells. B) Insulin is secreted by the beta cells of the islets of Langerhans in the pancreas. The binding of insulin to receptors facilitates the opening of insulin-dependent glucose transporters, resulting in an influx of glucose into peripheral cells, such as adipocytes. C) In type I DM, beta cells are destroyed; consequently, insulin is not produced, which to hyperglycaemia. D) In type II DM, insulin receptors exhibit reduced sensitivity to insulin, leading to hyperglycaemia. Created with (Biorender, 2024).

1.1.3 Current treatments and Challenges

The first line treatment of DM type II starts with lifestyle modification such as diet and increase physical exercises with prescriptions of monotherapy (usually starts with Metformin) in case of presence of risk factors. Patients are advised to repeat the HbA1c test every 3 or 6 months. If HbA1c results shows persistent hyperglycaemia, a second antidiabetic medication (such as sulfonylurea) is added with monitoring the HbA1c after 3 or 6 months. If hyperglycaemia persists, a third medication is added or insulin therapy is initiated (NICE, 2022). However,, the treatment protocol for DM type I commences with insulin supplementation (NICE, 2022). Oral medications, such as metformin, are exclusively recommended for use in conjunction with insulin therapy and solely within the context of research studies, as this combination has not been demonstrated to enhance glycaemic control in DM type I.

DM type II is more common than DM type I. Moreover, there are two main challenges associated with current DM-II treatments. It is difficult to control hyperglycaemia with current DM medications (Higgins et al., 2016).

As insulin prescriptions and number of antidiabetic medication prescriptions per patient have increased, with only minimal improvement in HbA1c levels (Higgins et al., 2016). Additionally, even if multiple therapy improves glycaemic control, there is an increased risk of hypoglycaemia and other adverse (Qian et al., 2018).

Failure to manage hyperglycaemia in both DM type I and II leads to many life-threatening complications (Ali et al., 2022; Kurkela et al., 2021).

1.1.4 Hyperglycaemic and DM complications

As described in section 1.1.2, the process of glucose uptake by insulin sensitive cells is disturbed in DM leading to persistent hyperglycaemic conditions. As a result of this disturbance, polyol (sorbitol) pathway is activated as an alternative route of glucose metabolism in hyperglycaemia (Yan, 2018). This pathway consists of two main enzymatic steps: In first step, glucose is converted to sorbitol by aldose reductase enzyme with using NADPH (nicotinamide adenine dinucleotide phosphate) as a cofactor (Yan, 2018); In second step, sorbitol is converted to fructose by sorbitol dehydrogenase enzyme with using NAD+ as cofactor (Yan, 2018).

The polyol pathway fulfils physiological roles in specific tissues; however, its activation during chronic hyperglycaemia can result in numerous complications, especially in the context of DM (Yan, 2018). Oxidative stress and osmotic stress are the primary mechanisms through which the polyol pathway induces complications (Yan, 2018).

Oxidative stress arises from the depletion of NADPH due to the overactivation of the polyol pathway (Volpe et al., 2018; Yan, 2018). NADPH is essential for sustaining the reduced state of glutathione, a crucial antioxidant within the cell (Yan, 2018). The reduction of NADPH levels impairs the cell's ability to counteract ROS, resulting in oxidative stress (Volpe et al., 2018; Yan, 2018).

Sorbitol, produced due to the overactivation of the polyol pathway, exhibits low membrane permeability and accumulates within cells, resulting in formation of advanced glycation end (AGE) products and osmotic stress (Yan, 2018). This osmotic imbalance can induce cellular swelling and tissue damage, particularly affecting the kidneys, retina, and nerves (Dănilă et al., 2024; Yan, 2018). Moreover, overproduction of fructose resulting from the hyperactivation of the polyol pathway can accumulate in tissues such as the retina, thereby contributing to additional cellular damage and complications (Dănilă et al., 2024; Yan, 2018).

Figure 1.2 summarises the main complication caused as a result of persistent hyperglycaemia and activation of polyol pathway. In the present study the focus is on peripheral neuropathy and peripheral vascular disease that led to poor wound and diabetic foot ulcer (DFU)

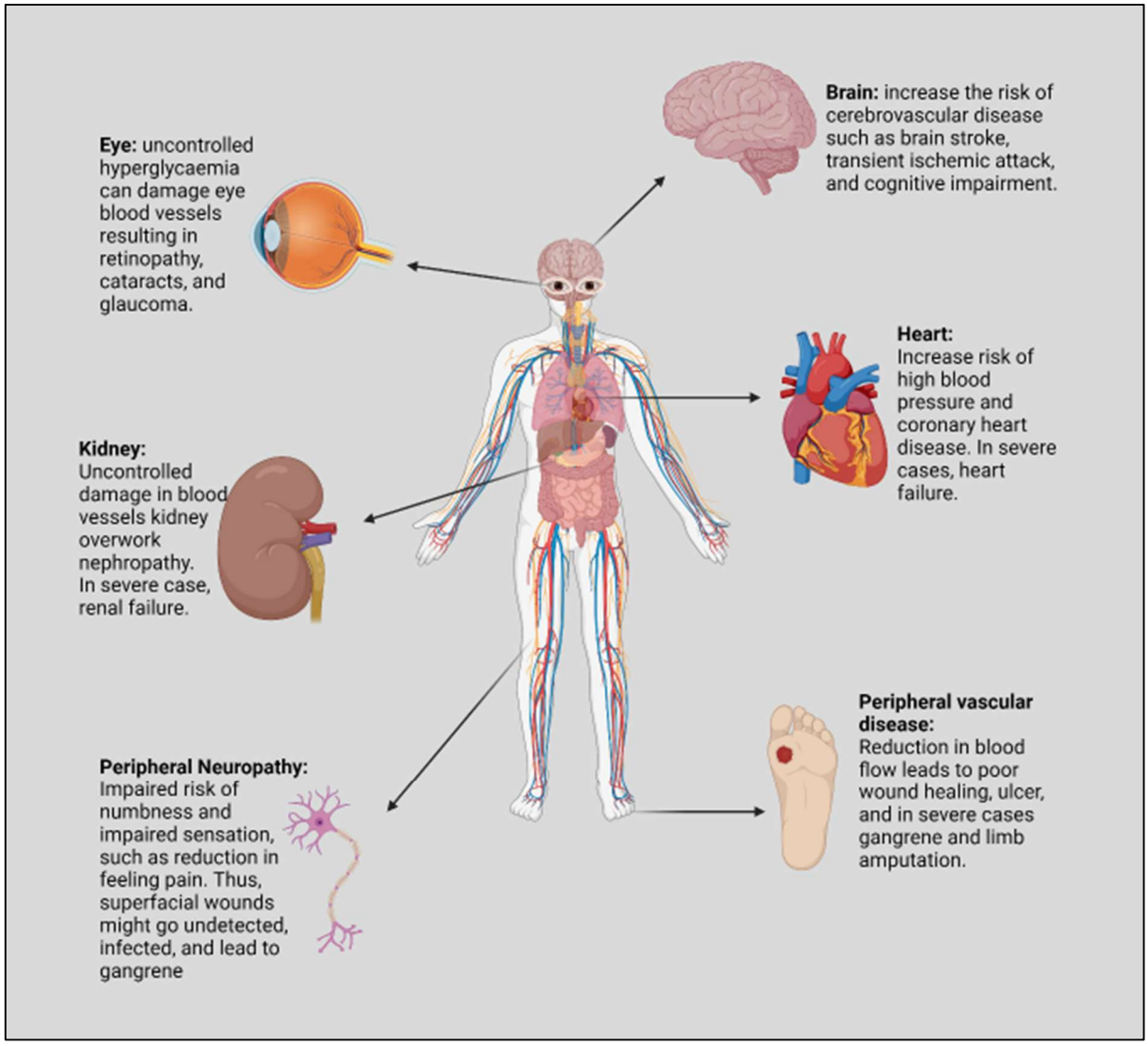

Figure 1.2: Primary complications of DM. Chronic uncontrolled hyperglycaemia results in activation of the polyol (sorbitol) pathway. This activation contributes to osmotic stress, oxidative stress, and cellular damage, leading to various complications. The figure illustrates the principal complications associated with DM. Created with (Biorender, 2024).

Peripheral neuropathy in DM results in both sensory and motor impairments within peripheral nervous system (Armstrong et al., 2023; Oh, 2020; Volpe et al., 2018). Sensory neuropathy is particularly significant in the context of ulcer formation, as it impairs the ability to detect alterations in pain, temperature, or pressure (Armstrong et al., 2023; Bandyk, 2018; Volpe et al., 2018). This loss of sensation prevents individuals from recognising injuries or irritation to their feet, which may remain undetected and exacerbate over time (Armstrong et al., 2023; Bandyk, 2018; Volpe et al., 2018).

Furthermore, diabetic neuropathy affects the autonomic nervous system, resulting in impaired sweat gland function and cutaneous dehydration (Armstrong et al., 2023; Oh, 2020). The diminished moisture content renders the skin more susceptible to fissuring and subsequent infection, thereby creating conditions conducive to ulcer formation (Armstrong et al., 2023; Bandyk, 2018). Moreover, motor neuropathy can result in muscular imbalances, altered pedal biomechanics, and the development of deformities such as hammertoes or Charcot foot, which exacerbate pressure on specific regions of the foot (Bandyk, 2018). These modified mechanical forces elevate the risk of cutaneous breakdown and ulceration (Armstrong et al., 2023; Bandyk, 2018).

Peripheral vascular disease, a significant complication of diabetes, is primarily attributed to the confluence of hyperglycaemia, dyslipidaemia, and hypertension (Bandyk, 2018). These factors, over time, contribute to the development of atherosclerosis, characterised by the hardening of blood vessels, which subsequently impedes blood flow to the extremities, particularly the lower limbs and feet (Bandyk, 2018). This diminished circulation compromises the body's wound healing capacity, rendering individuals with diabetes more susceptible to the development of chronic ulcers (Bandyk, 2018).

Chronic ischemia resulting from vascular disease impedes the delivery of oxygen, nutrients, and immune cells essential for tissue repair, thereby delaying wound healing (Levy et al., 2008). Moreover, impaired blood flow also diminishes the capacity to eliminate waste products from tissues, potentially leading to an accumulation of toxic metabolites that further compromise skin and soft tissue integrity (Levy et al., 2008). This process exacerbates the formation of diabetic foot ulcers, frequently in areas

subjected to high pressure or friction, such as the heels or toes (Bandyk, 2018; Levy et al., 2008).

The interaction between diabetic neuropathy and vascular disease exacerbates the risk of ulcer development (Kim, 2023). The presence of both conditions increases the likelihood of ulceration, and that ulcers in individuals with both neuropathy and poor circulation tend to be more severe and less responsive to treatment (Kim, 2023). Specifically, sensory neuropathy impairs the detection of early signs of skin injury, whilst vascular disease hinders the healing process (Kim, 2023). These conditions create a synergistic effect, wherein neuropathy increases the risk of injury, and vascular disease impairs recovery, resulting in chronic wounds that may become infected and resistant to healing (Kim, 2023) .

1.2 Wounds

1.2.1 Main Phases of Wound Healing Process

The skin is a complex ecosystem that provides mechanical and chemical protection against the invasion of pathogenic microbes (Kwiecien et al., 2019). It is divided into three main layers: the epidermis, the dermis, and the hypodermis. Each layer consists of different types of cells that play a crucial role in maintaining healthy function of skin (Kwiecien et al., 2019). Skin wound healing is a complex process that is divided into four main phases: 1- haemostasis, 2-inflammation, 3-proliferation, 4-remoding (Kwiecien et al., 2019) (Figure 1.3).

The haemostasis phase starts immediately following injury, and is characterised by the recruitment of circulating coagulant factors and platelets to the wound site to induce the formation of clots (Clark, 2001). During this stage, platelets release various cytokines and growth factors that are important to initiate the healing process (Diegelmann & Evans, 2004). Platelet- derived growth factor (PDGF) and transforming growth factor beta (TGF-β) are the two main factors released in homeostasis (Diegelmann & Evans, 2004). Both initiate the healing cascade by chemotaxis of macrophages, neutrophils, fibroblasts, and smooth muscle cells (Diegelmann & Evans, 2004). Moreover, TGF-β stimulates the macrophages to secrete additional cytokines such as tumour necrosis alpha (TNF-α), interleukin-1 (IL-1), fibroblast growth factor (FGF), and PDGF, which are important to initiate the following stages of wound healing (Diegelmann & Evans, 2004). Following clotting, an inflammatory response is induced, which is characterised mainly by recruitment of neutrophils, macrophages, and T-lymphocytes to the wound site and phagocytosis of damaged tissue and pathogenic microbes (Hart, 2002; Sylvia, 2003). In addition to phagocytosis, several chemokines and cytokines are secreted by immune cells, such as PDGF and TGF-β, that induces the transition from the inflammatory state to proliferative phase (Hart, 2002; Sylvia, 2003).

The proliferation phase is divided into two main processes: a- Reepithelialisation and b- Reconstitution of the dermis (Diegelmann & Evans, 2004). Reepithelialisation is a process of restoring the epidermal layer of the skin, which is characterised mainly by migration of keratinocytes to the site of wound, increase of keratinocytes proliferation, and repair of the intact basement membrane zone, a membrane that connect the

epidermis to the underlying dermis (Diegelmann & Evans, 2004). Dermal reconstitution process characterised by formation of granulation tissue to replace the clot formed in early stage of wound healing. The process of granulation tissue formation involves the migration and proliferation of fibroblasts, secretion of collagen, fibronectin and other extracellular matrix proteins, as well as the formation of new blood vessels (angiogenesis) (Diegelmann & Evans, 2004; Phillips, 2000). The main cytokines involved in proliferation phase are TGF-β, FGF, interleukins, and TNF-α (Diegelmann & Evans, 2004). Local factors in the wound microenvironments, such as low oxygen tension, acidic medium, and lactate, play a vital role in stimulating the process of angiogenesis and promote wound healing (Gethin, 2007; Haller et al., 2021; Percival et al., 2014; Saghiri et al., 2020)

In the final stage, the remodelling phase, fibroblasts start to differentiate into contractile myofibroblasts that cause contraction of the wound. Also, the deposited collagen III in the extracellular matrix is replaced with collagen I which has a higher tensile strength (Diegelmann & Evans, 2004).

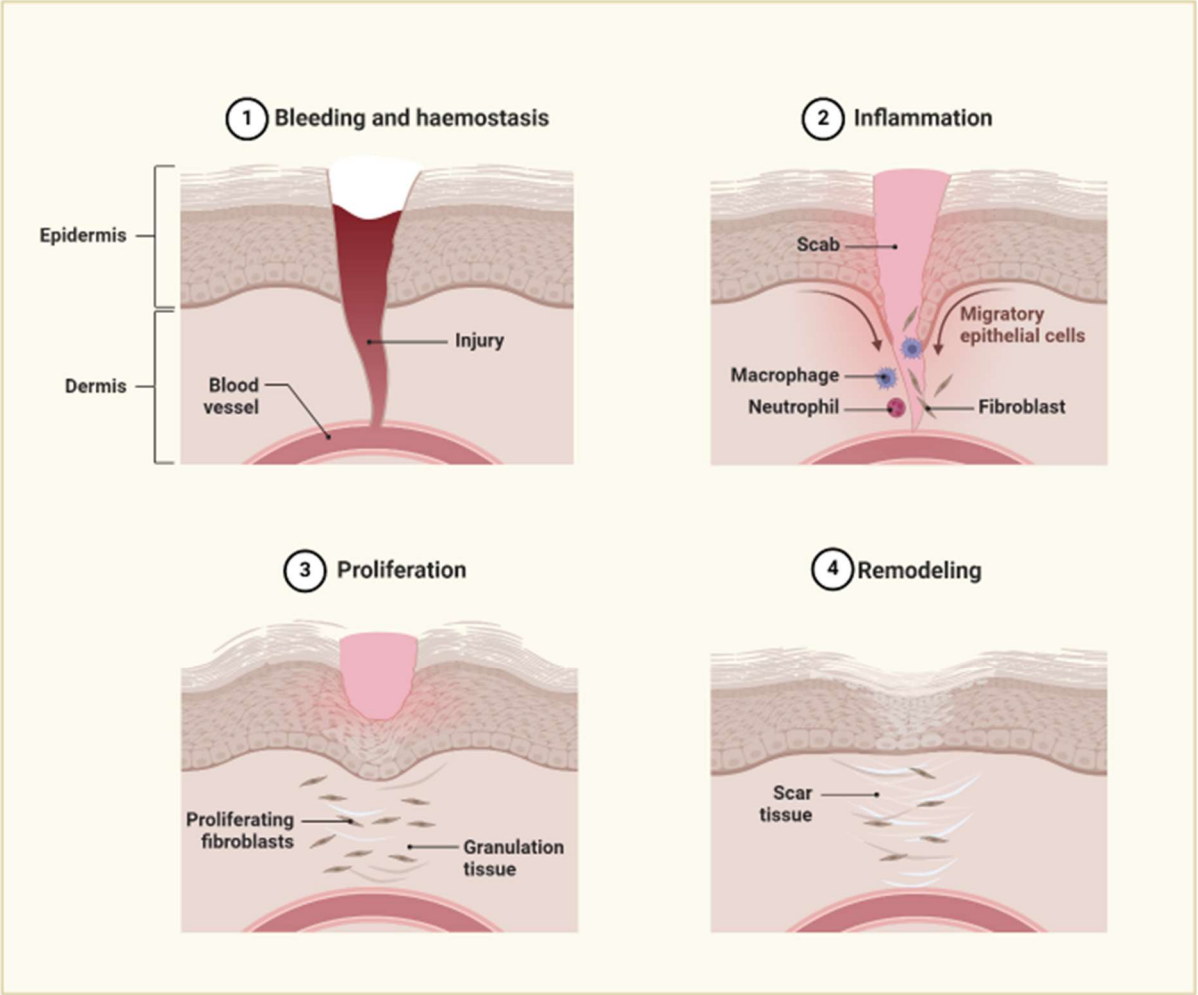

Figure 1.3: Four phases of acute wound healing. 1-Hemostasis characterised by the recruitment of platelets and coagulant factors (i.e., formation of clots). 2-Inflammation is characterised by the recruitment of neutrophils and macrophages to the wound site. Phagocytosis in damaged tissues and pathogenic microbes. Secretion of chemokines and cytokines to induce skin cell proliferation. 3-Proliferation: Characterised by keratinocyte and fibroblast proliferation and migration. 4-Remodeling: Fibroblasts begin to differentiate into contractile myofibroblasts that contract the wound, and collagen III is deposited in the extracellular matrix. Created with (Biorender, 2024).

1.2.2 Chronic wounds in DM

Untreated hyperglycaemia causes alterations in the functions of skin cells lead to formation of chronic wounds and increased risk of wound infections (Falanga, 2005; Kim et al., 2018). Alteration in vascular permeability and reduction in blood supply are two of the main aetiologies of impaired wound healing in DM (Falanga, 2005).These abnormalities involve thickening of the capillary basement membrane and a reduction of capillary size (Chen et al., 2010; Falanga, 2005)

As a result of these capillary abnormalities, the inflammatory phase is altered in diabetic patients (Falanga, 2005; LoGerfo Frank & Coffman Jay, 1984). The abnormal thickening of blood vessels causes a disturbance in the number of inflammatory cells reaching the site of injury and thus increases the risk of infections (Maruyama et al., 2007; Okizaki et al., 2015; Spampinato et al., 2020). Moreover, even if the inflammatory cells are present, an impairment in their function was observed (Falanga, 2005; Maruyama et al., 2007). For example, even if macrophage and leucocytes are present in diabetic wounds, their phagocytosis ability is reported to be impaired (Kidman, 2008; Lioupis, 2005; Maruyama et al., 2007; Okizaki et al., 2015). One of the main mechanisms by which DM causes disturbed wound healing is through promoting continued inflammation, rather than progressing to proliferative phase of wound healing (Andrade et al., 2017; Krisp et al., 2013). This is because the body may secrete more inflammatory cytokines in response to disturbed inflammatory response in hyperglycaemia, which may persist in the diabetic wound and prolong the inflammatory process longer than in healthy individuals (Kidman, 2008; Krisp et al., 2013; Wetzler et al., 2000).

The proliferative phase has been reported to be altered in DM as a results of alteration inflammatory response (Kim et al., 2018). There is a decrease in the factors which promote proliferation, with pro-inflammatory cytokines dominating the proliferative cytokines (Lobmann et al., 2002). This leads to alteration proliferation and migration of both keratinocytes and fibroblasts. However, contradicting results were reported on how the proliferation is altered. For example, Keratinocyte proliferation was reported to be reduced in diabetic mice (Sakai et al., 2003) and in human keratinocytes cell lines exposed to glycated albumin (Chen et al., 2010). However, no alteration was observed in another study investigating keratinocyte differentiation in rats (Park et al., 2011). Moreover, growing keratinocytes in different glucose concentrations revealed

that high glucose level concentration induces keratinocyte differentiation whilst lowering the proliferation rate (Spravchikov et al., 2001). This disturbance in keratinocytes proliferation-differentiation balance might be the mechanism by which hyperglycaemia causes impaired wound healing in DM (Spravchikov et al., 2001). Moreover, there is also a suggestion that fibroblasts are less responsive to growth factors in DM (Loots et al., 2002).

The final stage of wound healing is reported to be disturbed in DM (Bermudez et al., 2011; Sharp & Clark, 2011). There is a reduction in collagen deposition and thus, reduced tensile strength and prolonged wound healing (Bermudez et al., 2011; Lioupis, 2005). Moreover, it has been reported that hyperglycaemia modify collagen and leads to production of advance glycated end products (Bermudez et al., 2011; Snedeker & Gautieri, 2014). A glycated collagen matrix has been reported to be more brittle and more rigid compared to a non-glycated collagen matrix (Ibuki et al., 2012; Quondamatteo, 2014; Sell et al., 2005). Table 1.1 summarises the main changes in wound healing cascade in DM.

Table 1.1: The main alteration in wound healing phases in DM (Dasari et al., 2021; Falanga, 2005)

Healthy wound healing stages	DM associated alteration
1- Haemostasis	**1- Poor blood supply.** **2- Increased infection.**
2- Inflammation	**1- Slow recruitment of macrophages and neutrophils** **2- Persistent inflammation rather than moving forward to the proliferative phase of healing.**
3- Proliferation	**1- Alteration in keratinocytes proliferation and migration.** **2- Alteration in fibroblasts proliferation, migration, and activity.** **3- Alteration in collagen deposition** **4- Reduced fibroblast activity**
4- Remodelling	**1- Formation of glycated collagen matrix has been reported to be more brittle and more rigid compared to a non-glycated collagen matrix** **2- Reduced tensile strength**

1.2.3 Current treatments for DFU in DM

Poor wound healing and diabetic foot ulcer (DFU); two of the most common complications of DM (IDF, 2024; McDermott et al., 2023). 40 to 60 million diabetic patients are diagnosed with diabetic foot ulcer worldwide (IDF, 2024; McDermott et al., 2023). The prevalence of DFU is higher in DM type II than DM type I (Zhang et al., 2017). Other common skin disorders associated with DM include skin inflammatory diseases such as psoriasis, bacterial and fungal infections, and xerosis (Demirseren et al., 2014). A clinical analysis of 750 diabetic patients revealed 79.2 of patients had skin disorders (Demirseren et al., 2014).

The treatment regimen of skin complications in DM involves prescribing antibiotics to heal the infection, wound debridement, wound dressing, and limb amputation in severe cases (NICE, 2024b). Unfortunately, treatment failure in DFU is common and this is due to an increase in wound infections with multidrug resistant bacteria (Vardakas et al., 2008). DFUs and limb amputation are surprisingly associated with high 5 years mortality rate which is similar to or higher than some of the common types of cancer (Armstrong et al., 2020; Armstrong et al., 2007). Thus, further studies are required to investigate to find novel products to heal or prevent diabetic wounds and reduce the risk of limb amputation (Rodríguez-Rodríguez et al., 2022).

1.3 The Human Skin Microbiota

1.3.1 Composition, Distribution, Diversity & Abundance in Healthy Individuals

The skin harbours various microorganisms. Bacteria were reported to be the most abundant kingdom in the skin microbiota (Oh et al., 2016). Fungi, viruses, and archaea were also found on skin but with less relative abundance compared to bacteria (Findley et al., 2013; Hannigan et al., 2015; Oh et al., 2014; Umbach Alexander et al., 2021)

The composition of skin bacterial communities was found to be mainly dependant on the physiology of skin site. Moreover, the alteration in distribution and relative abundance of the bacterial communities was reported to be based on alteration in the distribution of sweat and sebaceous glands (Costello et al., 2009; Oh et al., 2014). For example, *Staphylococcus* and *Corynebacterium* species (spp.) are mostly found in the moist areas of the skin such as the axilla (Callewaert et al., 2013), bend of elbow and in feet, whereas the oily sites of the skin harbours *Propionibacterium* spp. such sebaceous sites and hair follicles (Grice et al., 2009).

In contrast to bacteria, the composition of fungal communities a was found to be similar across the body core regardless of distribution of sweat and sebaceous glands (Findley et al., 2013). *Malassezia* found predominant at the core body and arms, whereas a diverse combination of *Aspergillus* spp., *Malassezia* spp., *Rhodotorula* spp., *Cryptococcus* spp., *Epicoccum* spp. and other fungal spp. were found in foot sites (Findley et al., 2013).

In contrast to fungi and bacteria, colonisation by viruses was specific to the individual rather than skin physiological site (Oh et al., 2016). Apart from bacteriophages, mainly those related to *Propionibacterium* spp. and *S.* spp., no other DNA viruses has been found in the skin of healthy individuals (Hannigan et al., 2015; Oh et al., 2016).

Archaea, mainly *Thaumarchaeota,* was also reported to be part of human skin microbiota mainly living on front torso of human skin (Probst et al., 2013). However, based on another study, archaea presence on human skin was found to be limited and uncommon (Umbach Alexander et al., 2021)

1.3.2 Skin Microbiota Function in Wound Healing

Although skin microbiota has been reported to play a vital role in maintaining healthy skin function, the role skin microbiota in different stages of wound healing is not yet fully understood (Tomic-Canic et al., 2020). To date, it appears that the main mechanisms by which some members of skin microbiota influences wound healing is through altering the immune response, and promoting the production of antimicrobial peptides (AMPs) that prevent the invasion of pathogenic microbes (Johnson et al., 2018; Tomic-Canic et al., 2020).

Staphylococcus epidermidis (S. epidermidis), which is found extensively on skin, is most widely investigated regarding its effect in wound healing (Linehan et al., 2018; Naik et al., 2015). Colonisation with *S. epidermidis* is reported to prevent wound infections by enhancing the innate barrier immunity. This is mainly though induction of immune cells such as skin T cells, downstream modulation of TNF-α and upregulation of toll-like receptors (TLR) (Linehan et al., 2018; Naik et al., 2015) . Also, *S. epidermidis* has been reported to protect the skin from the invasion of pathogenic bacteria by stimulating keratinocytes to secrete AMPs such as modulin and beta-defensin (Cogen et al., 2010; Nakatsuji et al., 2017; Simanski et al., 2019). In addition to preventing pathogenic infections, when applied to a breached skin barrier model, *S. epidermidis* was found to promote wound healing by alteration of keratinocyte immune function and differentiation (Duckney et al., 2013). Interesting, it is reported that the CD8+ T cells induced by *S. epidermidis* promotes skin re-epithelialisation and wound healing following injury (Linehan et al., 2018)

Moreover, *S. epidermidis* has been reported to produce short chain fatty acids (SCFAs) which have been reported to have an antimicrobial effect against methicillin-resistant *S. aureus* (Alva-Murillo et al., 2012; Schwarz et al., 2017). *S. epidermidis* has been reported to improve wound healing though secretion of different acids that have many healing effects. For example, Lipoteichoic acid inhibits inflammatory cytokine production from keratinocytes and inflammation following injury though a TLR-2 mechanism (Lai et al., 2009). However, murine wound models have reported that *S. epidermidis* biofilms decreases re-epithelialisation in wounds, and this has been revealed to be influenced by quorum sensing (Schierle et al., 2009).

The presence of biofilms of *Staphylococcus aureus* (*S. aureus)* resulted in significant reduction in scratch closure in keratinocytes and fibroblasts cultures (Kirker et al., 2009; Kirker et al., 2012). Moreover, *S. aureus* biofilm increased the release of TNF-α and decreased the release of IL-6, matrix metalloproteinase (MMP-3) and VEGF from human dermal fibroblasts which leads to poor wound healing (Secor et al., 2011). Murine wound models have reported that *S. aureus* biofilms decrease re-epithelialisation in wounds, and this has been reported to be influenced by quorum sensing (Schierle et al., 2009). However, *S. aureus* has been shown to protect the skin from invasion of pathogenic bacteria though stimulating the innate immune response of skin via production of AMPs such as Human β defensins (Midorikawa et al., 2003, Wanke et al., 2011).

Propionibacterium acnes (P. acnes) are found to induce differentiation of keratinocytes when applied to breached skin barrier models, suggesting it has potential to induce barrier repair in response to injuries (Duckney et al., 2013). Moreover, *P. acnes* induce the secretion of bacteriocins which protect the sebaceous ducts from other pathogenic inhabitants. Also, it modulates the immune response though induction of expression of TLR2 and TLR4 in keratinocytes (Johnson et al., 2018).

In summary, various skin commensal bacteria might have both advantageous and damaging effects on skin cells in wounds, which may dictate whether these microbes take on the role of skin pathogen or skin commensal in healing wounds (Johnson et al., 2018; Tomic-Canic et al., 2020). Further studies are needed to understand the role skin commensal bacteria on skin cell function in wound healing, as this will help in identifying novel pathways to heal chronic wounds such as diabetic wounds.

1.4 The Human Skin Microbiota in DM

1.4.1 Composition, Distribution, Diversity, and Abundance in Intact Non-Injured Skin of Diabetic Patients and Individuals with Risk of DM

Both microbiological culture and next generation sequencing studies support a significant dysbiosis in microbiota of intact non-injured skin of diabetic patients leading to increased risk of skin infections (Pam et al., 2006; Redel et al., 2013; Thimmappaiah Jagadeesh et al., 2017) (Figure 1.4 A & B).

The skin microbiota in DM was reported to be more diverse and had different composition in comparison to healthy individuals (Redel et al., 2013; Thimmappaiah Jagadeesh et al., 2017).

Cultural and biochemical investigations reported that *S. epidermidis* was significantly more frequent in armpits of diabetic patients in comparison to healthy individuals (Pam et al., 2006). Moreover, *S. epidermidis* is significantly more prevalent in the toe-web space of diabetic patients in comparison to healthy individuals (Thimmappaiah Jagadeesh et al., 2017). In both skin regions, the armpits and toe-web space, *S. aureus* was the second most prevalent bacterial spp. isolated from different regions of intact diabetic skin (Pam et al., 2006; Thimmappaiah Jagadeesh et al., 2017).

However, contradicting results were reported when performing a quantitative polymerase chain reaction (PCR) and high throughput 16S ribosomal RNA of foot swabs compared to cultured and biochemical investigations, as a significant decrease in the quantity of coagulase negative *Staphylococcus* spp., such as *S. epidermidis*, with significant increase in the more virulent *S. aureus* in foot of diabetic patients in comparison to healthy individuals was observed (Redel et al., 2013). These alterations were reported to be a significant factor in increasing the risk of infections and developments of ulcers in diabetic skin (Redel et al., 2013).

The abundance of *Corynebacterium* was higher in the foot on the diabetic patients in comparison to healthy individuals (Redel et al., 2013). Moreover, the relative abundance of *Corynebacterium* spp. was higher in the skin of obese individuals (Brandwein et al., 2019). As obesity is considered one of the risk factors of DM, it is suggested that the alteration in *Corynebacterium abundance* might be used as a

marker for obesity and other manifestations of the metabolic syndrome (Brandwein et al., 2019).

1.4.2 Composition, Distribution, Diversity & Abundance of Skin Microbiota in DFU

Different microbiological culture and next generation sequencing have been used to assess and identify the composition of microbiota in DFU. Variation in the composition and abundance of skin microbiota was observed among the published articles (Figure 1.4 C & D).

Culture analysis revealed that bacteria was the most common microbe isolated from the DFU. Fungi were also found in DFU, however, was isolated to lower extend compared to bacteria (Bansal et al., 2008). *K. pneumonia, P. aeruginosa, E. coli, AND S. aureus* was the most predominant bacterial spp. in DFU, whereas *Aspergillus flavus, Candida tropicalis, Aspergillus Niger, Candida albicans* and *Fusarium spp*. were the most common fungal spp. found in DFU (Bansal et al., 2008). Only bacterial spp. was detected in another culture analysis study with *Staphylococcus, Streptococcus, Proteobacteria*, and *anaerobes* being the most predominant spp. in the neuropathic DFU (Gardner et al., 2013).

96% of the microbiota genome in DFU was detected to belong bacterial spp. by shotgun metagenomic and 16S rRNA sequencing with *S.* (particularly *S. aureus)*, *Corynebacterium spp.* (mainly *C. stratum*), *Pseudomonas* spp. (particularly *P. alcaliphila* and *P. aeruginosa*), and *Streptococcus* spp. (particularly *S. agalactiae*, *S. anginosus* and *S. dysgalactiae*) being the most abundant spp. (Kalan et al., 2019). Another qPCR and pyrosequencing 16S rRNA analysis revealed that *Staphylococcus, Finegoldia, Streptococcus, Corynebacterium and Pseudomonas* are the dominant bacterial genera in DFUs (Gardiner et al., 2017; Loesche et al., 2017). Although, another 16S rRNA sequencing study of neuropathic DFUs reported the dominance of *Staphylococcus, Proteobacteria, Anaerobes, Streptococcus* bacteria in the DFU (Gardner et al., 2013). Moreover, Culturomics analysis of DFU reported that *S. aureus, S. epidermidis, E. cloacae, S. lugdunensis, E. faecalis P. mirabilis, F. magna* are the most prevalent microbiota in DFU (Jneid et al., 2018).

Interestingly, ITS1 high throughout sequencing reported that fungal communities were found in 80% of DFUs. *Basidiomycota* (mainly *T. asahii* and *R. diobovatum)* and

Ascomycota (mainly *C. herbarum* and *C. albicans)* were the main isolated fungal communities in DFU (Kalan et al., 2016).

To further understand the role of skin microbiota in DFU, the composition of skin microbiota in DFU were compared to contralateral healthy skin tissue and healthy control (Gardiner et al., 2017). The composition of skin microbiota in DFU was reported to be significantly altered in comparison to contralateral healthy skin tissue and healthy control (Gardiner et al., 2017). Based on DNA sequencing and eubacterium-specific PCR-denaturing gradient gel electrophoresis comparing wound microbiota to adjacent healthy skin, *S. aureus* were reported to be most abundant microbiota in DFU (Oates et al., 2012). *Streptococcus, pseudomonas* and *candida* were less prevalent in DFU (Oates et al., 2012). Moreover, another study found *Pseudomonas, Bacteroides,* and *Enterococcus* were reported to be significantly more abundant in DFUs compared to adjacent healthy skin (Park et al., 2019). However, *Staphylococcus, Sphingomonas, Paracoccus, Rothia, Methylobacterium, Micrococcus Propionibacterium, Lactobacillus, Brevibacterium, Streptococcus, Acinetobacter, and Corynebacterium* were more abundant in the contralateral healthy skin in comparison to DFU (Park et al., 2019).

The present study highlights the microbiota composition of DFU is widely investigated. Thus, to add valuable knowledge to microbiome, wound, and DM research. The present study recommends further studies need to focus on investigating the effect of specific members of skin microbiota on skin cells function and wound healing in an experimentally designed diabetic condition. Particularly focusing on the bacterial isolates that identifies in DFU in published articles. As this will add a valuable knowledge to published data and help in identifying novel therapeutics to treat DFU. In present study, the effect of *S. epidermidis, S. aures*, and *C. jeikeium* on the function of human skin cells will be studied in an experimentally designed diabetic condition.

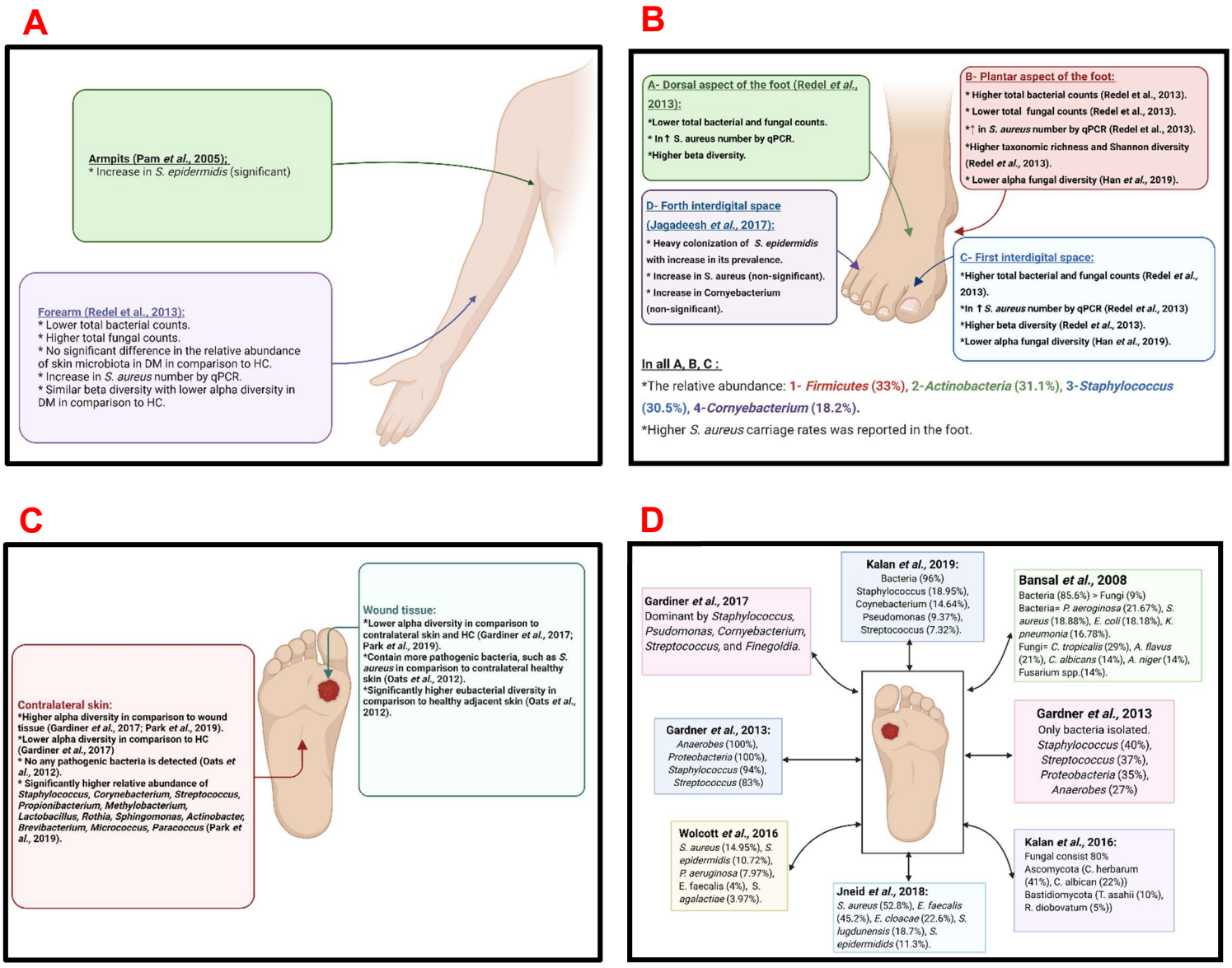

***Figure 1.4*: Distribution of predominant skin microbiota in DM.** A-Skin microbiota in non-injured skin at the axillary and antebrachial regions in DM; B-Skin microbiota in non-injured pedal skin in DM. C-Comparative analysis of DFU with contralateral healthy skin. D-Skin microbiota isolated from DFUs. Created with (Biorender, 2020).

1.4.3 Skin Microbiota Function in DFU Healing

Although different stages of wound healing process are now well characterised and the molecular and cellular mechanisms of impaired wound healing in DM was widely investigated (Section 1.2.1 & 1.2.2). The role of skin microbiota in each stage of wound healing in chronic diabetic wound is not yet fully understood (Tomic-Canic et al., 2020). To date, the available knowledge has mainly focused on linking the specific members of microbiota to clinical manifestation of wounds. Table 2 summarises the association of skin microbiota and the prognosis of diabetic wounds (Sabir, 2020).

A reduction in diversity of microbiota alongside increase in its abundance were reported as the severity of DFU increased (Bansal et al., 2008; Park et al., 2019). The duration of infection, wound size and healing status were not correlated to the abundance of any bacterial spp. by a study (Gardiner et al., 2017). However, based on another metagenomic studies the relative abundance of specific microbiota might be correlated to the duration of DFU (Gardner et al., 2013). For example, the presence of higher level of proteobacteria and anaerobic bacteria was associated with deep and persistent DFU. Whilst new and superficial ulcers was associated with higher abundance of *S.* spp. (Gardner et al., 2013). Interestingly, another study reported that higher relative abundance of *Firmicutes* was observed in superficial DFU. Whereas higher relative abundance of *Peptoniphilus, Bacteroidetes, Dialister Porphyromonas, and Prevotella* were associated with deep DFU (Park & Lee, 2017).

Culturomics, shotgun and 16S rRNA sequencing revealed that *S. aureus* was associated poor prognosis of DFU (Jneid et al., 2018; Kalan et al., 2019). Principle component analysis reported that a positive correlation between the presence *E. faecalis, S. epidermidis* and *S. lugdunensis* and wound recovery, whereas the presence of *F. magna* in DFWs was the main factor linked to the wound poor prognosis (Jneid et al., 2018)

Shotgun and 16S rRNA sequencing revealed that a positive correlation between *Corynebacterium striatum* and DFU duration (Kalan et al., 2019).

Lower relative abundance of *Ascomycota* was correlated with wound healing after 8 weeks. This suggest that quantifying the amount of *Ascomycota* on initial patients' admission might help in predicting the healing time of DFUs (Kalan et al., 2019).

Moreover, the presence of yeast biofilm was correlated with wound necrosis and poor prognosis of DFU (Kalan et al., 2019).

DFU with ischemic aetiology had different microbiota community structure due to lower oxygen level. However, the number and microbial community structure was not associated to oxygen level in DFU with neuropathic aetiology (Gardner et al., 2013). Interestingly, higher fungal diversity was correlated with reduction in tissue oxygenation, which lead to poor DFU prognosis (Kalan et al., 2016). Moreover, the relative abundance of *Anaerococcus* was higher in DFU caused due to neuropathic pain in comparison to DFU with ischemic aetiology (Park et al., 2019)

16S rDNA pyrosequencing of different types of chronic wounds revealed that bacterial composition of chronic wound was not influenced by neither wound type nor patient demographics (Wolcott et al., 2016). However, several patients' demographic factors were reported to have a great effect on microbiota of DFU by another study such as personal hygiene, severity of wounds, glycaemic control and previous antibiotics intake (Jneid et al., 2018).

The predicted function of skin microbiota was significantly altered among diabetic patients with different clinical factors. For example, ascorbate and aldarate metabolism were higher in mild DFU, whilst lipopolysaccharide biosynthesis was higher in severe DFU. Higher level of arachidonic acid metabolism was observed diabetic patients with HA1c was higher that 8%, whereas glutathione metabolism was significantly higher in patients with HA1c was lower that 8% (Park et al., 2019).

Poor wound healing was reported to be associated with the presence of microbiota biofilm, such as *Staphylococcus* biofilm, and existence of virulent metabolism pathways, such as biosynthesis of polysaccharide and energy production though the non-glycolytic pathway (Kalan et al., 2019) Some DFU were found to harbour mixed bacteria-fungi biofilm. For example, mixed yeast and bacteria biofilm was found (Kalan et al., 2019).

Pathogenic and allergenic fungal taxa were both isolated from the DFU. Interestingly, deep DFU was associated with presence of pathogenic fungi, whilst controlled hyperglycaemia and low systematic inflammation were associated with existence of allergenic fungi (Kalan et al., 2019).

Table 1.2 : Summary of the results of the microbiota associated with the clinical factors of DFUs (Sabir, 2020)

Clinical factors	Associated with	Reference
Deep DFUs & persistence for longer time (Severe)	Increase in the prevalence of skin microbiota.	(Bansal et al., 2008)
	Reduction in diversity of skin microbiota	(Park et al., 2019)
	higher level of *proteobacteria, anaerobic,* *S. aureus & F. magna* associated with poor prognosis	(Gardner et al., 2013) (Jneid et al., 2018) (Kalan et al., 2019)
	Corynebacterium striatum positively correlated with DFUs duration	(Kalan et al., 2019)
	Wound highly associated with the formation of yeast biofilm and pathogenic fungi biofilm.	(Kalan et al., 2019)
	*The structure and number of microbial communities is not associated with oxygen level of wound tissue in DFU with neuropathic aetiology. *Decrease in tissue oxygenation was correlated with higher the fungal diversity	(Gardner et al., 2013) (Kalan et al., 2016)
	Delayed wound healing were correlated with increased in stability of bacterial communities in comparison with the faster healing DFUs.	(Loesche et al., 2017)
	The increase in stability of fungal communities was positively correlated with increase in microbiota biofilm formation.	(Kalan et al., 2016)
	DFU of ischemic aetiology was associated with significantly lower relative abundance *Anaerococcus* in comparison DFU of neuropathic aetiology	(Park et al., 2019)
	Formation of mixed bacteria-fungi biofilm, for example, formation of biofilm by bacteria and yeast.	(Kalan et al., 2019)

Poor glycaemic control	High relative abundance of *S.* and *Streptococcus, Bacteroidetes, Peptoniphilus* in DFUs.	(Gardner et al., 2013) (Park et al., 2019)
Diabetic patients diagnosed with end stage renal disease (ESRD)	lower relative abundance of *Bacteroidetes, Prevotella, Peptoniphilus*, and *Porphyromonas* in DFUs tissue	(Park et al., 2019)
The predicted function of skin microbiota	Significantly different among diabetic patients	(Park et al., 2019) (Kalan et al., 2019)
Superficial and newly diagnosed DFU	Increase in the abundance of *S.* spp., *Firmicutes, Bacteroidetes, Prevotella, Peptoniphilus, Porphyromonas, and Dialister.*	(Gardner et al., 2013) (Park & Lee, 2017)
Wound recovery	*Higher level *of S. epidermidis, S. lugdunensis, E. faecalis.* *Lower relative abundance of *Ascomycota.*	(Jneid et al., 2018) (Kalan et al., 2019)

1.5 *S. epidermidis*

1.5.1 Distribution & abundance

S. epidermidis is considered one of the most abundant colonisers of skin and it can be isolated from different skin microenvironments including moist, dry, sebaceous and l region (Brown & Horswill, 2020; Byrd et al., 2018).

1.5.2 Metabolism & physiology

S. epidermidis is a gram-positive, coagulase-negative, *staphylococci* (Constantinides et al.). Coagulase is an extracellular protein which binds to prothrombin in the host to form *staphylothombin*. Thrombin has protease activity, which allows it to convert fibrinogen to fibrin and induce the formation of clots. Thus, as a results of lacking the coagulase, *S. epidermidis* cannot induce clots (Otto, 2009)

Some *S. epidermidis* strains produce biofilms that consist mainly of extracellular DNA proteinaceous factors (Bhp, Aap, and Embp), polysaccharide intracellular adhesion (PIA), extracellular DNA and teichoic acids (Otto, 2009; Wanke et al., 2011).

1.5.3 Secreted factors

S. epidermidis secretes AMPs and acids production, which are believed to have many impacts on skin function and protect the skin from the invasion of pathogenic microbes.

The main AMPs secreted by *S. epidermidis* are modulin and lantibiotics, both reported to enhance the killing of pathogen bacteria such as *S. aureus* and *Streptococcus pyogenes* (Cogen et al., 2010).

The main acids produced by *S. epidermidis* are lipoteichoic acids, lipopeptide LP78 and SCFAs (Kao et al., 2017). Lipoteichoic acids and lipopeptide LP78 are both reported to induce inflammatory response in a Toll-like receptor (TLR)-3-dependent mechanism (Lai et al., 2009).

SCFAs produced by *S. epidermidis* have been reported to have many beneficial effects such as having antimicrobial effect against methicillin-resistant *S. aureus* and *P. acnes* , suppress cutaneous inflammation by promoting skin T-regulatory cells, and improve the skin barrier properties (Kao et al., 2017; Park et al., 2021; N. Salgaonkar et al., 2022; Schwarz et al., 2017; Wang et al., 2014)

1.5.4 Interactions with host

The current available knowledge on *S. epidermidis* skin interaction has mainly focused on its interaction with immune cells and keratinocytes.

S. epidermidis can modulate both adaptive and/or innate immune responses. *S. epidermidis* is reported to accelerate keratinocyte progression through initiation of immune response such as inducing skin T cells, downstream modulation of TNF-α and upregulation of toll-like receptors (TLR) (Linehan et al., 2018; Naik et al., 2015). Some *S. epidermidis* strains reduces the *S. aureus* induced cytokine production and neutrophil recruitment thus could potentially be protective against severe skin infections (Bitschar et al., 2020). In addition to positive effects on innate immune responses, *S. epidermidis* participates in development and priming of adaptive immune system (Brown & Horswill, 2020). For example, *S. epidermidis* skin colonisation is necessary for development and function of effector T cells (Naik et al., 2012) and early priming and localisation of mucosal associated invariant T cells (MAIT cells) (Constantinides et al., 2019). Moreover, it is reported that *S. epidermidis* stimulates the accumulation of CD8+ T lymphocytes in sites of injury in skin by antigen presentation in dendritic cells (Linehan et al., 2018). Interestingly, genome analysis of *S. epidermidis* in combination with *in vitro* experiments reported that main interaction with dendritic cells were by N-formyl methionine peptides secreted by *S. epidermidis* to T lymphocytes (Linehan et al., 2018). It appears from current knowledge that the *S. epidermidis* has a vital role in the immune response of the skin. Although immune response plays an important role in wound healing, the effect of *S. epidermidis* on inflammatory response of wound healing is yet not fully understood.

The main interaction of *S. epidermidis* with keratinocytes is through affecting the proliferation and antimicrobial production of keratinocyte (Duckney et al., 2013; Simanski et al., 2019; Wanke et al., 2011). *S. epidermidis* is reported to induce proliferation and differentiation of keratinocytes when applied to breached skin barrier models, suggesting that it might induce barrier repair response in injuries (Duckney et al., 2013). Moreover *S. epidermidis* has been reported to protect the skin from the invasion of pathogenic bacteria by stimulating keratinocytes to secrete antimicrobial peptides such as and beta-defensin (Simanski et al., 2019; Wanke et al., 2011).

1.5.5 Potential for virulence

S. epidermidis does not produce aggressive virulence factors and is considered to have commensal relationship with the skin (Otto, 2009). However, some pathogenic strains of *S. epidermidis* are virulent and cause various hospital acquired infections (Chabi & Momtaz, 2019). This is mainly through production of biofilms which are reported to resist damage by host immune system and are antibiotics resistant (Otto, 2009). In addition to antibiotic resistance, genome analysis of some pathogenic *S. epidermidis* strains showed the existence of various virulence factor genes such as exfoliative toxins A and B (eta and etb) (Chabi & Momtaz, 2019). The main toxin secreted by both commensal and pathogenic *S. epidermidis* is phenol soluble modulins PSMs. Some types of PSMs produced by *S. epidermidis* are cytolytic and can lyse human neutrophils similar to the PSM produced by the *S. aureus* (Wang et al., 2007; Yao et al., 2005). However, other types of PSMs are moderately or non-cytolytic types. The toxin production pattern of *S. epidermidis* shows higher production of the moderately or non-cytolytic than the highly cytolytic PSM (Wang et al., 2007; Yao et al., 2005). This might be the reason for low aggressiveness of *S. epidermidis*, in comparison to the other PSMs produced *staphylococci* such as *S. aureus* (Otto, 2009; Wang et al., 2007; Yao et al., 2005).

1.6 *S. aureus*

1.6.1 Distribution & abundance

S. aureus is both commensal bacteria and human pathogen. It is suggested that 30% of human population is colonised with commensal *S. aureus.* However, this bacteria is reported to causes severe infections such as bacteraemia, soft tissue and skin endocarditis, pleuropulmonary, osteoarticular, and device-related infections (Tong et al., 2015).

1.6.2 Metabolism & physiology

S. aureus is a gram-positive coccus. Unlike *S. epidermidis*, *S. aureus* is coagulase positive bacteria. Two different types of coagulases are produced by *S. aureus*: *staphylocoagulase* and von Willebrand factor binding protein. Both are reported to induce the formation of clots though conversion of prothrombin to fibrin. This unique ability of *S. aureus* to induce clotting are the main mechanism by which it causes severe cardiovascular infections such as endocarditis, that *S. epidermidis* lacks (Peetermans et al., 2015).

Biofilm formations are reported by many *S. aureus* strains, which appears to have multiple antibiotics resistance and causes severe chronic infections such as poor wound healing, endocarditis, and osteomyelitis. The structure of *S. aureus* biofilm is composed of proteins, external DNA, and polysaccharide and found to secrete many exotoxins such as toxic shock syndrome toxin-1 (TSST-1) (Parastan et al., 2020; Schlievert & Davis, 2020).

1.6.3 Secreted factors

S. aureus can be found on healthy skin and does not cause any infections in healthy conditions. However, in immune compromised patients or if it allowed to enter inside the body such, e.g., though injuries, it might cause several infections such as infective endocarditis or toxic shock syndrome (Rasigade & Vandenesch, 2014). Although *S. aureus* can be found on healthy skin, it is quite challenging to understand whether commensal *S. aureus* secrete any product that might be useful for skin function or not (Rasigade & Vandenesch, 2014). This is because most of the published articles have investigated the toxins and virulence factors secreted by pathogenic strains of *S. aureus* (Section 1.3.3.5). The role of commensal *S. aureus* on skin function is poorly

investigated. Interestingly, commensal *S. aureus* was found to have ability to inhibit the growth of more pathogenic methicillin resistance *S. aureus* strain such as USA300. This is mainly though fermentation of glycerol and production of short chain fatty acids (Yang et al., 2018). Thus, the present study suggest that further studies are required to understand the role secreted factors of commensal *S. aureus* on skin function.

1.6.4 Interaction with host

S. aureus has been reported to initiate adaptive and innate immune response though induction of toll like receptors which leads to production of various cytokines and chemokines and recruitment of immune cells (Krishna & Miller, 2012; Miller & Cho, 2011). Interestingly, *S. aureus* have been reported to escape being killed by immune system and causes chronic infections. This is mainly though survival within neutrophils and macrophages after phagocytosis and disseminate to different parts of the body within these immune cells (Horn et al., 2018). In addition to persistence within immune cells, *S. aureus* induces its uptake by non-phagocytic cells to ensure intracellular cytotoxicity leading to further induction to immune envision and formation of chronic infections (Horn et al., 2018).

In addition to induction of immune responses*, S. aureus* is reported to induce protease secretion in keratinocytes leading to disturbance in integrity of skin barrier and increase the severity of skin infections such as atopic dermatitis (Williams et al., 2017). Moreover, the secretion of some antimicrobial peptides by keratinocytes, such as β-defensins, is increased upon exposure to viable and heat-killed *S. aureus* (Menzies & Kenoyer, 2005).

1.6.5 Potential for virulence

Although *S. aureus* might be found on healthy skin, its main pathogenicity is due to secretion of various toxins and other virulence factors that can cause severe infections (Cheung et al., 2021). The toxins produced by *S. aureus* can be divided into two main groups: 1-cytotoxins, which target host cells membrane and induces inflammation, 2-superantigens, which induces massive inflammatory response though induction of cytokine secretion stimulating T and B cells proliferation (Cheung et al., 2021).

Alpha toxin (α-toxin) is one of the major cytotoxins secreted by *S. aureus*, which are believed to initiate infections by two main mechanisms: 1-breaking the adherent junction of epithelial and endothelial cells (Popov et al., 2015), 2- formation of

heptameric pores in target cells (Inoshima et al., 2011). Both mechanisms are done though binding of α-toxin to ADAM10 receptor (Inoshima et al., 2012). Interestingly, similar to *S. epidermidis*, phenol-soluble modulins (PSMs) are one of the major cytotoxin secreted by *S. aureus*. However, modulins produced by *S. aureus* are consider to more pathogenic, have cytolytic activity and activates mast cells which might contribute to development of skin diseases such as atopic dermatitis (Hodille et al., 2016; Nakamura et al., 2013).

Enterotoxins are one of the major superantigen toxins secreted by *S. aureus,* that believed to cause acute *Staphylococcus* food poisoning. The main mechanism by which *S. aureus* enterotoxins cause infections is though inducing intestinal mast cells to secret histamine and induction of inflammatory response mainly though activation of T-cells in a non-specific manner (Fisher et al., 2018; Senn et al., 2016). Toxic shock syndrome toxin-1 (TSST-1) is another example of superantigens secreted from some *S. aureus strain* biofilm that are reported to cause of *staphylococcal* toxic shock syndrome (TSS) (Schlievert & Davis, 2020).

1.7 *C. jeikeium*

1.7.1 Distribution & abundance

C. jeikeium is one of the skin microbiota members that found extensively in moist area of the skin such as axilla (Olson et al., 2009). Although these bacteria are part of skin microbiota, *C. jeikeium* might cause severe infections in immunocompromised patients such as endocarditis, meningitis, osteomyelitis, and pneumonia (Gupta et al., 2021; Ifantidou et al., 2010).

1.7.2 Metabolism & physiology

C. jeikeium is catalase-positive, gram positive, aerobic, mainly non-motile rods. It is considered are lipophilic bacteria as its genome sequencing lacks fatty acid synthase and its growth enhanced in the presence of lipids (Ifantidou et al., 2010; Tauch et al., 2005). Unfortunately, *C. jeikeium* is reported to harbour a number of antibiotic resistance genes (Tauch et al., 2005).

1.7.3 Secreted factors

To date, it not clear whether *C. jekeium* secretes any beneficial products to skin function or not. Most of published articles are focusing on the toxins secreted by *C. jeikeium* (Section 1.3.4.5). The present study suggest that further studies are required to understand whether commensal *C. jeikeium* species can secrete any factors that have any effect on skin or not.

1.7.4 Interaction with host

It is reported that *C. jeikeium* escape being killed by immune cells though damaging the cell membrane of various immune cells (Tauch et al., 2005). To date, the interaction of *C. jeikeium* with human cells are not fully understood. Interestingly, it is reported that *Corynebacterium* spp. are significantly increased in the skin of obese individuals (Brandwein et al., 2019). This might be because of its lipophilic activity (Ifantidou et al., 2010; Tauch et al., 2005). However, the present study suggest that further studies are required to understand how this increase might influence the immune response and development of human skin diseases.

1.7.5 Potential for virulence

The main mechanism of *C. jeikeium* pathogenicity is due to secretion of some lipolytic enzymes, such as ceramidase, that cleave the cell membrane and downregulate the

activity of immune cells such macrophages (Tauch et al., 2005). In addition, *C. jeikeium* is reported to secrete Bacteriocins that inhibit the growth of other species of *Corynebacterium* (Tauch et al., 2005).

1.8 Gap in current knowledge

Hyperglycaemia causes alteration in human skin cell function leading to impaired wound healing through multiple mechanisms (Section 1.2.2). One of the primary mechanisms is the alteration in proliferation and migration of both human skin fibroblasts and keratinocytes (Section 1.2.2). Certain members of human skin microbiota, particularly skin commensal bacteria, have been found to influence the wound healing process under healthy conditions (Section 1.3.2). In diabetes mellitus (DM), dysbiosis in skin microbiota has been observed by numerous studies (Section 1.4.2). Furthermore, some studies have identified a correlation between human skin commensal bacteria and wound healing in diabetic patients (Section 1.4.3). Although proliferation and migration of both fibroblasts and keratinocytes are crucial in wound healing and are disrupted in DM, the present study emphasises that it is not yet fully understood how skin commensal bacteria affect the proliferation and migration of both fibroblasts and keratinocytes in healthy and hyperglycaemic conditions.

Moreover, several studies have been published investigating the role of bacterial lysate and cell-free supernatant, prepared from *Lactobacillus* spp., on the wound healing process. For instance, lysate prepared from *Lactobacillus rhamnosus*, Lactobacillus plantarum, and Lactobacillus salivarius accelerates re-epithelialisation by stimulating keratinocyte migration (Brandi et al., 2020; Mohammedsaeed et al., 2015). Cell-free supernatant prepared from *Lactobacillus acidophilus* and *Lactobacillus plantarum* inhibits infections by suppressing the growth of *Escherichia coli* (Kaewchomphunuch et al., 2022). The present study questions if lysate and cell-free supernatant from certain *Lactobacillus* spp. promote wound healing, such as inducing keratinocyte migration and possessing antibacterial effects, how lysate prepared from skin commensal bacteria would influence the migration and proliferation of both keratinocytes and fibroblasts in healthy and hyperglycaemic conditions. The present study emphasises that understanding and investigating this interaction is essential as it will provide a valuable contribution to microbiome, DM, and medical research. Figure 1.5 provides a summary of the gap in current knowledge and poses an important question that will contribute valuable knowledge to current published articles.

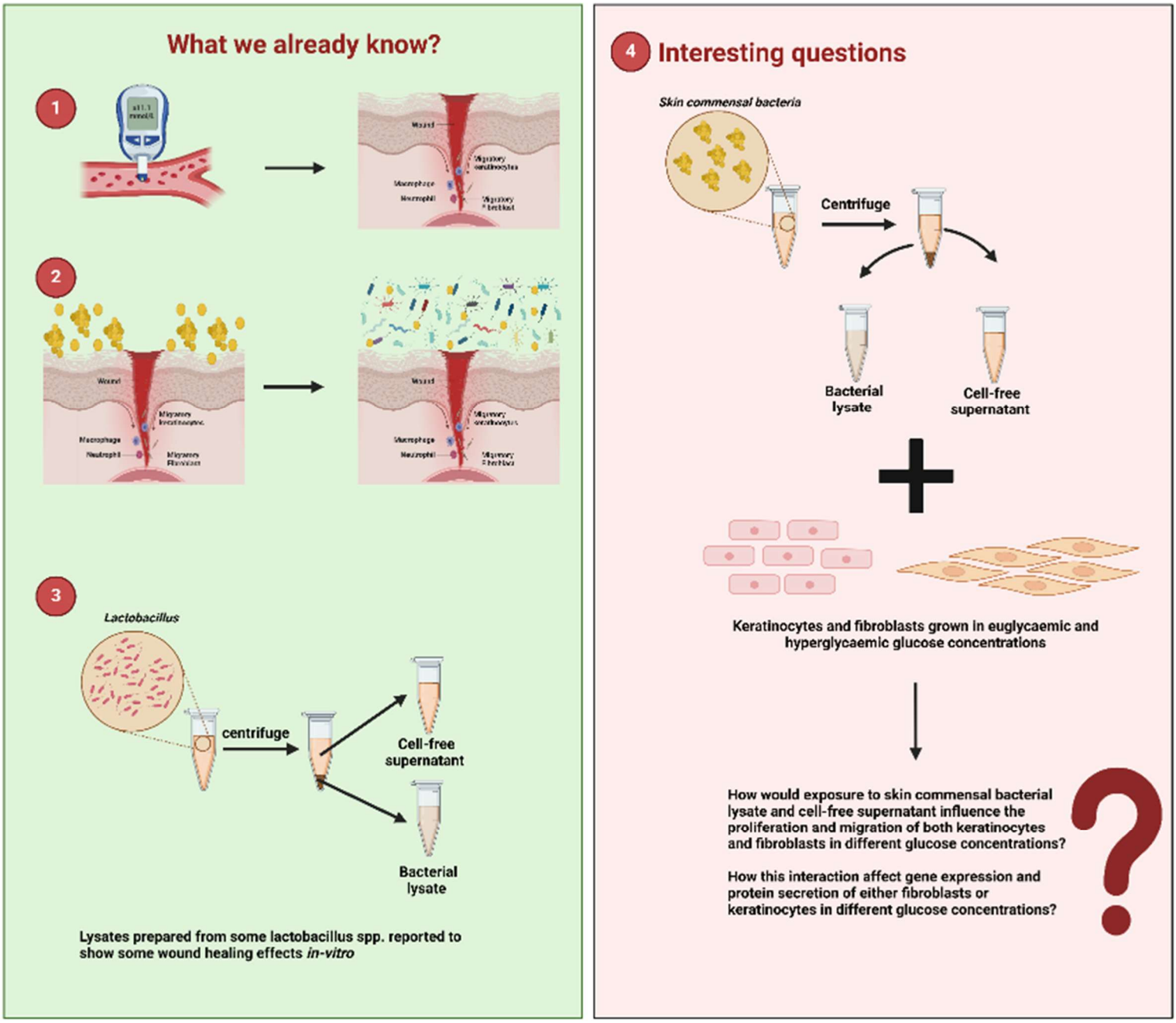

Figure 1.5: Gaps in current knowledge. The scientific figure presents a summary of extant knowledge and published literature regarding the skin microbiota in wound healing in DM. Furthermore, it highlights a pertinent research question to be investigated in this study. 1- Uncontrolled hyperglycaemia is the primary cause of DM complications **(Section 1.1.2).** For instance, impairment in proliferation and migration of fibroblasts and keratinocytes results in poor wound healing and DFU **(Section 1.2.2).** 2- Certain members of the human skin microbiota, predominantly skin commensal bacteria, have been found to influence the wound healing process under healthy conditions **(Section 1.3.2).** Dysbiosis in the human skin microbiota has been reported in DM. Moreover, a correlation between the high relative abundance of specific members of the skin microbiota and positive prognosis of DFU has been reported in other studies **(Section 1.4).** 3- Lysate and cell-free supernatants prepared from select Lactobacillus spp. were found to promote wound healing by enhancing the migration of keratinocytes under healthy conditions (Brandi et al., 2020; Mohammedsaeed et al., 2015). 4- It is crucial to investigate how lysates and cell-free supernatants influence the proliferation and migration of keratinocytes and fibroblasts at varying glucose concentrations. Additionally, it is important to examine how exposure to lysate or cell-free supernatant will affect the gene expression and protein secretions of fibroblasts and keratinocytes in different glucose concentrations.

1.9 Hypothesis

Uncontrolled hyperglycaemia in DM affects some cellular processes in human skin cells, which contributes to poor wound healing. In particular, the proliferation and migration of human skin fibroblasts and keratinocytes are altered. Lysate or cell-free supernatants prepared from some skin commensal bacteria might ameliorate these effects.

1.10 Aim

To investigate how specific skin commensal bacteria affect key wound healing processes in human skin fibroblasts and keratinocytes under varying glucose concentrations.

1.11 Objectives

To prepare bacterial lysate and cell-free supernatant from specific skin commensal bacteria, with an emphasis on *S. epidermidis, S. aureus, and C. jeikeium*.

To investigate the effect of the prepared bacterial lysate and cell-free supernatant on the proliferation of human skin fibroblasts and keratinocytes under varying glucose conditions.

To investigate the effect of the prepared bacterial lysate or cell-free supernatant on the migration of human skin cells, fibroblasts and keratinocytes, under varying glucose concentrations.

To study how the prepared bacterial lysate or cell-free supernatant influence genes expression and protein secretion in fibroblasts or keratinocytes under varying glucose concentrations.

Chapter 2: Methodology

2.1 Ethical approval

The present study was reviewed and approved by the ethical panel of Salford University. The application reference number was 1577.

2.2 Bacterial strains

Freeze-dried bacterial strains were purchased from National Collection of Type of Cultures (NCTC) by Public Health of England; *S. epidermidis* (NCTC11047), *S. aureus* (NCTC8532), and *C. jeikieum* (NCTC11913).

2.3 Chemicals

Nutrient agar (NCM0033A), nutrient broth (NCM0110A), Columbia agar base (NCM0038A), and Mueller Hinton broth (70192-500G) were all purchased from Neogen, Lansing, USA.

Glycerol, 99+%, Certified AR for Analysis, Fisher Chemical™ 500 mL (10579570), phosphate buffered saline Dulbecco A tablets (PBS) (BR0014G), and Pierce™ modified lowry assay kit (23240) were purchased from Fisher Scientific, Loughborough, UK.

Lysostaphin from *S. staphylolyticus* freeze-dried powder (L7386-5MG), Phenol red (P3532-25G), and defibrinated horse blood (MED1302) were purchased from Scientific Laboratory Supplies, Nottingham, UK.

2.4 Media preparation

2.4.1 Mueller Hinton Agar (MHA)

38 g of agar was dissolved in 1 L of purified water and sterilised by autoclave at 121˚C for 15 minutes before pouring to agar plates under aseptic conditions.

2.4.2 Mueller Hinton Broth (MHB)

21 g of broth was dissolved in 1 L of purified water and sterilised by autoclave at 121˚C for 15 minutes before pouring to agar plates under aseptic conditions.

2.4.3. Nutrient Broth (NB)

8 g of broth was dissolved in 1 L of purified water and sterilised by autoclave at 121˚C for 15 minutes before pouring to glass vial tubes under aseptic conditions.

2.4.4. Nutrient Agar (NA)

28 g of agar was dissolved in 1 L of purified water and sterilised by autoclave at 121˚C for 15 minutes before pouring to agar plates under aseptic conditions.

2.4.5. Columbia Blood Agar (CBA)

41 g of gar was dissolved in 1 L of purified water and sterilised by autoclave at 121˚C for 15 minutes. Blood agar (5%) was prepared by adding 50 mL of defibrinated horse blood to 1 L of the agar. The agar was poured to agar plates under aseptic condition.

2.5 Growing freeze-dried bacteria

Freeze-dried bacterial strains were reconstituted in 0.5 mL of NB enriched with 100 µL of defibrinated horse blood. All the strains were allowed to rehydrate for 2 minutes and mixed gently. The strains were then sub-cultured to a solid agar. *S. aureus,* and *S. epidermidis* were all sub-cultured to NA, whereas *C. jeikeium* was sub-cultured to CBA. *S. aureus, S. epidermidis,* and *C. jeikeium* were all incubated aerobically at 37 ˚C for 24 h in orbital shaker.

2.6 Storage of bacterial strains

For short term storage, all bacterial strains were stored on MHB at 4˚C for up to a month and propagated by subculturing to a new media.

For long term storage, all bacterial strains were stored as glycerol stocks. Glycerol (50%) were prepared by adding glycerol (50 mL) to distilled water (50 mL) and autoclaved at 121˚C for 15 minutes. All bacterial isolates were grown to stationary phase overnight in MHB. Bacterial glycerol stocks were prepared by adding the autoclaved glycerol (1 mL) to overnight bacterial suspension (1 mL). Glycerol stocks were stored in – 80 ˚C freezer.

2.7 Preparation of bacterial lysate

2.7.1 Growth curve

The growth curves of bacteria were studied in three different media: 1) Mueller-Hinton Broth (MHB) without supplements, 2) MHB supplemented with glycerol (2%), and 3) MHB supplemented with glucose (20 mM).

MHB was prepared as described in section 2.4.2. To prepare MHB supplemented with glycerol (2%), glycerol (2 mL) was added to MHB (98 mL). To prepare MHB supplemented with glucose (20 mM), glucose (0.4 g) was dissolved in MHB (100 mL).

S. aureus, S. epidermidis, and *C. jeikeium* were cultured overnight in MHB at 37˚C on an orbital shaker (100 rpm). Subsequently, all bacterial isolates were diluted (1:100) in fresh MHB. The dilution (1:100) was achieved by adding 1000 µL of bacterial overnight culture to 100 mL of fresh MHB broth. Bacterial dilutions were prepared in MHB without supplements, MHB supplemented with glycerol (2%), and MHB supplemented with glucose (20 mM). In 96-well microtiter plates, 200 µL of the prepared bacterial dilution was aliquoted. Additionally, 200 µL of fresh broth was prepared and added as a blank. Mean absorbance at four different points per well was measured using a FLUOstar omega microplate reader (BMG LAB TECH, Ortenberg, Germany). The temperature was maintained at 37˚C with continuous shaking (100 rpm). The absorbance was measured at 600 nm every 30 minutes for 48 hours.

2.7.2 Preparation of bacterial lysate by freeze-thawing

S. epidermidis, S. aureus, and *C. jeikeium* were cultured in MHB for 18 h. All bacterial suspensions (50 mL) were centrifuged at 4000 g at 4 °C for 15 minutes using a Beckman Coulter Avanti J-E centrifuge. The supernatant was discarded. The pellet was resuspended in PBS (2 mL) and centrifuged again at 4000 g at 4 °C for 15 minutes (washing step). The supernatant was discarded, and the pellet was resuspended in PBS (1 mL). The pellets were subjected to a freeze-thaw cycle by immersion in a dry ice/ethanol bath at -80 °C for 10 minutes, followed by thawing in an ice/water bath at 0 °C for 20 minutes. This freeze-thaw cycle was repeated twice. All prepared lysates were filtered through a syringe filter (0.45 µm) to remove non-lysed bacteria. Lysates were stored at -80 °C for subsequent experiments.

2.7.3 Preparation of bacterial lysate by sonication

S. epidermidis, S. aureus, and *C. jeikeium* were cultured in MHB for 18 h. All bacterial suspensions (50 mL) were centrifuged at 4000 g at 4 ˚C for 15 minutes using a Beckman Coulter Avanti J-E centrifuge. The supernatant was discarded. The pellet was resuspended in PBS (2 mL) and centrifuged again at 4000 g at 4 ˚C for 15 minutes (washing step). The supernatant was discarded, and the pellet was resuspended in PBS (1 mL). Sonication was performed using a compact ultrasonic laboratory device (UP50H, Hielscher, Germany). Amplitude power (80%) for 12 cycles was applied to the resuspended pellet. All prepared lysates were filtered through a syringe filter (0.45 µm) to remove non-lysed bacteria. Lysates were stored at – 80 ˚C for subsequent experiments.

2.7.4 Preparation of bacterial lysate by bead-beating

S. epidermidis, S. aureus, and *C. jeikeium* were cultured in MHB for 18 h. All bacterial suspensions (50 mL) were centrifuged at 4000 g at 4 ˚C for 15 minutes in a Beckman Coulter, Avanti J-E centrifuge. The supernatant was discarded. The pellet was resuspended in PBS (2 mL) and centrifuged again at 4000 g at 4 ˚C for 15 minutes (washing step). The supernatant was discarded, and the pellet was resuspended in PBS (1 mL). The resuspended pellets were transferred to microcentrifuge tubes containing acid-washed glass beads (50 mg). Two different sizes of acid-washed glass beads were evaluated, (425- 600) µm & (212-300) µm. Glass beads (G8772 and G1277) were obtained from Sigma Aldrich (Dorset, UK). The microcentrifuge tubes

were placed in the homogeniser (TissueLyser adaptor set 2×24). The TissueLyser was operated at 30 Hz for 5 minutes. All prepared lysates were filtered through a syringe filter (0.45 µm) to remove non-lysed bacteria. Lysates were stored at -80 ˚C for further experiments.

2.7.5 Preparation of bacterial lysate by enzymatic lysis

S. epidermidis, S. aureus, and *C. jeikeium* were cultured in MHB for 18 h. All bacterial suspensions (50 mL) were centrifuged at 4000 g at 4 ˚C for 15 minutes using a Beckman Coulter Avanti J-E centrifuge. The supernatant was discarded. The pellet was resuspended in PBS (2 mL) and centrifuged again at 4000 g at 4 ˚C for 15 minutes (washing step). The supernatant was discarded, and the pellet was resuspended in PBS (1 mL). Lysostaphin (0.5 mg/mL) was added to the resuspended pellet. The microcentrifuge tube was incubated in a water bath at 37 ˚C for 20 minutes. PBS (2 mL) was added to the lysed cells to reduce the viscosity of the lysate. All prepared lysates were filtered through a syringe filter (0.45 µm) to remove non-lysed bacteria. Lysates were stored at – 80 ˚C for subsequent experiments

2.8 Checking the efficacy of lysate preparation

2.8.1 Measuring absorbance before and after lysis

For all lysis procedures (section 2.7.2, 2.7.3, 2.7.4, 2.7.5), the absorbance before and after lysis was measured at 600 nm using a FLUOstar omega microplate reader (BMG LAB TECH, Ortenberg, Germany). The measurement before lysis represents the absorbance of the washed and resuspended bacterial pellet in PBS. The measurement after lysis represents the absorbance of the prepared lysate following the completion of the lysis procedure (Diagenode, 2021; Saeidi et al., 2011).

The percentage optical density (OD600%) was calculated using the following equation:

$$(\mathrm{OD600\%}) = \frac{\mathrm{OD600\ of\ specific\ bacteria\ after\ lysis}}{\mathrm{Average\ OD600\ of\ specidic\ bacteria\ before\ lysis}} \times 100$$

This percentage was utilised to assess bacterial viability. A reduction in OD600% indicates lysis of bacterial cells.

2.8.2 Checking for absence of live bacteria in lysate

For all bacterial lysates prepared in (section 2.7.2, 2.7.3, 2.7.4, 2.7.5), the absence of viable bacteria was verified by inoculating 20 µL of lysate onto MHA and incubating overnight at 37 ˚C.

2.8.3 Quantification of protein level in lysate

The Pierce™ modified Lowry assay was conducted according to the manufacturer's protocol (Fisher Scientific, Loughborough, UK). A standard curve of bovine serum albumin (BSA) was generated by preparing various concentrations of BSA (0-1500 µg/mL) from a BSA stock solution (2 mg/mL) in distilled water. Table 2.1 delineates the volumes (µL) of BSA and diluents utilised to prepare different BSA concentrations. Bacterial lysate (40 µL) and each of the prepared standard concentrations (40 µL) were placed in a 96-well plate. Modified Lowry assay reagent (200 µL) was added to all sample and standard wells. The plate was covered, mixed for 30 seconds, and incubated at room temperature for 10 minutes. Concurrently, Folin-Ciocalteu reagent (1N) was prepared by diluting the provided (2N) reagent with ultrapure water at a ratio

of 1:1. After 10 minutes, the diluted Folin-Ciocalteu reagent (20 µL) was added to each well, mixed for 30 seconds, and incubated at room temperature for 30 minutes. The absorbance was measured at 750 nm using a FLUOstar Omega microplate reader (BMG LABTECH, Ortenberg, Germany).

Table 2.1: Preparation of different BSA concentrations for standard curve. BSA stock solution (2 mg/mL) was used to prepare seven standard concentrations of BSA (0-1500) µg/mL.

Vial	**Volume of BSA stock (µL)**	**Volume of diluent (water) (µL)**	**Final BSA concentration (µg/mL)**
1	750 µL of stock	250 µL	1500 µg/mL
2	625 µL of stock	625 µL	1000 µg/mL
3	310 µL of vial A	310 µL	750 µg/mL
4	625 µL of vial B	625 µL	500 µg/mL
5	625 µL of vial D	625 µL	250 µg/mL
6	625 µL of vial E	625 µL	125 µg/mL
7	0	1000 µL	0 µg/mL

2.9 Preparation of cell free supernatant

2.9.1 Preparation of cell free supernatant in MHB

S. epidermidis, S. aureus, and C. jeikeium were cultured in MHB for 18 h. All bacterial suspensions (50 mL) were centrifuged at 4000 g at 4 °C for 15 minutes using a Beckman Coulter Avanti J-E centrifuge. The pellet was discarded, and the supernatant was filtered through syringe filters (0.45 µm) and stored at -80 °C for subsequent experiments.

2.9.2 Preparation of cell free supernatant in MHB supplemented with glycerol (2%)

S. epidermidis, S. aureus, and *C. jeikeium* were cultivated in MHB supplemented with 2% glycerol (Wang et al., 2014) for 24 h. All bacterial suspensions (50 mL) were centrifuged at 4000 g at 4 °C for 15 minutes using a Beckman Coulter Avanti J-E centrifuge. The pellet was discarded, and the supernatant was filtered through syringe filters (0.45 µm) and stored at -80 °C for subsequent experiments

2.9.3 Preparation of cell free supernatant in MHB supplemented with glucose (20 mM)

S. epidermidis, S. aureus, and *C. jeikeium* were cultured in MHB supplemented with 20 mM for 18 h. All bacterial suspensions (50 mL) were centrifuged at 4000 g at 4 °C for 15 minutes using a Beckman Coulter Avanti J-E centrifuge. The pellet was discarded, and the supernatant was filtered through syringe filters (0.45 µm) and stored at -80 °C for subsequent experiments.

2.9.4 Checking for absence of live bacteria in cell-free supernatant

For all prepared cell-free supernatant in sections (2.9.1, 2.9.2, 2.9.3), the absence of viable bacteria was verified by inoculating 20 µL of the cell-free supernatant onto Mueller-Hinton agar (MHA) and incubating overnight at 37 ˚C.

2.9.5 Checking acid production in cell-free supernatant prepared in MHB supplemented with glycerol (2%) and MHB supplemented with glucose (20 mM)

All prepared cell-free supernatant in media supplemented with glycerol (2%) and glucose (20 mM) were analysed for acid production. This analysis was conducted by

measuring the pH of the cell-free supernatant. Additionally, media were supplemented with 0.001% (W/V) phenol red. The conversion of media colour from red-orange to yellow indicates the formation of acids (Wang et al., 2014).

2.10 Bacterial Enumeration

S. epidermidis were inoculated and cultured overnight in MHB at 37˚C on an orbital shaker (100 rpm). Subsequently, all bacterial isolates were diluted (1:100) in fresh MHB. The dilution (1:100) was prepared by adding 1000 µL of bacterial overnight culture to 100 mL of fresh MHB. Serial dilution was performed in a 96-well plate. 180 µL of fresh MHB was added to 10 wells. 20 µL of diluted bacterial suspension was added to the first well and thoroughly mixed. Serial dilution was conducted by transferring 20 µL from the first well to the subsequent well. This procedure was repeated for the following 10 wells. Upon completion of the serial dilution, 20 µL of each prepared bacterial diluent was spread on Mueller-Hinton Agar (MHA) and incubated at 37˚C in an incubator overnight. The following day, plates with easily countable colonies (approximately 30–100) were enumerated. The number of *S. epidermidis* per mL was calculated using the following equation:

Number of *S. epidermidis* colony forming unit per mL (CFU/mL) = number of counted colonies × dilution of sample

1×10^6 CFU/mL of *S. epidermidis* was counted used for experiments in section 2.13. and 2.14.

2.11 Fibroblast

2.11.1 Source

Human skin fibroblast cell line (CCD-1070Sk) derived from healthy donors' foreskin was obtained from the American Type of Cell Culture Collection (Middlesex, UK). Modified Eagle's minimum essential medium (EMEM) (30-2003™), Fetal Bovine Serum (FBS) (F7524-500ML), and Trypsin-EDTA Solution (59417C-500M) (0.05% trypsin, 0.02% EDTA), Dimethyl sulfoxide (DMSO) (D2650-5X5ML) were procured from Fisher Scientific (Leicestershire, UK).

2.11.2 Resuspending Frozen cells

The cell vial was thawed via gentle agitation in a 37°C water bath. The vial was subsequently decontaminated with 70% ethanol. Under stringent aseptic conditions, the vial contents were transferred to a centrifuge tube containing 9.0 mL EMEM supplemented with FBS (10%) and centrifuged at approximately 125 g for 5 minutes. The supernatant was discarded. The cell pellet was resuspended in 10 mL EMEM supplemented with FBS (10%) and transferred to a T-25 cell culture flask. The cell culture was incubated at 37°C and 5% CO_2 air atmosphere in a humidified incubator. The cell culture was examined microscopically on a daily basis to assess confluency. When the confluency of cells reached approximately 75%, the cells were subcultured to a T75 flask.

2.11.3 Subculture of fibroblasts

All cell culture medium was removed using a 10 mL graduated pipette. The cells were subsequently washed with 5 mL PBS. A volume of 1.5 mL of Trypsin-EDTA (0.05%-0.02%) was added and incubated for 5 minutes at 37°C and 5% CO_2 air atmosphere in a humidified incubator. Following incubation, the cells were examined under a microscope to assess their detachment from the cell flask. To neutralise the effect of the Trypsin, 1 mL of prewarmed medium was immediately added to the flask. The cells were subcultured at a 1:3 ratio. To achieve this ratio, 3 mL of prewarmed media was added to the cell culture. Subsequently, 1 mL of the cell culture solution was transferred to a T-75 cell culture flask containing 9 mL of fresh media. The cell medium was replenished every 3 to 4 days.

2.11.4 Cryopreservation of fibroblasts

To prepare 5% freezing media, 0.5 mL of DMSO was added to 19.5 mL FBS. All cell culture medium was aspirated using a 10 mL graduated pipette. The cells were washed with 5 mL PBS. 1.5 mL of Trypsin 0.05% was added and incubated for 5 minutes at 37°C and 5% CO_2 air atmosphere in a humidified incubator. Following incubation, the cells were centrifuged at 130 g for 5 minutes. The supernatant was discarded. The pellet was resuspended in 3 mL of freezing media. 1 mL of prepared freezing media containing cells was transferred to each cryovial. The cryovial was placed on dry ice and immediately transferred to a -80°C freezer.

2.11.5 Preparation of hyperglycaemic media for fibroblasts

A glucose concentration of 5.5 mM was utilised to simulate euglycemic conditions (Lan, 2008; Li et al., 2019). Concentrations of 15, 20, and 25 mM were employed to replicate hyperglycaemic conditions (Lan, 2008; Li et al., 2019). The commercially available EMEM media inherently contain 5.5 mM glucose. The other concentrations were calculated using the following equation: Moles = volume of solution (L) × Molarity, Mass (g) = moles × molecular weight. The hyperglycaemic concentrations were prepared as follows: 15 mM: 0.07 g of glucose was dissolved in 25 mL of EMEM. 20 mM: 0.09 g of glucose was dissolved in 25 mL of EMEM. 25 mM: 0.1 g of glucose was dissolved in 25 mL of EMEM. All media were filtered using 0.22 µm syringe filters prior to use.

2.12 Keratinocytes

2.12.1 Source

Immortalised human skin keratinocytes (HaCaT) were obtained from AddexBio (CA, USA). Dulbecco's Modified Eagle Medium (DMEM) (Gibco™ 11965092) supplemented with low (5.5 mM) and high (24 mM) glucose concentrations, fetal bovine serum (FBS) (F7524-500ML), and Trypsin-EDTA Solution (Gibco™ 25200072) (0.25% trypsin, 0.02% EDTA) were utilised. Dimethyl sulfoxide (DMSO) (D2650-5X5ML) was procured from Fisher Scientific (Leicestershire, UK).

2.12.2 Resuspending frozen cells

Frozen cells were cultured based on supplier protocol AddexBio (CA, USA). The vial of cells was thawed via gentle agitation in a 37°C water bath. Subsequently the vial contents were transferred to 9 mL of high glucose DMEM (24 mM) supplemented with FBS (10%). The cell suspension was centrifuged at approximately 125g for 5 minutes. The resultant cell pellet was resuspended and transferred to a T25 flask.

The cell culture was incubated at 37°C and 5% CO_2 in a suitable humidified incubator for 24-48 h to facilitate cell attachment. The cell culture was examined microscopically on a daily basis to assess confluency. Upon reaching approximately 75% confluency, the cells were subcultured into a T75 flask. The turbidity of the media was evaluated to confirm the absence of bacterial and fungal contamination.

2.12.3 Subculture of keratinocytes

The cell culture medium (DMEM high glucose 24 mM) was completely removed using a 10 mL graduated pipette. Subsequently, the cells were washed with 10 mL PBS. A volume of 1.5 mL of 0.25% trypsin was added, and the culture was incubated for 5 minutes at 37°C and 5% CO_2 in a humidified incubator. Following incubation, the cells were examined under a microscope to assess their detachment from the cell flask. To neutralise the effect of trypsin, 1 mL of prewarmed medium was immediately added to the flask. The cells were subcultured at a 1:3 ratio. To achieve this ratio, 3 mL of prewarmed media was added to the cell culture. Subsequently, 1 mL of the cell culture media was transferred to a T-75 cell culture flask containing 9 mL of fresh media. The cell media was replenished every 1 to 2 days.

2.12.4 Cryopreservation of keratinocytes

To prepare 5% freezing media, 0.5 mL of dimethyl sulfoxide was added to 19.5 mL FBS. All cell culture medium was aspirated using a 10 mL graduated pipette. The cells were washed with 5 mL PBS. Subsequently, 1.5 mL of Trypsin 0.25% was added and incubated for 5 minutes at 37°C and 5% CO_2 air atmosphere. Following incubation, the cells were centrifuged at 130 g for 5 minutes. The supernatant was discarded, and the pellet was resuspended in 3 mL of freezing media. One millilitre of prepared freezing media containing cells was transferred to each cryovial. The cryovials were placed on dry ice and immediately transferred to a -80°C freezer.

2.12.5 Preparation of hyperglycaemic media for keratinocytes

A glucose concentration of 5.5 mM was utilised to simulate euglycemic conditions (Li et al., 2019). 24 mM, 50 mM, 70 mM, and 100 mM were employed to represent hyperglycaemic glucose concentrations.

A concern regarding the preparation of euglycemic and hyperglycaemic conditions for the immortalised keratinocytes utilised in the present study was the necessity to thaw and culture frozen cell stocks in high glucose DMEM media (24 mM), as recommended by suppliers' protocols (Section 2.12.2 & 2.12.3). Consequently, in the present study, even though 5.5 mM was used to represent a healthy level of glucose (control) (Lan, 2008; Li et al., 2019)., the control cells were initially exposed to high glucose (24 mM) prior to seeding in 5.5 mM media. Furthermore, whilst the selected hyperglycaemic glucose concentrations were significantly higher than those observed in DM (Lan, 2008; Li et al., 2019), numerous studies investigating the effect of high glucose on various types of keratinocytes have employed concentrations within the range of 24 mM – 110 mM to elicit a response (Furukawa et al., 2020; Shi et al., 2022; Yamada et al., 2017).

DMEM containing 5.5 mM and 24 mM glucose was obtained from Fisher Scientific, UK. Additional glucose concentrations were prepared using the following equations: Moles = volume of solution (L) × Molarity (M), Mass (g) = moles × molecular weight. To achieve a 50 mM concentration, 0.2 g of glucose was dissolved in 25 mL of DMEM (5.5 mM). For 70 mM, 0.3 g of glucose was dissolved in 25 mL of DMEM (5.5 mM). To prepare 100 mM, 0.4 g of glucose was dissolved in 25 mL of DMEM (5.5 mM). All media were filtered using 0.22 µm syringe filters prior to use.

2.13 Cell proliferation assay

2.13.1 Fibroblasts proliferation assay

5000 cells/well were seeded in a 96-well plate and incubated for 2 days at 37 ˚C and 5% CO_2. Subsequently, the EMEM media were replaced with fresh EMEM media (200 µL). To examine the effect of different glucose concentrations on fibroblast proliferation, various glucose concentrations were prepared (section 2.11.5), and 200 µL of each prepared EMEM media was placed into relevant wells in the 96-well plate. To investigate the effect of bacterial lysate on fibroblast proliferation in different glucose concentrations, 100 µL of each prepared bacterial lysate (prepared in section 2.7.5) were added to fibroblasts in EMEM media (200 µL) containing different glucose concentrations in the 96-well plate. To investigate the effect of cell-free supernatant on fibroblast proliferation in different glucose concentrations, 100 µL of each prepared cell-free supernatant (from Section 2.9) were added to fibroblasts cultured in EMEM media (200 µL) containing different glucose concentrations in the 96-well plate. Fibroblasts were incubated with bacterial lysate and cell-free supernatant in different glucose concentrations for 24 h at 37 ˚C and 5% CO_2. CellTiter 96® AQueous Non-Radioactive Cell Proliferation Assay (MTS) was performed on the following day according to the manufacturer's protocol (Promega, UK). The principle of this assay is based on the reduction of tetrazolium compound by NAD(P)H-dependent dehydrogenase enzymes in metabolically active cells(Promega, 2022). Media was removed and replaced with fresh EMEM media (100 µL). MTS reagent (20 µL) was added to each well. The plate was covered with foil and incubated for 3 h at 37 ˚C and 5% CO_2. The absorbance was measured at 490 nm and blank corrected. The percentage of viability (%) was calculated by normalising the sample data to a control.

To investigate the effect of live *S. epidermidis* secretions on fibroblast proliferation, Corning™ Transwell™ Multiple Well Plate with Permeable Polyester Membrane Inserts (0.4 µm) (Fisher scientific, Leicestershire, UK) was utilised to separate live bacteria from fibroblasts. 1×105 cells/well were seeded in a 6-well plate. The cells were incubated for 48 h at 37 ˚C and 5% CO_2. After two days, the EMEM media were replaced with fresh EMEM media (2 mL) containing different glucose concentrations. 106 CFU/mL live *S. epidermidis* was enumerated (section 2.10) and added to the transwell. Fibroblasts were incubated with live bacteria for 24 h at 37 ˚C and 5% CO_2,

and CellTiter 96® AQueous Non-Radioactive Cell Proliferation Assay (MTS) was performed according to the manufacturer's protocol on the following day. Media was removed and replaced with fresh EMEM media (1 mL). MTS reagent (200 µL) was added to each well. The absorbance was measured at 490 nm. The percentage of viability (%) was calculated by normalising the sample data to a control.

2.13.2 keratinocytes proliferation assay

5000 cells/well were seeded in a 96-well plate and incubated for 1 day at 37 ˚C and 5% CO_2. After 24 h, the DMEM media were replaced with fresh DMEM media (200 µL). To examine the effect of different glucose concentrations on keratinocyte proliferation, various glucose concentrations were prepared in DMEM media (section 2.11.5), and 200 µL of each prepared DMEM media was placed into relevant wells in the 96-well plate. *S. epidermidis* lysate (100 µL) was placed into each relevant well. The plates were incubated for 24 h at 37 ˚C and 5% CO_2. CellTiter 96® AQueous Non-Radioactive Cell Proliferation Assay (MTS) was performed on the following day according to the manufacturer's protocol (Promega, UK). Media were removed and replaced with fresh DMEM media (100 µL). MTS reagent (20 µL) was added to each well. The plate was covered with foil and incubated for 3 h at 37 ˚C and 5% CO_2. The absorbance was measured at 490 nm and blank-corrected. The percentage of viability (%) was calculated by normalising the sample data to a control.

2.14 Scratch migration assay

2.14.1 Fibroblasts scratch migration assay

5000 cells/well were seeded in a 96-well plate and incubated for 2 days at 37 ˚C and 5% CO_2. After 48 h, cells were subjected to starvation for 1 h by replacing the media with EMEM containing different glucose concentrations and 0% FBS. The starvation process was implemented to halt cell proliferation. The efficacy of starvation was assessed using the CellTiter 96® AQueous Non-Radioactive Cell Proliferation Assay (MTS) following the manufacturer's protocol (Section 2.13.1).

Following starvation, a scratch was created in each well using p200 micropipette tips. The media were removed, and cells were washed twice with PBS (200 µL). Subsequently, the cells were treated with EMEM media (0% FBS, 200 µL) containing different glucose concentrations. To investigate the effect of *S. epidermidis* lysate on fibroblast migration, 100 µL of lysate were added to each relevant well. Micrographic images of the scratch were captured using Cytation (Agilent, UK) every 6 h for 48 h. The area of the scratch was measured using ImageJ. The percentage of scratch closure was calculated as follows:

Percentage of Scratch Closure= $\frac{Area\ at\ t=t - Area\ at\ t=0}{Area\ at\ t=0}$ ×100, where t = (6,12,18, 24, 48) h

To investigate the effect of live *S. epidermidis* secretions on fibroblast proliferation, Corning™ Transwell™ Multiple Well Plate with Permeable Polyester Membrane Inserts (0.4 µm) (Fisher scientific, Leicestershire, UK) was utilised to separate live bacteria from fibroblasts. 1×105 cells/well were seeded in a 6-well plate. The cells were incubated for 48 h at 37 ˚C and 5% CO_2. After 48 h, cells were subjected to starvation for 1 h by replacing the media with EMEM in different glucose concentrations and at 0% FBS. *S. epidermidis* (106 CFU/mL) in 2 mL MHB was enumerated (based on section 2.9.) and added directly to the transwell. The cells were incubated with live bacteria at 37 ˚C and 5% CO_2 for 12 h. Images were captured by microscope at 12 h.

The area of scratch was measured using ImageJ. The percentage of scratch closure was calculated as follows:

Percentage of Scratch Closure= $\frac{Area\ at\ t=0 - Area\ at\ t=t}{Area\ at\ t=0} \times 100$, where t = 12 h

2.14.2 Keratinocytes scratch migration assay

10,000 cells per well were seeded in a 96-well plate. The cells were incubated for 24 h at 37 ˚C and 5% CO_2. Subsequently, cells were subjected to starvation for 1 h by replacing the media with EMEM containing different glucose concentrations and 0% FBS. The starvation procedure was implemented to halt cell proliferation. The efficacy of the starvation process was assessed using the CellTiter 96® AQueous Non-Radioactive Cell Proliferation Assay (MTS) following the manufacturer's protocol (Section 2.13.2).

The cells were incubated for 48 h at 37 ˚C and 5% CO_2. Following this period, cells were subjected to starvation for 1 h by replacing the media with DMEM containing different glucose concentrations and 0% FBS. The starvation procedure was implemented to halt cell proliferation. Subsequently, a scratch was created using p200 micropipette tips. The media were removed, and the cells were washed twice with PBS (200 µL). After washing, the cells were treated with 200 µL DMEM media containing different glucose concentrations in 0% FBS. To investigate the effect of *S. epidermidis* lysate on keratinocyte migration, 100 µL of lysate were added to each well. Micrographic images of the scratch were captured using Cytation (Agilent, UK) every 6 h for 48 h. The area of the scratch was measured using ImageJ. The percentage of scratch closure was calculated as follows:

Percentage of Scratch Closure= $\frac{Area\ at\ t=t - Area\ at\ t=0}{Area\ at\ t=0} \times 100$, where t= (6,12,18, 24, 48) h

2.15. Transcriptomic analysis (whole mRNA sequencing)

2.15.1. RNA extraction

Human skin fibroblasts were seeded (1×10^6) cells per well in 6 well plate. Cells were grown in 5.5 mM and 20 mM glucose concentrations. A scratch was introduced by p200 filter tip and cells were exposed to *S. epidermidis* lysate (1 mL) for 12 h. RNA was extracted after 12 h of exposure using RNeasy Micro Kit (Qiagen) following the manufacturer's protocol.

Fibroblasts were directly lysed in 6 well plates by adding 350 µL of Guanidine-thiocyanate-containing RLT lysis buffer followed by 350 µL of 70% ethanol. The lysate was transferred to RNeasy MinElute spin column and centrifuged at 10000 *g* for 15 s. The flow-though was discarded. The main purpose of adding Guanidine-thiocyanate and ethanol is to facilitates the binding of RNA to silica membrane of the RNeasy MinElute spin column. The silica membrane bound RNA was then washed by adding 350 µL of RW1 wash buffer to the spin column and centrifugation at 10000 *g* for 15 s. Flow-though was discarded. To remove traces of DNA that may copurify, 80 µl of DNase I incubation mix was directly placed to the spin column membrane and left in to incubate in room temperature (20–30)°C for 15 min. The DNase I incubation mix was prepared by adding 10 µl DNase I stock solution to 70 µl RDD Buffer. The silica membrane bound RNA was then washed with 350 µL RW1 buffer and centrifuge at 10000 *g* for 15 s. The flow-though was discarded. To remove all salt traces left on the column due to buffers added in earlier steps. 500 µl of RPE buffer was added to the spin column and centrifuged at 10000 *g* for 15 s. The flow-though was discarded. RPE buffer was prepared by adding 1 mL of the Buffer was diluted with absolute ethanol (100%). 500 µl of 80% ethanol was then added to the RNeasy MinElute spin column and centrifuged at 10000 g for 15 s. The flow-though was discarded. RNeasy MinElute spin column was placed in a new 2 ml collection tube and centrifuge at 10000 g for 5 min to dry the membrane. To elute the RNA, the RNeasy MinElute spin column was placed in a new 1.5 ml collection tube and 14 µl RNase-free water was added directly to the centre of the spin column membrane and centrifuged at 10000 g for 15 s. The concentration and purity of RNA were measured using NanoDrop 2000 (Thermo Fisher Scientific, Wilmington, DE). The required concentration per sample for mRNA sequencing was (≥ 30 ng/µL) per sample (BMKGENE, 2023). RNA samples were

considered pure if the measured absorbance ratio was as follow: OD260/280=1.7-2.5 and OD260/230=0.5-2.5 (BMKGENE, 2023). The prepared RNA was stored in – 80 ˚C.

Following extraction, purification, and quantification of RNA all genomics work was carried out by Biomarker Technologies at Münster, Germany (BMKGENE, 2023).

2.15.2 RNA Quality assessment, performed by (BMKGENE, 2023)

RNA integrity was assessed using the RNA Nano 6000 Assay Kit the Agilent Bioanalyzer 2100 system (Agilent Technologies, CA, USA). RNA integrity per sample is required to be higher than 7 (BMKGENE, 2023).

2.15.3 Whole mRNA sequencing (mRNA-seq), performed by (BMKGENE, 2023)

Sequencing libraries were generated using NEB Next UltraTM RNA Library Prep Kit for Illumina (NEB, USA) following manufacturer's protocol and index codes were added to attribute sequences to each sample.

Only qualified RNA samples were process for library preparations. RNA (1 μg) per sample was used as input material. At first, mRNA was purified from total RNA using poly-T oligo-attached magnetic beads. Then, fragmentation of mRNA was performed using divalent cations under elevated temperature in NEBNext First Strand Synthesis Reaction Buffer (5X).

M-MuLV Reverse Transcriptase and random hexamer primer were used to synthesise first strand cDNA from mRNA fragments using. Second strand cDNA synthesis was subsequently performed using DNA Polymerase I and RNase H. After adenylation of 3' ends of DNA fragments, NEBNext Adaptor with hairpin loop structure were ligated to prepare for hybridisation. To select cDNA fragments of 240 bp in length, the library fragments were purified with AMPure XP system (Beckman Coulter, Beverly, USA). Then, USER Enzyme (3 μl) (NEB, USA) was used with size-selected, adaptor-ligated cDNA at 37°C for 15 min followed by 5 min at 95°C.

PCR was conducted with Phusion High-Fidelity DNA polymerase, Index (X) Primer and Universal PCR primers. Finally, PCR products were purified (AMPure XP system) and library quality was assessed on the Agilent Bioanalyzer 2100 system.

The clustering of the index-coded samples was carried out on a cBot Cluster Generation System using TruSeq PE Cluster Kit v4-cBot-H (Illumina) according to the manufacturer's manual. Library preparations were sequenced on an Illumina platform and paired-end reads were successfully generated.

Raw data (raw reads) of fastq format were initially processed though in-house perl scripts. Only clean reads were obtained. This was performed by removing reads containing adapter, reads containing ploy-N and low-quality reads from raw data. At the same time, GC-content, Quality score 30, and sequence duplication level of the clean data were calculated. $Q = -10 \times \log_{10}P$ Base with high Q-scores are more reliable and less likely to be error base. Q30 is equivalent to the probability of one incorrect base call in 1000 times. All the downstream analyses were based on clean data with high quality.

2.15.4 Bioinformatic analysis, performed by (BMKGENE, 2023)

Clean data reads were mapped to the reference genome (GRCh38.p14) by using Hisat2 tools software. The number of mapped reads was normalised by the length of its transcripts by measuring Fragments per kilobase of transcript per million fragments mapped (FPKM) stringTie software by using following equation:

The equation for FPKM= $\frac{\text{cDNA Fragments}}{\text{Mapped Fragments (Millions)} * \text{Transcript Length (kb)}}$

To check the reproducibility between biological replicates, Principal component analysis (PCA) and Pearson correlation coefficient R (Pearson's Correlation Coefficient) (PCC) were performed on the FPKM of each sample. In PCA, similarity among samples were displayed by reducing dimensionality into two or three principal components. Whilst in PCC, a closer value to 1 indicates better reproducibility between the two samples.

Differential expression analysis was performed in DESeq2 software to identify differentially expressed genes (DEG). Negative binomial distribution was used, and the resulted *P* values were adjusted using the Benjamini and Hochberg's approach for controlling the false discovery rate. DEG were identified based on the criteria Fold Change (FC)≥2 and false discovery rate (FDR<0.01).

Three main comparison groups were made on DEG. The first group (F20_vs_F5) represent a comparison between DEG expressed in fibroblasts grown in high (20 mM) compared to fibroblasts grown in healthy level of glucose (5.5 mM) with no addition of *S. epidermidis* lysate. The second comparison (FSe5_vs_F5) represent a comparison between DEG in fibroblasts exposed to *S. epidermidis* lysate in 5.5 mM glucose concentration compered to no-lysate control. The third comparison group (FSe20_vs_F20) represent a comparison between DEG in fibroblasts exposed to *S. epidermidis* lysate in 5.5 mM glucose concentration compered to no-lysate control.

To understand the biological process (BP), cellular component (CC), and molecular function (MF) of DEG, Gene Ontology (GO) enrichment analysis of DEG was performed using GOseq R packages based Wallenius non-central hyper-geometric distribution (Young et al, 2010). The top 20 enriched term in each BP, CC, and MF was presented as bubble chart ranked based on q-value (adjusted p-value) and Enrichment factor (EF). The smaller the q-value, the more significant the EF is. EF was calculated by following equation:

$$\text{EF}= \frac{\text{Ratio of DEG annotated to the term over all DEG}}{\text{Ratio of genes annotated to the term over all genes}}$$

For further investigations GO analysis, Gene Set Enrichment Analysis (GSEA) (Subramanian et al., 2005) was performed on DEG. In this analysis, genes terms of GO were applied as gene sets of interest. GO identified significant terms in BP, CC, and MF based on up- or down-regulated genes with statistical significancy. This masks the genes, which are altered slightly without significancy but play vital role in biological functions. Thus, GSEA was used to overcome this issue (Subramanian et al., 2005).

For further investigations of DEG cellular function, KEGG (Kanehisa *et al.,* 2008) and KOBAS (Mao et al., 2005) software were used to test the statistical enrichment of differential expression genes in KEGG pathways. The top 20 enriched term of each significant was presented as bubble chart ranked based on q-value (adjusted p-value) and Enrichment factor (EF). The smaller the q-value, the more significant the EF is. EF was calculated by following equation: $\text{EF}= \frac{\text{Ratio of DEG annotated to the term over all DEG}}{\text{Ratio of genes annotated to the term over all genes}}$

2.16 Enzyme-linked immunosorbent assay (ELISA)

2.16.1 IL-17A

Human skin fibroblasts were cultured in EMEM media supplemented with 5.5 mM and 20 mM glucose concentrations. A total of 5000 cells were seeded in a 96-well plate. A scratch was introduced using a pipette tip (p200). Cells were washed twice with 200 µL of PBS. Subsequently, 200 µL of EMEM media was added to each well in a six-well plate. 100 µL of *S. epidermidis* lysate was added to each well. The protein level of IL-17A was quantified by ELISA after 12 h, following the manufacturer's protocol (Fisher Scientific, Leicestershire, UK).

A standard curve of IL-17A was prepared using Human IL-17A freeze-dried powder. The stock solution was prepared by reconstituting the powder in 414 µL of distilled water. The vial was gently agitated to ensure proper and homogeneous solubilisation of the freeze-dried powder. A stock solution (30 pg/mL) was prepared by diluting the reconstituted IL-17A powder with sample diluent (1:6.7). Serial dilution was performed in a microwell plate. 100 µL of sample diluent was added to all standard curve wells in triplicates. To prepare the first standard (S1) concentration (15 pg/mL), 100 µL of IL-17 stock solution was added to the first three wells. The subsequent six standard concentrations (7.5, 3.75, 1.88, 0.94, 0.47, 0.23) pg/mL were prepared by serial dilution of S1 in the microwell plate.

Assay buffer was prepared by diluting 5 mL of concentrated assay buffer with 95 mL of distilled water.

Wash buffer was prepared by diluting 50 mL of concentrated wash buffer with 950 mL of distilled water.

Biotin-Conjugate solution was prepared by diluting 60 µL of concentrated Biotin-Conjugate with 5.94 mL of assay buffer.

Streptavidin-HP solution was prepared by diluting 60 µL of concentrated Streptavidin-HP solution with 11.94 mL of assay buffer.

Amplification diluent was prepared by diluting 6 mL of concentrated amplification diluent solution with 6 mL of distilled water.

Amplification Reagent I was prepared by diluting 75 µL of concentrated amplification Reagent I with 2.25 mL of amplification diluent.

Amplification Reagent II was prepared by diluting 15 µL of concentrated amplification Reagent II with 2.85 mL of amplification diluent.

Microwell strips were washed twice by adding 400 µL of wash buffer per well. 50 µL of sample diluent was added to sample wells. 50 µL of sample was added to sample wells. 100 µL of sample diluent was added to blank wells. 50 µL of Biotin-conjugate was added to all wells. The microplate was covered with an adhesive film and incubated in darkness at room temperature (18-25) ˚C overnight.

On the subsequent day, the microwell strips were washed twice by adding 400 µL of wash buffer per well. Subsequently, 100 µL of diluted Streptavidin-HP was added to each well. The microplate was covered with an adhesive film and incubated in darkness at room temperature (18-25) ˚C for 1 h on a microplate shaker.

Microwell strips were washed twice by adding 400 µL of wash buffer per well. 100 µL of amplification solution I was added to each well. The microplate was covered with an adhesive film and incubated on a microplate shaker in darkness at room temperature (18-25) ˚C for 15 minutes.

The microwell strips were washed twice by adding 400 µL of wash buffer per well. 100 µL of amplification solution II was added to each well. The microplate was covered with an adhesive film and incubated on a microplate shaker in darkness at room temperature (18-25) ˚C for 30 minutes.

The microwell strips were washed twice by adding 400 µL of wash buffer per well. 100 µL of substrate solution was added to each well. The microplate was covered with an adhesive film and incubated on a microplate shaker in darkness at room temperature (18-25) ˚C for 15 minutes.

100 µL of substrate solution was added to each well. The absorbance of each microwell was measured at 450 nm using a microplate reader.

2.16.2 CXCL6

Human skin fibroblasts were cultured in EMEM media supplemented with 5.5 mM and 20 mM glucose concentrations. 5000 cells were seeded in a 96-well plate. For blocker wells, the cells were exposed to brodalumab (143 ng/mL) for 1 h. A scratch was introduced using a pipette tip (p200). Cells were washed with PBS (200 µL) twice. Fresh EMEM media (200 µL) was added per well in the 96-well plate. For IL-17A wells, 100 µL of human IL-17A (1.5 ng/mL) was added per well. *S. epidermidis* lysate (100 µL) was added to relevant wells. After 12 h, the protein level of CXCL6 was measured by ELISA following the manufacturer's protocol (Abcam Limited, UK).

Wash buffer was prepared by adding 5 mL of wash buffer to 45 mL of deionised water. To prepare the antibody cocktail, 300 µL of capture antibody was mixed with 300 µL of detector antibody and added to 2.5 mL of antibody diluent.

The standard curve of CXCL6 protein (Granulocyte Chemotactic Protein) was prepared by reconstituting freeze-dried powder in 500 µL of distilled water. The vial was gently agitated to ensure proper and homogeneous solubilisation of the freeze-dried powder. The vial was left at room temperature for 10 minutes. The concentration of the stock solution was 32000 pg/mL.

To prepare the first standard (S1) concentration (1600 pg/mL), 20 µL of stock solution was added to 350 µL of sample diluent. 150 µL of sample diluent was added to each of the six Eppendorf tubes. The following six standard concentrations (800, 400, 200, 100, 50, 25 pg/mL) were prepared by serial dilution of standard (S1) in Eppendorf tubes.

50 µL of all samples or standards were added to wells of microplate strips. 50 µL of the Antibody Cocktail was placed in each well. The plate was sealed with an adhesive film and incubated for 1 hour at room temperature on a plate shaker set to 400 rpm. The microwell strips were washed twice by adding 350 µL of wash buffer per well. 100 µL of TMB Development Solution was added to each well and incubated for 10 minutes in the dark on a 400 rpm plate shaker. 100 µL of Stop Solution was added to each well. The plate was agitated on a plate shaker for 1 minute to mix. The absorbance was measured at 450 nm.

2.17 Statistical Analysis

All assay experiments were performed a minimum of three times, with thee replicates technical within each experiment. Data generated were analysed by two-way analysis of variance (ANOVA) and post hoc Tukey test using GraphPad prism 9. Results were considered significant if the P value was ≤ 0.05. Data are expressed as mean ± standard error of the means (SEM).

Chapter 3: Optimisation of bacterial lysate and cell-free supernatant suitable for in-vitro experiments

3.1 Introduction

3.1.1 Manipulating skin microbiota to restore healthy skin function

Manipulating the skin microbiota can restore the healthy function of skin and demonstrates potential for treating dermatological disorders (Gebrayel et al., 2022). This is attributed to the crucial role that skin microbiota plays in maintaining the healthy function of the skin (Chen et al., 2018). Furthermore, various skin diseases are associated with dysbiosis of the skin microbiota (Blicharz et al., 2021; Hrestak et al., 2022).

Skin microbiota alters skin function through various mechanisms, including: 1- stimulating skin cells to produce metabolites or proteins that are essential for healthy skin function. For instance, *staphylococci* induce human skin keratinocytes to produce β-defensin, an antimicrobial peptide (Ommori et al., 2013). 2- Secreting metabolites or proteins that are crucial for healthy skin function. For example, lantibiotics produced by *S. epidermidis* and *S. hominis* were found to protect the skin from pathogenic infections of *S. aureus* (Teruaki Nakatsuji et al., 2017). 3- Metabolising and fermenting indigenous skin compounds. For instance, glycerol, a natural component in the skin that aids in maintaining skin moisture and hydration(Fluhr et al., 2008), is fermented by *S. epidermidis* to produce short chain fatty acids that inhibit the growth of *P. acnes* (Wang et al., 2014).

As reviewed by (Hemarajata & Versalovic, 2013), one method to partially modulate the microbiome is through the application of probiotics and prebiotics to restore the healthy function of human cells. For instance, *S. epidermidis* can be utilised in the formulation of probiotics to treat acne, as this bacterium ferments glycerol to succinic acid, which exhibits antibacterial effects against *P. acnes* (Wang et al., 2014). Furthermore, another approach to restore the healthy function of skin by bacteria is through the application of bacterial extracts such as lysates and cell-free supernatants, as reviewed by (Boxberger et al., 2021). For example, a positive impact on the skin barrier function was observed when *Lactobacillus reuteri* lysate was applied in an ultraviolet-induced inflammation model (Khmaladze et al., 2019).

3.1.2 Bacterial lysate

Bacterial lysate, which can be prepared from pathogenic or commensal bacterial species, has been extensively investigated for its immunomodulatory effects, particularly in respiratory tract infections (Braido et al., 2011; M. Cazzola et al., 2012; Esposito et al., 2018; Triantafillou et al., 2019). As reviewed by Kearney et al. (2015), the primary immunomodulatory effects of bacterial lysate occur through the interaction of immune cells with bacterial cell wall components, such as antigens, proteoglycans, or lipopolysaccharides.

A notable example of a commercially available bacterial lysate is the Broncho-Vaxom medication, which is utilised for the treatment and prevention of upper respiratory tract infections. This medication is derived from eight bacterial species (*Klebsiella pneumoniae, Neisseria catarrhalis, Streptococcus viridans, S. aureus, Diplococcus pneumoniae, Haemophilus influenzae, Streptococcus pyogenes, and Klebsiella ozaenae*) (Triantafillou et al., 2019).

In contrast to the extensive research on bacterial lysate used for respiratory tract infections, there is limited knowledge regarding its application in wound healing (Brandi et al., 2020; Mohammedsaeed et al., 2015). Lysate prepared from *Lactobacillus rhamnosus, Lactobacillus plantarum, and Lactobacillus salivarius* has been observed to accelerate re-epithelialisation by stimulating keratinocyte migration (Brandi et al., 2020; Mohammedsaeed et al., 2015).

Bacterial lysate can be prepared as chemically degraded freeze-dried bacterial cells or mechanically fractioned particles (Braido et al., 2011; Mario Cazzola et al., 2012; Jung et al., 2019). Consequently, one of the primary challenges in the preparation of bacterial lysate is the reproducibility of its physiological effects due to variations in preparation methods (Braido et al., 2011; Mario Cazzola et al., 2012; Jung et al., 2019). As reviewed by Suárez et al. (2020), a significant consideration in the preparation of bacterial lysate is the selection of the most appropriate preparation method, as certain methods such as chemical lysis may potentially disrupt some bacterial antigens.

In alkaline lysis, sodium hydroxide is utilised to disrupt the bacterial cell membrane (Braido et al., 2014). Lantigen B exemplifies a commercially available bacterial lysate prepared through alkaline lysis. This medication is derived from *S. pneumoniae, S.*

aureus, M. catarrhalis, K. pneumoniae, H. influenzae, and *S. pyogenes*. Administered as oral drops, it is employed to reduce recurrent respiratory tract infections (Braido et al., 2014).

Mechanical disruption involves lysing bacterial cells by applying high pressure to break the cell wall. Examples of mechanical disruption include high pressure homogenisation and ultra-sonication (Mario Cazzola et al., 2012). Ismigen PBML represents a commercially available bacterial lysate prepared through mechanical disruption. This lysate is composed of *K. pneumoniae, S. pyogenes, M. catarrhalis, S. aureus, S. viridans, S. pneumoniae, H. influenzae,* and *K. ozaenae,* prescribed as sublingual tablets to reduce the intensity of exacerbation in patients with chronic obstructive pulmonary diseases (Braido et al., 2015).

An additional method employed for bacterial lysis is the freeze-thawing method in conjunction with buffer usage (Didovyk et al., 2017). To the best of our knowledge, no commercially available bacterial lysate is prepared by this method. However, it is utilised for cell-free gene expression (Didovyk et al., 2017).

In the context of DM, *S. epidermidis* has been associated with a positive prognosis for wound healing (Jneid et al., 2018), *S. aureus* has been identified as the primary pathogen isolated from diabetic wounds (Redel et al., 2013), and *Corynebacterium* spp. has been found to be the most abundant species in the skin of obese individuals, a primary risk factor for DM (Brandwein et al., 2019). The present study suggests that valuable knowledge in wound and microbiome research can be gained by investigating the role of *S. epidermidis, S. aureus,* and *C. jeikeium* lysate on fibroblast and keratinocyte function under varying glucose concentrations. Furthermore, this study proposes that these investigations should commence with the proper preparation and optimisation of lysate preparation methods.

3.1.2 Cell-free supernatant

As reviewed by (Mani-López et al., 2022), cell-free supernatant is a liquid enriched with bacterial metabolites resulting from bacterial growth and the remaining nutrients of media used for growth. Cell-free supernatant has been extensively investigated for its antibacterial and antifungal activity (Scillato et al., 2021). For instance, cell-free supernatant of *Lactobacillus gasseri* has been shown to inhibit the growth of various multi-drug-resistant pathogenic bacteria such as *S. aureus, E. coli, P. aeruginosa*, and *K. pneumonia* (Scillato et al., 2021). Cell-free supernatant of *Lactobacillus plantarum* has been found to have antifungal effects and inhibit the growth of *Aspergillus parasiticus* (Poornachandra Rao et al., 2019).

The primary mechanism of cell-free supernatant is attributed to the presence of flavonoid and phenolic compounds that, for example, demonstrate anti-inflammatory and antioxidant activity in RAW 264.7 cells (Sornsenee et al., 2021). A significant finding is that the presence of different substrates in the bacterial growth media affects the type of metabolites produced (Zhang et al., 2014). For example, the addition of phenyl pyruvic acid to Lactobacillus plantarum growth medium leads to the production of phenyl lactic acid, a metabolite with strong antimicrobial activity (Zhang et al., 2014). Therefore, to ensure proper investigation of cell-free supernatant of skin commensal bacteria in DM, the supernatant was prepared in MHB with different supplements, specifically: 1- MHB with glucose (20 mM), and 2- MHB with glycerol (2%).

As DM is associated with hyperglycaemia (NICE, 2022), the present study suggests it is important to prepare cell-free supernatant of skin commensal bacteria in high glucose concentration (20 mM). This approach aims to study the effect of cell-free supernatant prepared in high glucose on the proliferation and migration of fibroblasts and keratinocytes in DM. In other words, the objective is to examine whether skin commensal bacteria will produce any metabolites when grown in high glucose that might influence the proliferation and migration of fibroblasts and keratinocytes.

Glycerol is a natural component of the skin(Fluhr et al., 2008), and *S. epidermidis* has been reported to ferment glycerol to produce short-chain fatty acids (Wang et al., 2014). The current study proposes the importance of preparing cell-free supernatant of skin commensal bacteria in media supplemented with glycerol (2%). This approach aims to investigate its effect on the proliferation and migration of fibroblasts and

keratinocytes in DM. In essence, the study seeks to examine whether skin commensal bacteria produce any metabolites when cultured in glycerol (2%) that may influence the proliferation and migration of fibroblasts and keratinocytes.

3.1.3 A critical consideration in the preparation of both bacterial lysate and cell-free supernatant

The growth of bacterial cells is divided into four main phases: lag, exponential (log), stationary, and death phases. The lag phase is a temporary initial phase in which bacterial cells do not divide but rather prepare for proliferation, and the bacterial growth rate is at its slowest (Bertrand, 2019). In the exponential (log) phase, the number of proliferating bacterial cells increases exponentially, and the growth rate and metabolic activity of bacterial cells are at their highest. In the stationary phase, bacterial proliferation begins to decline, and the overall growth rate appears steady. In the final death phase, the number of bacterial cells decreases exponentially (Kumakura et al., 2023).

The present study suggests that the preparation of bacterial lysate or cell-free supernatant should commence with an examination of the growth dynamics of bacterial cells. This approach is warranted because bacteria grow in distinct phases, and bacterial growth dynamics allow for proper characterisation and study of the duration of each growth phase (Cuevas & Edwards, 2017). Furthermore, the metabolic activity and transcription analysis of bacteria can vary in each bacterial phase (Bertrand, 2019; Kumakura et al., 2023). Consequently, the composition and concentrations of components in bacterial lysate and cell-free supernatant will differ in each growth phase (Tenea & Barrigas, 2018). For instance, the production of bacteriocin by Lactobacillus plantarum was detected after 3 h of growth, Whilst its production reached its peak after 24 h (i.e., when bacteria reached the stationary phase) (Tenea & Barrigas, 2018).

3.2 Aim of Chapter

To optimise and ensure bacterial lysates and cell-free supernatants prepared from skin commensal bacteria are suitable for further in vitro cell culture experiments.

3.3 Objectives of Chapter

To investigate the bacterial growth dynamics of *S. epidermidis, S. aureus*, and *C. jeikeium* in MHB without supplements.

To develop and evaluate various methods for bacterial lysate preparation and determine the optimal preparation method.

To assess the efficacy of the selected lysis method for bacterial lysate preparation.

To generate cell-free supernatant in MHB without supplements.

To examine the bacterial growth dynamics of *S. epidermidis, S. aureus,* and *C. jeikeium* in MHB supplemented with glycerol (2%).

To produce cell-free supernatant in MHB supplemented with glycerol (2%).

To analyse the presence of acids in the prepared cell-free supernatant in MHB supplemented with glycerol (2%).

To investigate the bacterial growth dynamics of *S. epidermidis, S. aureus,* and *C. jeikeium* in MHB supplemented with glucose (20 mM).

To generate cell-free supernatant in MHB supplemented with glucose (20 mM).

To analyse the presence of acids in the prepared cell-free supernatant in MHB supplemented with glucose (20 mM).

3.4 Optimisation of bacterial lysate

3.4.1 Growth dynamics of skin commensal bacteria in MHB for 48 h

The growth curves of all skin commensal bacteria were measured as the initial step in bacterial lysate preparation (Figure 3.1). This procedure was conducted to determine the duration of each bacterial growth phase. Additionally, to ensure consistency in various in vitro experiments, the lysates were prepared from bacteria in the same growth phase.

For *S. epidermidis*, the initial lag phase persisted for 2 h. Subsequently, the bacteria entered the exponential (log) phase, which lasted for 14 h. The stationary phase commenced after 14 h (Figure 3.1 A).

For *S. aureus*, the initial lag phase endured for 2 h. The bacteria then entered the exponential (log) phase, which continued for 12 h. The stationary phase initiated after 12 h (Figure 3.1 B).

For *C. jeikeium*, the initial lag phase extended for 2 h. The bacteria subsequently entered the exponential (log) phase, which persisted for 17 h. The stationary phase began after 17 h (Figure 3.1 C).

Lysates of all bacteria were prepared from cells cultured in MHB for 18 h. This indicates that all bacterial lysates in the present study were derived from bacterial cells in the stationary phase of growth.

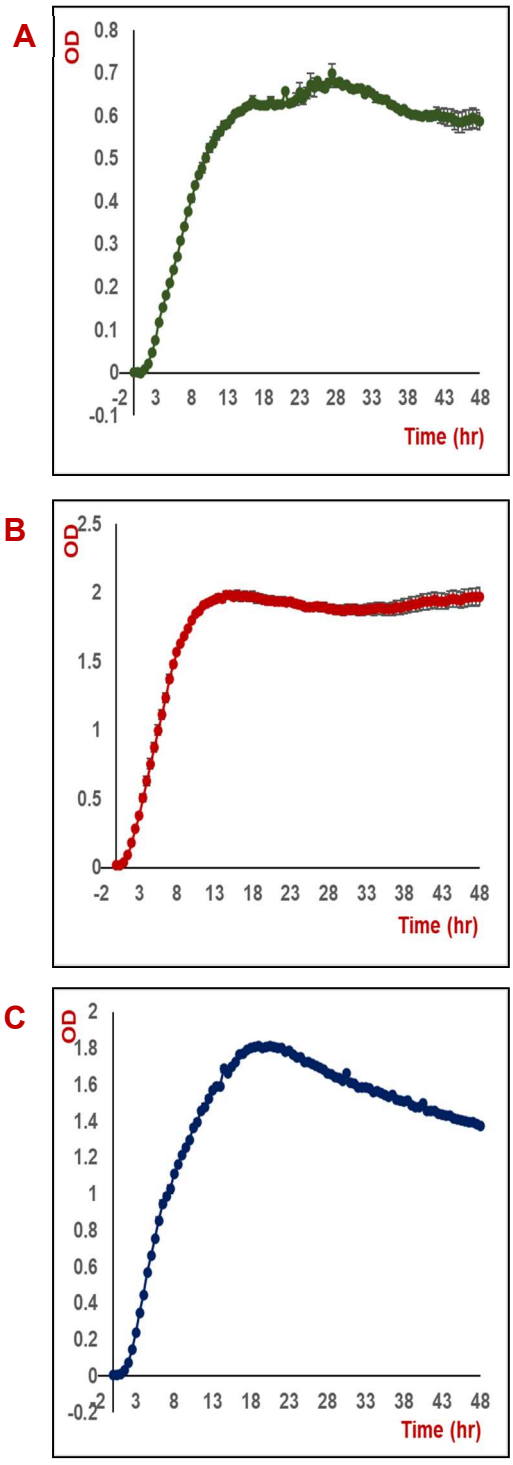

Figure 3.1: Growth curve of A) *S. epidermidis*, B) *S. aureus*, C) *C. jeikeium* in MHB without supplements. All bacterial strains were cultured at 37 ˚C with continuous agitation (100 rpm). OD600 measurements were obtained at 600 nm using a FLUOstar omega microplate reader (BMG LAB TECH, Ortenberg, Germany) at 30-minute intervals over a 48-hour period. Sterile broth served as a control. Data were blank corrected. Each data point represents the mean OD of three replicates from three independent experiments. Error bars indicate ±SEM.

3.4.2 Preparation of bacterial lysate by freeze-thawing

The bacterial cell lysis process was ineffective, as evidenced by the absence of a statistically significant change in optical density (OD600%) observed post-lysis compared to pre-freeze-thawing (Figure 3.2) [OD600%; *S. epidermidis* 99.83% ± 2.8 ($p>0.05$, n=3); *S. aureus* 99.84% ± 9.9 ($p>0.05$, n=3); *C. jeikeium* 99.85% ± 21.3 ($p>0.05$, n=3)].

Moreover, the presence of viable bacteria in the lysate prepared by the freeze-thawing method was confirmed, as inoculation of 20 µL of lysate on MHA resulted in bacterial growth.

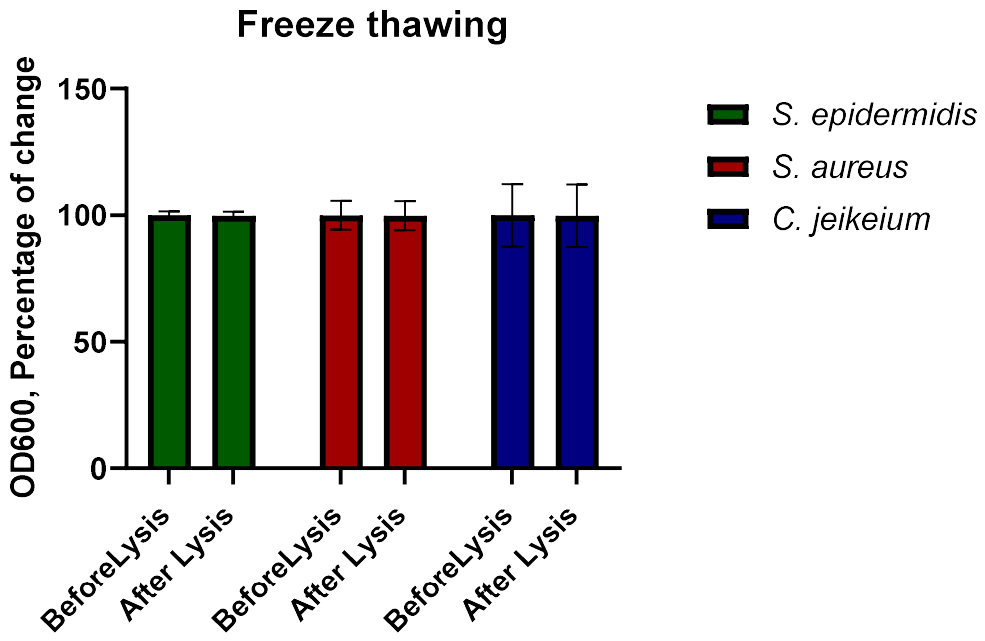

Figure 3.2: OD600% observed post-lysis compared to pre-freeze-thawing. No reduction was observed for any of the samples. The OD was measured at 600 nm using a FLUOstar omega microplate reader (BMG LAB TECH, Ortenberg, Germany). All experiments were conducted in triplicate with three technical replicates per experiment. Results are presented as mean ± standard error of the mean (SEM). n=3; error bars represent ± SEM. Statistical analysis was performed using two-way analysis of variance (ANOVA) followed by post-hoc Tukey test.

3.4.3 Preparation of bacterial lysate by sonication

Sonication at 80% amplitude and 12 cycles was performed to prepare lysate. Bacterial cells were not effectively lysed, as no significant alteration in OD600% was observed after the lysis process compared to before lysis (Figure 3.3) [OD600%; *S. epidermidis* 98.1% ± 2.6 ($p>0.05$, n=3); *S. aureus* 94.2% ± 7.2 ($p>0.05$, n=3); *C. jeikeium* 91.1% ± 1.2 ($p>0.05$, n=3)].

Furthermore, viable bacteria were present in the prepared lysate obtained through the sonication method, as evidenced by bacterial growth when 20 µL of lysate was spread on MHA.

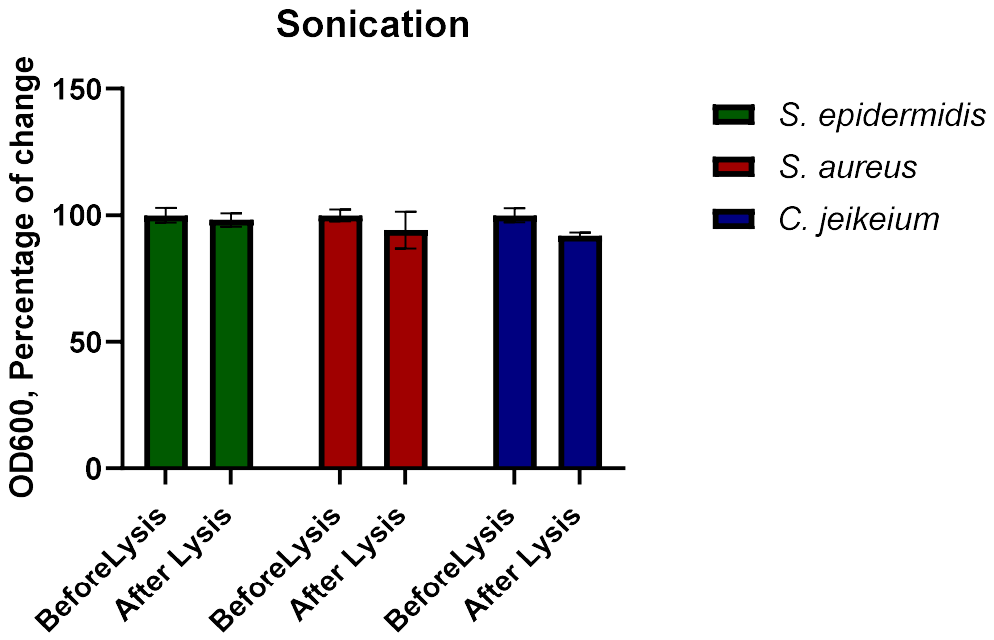

Figure 3.3: OD600% observed post-lysis compared to pre-sonication. No reduction in OD600% was observed in all samples. OD was measured at 600 nm in FLUOstar omega microplate reader (BMG LAB TECH, Ortenberg, Germany). All experiments were repeated for three times, with three technical replicates per experiments. Results are expressed as mean ± SEM. n=3, error bars represent +/- SEM, two-way analysis of variance (ANOVA) and post hoc Tukey test was performed.

3.4.4 Preparation of bacterial lysate by bead beating

Two primary bead sizes were utilised for bacterial lysis: (212-300) µm and (425-600) µm. However, bacterial cells were not effectively lysed. Bacterial cells were not effectively lysed, as no significant alteration in OD600% was observed after the lysis process compared to before lysis (Figure 3.4). [OD600% after lysis by bead beating size (212-300) µm of *S. epidermidis* 98.3% ± 2.7 ($p>0.05$, n=3); *S. aureus* 94.1% ± 11.6 ($p>0.05$, n=3); *C. jeikeium* 95.9% ± 2.1 ($p>0.05$, n=3)]; [OD% after lysis by bead beating size (425-600) µm of *S. epidermidis*=91.7% ± 1.8 ($p>0.05$, n=3); *S. aureus* 96.7% ± 1.8 ($p>0.05$, n=3); *C. jeikeium* 93.2% ± 2.2 ($p>0.05$, n=3)]

Furthermore, viable bacteria were present in the lysate prepared using this method with two different bead sizes, as evidenced by bacterial growth when 20 µL of lysate was spread on MHA.

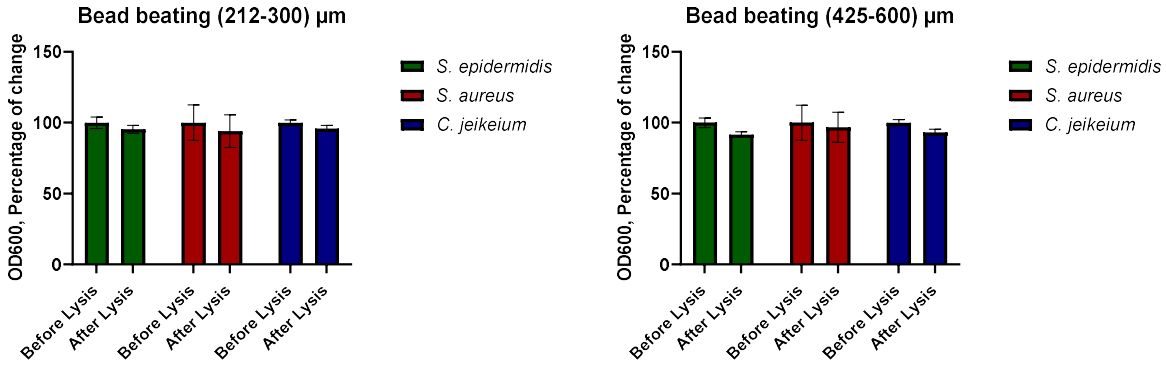

Figure 3.4: OD600% post-lysis compared to pre-bead beating using two different bead sizes. No reduction in OD600% was observed in all samples. OD was measured at 600 nm in FLUOstar omega microplate reader (BMG LAB TECH, Ortenberg, Germany). All experiments were repeated for three times, with three technical replicates per experiments. Results are expressed as mean ± SEM. n=3, error bars represent +/- SEM, two-way analysis of variance (ANOVA) and post hoc Tukey test was performed.

3.4.5 Preparation of bacterial lysate by enzymatic lysis

All skin commensal bacterial species were successfully lysed following incubation with lysostaphin (0.5 mg/mL) at 37°C for 20 min. This was confirmed by the significant decrease in OD600% in all bacterial samples post-lysis compared to pre-lysis [OD% after lysis of *S. epidermidis* 33.6% ± 2.4 ($p<0.001$, n=3); *S. aureus* 24.6% ± 2.8 ($p<0.0001$, n=3); *C. jeikeium* 33.8% ± 6.5 ($p<0.001$, n=3)] (Figure 3.5).

Furthermore, viable bacteria were not detected in the lysate prepared by this method, as inoculation of 20 µL of lysate on MHA resulted in no bacterial growth.

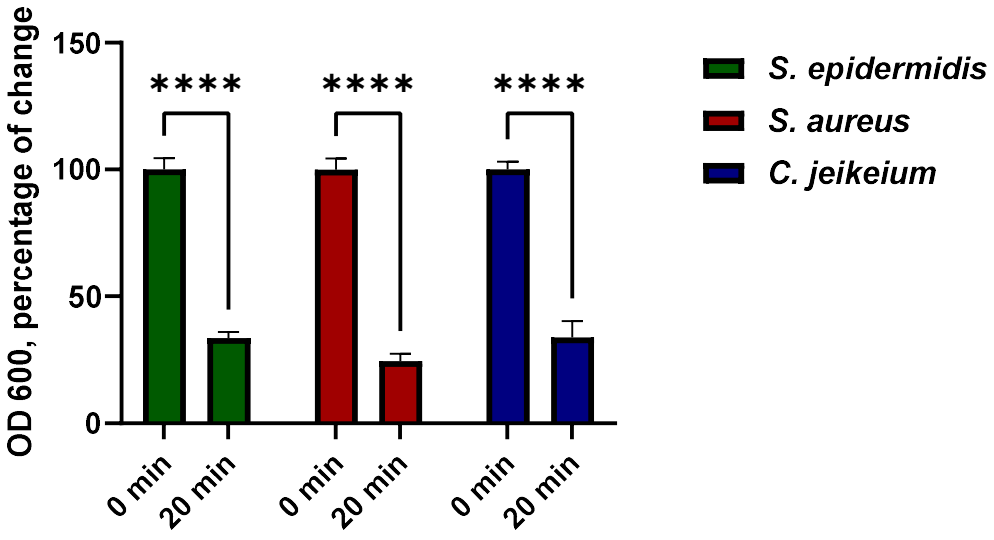

Figure 3.5: OD600% observed post-lysis compared to pre-enzymatic lysis. A significant reduction in OD% was observed in all samples. This observation indicates successful lysis of all skin commensal bacteria following treatment with lysostaphin (0.5 mg/mL) at 37 ˚C for 20 minutes. OD600 was measured at 600 nm using a FLUOstar omega microplate reader (BMG LAB TECH, Ortenberg, Germany). All experiments were conducted in triplicate, with three technical replicates per experiment. Results are expressed as mean ± SEM. n=3, error bars represent +/- SEM, two-way analysis of variance (ANOVA) and post hoc Tukey test was performed, **** $p<0.0001$.

3.4.6 Measuring protein concentration level in bacterial lysate

Protein concentration in the lysate prepared by enzymatic lysis was quantified using a Modified Lowry assay. This experiment was conducted to assess the reproducibility and consistency of protein production during the lysis process among the different experimental replicates. The concentration of protein in *S. epidermidis* lysate was 573.3 µg/mL ± 35 (n=3), in *S. aureus* lysate was 638.3 µg/mL ± 32.9 (n=3), and in *C. jeikeium* lysate was 596.1 ± 85.6 µg/mL (n=3) (Figure 3.6).

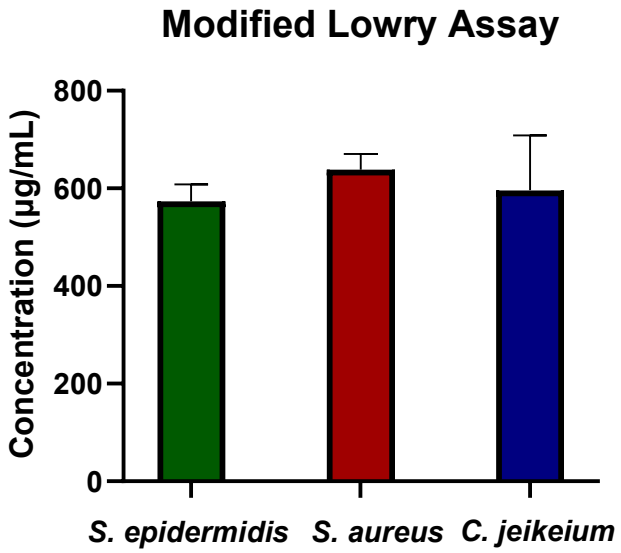

Figure 3.6: Concentration of protein in skin commensal bacterial lysates. The protein concentration of skin commensal bacterial lysates following a 20-minute treatment with 100 µL of lysostaphin (0.5 mg/mL) was quantified using a modified Lowry assay. Absorbance was measured at 750 nm, and data were corrected for blank values. Blanks consisted of PBS with lysostaphin. The concentration of bacterial lysate protein was calculated based on the standard curve, (Concentration (µg/mL) = (Absorbance (750 nm) - 0.0706)/0.0008). All experiments were conducted in triplicate, with three technical replicates per experiment. Results are expressed as mean ± SEM. n=3, error bars represent +/- SEM.

3.5 Optimisation of cell-free supernatant in MHB without any supplements

Cell-free supernatant was prepared by centrifugation at 4000 g, at 4 °C, for 15 min of bacterial cells grown in MHB without any supplements for 18 h. The cell pellet was used for lysate preparation (as described in Section 3.4). The supernatant was filtered using a syringe filter (0.45 µm). Viable bacteria were not detected in the cell-free supernatant prepared using this method, as inoculation of 20 µL of the supernatant on MHA resulted in no bacterial growth.

3.6 Optimisation of cell-free supernatant in MHB supplemented with glycerol (2%)

3.6.1 Growth dynamics

Growth curves of all skin commensal bacteria were measured as a first step in preparation of cell-free fermented glycerol supernatant. This is to determine whether skin commensal bacteria can survive in media containing glycerol (2%). Also, to identify the duration of each bacterial growth phase, and ensure the cell-free supernatant, which will be used in various *in-vitro* experiments, are always made from the same growth phase.

For *S. epidermidis,* the initial lag phase lasted for 3 h. Subsequently, bacterial cell division commenced, and the population remained in the exponential (log) phase for approximately 16 h. The stationary phase initiated after 16 h (Figure 3.7 A).

For *S. aureus*, the initial lag phase lasted for 3.5 h. Subsequently, bacterial cell division commenced, and the population remained in the exponential (log) phase for approximately 19 h. The stationary phase started after 19 h (Figure 3.7 B).

For *C. jeikeium* The initial lag phase lasted for 3 h. started to divide and remained in exponential (log phase) lasted for 19 h. The stationary phase initiated after 19 h (Figure 3.7 C).

Cell-free supernatants of all samples were prepared from bacterial suspensions cultured in MHB supplemented with glycerol (2%) for 24 h. This observation indicated that all cell-free supernatants in the present study were derived from bacterial cells grown in the stationary phase.

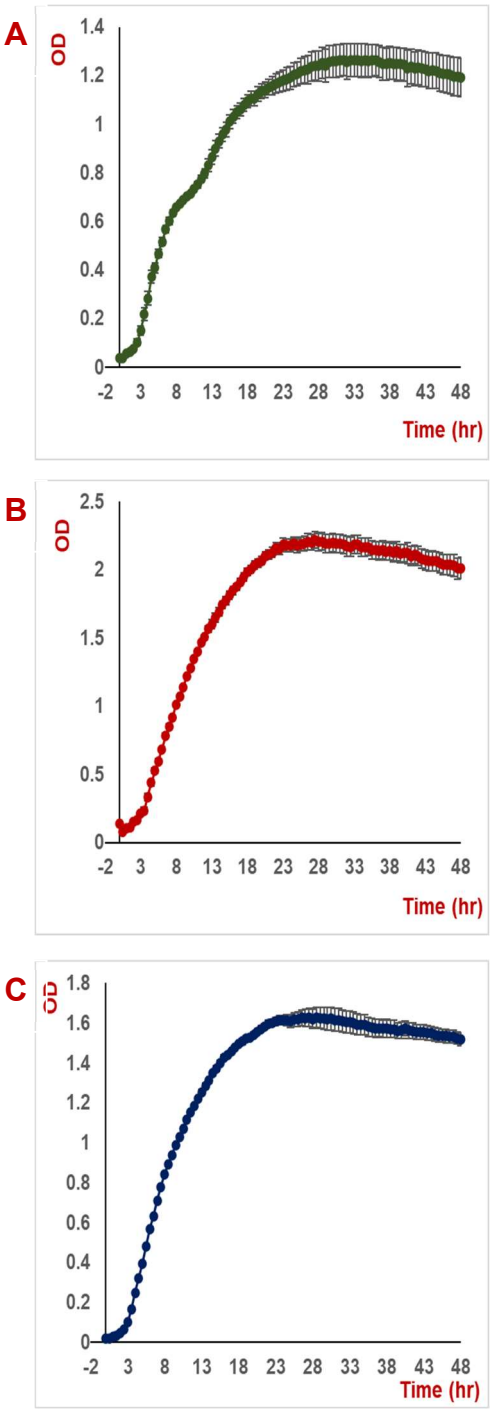

Figure 3.7: Growth curve of A) *S. epidermidis,* B) *S. aureus,* C) *C. jeikeium* in MHB supplemented with glycerol (2%). All bacterial strains were cultured at 37 ˚C with continuous agitation (100 rpm). OD600 measurements were obtained at 600 nm using a FLUOstar omega microplate reader (BMG LAB TECH, Ortenberg, Germany) at 30-minute intervals over a 48-hour period. Sterile broth served as a control. Data were blank corrected. Each data point represents the mean OD of three replicates from three independent experiments. Error bars indicate ±SEM.

3.6.2 Assessing the presence of acids in the cell-free supernatant prepared in MHB supplemented with glycerol (2%)

To determine the production of acid during the fermentation of glycerol (2%), *S. epidermidis, S. aureus*, and *C. jeikeium* were cultured in MHB in the presence and absence of glycerol (2%). The change in pH was subsequently measured using a pH meter and phenol red at 24 h. In pH meter, pH values below 7 are acidic, whilst those above 7 are basic, and a pH of 7 is neutral (Sarkawi, 2015; Weiskirchen et al., 2023). Phenol red, a pH indicator, undergoes a colour transition from red to yellow under acidic conditions (Wang et al., 2014; Weiskirchen et al., 2023).

In the present study, a pH reduction was observed exclusively when bacteria were cultured with glycerol (2%), indicating acid formation (Figure 3.8). Moreover, colour change was observed solely when bacteria were cultured with glycerol (2%) (Figure 3.9). This observation provided additional confirmation of acid production.

A

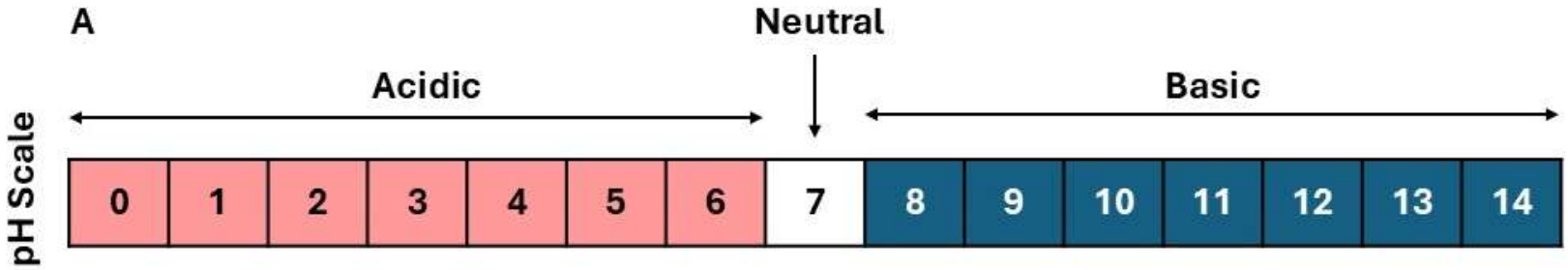

B

Growth medium	*S. epidermidis*	*S. aureus*	*C. Jeikeium*	No bacteria
MHB + glycerol	4.96 ± 0.15	5.34 ± 0.10	6.40 ± 0.12	7 ±0.058
MHB	7.91 ± 0.10	7.57 ± 0.14	7.49 ± 0.056	7.3 ± 0.058

Figure 3.8: pH measurement of cell-free supernatant prepared in MHB supplemented with glycerol (2%) by pH meter. A) pH scale pH values below 7 are acidic, whilst those above 7 are basic, and a pH of 7 is neutral (Sarkawi, 2015; Weiskirchen et al., 2023). B) Skin commensal bacteria were cultured in MHB in the presence and absence of glycerol (2%), and the pH was measured after 24 h using a pH meter. The pH of the growth medium without bacterial inoculation was also measured. A decrease in pH was observed only when the bacteria were cultured in the presence of glycerol (2%). This observation indicated the production of acids when the bacteria were exposed to glycerol (2%).

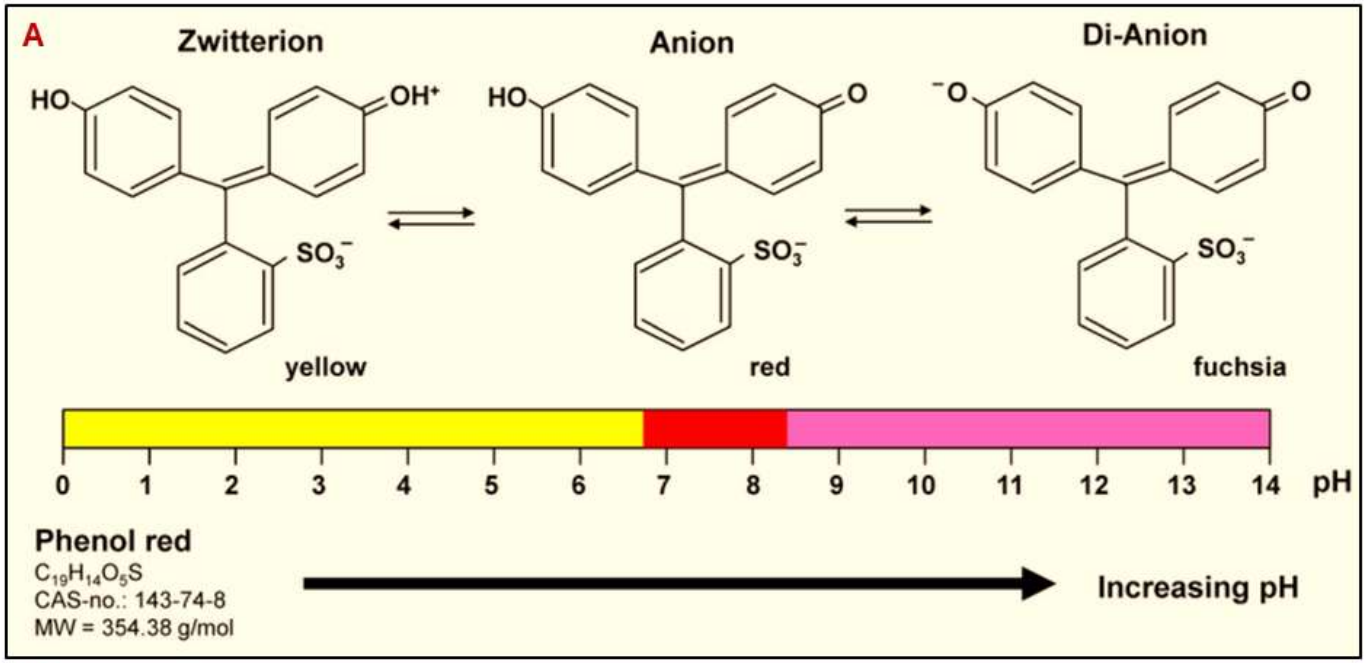

B

Growth medium	*S. epidermidis*	*S. aureus*	*C. Jeikeium*	No bacteria
MHB + glycerol	Yellow	Yellow	Yellow	Red
MHB	Red	Red	Red	Red

Figure 3.9: pH measurement of cell-free supernatant prepared in MHB supplemented with glycerol (2 %) using phenol red. A) pH scale, pH values below 7 are acidic, whilst those above 7 are basic, and a pH of 7 is neutral. With increase in pH value, the colour of phenol red change from yellow to pinkish red (Wang et al., 2014; Weiskirchen et al., 2023). B) Skin commensal bacteria were cultured in MHB in the presence and absence of glycerol (2%), and pH was measured after 24 h using phenol red. The pH of the growth medium without bacterial inoculation was measured. A decrease in pH was observed only when the bacteria were cultured in the presence of glycerol (2%). This observation indicated the production of acids when the bacteria were exposed to glycerol (2%).

3.7 Optimisation of cell-free supernatant in MHB supplemented with glucose (20 mM)

3.7.1 Growth curve

The growth curves of all skin commensal bacteria were measured as the initial step in the preparation of the cell-free fermented glycerol supernatant. This procedure was conducted to determine whether commensal skin bacteria can survive in media containing glucose (20 mM). Additionally, we aimed to elucidate the duration of each bacterial growth phase and ensure that the cell-free supernatant, which would be used in various in vitro experiments, was consistently produced from the same growth phase.

For *S. epidermidis*, the initial lag phase lasted for 2.5 h. Subsequently, bacterial cells commenced division and remained in the exponential (log) phase for approximately 13 h. The stationary phase commenced after 13 h (Figure 3.10 A).

For *S. aureus*, the initial lag phase lasted for 1.5 h. Subsequently, bacterial cells commenced division and remained in the exponential (log) phase for approximately 7 h. The stationary phase commenced after 7 h (Figure 3.10 B).

For *C. jeikeium*, the initial lag phase lasted for 2 h. Subsequently, bacterial cell division commenced, and the population remained in the exponential (log) phase for approximately 9 h. The stationary phase endured for 9 h (Figure 3.10 C).

Cell-free supernatant of all bacteria was prepared from bacterial suspensions cultured in MHB supplemented with glucose (20 mM) for 18 h. This procedure indicates that all cell-free supernatants in the present study were derived from bacterial cells grown to stationary phase.

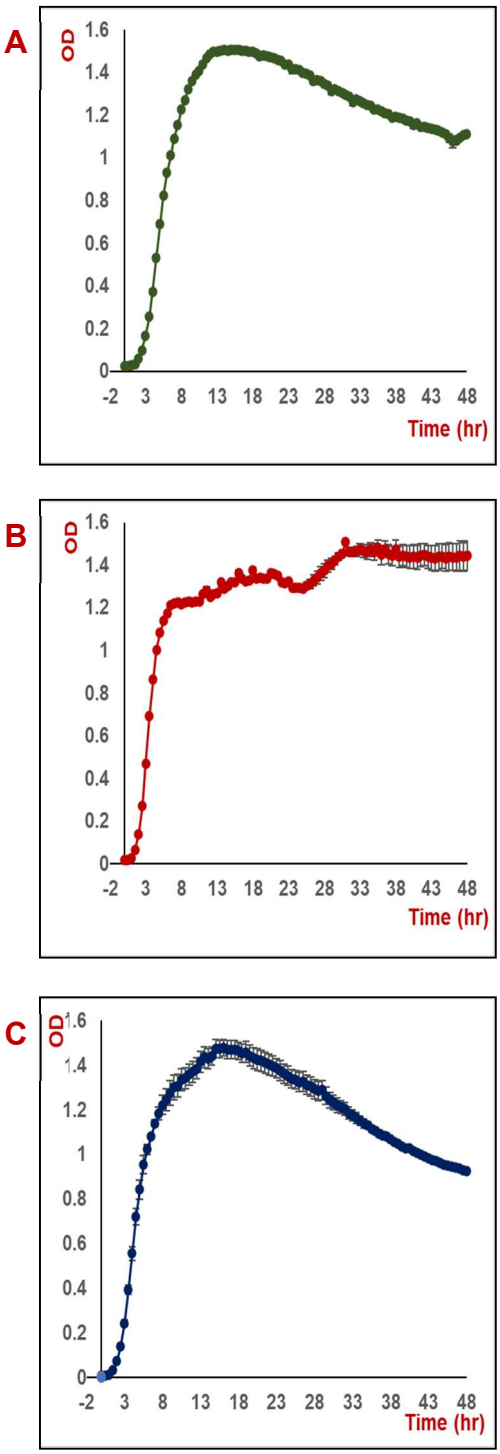

Figure 3.10: Growth curve of A) *S. epidermidis,* B) *S. aureus,* C) *C. jeikeium* in MHB supplemented with glucose (20 mM). All bacterial strains were cultured at 37 ˚C with continuous agitation (100 rpm). OD600 measurements were obtained at 600 nm using a FLUOstar omega microplate reader (BMG LAB TECH, Ortenberg, Germany) at 30-minute intervals over a 48-hour period. Sterile broth served as a control. Data were blank corrected. Each data point represents the mean OD of three replicates from three independent experiments. Error bars indicate ±SEM.

3.7.2 Evaluation of acid presence in the cell-free supernatant prepared in MHB supplemented with glucose (20 mM)

To determine the production of acid during the fermentation of glucose (20 mM), *S. epidermidis, S. aureus,* and *C. jeikeium* were cultured in MHB in the presence and absence of glucose (20 mM). The change in pH was subsequently measured using a pH meter and phenol red at 18 h. In pH meter, pH values below 7 are acidic, whilst those above 7 are basic, and a pH of 7 is neutral (Sarkawi, 2015; Weiskirchen et al., 2023). Phenol red, a pH indicator, undergoes a colour transition from red to yellow under acidic conditions (Wang et al., 2014; Weiskirchen et al., 2023).

In the present study, a pH reduction was observed exclusively when bacteria were cultured with glucose (20 mM), indicating acid formation (Figure 3.11). Moreover, colour change was observed solely when bacteria were cultured with glucose (20 mM) (Figure 3.12). This observation provided additional confirmation of acid production.

A

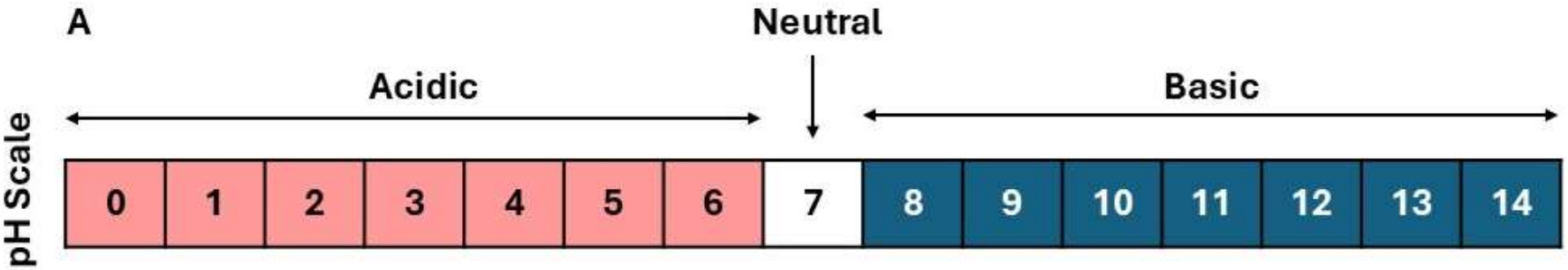

B

Growth medium	*S. epidermidis*	*S. aureus*	*C. Jeikeium*	No bacteria
MHB + glucose	4.71 ± 0.075	4.71 ± 0.05	4.96 ± 0.105	7 ±0.058
MHB	7.91 ± 0.101	7.57 ± 0.14	7.49 ± 0.056	7.3 ± 0.058

Figure 3.11: pH measurement of cell-free supernatant prepared in MHB supplemented with glucose (20 mM) using pH meter. A) pH scale, pH values below 7 are acidic, whilst those above 7 are basic, and a pH of 7 is neutral (Sarkawi, 2015; Weiskirchen et al., 2023). B) Skin commensal bacteria were cultured in MHB in the presence and absence of glucose (20 mM), and the pH was measured after 18 h using a pH meter. The pH of the growth medium without bacterial inoculation was also measured. A decrease in pH was observed only when the bacteria were cultured in the presence of glucose (20 mM). This observation indicated the production of acids when the bacteria were exposed to glucose (20 mM).

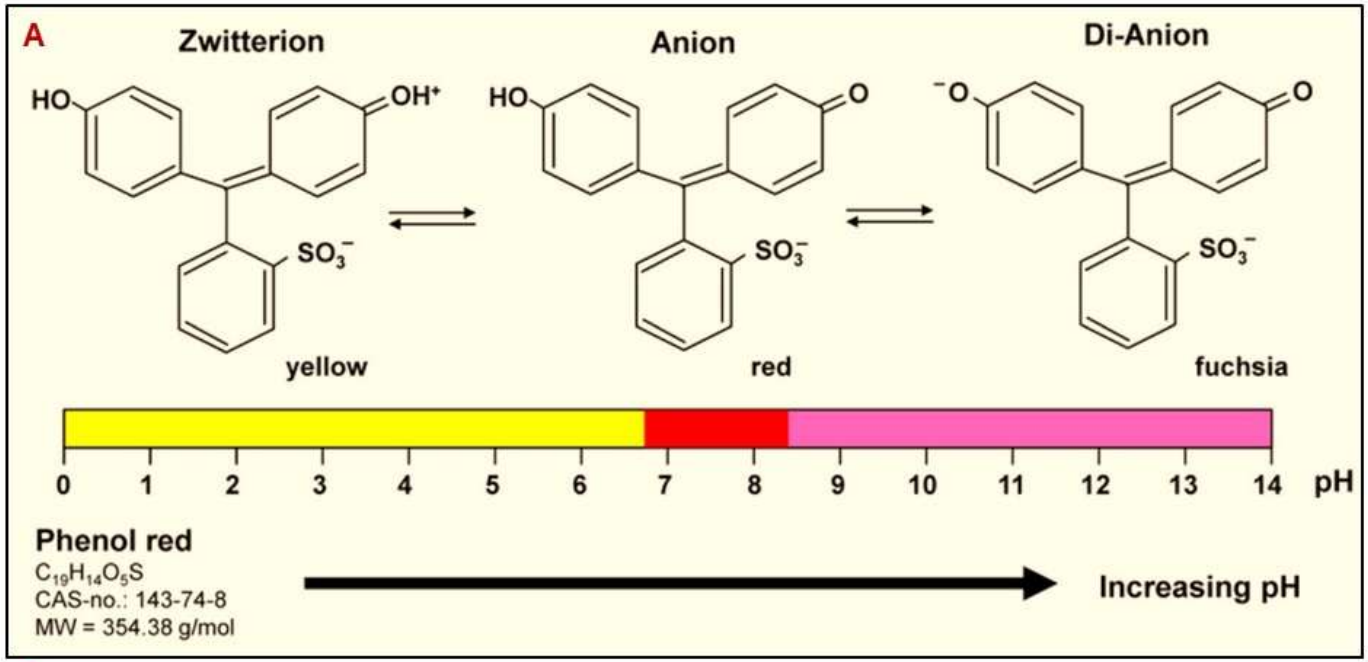

B

Growth medium	*S. epidermidis*	*S. aureus*	*C. Jeikeium*	No bacteria
MHB + glucose	Yellow	Yellow	Yellow	Red
MHB	Red	Red	Red	Red

Figure 3.12: pH measurement of cell-free supernatant prepared in MHB supplemented with glucose (20 mM) using phenol red. A) pH scale, pH values below 7 are acidic, whilst those above 7 are basic, and a pH of 7 is neutral. With increase in pH value, the colour of phenol red change from yellow to pinkish red (Wang et al., 2014; Weiskirchen et al., 2023). B) Skin commensal bacteria were cultured in MHB in the presence and absence of glucose (20 mM), and pH was measured after 18 h using phenol red. The pH of the growth medium without bacterial inoculation was measured. A decrease in pH was observed only when the bacteria were cultured in the presence of glucose (20 mM). This observation indicated the production of acids when the bacteria were exposed to glucose (20 mM).

3.8 Discussion

Bacterial lysate and cell-free supernatant of certain bacterial species, such as *Lactobacillus* spp., have been found to promote healthy function of skin through various mechanisms, including antifungal (Poornachandra Rao et al., 2019) and antibacterial effects (Scillato et al., 2021), as well as the induction of keratinocyte migration (Mohammedsaeed et al., 2022). In this chapter, bacterial lysate and cell-free supernatant were prepared from three primary skin commensal bacteria: *S. epidermidis, S. aureus,* and *C. jeikeium*. The objective of this chapter was to optimise the preparation of both bacterial lysate and cell-free supernatant to ensure their suitability for subsequent in-vitro cell culture experiments.

The present study identifies that the most effective method for preparing bacterial lysate from *S. epidermidis, S. aureus,* and *C. jeikeium* is through enzymatic lysis, specifically using lysostaphin in PBS buffer. This method was the only one that resulted in a significant reduction in the percentage change of optical density (OD) at 600 nm. Bacterial growth can be detected by measuring absorbance at a wavelength of 600 nm (Mira et al., 2022). Thus, a significant reduction in absorbance indicates proper lysis of bacteria (Saeidi et al., 2011). Furthermore, in the present study, proper lysis was also confirmed by the absence of live bacterial growth in the lysate, as no bacterial growth was observed when spreading the lysate on MHA. As reviewed by Kearney et al. (2015), the main composition of bacterial lysate consists of cell wall components, such as antigens, proteoglycans, or lipopolysaccharides. Therefore, in the present study, proper lysis was additionally confirmed by the detection of proteins in the lysate using a modified Lowry assay.

It is important to note that sonication or other lysis methods might lyse bacterial cells effectively if a stronger lysis buffer, such as Triton X-100, is used (Q. Li et al., 2015). However, the present study suggests that using PBS is the optimal buffer choice for lysate preparation intended for use in further cell-culture experiments. This is to prevent lysis of skin cells by stronger lysis buffers, such as Triton X-100, when the lysate is added to cells (Waise et al., 2019).

In the present study, when skin commensal bacteria were exposed to media supplemented with glycerol and glucose, acid was the primary by-product produced. However, no acid was detected when bacteria were grown in media without any

supplements. This was determined by measuring the pH value using a pH meter and phenol red indicator. As pH has been reported to play a crucial role in the wound healing process (Percival et al., 2014), the present study hypothesises that one of the mechanisms by which skin commensal bacteria affect wound healing is through the production of acids.

As the metabolomics and transcriptomic analysis of bacteria differs in each bacterial growth phase (Bertrand, 2019; Kumakura et al., 2023), the composition and concentration of both bacterial lysate and cell-free supernatant change based on the growth phase of bacteria (Tenea & Barrigas, 2018). Thus, to avoid heterogeneity of data between different replicates of each in-vitro cell culture experiment planned for subsequent chapters, both lysate and cell-free supernatant were prepared in the stationary phase only.

Wound healing is a complex process that comprises numerous molecular and biological mechanisms (Section 1.2.1). Although it appears that skin commensal bacteria may play a vital role in wound healing in healthy and diabetic patients (Section 1.3.2 & 1.4), the cellular mechanisms by which skin commensal bacteria affect wound healing are not yet fully understood. Therefore, the present study reports that it is challenging to determine which cellular mechanisms, i.e., which in-vitro method, should be investigated initially to understand the effect of skin commensal bacterial lysate and cell-free supernatant on wound healing in DM. A flow chart assisting researchers in selecting the most appropriate experimental methods for assessing the effect of any agent on the wound healing process is reviewed by Masson-Meyers et al. (2020) (Figure 3.13). In the present study, this review flow chart was used as a guideline to select the most appropriate experimental investigations to understand the effect of both bacterial lysate and cell-free supernatant on fibroblasts and keratinocytes in DM (Figure 3.14). Initially, the effect of bacterial lysate and cell-free supernatant on the proliferation of fibroblasts and keratinocytes in different glucose concentrations will be investigated (chapter 4). Based on the significance of proliferation assay results, either lysate or cell-free supernatant will be investigated for its effect on the migration of fibroblasts and keratinocytes (chapter 5). Based on migration assay results, further transcriptomic analysis will be performed to understand the mechanism of selected bacterial action on the selected human skin cell line, either fibroblasts or keratinocytes.

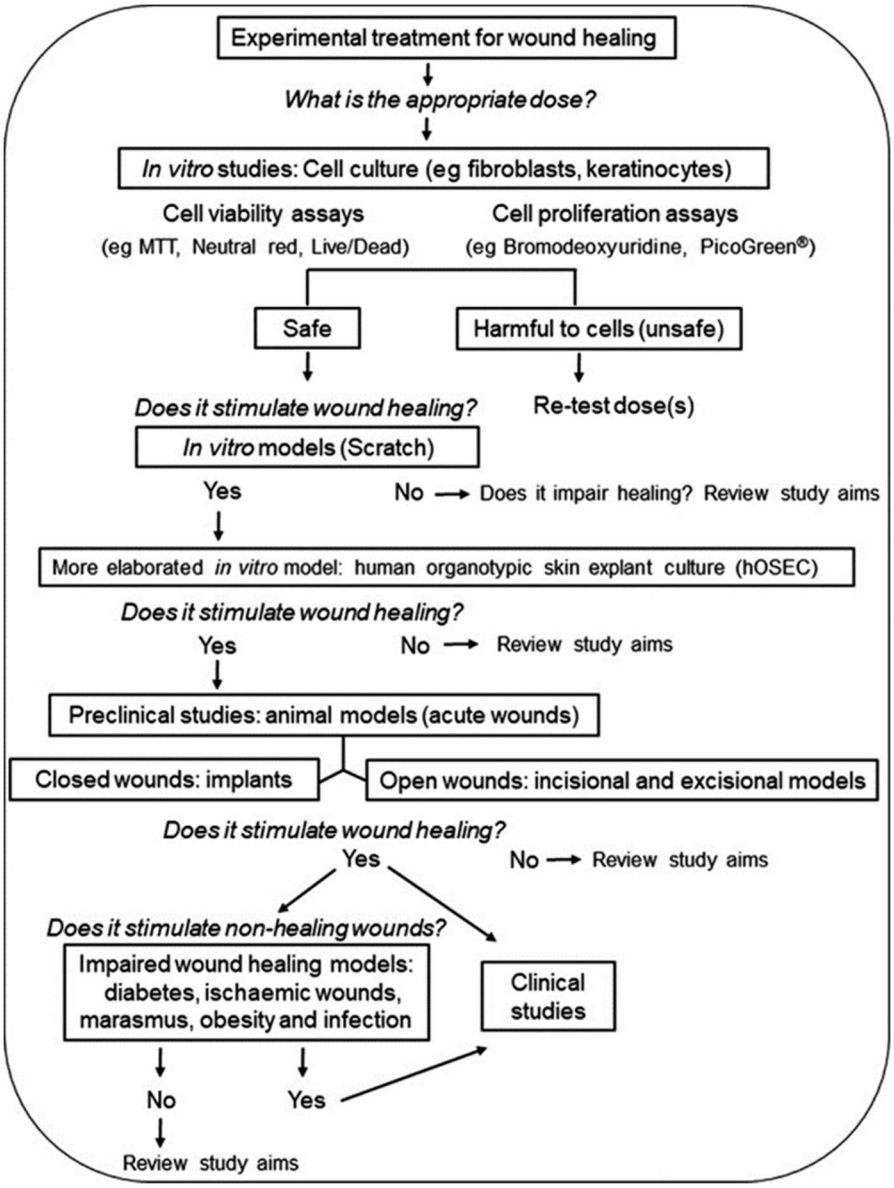

Figure 3.13: Experimental models and methodologies for the evaluation of cutaneous wound healing. The schematic diagram illustrates the principal experimental procedures that can be implemented to elucidate the effects of various agents on the wound healing process (Masson-Meyers et al., 2020).

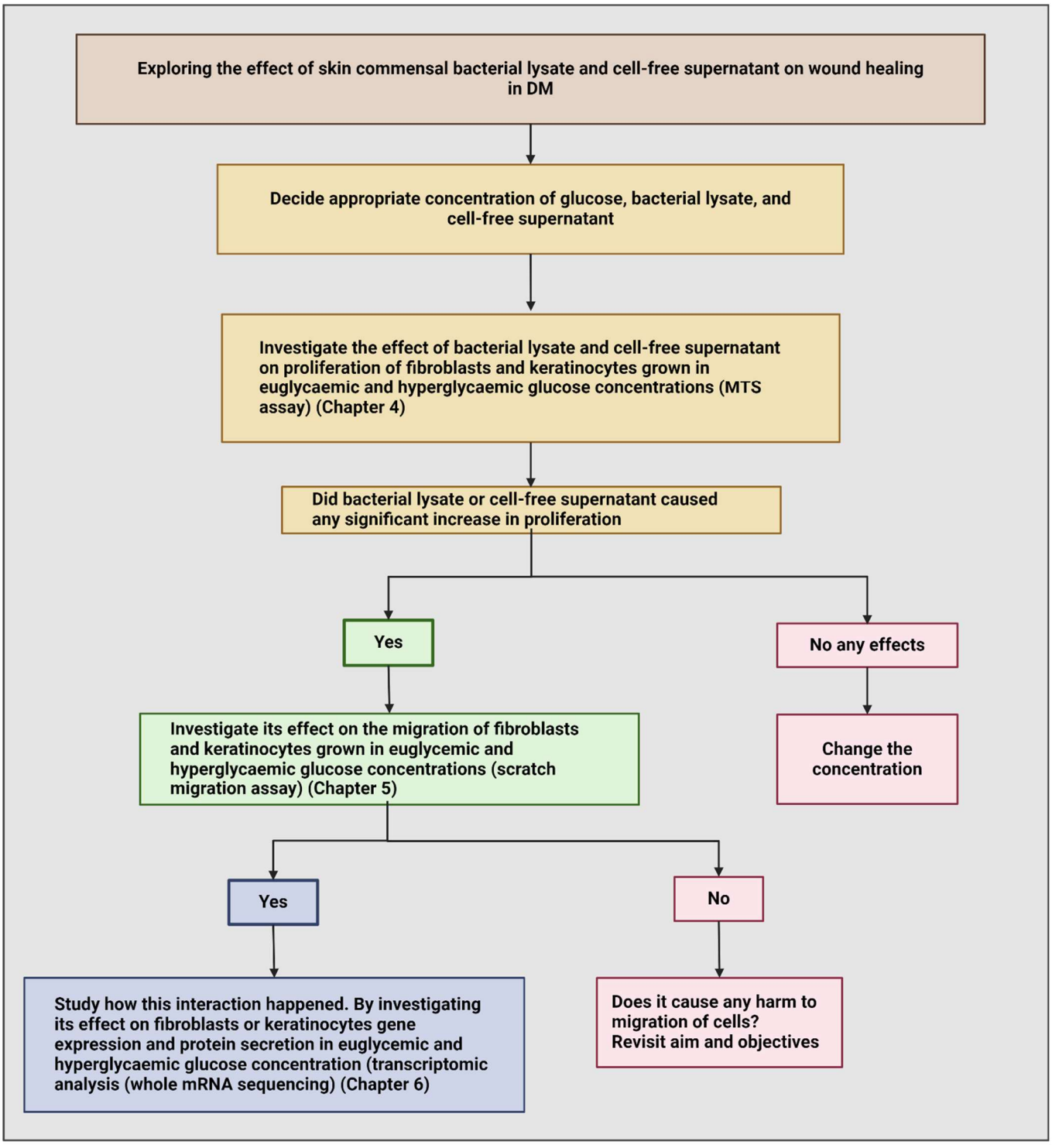

Figure 3.14: Investigation of the effect of bacterial lysate and cell-free supernatant on wound healing in DM. The flow chart illustrates the primary steps to be executed in the subsequent chapter of the present study to elucidate the impact of bacterial lysate and cell-free supernatant on wound healing in DM. Generated using (Biorender, 2024)

Chapter 4: Effect of Bacterial Lysate and Cell-Free Supernatant on the Proliferation of Human Skin Cells, Fibroblasts, and Keratinocytes in Various Glucose Concentrations

4.1 Introduction

Cell proliferation and cytotoxicity assays are essential components of most in vitro studies, particularly when investigating the safety of therapeutic products (Adan et al., 2016). These assays facilitate the determination of the optimal dosage of potential drugs by measuring the rate of cell proliferation in the presence of the compound (Adan et al., 2016). Furthermore, as reviewed by Masson-Meyers et al. (2020), in vitro investigations of the influence of any agent on the wound healing process should begin with an examination of its effect on cell proliferation. The proliferation of keratinocytes and fibroblasts promotes wound regeneration and closure, which is crucial for proper wound healing (Landén et al., 2016; Pastar et al., 2014; Schultz & Wysocki, 2009; Sorg et al., 2017).

In DM, the proliferation of these cells has been demonstrated to be impaired as a consequence of various factors, such as elevated blood glucose levels, peripheral neuropathy and vascular disease, resulting in delayed wound healing and chronic infections (David et al., 2023). However, the precise mechanisms by which keratinocyte and fibroblast proliferation is altered in diabetic wounds remain unclear (Chen et al., 2010; Sakai et al., 2003). Heterogeneity exists in the published data regarding the effects of hyperglycaemia on keratinocyte and fibroblast proliferation (Chen et al., 2010; Sakai et al., 2003). For instance, an in vitro investigation of human keratinocytes cultured under hyperglycaemic conditions and diabetic mouse model wounds showed reduced keratinocyte proliferation (Chen et al., 2010; Sakai et al., 2003). Conversely, another study examining the proliferation of keratinocytes in wounds in a diabetic rat model did not observe any changes (Park et al., 2011). The proliferation of fibroblasts extracted from the skin of diabetic patients is not significantly different from that of healthy donors (Nickel et al., 2021). However, the proliferation of human foreskin primary fibroblasts was significantly reduced when cultured under experimentally designed diabetic conditions (Xuan et al., 2014). Further studies are

necessary to elucidate the effects of hyperglycaemia on fibroblast and keratinocyte proliferation.

Understanding the impact of skin microbiota on the proliferation of skin cells in wound healing presents significant challenges, as current published knowledge regarding skin microbiota-host interactions primarily focuses on the immune response of cells rather than elucidating the proliferation of skin cells (Linehan et al., 2018; Naik et al., 2015; T. Nakatsuji et al., 2017; Simanski et al., 2019). Limited research has been conducted on the effects of skin microbiota on cell proliferation. For instance, co-culturing keratinocytes with *S. epidermidis* did not adversely affect their viability (Mohammedsaeed & Manzoor, 2022). Similarly, topical application of *S. epidermidis* to reconstructed human epidermal skin models did not affect keratinocyte viability. However, in breached reconstructed human epidermis skin models, *S. epidermidis* induced keratinocyte cytotoxicity (Duckney et al., 2013). The viability of keratinocytes was significantly reduced when co-cultured with *S. aureus* in vitro or when high concentrations of *S. aureus* were applied to a reconstructed human epidermal skin model (Duckney et al., 2013; Mohammedsaeed & Manzoor, 2022).

To date, no study has investigated the impact of the skin microbiota on the viability of skin fibroblasts. Research has demonstrated that pathogenic isolates of *S. epidermidis* associated with prosthetic joint infection can persist intracellularly within human fibroblasts, primarily within acidic phagolysosomes, potentially leading to chronic or delayed infections (Perez & Patel, 2018). Consequently, it is crucial to elucidate how commensal *S. epidermidis* isolates and other commensal members of the skin microbiota influence fibroblast viability in wounds, as this understanding will contribute to determining whether these species exert healing or pathogenic effects on the wound healing process.

Moreover, the currently available literature on bacterial lysates and cell-free supernatants primarily focuses on lysates prepared from Lactobacillus spp. Limited knowledge exists regarding the effects of skin commensal lysates on the proliferation of both skin fibroblasts and keratinocytes. A significant enhancement of keratinocyte proliferation was observed when keratinocytes were incubated with various *Lactobacillus* lysates, including *Lactobacillus paracasei, Lactobacillus plantarum, Lactobacillus fermentum, Lactobacillus brevis, Lactobacillus casei, Lactobacillus*

salivarius, Lactobacillus rhamnosus GG, and *Lactobacillus reuteri* (Brandi et al., 2020; Mohammedsaeed et al., 2015). Exposure to *S. epidermidis* lysate did not elicit any effect on keratinocyte proliferation in vitro (Mohammedsaeed & Manzoor, 2022). However, exposure to *S. epidermidis* lysate in an ex vivo skin model demonstrated an increase in the number of cells per unit area of skin, as well as increased expression of the proliferation marker Ki-67, compared to the untreated control (Mohammedsaeed et al., 2022). This finding suggests that *S. epidermidis* lysate induces skin cell proliferation in an ex vivo model (Mohammedsaeed et al., 2022).

To date, no study has examined the effects of lysates prepared from commensal skin bacteria on the viability of skin fibroblasts. Further research is necessary to elucidate how lysates prepared from skin commensal bacteria, particularly skin commensal bacteria, influence fibroblast proliferation. In this study, human skin fibroblasts and keratinocytes were treated with *S. epidermidis, S. aureus,* and *C. jeikeium* lysates at varying glucose concentrations. Subsequently, fibroblast proliferation was assessed at different time points using the MTS assay. This approach aimed to investigate the impact of *S. epidermidis, S. aureus,* and *C. jeikeium* lysates on fibroblast and keratinocyte proliferation under euglycemic and hyperglycaemic conditions.

Certain members of skin commensal bacteria have been reported to produce various products that influence skin physiology. For instance, *S. epidermidis* has been shown to produce SCFAs through the fermentation of glycerol in the stratum corneum of the skin, which is believed to confer various beneficial effects on the skin (Neha Salgaonkar et al., 2022; Wang et al., 2017). Wound pH plays a crucial role in the healing process (Metcalf et al., 2019; Sim et al., 2022). The optimal wound healing process involves alteration of the wound environment from alkaline to neutral to acidic during healing (Percival et al., 2014). An acidic wound environment is essential for inhibiting bacterial growth and promoting wound closure, whereas an alkaline wound can impede healing and increase infection risk (Metcalf et al., 2019; Sim et al., 2022). The optimal pH for fibroblast and keratinocyte proliferation is reported to be between 7.2 and 8.3 (Percival et al., 2014). Despite extensive investigations into the effects of pH on wounds, limited knowledge is available regarding how acids produced by skin commensal bacteria might alter wound pH and influence wound healing. Given that wound pH is important for proper healing, and skin commensal bacteria already

produce acids through fermentation of glycerol or glucose, one of the mechanisms by which skin commensal bacteria affect wounds might be through the alteration of skin cell proliferation via acid production. In this chapter, human skin fibroblasts were treated with different cell-free supernatants prepared from skin commensal bacteria grown in media with various supplements, such as glycerol and glucose, at different glucose concentrations. Subsequently, fibroblast proliferation was assessed at different time points using the MTS assay. This approach aimed to elucidate the effect of acids produced by skin commensal bacteria on fibroblast proliferation under euglycemic and hyperglycaemic conditions.

4.2 Aim of chapter

To investigate the impact of specific bacterial lysate and cell-free supernatant on fibroblast and keratinocyte proliferation under varying glucose concentrations.

4.3 Objectives of Chapter

To investigate the effects of varying glucose concentrations on the proliferation of fibroblasts and keratinocytes.

To investigate the effect of various bacterial lysates on fibroblast proliferation under different glucose concentrations.

To examine the effect of cell-free supernatant on fibroblast proliferation under different glucose concentrations.

To assess the effect of viable *S. epidermidis* on fibroblast proliferation under different glucose concentrations.

To evaluate the effect of *S. epidermidis* lysate on keratinocyte proliferation under different glucose concentrations.

4.4 Effect of varying glucose concentrations on human skin fibroblast viability at different time points

MTS assay was conducted on human skin fibroblasts cultured in glucose concentrations of 5.5 mM, 15 mM, 20 mM, and 25 mM for 24 h, 48 h, and 72 h. A glucose concentration of 5.5 mM was considered as the control, representing euglycemic conditions, whilst concentrations of 15 mM, 20 mM, and 25 mM were selected to represent hyperglycaemic glucose concentrations (Li et al., 2019).

Media containing 15 mM, 20 mM, and 25 mM glucose did not significantly affect the mean percentage viability of fibroblasts at 24 h, 48 h, and 72 h of treatment compared to 5.5 mM glucose (Figure 4.1).

A

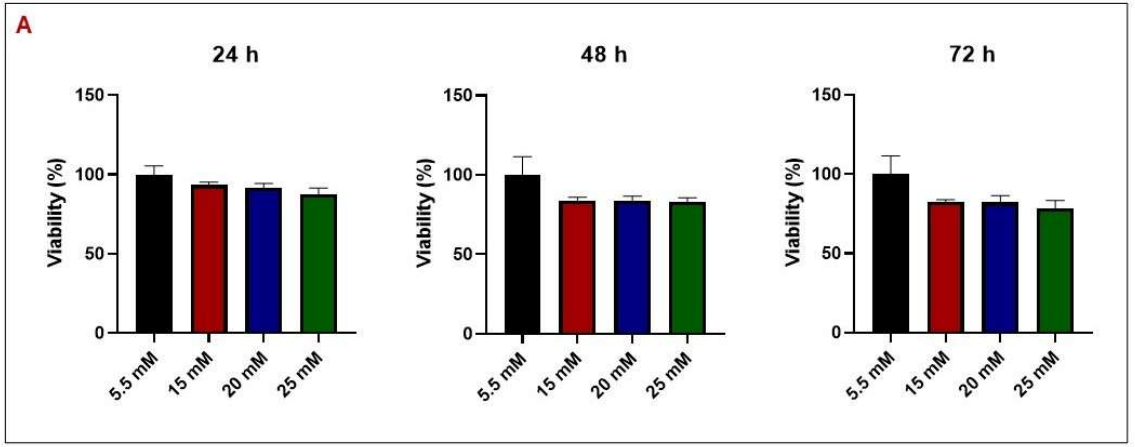

B

Glucose concentration (mM)	24 h	48 h	72 h
5.5 mM	100 ± 5.39	100.00 ± 11.43	99.98 ± 11.58
15 mM	93.36 ± 1.79	83.66 ± 2.30	82.74 ± 1.20
20 mM	91.84 ± 2.51	83.60 ± 3.04	82.21 ± 4.39
25 mM	87.43 ± 4.05	83.31 ± 2.34	78.62 ± 4.84

Figure 4.1: The viability (%) of human skin fibroblast in different glucose concentrations at different timepoints 24 h, 48 h, 72 h. There were no significant changes observed. Fibroblasts were plated at 5000 cells per well in 96-well plate and grown in different glucose concentrations (5.5, 15, 20, 25) mM. Glucose concentration (5.5 mM) was considered as control, reflecting euglycemic concentration, whereas 15 mM, 20 mM, and 25 mM were chosen to represent hyperglycaemic glucose concentrations. MTS assay was performed after 24 h, 48 h, 72 h. Absorbance was measured at 490 nm and blank corrected. To calculate the percentage of viability, all data were normalised to control of each timepoint (i.e., 5.5 mM glucose concentration of each 24 h, 48 h, 72 h. Results are expressed as mean of viability (%) ± SEM, n=3, error bars represent +/- SEM, Statistical analysis two-way analysis of variance (ANOVA) and post hoc Tukey test was performed. The data are presented in two components: A) A graphical representation of the results, and B) A table of raw numerical data.

4.5 Effect of skin commensal bacterial lysate on human skin fibroblasts viability in different glucose concentrations at 24 h

An MTS assay was performed on human skin fibroblasts cultured in glucose concentrations of 5.5 mM, 15 mM, 20 mM, and 25 mM and subsequently exposed to 100 µL of *S. epidermidis, S. aureus, and C. jekeium* lysate for 24 h. The effect of lysostaphin on fibroblasts at varying glucose concentrations was also investigated to verify that the observed effects were solely due to the lysate (Figure 4.2).

Exposure to *S. epidermidis* lysate resulted in significant increases in the mean percentage of fibroblast viability at glucose concentrations of 15 mM, 20 mM, and 25 mM compared to the no-lysate control at the same glucose concentrations. However, no change was observed at 5.5 mM glucose concentration.

Exposure to *S. aureus* and *C. jeikeium* lysate did not significantly affect the percentage of fibroblast viability across any of the glucose concentrations examined in comparison to the no-lysate control.

Exposure to lysostaphin did not significantly affect the percentage of fibroblast viability at any of the glucose concentrations examined in comparison to the no-lysostaphin control. Furthermore, exposure to *S. epidermidis* lysate resulted in significant increases in the mean percentage of fibroblast viability at glucose concentrations of 20 mM and 25 mM compared to lysostaphin.

Upon comparing the effects of various commensal bacterial lysates on skin fibroblast viability at 24 h, a statistically significant increase was observed in fibroblasts exposed to the *S. epidermidis* lysate compared to those exposed to the *S. aureus* lysate across all investigated glucose concentrations. However, a statistically significant increase was observed in fibroblasts exposed to the *S. epidermidis* lysate compared to those exposed to *C. jeikeium* only at 25 mM. In addition, a significant increase in percentage of fibroblast viability was observed when exposed *C. jeikeium* lysate in comparison to *S. aureus* lysate

A

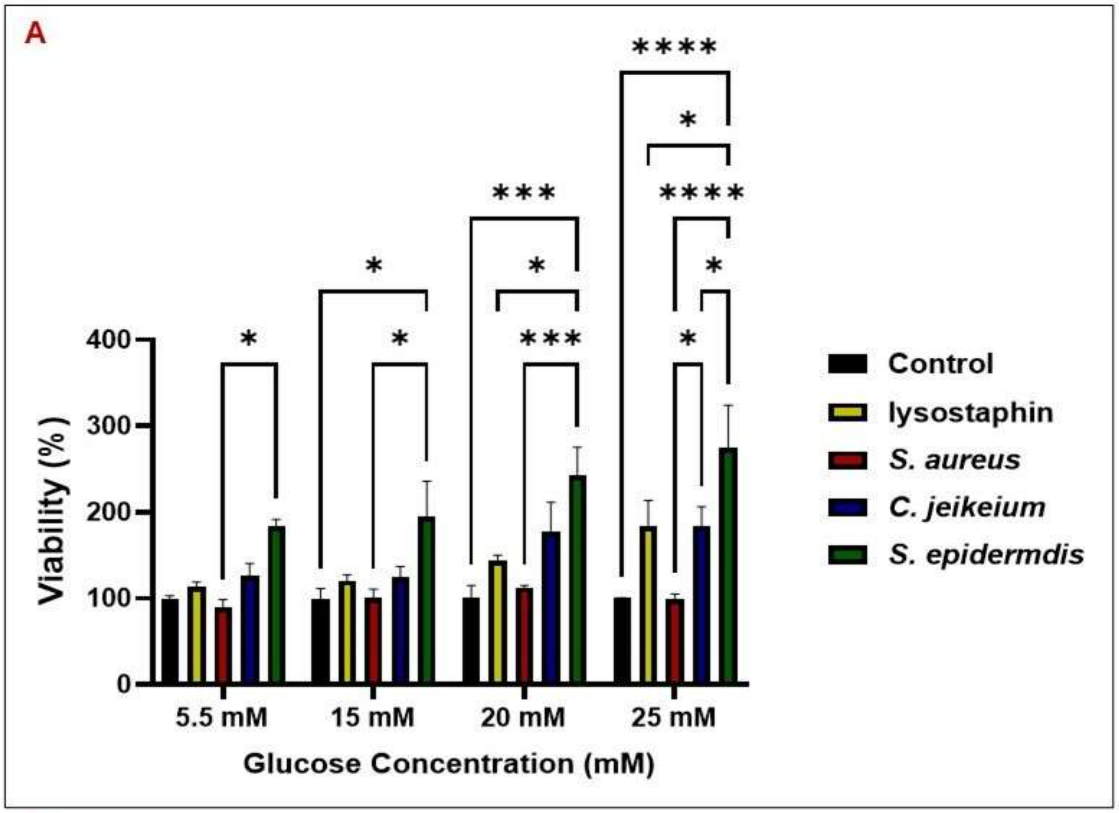

B

Glucose concertation (mM)	Control	Lysostaphin	*S. aureus*	*C. jeikeium*	*S. epidermidis*
5.5 mM	100 ± 3.29	113.74 ± 5.10	89.26 ± 9.18	126.44 ± 13.95	183.85 ± 7.91
15 mM	100 ± 11.44	120.43 ± 7.23	100.86 ± 10.11	124.33 ± 12.91	194.41 ± 41.50
20 mM	100 ± 14.67	143.70 ± 6.40	112.52 ± 2.68	177.13 ± 34.23	242.75 ± 32.83
25 mM	100 ± 0.78	183.69 ± 29.72	98.99 ± 6.08	184.59 ± 21.85	274.19 ± 50.11

Figure 4.2: **The viability (%) of human skin fibroblast in different glucose concentrations exposed to skin commensal bacterial lysates for 24 h.** Fibroblasts were plated at 5000 cells per well in 96-well plate and grown in different glucose concentrations 5.5 mM, 15 mM, 20 mM, 25 mM. Glucose concentration 5.5 mM was considered as control, reflecting euglycemic concentration, whereas 15 mM, 20 mM, and 25 mM were chosen to represent hyperglycaemic glucose concentrations. Fibroblasts were exposed to of skin commensal bacterial lysates (100 µL) and MTS assay was performed after 24 h. Absorbance was measured at 490 nm and blank corrected. To calculate the percentage of viability, all data were normalised based on control of each glucose concentration (i.e., 5.5, 15, 20 ,25) mM. Results are expressed as mean of viability (%) ± SEM, n=3, error bars represent +/- SEM, Statistical analysis two-way analysis of variance (ANOVA) and post hoc Tukey test was performed. The data were presented in two components: A) A graphical representation of the results, *p<0.05, ***p< 0.001. **** p<0.0001, and B) A table of raw numerical data.

4.6 Effect of skin commensal bacteria cell-free supernatant on human skin fibroblasts viability in different glucose concentrations at 24 h

To investigate the effect of the secreted metabolites and proteins of each bacterium on fibroblasts, *S. epidermidis, S. aureus*, and *C. jeikeium* were cultured in MHB for 18 h. Cell-free bacterial supernatant was isolated from live bacterial cells by centrifugation at 4000 × g at 4 °C for 15 min. MTS assay was conducted on human skin fibroblasts cultivated with various glucose concentrations 5.5 mM, 15 mM, 20 mM, and 25 mM and exposed to skin commensal bacterial supernatant (100 µL) for 24 h. A glucose concentration of 5.5 mM was used as the control, representing euglycemic concentrations, whereas 15 mM, 20 mM, and 25 mM were selected to represent hyperglycaemic glucose concentrations (Li et al., 2019) (Figure 4.3).

The cell-free supernatants of *S. epidermidis, S. aureus,* and *C. jeikeim* did not elicit any significant alterations in fibroblast viability at any of the glucose concentrations examined (Figure 4.3.).

A

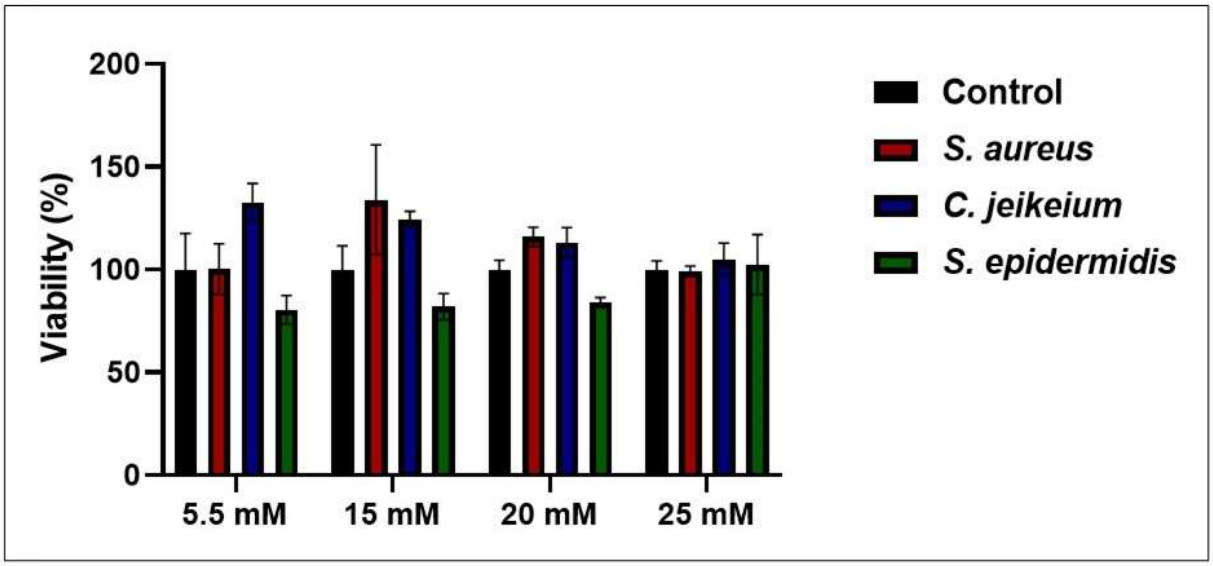

B

Glucose concentration (mM)	Control	*S. aureus*	*C. jeikeium*	*S. epidermidis*
5.5 mM	100.00 ± 17.56	100.21 ± 12.34	132.80 ± 9.10	80.55 ± 6.93
15 mM	100.00 ± 11.66	133.94 ± 26.77	124.38 ± 4.00	82.00 ± 6.41
20 mM	100.01 ± 4.49	116.04 ± 4.58	113.22 ± 7.25	84.02 ± 2.36
25 mM	100.03 ± 4.26	99.33 ± 2.49	104.92 ± 7.91	102.47 ± 14.57

Figure 4.3: **The viability (%) of human skin fibroblast in different glucose concentrations exposed to skin commensal bacterial supernatant for 24 h.** There were no significant changes observed. Fibroblasts were plated at 5000 cells per well in 96-well plate and grown in different glucose concentrations (5.5, 15, 20, 25) mM. Glucose concentration (5.5 mM) was considered as control, reflecting euglycemic concentration, whereas (15, 20, and 25) mM were chosen to represent hyperglycaemic glucose concentrations. Fibroblasts were exposed to 100 µL of skin commensal bacterial supernatant and MTS assay was performed after 24 h. Absorbance was measured at 490 nm and blank corrected. To calculate the percentage of viability, all data were normalised based on control of each glucose concentration (i.e., 5.5, 15, 20 ,25) mM. Results are expressed as mean of viability (%) ± SEM, n=3, error bars represent +/- SEM, Statistical analysis two-way analysis of variance (ANOVA) and post hoc Tukey test was performed. The data were presented in two components: A) A graphical representation of the results, and B) A table of raw numerical data.

4.7 Effect of various cell-free fermented bacterial supernatants on fibroblast viability in varying glucose concentrations over a 24-hour period

4.7.1 Cell-free glycerol fermented supernatant

To investigate the effect of cell-free fermented glycerol supernatant from each bacterium on fibroblast viability, *S. epidermidis, S. aureus,* and *C. jeikeium* were cultured in MHB supplemented with glycerol (2%) for 24 h. Cell-free bacterial supernatant was isolated from live bacterial cells by centrifugation at 4000 × g at 4 °C for 15 min. MTS assay was conducted on human skin fibroblasts cultivated with various glucose concentrations 5.5 mM, 15 mM, 20 mM, and 25 mM and exposed to cell-free fermented glycerol supernatant (100 µL) for 24 h. A glucose concentration of 5.5 mM was used as the control, representing euglycemic concentrations, whereas 15 mM, 20 mM, and 25 mM were selected to represent hyperglycaemic glucose concentrations (Li et al., 2019) (Figure 4.4).

Cell-free fermented glycerol supernatant produced by *S. epidermidis* resulted in a significant increase in fibroblast viability at 5.5 mM glucose concentration compared to the supernatant-free control. However, no significant effect was observed at 15 mM and 20 mM. Moreover, a significant decrease was observed at 25 mM glucose concentrations when exposed to cell-free fermented glycerol supernatant produced by *S. epidermidis* compared to the supernatant-free control at the same glucose concentration.

Cell-free fermented glycerol supernatant produced by *C. jeikeium* resulted in a significant decrease in the viability of fibroblasts across all glucose concentrations.

Cell-free fermented glycerol supernatant produced by *S. aureus* did not affect the viability of fibroblasts under any of the glucose conditions investigated.

A

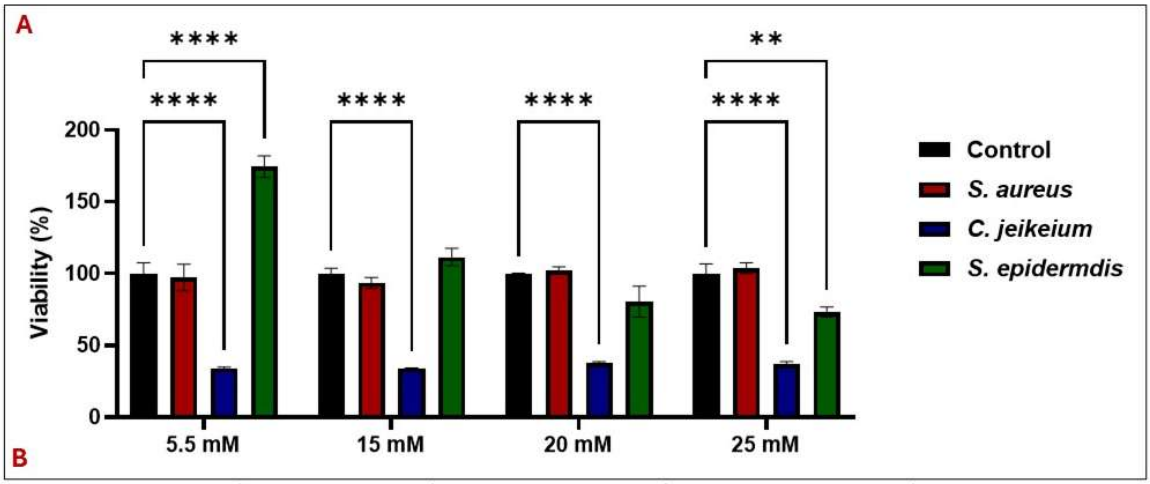

B

Glucose concentration (mM)	Control	*S. aureus*	*C. jeikeium*	*S. epidermidis*
5.5 mM	99.94 ± 7.56	97.38 ± 9.28	34.07 ± 0.65	174.40 ± 7.47
15 mM	99.94 ± 3.86	93.55 ± 3.74	34.09 ± 0.24	111.50 ± 6.07
20 mM	99.93 ± 0.26	102.10 ± 2.65	37.96 ± 0.69	80.45 ±10.77
25 mM	100.00 ± 6.81	103.72 ± 3.64	36.71 ± 1.87	73.19 ± 3.61

Figure 4.4: The viability (%) of human skin fibroblasts in various glucose concentrations exposed to cell-free fermented glycerol supernatant derived from skin commensal bacteria for 24 h. Fibroblasts were plated at 5000 cells per well in 96-well plate and grown in different glucose concentrations 5.5 mM, 15 mM, 20 mM, 25 mM. Glucose concentration 5.5 mM was considered as control, reflecting euglycemic concentration, whereas 15 mM, 20 mM, and 25 mM were chosen to represent hyperglycaemic glucose concentrations. Fibroblasts were exposed to of fermented glycerol media (80 µL) and MTS assay was performed after 24 h. Absorbance was measured at 490 nm and blank corrected. To calculate the percentage of viability, all data were normalised based on control of each glucose concentration (i.e., 5.5, 15, 20 ,25) mM. Results are expressed as mean of viability (%) ± SEM, n=3, error bars represent +/- SEM, Statistical analysis two-way analysis of variance (ANOVA) and post hoc Tukey test was performed. The data were presented in two components: A) A graphical representation of the results, **** $p<0.0001$, and B) A table of raw numerical data

4.7.2. Cell-free glucose fermented supernatant

To investigate the effect of cell-free fermented glucose supernatant from each bacterium on fibroblast viability, *S. epidermidis, S. aureus, and C. jeikeium* were cultured in MHB supplemented with glucose (20 mM) for 18 h. Cell-free bacterial supernatant was isolated from live bacterial cells by centrifugation at 4000 × g at 4 °C for 15 min. MTS assay was conducted on human skin fibroblasts cultivated with various glucose concentrations 5.5 mM, 15 mM, 20 mM, and 25 mM and exposed to cell-free fermented glucose supernatant (100 µL) for 24 h. A glucose concentration of 5.5 mM was used as the control, representing euglycemic concentrations, whereas 15 mM, 20 mM, and 25 mM were selected to represent hyperglycaemic glucose concentrations (Li et al., 2019) (Figure 4.5).

Exposure to cell-free fermented glucose supernatant produced by *S. aureus* and *C. jeikeim* resulted in a significant decrease in fibroblast viability compared with the supernatant-free control at all glucose concentrations. However, the cell-free fermented glucose supernatant produced by *S. epidermidis* exhibited no statistically significant effect on the mean percentage of fibroblast viability compared with the non-supernatant control.

A

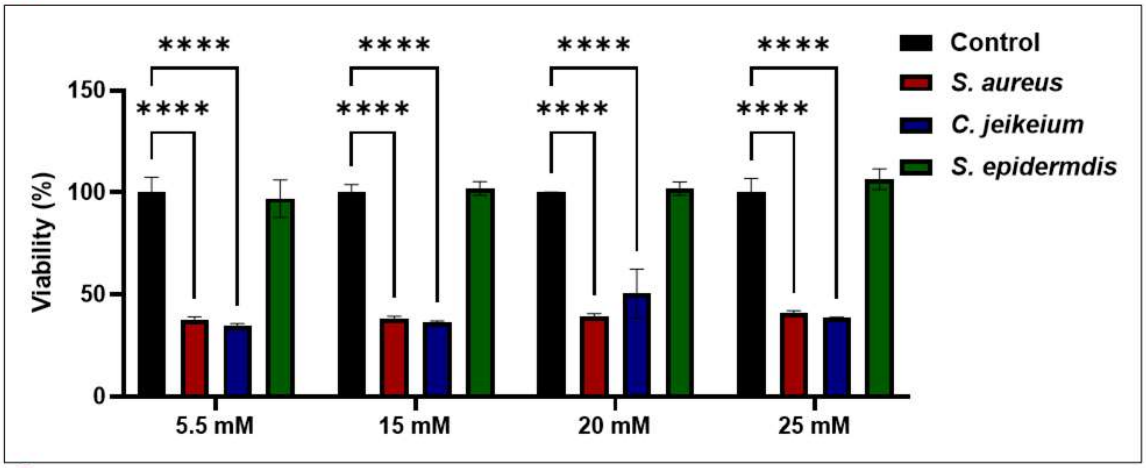

B

Glucose concentration (mM)	Control	*S. aureus*	*C. jeikeium*	*S. epidermidis*
5.5 mM	99.94 ± 7.56	37.50 ± 1.53	34.50 ± 1.18	97.02 ± 9.16
15 mM	99.94 ± 3.86	38.30 ± 0.97	36.54 ± 0.53	101.93 ± 3.40
20 mM	99.93 ± 0.26	39.12 ± 1.41	50.45 ± 11.96	101.84 ± 3.32
25 mM	100.00 ± 6.81	41.22 ± 0.73	38.63 ± 0.36	106.49 ± 5.07

Figure 4.5: The viability (%) of human skin fibroblasts in various glucose concentrations exposed to cell-free fermented glucose supernatant derived from skin commensal bacteria for 24 h. Fibroblasts were plated at 5000 cells per well in 96-well plate and grown in different glucose concentrations 5.5 mM, 15 mM, 20 mM, 25 mM. Glucose concentration 5.5 mM was considered as control, reflecting euglycemic concentration, whereas 15 mM, 20 mM, and 25 mM were chosen to represent hyperglycaemic glucose concentrations. Fibroblasts were exposed to cell-free fermented glucose supernatant (80 µL) and MTS assay was performed after 24 h. Absorbance was measured at 490 nm and blank corrected. To calculate the percentage of viability, all data were normalised based on control of each glucose concentration (i.e., 5.5, 15, 20 ,25) mM. Results are expressed as mean of viability (%) ± SEM, n=3, error bars represent +/- SEM, Statistical analysis two-way analysis of variance (ANOVA) and post hoc Tukey test was performed. The data were presented in two components: A) A graphical representation of the results, **** $p<0.0001$, and B) A table of raw numerical data.

4.8 effect of viable *S. epidermidis* on human skin fibroblast viability in 5.5 mM and 20 mM glucose concentrations at 24 h

To further investigate the effect of *S. epidermidis* secretions on fibroblast viability, an MTS assay was conducted on human skin fibroblasts cultured in 5.5 mM and 20 mM glucose concertation and exposed to (1×10^6) CFU/mL ± 2.8×10^5 of S. epidermidis for 24 h using a transwell (0.45 µm pore size). A glucose concentration of 5.5 mM was utilised as the control, representing euglycemic conditions, whereas 20 mM was selected to represent hyperglycaemic glucose concentrations (Li et al., 2019) (Figure 4.6)

Exposure to viable *S. epidermidis* separated a transwell demonstrated no significant effect on fibroblast viability compared to the no-bacteria control at both glucose concentrations tested.

A

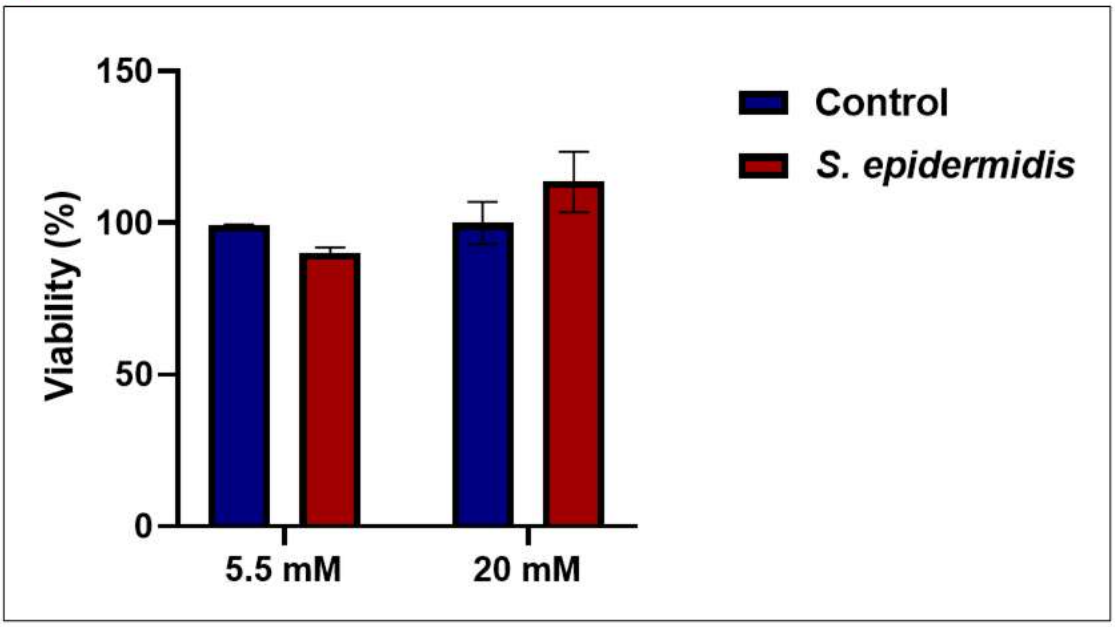

B

Glucose concentration (mM)	Control	*S. epidermidis* lysate
5.5 mM	99.36 ± 0.05	90.19 ± 1.80
20 mM	100.00 ± 6.88	113.50 ± 9.96

Figure 4.6: The viability (%) of human skin fibroblasts exposed to viable *S. epidermidis* in transwell in 5.5 mM and 20 mM glucose concentrations for 24 h. No significant changes were observed. Fibroblasts were plated at a density of cells per well in 6-well plates at euglycemic (5.5 mM) and hyperglycaemic (20 mM) glucose concentrations. Fibroblasts were exposed to (1×10^6) CFU/mL ± 2.8×10^5 *S. epidermidis* grown in transwell, and an MTS assay was performed after 24 h. Absorbance was measured at 490 nm and the absorbance was blank-corrected. To calculate the percentage viability, all data were normalised based on the control for each glucose concentration (i.e., 5.5mM and 20 mM). Results are expressed as mean viability (%) ± SEM, n=3, with error bars representing ± SEM. Statistical analysis was performed using two-way analysis of variance (ANOVA) and post-hoc Tukey test. The data were presented in two components: A) a graphical representation of the results and B) a table of raw numerical data.

4.9 Effect of *S. epidermidis* lysate on immortalised human skin keratinocytes viability in different glucose concentrations at 24 h

To investigate the effect of *S. epidermidis* lysate on the viability of keratinocytes, an MTS assay was performed on immortalised human skin keratinocytes cultured in various glucose concentrations (5.5, 24, 50, 70, and 100 mM) and exposed to 100 µL of *S. epidermidis* lysate for 24 h. Glucose concentrations of 5.5 mM was considered as control (Figure 4.7).

Culturing keratinocytes in different glucose concentrations (24, 50, 70, 100 mM) did not significantly affect the mean viability percentage of Keratinocytes compared to the 5.5 mM glucose concentration control. Moreover, exposure of keratinocytes to *S. epidermidis* lysate did not alter the mean viability percentage of keratinocytes compared to the no-lysate control across all glucose concentrations.

A

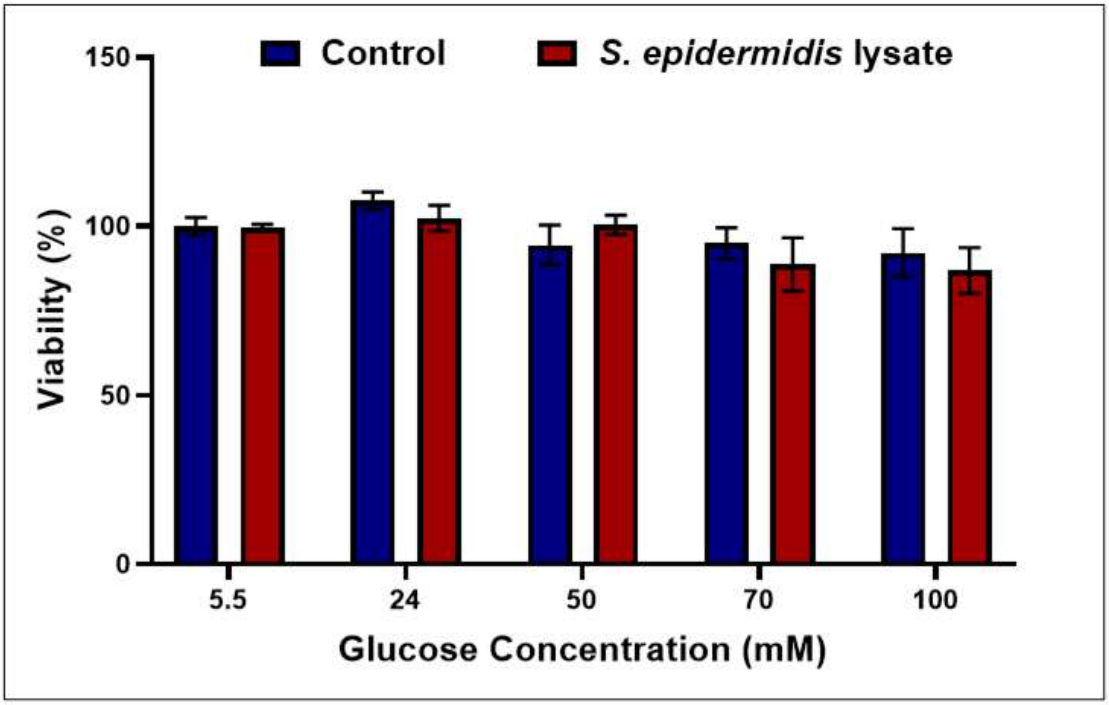

B

Glucose concentration (mM)	Control	*S. epidermidis* lysate
5.5 mM	100 ± 2.62	99.69 ± 0.84
24 mM	107.61 ± 2.58	102.37 ± 3.81
50 mM	94.42 ± 5.93	100.40 ± 2.87
70 mM	94.99 ± 4.57	88.74 ± 7.87
100 mM	92.17 ± 7.11	86.90 ± 6.80

Figure 4.7: The viability (%) of immortalised human keratinocytes in different glucose concentrations exposed to *S. epidermidis* lysate at 24 h. There were not significant changes observed. Cells were plated at 10000 cells per well in 96-well plate. Glucose concentration 5.5 mM was considered as control The cells were exposed to 100 µL of *S. epidermidis* lysate and MTS assay was performed after 24 h. Absorbance was measured at 490 nm and blank corrected. To calculate the percentage of viability, all data were normalised based on control. Results are expressed as mean of viability (%) ± SEM, n=3, error bars represent +/- SEM, Statistical analysis two-way analysis of variance (ANOVA) and post hoc Tukey test was performed. The data were presented in two components: A) A graphical representation of the results, and B) A table of raw numerical data.

4.10 Discussion

This chapter investigated the influence of different glucose concentrations on the proliferation of human skin fibroblasts and keratinocytes. Additionally, it examined whether these effects were modulated by the presence of bacterial lysate or cell-free supernatant derived from three principal skin commensal bacteria: *S. epidermidis, S. aureus,* and *C. jeikeium*. The study focused on elucidating how these factors, both independently and in combination, affected the proliferation of skin cells under different glucose conditions.

4.10.1 Understanding the proliferation of fibroblasts and keratinocytes in euglycemic and hyperglycaemic glucose concentration

In the present chapter, 5.5 mM was utilised to represent euglycemic glucose concentration. The normal plasma level of glucose is approximately 5.8 mM, and subcutaneous glucose concentration closely resembles that in plasma (Lan, 2008; Li et al., 2019). Therefore, it is appropriate to employ 5.5 mM as the healthy glucose concentration (Lan, 2008; Li et al., 2019).

As described in section 1.1.2, a random blood glucose level of 11.1 mM or higher and a fasting blood glucose level of 7 mM or higher is diagnosed as DM. Furthermore, subcutaneous glucose concentration closely resembled that in plasma (Lan, 2008; Li et al., 2019). Therefore, in the present chapter, for fibroblasts experiments, it is reasonable to select 15 mM, 20 mM, and 25 mM to represent hyperglycaemic glucose concentrations. This selection aligns with other studies that utilised glucose concentrations in the range of 10 mM - 25 mM for hyperglycaemic conditions (Lan, 2008; Li et al., 2019).

In the present study, keratinocytes were thawed and cultures in a glucose concentration of 24 mM, as specified by the supplier manual for the specific type of keratinocytes utilised in the present study (Section 2.12.5). To evaluate the impact of hyperglycaemia, glucose concentrations of 50 mM, 70 mM, and 100 mM were selected based on previous studies investigating the effects of high glucose on different types of keratinocytes (Furukawa et al., 2020; Shi et al., 2022; Yamada et al., 2017). These

concentrations were chosen as they fall within the range reported in the literature to elicit cellular responses under high glucose conditions. Although these levels are substantially higher than the physiological glucose levels observed under diabetic conditions, they have been demonstrated to induce stress responses in some other types of keratinocytes (Lan, 2008; Li et al., 2019).

In the present study, all the selected hyperglycaemic glucose concentrations did not affect the proliferation of fibroblasts and keratinocytes at any of the time points investigated (Figure 4.1, 4.7). Multiple studies utilising various glucose concentrations also reported nonsignificant alterations in fibroblast and keratinocyte proliferation (Li et al., 2019; Nickel et al., 2021; Xuan et al., 2014).

A significant decrease in proliferation of fibroblasts was only observed in some studies when the concentration of FBS was reduced or very high glucose concentrations, such as 90 mM, were used (Xuan et al., 2014). Moreover, a study by (Nakai et al., 2003) found a significant decrease in the proliferation of immortalised keratinocytes after one week of treatment with glucose concentration (25 mM) using the CCK-8 assay. Additionally, a meta-analysis and systematic review found that diabetic foot ulcers (DFU) were more prevalent in older patients with diabetes for longer durations than in younger and newly diagnosed diabetic patients (Zhang et al., 2017). The present study hypothesises the non-significant effects of glucose on the proliferation of fibroblasts and keratinocytes observed here might be due to the short duration of treatment of cells with glucose. Further studies are required to identify the correlation between the duration of exposure to high glucose and the proliferation of fibroblasts and keratinocytes, as this will provide additional insights into DFU pathophysiology in DM.

4.10.2 Understanding the effect of bacterial lysates on proliferation of fibroblasts and keratinocytes in euglycemic and hyperglycaemic glucose concentrations

Notably, in the present study, *S. epidermidis* lysate induced a significant increase in fibroblast proliferation under hyperglycaemic conditions (i.e.,15 mM, 20 mM, and 25 mM). In contrast, neither *S. aureus* nor *C. jeikeium* lysate exhibited any effect on fibroblast proliferation under either euglycemic or hyperglycaemic conditions (Figure 4.2). Exposure to lysostaphin did not cause any significant effects on viability of fibroblasts at any investigated glucose concentration (Figure 4.2). Thus, the observed results of present study are solely due to bacterial lysate. To the best of our knowledge, this finding has not been previously reported in any in vitro experiments. Only one ex vivo study was identified, which reported *S. epidermidis* lysate promotes reepithelialisation in both diabetic and healthy skin (Mohammedsaeed et al., 2022).

On interesting question in this context is why only *S. epidermidis* lysate elicited this significant effect and why it was only observed exclusively under hyperglycaemic conditions. Further investigations into the components of *S. epidermidis* lysate are necessary to elucidate the potential interaction between bacterial lysate and host cell pathways. Notably, a study suggested that two primary *S. epidermidis*-derived N-Formyl Methionine Peptides (f-MFLLVN and f-MIIINA) were responsible for inducing an immune response in the skin in vitro. Consequently, the present study proposes conducting additional research to characterise the effect of *S. epidermidis*-derived peptides on fibroblast proliferation under varying glucose concentrations. This approach will contribute to the understanding of potential interactions between bacterial lysate and host cell pathways in varying glucose concentration. Moreover, this will help to understand how lysate may modulate cellular behaviours such as proliferation under hyperglycaemic conditions.

As *S. epidermidis* lysate caused significant alteration in fibroblast proliferation, further investigation of its effect on keratinocyte proliferation was conducted in the present study. Notably, *S. epidermidis* lysate did not elicit any significant effect on keratinocytes proliferation. Interestingly, a study hypothesised that keratinocytes in reconstructed human epidermal models treated with live skin commensal bacteria to proliferate more rapidly to elicit a stronger immune response (Duckney et al., 2013).

However, it appears that keratinocytes prioritise differentiation and barrier repair over regeneration and proliferation (Duckney et al., 2013). Consequently, the present study strongly recommends investigating the effect of *S. epidermidis* lysate on the differentiation and barrier repair of keratinocytes The primary influence of *S. epidermidis* on keratinocytes may be through its impact on keratinocyte differentiation rather than cellular proliferation.

4.10.3 Understanding the effect of cell-free supernatant on proliferation of fibroblasts and keratinocytes in euglycemic and hyperglycaemic glucose concentrations

S. epidermidis, S. aureus, and *C. jeikieum* did not appear to secrete any substances that influence the proliferation of fibroblasts at both euglycemic and hyperglycaemic levels of glucose. This conclusion is supported by the observation that cell-free supernatant of all bacteria species, prepared in MHB without supplements, did not elicit any significant effects on fibroblast proliferation at euglycemic and hyperglycaemic levels of glucose (Figure 4.3). Moreover, exposure to viable *S. epidermidis* separated by a transwell did not influence the percentage of viability of fibroblasts at euglycemic and hyperglycaemic glucose concentrations (Figure 4.6). The present study suggests characterising the components of bacterial cell-free supernatant and examining the effects of different doses of cell-free supernatant on human skin cells separately, as the non-significant results observed here may be attributed to the low concentration of components within the applied cell-free supernatant.

Notably, when fibroblasts were exposed to cell-free supernatant prepared in media supplemented with glycerol, the proliferation of fibroblasts was affected in various ways (Figure 4.4). Specifically, when fibroblasts were exposed to cell-free supernatant prepared from *S. epidermidis* growing in media supplemented with glycerol, a significant increase in fibroblast proliferation was observed at a normal glucose level. However, the proliferation of fibroblasts began to decrease under hyperglycaemic conditions (15 and 20 mM) and significantly diminished at 25 mM glucose concentration (Figure 4.4). In contrast, no alteration in fibroblast proliferation was observed when exposed to cell-free supernatant prepared from *S. aureus* growing in media supplemented with glycerol, at both euglycemic and hyperglycaemic glucose levels (Figure 4.4). However, a significant reduction in fibroblast proliferation was observed when fibroblasts were exposed to cell-free supernatant prepared from *C. jeikeium* growing in media supplemented with glycerol (Figure 4.4).

In the present study, pH measurements during glycerol fermentation exhibited variation when different bacterial species were utilised for glycerol fermentation (Figure 3.8). Consequently, the present study suggests the observed differences in

fibroblast proliferation exposed to cell-free supernatant (Figure 4.4) may be attributed due to variations in pH (Figure 3.8). Furthermore, the disparities in pH measurements potentially indicate the formation of distinct acid types when different bacterial species are employed. As different acids have varying pH levels (Yang et al., 2014). Consequently, this study proposes an additional factor contributing to the observed variation in proliferation results (Figure 4.4) could be the differences in the types and concentrations of acids present in the cell-free supernatant generated through the fermentation of glycerol by each bacterial species.

The biochemical pathway of glycerol fermentation is summarised in Figure 4.8 Succinate, butyrate, acetate, and ethanol may be produced as by-products in glycerol fermentation (Serwańska-Leja et al., 2011). Moreover, variations in different acid by-products have been reported among diverse studies based on the utilisation of different bacterial species and fermentation conditions. In *Escherichia coli*, glycerol can be fermented in a pH-dependent manner (Dharmadi et al., 2006). The primary products of glycerol fermentation in *Escherichia coli* are ethanol and succinate, constituting 93% of the product mixture (Dharmadi et al., 2006). *Paenibacillus macerans*, previously considered incapable of fermenting glycerol, has been demonstrated to grow fermentatively on glycerol, producing ethanol, formate, acetate, succinate, and 1,2-propanediol (Gupta et al., 2009). *Halanaerobium saccharolyticum* subspecies can produce hydrogen, carbon dioxide, and acetate from glycerol fermentation, with subspecies *saccharolyticum* also producing 1,3-propanediol, butyrate, and ethanol (Kivistö et al., 2010).

Interestingly, acetic, butyric, and succinic acids were the primary acids produced in glycerol fermentation by *S. epidermidis* (Wang et al., 2017). However, another study reported the formation of lactic acids when glycerol was fermented by *S. epidermidis* (N. Salgaonkar et al., 2022). The main difference between the methodologies of both studies was that one fermented the glycerol in aerobic media for 24 h and 72 h (N. Salgaonkar et al., 2022), whilst the other study fermented it in anaerobic media for six days (Wang et al., 2017). This suggests that different growth conditions may influence the type of acids produced by each bacterial species. Thus, the present study indicates that further experiments are necessary to determine the type and concentration of acid produced in glycerol fermentation by each skin commensal bacterium. Subsequently, it is essential to study the effect of each produced acid on the proliferation of fibroblasts

separately. This is crucial to understand the effect of acids produced by skin commensal bacteria on wound healing in DM. Additional studies are required to conduct this investigation.

A study found that high concentrations (5 mM and 10 mM) of butyrate reduced porcine jejunal epithelial cells; however, lower concentrations such as 0.5 mM or 1 mM did not (Qiu et al., 2017). As butyrate is one of the products in glycerol fermentation (Figure 4.8) (Serwańska-Leja et al., 2011), the present study hypothesises that the observed results might be due to the presence of high concentrations of butyrate. However, further studies are required to investigate this hypothesis.

Moreover, a study demonstrated that topical application of sodium butyrate with epidermal growth factor and platelet-derived growth factor-BB promoted wound healing in diabetic mice by inducing skin cell differentiation (Keshava & Gope, 2015). As butyrate is one of the glycerol fermentation by-products and there is evidence of its significance in diabetic wound healing (Keshava & Gope, 2015), the present study suggests that further investigation of the effect of skin commensal bacteria on wound healing in DM is necessary to elucidate the relationships between different acids produced by skin commensal bacteria and their role in the wound healing process.

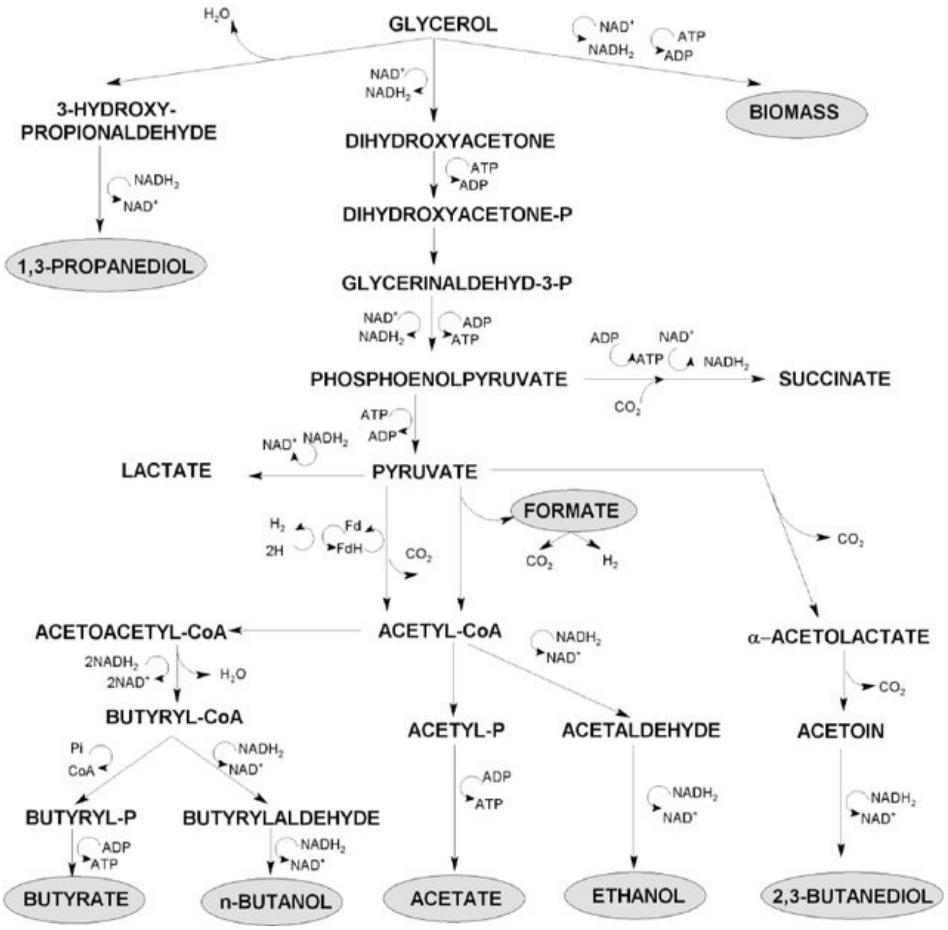

Figure 4.8: The biochemical fermentation pathway of glycerol (Serwańska-Leja et al., 2011)

As DM is associated with sustained hyperglycaemia (NICE, 2022), it is essential to elucidate how skin commensal bacteria respond to this elevated glucose concentration and how the by-product of glucose metabolism by *S. epidermidis* influences wound healing in DM. In the present study, cell-free supernatant prepared in media supplemented with glucose (20 mM) and the effect of this supernatant on fibroblast proliferation in euglycemic and hyperglycaemic glucose concentrations were investigated. Similar to glycerol, a variation in the influence of cell-free supernatant prepared in media supplemented with glucose on the viability of fibroblasts was also observed among different bacterial species. No significant alteration in fibroblast proliferation was observed when exposed to cell-free supernatant prepared from *S. epidermidis* cultured in media supplemented with glucose (Figure 4.5). However, the proliferation of fibroblasts was significantly reduced when exposed to cell-free supernatant prepared from *S. aureus* and *C. jeikeium* cultured in media supplemented with glucose (Figure 4.5).

Although pH measurements during glucose fermentation exhibited slight variation when different bacterial species were utilised for glucose fermentation (Figure 3.12). The present study suggests the observed differences in fibroblast proliferation exposed to cell-free supernatant (Figure 4.5) may be attributed due to this slight change in variations in pH (Figure 3.12). Furthermore, the disparities in pH measurements potentially indicate the formation of distinct acid types when different bacterial species are employed. As different acids have varying pH levels (Yang et al., 2014).

Figure 4.9 summarises the fermentation pathway of glucose. The main products of glucose fermentation might be ethanol or lactate (Boumba et al., 2008). Different bacteria exhibit diverse glucose fermentation patterns, resulting in varied metabolic products and physiological responses. *Lactobacillus brevis* strains aggregate upon glucose addition, leading to pH decrease and partial detachment of surface layer proteins (Saito et al., 2019). Interestingly, *Vibrio cholerae* O1 serogroup strains show biotype-specific glucose fermentation. Classical biotype strains perform organic acid-producing fermentation, whilst *El Tor biotype* strains use a neutral fermentation pathway (Lee et al., 2020). However, current Wave 2 and Wave 3 atypical El Tor strains have lost this neutral fermentation ability due to a genetic mutation (Lee et al., 2020). In *Saccharomyces* strains engineered for xylose fermentation, genetic

background significantly affects glucose and xylose metabolism, resulting in varied performance between strains (Lopes et al., 2017).

Therefore, the present study suggests that further experiments are necessary to investigate the types of acids and metabolites produced during glucose fermentation by skin commensal bacteria. This investigation will contribute to identifying the secretion patterns of skin commensal bacteria in diabetic environments and elucidate the effects of skin commensal bacteria on wound healing in DM.

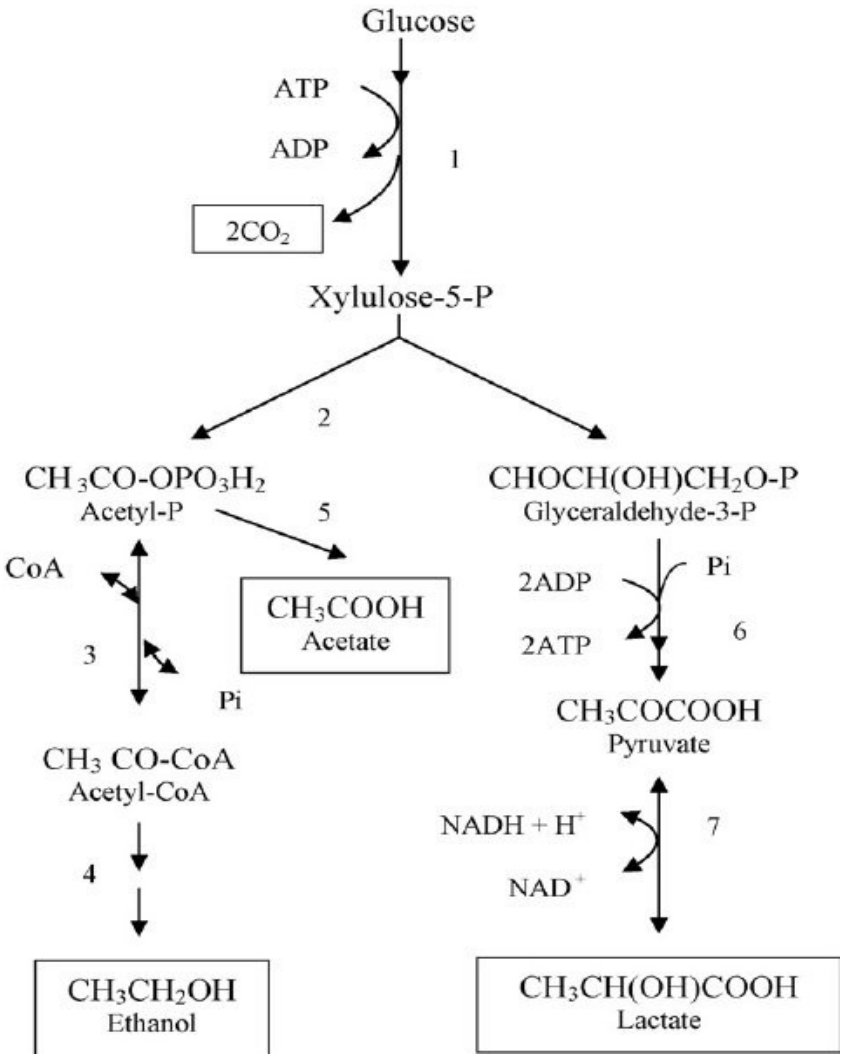

Figure 4.9.: The biochemical fermentation pathway of glucose (Boumba et al., 2008).

4.10.4 Conclusion and Future Direction

S. epidermidis lysate demonstrated a significant effect on fibroblast proliferation under hyperglycaemic glucose concentrations. Consequently, Chapter 5 will exclusively focus on investigating the influence of *S. epidermidis* on fibroblast and keratinocyte migration under both euglycemic and hyperglycaemic conditions. Subsequently, Chapter 6 will elucidate the alterations in gene expression of fibroblasts exposed to *S. epidermidis* lysate under varying glucose concentrations. This will help to clarify how *S. epidermidis* lysate modulate cellular pathways of fibroblasts under varying glucose concentrations.

Chapter 5: Exploring the effect of *S. epidermidis* on human skin fibroblasts and keratinocytes migration in euglycemic and hyperglycaemic glucose concentrations.

5.1 Introduction

Cell migration is a critical process that is involved in human body development, disease, and homeostasis (Guak & Krawczyk, 2020; Ridley et al., 2003). Coordinated migration of precursor cells is essential for generating the embryo in normal embryogenesis (Ridley et al., 2003). Migration of immune cells to the site of infection is crucial for controlling infections (Guak & Krawczyk, 2020). Migration of keratinocytes and fibroblasts contributes to proper wound closure and tissue regeneration (Cialdai et al., 2022; Raja et al., 2007). Furthermore, disturbances in migration are implicated in the prognosis of various diseases, such as cancer cell metastasis and impaired wound healing (Olson & Sahai, 2009; Raja et al., 2007). Therefore, modulation of cell migration may potentially aid in the treatment of numerous chronic conditions, including chronic wounds (Raja et al., 2007).

The migration assay is a technique utilised to investigate cellular movement in response to specific stimuli. This methodology is frequently employed in research to examine cell migration, wound healing processes, and the metastatic potential of cancer cells (Pijuan et al., 2019).

A transwell migration assay is a prevalent method for studying cell migration, which employs two medium-filled compartments to establish a chemoattractant gradient that induces chemotaxis of cells through a porous membrane (Justus et al., 2023). The fundamental principle of this method involves creating a gradient of the stimulus and observing the subsequent migration of cells towards or away from it (Pijuan et al., 2019). The scratch migration assay is an alternative methodology for investigating cell migration, which entails the introduction of a wound in a confluent cell monolayer (Cappiello et al., 2018; Pijuan et al., 2019). The essential steps of this assay comprise introducing a wound in a monolayer of cells, followed by capturing microscopic images of the wound at the initial timepoint and at regular intervals thereafter, and subsequently comparing these images to quantify the migration rate of cells (Cappiello et al., 2018; Pijuan et al., 2019).

The selection of a migration assay should be based on the specific research objectives and available resources. As a transwell assay measures cell migration through a porous membrane gradient, this method is typically employed to study the metastasis of cancer cells under various conditions (Kovaříková et al., 2014). In contrast, the scratch assay involves creating a wound in a cell monolayer and measuring the closure of the wound over time. This type of migration assay is widely utilised to investigate cell migration in wound healing as it provides a strong directional migratory response (Masson-Meyers et al., 2020).

Cell starvation is necessary to ensure proper study of cell migration in the scratch assay. This procedure ensures that wound closure results from cell migration rather than cell proliferation (Vang Mouritzen & Jenssen, 2018). One of the commonly used methods to inhibit cell proliferation is supplementation with mitomycin. However, as mitomycin exhibits antibacterial effects (Pacios et al., 2021), it was not used in the present study. Instead, cell proliferation was inhibited by removing FBS from the media, and cell proliferation was monitored in a time-dependent manner.

5.2 Aim of chapter

To investigate the influence of *S. epidermidis* on the migration of fibroblasts and keratinocytes under varying glucose concentrations

5.3 Objectives of chapter

To examine the migration of fibroblasts and keratinocytes in varying glucose concentrations

To assess the impact of *S. epidermidis* lysate on fibroblast migration in varying glucose concentrations

To evaluate the influence of *S. epidermidis* lysate on keratinocyte migration in varying glucose concentrations

5.4 Investigating the effect of *S. epidermidis* on human skin fibroblast migration in 5.5 mm and 20 mm glucose concentrations

5.4.1 Investigating the effect of serum starvation on fibroblasts proliferation for 72 h: a crucial preparatory step for migration assay

Human skin fibroblasts were initially subjected to serum starvation by culturing them in EMEM media devoid of FBS for 1 h, after which the migration assay was conducted in the absence of FBS for 48 h. Serum starvation constitutes a crucial preliminary step to ensure that the observed results are due to cell movement rather than cell proliferation (Jiang et al., 2022).

To verify the efficacy of the starvation process, an MTS assay was conducted on human skin fibroblasts cultured in EMEM media without FBS at two distinct glucose concentrations: 5.5 mM and 20 mM. The assay was performed at 24 h, 48 h, and 72 h time points (Figure 5.1). The 5.5 mM glucose concentration served as the control, representing euglycemic conditions, whilst the 20 mM concentration was selected to simulate hyperglycaemic conditions.

Serum starvation with FBS did not affect mean percentage viability for 48 hours at both glucose concentrations of 5.5 mM and 20 mM. However, a significant reduction in mean percentage viability was observed after 72 hours at both glucose concentrations of 5.5 mM and 20 mM.

A

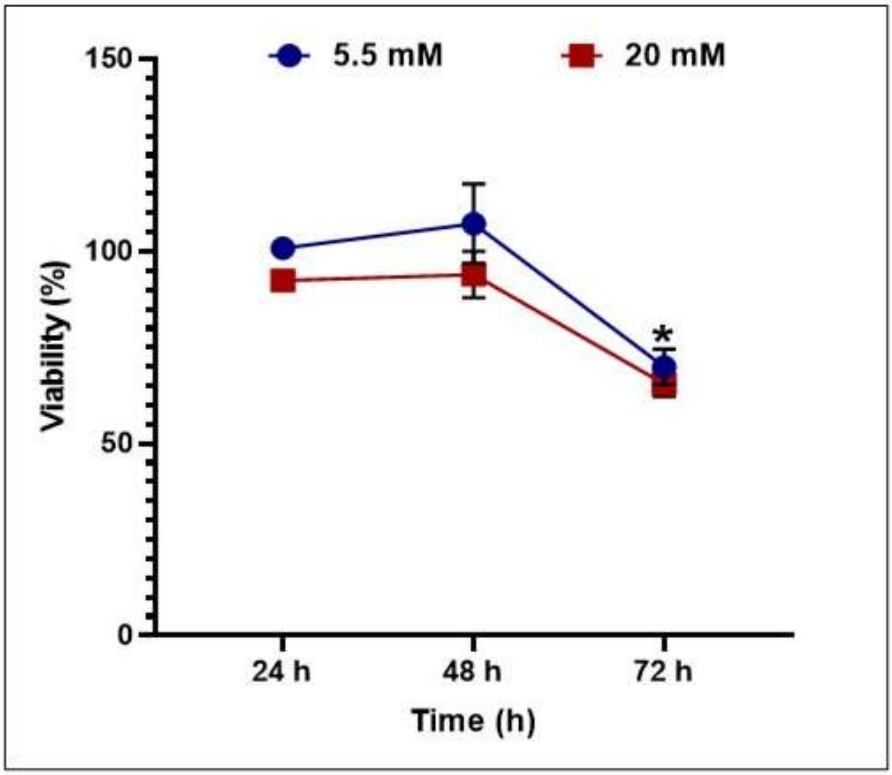

B

Time (h)	5.5 mM	20 mM
24	100.79 ± 0.84	92.41 ± 1.90
48	107.22 ± 10.32	93.98 ± 6.00
72	69.95 ± 4.57	65.51 ± 3.34

***Figure 5.1*: The percentage of viability of human skin fibroblast in healthy (5.5 mM) and hyperglycaemic (20) mM glucose concentration.** Fibroblasts were plated at 5000 cells per well and grown in different glucose concentrations in 0% FBS for (24, 48, 72) h. In both 5.5 mM and 20 mM glucose concentrations. No significant decrease in fibroblasts viability was observed over 48 h. Significant decrease in viability was observed at 72 h. The viability was determined by MTS assay and all results were normalised to control (i.e. fibroblasts at 24 h of each glucose concentration 5.5 mM and 20 mM). The viability of human fibroblasts is expressed as mean viability percentage± SEM, n=3, error bars represent +/- SEM, two-way analysis of variance (ANOVA) and post hoc Tukey test was performed * $p<0.05$. The data were presented in two components: A) a graphical representation of the results and B) a table of raw numerical data.

5.4.2. Investigating the effect of 5.5 mM and 20 mM glucose on the migration of human skin fibroblast for 48 h

A scratch migration assay was conducted on human skin fibroblasts cultured in 5.5 mM and 20 mM glucose for 48 h. Images of the scratch were captured using Cytation (Agilent, UK) at 6 h, 12 h, 18 h, 24 h, and 48 h (Figure 5.2, 5.3, and 5.8). A glucose concentration of 5.5 mM was used as a control, representing euglycemic conditions, whereas 20 mM was selected to represent hyperglycaemic conditions.

High glucose concentrations (20 mM) significantly reduced the percentage of fibroblast scratch closure at 12 h and 18 h compared to the euglycemic control (5.5 mM) [20 mM vs 5.5 mM; 12 h= 40.7%± 15.8 vs 76.6% ±14.7 ($p<0.05$, n=3), at 18 h= 56.9%±16.1 vs 92.3%± 6.5 ($p<0.05$, n=3)]. However, no significant difference was observed between the two glucose concentrations at 6 h, 24 h, and 48 h [high glucose (20 mM) vs low glucose (5.5 mM) control; 6 h= 20.6% ± 7.1 vs 42.1% ±12.1 ($p>0.05$, n=3), 24 h= 71.6%±11.5 vs 96.9%±3.1 ($p>0.05$, n=3), at 48 h= 94.8%± 2.9 vs 100%± 0 ($p>0.05$, n=3)].

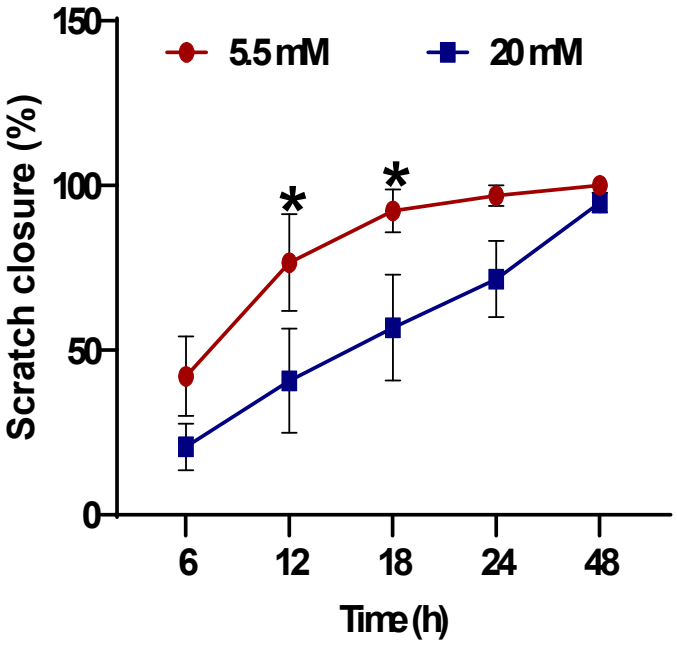

Figure 5.2: **The percentage of scratch closure in human skin fibroblast grown in healthy (5.5 mM) and hyperglycaemic (20 mM) glucose concentration.** Fibroblasts were plated at 5000 cells per well in 5.5 mM and 20 mM glucose concentrations. Cells were starved in 0% FBS for 1 h prior introduction of scratch. Image of scratch was taken by cytation (Agilent, UK). ImageJ was used to calculate the area of scratch at different timepoints. The percentage of Scratch closure % was calculated by equation (Scratch Closure= (Area at (t=t)- Area at t=0)/ Area at (t=0) ✕100). Results are expressed as mean scratch closure percentage± SEM, n=3, error bars represent +/- SEM, two-way analysis of variance (ANOVA) and post hoc Tukey test was performed *p> 0.05.

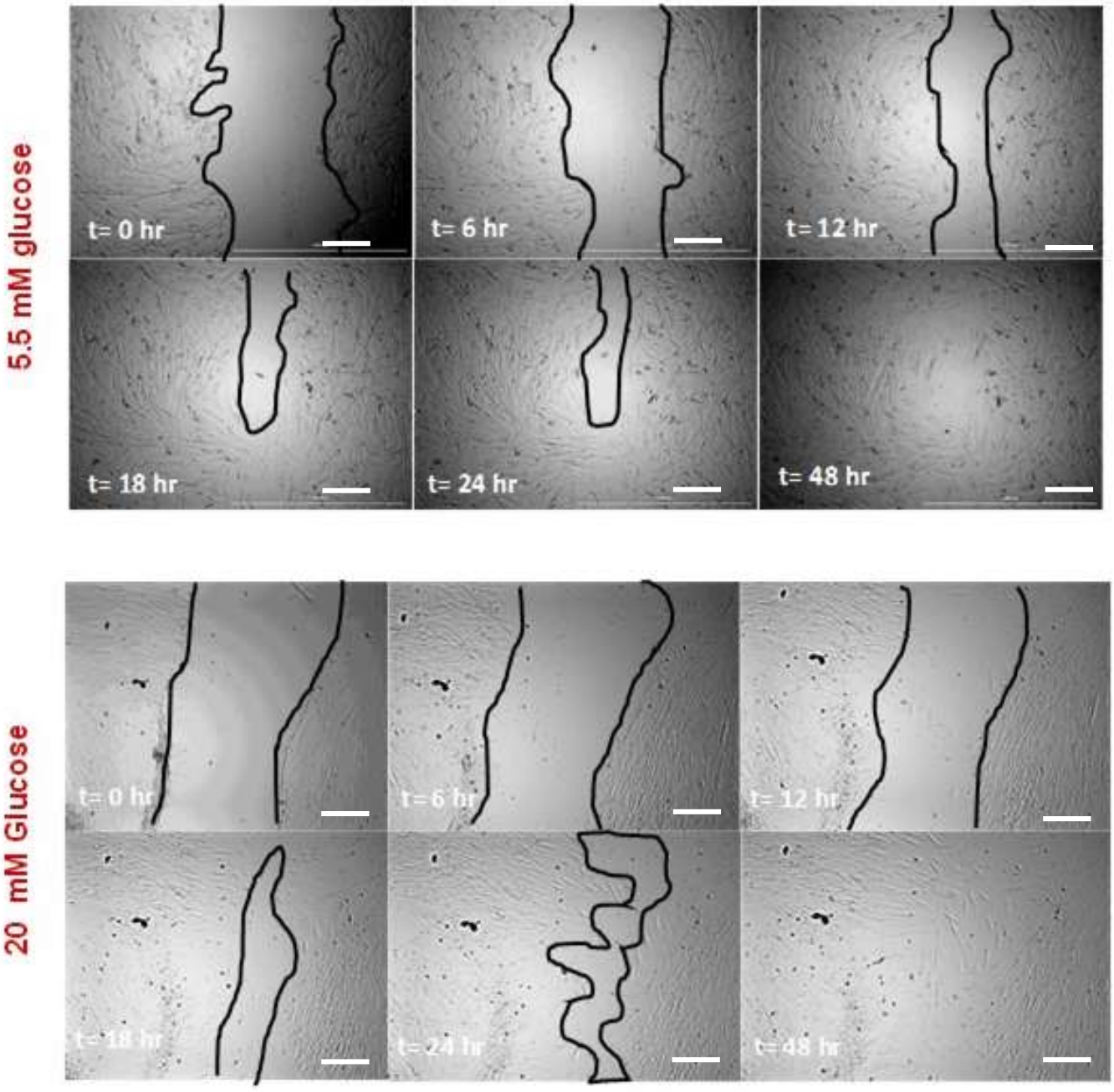

Figure 5.3: Image of scratch of human skin fibroblasts grown in 5.5 mM and 20 mM. Fibroblasts were plated at 5000 cells per well in 5.5 mM and 20 mM glucose concentrations and. Cells were starved in 0% FBS for 1 h prior introduction of scratch. A scratch was introduced, and microscopic pictures (at 40X magnification) was taken by citation (Agilent, UK) at 0 h, 6 h, 12 h, 18 h, 24 h, 48 h. Scale bar=0.01 mm.

5.4.3. Investigating the effect of *S. epidermidis* lysate on human skin fibroblast migration in (5.5 mM) glucose concentration for 48 h

A scratch migration assay was conducted on human skin fibroblasts exposed to *S. epidermidis* lysate at 5.5 mM for 48 h. Images of the scratch were captured using Cytation (Agilent, UK) at 0 h, 6 h, 12 h, 18 h, 24 h, and 48 h (Figure 5.4, 5.5, and 5.8).

Exposure to *S. epidermidis* demonstrated no statistically significant effect on the percentage of scratch closure in fibroblasts compared to the no-lysate glucose control at 5.5 mM glucose concentration [*S. epidermidis* lysate vs no-lysate control; 6 h= 42% ± 3.5 vs 42.1% ± 12.1 ($p>0.05$, n=3), 12 h=89.5%± 5.4 vs 76.6% ± 14.7 ($p>0.05$, n=3), 18 h= 96.2%± 2.2 vs 92.3% ± 6.5 ($p>0.05$, n=3), 24 h=99.1%±1 vs 96.9% ± 3.1 ($p>0.05$, n=3), 48 h= 100% vs 100 % ($p>0.05$, n=3)].

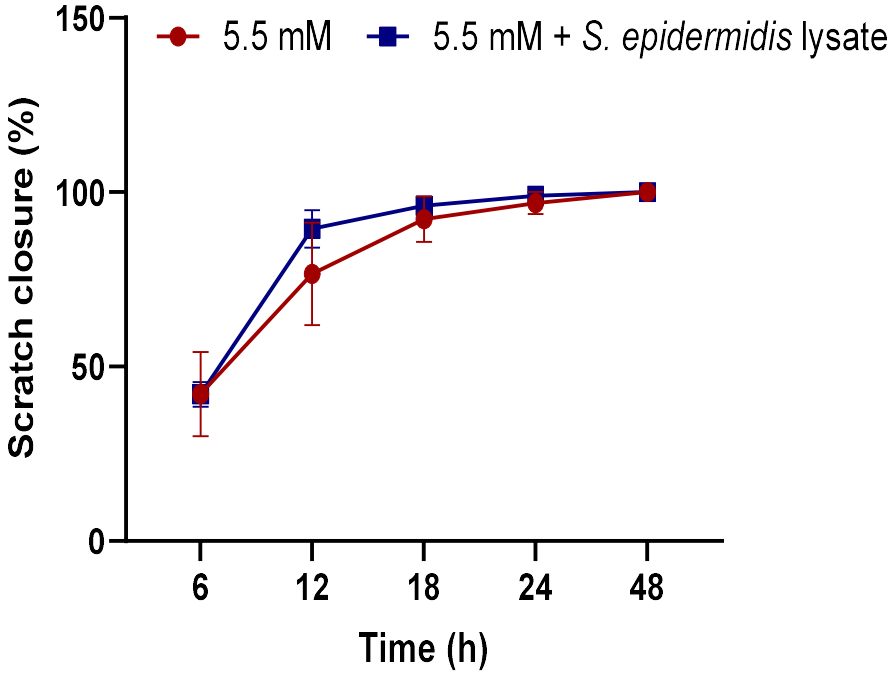

Figure 5.4: **The percentage of scratch closure of human skin fibroblast exposed to *S. epidermidis* lysate in healthy (5.5 mM).** Fibroblasts were plated at 5000 cells per well in 5.5 mM glucose concentrations and exposed to 100 µL of *S. epidermidis* lysate. Cells were starved in 0% FBS for 1 h prior introduction of scratch. Image of scratch was taken by citation (Agilent, UK) at different timepoints. ImageJ was used to calculate the area of scratch at different timepoints. The percentage of Scratch closure % was calculated by equation (Scratch Closure= (Area at (t=t)- Area at t=0)/ Area at (t=0) ✕100). Results are expressed as mean scratch closure percentage± SEM, n=3, error bars represent +/- SEM, two-way analysis of variance (ANOVA) and post hoc Tukey test was performed.

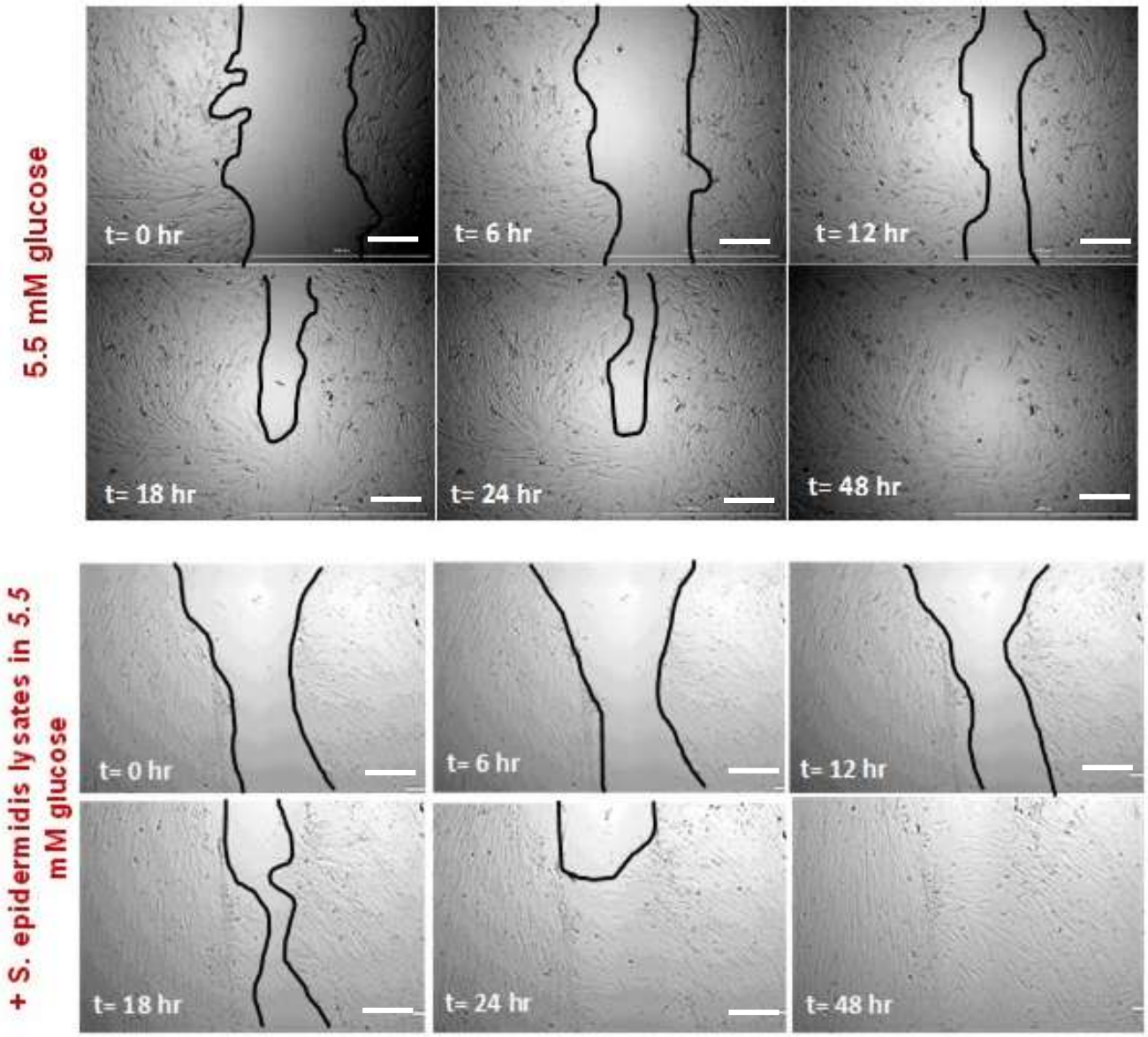

***Figure* 5.5: Image of scratch of human skin fibroblasts exposed to *S. epidermidis* lysate grown in 5.5 mM.** Fibroblasts were plated at 5000 cells per well in 5.5 mM glucose concentrations and exposed to *S. epidermidis* lysate. Cells were starved in 0% FBS for 1 h prior introduction of scratch. A scratch was introduced, and microscopic pictures (at 40X magnification) was taken by cytation (Agilent, UK) at 0 h, 6 h, 12 h, 18 h, 24 h, 48 h. Scale bar=0.01 mm.

5.4.4. Investigating the effect of *S. epidermidis* lysate on human skin fibroblast migration in (20 mM) glucose concentration for 48 h

A scratch migration assay was conducted on human skin fibroblasts exposed to *S. epidermidis* lysate at 20 mM for 48 h. Images of the scratch were captured using Cytation (Agilent, UK) at 0 h, 6 h, 12 h, 18 h, 24 h, and 48 h (Figure 5.6, 5.7, and 5.8).

Exposure to *S. epidermidis* lysate significantly increased the percentage of scratch closure in fibroblasts compared to the no-lysate control in 20 mM glucose concentrations at 12 h and 18 h. However, exposure to *S. epidermidis* lysate had no significant effect on the percentage of scratch closure at 6 h, 24 h, and 48 h [*S. epidermidis* lysate vs no-lysate control at 6 h=46%± 4.9 vs 20.6% ± 7.1 ($p>0.05$, n=3), 12 h=89.9% ± 3.2 vs 40.7% ± 15.8 ($p<0.001$, n=3), 18 h= 98%± 2 vs 56.9% ± 16.1 ($p<0.01$, n=3), 24 h=99 % ± 0.7 vs 71.6% ± 11.5 ($p>0.05$, n=3), 48 h= 100% vs 94.8%± 2.9 ($p>0.05$, n=3)].

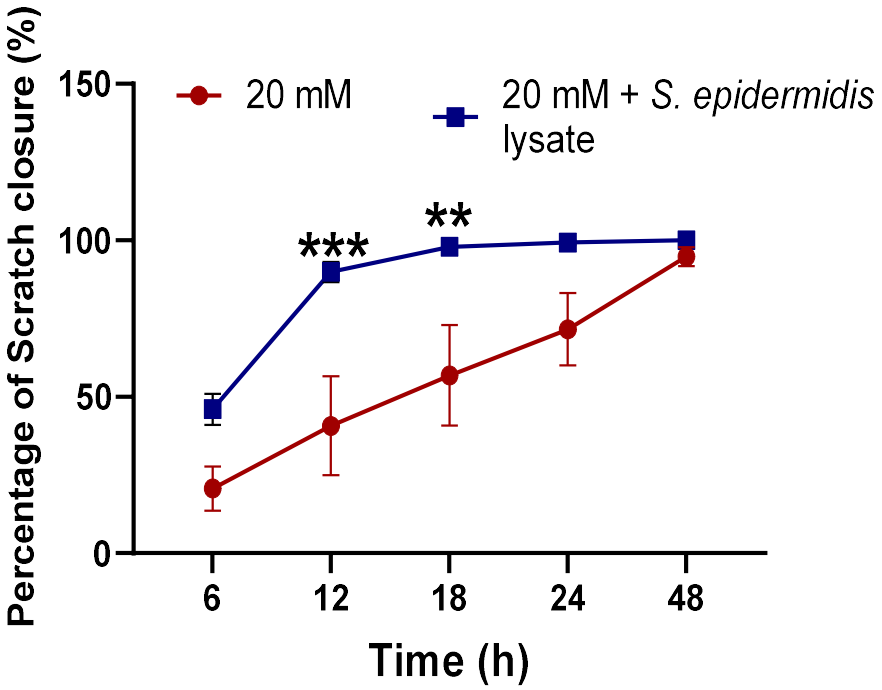

Figure 5.6: **The percentage of scratch closure of human skin fibroblast exposed to *S. epidermidis* lysate in hyperglycaemic (20) mM glucose concentration.** Fibroblasts were plated at 5000 cells per well in 20 mM glucose concentrations and exposed to 100 µL of *S. epidermidis* lysate. Cells were starved in 0% FBS for 1 h prior introduction of scratch. Image of scratch was taken by cytation (Agilent, UK) at different timepoints. ImageJ was used to calculate the area of scratch at different timepoints. The percentage of Scratch closure % was calculated by equation (Scratch Closure= (Area at (t=t)- Area at t=0)/ Area at (t=0) ✕100). Results are expressed as mean scratch closure percentage± SEM, n=3, error bars represent +/- SEM, two-way analysis of variance (ANOVA) and post hoc Tukey test was performed **p<0.01.***p<0.001.

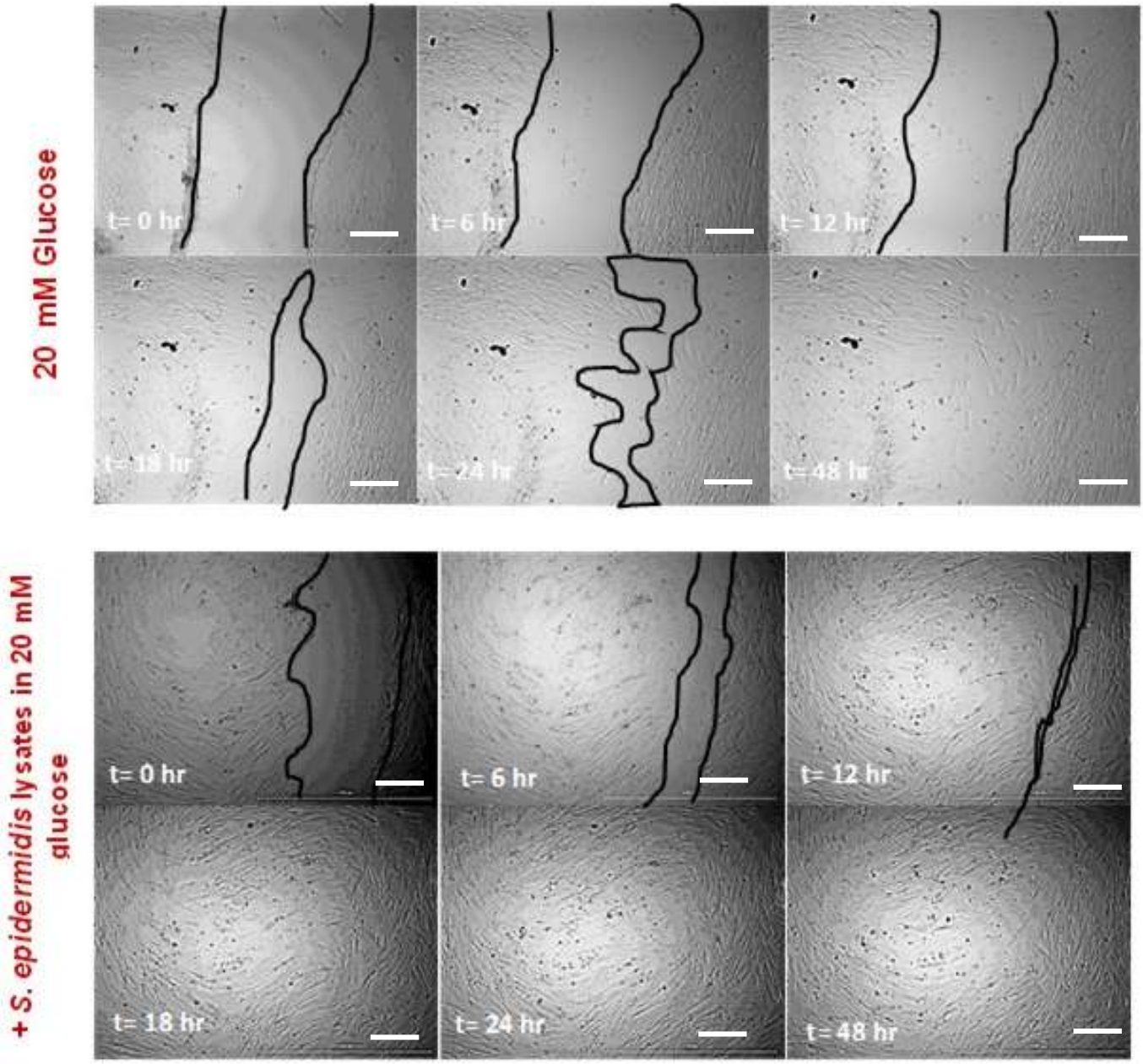

Figure 5.7: Image of scratch of human skin fibroblasts exposed to *S. epidermidis* lysate grown in 20 mM. Fibroblasts were plated at 5000 cells per well in 20 mM glucose concentrations and exposed to *S. epidermidis* lysate. Cells were starved in 0% FBS for 1 h prior introduction of scratch. A scratch was introduced, and microscopic pictures (at 40X magnification) was taken by cytation (Agilent, UK) at 0 h, 6 h, 12 h, 18 h, 24 h, 48 h. Scale bar=0.01 mm.

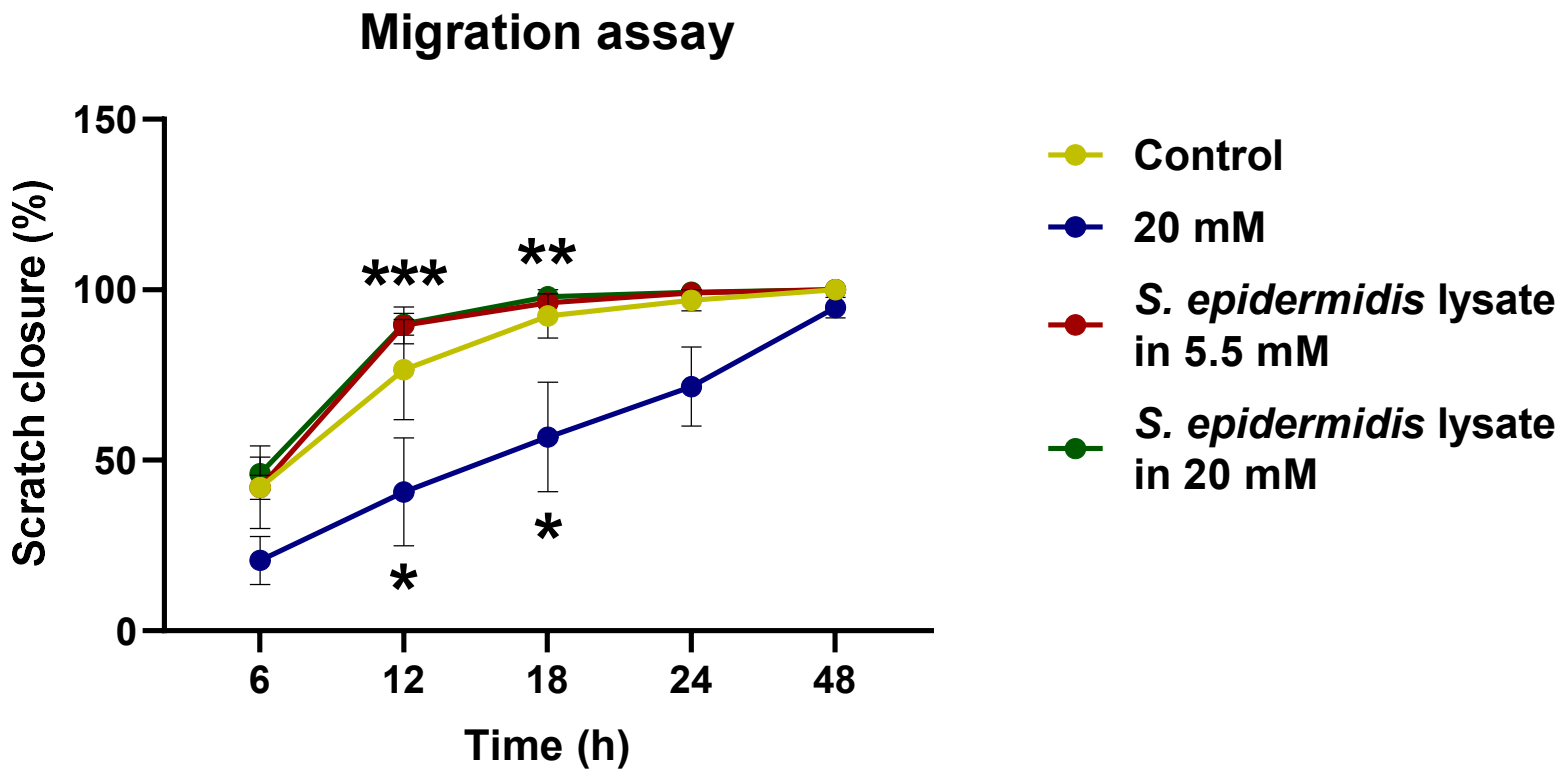

Figure 5.8: *S. epidermidis* lysate stimulates fibroblasts migration in hyperglycaemic conditions in-vitro. The figure combines data from Figures 5.2, 5.4, and 5.6. Human fibroblasts were cultured in 5.5 mM and 20 mM glucose concentrations and subsequently exposed to *S. epidermidis* lysates for 48 hours. Microscopic images were captured at 6-hour intervals for a duration of 24 hours using Cytation (Agilent, UK). Image of scratch was taken by cytation at different timepoints. ImageJ was used to calculate the area of scratch at different timepoints. The percentage of Scratch closure % was calculated by equation (Scratch Closure= (Area at (t=t)- Area at t=0)/ Area at (t=0) ✕100). Results are expressed as mean scratch closure percentage± SEM, n=3, error bars represent +/- SEM, two-way analysis of variance (ANOVA) and post hoc Tukey test was performed*p<0.05, **p<0.01, ***p< 0.001, **** p<0.0001.

5.4.5 Investigating the effect of viable *S. epidermidis* on human skin fibroblast migration in (5.5 mM) glucose concentration at 12 h

To further elucidate the effect of *S. epidermidis* on fibroblast migration, a scratch migration assay was conducted on fibroblasts cultured in 5.5 mM glucose and exposed to 1×10^6 CFU/mL ± 2.8×10^5 viable S. epidermidis. Bacterial cells were separated from the fibroblasts by a transwell (0.45 µm pore size). Images of the scratch were captured via microscopy at 12 h (Figure 5.9).

Exposure to S. epidermidis demonstrated no significant effect on the percentage of scratch closure compared with the no-bacteria control in 5.5 mM glucose concentration [viable *S. epidermidis* vs no-bacteria control; 12 h= 45.8% ± 6.1 vs 68% ± 8 ($p>0.05$, n=3)].

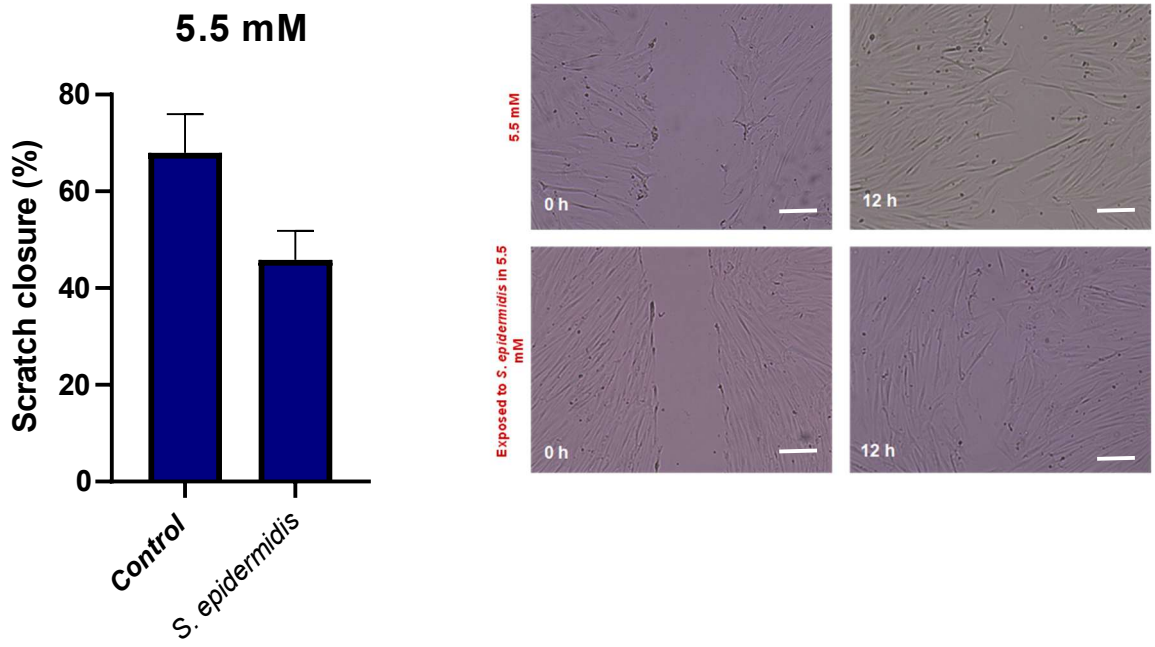

Figure 5.9: **The percentage of scratch closure of human skin fibroblast exposed to viablr *S. epidermidis* in 5.5 mM glucose.** Fibroblasts (10^5) were plated at cells per well in 6-well plate in 5.5 mM. Fibroblasts were exposed to (1×10^6) CFU/mL ± 2.8×10^5 *S. epidermidis* grown in transwell. Cells were starved in 0% FBS for 1 h prior introduction of scratch. Image of scratch was taken by microscope at 12 h. ImageJ was used to calculate the area of scratch. The percentage of Scratch closure % was calculated by equation (Scratch Closure= (Area at (t=t)- Area at t=0)/ Area at (t=0) ×100). Results are expressed as mean scratch closure percentage± SEM, n=3, error bars represent +/- SEM, two-way analysis of variance (ANOVA) and post hoc Tukey test was performed.

5.4.6 Investigating the effect of viable *S. epidermidis* secretions on human skin fibroblast migration in (20 mM) glucose concentration at 12 h

To further elucidate the effect of *S. epidermidis* on fibroblast migration, a scratch assay was conducted on fibroblasts cultured in 20 mM glucose concentration and exposed to (1×10^6) CFU/mL ± 2.8×10^5 of viable *S. epidermidis*. Bacterial cells were separated from the fibroblasts using a transwell (0.45 µm pore size). Images of the scratch were captured by microscopy at 12 h (Figure 5.10).

Exposure to *S. epidermidis* did not significantly affect the percentage of scratch closure compared to the no-bacteria control in 20 mM glucose concentration [Viable *S. epidermidis* vs no-bacteria control; 12 h= 43.1% ± 9.2 vs 38.5% ± 0.7 ($p>0.05$, n=3)].

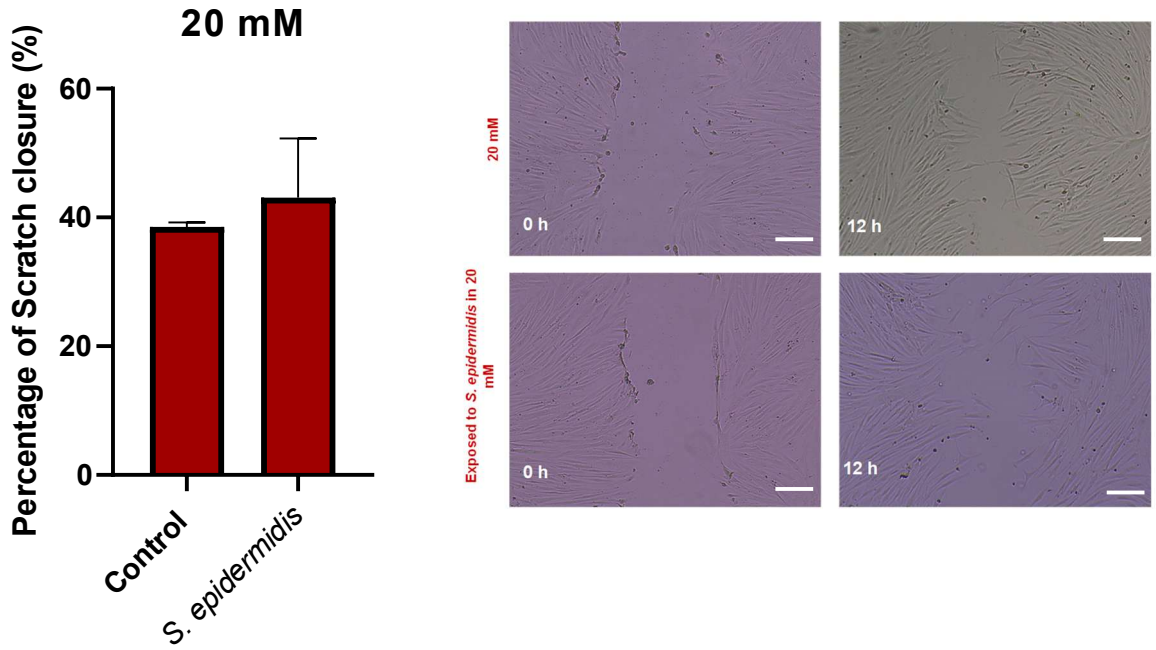

Figure 5.10: **The percentage of scratch closure of human skin fibroblast exposed to live *S. epidermidis* in 20 mM glucose concentration.** Fibroblasts were plated at cells per well in 6-well plate in 20 mM. Fibroblasts were exposed to (1×10^6) CFU/mL±2.8×10^5 *S. epidermidis* grown in transwell. Cells were starved in 0% FBS for 1 h prior introduction of scratch. Image of scratch was taken by microscope. ImageJ was used to calculate the area of scratch at different timepoints. The percentage of Scratch closure % was calculated by equation (Scratch Closure= (Area at (t=t)- Area at t=0)/ Area at (t=0) ×100). Results are expressed as mean scratch closure percentage± SEM, n=3, error bars represent +/- SEM, two-way analysis of variance (ANOVA) and post hoc Tukey test was performed.

5.5 Investigating the effect of *S. epidermidis* lysate on human keratinocyte migration in 24 mM and 50 mM glucose concentrations

5.5.1 Investigating the effect of serum starvation on keratinocytes proliferation for 72 h: a crucial preparatory step for migration assays

Immortalised human skin keratinocytes were initially subjected to serum starvation by culturing them in DMEM media devoid of FBS for 1 h, after which the migration assay was conducted in the absence of FBS for 72 h. Serum starvation constitutes a crucial preliminary step to ensure that the observed results are due to cell movement rather than cell proliferation (Jiang et al., 2022).

To verify the efficacy of the starvation process, an MTS assay was conducted on immortalised human skin keratinocytes cultured in two primary glucose concentrations (24 mM and 50 mM) for 24 h, 48 h, and 72 h (Figure 5.11). The absence of FBS resulted in a significant reduction in the mean percentage viability at 48 h and 72 h compared to the 24 h control at glucose concentrations of 24 mM and 50 mM.

A

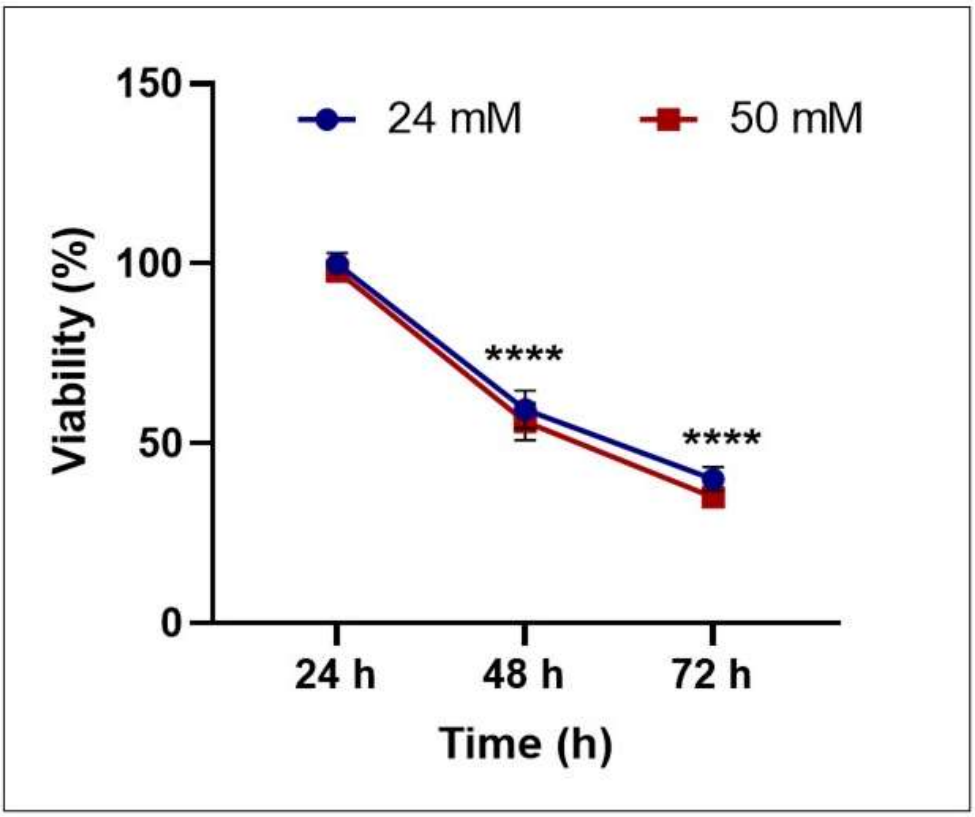

B

Time (h)	24 mM	50 mM
24	100.00 ± 2.97	97.88 ± 2.82
48	59.45 ± 5.21	56.08 ± 5.08
72	40.12 ± 3.34	35.06 ±2.34

***Figure 5.11*: The percentage of viability of immortalised human skin keratinocytes in 24 mM and 50 mM glucose concentration.** Keratinocytes were plated at 10000 cells per well and grown in different glucose concentrations in 0% FBS for (24, 48, 72) h. No significant decrease in fibroblasts viability was observed after 24 h. Significant decrease in viability was observed at 24 h and 72 h. The viability was determined by MTS assay and all results were normalised to control (i.e. keratinocytes at 24 h of each glucose concentration 24 mM and 50 mM). The viability of human fibroblasts is expressed as mean viability percentage± SEM, n=3, error bars represent +/- SEM, two-way analysis of variance (ANOVA) and post hoc Tukey test was performed ****p<0.0001. The data were presented in two components: A) a graphical representation of the results and B) a table of raw numerical data.

5.5.2. Investigating the effect of 24 mM and 50 mM glucose concentrations on migration of immortalised human skin keratinocytes migration for 48 h

Scratch migration assay was performed on immortalised human skin keratinocytes grown in low (24 mM) and high (50 mM) glucose concentration for 48 h. Image of scratch was taken by Cytation (Agilent, UK) at 6 h, 12 h, 18 h, 24 h, 48 h (Figure 5.12 and 5.13).

High glucose concentrations (50 mM) significantly reduced percentage of scratch closure only at 6 h in comparison to lower glucose concentration (24 mM). However, no significant difference was observed at 12 h, 24 h, and 48 h [50 mM vs euglycemic control 24 mM; 6 h=11.9%± 2.03 vs 28.6% ± 4.5 ($p>0.05$, n=3), 12 h= 29.5% ± 3.9 vs 39.2% ± 4.4 ($p<0.05$, n=3), at 18 h=39.3% ± 5 vs 44.8% ± 3.2 ($p<0.05$, n=3), at 24 h= 45.1% ± 3.9 vs 46.4%± 2.9 ($p>0.05$, n=3), at 48 h= 58.3% ± 4.4 vs 50.6 % ± 3.7 ($p>0.05$, n=3)].

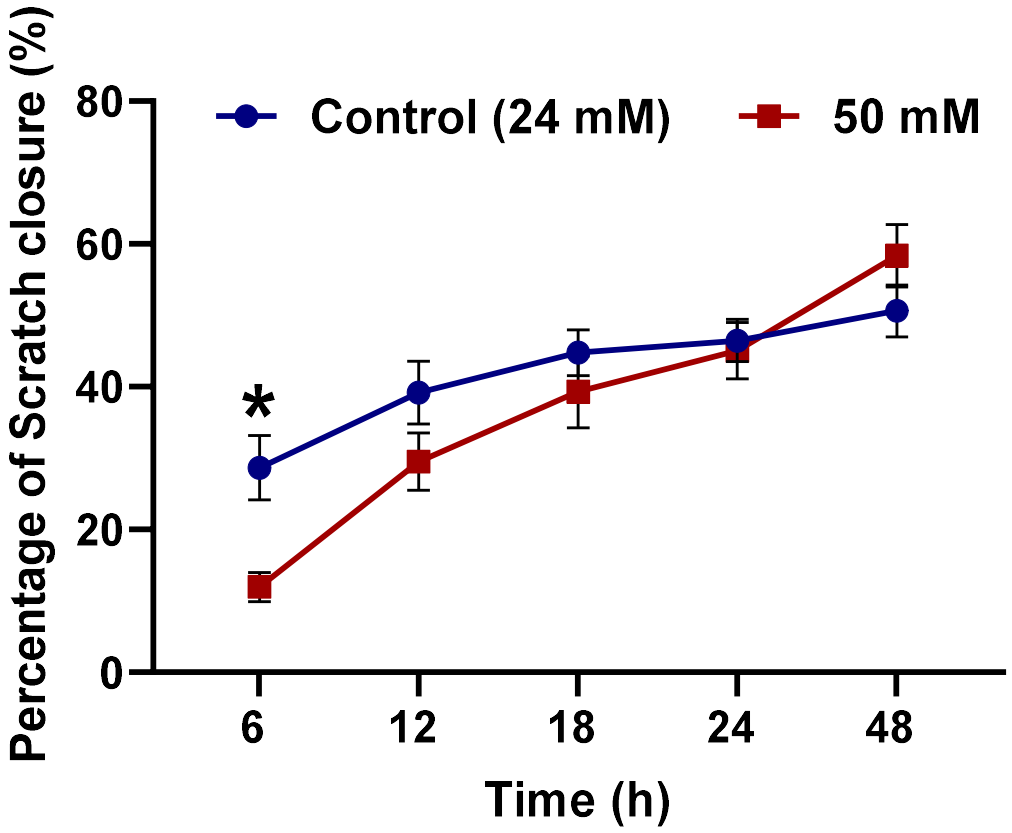

Figure 5.12: **The percentage of scratch closure in immortalised human keratinocytes grown in healthy (24 mM) and hyperglycaemic (50 mM) glucose concentration.** Keratinocytes were plated at 10000 cells per well in 24 mM and 50 mM glucose concentrations. Cells were starved in 0% FBS for 1 h prior introduction of scratch. Image of scratch was taken by cytation (Agilent, UK). ImageJ was used to calculate the area of scratch at different timepoints. The percentage of Scratch closure % was calculated by equation (Scratch Closure= (Area at (t=t)- Area at t=0)/ Area at (t=0) ✕100). Results are expressed as mean scratch closure percentage± SEM, n=3, error bars represent +/- SEM, two-way analysis of variance (ANOVA) and post hoc Tukey test was performed *p< 0.05.

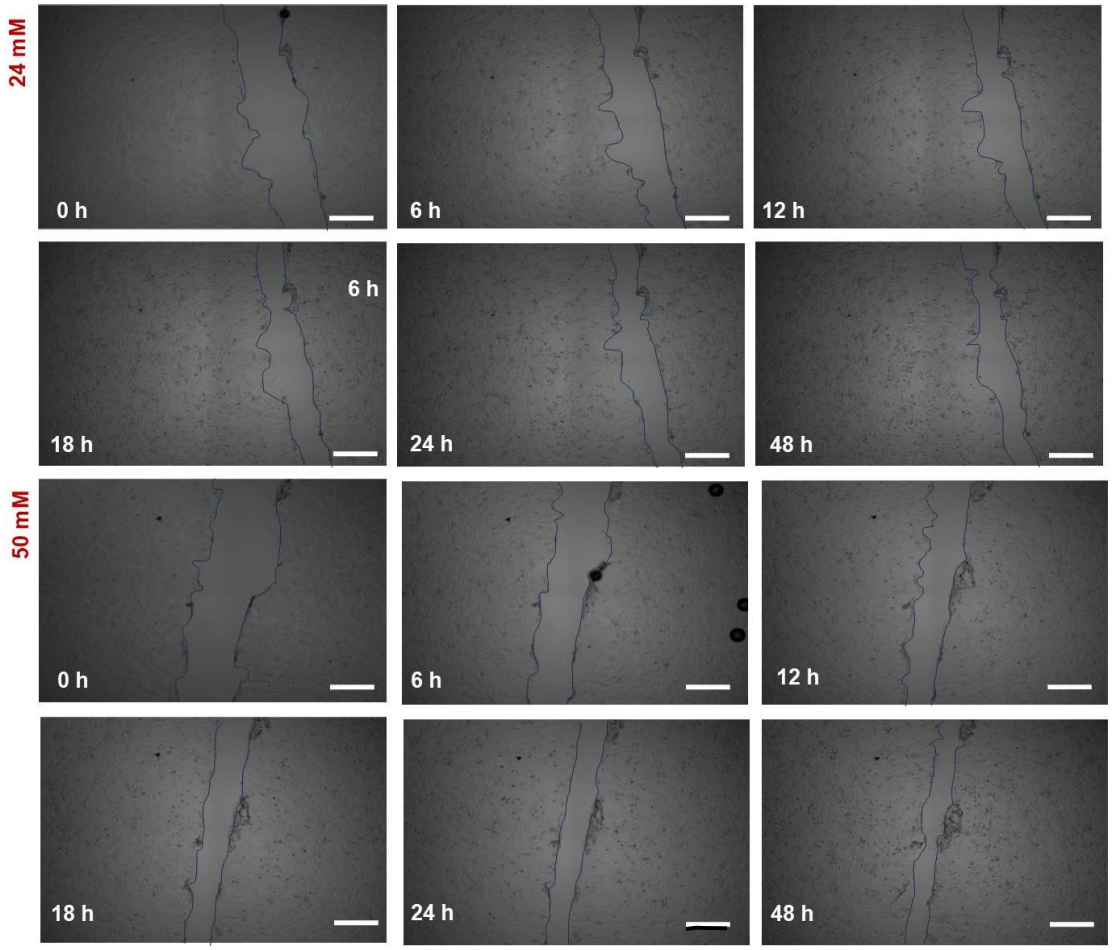

Figure 5.13: Image of scratch of immortalised human skin keratinocytes grown in 24 mM and 50 mM glucose concentrations. Keratinocytes were plated at 10000 cells per well in 24 mM and 50 mM glucose concentrations. Cells were starved in 0% FBS for 1 h prior introduction of scratch. A scratch was introduced, and microscopic pictures (at 40X magnification) was taken by cytation (Agilent, UK) at 0 h, 6 h, 12 h, 18 h, 24 h, 48 h. Scale bar=0.01 mm.

5.5.4 Investigating the effect of *S. epidermidis* lysate on immortalised human skin keratinocytes migration in 24 mM glucose concentrations

Scratch migration assay was performed on immortalised human skin keratinocytes grown in low (24 mM) and exposed to *S. epidermidis* lysate for 48 h. Image of scratch was taken by Cytation (Agilent, UK) at 6 h, 12 h, 18 h, 24 h, 48 h (Figure 5.14 and 5.15).

Exposure to *S. epidermidis* lysate had no significant effect on percentage of scratch closure in keratinocytes in 24 mM glucose concentrations compared to no lysate control at all timepoints (6, 12, 18, 24, 48) h [*S. epidermidis* lysate vs no-lysate control: 6 h=27.1% ± 2.6 vs 28.6% ± 4.5 ($p<0.05$, n=3), 12 h= 39.8% ± 4.9 vs 39.2% ± 4.4 ($p<0.05$, n=3), at 18 h= 44% ± 4.9 vs 44.8%± 3.2 ($p<0.05$, n=3), at 24 h= 49.2% ± 4.9 vs 46.4%± 2.9 ($p>0.05$, n=3), at 48 h= 51.8% ± 5.1 vs 50.6 % ± 3.7 ($p>0.05$, n=3)].

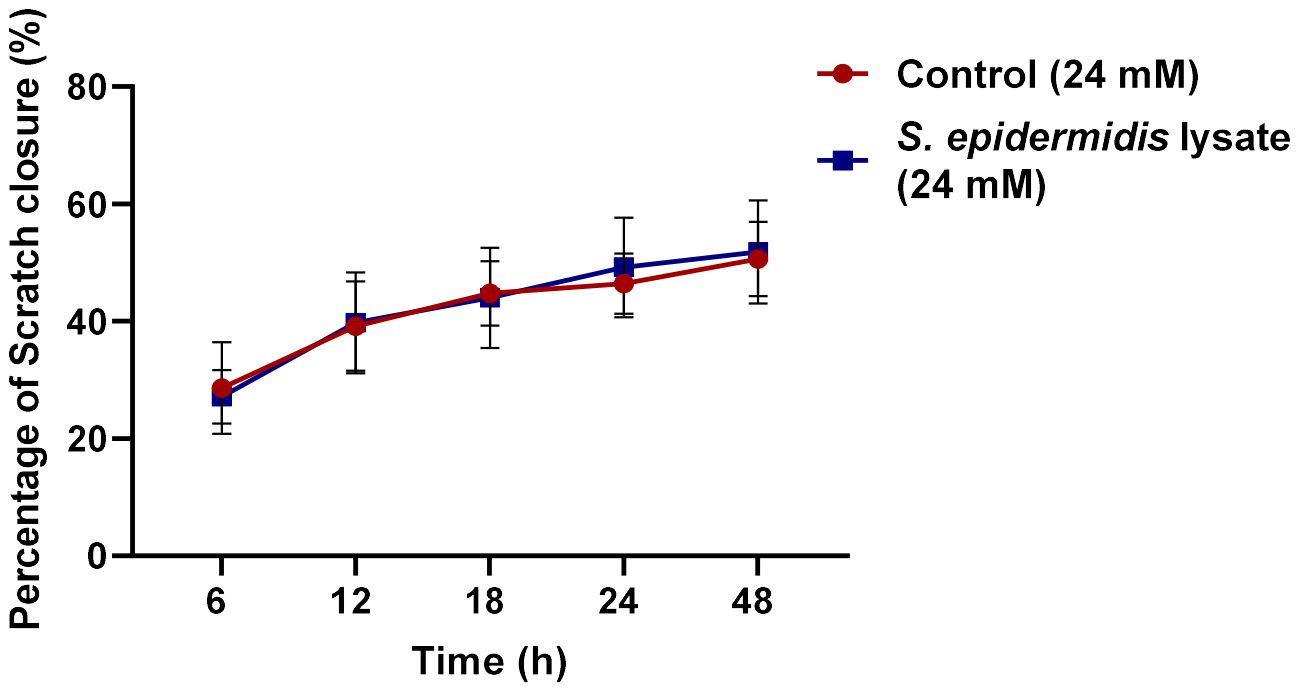

Figure 5.14: **The percentage of scratch closure in immortalised human skin keratinocytes grown in 24 mM glucose concentration.** Keratinocytes were plated at 10000 cells per well in 24 mM glucose concentrations and exposed to 100 µL of *S. epidermidis* lysate. Cells were starved in 0% FBS for 1 h prior introduction of scratch. Image of scratch was taken by cytation (Agilent, UK). ImageJ was used to calculate the area of scratch at different timepoints. The percentage of Scratch closure % was calculated by equation (Scratch Closure= (Area at (t=t)- Area at t=0)/ Area at (t=0) ✕100). Results are expressed as mean scratch closure percentage± SEM, n=3, error bars represent +/- SEM, two-way analysis of variance (ANOVA) and post hoc Tukey test was performed.

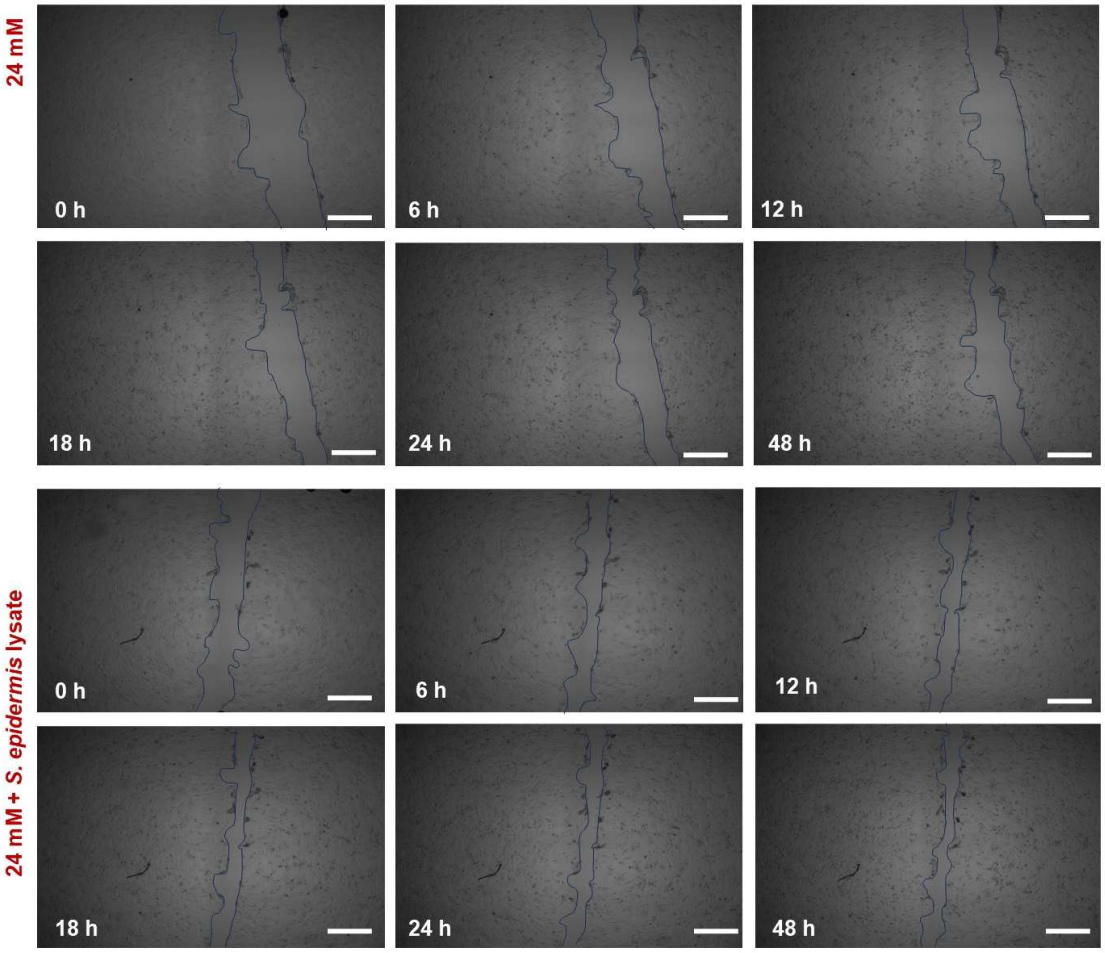

***Figure* 5.15: Image of scratch of immortalised human skin keratinocytes grown in 24 mM and exposed to *S. epidermidis* lysate.** Cells were plated at 10000 cells per well in 24 mM and 50 mM glucose concentrations. Cells were starved in 0% FBS for 1 h prior introduction of scratch. A scratch was introduced, and microscopic pictures (at 40X magnification) was taken by cytation (Agilent, UK) at 0 h, 6 h, 12 h, 18 h, 24 h, 48 h. Scale bar=0.01 mm.

5.5.5 Investigating the effect of *S. epidermidis* lysate on immortalised human skin keratinocytes migration in 50 mM glucose concentrations

Scratch migration assay was performed on immortalised human skin keratinocytes grown in low (50 mM) and exposed to *S. epidermidis* lysate for 48 h. Image of scratch was taken by Cytation (Agilent, UK) at 6 h, 12 h, 18 h, 24 h, 48 h (Figure 5.16 and 5.17).

Exposure to *S. epidermidis* lysate had no significant effect on percentage of scratch closure in keratinocytes in 50 mM glucose concentrations compared to no lysate control at all timepoints (6, 12, 18, 24, 48) h [*S. epidermidis* lysate vs no-lysate control: 6 h=18.9% ± 3.9 vs 11.9%± 2.03 ($p<0.05$, n=3), 12 h= 34.8% ± 5.7 vs 29.5% ± 3.9 ($p<0.05$, n=3), at 18 h= 41.4% ± 4.5 vs 39.3 %± 5 ($p<0.05$, n=3), at 24 h= 45.3% ± 2.9 vs 45.1% ± 3.9 ($p>0.05$, n=3), at 48 h= 50.5% ± 2.4 vs 58.3% ± 4.4 ($p>0.05$, $p<0.05$, n=3),

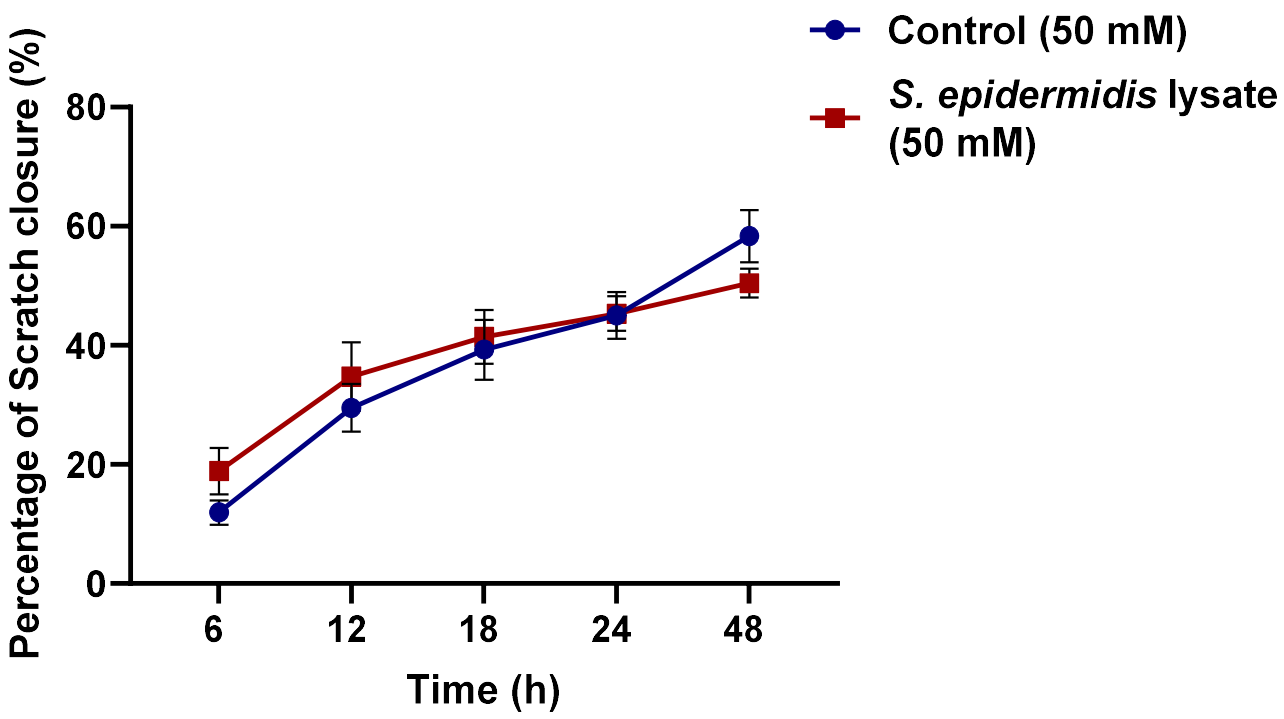

Figure 5.16: **The percentage of scratch closure in immortalised human skin keratinocytes grown in 50 mM glucose concentration.** Cells were plated at 10000 cells per well in 50 mM glucose concentrations and exposed to 100 µL of *S. epidermidis* lysate. Cells were starved in 0% FBS for 1 h prior introduction of scratch. Image of scratch was taken by cytation (Agilent, UK). ImageJ was used to calculate the area of scratch at different timepoints. The percentage of Scratch closure % was calculated by equation (Scratch Closure= (Area at (t=t)- Area at t=0)/ Area at (t=0) ✕100). Results are expressed as mean scratch closure percentage± SEM, n=3, error bars represent +/- SEM, two-way analysis of variance (ANOVA) and post hoc Tukey test was performed.

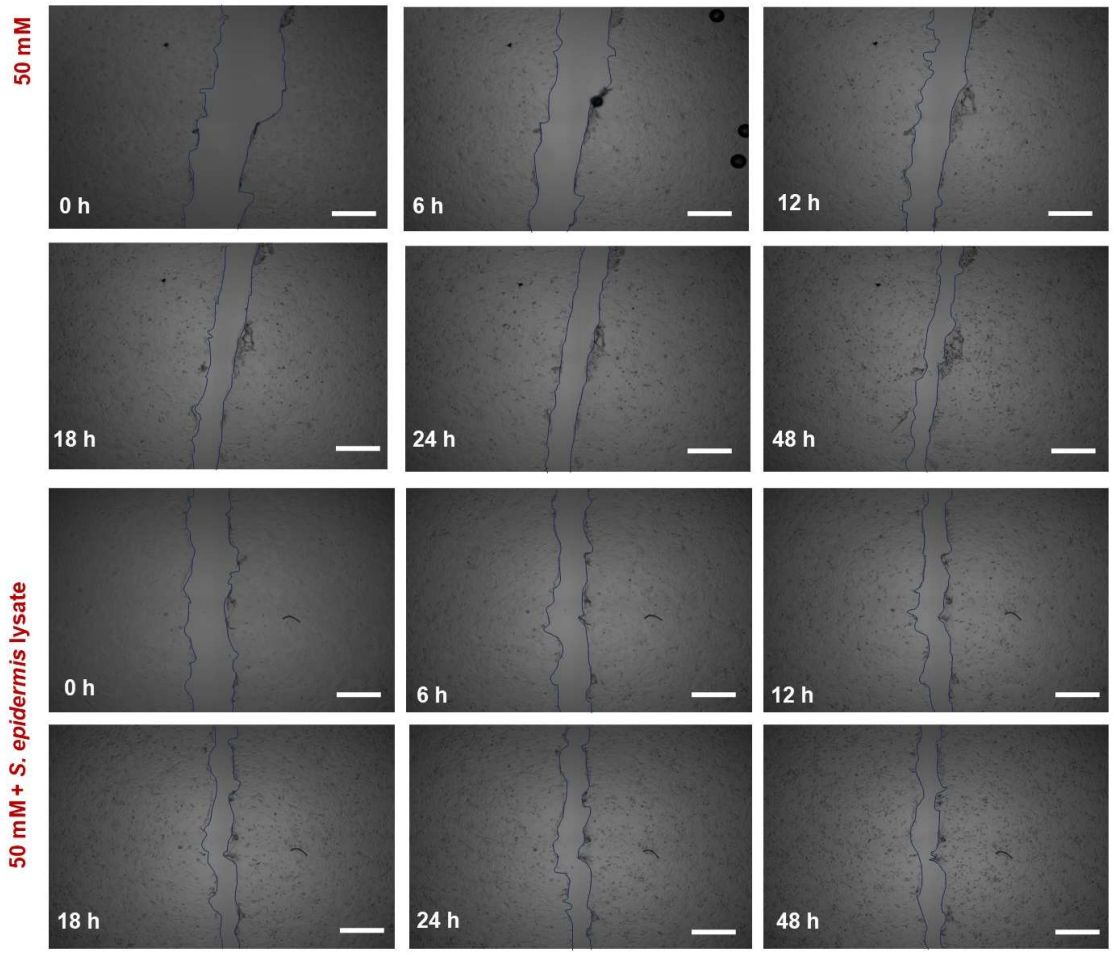

***Figure* 5.17: Image of scratch of immortalised human skin keratinocytes grown in 50 mM and exposed to *S. epidermidis* lysate.** Cells cells were seeded at a density of 10,000 cells per well in 50 mM glucose concentrations and exposed to 100 µL of *S. epidermidis* lysate. Cells were serum-starved in 0% FBS for 1 h prior to the introduction of the scratch. A scratch was introduced, and microscopic images (at 40X magnification) were captured using a Cytation imaging system (Agilent, UK) at 0 h, 6 h, 12 h, 18 h, 24 h, and 48 h. Scale bar = 0.01 mm.

5.6 Discussion

The migration of fibroblasts and keratinocytes serves as a crucial indicator in evaluating the effects of products on the wound healing process (Masson-Meyers et al., 2020). This significance stems from the fact that the proper migration of both fibroblasts and keratinocytes is essential for effective wound healing (Cialdai et al., 2022; Raja et al., 2007). Furthermore, DM is associated with impaired migration of both fibroblasts and keratinocytes (Lan et al., 2008; Xuan et al., 2014). In this chapter, to further investigate the effect of *S. epidermidis* lysate on wound healing in DM, fibroblasts and keratinocytes were exposed to *S. epidermidis* lysate under both normal and hyperglycaemic glucose conditions, and cell migration was assessed using the scratch migration assay.

5.6.1 Understanding the effect of *S. epidermidis* on human fibroblasts migration in 5.5 mM and 20 mM

In the present study, hyperglycaemic levels of glucose (20 mM) resulted in a significant decrease in the migration of human skin fibroblasts (Figure 5.2, 5.3, and 5.8). This finding aligns with another study that reported a significant reduction in the migration of primary human foreskin fibroblasts at 30 mM glucose concentration (Xuan et al., 2014). Furthermore, a significant reduction in fibroblast migration in adult diabetic mice was observed in an additional study (Lerman et al., 2003).

The mechanism behind impaired fibroblast migration in high glucose involves multiple factors. Oxidative stress plays a crucial role, as hyperglycaemia found to enhances ROS production and represses c-Jun N-terminal kinases (JNK) phosphorylation, which is important for bFGF-regulated fibroblast migration (Xuan et al., 2014). High glucose also alters the expression of extracellular matrix and adhesion genes, affecting cell migration (Wright et al., 2012).

Moreover, this study demonstrates that exposure to *S. epidermidis* lysate resulted in a significant increase in the migration of human skin fibroblasts in hyperglycaemic glucose concentration (20 mM) (Figure 5.6, 5.7, 5.8) with no significant effects in euglycemic glucose concentration (Figure 5.4, 5.5, 5.8). These findings suggest that *S. epidermidis* lysate counteracted hyperglycaemia-induced deterioration of human skin fibroblast migration. Consequently, *S. epidermidis* lysate may have potential as a novel therapeutic agent to stimulate proper wound healing in diabetic patients. However, further ex-vivo and in-vivo studies are necessary to evaluate the efficacy of *S. epidermidis* lysate in wound healing in DM. At present, only one study has reported that *S. epidermidis* lysate promotes wound healing in an ex-vivo human diabetic wound model (Mohammedsaeed et al., 2022).

One interesting question in this context is why only *S. epidermidis* lysate elicited this significant effect exclusively under hyperglycaemic conditions. Further investigations into the components of *S. epidermidis* lysate are necessary to elucidate the potential interaction between bacterial lysate and fibroblast migration. Notably, a study suggested that two primary *S. epidermidis*-derived N-Formyl Methionine Peptides (f-MFLLVN and f-MIIINA) were responsible for inducing an immune response in skin in vitro. Consequently, the present study proposes conducting additional research to

characterise the effect of *S. epidermidis*-derived peptides on fibroblast migration under varying glucose concentrations. This approach will contribute to the understanding of potential interactions between bacterial lysate and fibroblast migration in varying glucose concentration. Moreover, this will help to understand how lysate may modulate fibroblast migration such as proliferation under hyperglycaemic conditions.

To further investigate whether *S. epidermidis* might secrete any metabolite which may influence the migration of fibroblasts. Human skin fibroblasts were exposed to live *S. epidermidis* separated by a transwell membrane. Surprisingly, no alteration in fibroblasts migration was observed in euglycemic and hyperglycaemic level of glucose (Figure 5.9 and 5.10). One might argue whether the reason of non-significant effect is due to presence of low concentrations of *S. epidermidis* metabolites. Characterising the type of metabolites secreted by *S. epidermidis* alongside investigating different concentrations of the metabolites on fibroblasts migrations are required to understand this effect.

5.6.2 Understanding the effect of *S. epidermidis* lysate on immortalised human keratinocytes migration in 24 mM and 50 mM

In the present study, a high glucose concentration (50 mM) resulted in a significant reduction in human immortalised keratinocytes migration compared to lower glucose concentrations (24 mM) (Figure 5.12 and 5.13). Various studies reported high glucose exposure disrupts keratinocyte migration through multiple interconnected mechanisms, including altered expression of migration-related proteins, dysregulation of signalling pathways, and changes in transcription factor activity. These impairments collectively contribute to the poor wound healing observed in diabetic patients (Lan, 2008; Li et al., 2019)

Keratinocytes cultured in hyperglycaemic conditions demonstrate reduced motility and decreased migration capacity (Lan, 2008; Lan, 2009). This impairment is progressive, with keratinocyte motility significantly decreasing over time under high glucose treatment (Lan, 2009). The molecular mechanisms involved include downregulation of matrix metalloproteinases (MMP-2 and MMP-9) and their activities, increased expression of tissue inhibitor of MMP (TIMP-1), and reduced expression of phosphorylated focal adhesion kinase (pp125FAK) (Lan, 2008). Additionally, high glucose suppresses the expression of keratinocyte activation marker K16 and downregulates α2β1 integrin and MMP-1, which are crucial for keratinocyte locomotion on collagen type I (Lan, 2009).

Interestingly, the effects of high glucose on keratinocyte migration involve multiple signalling pathways. The p38/MAPK pathway, which normally promotes keratinocyte migration, is downregulated under high glucose conditions, accompanied by inactivation of autophagy (Li et al., 2019). High glucose also inhibits the Erk signalling pathway in a reactive oxygen species (ROS)-dependent manner, further impairing keratinocyte migration (M. Li et al., 2015). Moreover, the forkhead box O1 (FOXO1) transcription factor, which enhances keratinocyte migration through TGFβ1 upregulation in normal glucose conditions, fails to bind to the TGFβ1 promoter in high glucose environments. Instead, FOXO1 enhances the expression of SERPINB2 and CCL20, which inhibit keratinocyte migration (Zhang et al., 2015).

Exposure to *S. epidermidis* lysate did not significantly affect immortalised human keratinocytes migration in either low (24 mM) or high (50 mM) glucose concentrations

(Figure 5.14, 5.15, 5.16, and 5.17). Previous research has reported that treatment of keratinocytes with live skin commensals induced keratinocyte differentiation and demonstrated barrier repair (Duckney et al., 2013). Consequently, this study strongly recommends investigating the effect of *S. epidermidis* lysate on the differentiation and barrier repair of keratinocytes, as this may elucidate the mechanism by which *S. epidermidis* influences keratinocytes in wound healing.

Lysates of certain *Lactobacillus* species have been observed to induce keratinocyte migration in vitro. Specifically, *Lactobacillus rhamnosus* lysate has been reported to accelerate re-epithelialisation in keratinocyte scratch assays, potentially through chemokine receptor pairs that stimulate keratinocyte migration (Mohammedsaeed et al., 2015). Moreover, *Lactobacillus plantarum* and *Lactobacillus salivarius* have been reported to accelerate wound re-epithelialisation by inducing keratinocyte (Brandi et al., 2020). Therefore, the present study proposes the preparation of a mixture comprising *S. epidermidis* lysate and *Lactobacillus* spp. lysate and recommends conducting further experiments to investigate the potential application of this lysate mixture in the treatment of diabetic wounds. This approach may contribute to the development of novel therapeutics to address delayed wound healing in diabetes mellitus (DM). However, the current study identifies a primary concern regarding the safety of utilising a bacterial lysate mixture. This concern arises from the observation that the primary cause of poor prognosis and metastasis in cancer is the increased migration of cancer cells (Tucci et al., 2012; Wang et al., 2021). Additional research is necessary to examine the association between the safety of bacterial lysate in patients diagnosed with DM and cancer.

5.6.3 Conclusion & Future Direction

The present study demonstrated that *S. epidermidis* lysate demonstrated a significant effect on fibroblast migration in hyperglycaemic glucose concentration, the subsequent chapter of this study will focus on elucidating the alterations in gene expression of fibroblasts exposed to *S. epidermidis* lysate under varying glucose concentrations. Understanding this will help to clarify how *S. epidermidis* lysate modulate cellular pathways in fibroblasts under varying glucose concentrations.

Chapter 6: Transcriptome analysis (whole mRNA sequencing) of Human skin Fibroblasts exposed to *S. epidermidis* lysate in euglycemic and hyperglycaemic glucose concentrations

6.1 Introduction

The interaction between human host cells and the skin microbiota is essential to maintaining healthy skin physiology (Chen et al., 2018). As the next-generation RNA sequencing technique is a powerful tool for identifying how gene expressions in cells are altered because of exposure to a compound or been grown in different conditions (Westermann & Vogel, 2021). It also allows understanding how the alteration in gene expression is linked to specific cellular function and the identification of novel genes (Westermann & Vogel, 2021). Next-generation RNA sequencing technique has become the primary technology for investigating host–microbe interactions (Colgan et al., 2017). The high sensitivity and resolution of this technique enables accurate measurement of gene expression and understanding the mechanisms of host-microbiota interaction and its physiological consequences (Colgan et al., 2017). Compared to other genomic techniques, RNA sequencing offers several advantages. It provides a more comprehensive and unbiased view of gene expression compared to microarray analysis (Tang et al., 2009). It has been reported next-generation RNA sequencing technique is capable to detect 75% more genes than microarray technique (Tang et al., 2009). It also allows for the detection of novel and rare transcripts (Ponce et al., 2012). However, next-generation RNA sequencing technique can be more expensive and computationally intensive, requiring specialised bioinformatics expertise for data analysis (Tang et al., 2009).

In wound healing, next-generation RNA sequencing technique provides a comprehensive view of the entire transcriptome, allowing researchers to identify and quantify all the genes and their expression levels in a wound (Liu et al., 2022). This information is crucial for understanding the complex molecular mechanisms underlying wound healing and can lead to the discovery of new therapeutic targets and personalised treatment options (Kanehisa et al., 2017; Liu et al., 2022). In the present study, next generation mRNA sequencing was used to understand how the expression of fibroblasts genes will alter because of exposure to *S. epidermidis* lysate

in euglycemic and hyperglycaemic glucose concentrations (Figure 6.1). Various bioinformatics tool can be used to study the function of differentially expressed genes. In present study, three main software was used Gene Ontology (GO) (Gaudet et al., 2021), Gene Set Enrichment Analysis (GSEA) (Subramanian et al., 2005), and Kyoto Encyclopaedia of Genes and Genomes (KEGG) (Kanehisa et al., 2017).

GO is a bioinformatic database that can be used to study the function of differentially expressed genes (Wood et al., 2020). This software can be divided link the differentially expressed genes to three main different groups: Biological process, Cellular function, and Molecular function (Thomas, 2017).

KEGG (Kyoto Encyclopaedia of Genes and Genomes) is another widely used bioinformatic resource for creating functional meaning to differentially expressed genes at a molecular level (Kanehisa et al., 2017).

Gene Set Enrichment Analysis (GSEA) is a bioinformatic tool that is used to analyse gene expression data and identify biological pathways or gene sets that are significantly enriched in each sample (Reimand et al., 2019). It helps researchers gain insights into the underlying biological mechanisms and pathways that are associated with a particular phenotype or condition (Reimand et al., 2019). GSEA calculates the enrichment score for each pathway or gene set by comparing the observed expression pattern of genes within the pathway or gene set to a null distribution generated by randomly permuting the gene labels (Reimand et al., 2019). This allows GSEA to determine if the genes in a particular pathway or gene set are co-ordinately upregulated or downregulated in a given sample, providing a measure of the pathway or gene set's enrichment in the sample (Zito et al., 2021). One advantage of using GSEA over other gene expression analysis methods is its ability to capture subtle but coordinated changes in gene expression across a pathway or gene set (Zito et al., 2021). This is particularly useful when studying complex diseases or conditions where multiple genes and pathways are involved. Additionally, GSEA provides a statistical significance measure for pathway enrichment, allowing researchers to prioritise and focus on the most relevant pathways for further investigation (Zito et al., 2021).

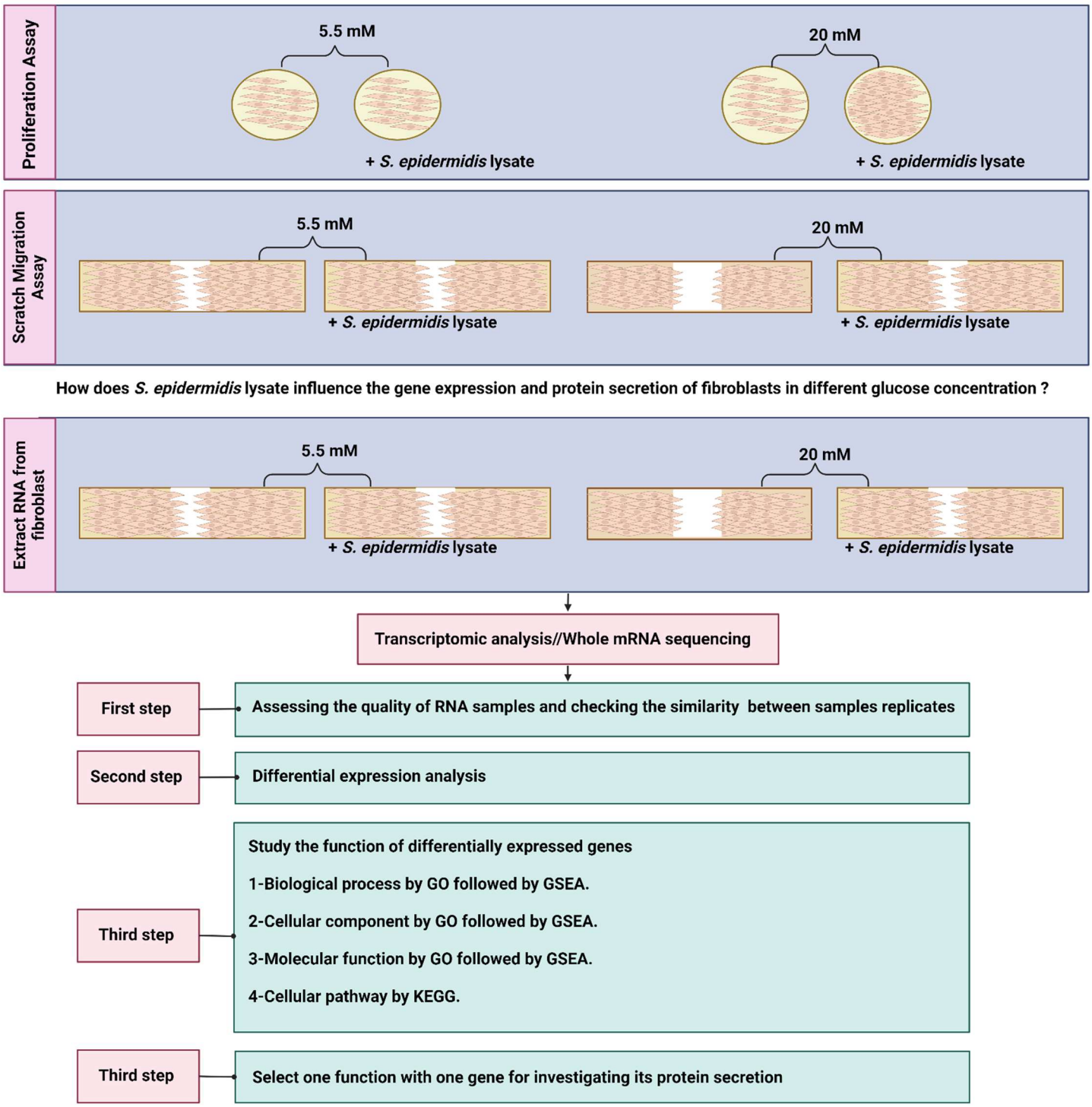

Figure 6.1: Transcriptomic analysis of present chapter. *S. epidermidis* lysate significantly induced the proliferation and migration of fibroblasts in high glucose concentrations (Chapter 4 & 5). Thus, in present study, it was selected for further analysis to understand how it alters the gene and protein expression of fibroblasts in euglycemic and hyperglycaemic glucose concentrations. RNA was extracted form fibroblasts exposed to *S. epidermidis* lysate in 5.5 mM and 20 mM glucose concentration. To understand the effect of high glucose on fibroblasts gene expression, RNA was also extracted form fibroblasts grown in 5.5 mM and 20 mM glucose concentration without exposure to *S. epidermidis* lysate. Differential expression analysis was performed. Then, biological process, cellular component, and molecular function of differentially expressed genes was studies in GO software and checked in GSEA. The cellular pathways of differentially expressed genes were also studied by using KEGG software. Only one function will be selected for further investigations. Moreover, the protein secretion of one gene will be investigated in present chapter.

6.2 Aim of chapter

To understand the effect on *S. epidermidis* lysate on fibroblast gene expression and protein secretions in different glucose concentrations.

6.3 Objectives of the chapter

To identify differentially expressed genes in fibroblasts when exposed to *S. epidermidis* lysate in 5.5 mM and 20 mM glucose concentrations.

To understand the function (biological process, cellular component, molecular function, and cellular pathways) of differentially expressed genes in fibroblasts when exposed to *S. epidermidis* lysate in 5.5 mM and 20 mM glucose concentrations.

To study the protein secretion of the highest significantly expressed gene in fibroblasts when exposed to *S. epidermidis* lysate in 5.5 mM and 20 mM glucose concentrations.

6.4 Quality control

6.4.1 Concentration, purity, and integrity of extracted RNA

Fibroblasts were grown in 5.5 mM or 20 mM glucose concentrations and exposed to *S. epidermidis* lysate. A scratch was introduced, and then RNA was extracted after 12 h. The concentration, quality, and integrity of RNA were measured. Figure 6.2 summarises the concentration, purity, and integrity results of extracted RNA.

The concentration of RNA required for transcriptomic analysis was (≥ 30 ng/mL). All RNA samples contained sufficient yield of RNA for analysis [The mean concentration of RNA extracted from fibroblasts grown in 5.5 mM glucose concentration was 263.3 ng/mL ± 49.2 (n=3); RNA extracted from fibroblasts grown in 20 mM glucose concentration 399.4 ng/mL ± 35.3 (n=3); from fibroblasts grown in 5.5 mM glucose concentration exposed to *S. epidermidis* lysate 231.2 ng/mL ± 10.9 (n=3); from fibroblasts grown in 20 mM glucose concentration exposed to *S. epidermidis* lysate 228.5 ng/mL ± 10.9 (n=3)].

All extracted RNA samples were pure, as the ratio of the absorbance 260/280 nm of all samples ranged 1.7 - 2.5 and ratio of the absorbance 260/280 ranged between 0.5 and 2.5. [The mean ratio of the absorbance 260/280 of RNA extracted from fibroblasts grown in 5.5 mM glucose concentration was 2.06 ± 0.007 (n=3); RNA extracted from fibroblasts grown in 20 mM glucose concentration 2.02 ± 0.015 (n=3); from fibroblasts grown in 5.5 mM glucose concentration exposed to *S. epidermidis* lysate 2.03 ± 0.012 (n=3); from fibroblasts grown in 20 mM glucose concentration exposed to *S. epidermidis* lysate 2.05 ± 0.015 (n=3)]. [The mean ratio of the absorbance 260/280 of RNA extracted from fibroblasts grown in 5.5 mM glucose concentration was 1.8 ± 0.1 (n=3); RNA extracted from fibroblasts grown in 20 mM glucose concentration 1.6 ± 0.2 (n=3); from fibroblasts grown in 5.5 mM glucose concentration exposed to *S. epidermidis* lysate 1.1 ± 0.5 (n=3); from fibroblasts grown in 20 mM glucose concentration exposed to *S. epidermidis* lysate 0.97 ± 0.4 (n=3)].

The RNA integrity of all samples was higher than (≥ 7) [The mean RNA integrity of RNA extracted from fibroblasts grown in 5.5 mM glucose concentration was 9.6 ± 0.1 (n=3); RNA extracted from fibroblasts grown in 20 mM glucose concentration 10 ± 0.0 (n=3); from fibroblasts grown in 5.5 mM glucose concentration exposed to *S.*

epidermidis lysate 9.7 ± 0.1 (n=3); from fibroblasts grown in 20 mM glucose concentration exposed to *S. epidermidis* lysate 9.8 ± 0.1 (n=3)].

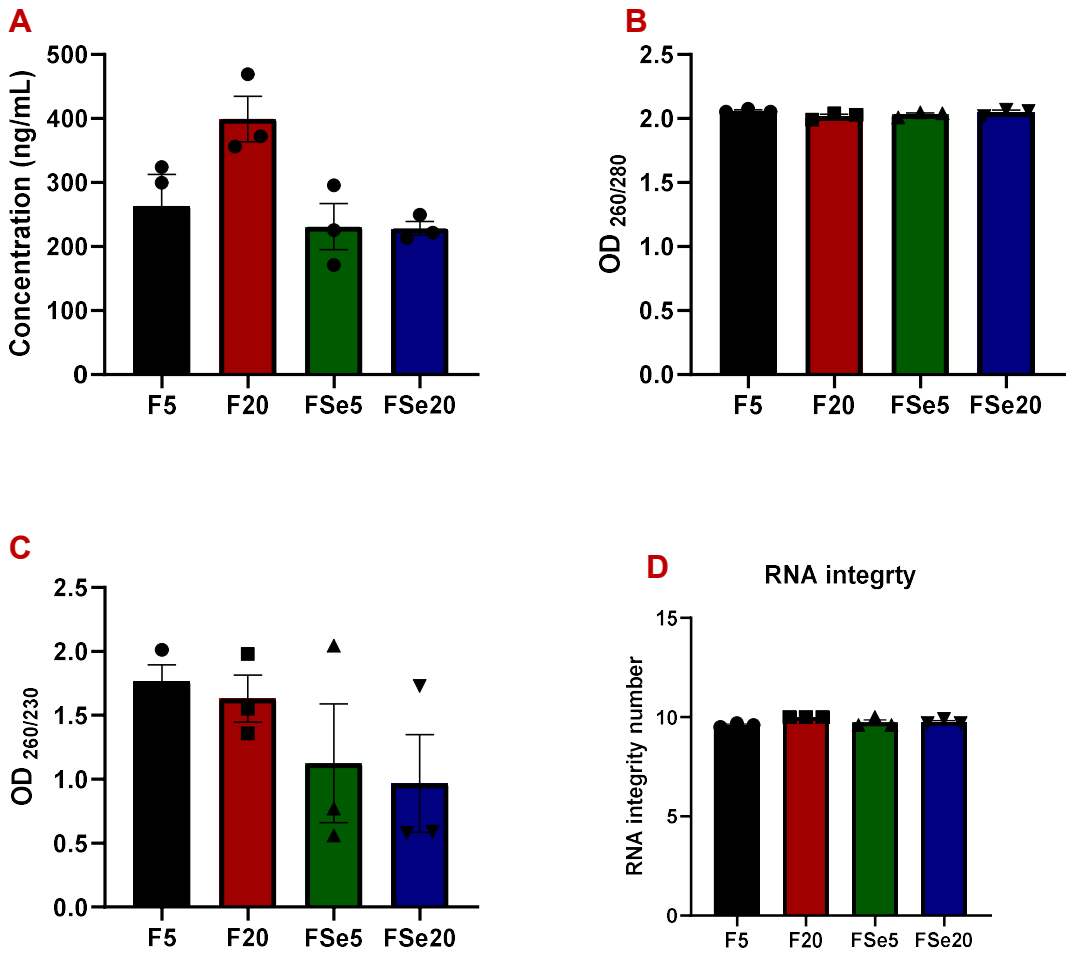

***Figure* 6.2: Concentration, purity, and integrity of RNA extracted from human skin fibroblasts.** Fibroblasts were grown in 5.5 mM and 20 mM glucose concentrations and exposed to *S. epidermidis* lysate. A scratch was introduced, and then RNA was extracted after 12 h. The A) concentration, B) absorbance (260/280), C) Absorbance (260/230), and D) RNA integrity was measured to determine the quality of extracted RNA. For transcriptomic analysis (whole mRNA sequencing), a concentration of (≥ 30 ng/mL), OD260/280:1.7-2.5 OD260/230:0.5-2.5, and RNA integrity (≥ 7) were required for each sample to ensure proper analysis (Biorender, 2024; BMKGENE, 2023). Results are expressed as mean value ± SEM, n=3, error bars represent +/- SEM.

6.4.2 Raw data quality control

A total of 1 µg per sample of 12 RNA samples were processed for transcriptome sequencing quality control. Sequencing base quality score (Q-scores) was measured and clean data with high quality was generated by filtering the raw data (i.e., removing adapter sequence and reads with low quality. Base with high Q-scores is more reliable. In present study percentage of Q-score 30 was measured which reflects the probability of one incorrect base call in 1000 times (i.e., 99.9% base call accuracy).

Quality control analysis generated 89.61 Gb Clean Data. At least 6.12 Gb clean data were generated for each sample. More than 92.73% of bases of each sample had a Q-score no less than Q-score 30, which mean 92.73% of base results are with 99.9% accuracy (Figure 6.3) [Q-score 30% in fibroblasts exposed to lysate; 5.5 mM= 94.2% ± 0.1 (n=3); 20 mM= 93.9 % ± 0.6 (n=3); Q-score 30% in fibroblasts not exposed to lysate; 5.5 mM= 94.1% ± 0.1 (n=3); 20 mM = 94.4% ± 0.2 (n=3)].

The percentage of guanine and cytosine (GC%) was also measured per sample to avoid the risk of false-positive results. The GC% of all samples ranged between 49.19% and 52.33% [GC% in fibroblasts exposed to lysate; 5.5 mM= 51.7% ± 0.2 (n=3); 20 mM= 51.6% ± 0.1 (n=3); GC% in fibroblasts not exposed to lysate; 5.5 mM= 49.5% ± 0.2 (n=3); 20 mM = 52.2% ± 0.1 (n=3)].

Once clean reads with high quality were selected of each sample, data was mapped to GRCh38.p14 reference genome. The mapping percentage ranged from 93.85% to 97.01% [The GC% of all samples ranged between 49.19% and 52.33% [Mapping (%) in fibroblasts exposed to lysate; 5.5 mM= 96.5 % ± 0.1 (n=3); 20 mM= 95.8% ± 0 (n=3); Mapping (%) in fibroblasts exposed to lysate not exposed to lysate; 5.5 mM= 94.4% ± 0.3 (n=3); 20 mM = 96.8 % ± 0.05 (n=3)].

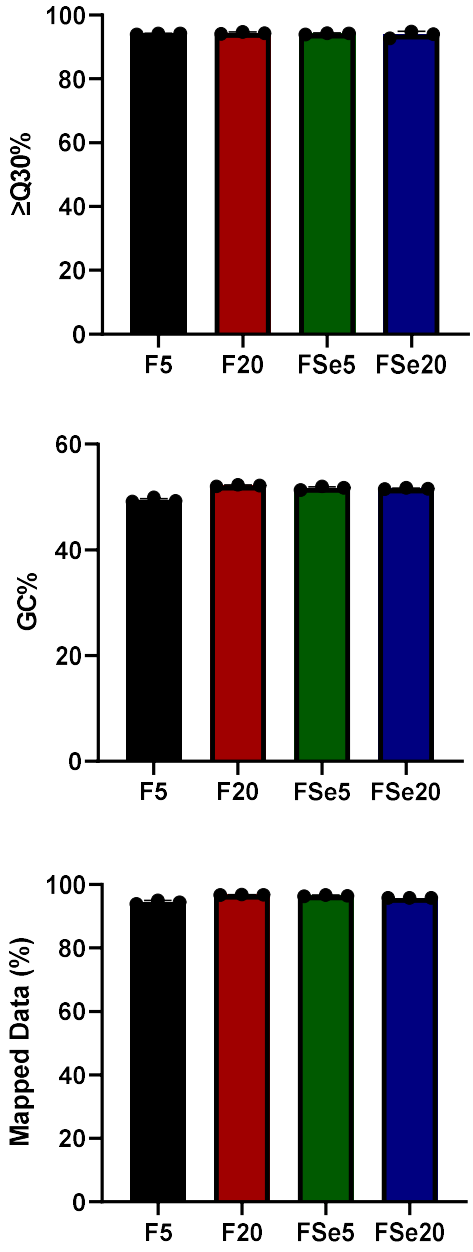

Figure 6.3: Row data quality control. The quality of row data was assessed before sequencing by measuring A) sequencing base quality control (Q ≥ 30%), and B) the percentage of Cytosine (C) and guanine (G) content. Only data with high quality was used for sequencing. Row data contains useless data such as primers, adapters…etc were removed. Once the quality of row data was confirmed, data was mapped to GRCh38.p14 reference genome and C) the percentage of reference genome was calculated. Results are expressed as mean value ± SEM, n=3, error bars represent +/- SEM (BMKGENE, 2023).

6.5 Analysing the correlation and similarity between biological replicates of each sample

Similarity between biological replicates of each sample studies by principal component analysis (PCA) and Pearson correlation coefficient (R) (Figure 6.4). Both analyses were performed on Fragments Per Kilobase of transcript per Million fragments mapped (FPKM) of each sample replicate. Reduction in dimensionality in PCA between sample replicates represent acceptable similarity between different replicates of each sample (Figure 6.4 A). R value also confirmed acceptable similarity between all sample replicates. This is because the R value was close to 1 for all replicates for each sample (Figure 6.4 B) [R value of three replicates of fibroblasts samples grown in 5.5 mM, F5-1_vs_F5-2=0.956, F5-2_vs_F5-3=0.947, F5-1_vs_F5-3=0.994; fibroblasts samples grown in 20 mM, F20-1_vs_F20-2=0.997, F20-2_vs_F20-3=0.987, F20-1_vs_F20-3=0.991; fibroblasts samples exposed to *S. epidermidis* lysate grown in 5.5 mM= FSe5-1_vs_FSe5-2=0.996, FSe5-2_vs_FSe5-3=0.926, FSe5-1_vs_FSe5-3=0.927; fibroblasts samples exposed to *S. epidermidis* lysate grown in 20 mM, F20-1_vs_F20-2=0.979, F20-2_vs_F20-3=0.997, F20-1_vs_F20-3=0.978].

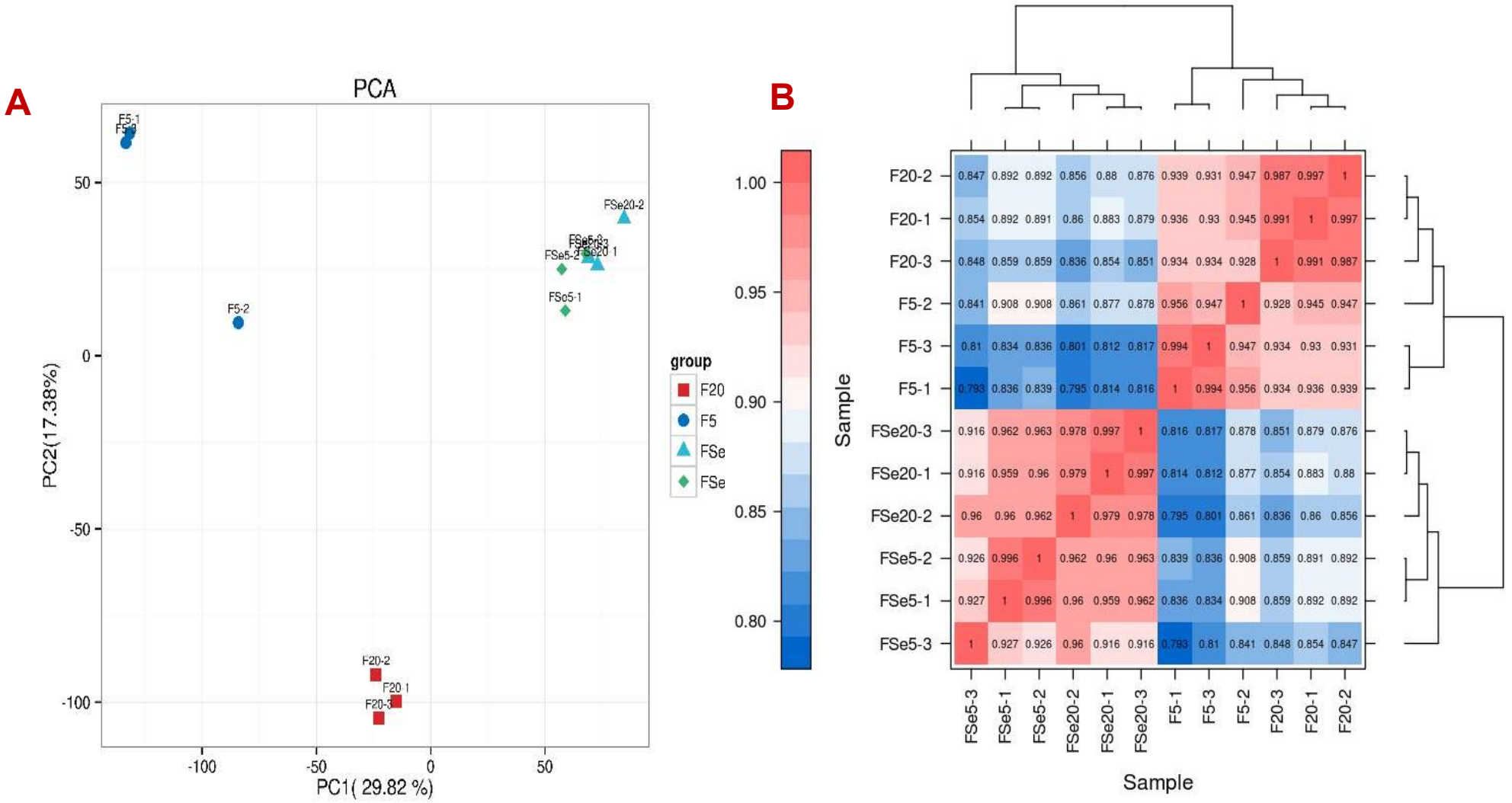

Figure 6.4: Exploring the similarity between biological replicates. A) principal component analysis (PCA) In the figure, PC1 and PC2 are two principal components; different colours and shapes represent different groups of biological replicates. Similarity among samples were displayed by reducing dimensionality. **B) Correlation heatmap between samples,** Pearson correlation coefficient R (Pearson's Correlation Coefficient) was applied in this project to evaluate reproducibility of biological replicates. X-axis: sample IDs, ; Y-axis: corresponding sample IDs. Clustering tree is presented on top and right of the heatmap. Colour indicates the correlation between samples, and its corresponding relationship is shown in the legend on the left. A closer R2 value to 1 indicates better reproducibility between the two samples. In both **A)** & **B)** F5 represent fibroblasts grown in euglycemia, F20 represent fibroblasts grown in hyperglycaemia, FSe5 represent fibroblasts grown in euglycemia exposed to *S. epidermidis* lysate, FSe20 represent fibroblasts grown in hyperglycaemia exposed to *S. epidermidis* lysate. The order of samples depends on clustering output (BMKGENE, 2023).

6.6 Differential expression analysis

Differentially expressed genes (DEG) were identified based on the criteria fold change (FC)≥2 and false discovery rate (FDR<0.01). DEG were classified into three main groups: Group 1: DEG in fibroblasts grown in high glucose (20 mM) compared to euglycemic control (5.5 mM) (F20_vs_ F5); Group 2: DEG in fibroblasts exposed to *S. epidermidis* lysate compared to no-lysate control in 5.5 mM glucose concentration (FSe5 _vs_F5); Group 3: DEG in fibroblasts exposed to *S. epidermidis* lysate compared to no-lysate control in 20 mM glucose concentration (FSe20 _vs_F20).

When fibroblasts were grown in high glucose (20 mM) and compared to low glucose (5.5 mM), 594 gene were differentially expressed, 406 upregulated and 188 downregulated. When fibroblasts were exposed to *S. epidermidis* lysate in 5.5 mM, the total number of differentially expressed genes were 1482. 1058 genes were upregulated, and 424 genes were downregulated. When fibroblasts were exposed to *S. epidermidis* lysate in 20 mM, the total number of differentially expressed genes were 970 gene respectively. 599 genes were upregulated, and 371 genes were downregulated (Figure 6.5 and Figure 6.6)

A list of all differentially expressed genes of each gene set group (F20_vs_F5; FSe5_vs_F5; FSe20_vs_F20) is summarised in appendix 2.

When comparing DEG in fibroblasts grown in 20 mM glucose concentration to euglycemic control (5.5 mM) (F20_vs_F5), the following 10 genes were the most upregulated genes: gene-TBC1D16-2 (FDR<0, log2FC=9.37, n=3); gene-MAMDC2-2 (FDR<0, log2FC=4.68, n=3); gene-LOC124905366 (FDR<0, log2FC=3.58, n=3); gene-TENM4 (FDR<0, log2FC=3.47, n=3); gene-NRK (FDR<0, log2FC=3.15, n=3); gene-FAM20C-4 (FDR<0, log2FC=2.71, n=3); gene-PGF (FDR<0, log2FC=2.70, n=3); gene-DLL4 (FDR<0, log2FC=2.65, n=3); gene-SLC7A8 (FDR<0, log2FC=2.55, n=3); gene-PTGER1 (FDR<0, log2FC=2.54, n=3).

When comparing DEG in fibroblasts exposed to *S. epidermidis* lysate to no-lysate control in 5.5 mM glucose concentration (FSe5_vs_F5), the following 10 genes were the most upregulated genes: gene-CXCL6 (FDR<0, log2FC=9.5, n=3); gene-RPS10-NUDT3 (FDR<0, log2FC=8.2, n=3); gene-SST (FDR<0, log2FC=7.5, n=3); gene-

CXCL3 (FDR<0, log2FC=6.9, n=3); gene-CSF3 (FDR<0, log2FC= 6.7, n=3); gene-CXCL1 (FDR<0, log2FC=6.4, n=3); gene-EGFL6 (FDR<0, log2FC=6.3, n=3); gene-NPTX1 (FDR<0, log2FC=5.9, n=3); gene-CXCL8 (FDR<0, log2FC=5.8, n=3); gene-PCSK9 (FDR<0, log2FC=5.4, n=3).

When comparing DEG in fibroblasts exposed to *S. epidermidis* lysate to no-lysate control in 20 mM glucose concentration (FSe20_vs_F20), the following 10 genes were the most upregulated genes: gene-ADH1B (FDR<0, log2FC=9.6, n=3); gene-CORO7-PAM16 (FDR<0, log2FC=9.3, n=3); gene-SST (FDR<0, log2FC=8.4, n=3); gene-RASL12 (FDR<0, log2FC=8.2, n=3); gene-CXCL6 (FDR<0, log2FC=7.1, n=3); gene-PDK4 (FDR<0, log2FC=6.8, n=3); gene-EGFL6(FDR<0, log2FC=6.6, n=3); gene-CXCL8 (FDR<0, log2FC=5.8, n=3); gene-DPT (FDR<0, log2FC=5.6, n=3); gene-FGF13 (FDR<0, log2FC= 5.4, n=3).

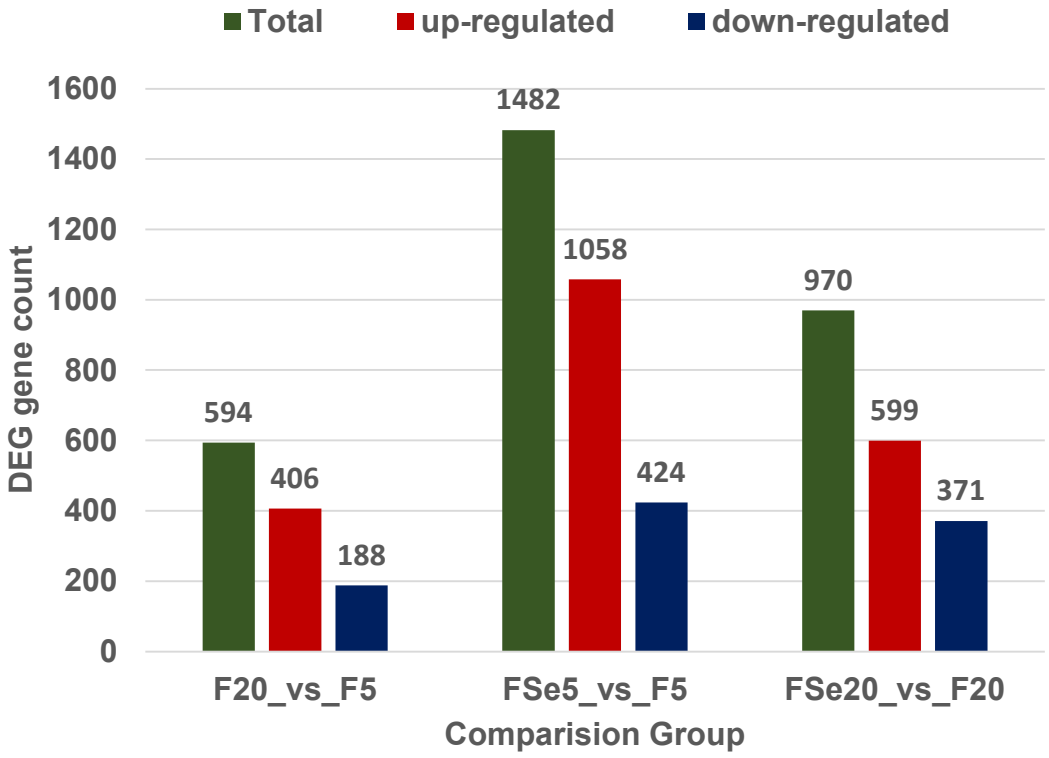

Figure 6.5: Statistics of DEG gene count. The number of total, upregulated, and downregulated genes were counted per the three main comparison group. Group 1: DEG in fibroblasts grown in high glucose (20 mM) compared to euglycemic control (5.5 mM) (F20_vs_ F5); Group 2: DEG in fibroblasts exposed to *S. epidermidis* lysate compared to no-lysate control in 5.5 mM glucose concentration (FSe5 _vs_F5); Group 3: DEG in fibroblasts exposed to *S. epidermidis* lysate compared to no-lysate control in 20 mM glucose concentration (FSe20 _vs_F20).

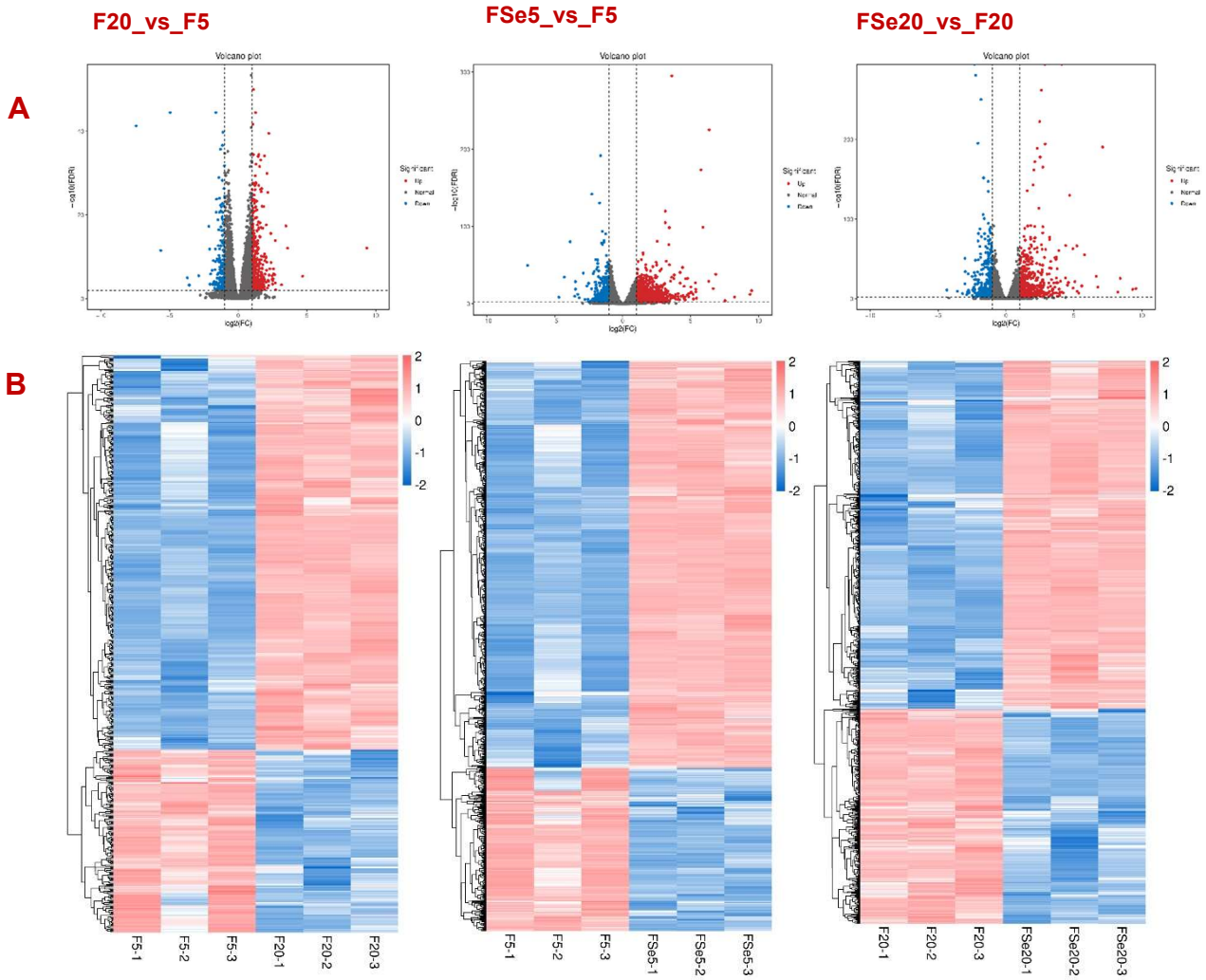

Figure 6.6: Differential expression analysis of fibroblasts exposed to *S. epidermidis* lysate in two main glucose concentrations; 5.5 mM and 20 mM. A) Volcano plot each dot correspond to a gene. X-axis: log2Fold change of expression; Y-axis: -log10(FDR) or -log10(P-value). Dots farther to y=0 represent genes with large difference in expression between two samples (fibroblasts in 20 mM glucose in comparison to control). Dots farther to x=0 means genes of which the difference is more reliable. Red dots are up-regulated ones, whilst blue dots are down-regulated genes and black dots represents genes without significant difference. **B) Hierarchical clustering of differentially expressed genes** Each column represents one sample, and rows represent genes. The expression level of genes (FPKM) was normalised by log10, i.e. log10（FPKM+0.000001 and illustrated as different colours based on scale bar. Red lines represent upregulated genes and blue lines represent down regulated genes. F5, fibroblasts in 5.5 mM; F20, Fibroblasts in 20 mM glucose; FSe20, Fibroblasts exposed to *S. epidermidis* lysate in 20 mM; In each sample, Number 1 represent replicate 1; Number 2 represent replicate 2; Number 3 represent replicate 3. Criteria for differentially expressed genes was set as Fold Change (FC)≥2 and FDR<0.01. Fold change (FC) defined as the ratio of gene expression in two samples. False Discovery Rate (FDR) refers to adjusted p-value, which is used to measure significancy of difference. (BMKGENE, 2023).

6.7 Understanding the function of DEGs

To understand the biological process, cellular component, and molecular function of DEG, genes were annotated in GO at first (Young et al., 2010). Top 20 significantly enriched terms (function) were selected based on enrichment factors (EF) and fisher test (q-value). The larger the enrichment factor indicates the more enrichment of the term. The smaller the q-value is, the more significant the enrichment is. GO results are represented in bubble chart are significantly enriched terms were ranked higher to lower based on the q value. Figure 8.1, 8.2, 8.3, 8.7, 8.8, 8.9, 8.13, 8.14, 8.15 in appendix 1 summarises 20 pathways in biological processes, cellular pathway, and molecular function of three main different groups (F20_vs_F5; FSe5_vs_F5; FSe20_vs_F20).

For further investigation of GO results, DEGs were also annotated in GSEA. This by using gene sets of GO biological process terms in GSEA. GO analysis focuses only on genes with statistical significance that are up- or down-regulated. In this case, the genes that are altered slightly without significance but play an important role in biological functions may be hidden. It is possible to detect modest changes in gene expression using GSEA without setting a threshold for fold change or significance (Nicolle et al., 2015). Figure 8.4, 8.5, 8.6, 8.10, 8.11, 8.12, 8.16, 8.17, 8.18 in appendix 1 summarises 20 pathways biological processes, cellular pathway, and molecular function of three main different groups (F20_vs_F5; FSe5_vs_F5; FSe20_vs_F20).

Moreover, KEGG was used to understand the functional pathways of DEG. Enrichment factors and fisher test were applied to determine enrichment factor (EF) and significancy of the pathway. Figure 8.19, 8.20, 8.21 in appendix 1 summarises 20 pathways in cellular pathways of three main different groups (F20_vs_F5; FSe5_vs_F5; FSe20_vs_F20). Larger EF indicates a more significant enrichment of the pathway. The colour of the dots stands for q-value (adjusted p-value). The smaller the q-value is, the more significant or reliable the enrichment factor is.

In present study, only one pathway was selected for further investigation.

6.8 IL-17 signalling pathway

6.8.1 Upregulated and downregulated genes within IL-17 signalling pathway

The name of each DEG linked to each term or pathway in GO, GSEA, and KEGG are summarised in appendix 3. Moreover, the FDR, log2FC and regulation of each DEGs are summarised in appendix 2.

In the present study, only IL-17 signalling pathway was selected for further investigations (Figure 6.7). IL-17 was significantly enriched pathway in fibroblasts when exposed to *S. epidermidis* lysate in both 5.5 mM and 20 mM glucose concentrations. But the type, log2FC, and regulation of DEGs linked to IL-17 signalling pathway were different when fibroblasts were exposed to *S. epidermidis* lysate in different glucose concentration. Moreover, IL-17 signalling pathway was not within the 20 most significantly enriched pathways when fibroblasts were grown in 20 mM glucose concentration and compared to euglycemic control (5.5 mM) without exposure to *S. epidermidis* lysate.

When fibroblasts were exposed to *S. epidermidis* lysate in 5.5 mM glucose concentrations, IL-17 signalling pathway was significantly enriched because of expression of 21 genes, 16 gene were up-regulated, and 5 genes were down-regulated. However, when fibroblasts were exposed to *S. epidermidis* lysate in 20 mM glucose concentrations, IL-17 signalling pathway was significantly enriched because of expression of 17 genes, 16 gene were up-regulated and only 1 gene were down-regulated.

In both glucose concentrations 5.5 mM and 20 mM, the following genes were all differentially expressed, but in a different fold change and regulation based on the concentration of glucose (Table 6.1) [Log2FC in FSe5_vs_F5 vs FSe20_vs_F20: Gene-CXCL6= 9.5 vs 7.1; gene-CASP3= -1.5 vs -1.1; gene-CCL11= 3.6 vs 1.3; gene-CXCL2= 5 vs 4.6; gene-CXCL3= 6.9 vs 4.9; gene-CXCL5= 4.3 vs 3.8; gene-CXCL8 = 5.8 vs 5.8; gene-CXCL1= 6.4 vs 5.2; gene-CCL7= 3.2 vs 2.2; gene-CILP= 3 vs 1.8; gene-CSF3= 6.7 vs 3.8; gene-FOS= 2.8 vs 2.8; gene-MMP-1= 3.1 vs 1.7; gene-IL1B= 4.2 vs 3, and gene-JUND= 2.2 vs 1.1].

Gene-CCL2 (log2FC=1.4), gene-CEBPB (log2FC=1.7), gene-PTGS2 (log2FC= -1.1), and gene-TRAF5 (log2FC= -1) were only found differentially expressed in fibroblasts when exposed to *S. epidermidis* lysate in 5.5 mM glucose concentration. However, gene-CCL20 (log2FC=2.2) and gene-FOSB (log2FC=1.1) were only found differentially expressed when fibroblasts were exposed to *S. epidermidis* lysate in 20 mM glucose concentration (Table 6.1).

Moreover, two new genes linked to IL-17 signalling pathway were only found downregulated when fibroblasts were exposed to *S. epidermidis* lysate in 5.5 mM glucose concentration [New Gene 3714 (log2FC=-4.3), New Gene 6000 (log2FC= -1.3)]. However, no new genes were linked to IL-17 when fibroblasts were exposed to *S. epidermidis* lysate in 20 mM glucose concentration (Table 6.1).

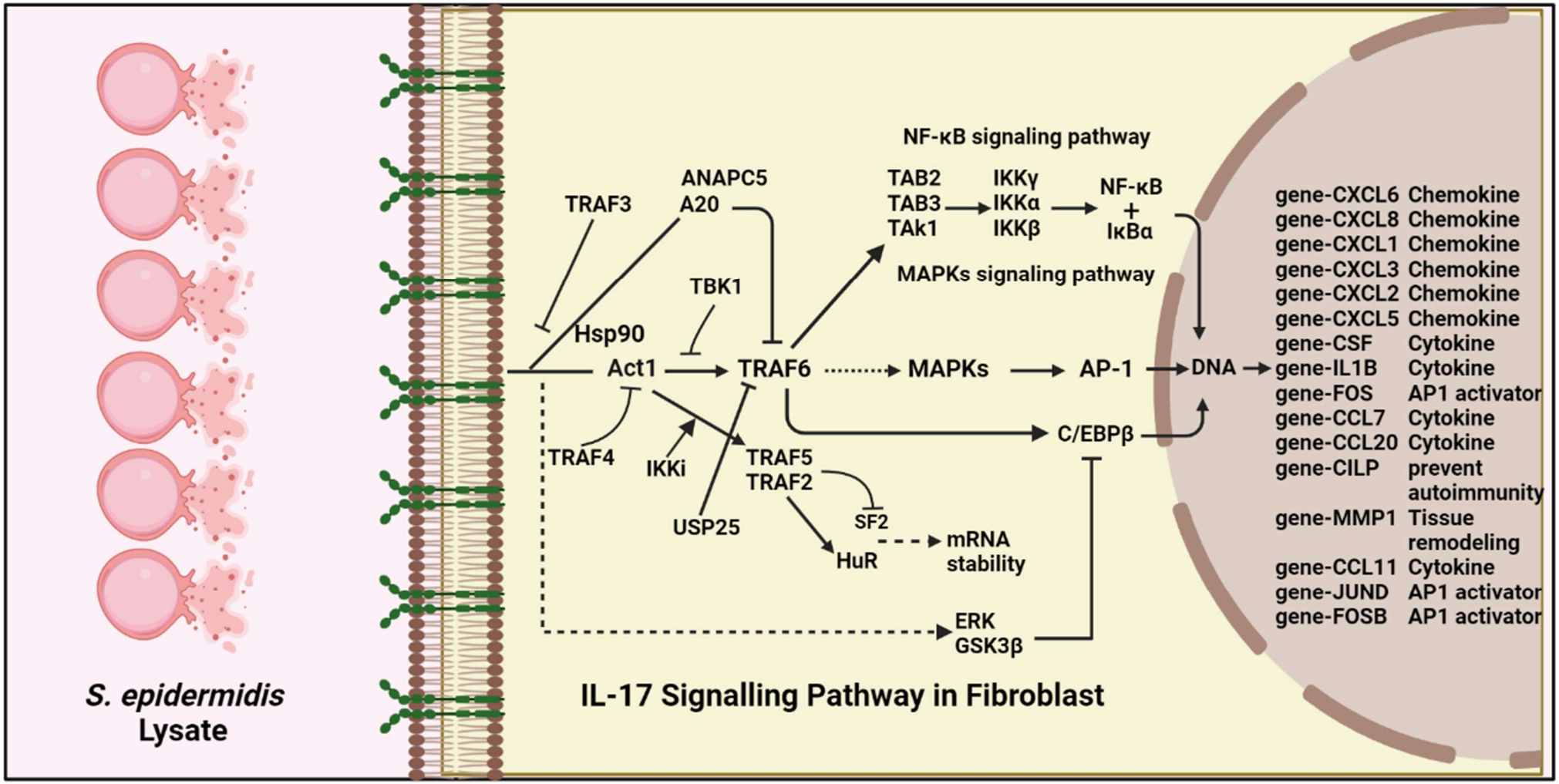

Figure 6.7: IL-17 signalling pathway in fibroblast exposed to *S. epidermidis* lysate in 5.5 mM and 20 mM glucose concentrations. **A)** The scientific illustrations summarises the main cellular pathways and genes linked to IL-17 signalling pathway based on KEGG results (BMKGENE, 2023) and drown by (Biorender, 2024). Exposure of fibroblasts to *S. epidermidis* lysate caused significant enrichment of IL-17 signalling pathway. However, the type and fold change of each DEGs linked to the pathway was different based on glucose concentration

Table 6.1: DEG linked to IL-17 signalling pathway. The table represent the false discovery rate (FDR), the log 2-fold change (log2FC), and the regulation of each DEG linked to IL-17 signalling pathway in fibroblasts exposed to *S. epidermidis* lysate in 5.5 mM (FSe5_vs_F5) and 20 mM (FSe20_vs_F20).

FSe5_vs_F5			
#ID	**FDR**	**log2FC**	**regulated**
gene-CXCL6	8E-18	9.5	up
gene-CXCL3	7E-39	6.9	up
gene-CSF3	2E-20	6.7	up
gene-CXCL1	6E-226	6.4	up
gene-CXCL8	3E-174	5.8	up
gene-CXCL2	8E-16	5.0	up
gene-CXCL5	3E-10	4.3	up
gene-IL1B	2E-41	4.2	up
gene-CCL11	3E-11	3.6	up
gene-CCL7	4E-13	3.2	up
gene-MMP1	1E-120	3.1	up
gene-CILP	3E-05	3.0	up
gene-FOS	2E-08	2.8	up
gene-JUND	8E-19	2.2	up
gene-CEBPB	7E-14	1.7	up
gene-CCL2	2E-13	1.4	up
gene-TRAF5	5E-19	-1.0	down
gene-PTGS2	4E-08	-1.1	down
NewGene_6000	1E-05	-1.3	down
gene-CASP3	8E-16	-1.5	down
NewGene_3714	3E-35	-4.3	down

FSe20_vs_F20			
#ID	**FDR**	**log2FC**	**regulated**
gene-CXCL6	2.05E-191	7.1	up
gene-CXCL8	6.32E-56	5.8	up
gene-CXCL1	3.54E-67	5.2	up
gene-CXCL3	9.61E-64	4.9	up
gene-CXCL2	3.94E-21	4.6	up
gene-CXCL5	1.38E-38	3.8	up
gene-CSF3	1.89E-12	3.5	up
gene-IL1B	6.79E-07	3.0	up
gene-FOS	8.30E-05	2.8	up
gene-CCL7	8.54E-06	2.2	up
gene-CCL20	1.44E-07	2.2	up
gene-CILP	3.82E-05	1.8	up
gene-MMP1	5.86E-31	1.7	up
gene-CCL11	0.007804843	1.3	up
gene-JUND	1.50E-26	1.1	up
gene-FOSB	0.005861131	1.1	up
gene-CASP3	8.28E-23	-1.1	down

6.8.2 IL-17A protein secretion by fibroblasts exposed to *S. epidermidis* lysate in 5.5 mM and 20 mM glucose concentrations

Fibroblasts were grown in 5.5 mM and 20 mM glucose concentrations and exposed to *S. epidermidis* lysate. A scratch was introduced, and the protein expression of IL-17A was measured by ELISA at 12 h.

In all condition, fibroblasts did not secrete IL-17A (Concentration of IL-17A in fibroblasts exposed to *S. epidermidis* lysate in 5.5 mM glucose= 0 pg/mL ($p>0.05$); Concentration of IL-17A in fibroblasts exposed to *S. epidermidis* lysate in 20 mM glucose= 0 pg/mL ($p>0.05$, $n=3$); Concentration of IL-17A in fibroblasts in 5.5 mM= 0 pg/mL ($p>0.05$, $n=3$); Concentration of IL-17A in fibroblasts in 20 mM= 0 pg/mL ($p>0.05$, $n=3$).

6.8.3 Protein secretion of CXCL6 by fibroblasts exposed to *S. epidermidis* lysate in 5.5 mM and 20 mM glucose concentrations

Human skin fibroblasts were grown in 5.5 mM and 20 mM glucose concentration and exposed to *S. epidermidis* lysate. A scratch was introduced and the secretion of CXCL6 was measured by ELISA at 12 h (Figure 6.8).

When fibroblasts were exposed to *S. epidermidis* lysate in 20 mM glucose concentration, a significant increase in the concentration of CXCL6 was observed in comparison to no-lysate control in same glucose concentration (Figure 6.29) [CXCL6 concentration, lysate vs no lysate in 20 mM =170.8 pg/mL ± 6.9 vs 67 pg/mL ± 18.6 ($p<0.01$, n=3)]. However, when fibroblasts were exposed to *S. epidermidis* lysate in 5.5 mM glucose concentrations, no significant alteration in CXCL6 secretion was observed in comparison to no-lysate control in same glucose concentration [CXCL6 concentration in 5.5 mM, lysate vs no lysate = 69.6 pg/mL ± 17 vs 59.3 pg/mL ± 18.5 ($p>0.05$, n=3)].

When fibroblasts were grown in 20 mM glucose concentration, no significant alteration in CXCL6 expression level was observed in comparison to fibroblast grown in 5.5 mM glucose concentration [CXCL6 concentration in 5.5 mM= 59.3 pg/mL ± 18.5 ($p>0.05$, n=3); CXCL6 concentration in 20 mM= 67 pg/mL ± 18.6 ($p>0.05$, n=3)].

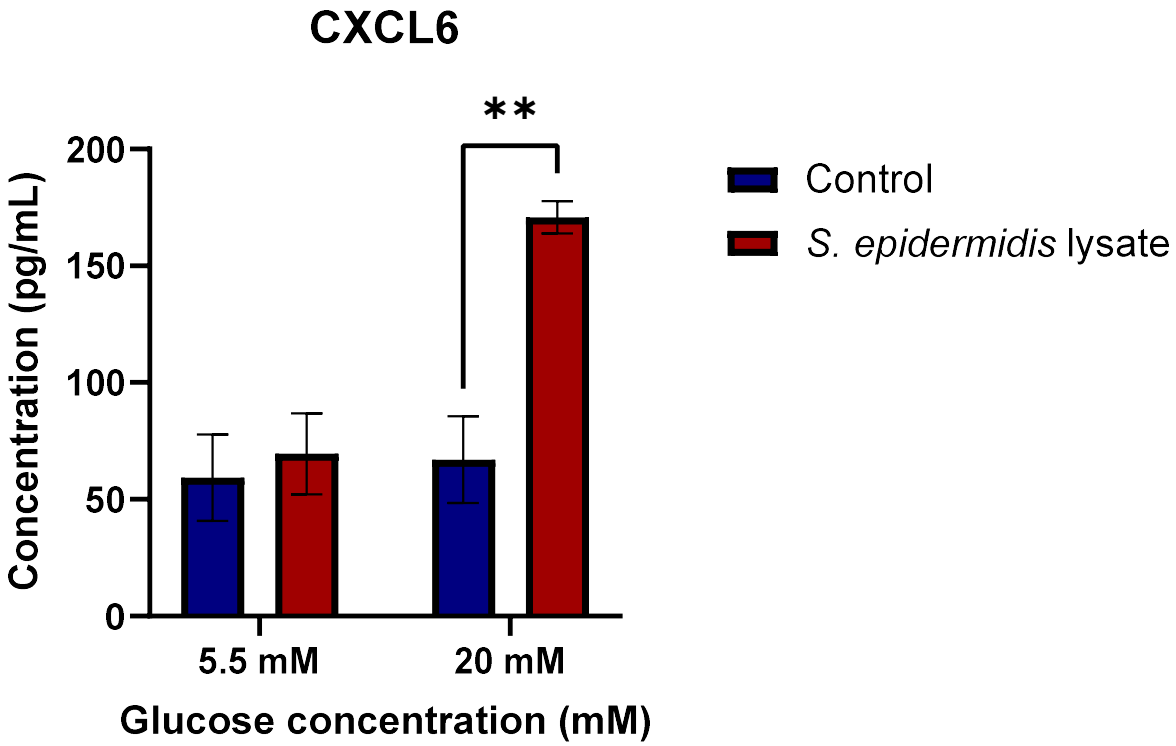

Figure 6.8: Significant induction of CXCL6 secretion in fibroblast as a result of exposure *S. epidermidis* lysate in hyperglycaemic conditions. Significant induction of CXCL6 secretion by fibroblast as a result of exposure *S. epidermidis* lysate in hyperglycaemic conditions. The figure shows the concentration of CXCL6 secreted by fibroblasts grown in euglycemic (5.5 mM) and hyperglycaemic glucose concentrations (20 mM) and exposed to of *S. epidermidis* lysate (100 µl). Fibroblasts were seeded in 96 well plates (5000 cells/ well). A scratch was introduced, and cells were exposed to *S. epidermidis lysate* in euglycemic and hyperglycaemic glucose concentrations. The level of CXCL6 secretion was measured by ELISA after 12 h of exposure. Results are expressed as mean of concentration (%) ± SEM, n=3, error bars represent +/- SEM, Statistical analysis two-way analysis of variance (ANOVA) and post hoc Tukey test was performed. **p<0.01

6.8.4 Protein secretion of CXCL6 by fibroblasts exposed to *S. epidermidis* lysate in 5.5 mM and 20 mM glucose concentrations

To investigate whether the significant induction of CXCL6 secretion by *S. epidermidis* lysate in 20 mM, observed in Section 6.7.4, was dependent on induction of IL-17 receptor or not, fibroblasts were cultured in euglycemic (5.5 mM) and hyperglycaemic levels of glucose (20 mM) and pretreated with IL-17A receptor antagonist, Brodalumab (143 ng/mL) for 1 h. Subsequently, cells were exposed to IL-17A (1.5 ng/mL) and *S. epidermidis* (100 µL) lysate. A scratch was introduced, and the secretion of CXCL6 was quantified by ELISA at 12 h (Figure 6.9).

In 5.5 mM glucose, exposure to *S. epidermidis* lysate resulted in a slight non-significant increase in expression of CXCL6 compared to control [294.9 pg/mL ± 54.7 vs 284.9 ± 35.8 ($p>0.05$, n=3)]. However, in 20 mM glucose concentration, exposure to *S. epidermidis* lysate resulted in a significant increase in CXCL6 expression [478.9 pg/mL ± 65.9 vs 234.6 ± 21.3 ($p<0.01$, n=3)].

When fibroblasts were pretreated with Brodalumab before exposure to *S. epidermidis* lysate, no significant effects on CXCL6 secretions were observed in both 5.5 mM and 20 mM glucose concentrations [Brodalumab vs no-brobalumab, in 5.5 mM = 195.1 pg/mL ± 20.04 vs 294.9 ± 54.7 ($p>0.05$, n=3); In 20 mM = 425.6 pg/mL ± 46.5 vs 478.9 ± 65.9 ($p>0.05$, n=3)].

No significant effects on CXCL6 secretion by fibroblasts were observed when treated with IL-17A in 5.5 mM glucose concentration compared to control [CXCL6 concentration vs control = 346.1 pg/mL ± 3.04 vs 284.9 ± 35.8 ($p>0.05$, n=3)]. However, pretreatment of cells with Brodalumab in 5.5 mM glucose concentration resulted in a significant decrease in CXCL6 secretion compared to cells that were exposed to IL-17 without pretreatment with Brodalumab [Brodalumab vs no-brobalumab= 146.6 pg/mL ± 9.6 vs 346.1 pg/mL ± 3.04 ($p<0.05$, n=3)].

No significant effect on CXCL6 secretion by fibroblasts was observed when treated with IL-17A in 20 mM glucose concentration compared to control [CXCL6 concentration vs control = 400.04 pg/mL ± 48.7 vs 234.6 pg/mL ± 21.3 ($p>0.05$, n=3)]. Pretreatment of cells with Brodalumab in 20 mM glucose concentration also did not cause any significant effects on CXCL6 secretion compared to cells that were exposed to IL-17 without pretreatment with Brodalumab [CXCL6 concentration Brodalumab vs

No-Brobalumab, in 20 mM = 340.9 pg/mL ± 62.5 vs. 400.04 pg/mL ± 48.7 (p>0.05, n=3)].

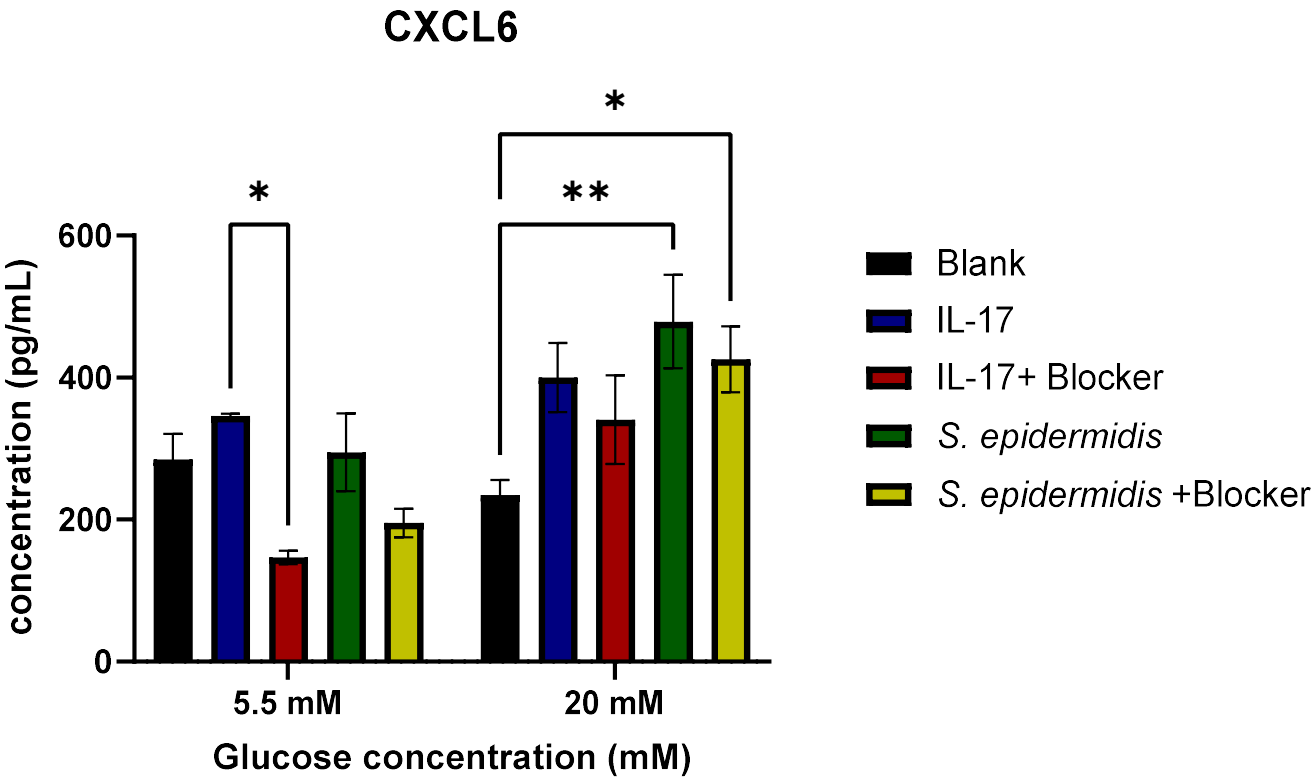

Figure 6.9: *S. epidermidis* lysate stimulated CXCL6 protein secretion in 20 mM glucose concentrations independently from IL-17A receptor. Fibroblasts were seeded at 5000 cells per well. Cells were grown in healthy (5.5 mM) and hyperglycaemic level of glucose (20 mM) and exposed to IL-17A (1.5 ng/mL), and *S. epidermidis* lysate (100 µL). In some relevant wells, fibroblasts were pretreated with Brodalumab (143 ng/mL) for 1 h before adding the lysate and IL-17A. A scratch was introduced and the concentration of $CXCL_6$ was measured after 12 h by ELISA. Results are expressed as mean +/- SEM. Two-way analysis of variance (ANOVA) and post hoc Tukey test was performed *p<0.05, **p<0.01.

6.9 Discussion

In the present study, transcriptomic analysis (whole mRNA-sequencing) was performed to elucidate the mechanism of *S. epidermidis* lysate action on fibroblasts cultured in 5.5 mM and 20 mM glucose concentrations. The 5.5 mM concentration was utilised to simulate euglycemic conditions, whilst 20 mM was employed to replicate hyperglycaemic conditions.

As previously established, evaluating the quality of extracted RNA is a crucial step prior to sequencing (Fleige & Pfaffl, 2006). Therefore, in the initial phase of this study, RNA quality was assessed by measuring the concentration, purity, and integrity of the extracted RNA. Subsequently, the quality of raw data and similarity among replicates of each sample were examined. All quality control results in this study indicated that RNA extraction was successfully executed, and all samples were deemed suitable for whole mRNA sequencing. Following confirmation of RNA quality, differential expression analysis was conducted, and the function of differentially expressed genes (DEGs) was investigated using Gene Ontology (GO), Gene Set Enrichment Analysis (GSEA), and Kyoto Encyclopedia of Genes and Genomes (KEGG) analyses. Various noteworthy functional terms and pathways were found to be altered in fibroblasts when exposed to *S. epidermidis* lysate under different glucose concentrations. In this study, only the IL-17 signalling pathway was selected for further investigation. This selection was based on the significant enrichment of this pathway in fibroblasts exposed to *S. epidermidis* lysate in both euglycemic and hyperglycaemic glucose concentrations. However, the degree of expression and type of genes associated with this pathway differed when fibroblasts were exposed to *S. epidermidis* lysate in 5.5 mM and 20 mM glucose concentrations. Notably, as reviewed by (McGeachy et al., 2019) IL-17 signalling can be either beneficial or detrimental depending on how IL-17 signals are received and transmitted within the responding cell. Thus, focusing on this pathway for further investigations will contribute valuable knowledge to the current body of published literature.

Several studies have reported that certain members of the skin microbiota, primarily *S. epidermidis*, induced immune cells, such as CD8+ T cells and innate lymphoid cells, to secrete IL-17 (Naik et al., 2015; Singh et al., 2021). The current study hypothesised that the observed induction of the IL-17 signalling pathway might be attributed to the

expression and secretion of IL-17 by fibroblasts when exposed to *S. epidermidis* lysate in varying glucose concentrations. However, contrary to expectations, neither was the IL-17 gene found to be differentially expressed in fibroblasts based on transcriptomic data, nor was IL-17 protein secreted based on ELISA results when exposed to *S. epidermidis* lysate in both euglycemic and hyperglycaemic glucose concentrations. Consequently, this study suggests that as fibroblasts did not secrete IL-17, *S. epidermidis* lysate may contain components capable of inducing the IL-17 signalling pathway. Furthermore, this may indicate that the upregulation of IL-17 observed in some published articles might not solely be due to the secretion of IL-17 by immune cells (Naik et al., 2015; Singh et al., 2021). Rather, *S. epidermidis* may possess components capable of directly stimulating the IL-17 signalling pathway in skin. Additional studies are necessary to characterise the components of *S. epidermidis* lysate and investigate their interaction with the IL-17 signalling pathway. Notably, a study suggested that two primary *S. epidermidis*-Derived N-Formyl Methionine Peptides (f-MFLLVN and f-MIIINA) might be responsible for inducing CD8+ T cells to produce IL-17A in vitro (Linehan et al., 2018). Therefore, further research is required to elucidate how *S. epidermidis*-Derived N-Formyl Methionine Peptides (f-MFLLVN and f-MIIINA) might influence the IL-17 signalling pathway in fibroblasts under euglycemic and hyperglycaemic glucose concentrations.

Granulocyte chemotactic protein-2 (GCP-2) (CXCL6) was the most upregulated gene in the IL-17 signalling pathway when fibroblasts were treated with *S. epidermidis* lysate in both 5.5 mM and 20 mM glucose concentrations. However, the CXCL6 gene was not significantly differentially expressed when fibroblasts were grown in 20 mM compared to 5.5 mM glucose and not exposed to *S. epidermidis* lysate. A notable observation was that *S. epidermidis* lysate induced higher gene expression of CXCL6 in 5.5 mM glucose concentration compared to 20 mM glucose concentration. However, the protein level of CXCL6 was significantly higher in 20 mM compared to 5.5 mM glucose concentration. Moreover, the protein level of CXCL6 was also not significantly different when fibroblasts were grown in 20 mM compared to 5.5 mM glucose. CXCL6 is reported to play an important role in inflammation by recruiting neutrophils to complete non-specific immunity(Dai et al., 2023). Notably, according to a clinical study, CXCL6 protein levels were higher in wound exudate from diabetic patients with rapidly healing wounds than in those with delayed wound healing(Wang et al., 2019). This

suggests that CXCL6 may serve as a novel biomarker and therapeutic target in diabetic foot ulcers (Wang et al., 2019). Thus, the present study hypothesised that *S. epidermidis* lysate might aid in diabetic wound healing through an increase in CXCL6 protein secretion and induction of the IL-17 signalling pathway. However, further studies are required to substantiate this hypothesis.

As CXCL6 was part of the IL-17 signalling pathway, the present study hypothesised that *S. epidermidis* lysate might induce CXCL6 secretion by binding to the IL-17A receptor. Consequently, fibroblasts were treated with the IL-17A receptor blocker brodalumab prior to exposure to *S. epidermidis* lysate. Unexpectedly, pretreatment with anti-IL-17A receptor (Brodalumab) did not result in a significant reduction of CXCL6 secretions induced by *S. epidermidis* lysate in both 5.5 mM and 20 mM glucose concentrations. This indicates that CXCL6 secretion induced by *S. epidermidis* lysate was independent of binding to the IL-17A receptor in euglycemic and hyperglycaemic glucose concentrations.

Moreover, in the present study, IL-17 was used as a positive control, and a comparison between IL-17 and *S. epidermidis* lysate to induce CXCL6 secretion by fibroblasts was performed in euglycemic and hyperglycaemic glucose concentrations. Unexpectedly, IL-17A did not cause any significant increase in CXCL6 production by fibroblasts in both 5.5 mM and 20 mM conditions. Only *S. epidermidis* lysate was found to induce a significant increase in CXCL6 protein levels in hyperglycaemic glucose concentrations. This indicates that *S. epidermidis* is more potent than IL-17A in inducing CXCL6 secretion by fibroblasts in both 5.5 mM and 20 mM conditions. However, in the present study, fibroblasts were exposed to 1.5 ng/mL of IL-17A. Thus, a comparison between *S. epidermidis* lysate and higher doses of IL-17A might be necessary before confirming this finding. Additionally, one might question how CXCL6 secretions would be altered if fibroblasts were exposed to another IL-17 cytokine dimer, such as IL-17F.

Furthermore, in the present study, the upregulation of CXCL6 was also linked to other pathways, such as the TNF signalling pathway. However, the significance and enrichment of this pathway were lower in comparison to the IL-17 signalling pathway. Therefore, the non-significant result observed when cells were pretreated with brodalumab might be due to stimulation of TNF receptors in addition to IL-17 receptors

by *S. epidermidis* lysate. Thus, further studies are required to understand the interaction between *S. epidermidis* lysate and TNF receptors. Interestingly, a study revealed that two main peptides of *S. epidermidis*-derived antigenic ligands containing N-formyl methionine (f-MIIINA and f-MFLLVN) could significantly induce the secretion of IL-17 and TNF-ɣ by immune cells (CD8 T cells) (Linehan et al., 2018). Consequently, further studies are necessary to characterise the components of *S. epidermidis* lysate and investigate their effect on TNF receptors in euglycemic and hyperglycaemic glucose concentrations. This is because these interactions might form fundamental mechanisms by which *S. epidermidis* lysate may be involved in healing diabetic wounds.

Another gene of interest that was found to be upregulated within the IL-17 signalling pathway when fibroblasts were exposed to *S. epidermidis* lysate in euglycemic and hyperglycaemic glucose concentrations was IL1B. However, this gene was not significantly expressed when fibroblasts were grown in hyperglycaemic glucose concentration without exposure to *S. epidermidis* lysate. Notably, a clinical study observed a higher abundance of M1 macrophages and overexpression of IL1B, S100A8, and S100A9 genes in the skin of diabetic patients with healed ulcers compared to non-healed patients (Theocharidis et al., 2022). Consequently, it can be hypothesised that *S. epidermidis* lysate might facilitate diabetic wound healing through increased IL1B gene expression alongside increased expression of CXCL6. Nevertheless, further studies are necessary to investigate the effect of *S. epidermidis* lysate on IL1B protein secretion by fibroblasts in low and high glucose concentrations.

7. Chapter 7: General Discussion and Future Plan

7.1 General Discussion

Poor wound healing and DFU are very common complications of DM (Demirseren et al., 2013). DFU and gangrene are two of the most common complications of DM (IDF, 2024; McDermott et al., 2023). 40 to 60 million diabetic patients are diagnosed with DFU worldwide (IDF, 2024; McDermott et al., 2023). DFU and limb amputation are surprisingly associated with high 5 years mortality rate which is like or higher than some of the common types of cancer (Armstrong et al., 2020; Armstrong et al., 2007). Unfortunately, treatment failure in DFU is common and this mainly due to increase of antibiotics resistance (Trivedi et al., 2014; Vardakas et al., 2008). Thus, the present study suggests that there is an urgent need to identify new therapeutic agents to help in healing DFUs. As lysate or cell- free supernatant of some *lactobacillus* spp. has been investigated widely and found to heal wounds in skin and gastrointestinal tract (Brandi et al., 2020; Halper et al., 2003; Mohammedsaeed et al., 2015) Moreover, some members of skin microbiota have been reported to play a vital role in proper wound healing by activating immune response (Schierle et al., 2009), and DM was associated with dysbiosis in skin microbiota (Redel et al., 2013; Thimmappaiah Jagadeesh et al., 2017). Thus, the present study hypothesised lysates and cell-free supernatant prepared from skin commensal bacteria might ameliorate some effects of hyperglycaemia induced alterations in skin cells function and promote wound healing in DM. Figure 7.1 summarises the main findings in present study.

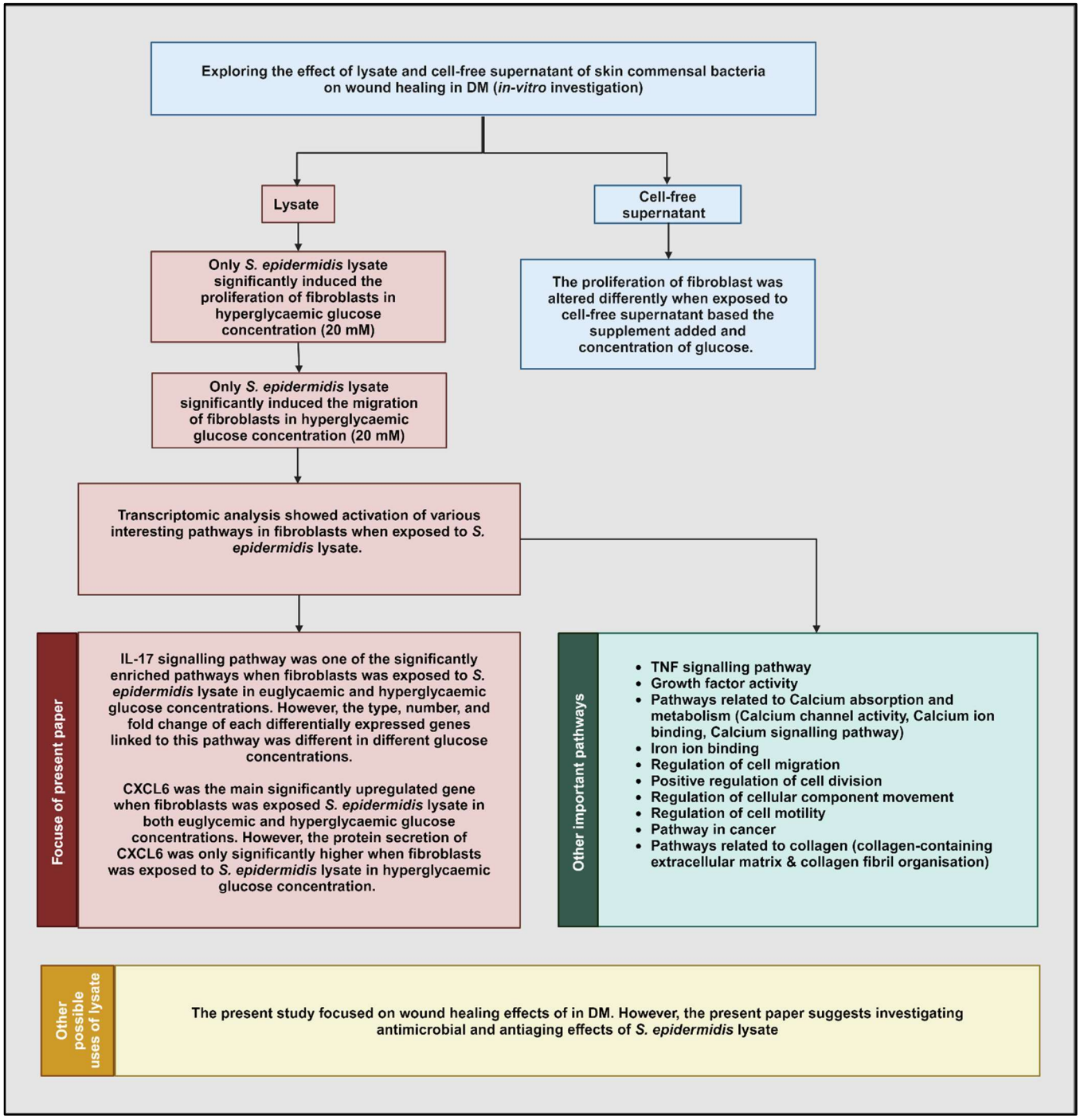

Figure 7.1: Summary of the main findings of the present study. *S. epidermidis* lysate induces proliferation and migration of fibroblasts in-vitro, only in 20 mM glucose concentration. Various pathways were significantly enriched in transcriptomic analysis of fibroblasts exposed to *S. epidermidis* lysate in euglycemic (5.5 mM) and hyperglycaemic (20 mM) glucose concentrations. The focus of present study is on IL-17 signalling pathway and CXCL6 protein secretion. However, the present study highlights some other important pathways for further studies to investigate with recommendations on further possible uses of *S. epidermidis* lysate.

7.1.1 Understanding the main significant finding of present study

One notable finding in the present study was that exposure to *S. epidermidis* lysate resulted in a significant increase in the proliferation and migration of fibroblasts in hyperglycaemic glucose concentration. However, exposure to *S. epidermidis* lysate did not cause significant alteration in proliferation and migration of fibroblasts in euglycemic glucose concentration. Another significant finding in the present study was that exposure to *S. epidermidis* lysate led to substantial enrichment in the IL-17 signalling pathway in both euglycemic and hyperglycaemic glucose concentrations. However, the type and degree of gene expression associated with the IL-17 signalling pathway differed based on the glucose concentration. As reviewed by (McGeachy et al., 2019), signals from the IL-17 pathway can be either beneficial or detrimental depending on how they are received and transmitted by cells responding to them under various conditions. Moreover, wound reepithelialisation, migration of wound tongue, and keratinocytes were found to depend on IL-17A-HIF1α signalling pathways (Konieczny et al., 2022). Additionally, the proliferation of fibroblasts was significantly increased when cocultured with IFN-γ+IL-17+Th17 secreting immune cells (Xing et al., 2020). Thus, the present study suggests that the observed heterogeneity in proliferation and migration of fibroblasts in different glucose concentrations was due to the activation of different genes in the IL-17 signalling pathway under varying glucose concentrations. However, further studies are required to investigate how the upregulation of each of the genes linked to the IL-17 signalling pathway will influence the proliferation and migration of fibroblasts in different glucose concentrations.

In the present study, only protein secretion of CXCL6 was investigated, as this gene exhibited the highest significant fold change within the IL-17 signalling pathway. Interestingly, in the current study, CXCL6 protein secretion was significantly upregulated only in hyperglycaemic glucose concentrations. CXCL6 has been reported to induce proliferation and migration of certain cancer cells (Ma et al., 2017). The present study suggests that the increase in CXCL6 protein secretion under hyperglycaemic conditions might be the cause of the significant increase in fibroblast migration observed in hyperglycaemia. However, further studies are necessary to investigate the effect of CXCL6 protein secretion on proliferation and migration of fibroblasts under varying glucose concentrations.

A notable observation in the present study was that gene-CCL20 exhibited upregulation exclusively when fibroblasts were exposed to *S. epidermidis* lysate in hyperglycaemic glucose concentration (20 mM). Gene-CCL20 did not demonstrate differential expression when fibroblasts were exposed to *S. epidermidis* lysate in euglycemic glucose concentration. Furthermore, in addition to its involvement in the IL-17 signalling pathway based on KEGG, gene-CCL20 was associated with various pathways, including regulation of cellular component movement, regulation of cell motility, cytokine-cytokine receptor interaction, and TNF signalling pathway. Previous research has reported that CCL20 induces the migration of immune cells (Zhai et al., 2023). The present study suggests that the absence of CCL20 upregulation in euglycemia might account for the non-significant results in fibroblast migration when exposed to *S. epidermidis* lysate in euglycemic glucose concentrations. Further investigations are necessary to elucidate how CCL20 influences migration and proliferation of fibroblasts in different glucose concentrations.

As reviewed by (McGeachy et al., 2019), activation of the IL-17 signalling pathway can produce either beneficial or detrimental effects depending on the manner in which IL-17 signals are received and transmitted by the responding cells. Notably, according to a clinical study, activation of the IL-17 signalling pathway was associated with healed DFUs in diabetic patients compared to non-healed DFUs (Theocharidis et al., 2022). Furthermore, the IL-17 signalling pathway was found to be downregulated in the skin of diabetic patients compared to healthy individuals (Takematsu et al., 2020). Additionally, CXCL6 secretion in wound exudates indicated proper wound healing in diabetics (Wang et al., 2019).

The significant enrichment of the IL-17 signalling pathway observed in the present study was accompanied by an increase in proliferation and migration of fibroblasts at 20 mM glucose. Considering the published evidence on the importance of the IL-17 signalling pathway and CXCL6 in proper wound healing in DM (Takematsu et al., 2020; Theocharidis et al., 2022; Wang et al., 2019), the present study suggests that the observed induction of the IL-17 signalling pathway by *S. epidermidis* lysate may have more beneficial than detrimental effects on fibroblasts in hyperglycaemic glucose concentrations. Consequently, *S. epidermidis* lysate may represent a potential novel therapeutic agent for healing diabetic wounds. However, the present study recommends further ex vivo, in vivo, and clinical studies to elucidate the effects of *S.*

epidermidis lysate on wound healing. To our knowledge, only one paper has been published investigating the effect of *S. epidermidis* lysate on diabetic wound healing using an ex vivo (punch-in-a-punch) model. *S. epidermidis* lysate promoted reepithelialisation by increasing epithelial tongue length, epidermal thickness, and the keratinocyte proliferation marker (Ki-67) in both diabetic and non-diabetic wound models (Mohammedsaeed et al., 2022). Further studies are warranted.

In addition to investigating the wound healing effect of *S. epidermidis* lysate, the present study suggests that this product requires assessment for its safety in cancer patients. This consideration is necessary because metastasis of cancer cells is associated with an increase in cancer cell migration (Tucci et al., 2012). Furthermore, based on transcriptomic analysis in the present study, pathways in cancers were significantly enriched when fibroblasts were exposed to *S. epidermidis* in hyperglycaemic glucose concentration (Figure 8.20 & 8.21). Consequently, the application of *S. epidermidis* lysate may not be an optimal choice for treating DFU in patients with comorbidities such as DM and cancer.

CXCL6 has been reported to have bactericidal effects on gram-negative (*P. aeruginosa* and *E. coli*) and gram-positive (*S. aureus, S. dysgalactiae* and *S. pyogenes*) bacteria (Linge et al., 2008). As the present study found CXCL6 significantly secreted by fibroblasts exposed to *S. epidermidis* lysate in hyperglycaemic glucose concentration, it is hypothesised that *S. epidermidis* lysate might protect diabetic wounds from chronic pathogenic bacterial infections by inducing CXCL6 in hyperglycaemic glucose concentrations. However, further studies are necessary to fully elucidate the antibacterial effects of *S. epidermidis* lysate in diabetic wounds.

A case report study found that deficiency in IL-17 receptor A in humans was one of the main aetiologies of persistent chronic infections of human skin with *Candida albicans* and *S. aureus* (Cho et al., 2010; Puel et al., 2011). *S. aureus* is considered a primary pathogen isolated in diabetic foot ulcers. *Candida* infection was also one of the main fungal infections in diabetic wounds. The present study suggests that further investigations are required to examine the antifungal and antibacterial properties of *S. epidermidis* lysate.

In the present study, the activation of the IL-17 signalling pathway was associated with significant enrichment of growth factor activity (Figure 8.14 & 8.15) when fibroblasts were exposed to *S. epidermidis* lysate in 5.5 mM and 20 mM glucose concentrations. Interestingly, a study reported that IL-17 derived from microbiota synergises with growth factor (FGF2) to induce proliferation of epithelial cells to heal damaged intestinal epithelium (Song et al., 2015). Moreover, deficiency in IL-17 or FGF2 resulted in disturbance of epithelial cell proliferation (Song et al., 2015). Thus, the present study hypothesises that exposure to *S. epidermidis* lysate might induce fibroblast proliferation by activation of genes involved in growth factor activation as a synergistic consequence of significant activation of the IL-17 signalling pathway. Further studies are required to understand the correlation between *S. epidermidis* lysate, IL-17 signalling pathway, and significant enrichment of genes involved in growth factor activity in fibroblasts grown in both 5.5 mM and 20 mM glucose concentrations.

In the present study, the activation of the IL-17 signalling pathway was associated with significant enrichment in the calcium signalling pathway, as demonstrated by KEGG, GO, and GSEA enrichment analyses (Figure 8.13, 8.14, 8.15, 8.16, 8.17, 8.19, 8.20, 8.21). The calcium signalling pathway has been reported to be important in the process of wound healing (Krizanova et al., 2022; Subramaniam et al., 2021). Although this pathway was also found to be significantly enriched in fibroblasts grown in 20 mM compared to 5.5 mM glucose concentration, the genes activated within this pathway differed. Epidermal growth factor was the primary gene of interest found to be altered. Epidermal growth factor (gene-EGF) was significantly reduced in all conditions. However, the expression of Epidermal growth factor-like 6 (gene-EGFL6) was only significantly upregulated when fibroblasts were exposed to *S. epidermidis* in both 5.5 mM and 20 mM glucose concentrations.

A study reported that EGF promotes wound healing by significantly increasing the proliferation of fibroblasts in vitro (Yu et al., 2012). Moreover, proliferation and migration were significantly increased when fibroblasts were exposed to EGF or its domain EGFL7 secreted by transfected mesenchymal stem cells (Yang et al., 2016; You & Nam, 2013). EGFL6 expression has been linked to cancer cell proliferation, migration, and tumour progression. In contrast, EGFL6 expression in normal conditions was found to be low, and blocking EGFL6 did not affect wound healing(Noh

et al., 2017; Su et al., 2022). The effect of EGFL6 on diabetic wounds remains unclear. In the present study, EGF was significantly lowered, and EGFL6 was not expressed in high glucose concentration. Furthermore, although EGF was also lowered when exposed to *S. epidermidis* lysate, EGFL6 was significantly higher. Thus, the present study suggests that *S. epidermidis* might counteract the significant reduction of EGF gene in fibroblasts in high glucose by significantly inducing the expression of EGFL6. Additionally, as EGFL6 has been found to induce proliferation and migration of tumour cells(Yang et al., 2016; You & Nam, 2013), this might be the mechanism by which *S. epidermidis* lysate induces the proliferation and migration of fibroblasts in high glucose concentrations. Further studies are required to investigate the role of EGFL6 in diabetic wounds. Moreover, as this gene was involved in the calcium signalling pathway, it is important to understand the correlation between calcium, *S. epidermidis* lysate, EGFL6, and fibroblast proliferation and migration in DM.

Moreover, in the present study, based on GO analysis, iron ion binding (Figure 8.15) was significantly enriched in molecular function when fibroblasts were exposed to *S. epidermidis* lysate in 20 mM glucose (Figure 8.3). Notably, a study reported significant dysregulation in iron gene expression, significant reduction in iron levels, and delayed extracellular matrix deposition. Furthermore, iron was found to be an important factor in the remodelling of extracellular matrix(Wilkinson et al., 2019). Thus, the present study suggests further investigation to understand the correlation between iron, *S. epidermidis* lysate, and fibroblast proliferation and migration in DM.

In the present study, various pathways were identified that were linked to collagen, such as collagen-containing extracellular matrix (Figure 8.8, 8.9), and collagen fibril organisation (Figure 8.3). Collagen is reported to play an important role in wound healing(Mathew-Steiner et al., 2021). Additionally, various collagen-based wound dressings showed improvement in DFU (Holmes et al., 2013). Thus, the present study suggests that one of the mechanisms by which *S. epidermidis* lysate might affect wound healing is through its effect on genes involved in collagen deposition and the remodelling phase of wound healing. Further studies are required to elucidate this mechanism.

7.1.2 Understanding the non-significant data of present study

The current study revealed no significant impact on keratinocyte proliferation and migration when exposed to *S. epidermidis* lysate under varying glucose concentrations. An intriguing question to consider is why *S. epidermidis* may exert its effects on fibroblasts in high-glucose conditions, whilst not exhibiting the same impact on keratinocytes under similar conditions.

The present study hypothesises this could be attributed to differences in glucose uptake and metabolism between the two cell types. Fibroblasts and keratinocytes exhibit distinct glucose uptake and metabolic patterns, which influence their functions under varying glucose conditions: Fibroblasts remain highly metabolically active even in a quiescent state, degrading and re-synthesising proteins and fatty acids, and secreting large amounts of protein into the extracellular environment (Lemons et al., 2010). They divert glucose to the pentose phosphate pathway, generating NADPH for detoxifying free radicals or synthesising fatty acids (Lemons et al., 2010). This metabolic activity is crucial for maintaining tissue homeostasis and supporting wound healing processes (Lemons et al., 2010).

In contrast, keratinocytes show a more dynamic response to glucose levels. Under high glucose conditions (20 mmol/l), keratinocytes downregulate glucose transport, whilst at low glucose levels (2 mmol/l), they increase transport rates (Spravchikov et al., 2001). These changes are associated with alterations in GLUT1 expression and transport affinity. High glucose exposure leads to decreased proliferation and enhanced calcium-induced differentiation in keratinocytes (Spravchikov et al., 2001). This glucose-dependent behaviour may be an adaptive mechanism to maintain epidermal barrier function under varying metabolic conditions (Spravchikov et al., 2001).

Metabolic reprogramming plays a crucial role in the response of fibroblasts and keratinocytes to varying glucose levels, significantly impacting their functions in tissue maintenance and wound healing. During wound healing, glucose metabolism is altered, with glucose transporters and key enzymes causing elevated metabolite levels (Wang et al., 2024). This glucose mediated oxidative stress drives the proinflammatory response and promotes wound healing. Keratinocytes and fibroblasts respond differently to these changes in glucose levels. Keratinocytes are particularly sensitive

to changes in their environment, including glucose levels, which can influence their rate of proliferation and migration (Wang et al., 2024). This sensitivity can be exploited to improve wound repair after tissue injury. Interestingly, whilst both cell types are affected by glucose levels, their responses can be quite different. For instance, high glucose concentrations impair keratinocyte proliferation, but this effect can be completely reversed by nerve growth factor (NGF) (Gostynska et al., 2020). In contrast, NGF has no effect on fibroblast proliferation, regardless of glucose levels. This difference in response highlights the complex interplay between metabolic factors and growth factors in regulating cellular functions during wound healing (Gostynska et al., 2020).

The present study hypothesises the metabolic state of these cells, influenced by glucose availability, may impact their ability to respond to skin commensal bacteria in high glucose concentrations. Moreover, the differences in glucose uptake and metabolism between fibroblasts and keratinocytes reflect their distinct roles in skin physiology. Fibroblasts maintain high metabolic activity for tissue maintenance (Lemons et al., 2010), whilst keratinocytes adapt their glucose utilisation based on environmental conditions (Spravchikov et al., 2001). These metabolic differences likely influence their interactions with each other with skin commensal bacteria in different glucose concentrations.

Thus, although the current study yielded non-significant findings when fibroblasts were exposed to cell-free supernatant from skin commensal bacteria, fermented supernatant, *S. aureus* lysate, and *C. jeikeium* lysate, it would be beneficial to investigate the effects of these substances on keratinocyte proliferation and migration. This area of research remains of interest and merits further investigation.

Interestingly, alterations in fibroblast activity can significantly impact keratinocyte behaviour and overall wound healing. For example, fibroblasts stimulated by certain compounds like glycitin can indirectly promote keratinocyte proliferation and migration through the secretion of growth factors such as TGF-β (Seo et al., 2017). Interestingly, keratinocytes also influence fibroblast behaviour in a reciprocal manner. Keratinocytes regulate fibroblast and mesenchymal stem cell proliferation, myofibroblast formation, and collagen matrix production through a FOXO1-induced TGF-β1/CTGF axis (Zhanng et al., 2017). This bidirectional communication highlights the complex

interplay between these cell types during wound healing (Seo et al., 2017; Zhanng et al., 2017). Therefore, it is pertinent to investigate how alterations in fibroblasts, observed in current study resulting from exposure to *S. epidermidis* lysate in high glucose, would influence keratinocyte function and the overall wound healing process in DM.

7.2 Future Direction

7.2.1 Future of bacterial lysate research

Current research in human microbiota primarily focuses on characterising and identifying the main species of human microbiota in healthy individuals, as well as establishing correlations between disease pathophysiology and alterations in human microbiota (Gilbert et al., 2018). It is now well-established that human microbiota is disrupted in various diseases. Consequently, modulating it may potentially alleviate these conditions. However, at present, limited research has been conducted on methods to manipulate human microbiota for therapeutic purposes (Sorbara & Pamer, 2022).

Furthermore, the current emphasis of microbiome-based therapeutics research is on utilising human gut microbiota to address human diseases (Sorbara & Pamer, 2022). Even in dermatological conditions, *Lactobacillus* probiotics have been extensively investigated for the treatment of skin diseases. However, there is limited knowledge regarding the potential utilisation of skin commensals in treating skin diseases (Yu et al., 2020). Therefore, the present study aims to investigate the possibility of developing novel therapeutics from skin microbiota to facilitate the healing of diabetic wounds. Notably, we have identified that *S. epidermidis* lysate can effectively counteract hyperglycaemia-induced alterations in human skin fibroblasts in vitro. This finding represents a significant contribution to microbiome-based therapeutics research, highlighting the importance of shifting focus from *Lactobacillus* spp. to skin microbiota spp. for the treatment of dermatological diseases. Additionally, the primary approaches to developing microbiota-based therapeutics currently involve investigating the preparation and use of prebiotics, probiotics, and faecal microbiota transplantation to modulate the microbiota and address diseases (Sorbara & Pamer, 2022). The findings of the present study encourage further investigation into the use of lysates prepared from human microbiota for the development of novel microbiome-based therapeutics, as opposed to live bacteria. This approach may potentially reduce the risk of bacterial overgrowth and gastrointestinal infections observed with some current probiotics (Dore et al., 2019). It may be worthwhile to consider the use of lysates in the preparation of ointments for treating dermatological diseases, rather than utilising oral probiotics encapsulated with live bacteria.

Although the primary focus of the present study was to identify the role of lysate in the treatment of diabetic wounds, the transcriptomic analysis reported in this paper reveals alterations in different pathways involved in collagen deposition in human skin fibroblasts exposed to *S. epidermidis* lysate in low and high glucose conditions. As collagen is reported to be altered in skin aging (Reilly & Lozano, 2021), it is worth considering whether *S. epidermidis* lysate could be utilised in the development of cosmetic agents for the prevention of skin aging. The present study warrants further investigation into the potential anti-aging effects of *S. epidermidis* lysate.

It has been widely reported that skin microbiota protects the skin from invasion by pathogens (Kwiecien et al., 2019). In the present study, *S. epidermidis* lysate induced an immune response, primarily through the upregulation of CXCL6 in the IL-17 signalling pathway. Interestingly, CXCL6 has been reported to have antibacterial and antifungal effects. Consequently, it is worth exploring whether *S. epidermidis* lysate could be utilised as a novel antibacterial agent (Linge et al., 2008). The present study provides a foundation for further investigation into the antibacterial effects of *S. epidermidis* lysate.

It is pertinent to consider the potential effects of lysates derived from various skin bacterial species on the healing processes of diverse dermatological conditions. For instance, lysate can be obtained from bacterial species that constitute the predominant bacterial groups identified on human skin, such as *Corynebacteria,* coagulase-negative *Staphylococcus,* and *Propionibacterium* (Grice et al., 2009) (Section 1.3.1), or from bacterial species associated with dysbiosis in DM (examples in section 1.4). Furthermore, lysate may be derived from common skin commensal fungal species, such as *Malassezia* spp. (Gao et al., 2010), or from primary fungal species that exhibit alterations in DM (examples in section 1.4). Furthermore, the present study suggests performing further investigation the synergistic effects of lysates prepared from different microbiota species on proliferation, migration and IL-17 signalling pathway in both fibroblasts and keratinocytes. As this will add valuable knowledge

7.2.2 Future of wound healing model for further lysate investigation

Wound healing is a multistage process that involves multiple cellular and molecular steps (Shevtsova, 2018). Thus, to investigate the effect of any healing agent on wound healing process, the experiment starts with in-vitro experiment focused on specific cellular process, followed by ex-vivo skin models and animal models (Masson-Meyers et al., 2020). The present study suggests further investigations of the effect of *S. epidermidis* lysate on wound healing by using either ex-vivo skin models (Yoon et al., 2019) or animal skin models (Sami et al., 2019).

The present study highlights that laboratory-based techniques are useful to understand the effect of healing agents on wounds. However, they are time-consuming. One might consider how, with the development of artificial intelligence (AI), AI can assist scientists in expediting the process of investigating the effect of an agent on wound healing process (Shevtsova, 2018). In the present study, bioinformatics tools were used to understand the mechanism of *S. epidermidis* lysate action on fibroblasts in low and high glucose concentrations. For instance, in the present study, employing bioinformatics tools allowed the identification of the IL-17 signalling pathway as one of the top 20 pathways enriched in fibroblasts exposed to *S. epidermidis* lysate. However, to our knowledge, there is no bioinformatic software that allows further investigation of how the alteration in this pathway will influence the overall wound healing process. Further research is required to design computer software that can predict the consequences of a laboratory finding on the overall wound healing process.

Moreover, the present study demonstrates that *S. epidermidis* lysate influences human skin fibroblast function in low and high glucose conditions. However, the composition of *S. epidermidis* lysate has not yet been fully investigated. Further studies are necessary to identify the components of *S. epidermidis* lysate and determine which component causes this effect. Current available methodologies may involve using mass spectrometry and chemical analysis to characterise the components of lysate (El-Chami et al., 2022). However, even if we characterise the components of lysate, it is challenging to understand which part of lysate is causing the observed results. It is also quite difficult and time-consuming to determine whether the observed effect is based on one individual component or is due to multiple actions by multiple molecules, i.e., proteins, antigens, or metabolites.

The development of computer software that can predict the function and interaction between each component of lysate and different molecular and cellular mechanisms might be beneficial. Network analysis, which can detect molecular alterations in healthy and disease conditions (Shevtsova, 2018), might be developed to understand how different *S. epidermidis* lysate components might interact with fibroblasts in low and high glucose concentrations. Examples of network analysis software include: PINA (protein interaction network analysis) database for protein–protein interactions (Wu et al., 2009); Intact-the European Molecular Biology Laboratory-European Bioinformatics Institute (EMBL-EBI) Protein Interaction DB (Kerrien et al., 2012); the BioGRID (biological general repository for interaction datasets) database for genetic and physical interactions (Stark et al., 2011).

7.2.3 Future of DM and DFU management

As discussed in section 1.2.2 of the present study, multiple investigations have indicated that disruptions in molecular and cellular pathways, including inflammatory response, proliferation, and migration of skin cells, are significant contributors to the development of diabetic foot ulcers (DFU). Despite this established knowledge, there is a relative paucity of treatment options targeting these molecular and cellular pathways in clinical practice (NICE, 2024b). As reviewed by Chakraborty et al. (2022), novel therapeutics targeting these molecular and cellular pathways could potentially enhance management protocols for the treatment of DFU in diabetes mellitus (DM). Consequently, this study proposes that further research is necessary to evaluate the safety and efficacy of *S. epidermidis* lysate, with recommendations for its potential integration into current guidelines for DFU management.

As mentioned in section 1.3.3., one of the primary challenges of DM is the inability to control hyperglycaemia using currently available medications, even with multiple medication prescriptions (Higgins et al., 2016). Failure to control hyperglycaemia results in various undesirable complications (Zheng et al., 2018). According to the NICE guideline, Metformin is utilised as first-line therapy to control hyperglycaemia in DM, followed by double and triple treatments in severe cases (NICE, 2024c). Several studies have reported that metformin exhibits antibacterial effects (Hegazy et al., 2021; Masadeh et al., 2021; Valadbeigi et al., 2023). Although some studies have reported dysbiosis of gut microbiota with metformin treatment leading to improvement in hyperglycaemia (Bauer et al., 2018; Sun et al., 2018), it remains unclear how skin microbiota is altered due to antidiabetic treatment, and how this alteration may contribute to poor wound healing in DM. The present study recommends conducting further research to elucidate how bacterial lysate can be used as a preventative agent to mitigate possible antidiabetic-induced dysbiosis in skin microbiota. This study hypothesises that bacterial lysate may serve as an effective option for preventing antidiabetic-induced dysbiosis in the skin microbiome. For instance, future research could investigate whether oral consumption of metformin exerts antibacterial effects on *S. epidermidis* in the skin, and how these effects influence the wound healing process in DM. Furthermore, it could examine whether applying *S. epidermidis* lysate is capable of counteracting metformin-induced dysbiosis and delayed wound healing.

7.3 Conclusion

S. epidermidis lysate significantly induces proliferation, migration, IL-17 signalling pathway activation, and CXCL6 secretion in fibroblasts cultured in hyperglycaemic glucose concentrations. These findings suggest that *S. epidermidis* lysate exhibits wound healing effects in DM. Further ex vivo, in vivo, and clinical studies are necessary to evaluate the efficacy and safety of using *S. epidermidis* lysate as a novel therapeutic agent for wound treatment in DM.

References

Adan, A., Kiraz, Y., & Baran, Y. (2016). Cell Proliferation and Cytotoxicity Assays. *Curr Pharm Biotechnol*, *17*(14), 1213-1221. https://doi.org/10.2174/1389201017666160808160513

Ali, M. K., Pearson-Stuttard, J., Selvin, E., & Gregg, E. W. (2022). Interpreting global trends in type 2 diabetes complications and mortality. *Diabetologia*, *65*(1), 3-13. https://doi.org/10.1007/s00125-021-05585-2

Alva-Murillo, N., Ochoa-Zarzosa, A., & López-Meza, J. E. (2012). Short chain fatty acids (propionic and hexanoic) decrease Staphylococcus aureus internalization into bovine mammary epithelial cells and modulate antimicrobial peptide expression. *Vet Microbiol*, *155*(2-4), 324-331. https://doi.org/10.1016/j.vetmic.2011.08.025

Andrade, T. A. M., Masson-Meyers, D. S., Caetano, G. F., Terra, V. A., Ovidio, P. P., Jordão-Júnior, A. A., & Frade, M. A. C. (2017). Skin changes in streptozotocin-induced diabetic rats. *Biochemical and Biophysical Research Communications*, *490*(4), 1154-1161. https://doi.org/https://doi.org/10.1016/j.bbrc.2017.06.166

Armstrong, D. G., Swerdlow, M. A., Armstrong, A. A., Conte, M. S., Padula, W. V., & Bus, S. A. (2020). Five year mortality and direct costs of care for people with diabetic foot complications are comparable to cancer. *J Foot Ankle Res*, *13*(1), 16. https://doi.org/10.1186/s13047-020-00383-2

Armstrong, D. G., Tan, T. W., Boulton, A. J. M., & Bus, S. A. (2023). Diabetic Foot Ulcers: A Review. *Jama*, *330*(1), 62-75. https://doi.org/10.1001/jama.2023.10578

Armstrong, D. G., Wrobel, J., & Robbins, J. M. (2007). Guest Editorial: are diabetes-related wounds and amputations worse than cancer? [https://doi.org/10.1111/j.1742-481X.2007.00392.x]. *International wound journal*, *4*(4), 286-287. https://doi.org/https://doi.org/10.1111/j.1742-481X.2007.00392.x

Bandyk, D. F. (2018). The diabetic foot: Pathophysiology, evaluation, and treatment. *Semin Vasc Surg*, *31*(2-4), 43-48. https://doi.org/10.1053/j.semvascsurg.2019.02.001

Bansal, E., Garg, A., Bhatia, S., Attri, A. K., & Chander, J. (2008). Spectrum of microbial flora in diabetic foot ulcers. *Indian J Pathol Microbiol*, *51*(2), 204-208. https://doi.org/10.4103/0377-4929.41685

Bauer, P. V., Duca, F. A., Waise, T. M. Z., Rasmussen, B. A., Abraham, M. A., Dranse, H. J., Puri, A., O'Brien, C. A., & Lam, T. K. T. (2018). Metformin Alters Upper Small Intestinal Microbiota that Impact a Glucose-SGLT1-Sensing Glucoregulatory Pathway. *Cell Metab*, *27*(1), 101-117.e105. https://doi.org/10.1016/j.cmet.2017.09.019

Bermudez, D. M., Herdrich, B. J., Xu, J., Lind, R., Beason, D. P., Mitchell, M. E., Soslowsky, L. J., & Liechty, K. W. (2011). Impaired biomechanical properties of diabetic skin implications in pathogenesis of diabetic wound complications. *Am J Pathol*, *178*(5), 2215-2223. https://doi.org/10.1016/j.ajpath.2011.01.015

Bertrand, R. L. (2019). Lag Phase Is a Dynamic, Organized, Adaptive, and Evolvable Period That Prepares Bacteria for Cell Division. *J Bacteriol*, *201*(7). https://doi.org/10.1128/jb.00697-18

Biorender. (2020). *Create Professional Scientific Figures in Minutes* https://biorender.com/

Biorender. (2024). *Create Professional Scientific Figures in Minutes* https://biorender.com/

Bitschar, K., Staudenmaier, L., Klink, L., Focken, J., Sauer, B., Fehrenbacher, B., Herster, F., Bittner, Z., Bleul, L., Schaller, M., Wolz, C., Weber, A. N. R., Peschel, A., & Schittek, B. (2020). Staphylococcus aureus Skin Colonization Is Enhanced by the Interaction of Neutrophil Extracellular Traps with Keratinocytes. *J Invest Dermatol*, *140*(5), 1054-1065.e1054. https://doi.org/10.1016/j.jid.2019.10.017

Blicharz, L., Rudnicka, L., Czuwara, J., Waśkiel-Burnat, A., Goldust, M., Olszewska, M., & Samochocki, Z. (2021). The Influence of Microbiome Dysbiosis and Bacterial Biofilms on Epidermal Barrier Function in Atopic Dermatitis-An Update. *Int J Mol Sci*, *22*(16). https://doi.org/10.3390/ijms22168403

BMKGENE. (2023). Biomarker Technologies (BMK)

https://doi.org/https://www.bmkgene.com/

Boumba, V., Ziavrou, K., & Vujuk, T. (2008). Biochemical pathways generating post-mortem volatile compounds co-detected during forensic ethanol analyses. *Forensic science international*, *174*, 133-151. https://doi.org/10.1016/j.forsciint.2007.03.018

Boutari, C., & Mantzoros, C. S. (2022). A 2022 update on the epidemiology of obesity and a call to action: as its twin COVID-19 pandemic appears to be receding, the obesity and dysmetabolism pandemic continues to rage on. *Metabolism*, *133*, 155217. https://doi.org/10.1016/j.metabol.2022.155217

Boxberger, M., Cenizo, V., Cassir, N., & La Scola, B. (2021). Challenges in exploring and manipulating the human skin microbiome. *Microbiome*, *9*(1), 125. https://doi.org/10.1186/s40168-021-01062-5

Braido, F., Melioli, G., Candoli, P., Cavalot, A., Di Gioacchino, M., Ferrero, V., Incorvaia, C., Mereu, C., Ridolo, E., Rolla, G., Rossi, O., Savi, E., Tubino, L., Reggiardo, G., Baiardini, I., di Marco, E., Rinaldi, G., Canonica, G. W., Accorsi, C., . . . Sclifò, F. (2014). The bacterial lysate Lantigen B reduces the number of acute episodes in patients with recurrent infections of the respiratory tract: the results of a double blind, placebo controlled, multicenter clinical trial. *Immunol Lett*, *162*(2 Pt B), 185-193. https://doi.org/10.1016/j.imlet.2014.10.026

Braido, F., Melioli, G., Cazzola, M., Fabbri, L., Blasi, F., Moretta, L., & Canonica, G. W. (2015). Sub-lingual administration of a polyvalent mechanical bacterial lysate (PMBL) in patients with moderate, severe, or very severe chronic obstructive pulmonary disease (COPD) according to the GOLD spirometric classification: A multicentre, double-blind, randomised, controlled, phase IV study (AIACE study: Advanced Immunological Approach in COPD Exacerbation). *Pulm Pharmacol Ther*, *33*, 75-80. https://doi.org/10.1016/j.pupt.2015.03.006

Braido, F., Schenone, G., Pallestrini, E., Reggiardo, G., Cangemi, G., Canonica, G. W., & Melioli, G. (2011). The relationship between mucosal immunoresponse and clinical outcome in patients with recurrent upper respiratory tract infections treated with a mechanical bacterial lysate. *J Biol Regul Homeost Agents*, *25*(3), 477-485.

Brandi, J., Cheri, S., Manfredi, M., Di Carlo, C., Vita Vanella, V., Federici, F., Bombiero, E., Bazaj, A., Rizzi, E., Manna, L., Cornaglia, G., Marini, U., Valenti, M. T., Marengo, E., & Cecconi, D. (2020). Exploring the wound healing, anti-inflammatory, anti-pathogenic and proteomic effects of lactic acid bacteria on keratinocytes. *Scientific Reports*, *10*(1), 11572. https://doi.org/10.1038/s41598-020-68483-4

Brandwein, M., Katz, I., Katz, A., & Kohen, R. (2019). Beyond the gut: Skin microbiome compositional changes are associated with BMI. *Human Microbiome Journal*, *13*, 100063. https://doi.org/https://doi.org/10.1016/j.humic.2019.100063

Brown, G. K. (2000). Glucose transporters: structure, function and consequences of deficiency. *J Inherit Metab Dis*, *23*(3), 237-246. https://doi.org/10.1023/a:1005632012591

Brown, M. M., & Horswill, A. R. (2020). Staphylococcus epidermidis-Skin friend or foe? *PLoS Pathog*, *16*(11), e1009026. https://doi.org/10.1371/journal.ppat.1009026

Bryant, N. J., & Gould, G. W. (2020). Insulin stimulated GLUT4 translocation - Size is not everything! *Curr Opin Cell Biol*, *65*, 28-34. https://doi.org/10.1016/j.ceb.2020.02.006

Byrd, A. L., Belkaid, Y., & Segre, J. A. (2018). The human skin microbiome. *Nature Reviews Microbiology*, *16*(3), 143-155. https://doi.org/10.1038/nrmicro.2017.157

Cabrera, O., Berman, D. M., Kenyon, N. S., Ricordi, C., Berggren, P. O., & Caicedo, A. (2006). The unique cytoarchitecture of human pancreatic islets has implications for islet cell function. *Proc Natl Acad Sci U S A*, *103*(7), 2334-2339. https://doi.org/10.1073/pnas.0510790103

Callewaert, C., Kerckhof, F.-M., Granitsiotis, M., Van Gele, M., Van de Wiele, T., & Boon, N. (2013). Characterization of Staphylococcus and Corynebacterium Clusters in the Human Axillary Region. *PLOS ONE*, *8*, e70538. https://doi.org/10.1371/journal.pone.0070538

Cappiello, F., Casciaro, B., & Mangoni, M. L. (2018). A Novel In Vitro Wound Healing Assay to Evaluate Cell Migration. *J Vis Exp*(133). https://doi.org/10.3791/56825

Cazzola, M., Anapurapu, S., & Page, C. P. (2012). Polyvalent mechanical bacterial lysate for the prevention of recurrent respiratory infections: A meta-analysis. *Pulmonary Pharmacology & Therapeutics*, *25*(1), 62-68. https://doi.org/https://doi.org/10.1016/j.pupt.2011.11.002

Cazzola, M., Capuano, A., Rogliani, P., & Matera, M. G. (2012). Bacterial lysates as a potentially effective approach in preventing acute exacerbation of COPD. *Curr Opin Pharmacol*, *12*(3), 300-308. https://doi.org/10.1016/j.coph.2012.01.019

Chabi, R., & Momtaz, H. (2019). Virulence factors and antibiotic resistance properties of the Staphylococcus epidermidis strains isolated from hospital infections in Ahvaz, Iran. *Tropical Medicine and Health*, *47*(1), 56. https://doi.org/10.1186/s41182-019-0180-7

Chen, X. F., Lin, W. D., Lu, S. L., Xie, T., Ge, K., Shi, Y. Q., Zou, J. J., Liu, Z. M., & Liao, W. Q. (2010). Mechanistic study of endogenous skin lesions in diabetic rats. *Exp Dermatol*, *19*(12), 1088-1095. https://doi.org/10.1111/j.1600-0625.2010.01137.x

Chen, Y. E., Fischbach, M. A., & Belkaid, Y. (2018). Skin microbiota-host interactions. *Nature*, *553*(7689), 427-436. https://doi.org/10.1038/nature25177

Cheon, C. K. (2018). Understanding of type 1 diabetes mellitus: what we know and where we go. *Korean J Pediatr*, *61*(10), 307-314. https://doi.org/10.3345/kjp.2018.06870

Cheung, G. Y. C., Bae, J. S., & Otto, M. (2021). Pathogenicity and virulence of Staphylococcus aureus. *Virulence*, *12*(1), 547-569. https://doi.org/10.1080/21505594.2021.1878688

Cho, J. S., Pietras, E. M., Garcia, N. C., Ramos, R. I., Farzam, D. M., Monroe, H. R., Magorien, J. E., Blauvelt, A., Kolls, J. K., Cheung, A. L., Cheng, G., Modlin, R. L., & Miller, L. S. (2010). IL-17 is essential for host defense against cutaneous Staphylococcus aureus infection in mice. *J Clin Invest*, *120*(5), 1762-1773. https://doi.org/10.1172/jci40891

Cialdai, F., Risaliti, C., & Monici, M. (2022). Role of fibroblasts in wound healing and tissue remodeling on Earth and in space. *Front Bioeng Biotechnol*, *10*, 958381. https://doi.org/10.3389/fbioe.2022.958381

Clark, R. A. (2001). Fibrin and wound healing. *Ann N Y Acad Sci*, *936*, 355-367. https://doi.org/10.1111/j.1749-6632.2001.tb03522.x

Cogen, A. L., Yamasaki, K., Muto, J., Sanchez, K. M., Crotty Alexander, L., Tanios, J., Lai, Y., Kim, J. E., Nizet, V., & Gallo, R. L. (2010). Staphylococcus epidermidis antimicrobial delta-toxin (phenol-soluble modulin-gamma) cooperates with host antimicrobial peptides to kill group A Streptococcus. *PLoS One*, *5*(1), e8557. https://doi.org/10.1371/journal.pone.0008557

Colgan, A. M., Cameron, A. D., & Kröger, C. (2017). If it transcribes, we can sequence it: mining the complexities of host-pathogen-environment interactions using RNA-seq. *Curr Opin Microbiol*, *36*, 37-46. https://doi.org/10.1016/j.mib.2017.01.010

Constantinides, M. G., Link, V. M., Tamoutounour, S., Wong, A. C., Perez-Chaparro, P. J., Han, S. J., Chen, Y. E., Li, K., Farhat, S., Weckel, A., Krishnamurthy, S. R., Vujkovic-Cvijin, I., Linehan, J. L., Bouladoux, N., Merrill, E. D., Roy, S., Cua, D. J., Adams, E. J., Bhandoola, A., . . . Belkaid, Y. (2019). MAIT cells are imprinted by the microbiota in early life and promote tissue repair. *Science*, *366*(6464). https://doi.org/10.1126/science.aax6624

Costello, E. K., Lauber, C. L., Hamady, M., Fierer, N., Gordon, J. I., & Knight, R. (2009). Bacterial community variation in human body habitats across space and time. *Science*, *326*(5960), 1694-1697. https://doi.org/10.1126/science.1177486

Cuevas, D. A., & Edwards, R. A. (2017). PMAnalyzer: a new web interface for bacterial growth curve analysis. *Bioinformatics*, *33*(12), 1905-1906. https://doi.org/10.1093/bioinformatics/btx084

Dai, C.-L., Yang, H.-X., Liu, Q.-P., Rahman, K., & Zhang, H. (2023). CXCL6: A potential therapeutic target for inflammation and cancer. *Clinical and Experimental Medicine*, *23*(8), 4413-4427. https://doi.org/10.1007/s10238-023-01152-8

Dănilă, A. I., Ghenciu, L. A., Stoicescu, E. R., Bolintineanu, S. L., Iacob, R., Săndesc, M. A., & Faur, A. C. (2024). Aldose Reductase as a Key Target in the Prevention and Treatment of Diabetic

Retinopathy: A Comprehensive Review. *Biomedicines*, *12*(4). https://doi.org/10.3390/biomedicines12040747

Dasari, N., Jiang, A., Skochdopole, A., Chung, J., Reece, E. M., Vorstenbosch, J., & Winocour, S. (2021). Updates in Diabetic Wound Healing, Inflammation, and Scarring. *Semin Plast Surg*, *35*(3), 153-158. https://doi.org/10.1055/s-0041-1731460

David, P., Singh, S., & Ankar, R. (2023). A Comprehensive Overview of Skin Complications in Diabetes and Their Prevention. *Cureus*, *15*(5), e38961. https://doi.org/10.7759/cureus.38961

Demirseren, D., Emre, S., Akoglu, G., Arpaci, D., Arman, A., Metin, A., & Cakir, B. (2013). Relationship Between Skin Diseases and Extracutaneous Complications of Diabetes Mellitus: Clinical Analysis of 750 Patients. *American journal of clinical dermatology*, *15*. https://doi.org/10.1007/s40257-013-0048-2

Demirseren, D. D., Emre, S., Akoglu, G., Arpacı, D., Arman, A., Metin, A., & Cakır, B. (2014). Relationship between skin diseases and extracutaneous complications of diabetes mellitus: clinical analysis of 750 patients. *Am J Clin Dermatol*, *15*(1), 65-70. https://doi.org/10.1007/s40257-013-0048-2

Dharmadi, Y., Murarka, A., & Gonzalez, R. (2006). Anaerobic fermentation of glycerol by Escherichia coli: a new platform for metabolic engineering. *Biotechnol Bioeng*, *94*(5), 821-829. https://doi.org/10.1002/bit.21025

Diagenode. (2021). *Bioruptor® Plus sonication device*.

Didovyk, A., Tonooka, T., Tsimring, L., & Hasty, J. (2017). Rapid and Scalable Preparation of Bacterial Lysates for Cell-Free Gene Expression. *ACS Synth Biol*, *6*(12), 2198-2208. https://doi.org/10.1021/acssynbio.7b00253

Diegelmann, R. F., & Evans, M. C. (2004). Wound healing: an overview of acute, fibrotic and delayed healing. *Front Biosci*, *9*, 283-289. https://doi.org/10.2741/1184

Dore, M. P., Bibbò, S., Fresi, G., Bassotti, G., & Pes, G. M. (2019). Side Effects Associated with Probiotic Use in Adult Patients with Inflammatory Bowel Disease: A Systematic Review and Meta-Analysis of Randomized Controlled Trials. *Nutrients*, *11*(12). https://doi.org/10.3390/nu11122913

Duckney, P., Wong, H. K., Serrano, J., Yaradou, D., Oddos, T., & Stamatas, G. N. (2013). The role of the skin barrier in modulating the effects of common skin microbial species on the inflammation, differentiation and proliferation status of epidermal keratinocytes. *BMC Res Notes*, *6*, 474. https://doi.org/10.1186/1756-0500-6-474

El-Chami, C., Choudhury, R., Mohammedsaeed, W., McBain, A. J., Kainulainen, V., Lebeer, S., Satokari, R., & O'Neill, C. A. (2022). Multiple Proteins of Lacticaseibacillus rhamnosus GG Are Involved in the Protection of Keratinocytes From the Toxic Effects of Staphylococcus aureus. *Front Microbiol*, *13*, 875542. https://doi.org/10.3389/fmicb.2022.875542

Esposito, S., Soto-Martinez, M. E., Feleszko, W., Jones, M. H., Shen, K. L., & Schaad, U. B. (2018). Nonspecific immunomodulators for recurrent respiratory tract infections, wheezing and asthma in children: a systematic review of mechanistic and clinical evidence. *Curr Opin Allergy Clin Immunol*, *18*(3), 198-209. https://doi.org/10.1097/aci.0000000000000433

Falanga. (2005). Wound healing and its impairment in the diabetic foot. *The Lancet*, *366*(9498), 1736-1743. https://doi.org/https://doi.org/10.1016/S0140-6736(05)67700-8

Findley, K., Oh, J., Yang, J., Conlan, S., Deming, C., Meyer, J. A., Schoenfeld, D., Nomicos, E., Park, M., Becker, J., Benjamin, B., Blakesley, R., Bouffard, G., Brooks, S., Coleman, H., Dekhtyar, M., Gregory, M., Guan, X., Gupta, J., . . . Program, N. I. H. I. S. C. C. S. (2013). Topographic diversity of fungal and bacterial communities in human skin. *Nature*, *498*(7454), 367-370. https://doi.org/10.1038/nature12171

Fisher, E. L., Otto, M., & Cheung, G. Y. C. (2018). Basis of Virulence in Enterotoxin-Mediated Staphylococcal Food Poisoning. *Front Microbiol*, *9*, 436. https://doi.org/10.3389/fmicb.2018.00436

Fleige, S., & Pfaffl, M. W. (2006). RNA integrity and the effect on the real-time qRT-PCR performance. *Mol Aspects Med*, *27*(2-3), 126-139. https://doi.org/10.1016/j.mam.2005.12.003

Fletcher, B., Gulanick, M., & Lamendola, C. (2002). Risk factors for type 2 diabetes mellitus. *J Cardiovasc Nurs*, *16*(2), 17-23. https://doi.org/10.1097/00005082-200201000-00003

Fluhr, J. W., Darlenski, R., & Surber, C. (2008). Glycerol and the skin: holistic approach to its origin and functions. *Br J Dermatol*, *159*(1), 23-34. https://doi.org/10.1111/j.1365-2133.2008.08643.x

Furukawa, M., Yamada, K., Kurosawa, M., Shikama, Y., Wang, J., Watanabe, M., Kanekura, T., & Matsushita, K. (2020). High concentration of glucose induces filaggrin-1 expression through AP-1 in skin keratinocytes. *J Dermatol Sci*, *98*(2), 137-140. https://doi.org/10.1016/j.jdermsci.2020.04.002

Gardiner, M., Vicaretti, M., Sparks, J., Bansal, S., Bush, S., Liu, M., Darling, A., Harry, E., & Burke, C. (2017). A longitudinal study of the diabetic skin and wound microbiome. *PeerJ*, *5*, e3543. https://doi.org/10.7717/peerj.3543

Gardner, S. E., Hillis, S. L., Heilmann, K., Segre, J. A., & Grice, E. A. (2013). The neuropathic diabetic foot ulcer microbiome is associated with clinical factors. *Diabetes*, *62*(3), 923-930. https://doi.org/10.2337/db12-0771

Gaudet, P., Logie, C., Lovering, R. C., Kuiper, M., Lægreid, A., & Thomas, P. D. (2021). Gene Ontology representation for transcription factor functions. *Biochimica et Biophysica Acta (BBA) - Gene Regulatory Mechanisms*, *1864*(11), 194752. https://doi.org/https://doi.org/10.1016/j.bbagrm.2021.194752

Gebrayel, P., Nicco, C., Al Khodor, S., Bilinski, J., Caselli, E., Comelli, E. M., Egert, M., Giaroni, C., Karpinski, T. M., Loniewski, I., Mulak, A., Reygner, J., Samczuk, P., Serino, M., Sikora, M., Terranegra, A., Ufnal, M., Villeger, R., Pichon, C., . . . Edeas, M. (2022). Microbiota medicine: towards clinical revolution. *J Transl Med*, *20*(1), 111. https://doi.org/10.1186/s12967-022-03296-9

Gethin, G. (2007). The significance of surface pH in chronic wounds. *Wounds UK*, *3*.

Gilbert, J. A., Blaser, M. J., Caporaso, J. G., Jansson, J. K., Lynch, S. V., & Knight, R. (2018). Current understanding of the human microbiome. *Nat Med*, *24*(4), 392-400. https://doi.org/10.1038/nm.4517

Gostynska, N., Pannella, M., Rocco, M. L., Giardino, L., Aloe, L., & Calzà, L. (2020). The pleiotropic molecule NGF regulates the in vitro properties of fibroblasts, keratinocytes, and endothelial cells: implications for wound healing. *Am J Physiol Cell Physiol*, *318*(2), C360-c371. https://doi.org/10.1152/ajpcell.00180.2019

Grice, E. A., Kong, H. H., Conlan, S., Deming, C. B., Davis, J., Young, A. C., Bouffard, G. G., Blakesley, R. W., Murray, P. R., Green, E. D., Turner, M. L., & Segre, J. A. (2009). Topographical and temporal diversity of the human skin microbiome. *Science*, *324*(5931), 1190-1192. https://doi.org/10.1126/science.1171700

Guak, H., & Krawczyk, C. M. (2020). Implications of cellular metabolism for immune cell migration. *Immunology*, *161*(3), 200-208. https://doi.org/10.1111/imm.13260

Gupta, A., Murarka, A., Campbell, P., & Gonzalez, R. (2009). Anaerobic fermentation of glycerol in Paenibacillus macerans: metabolic pathways and environmental determinants. *Appl Environ Microbiol*, *75*(18), 5871-5883. https://doi.org/10.1128/aem.01246-09

Gupta, R., Popli, T., Ranchal, P., Khosla, J., Aronow, W. S., Frishman, W. H., & El Khoury, M. Y. (2021). Corynebacterium Jeikeium Endocarditis: A Review of the Literature. *Cardiol Rev*, *29*(5), 259-262. https://doi.org/10.1097/crd.0000000000000355

Guthrie, R. A., & Guthrie, D. W. (2004). Pathophysiology of Diabetes Mellitus. *Critical Care Nursing Quarterly*, *27*(2). https://journals.lww.com/ccnq/fulltext/2004/04000/pathophysiology_of_diabetes_mellitus.3.aspx

Haller, H. L., Sander, F., Popp, D., Rapp, M., Hartmann, B., Demircan, M., Nischwitz, S. P., & Kamolz, L. P. (2021). Oxygen, pH, Lactate, and Metabolism-How Old Knowledge and New Insights Might

Be Combined for New Wound Treatment. *Medicina (Kaunas)*, *57*(11). https://doi.org/10.3390/medicina57111190

Halper, J., Leshin, L. S., Lewis, S. J., & Li, W. I. (2003). Wound healing and angiogenic properties of supernatants from Lactobacillus cultures. *Exp Biol Med (Maywood)*, *228*(11), 1329-1337. https://doi.org/10.1177/153537020322801111

Hannigan, G. D., Meisel, J. S., Tyldsley, A. S., Zheng, Q., Hodkinson, B. P., SanMiguel, A. J., Minot, S., Bushman, F. D., & Grice, E. A. (2015). The human skin double-stranded DNA virome: topographical and temporal diversity, genetic enrichment, and dynamic associations with the host microbiome. *mBio*, *6*(5), e01578-01515. https://doi.org/10.1128/mBio.01578-15

Hart, J. (2002). Inflammation. 1: Its role in the healing of acute wounds. *J Wound Care*, *11*(6), 205-209. https://doi.org/10.12968/jowc.2002.11.6.26411

Hegazy, W. A. H., Rajab, A. A. H., Abu Lila, A. S., & Abbas, H. A. (2021). Anti-diabetics and antimicrobials: Harmony of mutual interplay. *World J Diabetes*, *12*(11), 1832-1855. https://doi.org/10.4239/wjd.v12.i11.1832

Hemarajata, P., & Versalovic, J. (2013). Effects of probiotics on gut microbiota: mechanisms of intestinal immunomodulation and neuromodulation. *Therap Adv Gastroenterol*, *6*(1), 39-51. https://doi.org/10.1177/1756283x12459294

Higgins, V., Piercy, J., Roughley, A., Milligan, G., Leith, A., Siddall, J., & Benford, M. (2016). Trends in medication use in patients with type 2 diabetes mellitus: a long-term view of real-world treatment between 2000 and 2015. *Diabetes Metab Syndr Obes*, *9*, 371-380. https://doi.org/10.2147/dmso.S120101

Hodille, E., Cuerq, C., Badiou, C., Bienvenu, F., Steghens, J. P., Cartier, R., Bes, M., Tristan, A., Plesa, A., Le, V. T., Diep, B. A., Lina, G., & Dumitrescu, O. (2016). Delta Hemolysin and Phenol-Soluble Modulins, but Not Alpha Hemolysin or Panton-Valentine Leukocidin, Induce Mast Cell Activation. *Front Cell Infect Microbiol*, *6*, 180. https://doi.org/10.3389/fcimb.2016.00180

Holmes, C., Wrobel, J. S., Maceachern, M. P., & Boles, B. R. (2013). Collagen-based wound dressings for the treatment of diabetes-related foot ulcers: a systematic review. *Diabetes Metab Syndr Obes*, *6*, 17-29. https://doi.org/10.2147/dmso.S36024

Horn, J., Stelzner, K., Rudel, T., & Fraunholz, M. (2018). Inside job: Staphylococcus aureus host-pathogen interactions. *International Journal of Medical Microbiology*, *308*(6), 607-624. https://doi.org/https://doi.org/10.1016/j.ijmm.2017.11.009

Hrestak, D., Matijašić, M., Čipčić Paljetak, H., Ledić Drvar, D., Ljubojević Hadžavdić, S., & Perić, M. (2022). Skin Microbiota in Atopic Dermatitis. *Int J Mol Sci*, *23*(7). https://doi.org/10.3390/ijms23073503

Ibuki, A., Akase, T., Nagase, T., Minematsu, T., Nakagami, G., Horii, M., Sagara, H., Komeda, T., Kobayashi, M., Shimada, T., Aburada, M., Yoshimura, K., Sugama, J., & Sanada, H. (2012). Skin fragility in obese diabetic mice: possible involvement of elevated oxidative stress and upregulation of matrix metalloproteinases. *Exp Dermatol*, *21*(3), 178-183. https://doi.org/10.1111/j.1600-0625.2011.01409.x

IDF. (2024). *IDF* https://www.diabetesatlas.org/

Ifantidou, A. M., Diamantidis, M. D., Tseliki, G., Angelou, A. S., Christidou, P., Papa, A., & Pentilas, D. (2010). Corynebacterium jeikeium bacteremia in a hemodialyzed patient. *International Journal of Infectious Diseases*, *14*, e265-e268. https://doi.org/https://doi.org/10.1016/j.ijid.2009.11.008

Inoshima, I., Inoshima, N., Wilke, G. A., Powers, M. E., Frank, K. M., Wang, Y., & Bubeck Wardenburg, J. (2011). A Staphylococcus aureus pore-forming toxin subverts the activity of ADAM10 to cause lethal infection in mice. *Nat Med*, *17*(10), 1310-1314. https://doi.org/10.1038/nm.2451

Inoshima, N., Wang, Y., & Bubeck Wardenburg, J. (2012). Genetic requirement for ADAM10 in severe Staphylococcus aureus skin infection. *J Invest Dermatol*, *132*(5), 1513-1516. https://doi.org/10.1038/jid.2011.462

Jiang, S., Ito-Hirano, R., Shen, T. N., Fujimura, S., Mizuno, H., & Tanaka, R. (2022). Effect of MNCQQ Cells on Migration of Human Dermal Fibroblast in Diabetic Condition. *Biomedicines*, *10*(10). https://doi.org/10.3390/biomedicines10102544

Jneid, J., Cassir, N., Schuldiner, S., Jourdan, N., Sotto, A., Lavigne, J. P., & La Scola, B. (2018). Exploring the Microbiota of Diabetic Foot Infections With Culturomics. *Front Cell Infect Microbiol*, *8*, 282. https://doi.org/10.3389/fcimb.2018.00282

Johnson, T. R., Gómez, B. I., McIntyre, M. K., Dubick, M. A., Christy, R. J., Nicholson, S. E., & Burmeister, D. M. (2018). The Cutaneous Microbiome and Wounds: New Molecular Targets to Promote Wound Healing. *International Journal of Molecular Sciences*, *19*(9).

Jung, Y.-O., Jeong, H., Cho, Y., Lee, E.-O., Jang, H.-W., Kim, J., Nam, K. T., & Lim, K.-M. (2019). Lysates of a Probiotic, Lactobacillus rhamnosus, Can Improve Skin Barrier Function in a Reconstructed Human Epidermis Model. *International Journal of Molecular Sciences*, *20*(17).

Justus, C. R., Marie, M. A., Sanderlin, E. J., & Yang, L. V. (2023). Transwell In Vitro Cell Migration and Invasion Assays. *Methods Mol Biol*, *2644*, 349-359. https://doi.org/10.1007/978-1-0716-3052-5_22

Kaewchomphunuch, T., Charoenpichitnunt, T., Thongbaiyai, V., Ngamwongsatit, N., & Kaeoket, K. (2022). Cell-free culture supernatants of Lactobacillus spp. and Pediococcus spp. inhibit growth of pathogenic Escherichia coli isolated from pigs in Thailand. *BMC Veterinary Research*, *18*(1), 60. https://doi.org/10.1186/s12917-022-03140-8

Kalan, L., Loesche, M., Hodkinson, B., Heilmann, K., Ruthel, G., Gardner, S., & Grice, E. (2016). Redefining the Chronic-Wound Microbiome: Fungal Communities Are Prevalent, Dynamic, and Associated with Delayed Healing. *mBio*, *7*. https://doi.org/10.1128/mBio.01058-16

Kalan, L. R., Meisel, J. S., Loesche, M. A., Horwinski, J., Soaita, I., Chen, X., Uberoi, A., Gardner, S. E., & Grice, E. A. (2019). Strain- and Species-Level Variation in the Microbiome of Diabetic Wounds Is Associated with Clinical Outcomes and Therapeutic Efficacy. *Cell Host & Microbe*, *25*(5), 641-655.e645. https://doi.org/https://doi.org/10.1016/j.chom.2019.03.006

Kanehisa, M., Furumichi, M., Tanabe, M., Sato, Y., & Morishima, K. (2017). KEGG: new perspectives on genomes, pathways, diseases and drugs. *Nucleic Acids Res*, *45*(D1), D353-d361. https://doi.org/10.1093/nar/gkw1092

Kao, M. S., Huang, S., Chang, W. L., Hsieh, M. F., Huang, C. J., Gallo, R. L., & Huang, C. M. (2017). Microbiome precision editing: Using PEG as a selective fermentation initiator against methicillin-resistant Staphylococcus aureus. *Biotechnol J*, *12*(4). https://doi.org/10.1002/biot.201600399

Kerrien, S., Aranda, B., Breuza, L., Bridge, A., Broackes-Carter, F., Chen, C., Duesbury, M., Dumousseau, M., Feuermann, M., Hinz, U., Jandrasits, C., Jimenez, R. C., Khadake, J., Mahadevan, U., Masson, P., Pedruzzi, I., Pfeiffenberger, E., Porras, P., Raghunath, A., . . . Hermjakob, H. (2012). The IntAct molecular interaction database in 2012. *Nucleic Acids Res*, *40*(Database issue), D841-846. https://doi.org/10.1093/nar/gkr1088

Keshava, R., & Gope, R. (2015). Sodium Butyrate Plus EGF and PDGF-BB Aids Cutaneous Wound Healing in Diabetic Mice. *Advances in Biology*, *2015*(1), 527231. https://doi.org/https://doi.org/10.1155/2015/527231

Khmaladze, I., Butler, É., Fabre, S., & Gillbro, J. M. (2019). Lactobacillus reuteri DSM 17938-A comparative study on the effect of probiotics and lysates on human skin. *Exp Dermatol*, *28*(7), 822-828. https://doi.org/10.1111/exd.13950

Kidman, K. (2008). Tissue repair and regeneration: The effects of diabetes on wound healing.

Kim, J.-H., Yoon, N. Y., Kim, D. H., Jung, M., Jun, M., Park, H.-Y., Chung, C. H., Lee, K., Kim, S., Park, C. S., Liu, K.-H., & Choi, E. H. (2018). Impaired permeability and antimicrobial barriers in type 2 diabetes skin are linked to increased serum levels of advanced glycation end-product. *Experimental Dermatology*, *27*(8), 815-823. https://doi.org/https://doi.org/10.1111/exd.13466

Kim, J. (2023). The pathophysiology of diabetic foot: a narrative review. *J Yeungnam Med Sci*, *40*(4), 328-334. https://doi.org/10.12701/jyms.2023.00731

Kivistö, A., Santala, V., & Karp, M. (2010). Hydrogen production from glycerol using halophilic fermentative bacteria. *Bioresource Technology*, *101*(22), 8671-8677. https://doi.org/https://doi.org/10.1016/j.biortech.2010.06.066

Konieczny, P., Xing, Y., Sidhu, I., Subudhi, I., Mansfield, K. P., Hsieh, B., Biancur, D. E., Larsen, S. B., Cammer, M., Li, D., Landén, N. X., Loomis, C., Heguy, A., Tikhonova, A. N., Tsirigos, A., & Naik, S. (2022). Interleukin-17 governs hypoxic adaptation of injured epithelium. *Science*, *377*(6602), eabg9302. https://doi.org/10.1126/science.abg9302

Kovaříková, P., Michalova, E., Knopfová, L., & Bouchal, P. (2014). [Methods for studying tumor cell migration and invasiveness]. *Klin Onkol*, *27 Suppl 1*, S22-27. https://doi.org/10.14735/amko20141s22 (Metody studia buněčné migrace a invazivity nádorových buněk.)

Krishna, S., & Miller, L. S. (2012). Innate and adaptive immune responses against Staphylococcus aureus skin infections. *Semin Immunopathol*, *34*(2), 261-280. https://doi.org/10.1007/s00281-011-0292-6

Krisp, C., Jacobsen, F., McKay, M. J., Molloy, M. P., Steinstraesser, L., & Wolters, D. A. (2013). Proteome analysis reveals antiangiogenic environments in chronic wounds of diabetes mellitus type 2 patients. *PROTEOMICS*, *13*(17), 2670-2681. https://doi.org/https://doi.org/10.1002/pmic.201200502

Krizanova, O., Penesova, A., Sokol, J., Hokynkova, A., Samadian, A., & Babula, P. (2022). Signaling pathways in cutaneous wound healing. *Front Physiol*, *13*, 1030851. https://doi.org/10.3389/fphys.2022.1030851

Kumakura, D., Yamaguchi, R., Hara, A., & Nakaoka, S. (2023). Disentangling the growth curve of microbial culture. *Journal of Theoretical Biology*, *573*, 111597. https://doi.org/https://doi.org/10.1016/j.jtbi.2023.111597

Kurkela, O., Forma, L., Ilanne-Parikka, P., Nevalainen, J., & Rissanen, P. (2021). Association of diabetes type and chronic diabetes complications with early exit from the labour force: register-based study of people with diabetes in Finland. *Diabetologia*, *64*(4), 795-804. https://doi.org/10.1007/s00125-020-05363-6

Kwiecien, K., Zegar, A., Jung, J., Brzoza, P., Kwitniewski, M., Godlewska, U., Grygier, B., Kwiecinska, P., Morytko, A., & Cichy, J. (2019). Architecture of antimicrobial skin defense. *Cytokine & Growth Factor Reviews*, *49*, 70-84. https://doi.org/https://doi.org/10.1016/j.cytogfr.2019.08.001

Lai, Y., Di Nardo, A., Nakatsuji, T., Leichtle, A., Yang, Y., Cogen, A. L., Wu, Z.-R., Hooper, L. V., Schmidt, R. R., von Aulock, S., Radek, K. A., Huang, C.-M., Ryan, A. F., & Gallo, R. L. (2009). Commensal bacteria regulate Toll-like receptor 3–dependent inflammation after skin injury. *Nature Medicine*, *15*(12), 1377-1382. https://doi.org/10.1038/nm.2062

Lan, C. C., Liu, I. H., Fang, A. H., Wen, C. H., & Wu, C. S. (2008). Hyperglycaemic conditions decrease cultured keratinocyte mobility: implications for impaired wound healing in patients with diabetes. *Br J Dermatol*, *159*(5), 1103-1115. https://doi.org/10.1111/j.1365-2133.2008.08789.x

Lan, L., Fang, Wen, Wu, . (2008). Hyperglycaemic conditions decrease cultured keratinocyte mobility: implications for impaired wound healing in patients with diabetes. *British Journal of Dermatology*, *159*(5), 1103-1115. https://doi.org/10.1111/j.1365-2133.2008.08789.x

Lan, W., Kuo, Huang, Chen, . (2009). Hyperglycaemic conditions hamper keratinocyte locomotion via sequential inhibition of distinct pathways: new insights on poor wound closure in patients with diabetes. *Br J Dermatol*, *160*(6), 1206-1214. https://doi.org/10.1111/j.1365-2133.2009.09089.x

Landén, N. X., Li, D., & Ståhle, M. (2016). Transition from inflammation to proliferation: a critical step during wound healing. *Cell Mol Life Sci*, *73*(20), 3861-3885. https://doi.org/10.1007/s00018-016-2268-0

Lee, D., Kim, E. J., Baek, Y., Lee, J., Yoon, Y., Nair, G. B., Yoon, S. S., & Kim, D. W. (2020). Alterations in glucose metabolism in Vibrio cholerae serogroup O1 El Tor biotype strains. *Scientific Reports*, *10*(1), 308. https://doi.org/10.1038/s41598-019-57093-4

Lemons, J. M. S., Pollina, E. A., Bennett, B. D., Legesse-Miller, A., Feng, X.-J., Rabitz, H. A., Raitman, I., Johnson, E. L., Coller, H. A., & Rabinowitz, J. D. (2010). Quiescent Fibroblasts Exhibit High Metabolic Activity. *PLoS Biology*, *8*(10), e1000514. https://doi.org/10.1371/journal.pbio.1000514

Lerman, O. Z., Galiano, R. D., Armour, M., Levine, J. P., & Gurtner, G. C. (2003). Cellular dysfunction in the diabetic fibroblast: impairment in migration, vascular endothelial growth factor production, and response to hypoxia. *Am J Pathol*, *162*(1), 303-312. https://doi.org/10.1016/s0002-9440(10)63821-7

Levy, B. I., Schiffrin, E. L., Mourad, J.-J., Agostini, D., Vicaut, E., Safar, M. E., & Struijker-Boudier, H. A. J. (2008). Impaired Tissue Perfusion. *Circulation*, *118*(9), 968-976. https://doi.org/10.1161/CIRCULATIONAHA.107.763730

Li, L., Zhang, J., Zhang, Q., Zhang, D., Xiang, F., Jia, J., Wei, P., Zhang, J., Hu, J., & Huang, Y. (2019). High Glucose Suppresses Keratinocyte Migration Through the Inhibition of p38 MAPK/Autophagy Pathway [Original Research]. *Frontiers in Physiology*, *10*(24). https://doi.org/10.3389/fphys.2019.00024

Li, M., Zhao, Y., Hao, H., Dai, H., Han, Q., Tong, C., Liu, J., Han, W., & Fu, X. (2015). Mesenchymal stem cell-conditioned medium improves the proliferation and migration of keratinocytes in a diabetes-like microenvironment. *Int J Low Extrem Wounds*, *14*(1), 73-86. https://doi.org/10.1177/1534734615569053

Li, Q., Richard, C.-A., Moudjou, M., & Vidic, J. (2015). Purification and Refolding to Amyloid Fibrils of (His)6-tagged Recombinant Shadoo Protein Expressed as Inclusion Bodies in E. coli. *Journal of Visualized Experiments*, *2015*. https://doi.org/10.3791/53432

Linehan, J., Harrison, O., Han, S., Byrd, A., Vujkovic-Cvijin, I., Villarino, A., Sen, S., Shaik, J., Smelkinson, M., Tamoutounour, S., Collins, N., Bouladoux, N., Dzutsev, A., Rosshart, S., Arbuckle, J., Wang, C. R., Kristie, T. M., Rehermann, B., Trinchieri, G., . . . Belkaid, Y. (2018). Non-classical Immunity Controls Microbiota Impact on Skin Immunity and Tissue Repair. *Cell*, *172*(4), 784-796.e718. https://doi.org/10.1016/j.cell.2017.12.033

Linge, H. M., Collin, M., Nordenfelt, P., Mörgelin, M., Malmsten, M., & Egesten, A. (2008). The human CXC chemokine granulocyte chemotactic protein 2 (GCP-2)/CXCL6 possesses membrane-disrupting properties and is antibacterial. *Antimicrob Agents Chemother*, *52*(7), 2599-2607. https://doi.org/10.1128/aac.00028-08

Lioupis, C. (2005). Effects of diabetes mellitus on wound healing: an update. *J Wound Care*, *14*(2), 84-86. https://doi.org/10.12968/jowc.2005.14.2.26738

Liu, Z., Zhang, L., Toma, M. A., Li, D., Bian, X., Pastar, I., Tomic-Canic, M., Sommar, P., & Xu Landén, N. (2022). Integrative small and long RNA omics analysis of human healing and nonhealing wounds discovers cooperating microRNAs as therapeutic targets. *Elife*, *11*. https://doi.org/10.7554/eLife.80322

Lobmann, R., Ambrosch, A., Schultz, G., Waldmann, K., Schiweck, S., & Lehnert, H. (2002). Expression of matrix-metalloproteinases and their inhibitors in the wounds of diabetic and non-diabetic patients. *Diabetologia*, *45*(7), 1011-1016. https://doi.org/10.1007/s00125-002-0868-8

Loesche, M., Gardner, S. E., Kalan, L., Horwinski, J., Zheng, Q., Hodkinson, B. P., Tyldsley, A. S., Franciscus, C. L., Hillis, S. L., Mehta, S., Margolis, D. J., & Grice, E. A. (2017). Temporal Stability in Chronic Wound Microbiota Is Associated With Poor Healing. *J Invest Dermatol*, *137*(1), 237-244. https://doi.org/10.1016/j.jid.2016.08.009

LoGerfo Frank, W., & Coffman Jay, D. (1984). Vascular and Microvascular Disease of the Foot in Diabetes. *New England Journal of Medicine*, *311*(25), 1615-1619. https://doi.org/10.1056/NEJM198412203112506

Loots, M. A. M., Kenter, S. B., Au, F. L., van Galen, W. J. M., Middelkoop, E., Bos, J. D., & Mekkes, J. R. (2002). Fibroblasts derived from chronic diabetic ulcers differ in their response to stimulation with EGF, IGF-I, bFGF and PDGF-AB compared to controls. *European Journal of Cell Biology*, *81*(3), 153-160. https://doi.org/https://doi.org/10.1078/0171-9335-00228

Lopes, D. D., Rosa, C. A., Hector, R. E., Dien, B. S., Mertens, J. A., & Ayub, M. A. Z. (2017). Influence of genetic background of engineered xylose-fermenting industrial Saccharomyces cerevisiae strains for ethanol production from lignocellulosic hydrolysates. *Journal of Industrial Microbiology and Biotechnology*, *44*(11), 1575-1588. https://doi.org/10.1007/s10295-017-1979-z

Ma, J. C., Sun, X. W., Su, H., Chen, Q., Guo, T. K., Li, Y., Chen, X. C., Guo, J., Gong, Z. Q., Zhao, X. D., & Qi, J. B. (2017). Fibroblast-derived CXCL12/SDF-1α promotes CXCL6 secretion and co-operatively enhances metastatic potential through the PI3K/Akt/mTOR pathway in colon cancer. *World J Gastroenterol*, *23*(28), 5167-5178. https://doi.org/10.3748/wjg.v23.i28.5167

Mani-López, E., Arrioja-Bretón, D., & López-Malo, A. (2022). The impacts of antimicrobial and antifungal activity of cell-free supernatants from lactic acid bacteria in vitro and foods. *Compr Rev Food Sci Food Saf*, *21*(1), 604-641. https://doi.org/10.1111/1541-4337.12872

Maruyama, K., Asai, J., Ii, M., Thorne, T., Losordo, D. W., & D'Amore, P. A. (2007). Decreased Macrophage Number and Activation Lead to Reduced Lymphatic Vessel Formation and Contribute to Impaired Diabetic Wound Healing. *The American Journal of Pathology*, *170*(4), 1178-1191. https://doi.org/10.2353/ajpath.2007.060018

Masadeh, M. M., Alzoubi, K. H., Masadeh, M. M., & Aburashed, Z. O. (2021). Metformin as a Potential Adjuvant Antimicrobial Agent Against Multidrug Resistant Bacteria. *Clin Pharmacol*, *13*, 83-90. https://doi.org/10.2147/cpaa.S297903

Masson-Meyers, D. S., Andrade, T. A. M., Caetano, G. F., Guimaraes, F. R., Leite, M. N., Leite, S. N., & Frade, M. A. C. (2020). Experimental models and methods for cutaneous wound healing assessment. *Int J Exp Pathol*, *101*(1-2), 21-37. https://doi.org/10.1111/iep.12346

Mathew-Steiner, S. S., Roy, S., & Sen, C. K. (2021). Collagen in Wound Healing. *Bioengineering (Basel)*, *8*(5). https://doi.org/10.3390/bioengineering8050063

McDermott, K., Fang, M., Boulton, A. J. M., Selvin, E., & Hicks, C. W. (2023). Etiology, Epidemiology, and Disparities in the Burden of Diabetic Foot Ulcers. *Diabetes Care*, *46*(1), 209-221. https://doi.org/10.2337/dci22-0043

McGeachy, M. J., Cua, D. J., & Gaffen, S. L. (2019). The IL-17 Family of Cytokines in Health and Disease. *Immunity*, *50*(4), 892-906. https://doi.org/10.1016/j.immuni.2019.03.021

Menzies, B. E., & Kenoyer, A. (2005). Staphylococcus aureus infection of epidermal keratinocytes promotes expression of innate antimicrobial peptides. *Infection and immunity*, *73*(8), 5241-5244. https://doi.org/10.1128/iai.73.8.5241-5244.2005

Metcalf, D. G., Haalboom, M., Bowler, P. G., Gamerith, C., Sigl, E., Heinzle, A., & Burnet, M. W. M. (2019). Elevated wound fluid pH correlates with increased risk of wound infection. *Wound Medicine*, *26*(1), 100166. https://doi.org/https://doi.org/10.1016/j.wndm.2019.100166

Miller, L. S., & Cho, J. S. (2011). Immunity against Staphylococcus aureus cutaneous infections. *Nat Rev Immunol*, *11*(8), 505-518. https://doi.org/10.1038/nri3010

Mira, P., Yeh, P., & Hall, B. G. (2022). Estimating microbial population data from optical density. *PLOS ONE*, *17*(10), e0276040. https://doi.org/10.1371/journal.pone.0276040

Mohammedsaeed, W., Bukhari, S., & Almaramhy, H. (2022). An ex-vivo study to investigate the potential of Staphylococcus epidermidis lysate to improve wound healing in diabetic patients. *Journal of Taibah University for Science*, *16*, 895-902. https://doi.org/10.1080/16583655.2022.2112489

Mohammedsaeed, W., Cruickshank, S., McBain, A. J., & O'Neill, C. A. (2015). Lactobacillus rhamnosus GG Lysate Increases Re-Epithelialization of Keratinocyte Scratch Assays by Promoting Migration. *Scientific Reports*, *5*(1), 16147. https://doi.org/10.1038/srep16147

Mohammedsaeed, W., & Manzoor, N. (2022). An in vitro investigation of the protective role of Staphylococcus Epidermidis extracts on Staphylococcus Aureus induced toxicity in human keratinocytes. *Indian J Med Microbiol*, *40*(2), 239-244. https://doi.org/10.1016/j.ijmmb.2022.01.005

Naik, S., Bouladoux, N., Linehan, J. L., Han, S.-J., Harrison, O. J., Wilhelm, C., Conlan, S., Himmelfarb, S., Byrd, A. L., Deming, C., Quinones, M., Brenchley, J. M., Kong, H. H., Tussiwand, R., Murphy, K. M., Merad, M., Segre, J. A., & Belkaid, Y. (2015). Commensal–dendritic-cell interaction specifies a unique protective skin immune signature. *Nature*, *520*(7545), 104-108. https://doi.org/10.1038/nature14052

Naik, S., Bouladoux, N., Wilhelm, C., Molloy, M. J., Salcedo, R., Kastenmuller, W., Deming, C., Quinones, M., Koo, L., Conlan, S., Spencer, S., Hall, J. A., Dzutsev, A., Kong, H., Campbell, D. J., Trinchieri, G., Segre, J. A., & Belkaid, Y. (2012). Compartmentalized control of skin immunity by resident commensals. *Science*, *337*(6098), 1115-1119. https://doi.org/10.1126/science.1225152

Nakai, K., Fujii, S., Yamamoto, A., Igarashi, J., Kubota, Y., & Kosaka, H. (2003). Effects of high glucose on NO synthesis in human keratinocyte cell line (HaCaT). *J Dermatol Sci*, *31*(3), 211-218. https://doi.org/10.1016/s0923-1811(03)00006-9

Nakamura, Y., Oscherwitz, J., Cease, K. B., Chan, S. M., Muñoz-Planillo, R., Hasegawa, M., Villaruz, A. E., Cheung, G. Y., McGavin, M. J., Travers, J. B., Otto, M., Inohara, N., & Núñez, G. (2013). Staphylococcus δ-toxin induces allergic skin disease by activating mast cells. *Nature*, *503*(7476), 397-401. https://doi.org/10.1038/nature12655

Nakatsuji, Chen, T. H., Narala, S., Chun, K. A., Two, A. M., Yun, T., Shafiq, F., Kotol, P. F., Bouslimani, A., Melnik, A. V., Latif, H., Kim, J. N., Lockhart, A., Artis, K., David, G., Taylor, P., Streib, J., Dorrestein, P. C., Grier, A., . . . Gallo, R. L. (2017). Antimicrobials from human skin commensal bacteria protect against Staphylococcus aureus and are deficient in atopic dermatitis. *Sci Transl Med*, *9*(378). https://doi.org/10.1126/scitranslmed.aah4680

Nakatsuji, T., Chen, T. H., Narala, S., Chun, K. A., Two, A. M., Yun, T., Shafiq, F., Kotol, P. F., Bouslimani, A., Melnik, A. V., Latif, H., Kim, J.-N., Lockhart, A., Artis, K., David, G., Taylor, P., Streib, J., Dorrestein, P. C., Grier, A., . . . Gallo, R. L. (2017). Antimicrobials from human skin commensal bacteria protect against Staphylococcus aureus and are deficient in atopic dermatitis. *Science Translational Medicine*, *9*(378), eaah4680. https://doi.org/10.1126/scitranslmed.aah4680

Nakatsuji, T., Chen, T. H., Narala, S., Chun, K. A., Two, A. M., Yun, T., Shafiq, F., Kotol, P. F., Bouslimani, A., Melnik, A. V., Latif, H., Kim, J. N., Lockhart, A., Artis, K., David, G., Taylor, P., Streib, J., Dorrestein, P. C., Grier, A., . . . Gallo, R. L. (2017). Antimicrobials from human skin commensal bacteria protect against Staphylococcus aureus and are deficient in atopic dermatitis. *Sci Transl Med*, *9*(378). https://doi.org/10.1126/scitranslmed.aah4680

Navale, A. M., & Paranjape, A. N. (2016). Glucose transporters: physiological and pathological roles. *Biophys Rev*, *8*(1), 5-9. https://doi.org/10.1007/s12551-015-0186-2

NICE. (2022). *When should I suspect type 2 diabetes in an adult?* https://cks.nice.org.uk/topics/diabetes-type-2/diagnosis/diagnosis-in-adults/

NICE. (2024a). *Diabetes - type 2: How common is it?* https://cks.nice.org.uk/topics/diabetes-type-2/background-information/prevalence/#:~:text=Diabetes%20is%20one%20of%20the%20most%20common%20chronic,diagnosed%20with%20diabetes%20%5B%20Diabetes%20UK%2C%202019b%20%5D.

NICE. (2024b). *Diabetic foot problems: prevention and management* https://bnf.nice.org.uk/treatment-summaries/diabetic-foot-infections-antibacterial-therapy/#:~:text=Treatment%20should%20be%20based%20on%20clinical%20assessment%2C%20infection,treatment.%20Review%20the%20need%20for%20continued%20antibacterials%20regularly.

NICE. (2024c). Type 2 diabetes in adults: management

https://doi.org/https://www.nice.org.uk/guidance/ng28/chapter/Recommendations#first-line-drug-treatment

Nickel, K., Wensorra, U., Wenck, H., Peters, N., & Genth, H. (2021). Evaluation of Immunomodulatory Responses and Changed Wound Healing in Type 2 Diabetes-A Study Exploiting Dermal Fibroblasts from Diabetic and Non-Diabetic Human Donors. *Cells*, *10*(11). https://doi.org/10.3390/cells10112931

Nicolle, R., Radvanyi, F., & Elati, M. (2015). CoRegNet: reconstruction and integrated analysis of co-regulatory networks. *Bioinformatics*, *31*(18), 3066-3068. https://doi.org/10.1093/bioinformatics/btv305

Noh, K., Mangala, L. S., Han, H. D., Zhang, N., Pradeep, S., Wu, S. Y., Ma, S., Mora, E., Rupaimoole, R., Jiang, D., Wen, Y., Shahzad, M. M. K., Lyons, Y., Cho, M., Hu, W., Nagaraja, A. S., Haemmerle, M., Mak, C. S. L., Chen, X., . . . Sood, A. K. (2017). Differential Effects of EGFL6 on Tumor versus Wound Angiogenesis. *Cell Rep*, *21*(10), 2785-2795. https://doi.org/10.1016/j.celrep.2017.11.020

Oates, A., Bowling, F. L., Boulton, A. J., & McBain, A. J. (2012). Molecular and culture-based assessment of the microbial diversity of diabetic chronic foot wounds and contralateral skin sites. *J Clin Microbiol*, *50*(7), 2263-2271. https://doi.org/10.1128/jcm.06599-11

Oh, J. (2020). Clinical spectrum and diagnosis of diabetic neuropathies. *Korean J Intern Med*, *35*(5), 1059-1069. https://doi.org/10.3904/kjim.2020.202

Oh, J., Byrd, A. L., Deming, C., Conlan, S., Kong, H. H., & Segre, J. A. (2014). Biogeography and individuality shape function in the human skin metagenome. *Nature*, *514*(7520), 59-64. https://doi.org/10.1038/nature13786

Oh, J., Byrd, A. L., Park, M., Kong, H. H., & Segre, J. A. (2016). Temporal Stability of the Human Skin Microbiome. *Cell*, *165*(4), 854-866. https://doi.org/10.1016/j.cell.2016.04.008

Okizaki, S.-i., Ito, Y., Hosono, K., Oba, K., Ohkubo, H., Amano, H., Shichiri, M., & Majima, M. (2015). Suppressed recruitment of alternatively activated macrophages reduces TGF-β1 and impairs wound healing in streptozotocin-induced diabetic mice. *Biomedicine & Pharmacotherapy*, *70*, 317-325. https://doi.org/https://doi.org/10.1016/j.biopha.2014.10.020

Olson, J., Nguyen, V., Yoo, J., & Kuechle, M. (2009). Cutaneous manifestations of Corynebacterium jeikeium sepsis. *International journal of dermatology*, *48*, 886-888. https://doi.org/10.1111/j.1365-4632.2008.03984.x

Olson, M. F., & Sahai, E. (2009). The actin cytoskeleton in cancer cell motility. *Clin Exp Metastasis*, *26*(4), 273-287. https://doi.org/10.1007/s10585-008-9174-2

Ommori, R., Ouji, N., Mizuno, F., Kita, E., Ikada, Y., & Asada, H. (2013). Selective induction of antimicrobial peptides from keratinocytes by staphylococcal bacteria. *Microbial Pathogenesis*, *56*, 35-39. https://doi.org/https://doi.org/10.1016/j.micpath.2012.11.005

Otto, M. (2009). Staphylococcus epidermidis--the 'accidental' pathogen. *Nat Rev Microbiol*, *7*(8), 555-567. https://doi.org/10.1038/nrmicro2182

Pacios, O., Fernández-García, L., Bleriot, I., Blasco, L., González-Bardanca, M., López, M., Fernández-Cuenca, F., Oteo, J., Pascual, Á., Martínez-Martínez, L., Domingo-Calap, P., Bou, G., & Tomás, M. (2021). Enhanced Antibacterial Activity of Repurposed Mitomycin C and Imipenem in Combination with the Lytic Phage vB_KpnM-VAC13 against Clinical Isolates of Klebsiella pneumoniae. *Antimicrob Agents Chemother*, *65*(9), e0090021. https://doi.org/10.1128/aac.00900-21

Pam, S., Mawak, J., & Chuhwak, E. K. (2006). Bacterial skin flora of diabetic patients in the Jos University Teaching Hospital, Jos. *Journal of Medicine in the Tropics*, *7*. https://doi.org/10.4314/jmt.v7i1.35177

Parastan, R., Kargar, M., Solhjoo, K., & Kafilzadeh, F. (2020). Staphylococcus aureus biofilms: Structures, antibiotic resistance, inhibition, and vaccines. *Gene Reports*, *20*, 100739. https://doi.org/https://doi.org/10.1016/j.genrep.2020.100739

Park, H., Arellano, K., Lee, Y., Yeo, S., Ji, Y., Ko, J., & Holzapfel, W. (2021). Pilot Study on the Forehead Skin Microbiome and Short Chain Fatty Acids Depending on the SC Functional Index in Korean Cohorts. *Microorganisms*, *9*(11). https://doi.org/10.3390/microorganisms9112216

Park, H. Y., Kim, J. H., Jung, M., Chung, C. H., Hasham, R., Park, C. S., & Choi, E. H. (2011). A long-standing hyperglycaemic condition impairs skin barrier by accelerating skin ageing process. *Exp Dermatol*, *20*(12), 969-974. https://doi.org/10.1111/j.1600-0625.2011.01364.x

Park, J. U., Oh, B., Lee, J. P., Choi, M. H., Lee, M. J., & Kim, B. S. (2019). Influence of Microbiota on Diabetic Foot Wound in Comparison with Adjacent Normal Skin Based on the Clinical Features. *Biomed Res Int*, *2019*, 7459236. https://doi.org/10.1155/2019/7459236

Park, Y. J., & Lee, H. K. (2017). The Role of Skin and Orogenital Microbiota in Protective Immunity and Chronic Immune-Mediated Inflammatory Disease. *Front Immunol*, *8*, 1955. https://doi.org/10.3389/fimmu.2017.01955

Pastar, I., Stojadinovic, O., Yin, N. C., Ramirez, H., Nusbaum, A. G., Sawaya, A., Patel, S. B., Khalid, L., Isseroff, R. R., & Tomic-Canic, M. (2014). Epithelialization in Wound Healing: A Comprehensive Review. *Adv Wound Care (New Rochelle)*, *3*(7), 445-464. https://doi.org/10.1089/wound.2013.0473

Peetermans, M., Verhamme, P., & Vanassche, T. (2015). Coagulase Activity by Staphylococcus aureus: A Potential Target for Therapy? *Semin Thromb Hemost*, *41*(4), 433-444. https://doi.org/10.1055/s-0035-1549849

Percival, S. L., McCarty, S., Hunt, J. A., & Woods, E. J. (2014). The effects of pH on wound healing, biofilms, and antimicrobial efficacy. *Wound Repair Regen*, *22*(2), 174-186. https://doi.org/10.1111/wrr.12125

Perez, K., & Patel, R. (2018). Survival of Staphylococcus epidermidis in Fibroblasts and Osteoblasts. *Infection and immunity*, *86*(10). https://doi.org/10.1128/iai.00237-18

Phillips, S. J. (2000). Physiology of wound healing and surgical wound care. *Asaio j*, *46*(6), S2-5. https://doi.org/10.1097/00002480-200011000-00029

Pijuan, J., Barceló, C., Moreno, D. F., Maiques, O., Sisó, P., Marti, R. M., Macià, A., & Panosa, A. (2019). In vitro Cell Migration, Invasion, and Adhesion Assays: From Cell Imaging to Data Analysis. *Front Cell Dev Biol*, *7*, 107. https://doi.org/10.3389/fcell.2019.00107

Ponce, R., Martinsen, L., Vicente, L. M., & Hartl, D. L. (2012). Novel Genes from Formation to Function. *International Journal of Evolutionary Biology*, *2012*(1), 821645. https://doi.org/https://doi.org/10.1155/2012/821645

Poornachandra Rao, K., Deepthi, B. V., Rakesh, S., Ganesh, T., Achar, P., & Sreenivasa, M. Y. (2019). Antiaflatoxigenic Potential of Cell-Free Supernatant from Lactobacillus plantarum MYS44 Against Aspergillus parasiticus. *Probiotics and Antimicrobial Proteins*, *11*(1), 55-64. https://doi.org/10.1007/s12602-017-9338-y

Popov, L. M., Marceau, C. D., Starkl, P. M., Lumb, J. H., Shah, J., Guerrera, D., Cooper, R. L., Merakou, C., Bouley, D. M., Meng, W., Kiyonari, H., Takeichi, M., Galli, S. J., Bagnoli, F., Citi, S., Carette, J. E., & Amieva, M. R. (2015). The adherens junctions control susceptibility to Staphylococcus aureus α-toxin. *Proc Natl Acad Sci U S A*, *112*(46), 14337-14342. https://doi.org/10.1073/pnas.1510265112

Probst, A. J., Auerbach, A. K., & Moissl-Eichinger, C. (2013). Archaea on human skin. *PLoS One*, *8*(6), e65388. https://doi.org/10.1371/journal.pone.0065388

Promega. (2022). *CellTiter 96® AQueous One Solution Cell Proliferation Assay (MTS)*.

Puel, A., Cypowyj, S., Bustamante, J., Wright, J. F., Liu, L., Lim, H. K., Migaud, M., Israel, L., Chrabieh, M., Audry, M., Gumbleton, M., Toulon, A., Bodemer, C., El-Baghdadi, J., Whitters, M., Paradis, T., Brooks, J., Collins, M., Wolfman, N. M., . . . Casanova, J. L. (2011). Chronic mucocutaneous candidiasis in humans with inborn errors of interleukin-17 immunity. *Science*, *332*(6025), 65-68. https://doi.org/10.1126/science.1200439

Qian, D., Zhang, T., Tan, X., Zheng, P., Liang, Z., Xie, J., Jiang, J., & Situ, B. (2018). Comparison of antidiabetic drugs added to sulfonylurea monotherapy in patients with type 2 diabetes

mellitus: A network meta-analysis. *PLOS ONE*, *13*(8), e0202563. https://doi.org/10.1371/journal.pone.0202563

Qiu, Y., Ma, X., Yang, X., Wang, L., & Jiang, Z. (2017). Effect of sodium butyrate on cell proliferation and cell cycle in porcine intestinal epithelial (IPEC-J2) cells. *In Vitro Cell Dev Biol Anim*, *53*(4), 304-311. https://doi.org/10.1007/s11626-016-0119-9

Quondamatteo, F. (2014). Skin and diabetes mellitus: what do we know? *Cell Tissue Res*, *355*(1), 1-21. https://doi.org/10.1007/s00441-013-1751-2

Raja, Sivamani, K., Garcia, M. S., & Isseroff, R. R. (2007). Wound re-epithelialization: modulating keratinocyte migration in wound healing. *Front Biosci*, *12*, 2849-2868. https://doi.org/10.2741/2277

Ramakant, P., Verma, A. K., Misra, R., Prasad, K. N., Chand, G., Mishra, A., Agarwal, G., Agarwal, A., & Mishra, S. K. (2011). Changing microbiological profile of pathogenic bacteria in diabetic foot infections: time for a rethink on which empirical therapy to choose? *Diabetologia*, *54*(1), 58-64. https://doi.org/10.1007/s00125-010-1893-7

Rasigade, J. P., & Vandenesch, F. (2014). Staphylococcus aureus: a pathogen with still unresolved issues. *Infect Genet Evol*, *21*, 510-514. https://doi.org/10.1016/j.meegid.2013.08.018

Redel, H., Gao, Z., Li, H., Alekseyenko, A. V., Zhou, Y., Perez-Perez, G. I., Weinstock, G., Sodergren, E., & Blaser, M. J. (2013). Quantitation and composition of cutaneous microbiota in diabetic and nondiabetic men. *J Infect Dis*, *207*(7), 1105-1114. https://doi.org/10.1093/infdis/jit005

Reilly, D. M., & Lozano, J. (2021). Skin collagen through the lifestages: importance for skin health and beauty. *Plastic and Aesthetic Research*, *8*, 2. https://doi.org/10.20517/2347-9264.2020.153

Reimand, J., Isserlin, R., Voisin, V., Kucera, M., Tannus-Lopes, C., Rostamianfar, A., Wadi, L., Meyer, M., Wong, J., Xu, C., Merico, D., & Bader, G. D. (2019). Pathway enrichment analysis and visualization of omics data using g:Profiler, GSEA, Cytoscape and EnrichmentMap. *Nat Protoc*, *14*(2), 482-517. https://doi.org/10.1038/s41596-018-0103-9

Ridley, A. J., Schwartz, M. A., Burridge, K., Firtel, R. A., Ginsberg, M. H., Borisy, G., Parsons, J. T., & Horwitz, A. R. (2003). Cell migration: integrating signals from front to back. *Science*, *302*(5651), 1704-1709. https://doi.org/10.1126/science.1092053

Rodríguez-Rodríguez, N., Martínez-Jiménez, I., García-Ojalvo, A., Mendoza-Mari, Y., Guillén-Nieto, G., Armstrong, D. G., & Berlanga-Acosta, J. (2022). Wound Chronicity, Impaired Immunity and Infection in Diabetic Patients. *MEDICC Rev*, *24*(1), 44-58. https://doi.org/10.37757/mr2021.V23.N3.8

Sabir, A., Latimer, J. (2020). *The association between skin microbiota and diabetes mellitus pathophysiology with recommandations for further studies: a systematic review and metaanalysis* University of Salford]. Unpublished taught master dissertation.

Saeidi, N., Wong, C. K., Lo, T. M., Nguyen, H. X., Ling, H., Leong, S. S. J., Poh, C. L., & Chang, M. W. (2011). Engineering microbes to sense and eradicate Pseudomonas aeruginosa, a human pathogen. *Molecular Systems Biology*, *7*(1), 521. https://doi.org/https://doi.org/10.1038/msb.2011.55

Saghiri, M. A., Asatourian, A., Morgano, S. M., Wang, S., & Sheibani, N. (2020). Moderately Acidic pH Promotes Angiogenesis: An In Vitro and In Vivo Study. *Journal of Endodontics*, *46*(8), 1113-1119. https://doi.org/https://doi.org/10.1016/j.joen.2020.04.005

Saito, K., Tomita, S., & Nakamura, T. (2019). Aggregation of Lactobacillus brevis associated with decrease in pH by glucose fermentation. *Bioscience, Biotechnology, and Biochemistry*, *83*(8), 1523-1529. https://doi.org/10.1080/09168451.2019.1584522

Sakai, S., Endo, Y., Ozawa, N., Sugawara, T., Kusaka, A., Sayo, T., Tagami, H., & Inoue, S. (2003). Characteristics of the epidermis and stratum corneum of hairless mice with experimentally induced diabetes mellitus. *J Invest Dermatol*, *120*(1), 79-85. https://doi.org/10.1046/j.1523-1747.2003.12006.x

Salgaonkar, N., Kadamkode, V., Kumaran, S., Mallemala, P., Christy, E., Appavoo, S., Majumdar, A., Mitra, R., & Dasgupta, A. (2022). Glycerol fermentation by skin bacteria generates lactic acid

and upregulates the expression levels of genes associated with the skin barrier function. *Exp Dermatol*, *31*(9), 1364-1372. https://doi.org/10.1111/exd.14604

Salgaonkar, N., Kadamkode, V., Kumaran, S., Mallemala, P., Christy, E., Appavoo, S., Majumdar, A., Mitra, R., & Dasgupta, A. (2022). Glycerol fermentation by skin bacteria generates lactic acid and upregulates the expression levels of genes associated with the skin barrier function. *Experimental Dermatology*, *31*(9), 1364-1372. https://doi.org/https://doi.org/10.1111/exd.14604

Sami, D. G., Heiba, H. H., & Abdellatif, A. (2019). Wound healing models: A systematic review of animal and non-animal models. *Wound Medicine*, *24*(1), 8-17. https://doi.org/https://doi.org/10.1016/j.wndm.2018.12.001

Sarkawi, S. (2015). *An Overview on pH Measurement Technique and Application in Biomedical and Industrial Process*. https://doi.org/10.1109/ICoBE.2015.7235898

Schierle, C. F., De la Garza, M., Mustoe, T. A., & Galiano, R. D. (2009). Staphylococcal biofilms impair wound healing by delaying reepithelialization in a murine cutaneous wound model. *Wound Repair Regen*, *17*(3), 354-359. https://doi.org/10.1111/j.1524-475X.2009.00489.x

Schlievert, P. M., & Davis, C. C. (2020). Device-Associated Menstrual Toxic Shock Syndrome. *Clin Microbiol Rev*, *33*(3). https://doi.org/10.1128/cmr.00032-19

Schultz, G. S., & Wysocki, A. (2009). Interactions between extracellular matrix and growth factors in wound healing. *Wound Repair Regen*, *17*(2), 153-162. https://doi.org/10.1111/j.1524-475X.2009.00466.x

Schwarz, A., Bruhs, A., & Schwarz, T. (2017). The Short-Chain Fatty Acid Sodium Butyrate Functions as a Regulator of the Skin Immune System. *J Invest Dermatol*, *137*(4), 855-864. https://doi.org/10.1016/j.jid.2016.11.014

Scillato, M., Spitale, A., Mongelli, G., Privitera, G. F., Mangano, K., Cianci, A., Stefani, S., & Santagati, M. (2021). Antimicrobial properties of Lactobacillus cell-free supernatants against multidrug-resistant urogenital pathogens. *Microbiologyopen*, *10*(2), e1173. https://doi.org/10.1002/mbo3.1173

Sell, D., Biemel, K., Reihl, O., Lederer, M., Strauch, C., & Monnier, V. (2005). Glucosepane is a major protein cross-link of the senescent human extracellular matrix - Relationship with diabetes. *The Journal of biological chemistry*, *280*, 12310-12315. https://doi.org/10.1074/jbc.M500733200

Senn, L., Clerc, O., Zanetti, G., Basset, P., Prod'hom, G., Gordon, N. C., Sheppard, A. E., Crook, D. W., James, R., Thorpe, H. A., Feil, E. J., & Blanc, D. S. (2016). The Stealthy Superbug: the Role of Asymptomatic Enteric Carriage in Maintaining a Long-Term Hospital Outbreak of ST228 Methicillin-Resistant Staphylococcus aureus. *mBio*, *7*(1), e02039-02015. https://doi.org/10.1128/mBio.02039-15

Seo, G. Y., Lim, Y., Koh, D., Huh, J. S., Hyun, C., Kim, Y. M., & Cho, M. (2017). TMF and glycitin act synergistically on keratinocytes and fibroblasts to promote wound healing and anti-scarring activity. *Exp Mol Med*, *49*(3), e302. https://doi.org/10.1038/emm.2016.167

Serwańska-Leja, K., Czaczyk, K., & Myszka, K. (2011). The use of microorganisms in 1, 3-Propanediol production. *African Journal of Microbiology Research*, *5*, 4652-4658.

Sharp, A., & Clark, J. (2011). Diabetes and its effects on wound healing. *Nurs Stand*, *25*(45), 41-47. https://doi.org/10.7748/ns2011.07.25.45.41.c8626

Shevtsova, O. (2018). Wound Healing Management Bioinformatics Approach. *Biostatistics and Biometrics Open Access Journal*, *7*. https://doi.org/10.19080/BBOAJ.2018.07.555709

Shi, J., Han, C., Chen, D., Trivedi, H. M., Bangash, H. I., & Chen, L. (2022). High Glucose Induces Late Differentiation and Death of Human Oral Keratinocytes. *Curr Issues Mol Biol*, *44*(9), 4015-4027. https://doi.org/10.3390/cimb44090275

Sim, P., Strudwick, X. L., Song, Y., Cowin, A. J., & Garg, S. (2022). Influence of Acidic pH on Wound Healing In Vivo: A Novel Perspective for Wound Treatment. *Int J Mol Sci*, *23*(21). https://doi.org/10.3390/ijms232113655

Simanski, M., Erkens, A. S., Rademacher, F., & Harder, J. (2019). Staphylococcus epidermidis-induced Interleukin-1 Beta and Human Beta-defensin-2 Expression in Human Keratinocytes is Regulated by the Host Molecule A20 (TNFAIP3). *Acta Derm Venereol*, *99*(2), 181-187. https://doi.org/10.2340/00015555-3073

Singh, T. P., Carvalho, A. M., Sacramento, L. A., Grice, E. A., & Scott, P. (2021). Microbiota instruct IL-17A-producing innate lymphoid cells to promote skin inflammation in cutaneous leishmaniasis. *PLoS Pathog*, *17*(10), e1009693. https://doi.org/10.1371/journal.ppat.1009693

Snedeker, J. G., & Gautieri, A. (2014). The role of collagen crosslinks in ageing and diabetes - the good, the bad, and the ugly. *Muscles Ligaments Tendons J*, *4*(3), 303-308.

Song, X., Dai, D., He, X., Zhu, S., Yao, Y., Gao, H., Wang, J., Qu, F., Qiu, J., Wang, H., Li, X., Shen, N., & Qian, Y. (2015). Growth Factor FGF2 Cooperates with Interleukin-17 to Repair Intestinal Epithelial Damage. *Immunity*, *43*(3), 488-501. https://doi.org/10.1016/j.immuni.2015.06.024

Sorbara, M. T., & Pamer, E. G. (2022). Microbiome-based therapeutics. *Nat Rev Microbiol*, *20*(6), 365-380. https://doi.org/10.1038/s41579-021-00667-9

Sorg, H., Tilkorn, D. J., Hager, S., Hauser, J., & Mirastschijski, U. (2017). Skin Wound Healing: An Update on the Current Knowledge and Concepts. *Eur Surg Res*, *58*(1-2), 81-94. https://doi.org/10.1159/000454919

Sornsenee, P., Chatatikun, M., Mitsuwan, W., Kongpol, K., Kooltheat, N., Sohbenalee, S., Pruksaphanrat, S., Mudpan, A., & Romyasamit, C. (2021). Lyophilized cell-free supernatants of Lactobacillus isolates exhibited antibiofilm, antioxidant, and reduces nitric oxide activity in lipopolysaccharide-stimulated RAW 264.7 cells. *PeerJ*, *9*, e12586. https://doi.org/10.7717/peerj.12586

Spampinato, S. F., Caruso, G. I., De Pasquale, R., Sortino, M. A., & Merlo, S. (2020). The Treatment of Impaired Wound Healing in Diabetes: Looking among Old Drugs. *Pharmaceuticals (Basel)*, *13*(4). https://doi.org/10.3390/ph13040060

Spravchikov, N., Sizyakov, G., Gartsbein, M., Accili, D., Tennenbaum, T., & Wertheimer, E. (2001). Glucose effects on skin keratinocytes: implications for diabetes skin complications. *Diabetes*, *50*(7), 1627-1635. https://doi.org/10.2337/diabetes.50.7.1627

Stark, C., Breitkreutz, B. J., Chatr-Aryamontri, A., Boucher, L., Oughtred, R., Livstone, M. S., Nixon, J., Van Auken, K., Wang, X., Shi, X., Reguly, T., Rust, J. M., Winter, A., Dolinski, K., & Tyers, M. (2011). The BioGRID Interaction Database: 2011 update. *Nucleic Acids Res*, *39*(Database issue), D698-704. https://doi.org/10.1093/nar/gkq1116

Su, G., Wang, W., Xu, L., & Li, G. (2022). Progress of EGFL6 in angiogenesis and tumor development. *Int J Clin Exp Pathol*, *15*(11), 436-443.

Subramaniam, T., Fauzi, M. B., Lokanathan, Y., & Law, J. X. (2021). The Role of Calcium in Wound Healing. *Int J Mol Sci*, *22*(12). https://doi.org/10.3390/ijms22126486

Subramanian, A., Tamayo, P., Mootha, V. K., Mukherjee, S., Ebert, B. L., Gillette, M. A., Paulovich, A., Pomeroy, S. L., Golub, T. R., Lander, E. S., & Mesirov, J. P. (2005). Gene set enrichment analysis: a knowledge-based approach for interpreting genome-wide expression profiles. *Proc Natl Acad Sci U S A*, *102*(43), 15545-15550. https://doi.org/10.1073/pnas.0506580102

Sun, L., Xie, C., Wang, G., Wu, Y., Wu, Q., Wang, X., Liu, J., Deng, Y., Xia, J., Chen, B., Zhang, S., Yun, C., Lian, G., Zhang, X., Zhang, H., Bisson, W. H., Shi, J., Gao, X., Ge, P., . . . Jiang, C. (2018). Gut microbiota and intestinal FXR mediate the clinical benefits of metformin. *Nat Med*, *24*(12), 1919-1929. https://doi.org/10.1038/s41591-018-0222-4

Sylvia, C. J. (2003). The role of neutrophil apoptosis in influencing tissue repair. *J Wound Care*, *12*(1), 13-16. https://doi.org/10.12968/jowc.2003.12.1.26458

Takematsu, E., Spencer, A., Auster, J., Chen, P. C., Graham, A., Martin, P., & Baker, A. B. (2020). Genome wide analysis of gene expression changes in skin from patients with type 2 diabetes. *PLoS One*, *15*(2), e0225267. https://doi.org/10.1371/journal.pone.0225267

Tang, F., Barbacioru, C., Wang, Y., Nordman, E., Lee, C., Xu, N., Wang, X., Bodeau, J., Tuch, B. B., Siddiqui, A., Lao, K., & Surani, M. A. (2009). mRNA-Seq whole-transcriptome analysis of a single cell. *Nature Methods*, *6*(5), 377-382. https://doi.org/10.1038/nmeth.1315

Tauch, A., Kaiser, O., Hain, T., Goesmann, A., Weisshaar, B., Albersmeier, A., Bekel, T., Bischoff, N., Brune, I., Chakraborty, T., Kalinowski, J., Meyer, F., Rupp, O., Schneiker, S., Viehoever, P., & Pühler, A. (2005). Complete genome sequence and analysis of the multiresistant nosocomial pathogen Corynebacterium jeikeium K411, a lipid-requiring bacterium of the human skin flora. *J Bacteriol*, *187*(13), 4671-4682. https://doi.org/10.1128/jb.187.13.4671-4682.2005

Tenea, G. N., & Barrigas, A. (2018). The efficacy of bacteriocin-containing cell-free supernatant from Lactobacillus plantarum Cys5-4 to control pathogenic bacteria growth in artesanal beverages. *International Food Research Journal*, *25*, 2131-2137.

Theocharidis, G., Thomas, B. E., Sarkar, D., Mumme, H. L., Pilcher, W. J. R., Dwivedi, B., Sandoval-Schaefer, T., Sîrbulescu, R. F., Kafanas, A., Mezghani, I., Wang, P., Lobao, A., Vlachos, I. S., Dash, B., Hsia, H. C., Horsley, V., Bhasin, S. S., Veves, A., & Bhasin, M. (2022). Single cell transcriptomic landscape of diabetic foot ulcers. *Nature Communications*, *13*(1), 181. https://doi.org/10.1038/s41467-021-27801-8

Thimmappaiah Jagadeesh, A., Prakash, P. Y., Karthik Rao, N., & Ramya, V. (2017). Culture characterization of the skin microbiome in Type 2 diabetes mellitus: A focus on the role of innate immunity. *Diabetes Research and Clinical Practice*, *134*, 1-7. https://doi.org/https://doi.org/10.1016/j.diabres.2017.09.007

Thomas, P. D. (2017). The Gene Ontology and the Meaning of Biological Function. *Methods Mol Biol*, *1446*, 15-24. https://doi.org/10.1007/978-1-4939-3743-1_2

Tomic-Canic, M., Burgess, J. L., O'Neill, K. E., Strbo, N., & Pastar, I. (2020). Skin Microbiota and its Interplay with Wound Healing. *Am J Clin Dermatol*, *21*(Suppl 1), 36-43. https://doi.org/10.1007/s40257-020-00536-w

Tong, S. Y. C., Davis, J. S., Eichenberger, E., Holland, T. L., & Fowler, V. G. (2015). Staphylococcus aureus Infections: Epidemiology, Pathophysiology, Clinical Manifestations, and Management. *Clinical Microbiology Reviews*, *28*(3), 603-661. https://doi.org/doi:10.1128/CMR.00134-14

Triantafillou, V., Workman, A. D., Patel, N. N., Maina, I. W., Tong, C. C. L., Kuan, E. C., Kennedy, D. W., Palmer, J. N., Adappa, N. D., Waizel-Haiat, S., & Cohen, N. A. (2019). Broncho-Vaxom® (OM-85 BV) soluble components stimulate sinonasal innate immunity. *Int Forum Allergy Rhinol*, *9*(4), 370-377. https://doi.org/10.1002/alr.22276

Trivedi, U., Parameswaran, S., Armstrong, A., Burgueno-Vega, D., Griswold, J., Dissanaike, S., & Rumbaugh, K. P. (2014). Prevalence of Multiple Antibiotic Resistant Infections in Diabetic versus Nondiabetic Wounds. *J Pathog*, *2014*, 173053. https://doi.org/10.1155/2014/173053

Tucci, P., Agostini, M., Grespi, F., Markert, E. K., Terrinoni, A., Vousden, K. H., Muller, P. A., Dötsch, V., Kehrloesser, S., Sayan, B. S., Giaccone, G., Lowe, S. W., Takahashi, N., Vandenabeele, P., Knight, R. A., Levine, A. J., & Melino, G. (2012). Loss of p63 and its microRNA-205 target results in enhanced cell migration and metastasis in prostate cancer. *Proc Natl Acad Sci U S A*, *109*(38), 15312-15317. https://doi.org/10.1073/pnas.1110977109

Umbach Alexander, K., Stegelmeier Ashley, A., & Neufeld Josh, D. (2021). Archaea Are Rare and Uncommon Members of the Mammalian Skin Microbiome. *mSystems*, *6*(4), 10.1128/msystems.00642-00621. https://doi.org/10.1128/msystems.00642-21

Valadbeigi, H., Khoshnood, S., Negahdari, B., Abdullah, M. A., & Haddadi, M. H. (2023). Antibacterial and Immunoregulatory Effects of Metformin against Helicobacter pylori Infection in Rat Model. *Biomed Res Int*, *2023*, 5583286. https://doi.org/10.1155/2023/5583286

van Gerwen, J., Shun-Shion, A. S., & Fazakerley, D. J. (2023). Insulin signalling and GLUT4 trafficking in insulin resistance. *Biochem Soc Trans*, *51*(3), 1057-1069. https://doi.org/10.1042/bst20221066

Vang Mouritzen, M., & Jenssen, H. (2018). Optimized Scratch Assay for In Vitro Testing of Cell Migration with an Automated Optical Camera. *J Vis Exp*(138). https://doi.org/10.3791/57691

Vardakas, K. Z., Horianopoulou, M., & Falagas, M. E. (2008). Factors associated with treatment failure in patients with diabetic foot infections: An analysis of data from randomized controlled trials. *Diabetes Research and Clinical Practice*, *80*(3), 344-351. https://doi.org/https://doi.org/10.1016/j.diabres.2008.01.009

Volpe, C. M. O., Villar-Delfino, P. H., Dos Anjos, P. M. F., & Nogueira-Machado, J. A. (2018). Cellular death, reactive oxygen species (ROS) and diabetic complications. *Cell Death Dis*, *9*(2), 119. https://doi.org/10.1038/s41419-017-0135-z

Waise, S., Parker, R., Rose-Zerilli, M. J. J., Layfield, D. M., Wood, O., West, J., Ottensmeier, C. H., Thomas, G. J., & Hanley, C. J. (2019). An optimised tissue disaggregation and data processing pipeline for characterising fibroblast phenotypes using single-cell RNA sequencing. *Scientific Reports*, *9*(1), 9580. https://doi.org/10.1038/s41598-019-45842-4

Wang, R., Braughton, K. R., Kretschmer, D., Bach, T. H., Queck, S. Y., Li, M., Kennedy, A. D., Dorward, D. W., Klebanoff, S. J., Peschel, A., DeLeo, F. R., & Otto, M. (2007). Identification of novel cytolytic peptides as key virulence determinants for community-associated MRSA. *Nat Med*, *13*(12), 1510-1514. https://doi.org/10.1038/nm1656

Wang, X., Li, J., Wang, Z., & Deng, A. (2019). Wound exudate CXCL6: a potential biomarker for wound healing of diabetic foot ulcers. *Biomark Med*, *13*(3), 167-174. https://doi.org/10.2217/bmm-2018-0339

Wang, Y., Kuo, S., Shu, M., Yu, J., Huang, S., Dai, A., Two, A., Gallo, R. L., & Huang, C. M. (2014). Staphylococcus epidermidis in the human skin microbiome mediates fermentation to inhibit the growth of Propionibacterium acnes: implications of probiotics in acne vulgaris. *Appl Microbiol Biotechnol*, *98*(1), 411-424. https://doi.org/10.1007/s00253-013-5394-8

Wang, Y., Zhang, L., Yu, J., Huang, S., Wang, Z., Chun, K. A., Lee, T. L., Chen, Y. T., Gallo, R. L., & Huang, C. M. (2017). A Co-Drug of Butyric Acid Derived from Fermentation Metabolites of the Human Skin Microbiome Stimulates Adipogenic Differentiation of Adipose-Derived Stem Cells: Implications in Tissue Augmentation. *J Invest Dermatol*, *137*(1), 46-56. https://doi.org/10.1016/j.jid.2016.07.030

Wang, Z., Liu, J., Huang, H., Ye, M., Li, X., Wu, R., Liu, H., & Song, Y. (2021). Metastasis-associated fibroblasts: an emerging target for metastatic cancer. *Biomark Res*, *9*(1), 47. https://doi.org/10.1186/s40364-021-00305-9

Wang, Z., Zhao, F., Xu, C., Zhang, Q., Ren, H., Huang, X., He, C., Ma, J., & Wang, Z. (2024). Metabolic reprogramming in skin wound healing. *Burns Trauma*, *12*, tkad047. https://doi.org/10.1093/burnst/tkad047

Wanke, I., Steffen, H., Christ, C., Krismer, B., Götz, F., Peschel, A., Schaller, M., & Schittek, B. (2011). Skin commensals amplify the innate immune response to pathogens by activation of distinct signaling pathways. *J Invest Dermatol*, *131*(2), 382-390. https://doi.org/10.1038/jid.2010.328

Weiskirchen, S., Schröder, S., Buhl, M., & Weiskirchen, R. (2023). A Beginner's Guide to Cell Culture: Practical Advice for Preventing Needless Problems. *Cells*, *12*, 682. https://doi.org/10.3390/cells12050682

Westermann, A. J., & Vogel, J. (2021). Cross-species RNA-seq for deciphering host–microbe interactions. *Nature Reviews Genetics*, *22*(6), 361-378. https://doi.org/10.1038/s41576-021-00326-y

Wetzler, C., Kämpfer, H., Stallmeyer, B., Pfeilschifter, J., & Frank, S. (2000). Large and sustained induction of chemokines during impaired wound healing in the genetically diabetic mouse: prolonged persistence of neutrophils and macrophages during the late phase of repair. *J Invest Dermatol*, *115*(2), 245-253. https://doi.org/10.1046/j.1523-1747.2000.00029.x

Whitmore, C. (2010). Type 2 diabetes and obesity in adults. *British Journal of Nursing*, *19*(14), 880-886. https://doi.org/10.12968/bjon.2010.19.14.49041

Wild, S., Roglic, G., Green, A., Sicree, R., & King, H. (2004). Global prevalence of diabetes: estimates for the year 2000 and projections for 2030. *Diabetes Care*, *27*(5), 1047-1053. https://doi.org/10.2337/diacare.27.5.1047

Wilkinson, H. N., Upson, S. E., Banyard, K. L., Knight, R., Mace, K. A., & Hardman, M. J. (2019). Reduced Iron in Diabetic Wounds: An Oxidative Stress-Dependent Role for STEAP3 in Extracellular Matrix Deposition and Remodeling. *J Invest Dermatol*, *139*(11), 2368-2377.e2367. https://doi.org/10.1016/j.jid.2019.05.014

Williams, M. R., Nakatsuji, T., Sanford, J. A., Vrbanac, A. F., & Gallo, R. L. (2017). Staphylococcus aureus Induces Increased Serine Protease Activity in Keratinocytes. *Journal of Investigative Dermatology*, *137*(2), 377-384. https://doi.org/https://doi.org/10.1016/j.jid.2016.10.008

Wolcott, R. D., Hanson, J. D., Rees, E. J., Koenig, L. D., Phillips, C. D., Wolcott, R. A., Cox, S. B., & White, J. S. (2016). Analysis of the chronic wound microbiota of 2,963 patients by 16S rDNA pyrosequencing. *Wound Repair Regen*, *24*(1), 163-174. https://doi.org/10.1111/wrr.12370

Wood, V., Carbon, S., Harris, M. A., Lock, A., Engel, S. R., Hill, D. P., Van Auken, K., Attrill, H., Feuermann, M., Gaudet, P., Lovering, R. C., Poux, S., Rutherford, K. M., & Mungall, C. J. (2020). Term Matrix: a novel Gene Ontology annotation quality control system based on ontology term co-annotation patterns. *Open Biol*, *10*(9), 200149. https://doi.org/10.1098/rsob.200149

Wright, C. S., Pollok, S., Flint, D. J., Brandner, J. M., & Martin, P. E. (2012). The connexin mimetic peptide Gap27 increases human dermal fibroblast migration in hyperglycemic and hyperinsulinemic conditions in vitro. *J Cell Physiol*, *227*(1), 77-87. https://doi.org/10.1002/jcp.22705

Wu, J., Vallenius, T., Ovaska, K., Westermarck, J., Mäkelä, T. P., & Hautaniemi, S. (2009). Integrated network analysis platform for protein-protein interactions. *Nat Methods*, *6*(1), 75-77. https://doi.org/10.1038/nmeth.1282

Xing, X., Li, A., Tan, H., & Zhou, Y. (2020). IFN-γ(+) IL-17(+) Th17 cells regulate fibrosis through secreting IL-21 in systemic scleroderma. *J Cell Mol Med*, *24*(23), 13600-13608. https://doi.org/10.1111/jcmm.15266

Xuan, Y. H., Huang, B. B., Tian, H. S., Chi, L. S., Duan, Y. M., Wang, X., Zhu, Z. X., Cai, W. H., Zhu, Y. T., Wei, T. M., Ye, H. B., Cong, W. T., & Jin, L. T. (2014). High-glucose inhibits human fibroblast cell migration in wound healing via repression of bFGF-regulating JNK phosphorylation. *PLoS One*, *9*(9), e108182. https://doi.org/10.1371/journal.pone.0108182

Yamada, K., Matsushita, K., Wang, J., & Kanekura, T. (2017). Topical Glucose Induces Claudin-1 and Filaggrin Expression in a Mouse Model of Atopic Dermatitis and in Keratinocyte Culture, Exerting Anti-inflammatory Effects by Repairing Skin Barrier Function. *Acta Dermato-Venereologica*, *98*(1), 19-25. https://doi.org/10.2340/00015555-2807

Yan, L. J. (2018). Redox imbalance stress in diabetes mellitus: Role of the polyol pathway. *Animal Model Exp Med*, *1*(1), 7-13. https://doi.org/10.1002/ame2.12001

Yang, C., Xue, X. S., Li, X., & Cheng, J. P. (2014). Computational study on the acidic constants of chiral Brønsted acids in dimethyl sulfoxide. *J Org Chem*, *79*(10), 4340-4351. https://doi.org/10.1021/jo500158e

Yang, J. J., Chang, T. W., Jiang, Y., Kao, H. J., Chiou, B. H., Kao, M. S., & Huang, C. M. (2018). Commensal Staphylococcus aureus Provokes Immunity to Protect against Skin Infection of Methicillin-Resistant Staphylococcus aureus. *Int J Mol Sci*, *19*(5). https://doi.org/10.3390/ijms19051290

Yang, R.-H., Qi, S.-H., Ruan, S.-B., Lin, Z.-P., Lin, Y., Zhang, F.-G., Chen, X.-D., & Xie, J.-L. (2016). EGFL7-overexpressing epidermal stem cells promotes fibroblast proliferation and migration via mediating cell adhesion and strengthening cytoskeleton. *Molecular and Cellular Biochemistry*, *423*. https://doi.org/10.1007/s11010-016-2812-0

Yao, Y., Sturdevant, D., & Otto, M. (2005). Genomewide Analysis of Gene Expression in Staphylococcus epidermidis Biofilms: Insights into the Pathophysiology of S. epidermidis Biofilms and the Role of Phenol-Soluble Modulins in Formation of Biofilms. *The Journal of infectious diseases*, *191*, 289-298. https://doi.org/10.1086/426945

Yoon, D., Fregoso, D., Nguyen, D., Chen, V., Strbo, N., Fuentes, J., Tomic-Canic, M., Crawford, R., Pastar, I., & Isseroff, R. (2019). A tractable, simplified ex vivo human skin model of wound infection. *Wound Repair and Regeneration*, *27*. https://doi.org/10.1111/wrr.12712

You, D., & Nam, M. (2013). Effects of human epidermal growth factor gene-transfected mesenchymal stem cells on fibroblast migration and proliferation. *Cell proliferation*, *46*, 408-415. https://doi.org/10.1111/cpr.12042

Young, M., Wakefield, M., Smyth, G., & Oshlack, A. (2010). Gene ontology analysis for RNA-SEQ: accounting for selection bias. *Genome biology*, *11*, R14. https://doi.org/10.1186/gb-2010-11-2-r14

Yu, A., Matsuda, Y., Takeda, A., Uchinuma, E., & Kuroyanagi, Y. (2012). Effect of EGF and bFGF on fibroblast proliferation and angiogenic cytokine production from cultured dermal substitutes. *J Biomater Sci Polym Ed*, *23*(10), 1315-1324. https://doi.org/10.1163/092050611x580463

Yu, Y., Dunaway, S., Champer, J., Kim, J., & Alikhan, A. (2020). Changing our microbiome: probiotics in dermatology. *Br J Dermatol*, *182*(1), 39-46. https://doi.org/10.1111/bjd.18088

Zhai, H., Zhang, N., Mo, D., & Qin, T. (2023). CCL20 is a potential therapeutic target associated with immune infiltration in breast cancer. *J Int Med Res*, *51*(8), 3000605231171762. https://doi.org/10.1177/03000605231171762

Zhang, C., Ponugoti, B., Tian, C., Xu, F., Tarapore, R., Batres, A., Alsadun, S., Lim, J., Dong, G., & Graves, D. T. (2015). FOXO1 differentially regulates both normal and diabetic wound healing. *Journal of Cell Biology*, *209*(2), 289-303. https://doi.org/10.1083/jcb.201409032

Zhang, P., Lu, J., Jing, Y., Tang, S., Zhu, D., & Bi, Y. (2017). Global epidemiology of diabetic foot ulceration: a systematic review and meta-analysis (†). *Ann Med*, *49*(2), 106-116. https://doi.org/10.1080/07853890.2016.1231932

Zhang, X., Zhang, S., Shi, Y., Shen, F., & Wang, H. (2014). A new high phenyl lactic acid-yielding Lactobacillus plantarum IMAU10124 and a comparative analysis of lactate dehydrogenase gene. *FEMS Microbiology Letters*, *356*(1), 89-96. https://doi.org/10.1111/1574-6968.12483

Zhanng, C., Lim, J., Liu, J., Ponugoti, B., Alsadun, S., Tian, C., Vafa, R., & Graves, D. T. (2017). FOXO1 expression in keratinocytes promotes connective tissue healing. *Scientific Reports*, *7*(1), 42834. https://doi.org/10.1038/srep42834

Zheng, Y., Ley, S. H., & Hu, F. B. (2018). Global aetiology and epidemiology of type 2 diabetes mellitus and its complications. *Nat Rev Endocrinol*, *14*(2), 88-98. https://doi.org/10.1038/nrendo.2017.151

Zito, A., Lualdi, M., Granata, P., Cocciadiferro, D., Novelli, A., Alberio, T., Casalone, R., & Fasano, M. (2021). Gene Set Enrichment Analysis of Interaction Networks Weighted by Node Centrality. *Front Genet*, *12*, 577623. https://doi.org/10.3389/fgene.2021.577623

Appendix 1

F20_vs_F5

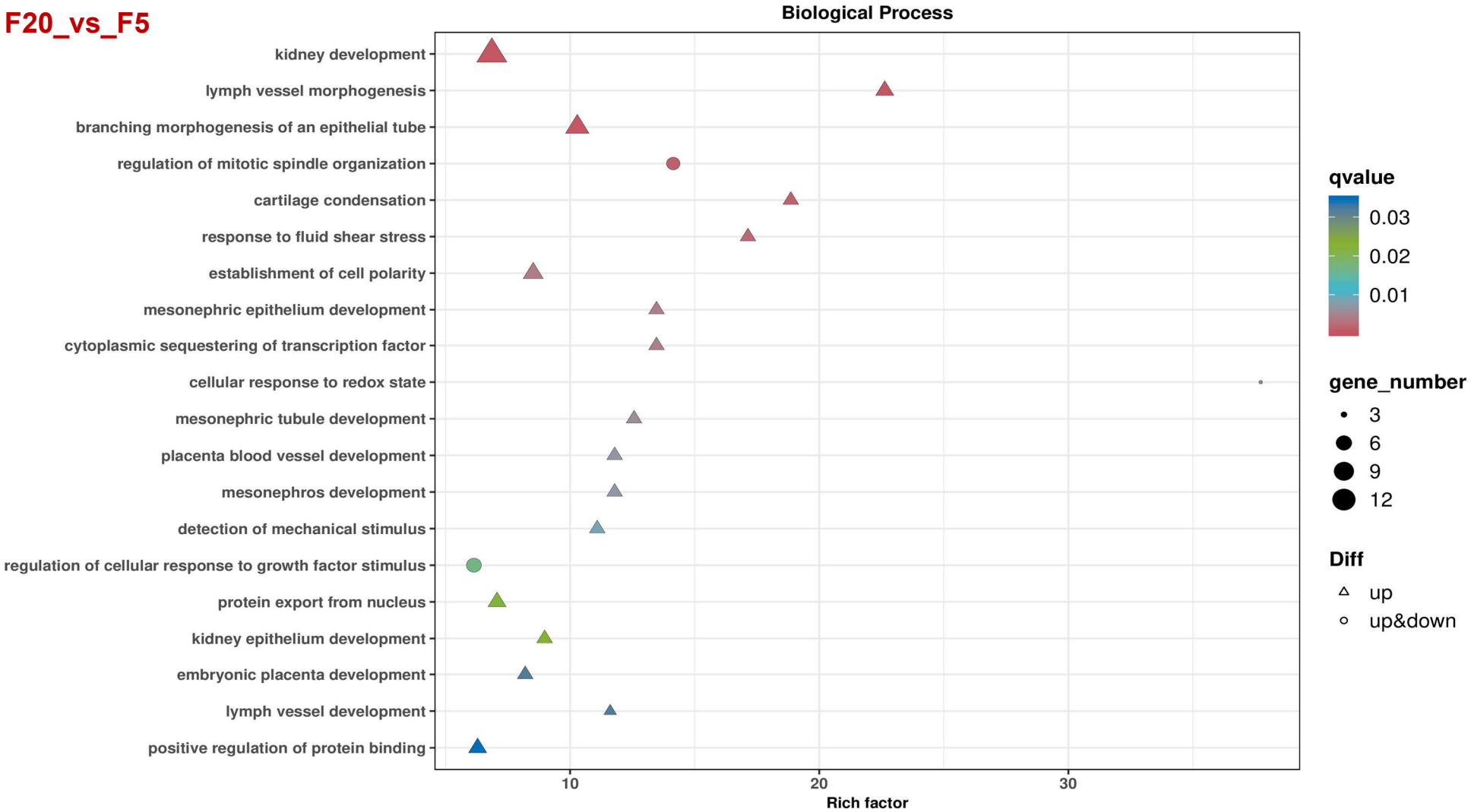

Figure 8.1: Biological process of DEGs in fibroblasts grown in 20 mM glucose concentration and compared to euglycemic control (5.5 mM) (F20_vs_F5). The Graph shows the top 20 significantly enriched biological processes found in fibroblasts growing in high glucose concentrations (20 mM) compared to fibroblasts growing in euglycemic glucose concentrations (5.5 mM). Each dot represents a biological process. Y-axis: Name of biological process; X-axis: Rich factor represent Enrichment factor that calculated as "Enrichment factor=(Ratio of DEG annotated to the term over all DEG)/(Ratio of genes annotated to the term over all genes)“ A larger enrichment factor indicates a more significant enrichment of the pathway. The colour of the dots stands for q-value (adjusted p-value). The smaller the q-value is, the more significant or reliable the enrichment is. The size of the dots represents the number of DEG enriched in this pathway. The larger the dot is, the more genes it contains. Graph created by (BMKGENE, 2023)

FSe5_vs_F5

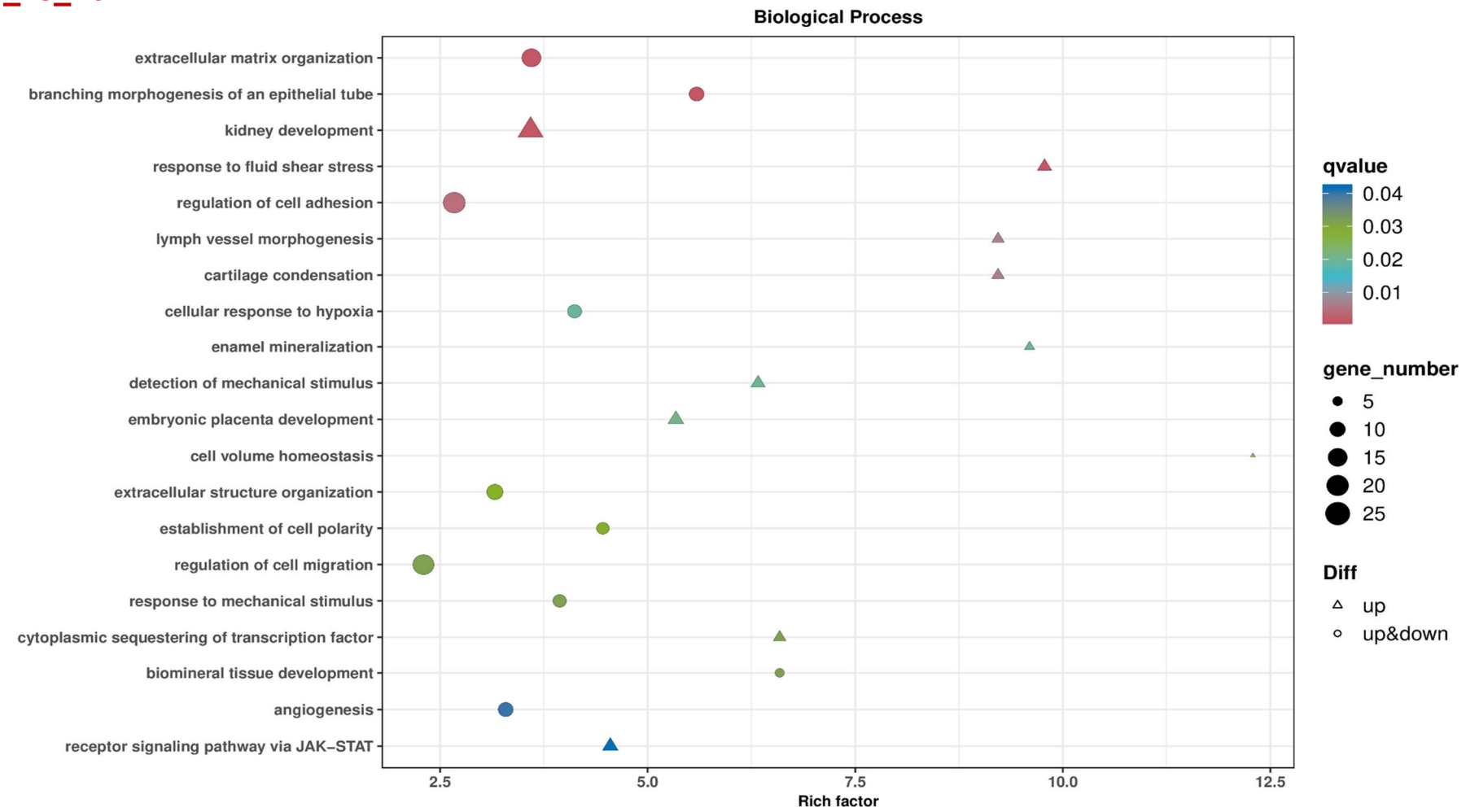

Figure 8.2: Biological process of DEGs in fibroblasts exposed to *S. epidermidis* lysate and compered to no-lysate control in 5.5 mM glucose concentration (FSe5_vs_F5). The Graph shows the top 20 significantly enriched biological processes found in fibroblasts treated with *S. epidermidis* lysate for 12 h in 5.5 mM glucose concentration compared no-lysate control in same glucose concentration. Each dot represents a biological process. Y-axis: Name of biological process; X-axis: Rich factor represent Enrichment factor that calculated as "Enrichment factor=(Ratio of DEG annotated to the term over all DEG)/(Ratio of genes annotated to the term over all genes)“ A larger enrichment factor indicates a more significant enrichment of the pathway. The colour of the dots stands for q-value (adjusted p-value). The smaller the q-value is, the more significant or reliable the enrichment is. The size of the dots represents the number of DEG enriched in this pathway. The larger the dot is, the more genes it contains. Graph created with (BMKGENE, 2023).

FSe20_vs_F20

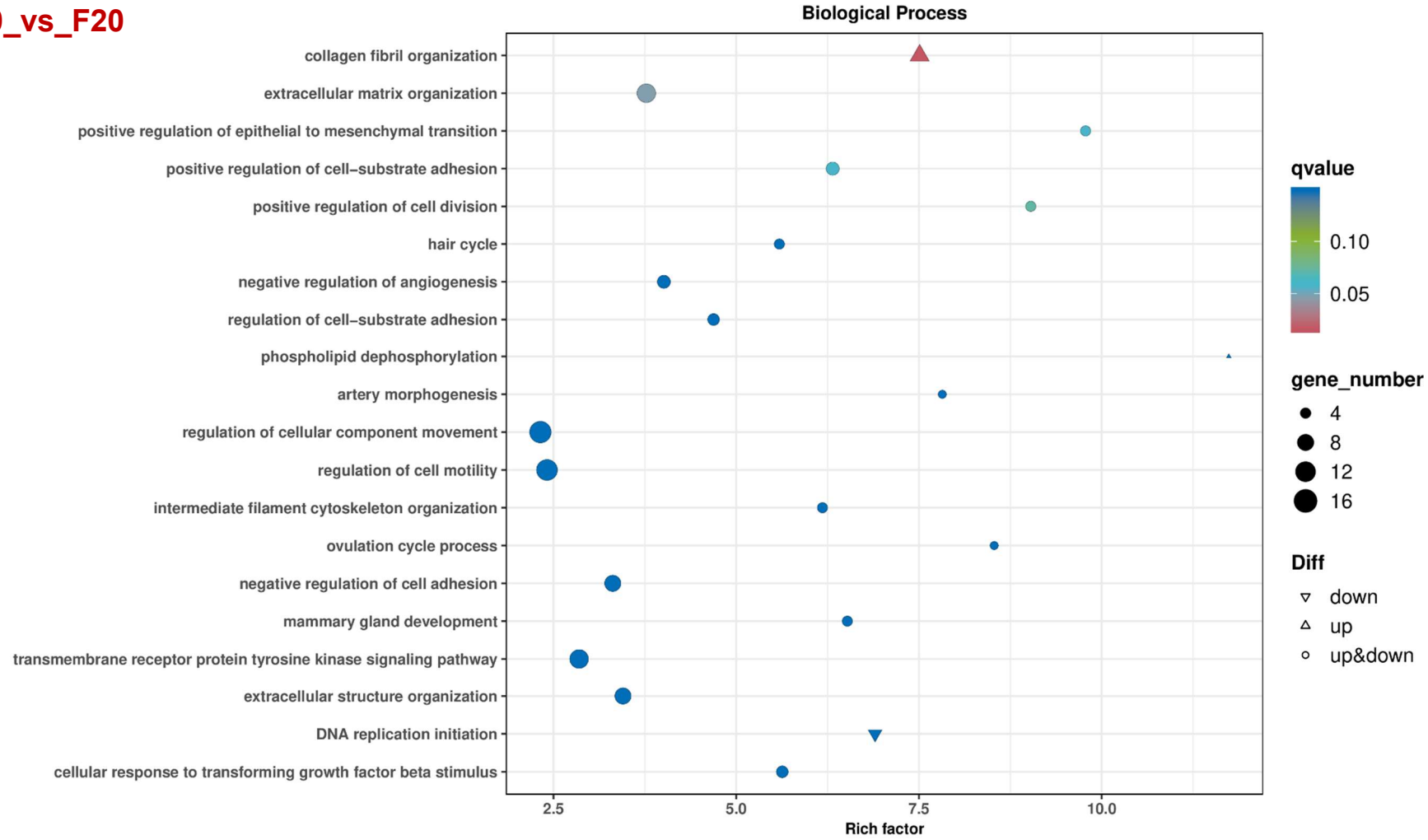

Figure 8.3: Biological process of DEGs in fibroblasts exposed to *S. epidermidis* lysate and compered to no-lysate control in 20 mM glucose concentration (FSe20_vs_F20). The Graph shows the top 20 significantly enriched biological processes found in fibroblasts treated with *S. epidermidis* lysate for 12 h in 20 mM glucose concentration compared no-lysate control in same glucose concentration. Each dot represents a biological process. Y-axis: Name of biological process; X-axis: Rich factor represent Enrichment factor that calculated as "Enrichment factor=(Ratio of DEG annotated to the term over all DEG)/(Ratio of genes annotated to the term over all genes)“ A larger enrichment factor indicates a more significant enrichment of the pathway. The colour of the dots stands for q-value (adjusted p-value). The smaller the q-value is, the more significant or reliable the enrichment is. The size of the dots represents the number of DEG enriched in this pathway. The larger the dot is, the more genes it contains. Graph created with (BMKGENE, 2023).

F20_vs_F5

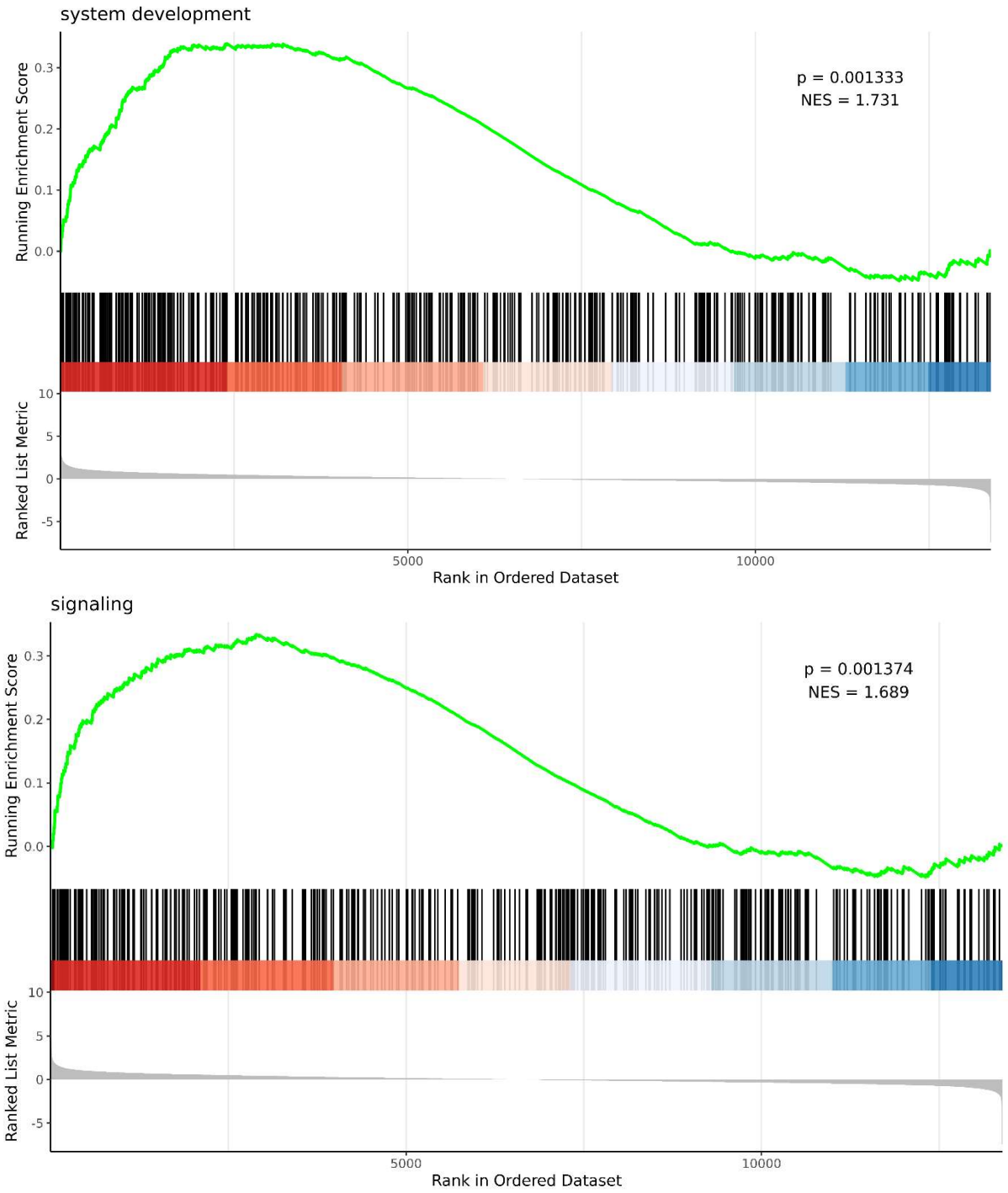

***Figure* 8.4: GSEA analysis of GO biological process of DEG in fibroblasts grown in 20 mM glucose concentration and compared to euglycemic control (5.5 mM) (F20_vs_F5).** GSEA can detect weak alterations in gene expression that cannot be detected by GO. Thus, to confirm GO results, GSEA was carried out and two most significant pathways were selected based on p-value<0.001 and FDR<0.05 (A & B). In both figures (A &B), the upper figure, X-axis: Position of gene set after ordering; Y-axis: Enrichment score; The lines on the top represent genes in the gene set. Green curve shows the enrichment score of each gene set across positions. In the lower figure, X-axis: Position of gene set after ordering. Y-axis: Score. Each line represents a gene in gene set. The length of lines indicates corresponding score. NES represent normalised enrichment score. Figure created by (BMKGENE, 2023).

FSe5_vs_F5

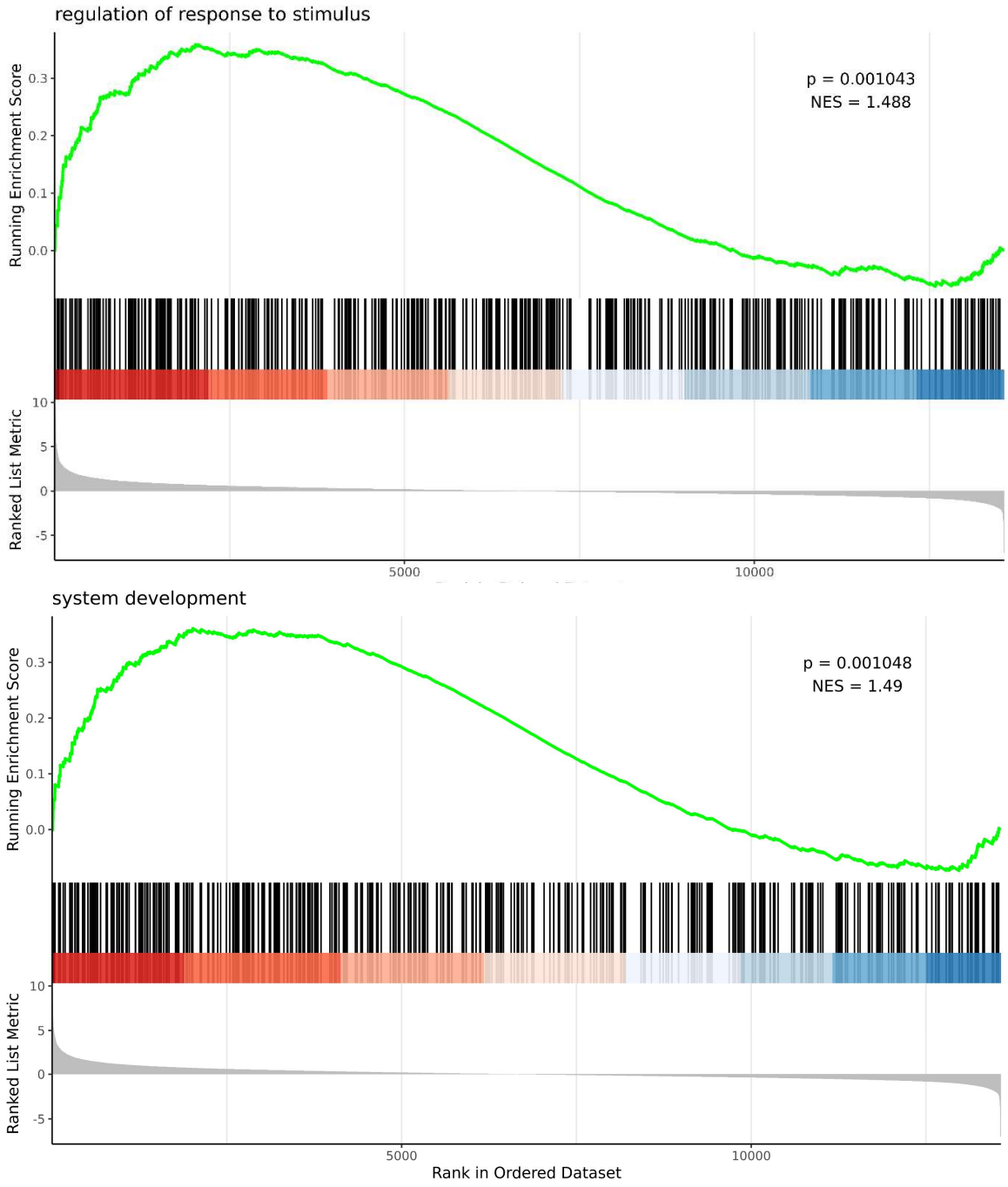

Figure 8.5: GSEA analysis of GO biological process of DEGs in fibroblasts exposed to *S. epidermidis* lysate and compered to no-lysate control in 5.5 mM glucose concentration (FSe5_vs_F5). GSEA can detect weak alterations in gene expression that cannot be detected by GO. Thus, to confirm GO results, GSEA was carried out and two most significant pathways were selected based on p-value<0.001 and FDR<0.05. In both figures (A &B), the upper figure, X-axis: Position of gene set after ordering; Y-axis: Enrichment score; The lines on the top represent genes in the gene set. Green curve shows the enrichment score of each gene set across positions. In the lower figure, X-axis: Position of gene set after ordering. Y-axis: Score. Each line represents a gene in gene set. The length of lines indicates corresponding score. NES represent normalised enrichment score. Figure created by (BMKGENE, 2023).

FSe20_vs_F20

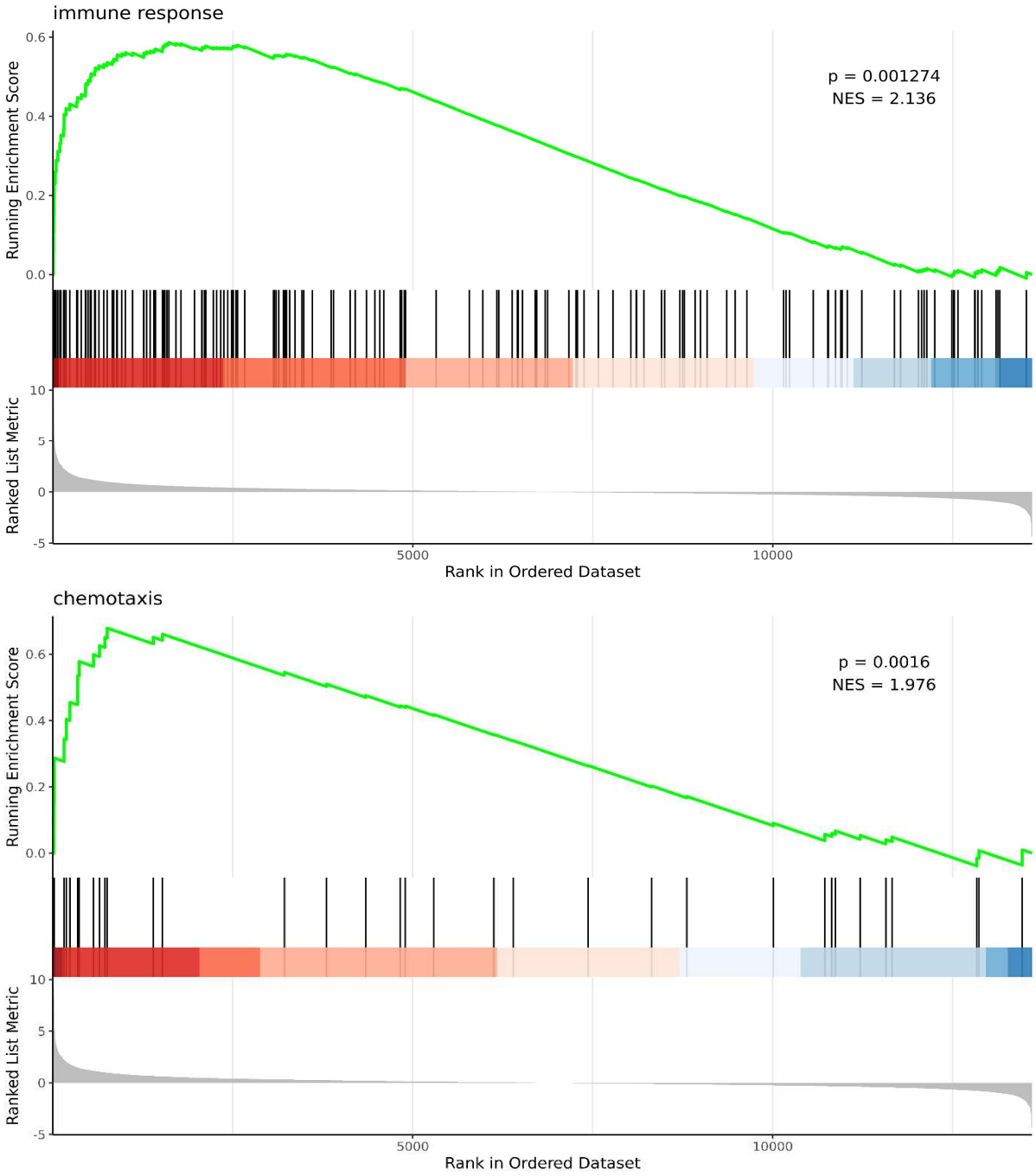

Figure 8.6: GSEA analysis of GO biological process of DEGs in fibroblasts exposed to *S. epidermidis* lysate and compered to no-lysate control in 20 mM glucose concentration (FSe20_vs_F20). GSEA can detect weak alterations in gene expression that cannot be detected by GO. Thus, to confirm GO results, GSEA was carried out and two most significant pathways were selected based on p-value<0.001 and FDR<0.05. In both figures (A &B), the upper figure, X-axis: Position of gene set after ordering; Y-axis: Enrichment score; The lines on the top represent genes in the gene set. Green curve shows the enrichment score of each gene set across positions. In the lower figure, X-axis: Position of gene set after ordering. Y-axis: Score. Each line represents a gene in gene set. The length of lines indicates corresponding score. NES represent normalised enrichment score. Figure created by (BMKGENE, 2023).

F20_vs_F5

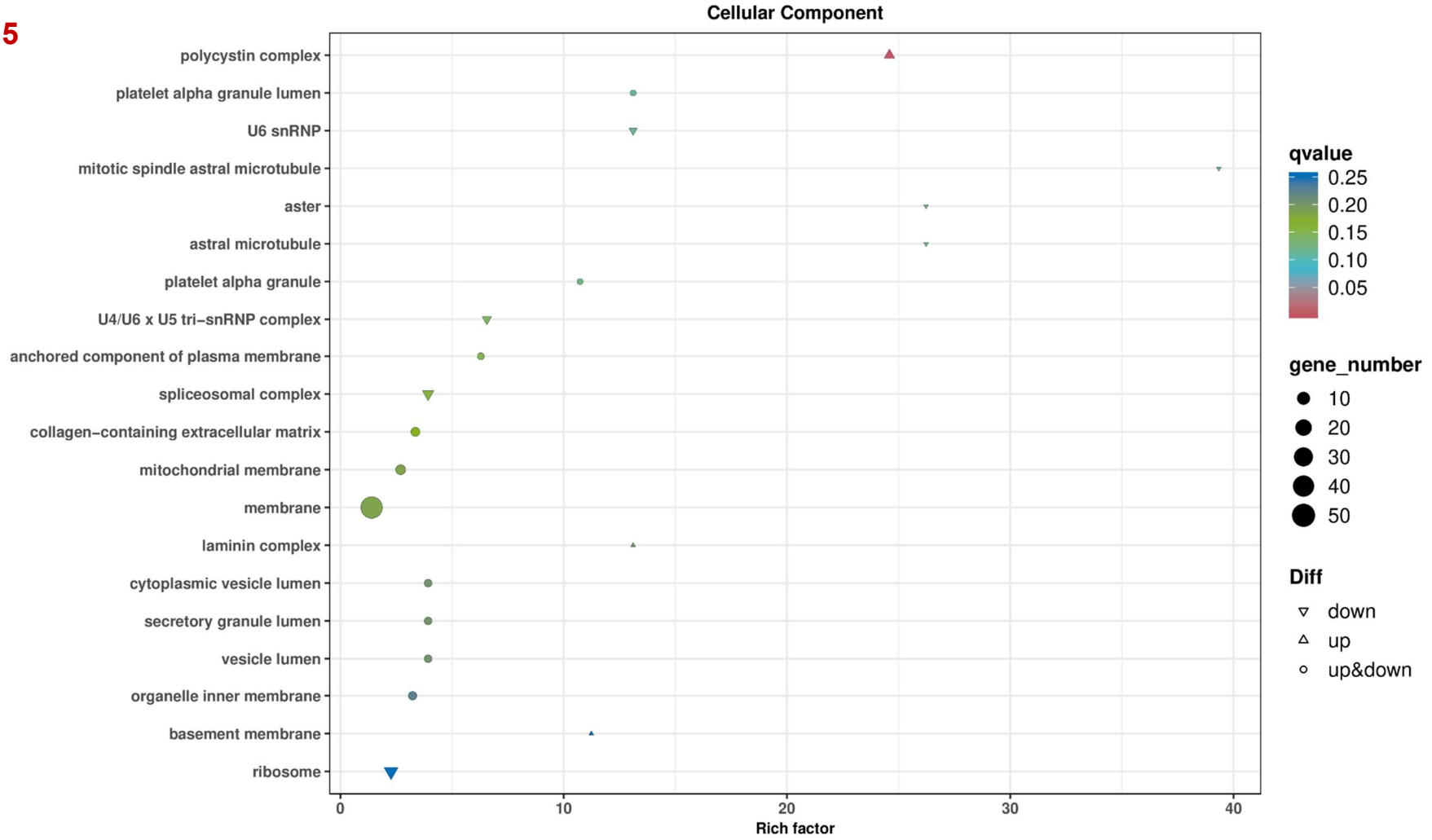

Figure 8.7: Cellular Component of DEGs in fibroblasts grown in 20 mM glucose concentration and compared to euglycemic control (5.5 mM) (F20_vs_F5). The Graph shows the top 20 significantly enriched terms of cellular component altered in fibroblasts growing in high glucose concentrations (20 mM) compared to fibroblasts growing in euglycemic glucose concentrations (5.5 mM). Analysis done in GO. Each dot represents a cellular component. Y-axis: Name of cellular component; X-axis: Rich factor represent Enrichment factor that calculated as "Enrichment factor=(Ratio of DEG annotated to the term over all DEG)/(Ratio of genes annotated to the term over all genes)“ A larger enrichment factor represent a more significant enrichment of the pathway. The colour of the dots stands for q-value (adjusted p-value). The smaller the q-value represent the more reliable and significant the enrichment is. The size of the dots represents the number of DEG enriched in this pathway. The larger the dot is, the more genes it contains. Graph created with (BMKGENE, 2023).

FSe5_vs_F5

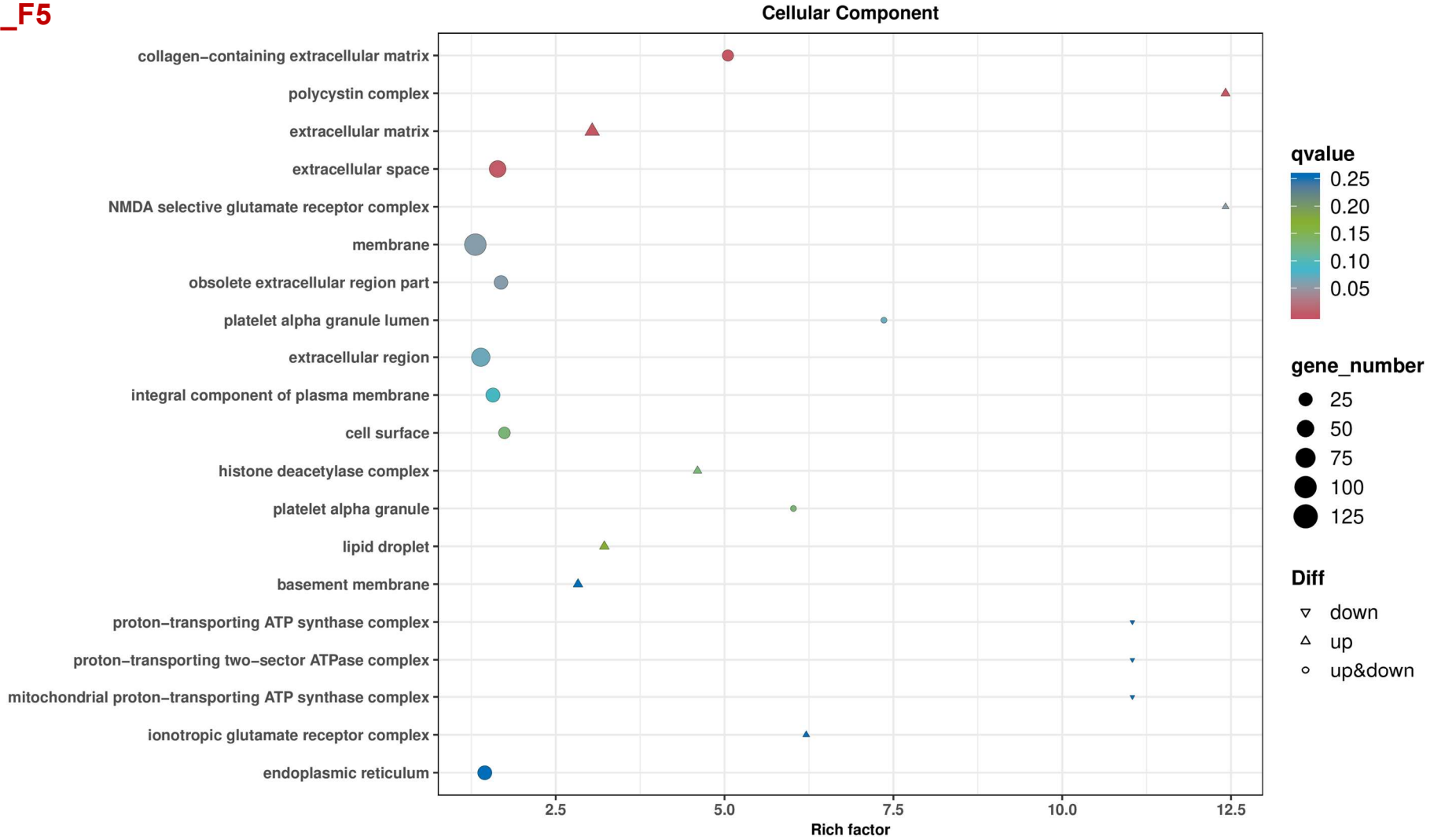

Figure 8.8: Cellular component of DEGs in fibroblasts exposed to *S. epidermidis* lysate and compered to no-lysate control in 5.5 mM glucose concentration (FSe5_vs_F5). The Graph shows the top 20 significantly enriched cellular component found in fibroblasts treated with *S. epidermidis* lysate for 12 h in 5.5 mM glucose concentration compared no-lysate control in same glucose concentration. Analysis done in GO. Each dot represents a cellular component. Y-axis: Name of cellular component; X-axis: Rich factor represent Enrichment factor that calculated as "Enrichment factor=(Ratio of DEG annotated to the term over all DEG)/(Ratio of genes annotated to the term over all genes)“ A larger enrichment factor represent a more significant enrichment of the pathway. The colour of the dots stands for q-value (adjusted p-value). The smaller the q-value represent the more reliable and significant the enrichment is. The size of the dots represents the number of DEG enriched in this pathway. The larger the dot is, the more genes it contains. Graph created by (BMKGENE, 2023)

FSe20_vs_F20

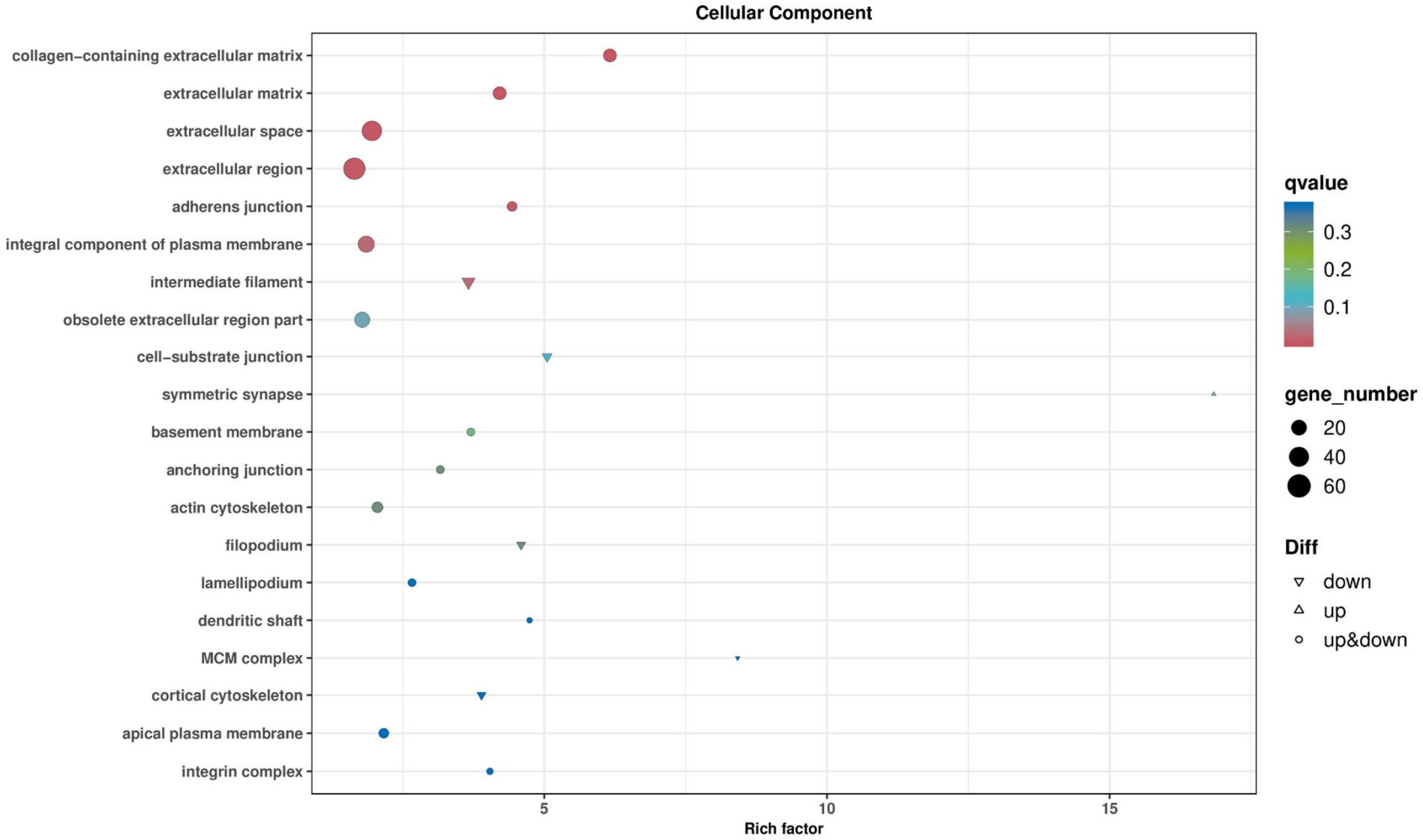

Figure 8.9: Cellular component of DEGs in fibroblasts exposed to *S. epidermidis* lysate and compered to no-lysate control in 20 mM glucose concentration (FSe20_vs_F20). The Graph shows the top 20 significantly enriched cellular component found in fibroblasts treated with *S. epidermidis* lysate for 12 h in 20 mM glucose concentration compared no-lysate control in same glucose concentration. Analysis done in GO. Each dot represents a cellular component. Y-axis: Name of cellular component; X-axis: Rich factor represent Enrichment factor that calculated as "Enrichment factor=(Ratio of DEG annotated to the term over all DEG)/(Ratio of genes annotated to the term over all genes)“ A larger enrichment factor represent a more significant enrichment of the pathway. The colour of the dots stands for q-value (adjusted p-value). The smaller the q-value represent the more reliable and significant the enrichment is. The size of the dots represents the number of DEG enriched in this pathway. The larger the dot is, the more genes it contains. Graph created by (BMKGENE, 2023).

F20_vs_F5

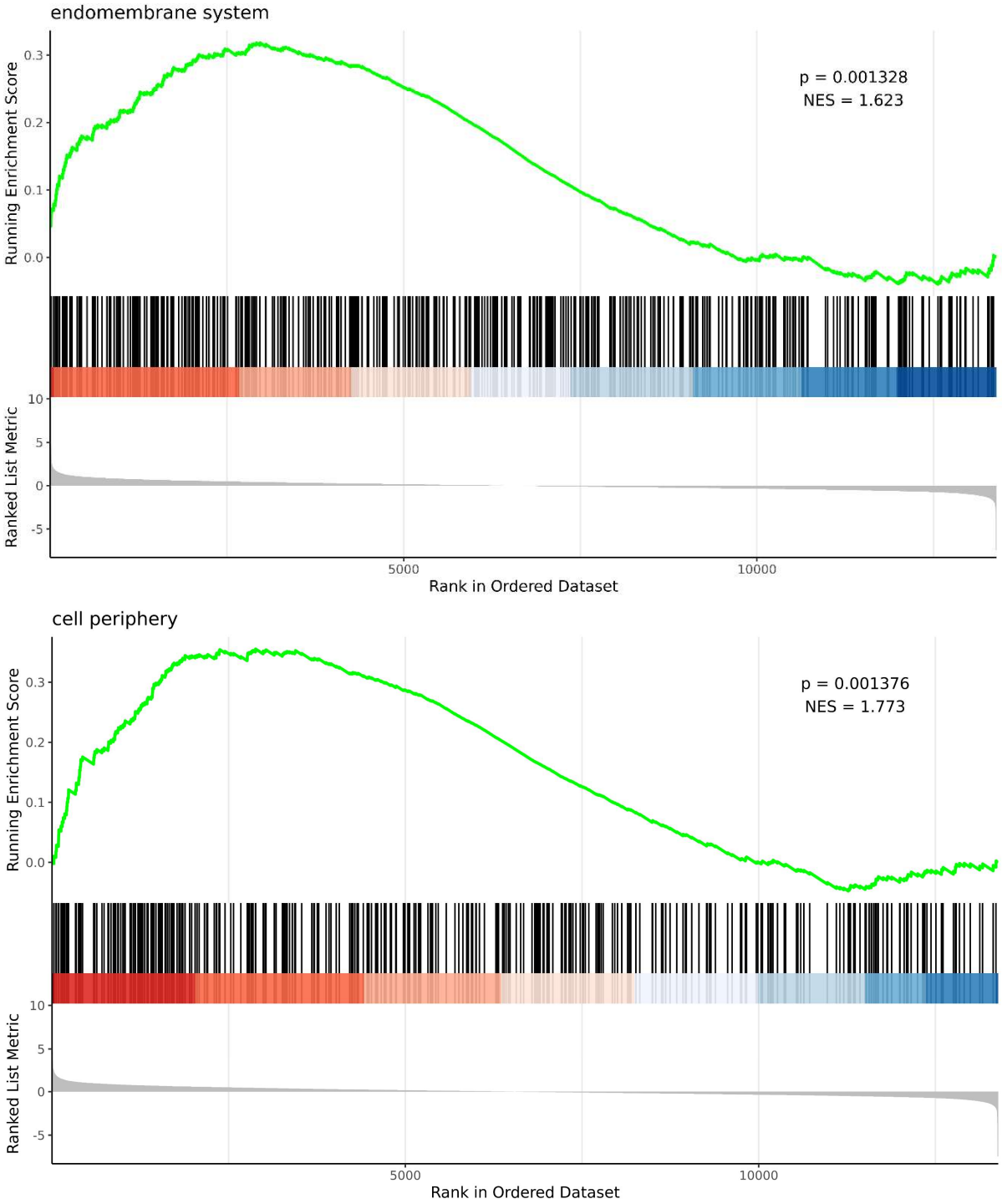

Figure 8.10: GSEA analysis of GO cellular component of DEG in fibroblasts grown in 20 mM glucose concentration and compared to euglycemic control (5.5 mM) (F20_vs_F5). GSEA can detect weak alterations in gene expression that cannot be detected by GO. Thus, to confirm GO results, GSEA was carried out and two most significant pathways were selected based on p-value<0.001 and FDR<0.05 (A & B). In both figures (A &B), the upper figure, Y-axis: Enrichment score; X-axis: Position of gene set after ordering; The lines on the top represent genes in the gene set. Green curve represents the enrichment score of each gene set across positions. In the lower figure, X-axis: Position of gene set after ordering. Y-axis: Score. Each line represents a gene in gene set. The length of lines indicates corresponding score. NES represent normalised enrichment score. Figure created by (BMKGENE, 2023)

FSe5_vs_F5

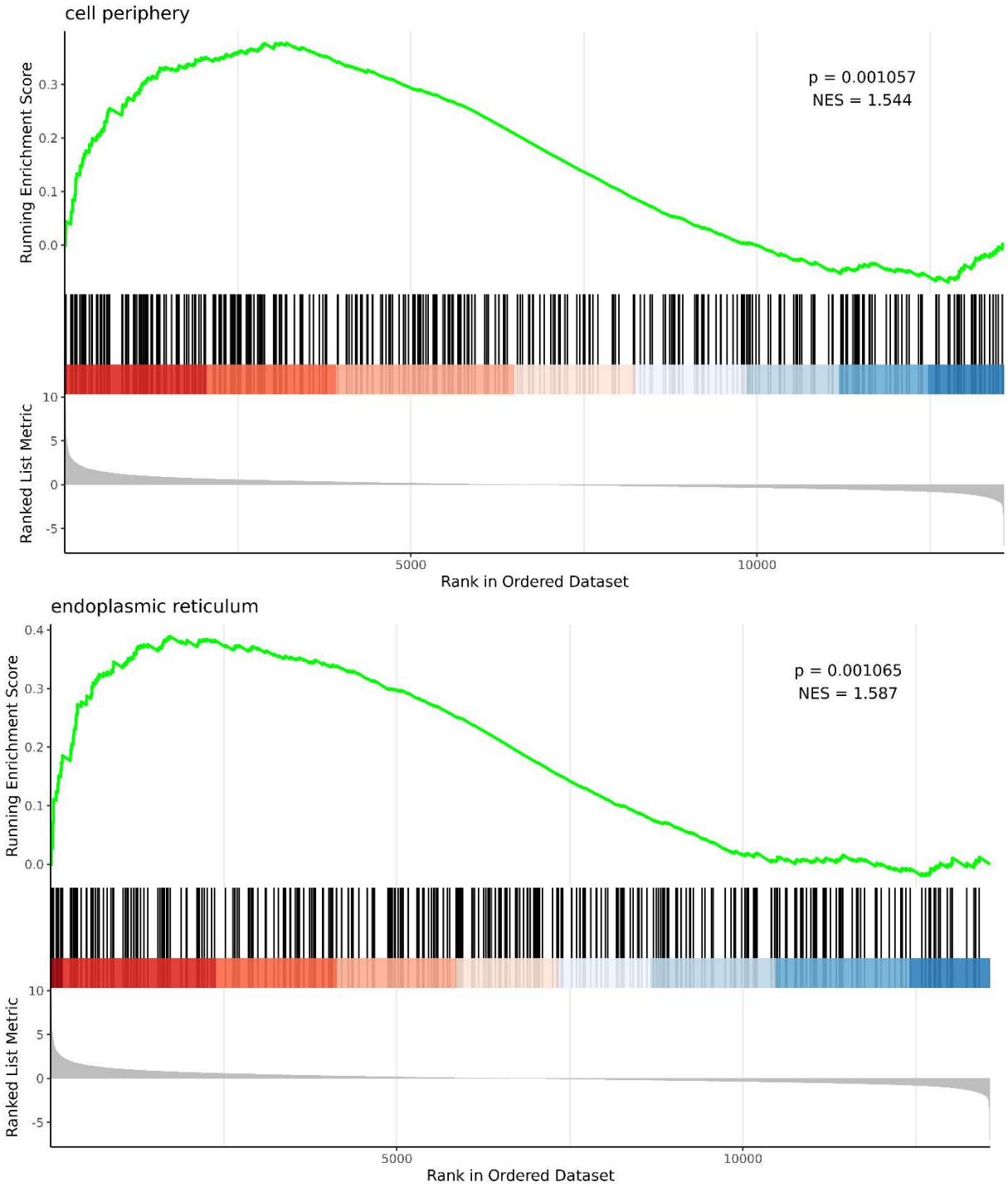

Figure 8.11: GSEA analysis of GO cellular component of DEGs in fibroblasts exposed to *S. epidermidis* lysate and compered to no-lysate control in 5.5 mM glucose concentration (FSe5_vs_F5). GSEA can detect weak alterations in gene expression that cannot be detected by GO. Thus, to confirm GO results, GSEA was carried out and two most significant pathways were selected based on p-value<0.001 and FDR<0.05. In both figures (A &B), the upper figure, Y-axis: Enrichment score; X-axis: Position of gene set after ordering; The lines on the top represent genes in the gene set. Green curve represents the enrichment score of each gene set across positions. In the lower figure, X-axis: Position of gene set after ordering. Y-axis: Score. Each line represents a gene in gene set. The length of lines indicates corresponding score. NES represent normalised enrichment score. Figure created by (BMKGENE, 2023).

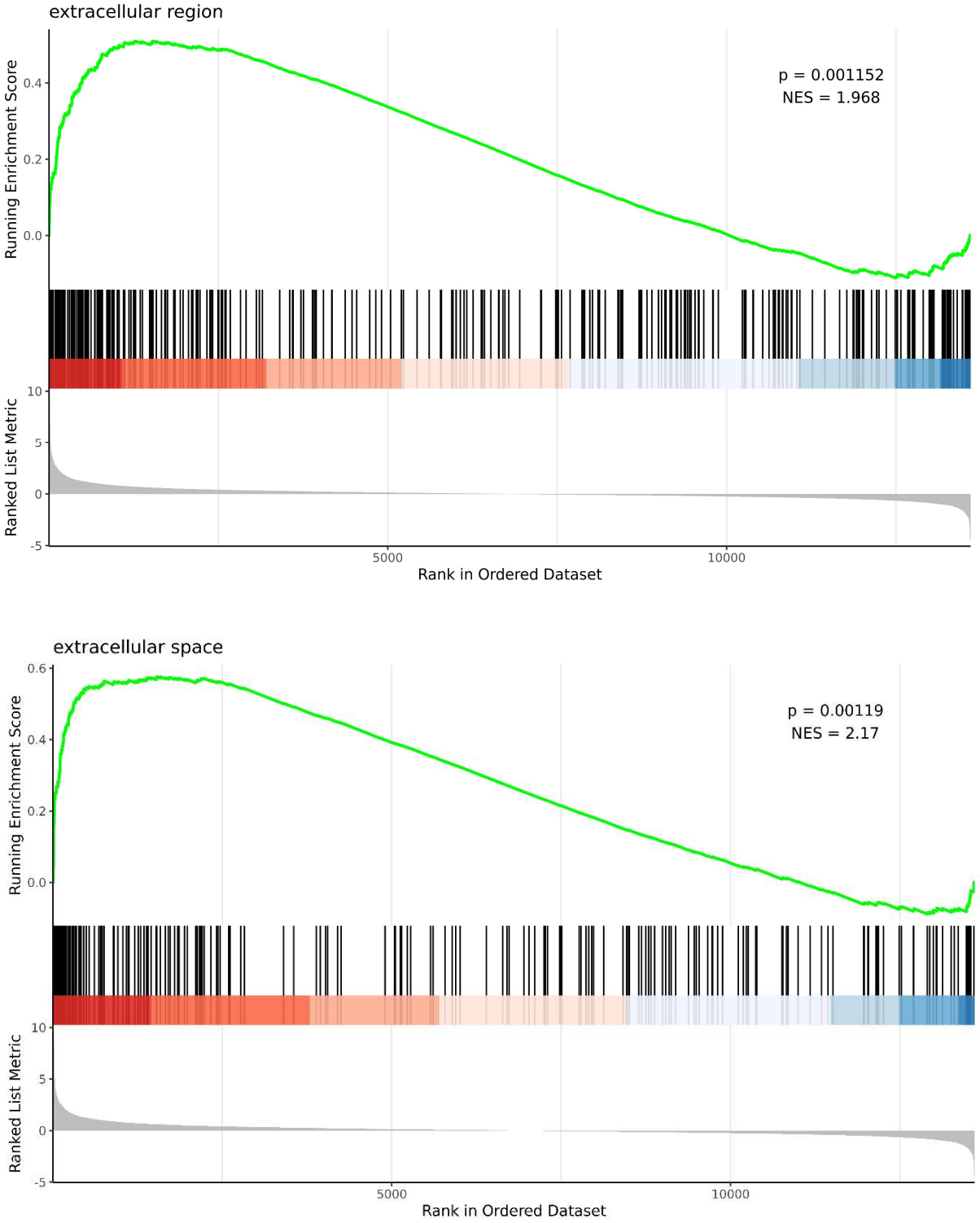

Figure 8.12: GSEA analysis of GO cellular component of DEGs in fibroblasts exposed to *S. epidermidis* lysate and compered to no-lysate control in 20 mM glucose concentration (FSe20_vs_F20). GSEA can detect weak alterations in gene expression that cannot be detected by GO. Thus, to confirm GO results, GSEA was carried out and two most significant pathways were selected based on p-value<0.001 and FDR<0.05. In both figures (A &B), the upper figure, Y-axis: Enrichment score; X-axis: Position of gene set after ordering; The lines on the top represent genes in the gene set. Green curve represents the enrichment score of each gene set across positions. In the lower figure, X-axis: Position of gene set after ordering. Y-axis: Score. Each line represents a gene in gene set. The length of lines indicates corresponding score. NES represent normalised enrichment score. Figure created by (BMKGENE, 2023)

F20_vs_F5

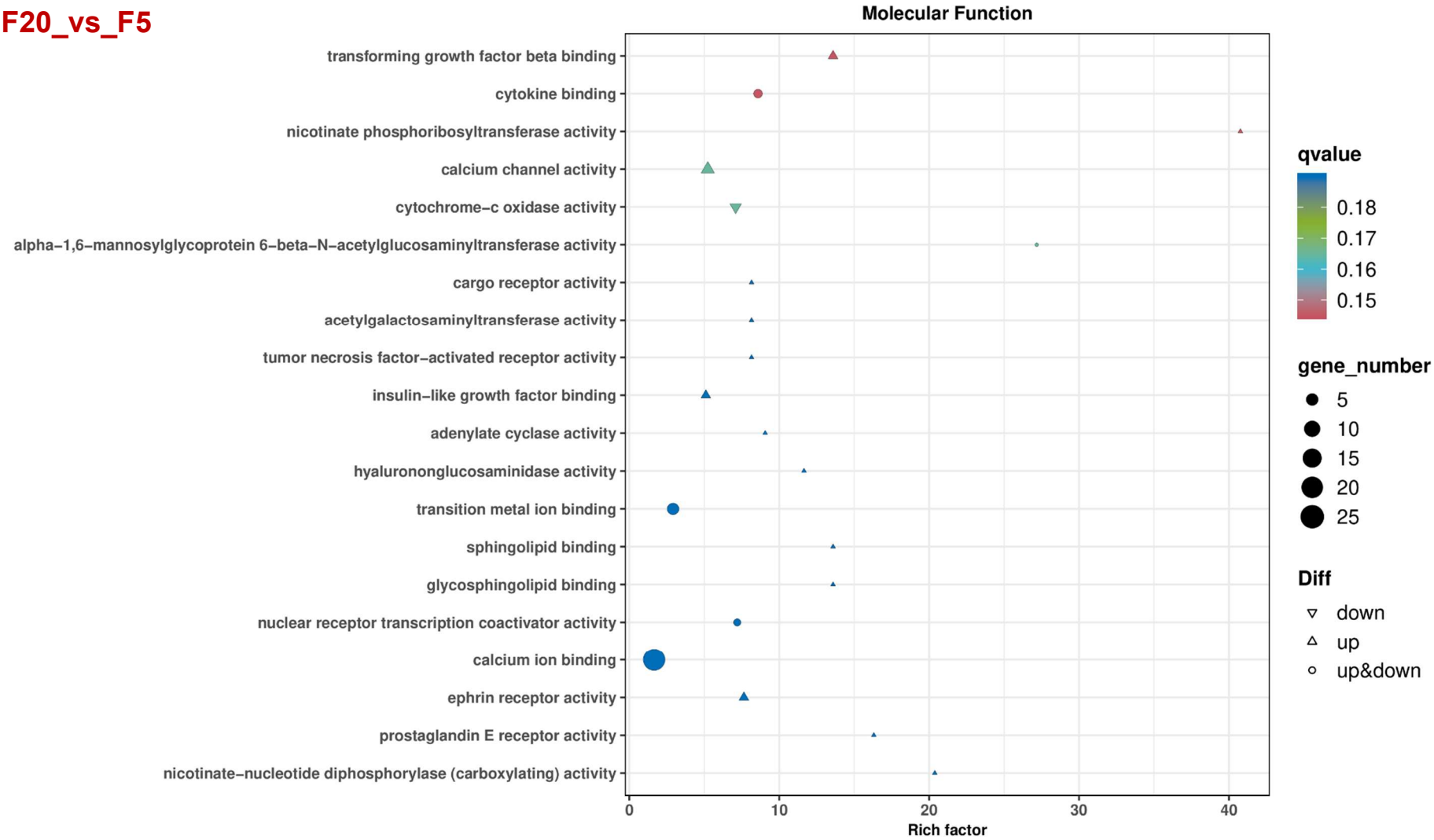

Figure 8.13: Molecular function in fibroblasts grown in 20 mM glucose concentration and compared to euglycemic control (5.5 mM) (F20_vs_F5). The Graph shows the top 20 significantly enriched terms of molecular function altered in fibroblasts growing in high glucose concentrations (20 mM) compared to fibroblasts growing in euglycemic glucose concentrations (5.5 mM). Analysis done in GO. Each dot represents a molecular function. Y-axis: Name of molecular function; X-axis: Rich factor represent Enrichment factor that calculated as "Enrichment factor=(Ratio of DEG annotated to the term over all DEG)/(Ratio of genes annotated to the term over all genes)“ A larger enrichment factor represent a more significant enrichment of the pathway. The colour of the dots stands for q-value (adjusted p-value). The smaller the q-value represent the more reliable and significant the enrichment is. The size of the dots represents the number of DEG enriched in this pathway. The larger the dot is, the more genes it contains. Graph created by (BMKGENE, 2023).

FSe5_vs_F5

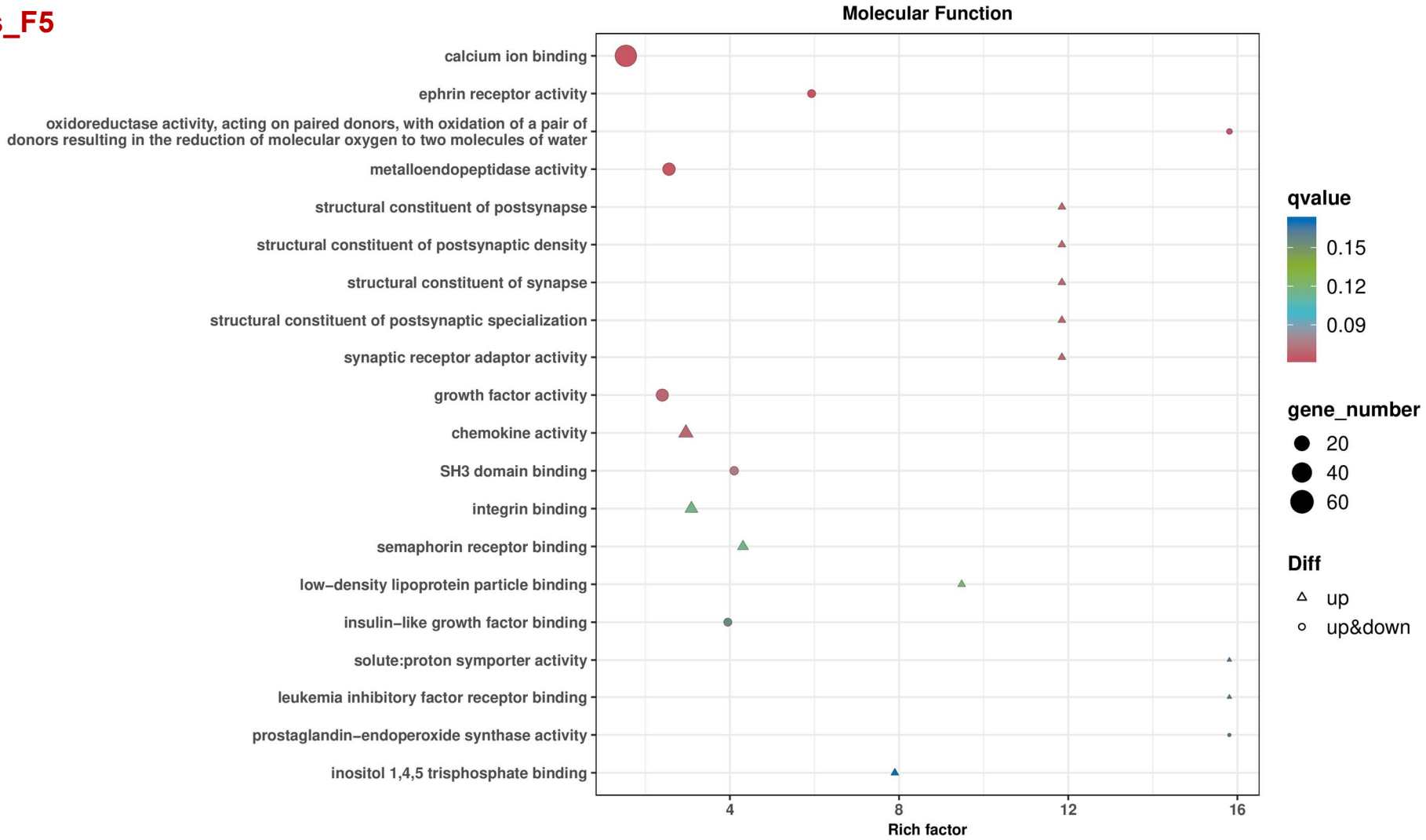

Figure 8.14: Molecular function of DEGs in fibroblasts exposed to *S. epidermidis* lysate and compered to no-lysate control in 5.5 mM glucose concentration (FSe5_vs_F5). The Graph shows the top 20 significantly enriched molecular function found in fibroblasts treated with *S. epidermidis* lysate for 12 h in 5.5 mM glucose concentration compared no-lysate control in same glucose concentration. Analysis done in GO. Each dot represents a molecular function. Y-axis: Name of molecular function; X-axis: Rich factor represent Enrichment factor that calculated as "Enrichment factor=(Ratio of DEG annotated to the term over all DEG)/(Ratio of genes annotated to the term over all genes)“ A larger enrichment factor represent a more significant enrichment of the pathway. The colour of the dots stands for q-value (adjusted p-value). The smaller the q-value represent the more reliable and significant the enrichment is. The size of the dots represents the number of DEG enriched in this pathway. The larger the dot is, the more genes it contains. Graph created by (BMKGENE, 2023).

FSe20_vs_F20

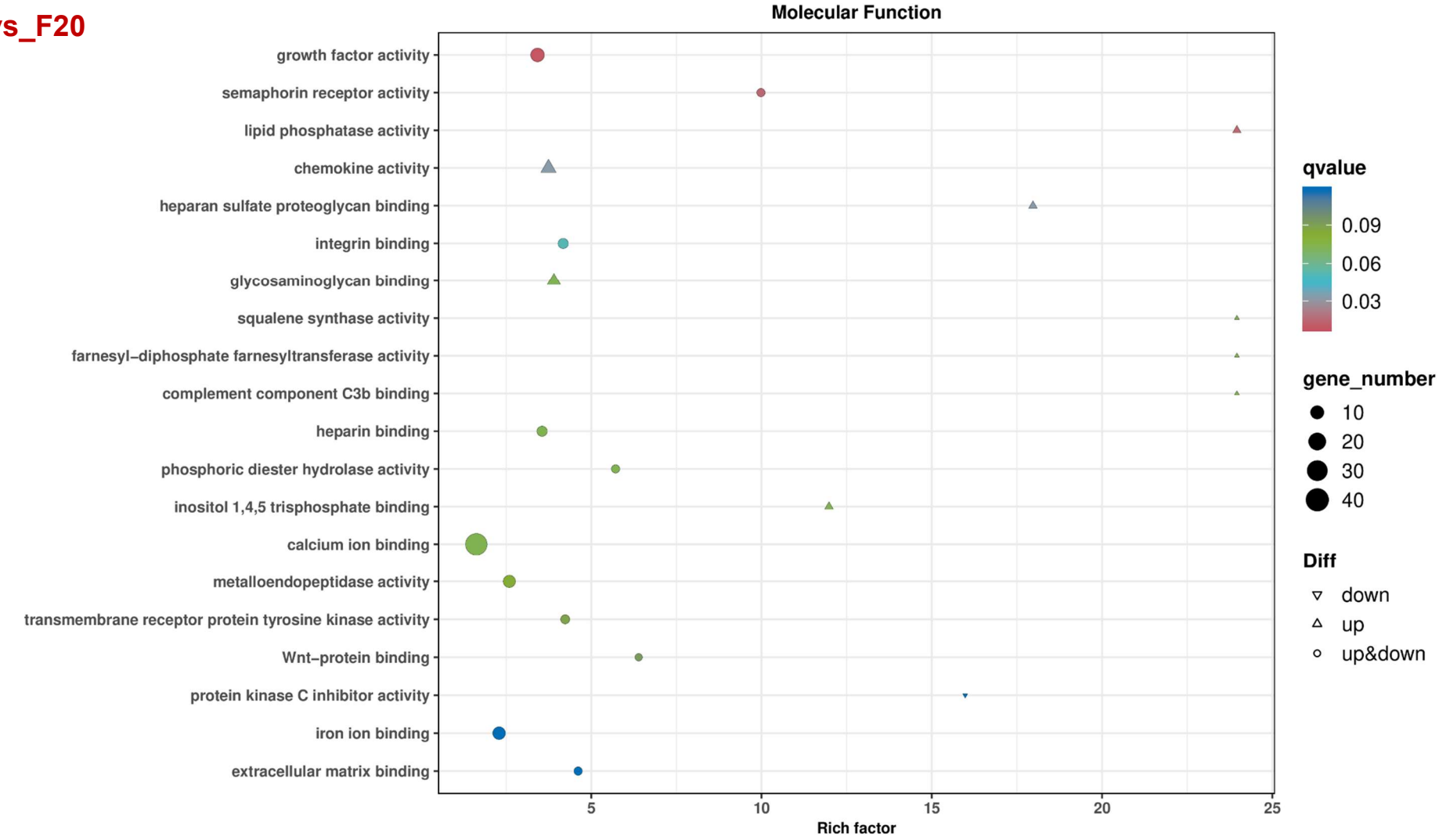

Figure 8.15: Molecular function of DEGs in fibroblasts exposed to *S. epidermidis* lysate and compered to no-lysate control in 20 mM glucose concentration (FSe20_vs_F20). The Graph shows the top 20 significantly enriched molecular function found in fibroblasts treated with *S. epidermidis* lysate for 12 h in 20 mM glucose concentration compared no-lysate control in same glucose concentration. Analysis done in GO. Each dot represents a molecular function. Y-axis: Name of molecular function; X-axis: Rich factor represent Enrichment factor that calculated as "Enrichment factor = (Ratio of DEG annotated to the term over all DEG)/(Ratio of genes annotated to the term over all genes)“ A larger enrichment factor represent a more significant enrichment of the pathway. The colour of the dots stands for q-value (adjusted p-value). The smaller the q-value represent the more reliable and significant the enrichment is. The size of the dots represents the number of DEG enriched in this pathway. The larger the dot is, the more genes it contains. Graph created by (BMKGENE, 2023).

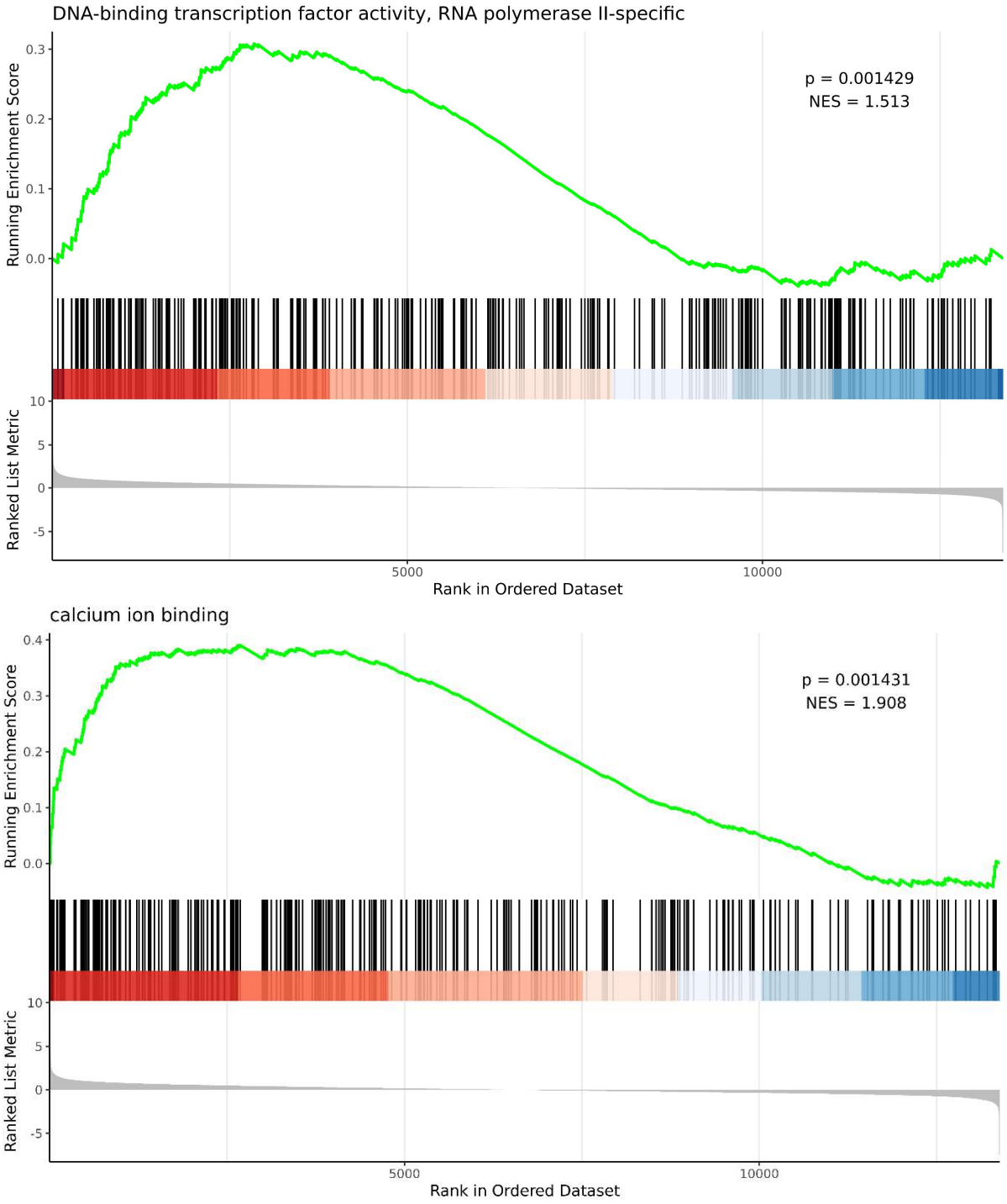

Figure 8.16: GSEA analysis of GO molecular function of DEG in fibroblasts grown in 20 mM glucose concentration and compared to euglycemic control (5.5 mM) (F20_vs_F5). GSEA can detect weak alterations in gene expression that cannot be detected by GO. Thus, to confirm GO results, GSEA was carried out and two most significant pathways were selected based on p-value<0.001 and FDR<0.05 (A & B). In both figures (A &B), the upper figure, Y-axis: Enrichment score; X-axis: Position of gene set after ordering; The lines on the top represent genes in the gene set. Green curve represents the enrichment score of each gene set across positions. In the lower figure, X-axis: Position of gene set after ordering. Y-axis: Score. Each line represents a gene in gene set. The length of lines indicates corresponding score. NES represent normalised enrichment score. Figure created by (BMKGENE, 2023).

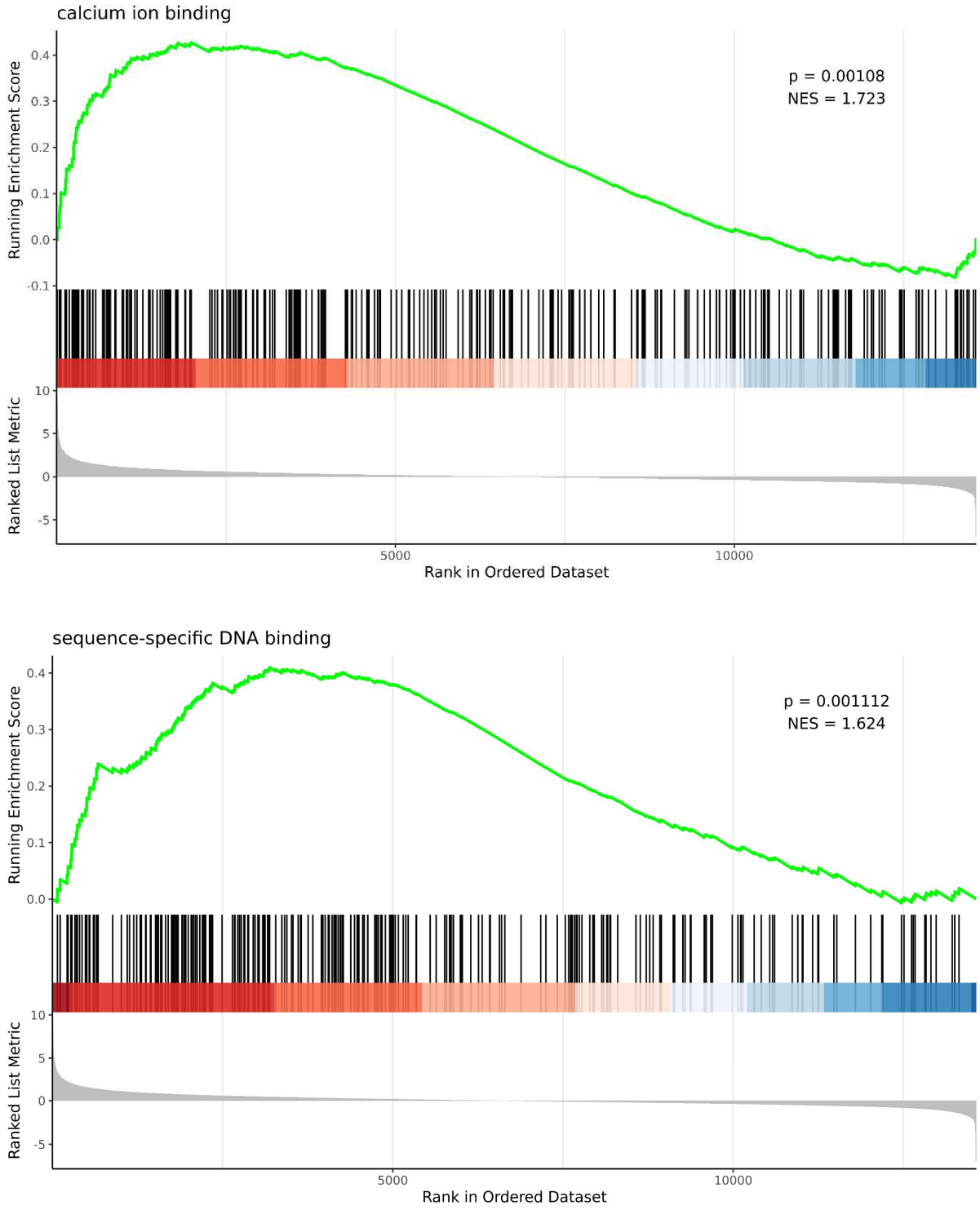

Figure 8.17: GSEA analysis of GO cellular component of DEGs in fibroblasts exposed to *S. epidermidis* lysate and compered to no-lysate control in 5.5 mM glucose concentration (FSe5_vs_F5). GSEA can detect weak alterations in gene expression that cannot be detected by GO. Thus, to confirm GO results, GSEA was carried out and two most significant pathways were selected based on p-value<0.001 and FDR<0.05. In both figures (A &B), the upper figure, Y-axis: Enrichment score; X-axis: Position of gene set after ordering; The lines on the top represent genes in the gene set. Green curve represents the enrichment score of each gene set across positions. In the lower figure, X-axis: Position of gene set after ordering. Y-axis: Score. Each line represents a gene in gene set. The length of lines indicates corresponding score. NES represent normalised enrichment score. Figure created by (BMKGENE, 2023).

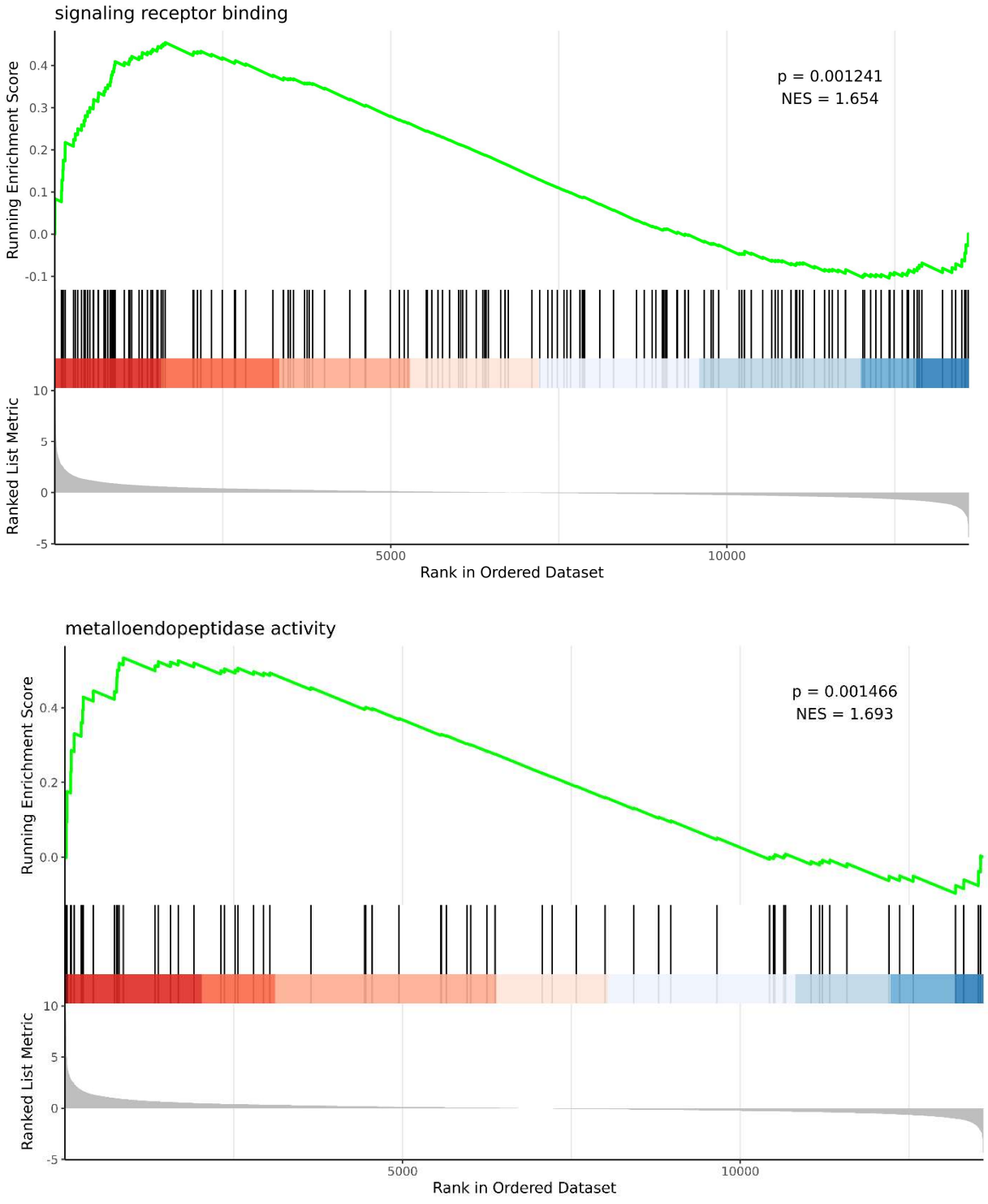

Figure 8.18: GSEA analysis of GO molecular function of DEGs in fibroblasts exposed to *S. epidermidis* lysate and compered to no-lysate control in 20 mM glucose concentration (FSe20_vs_F20). GSEA can detect weak alterations in gene expression that cannot be detected by GO. Thus, to confirm GO results, GSEA was carried out and two most significant pathways were selected based on p-value<0.001 and FDR<0.05. In both figures (A &B), the upper figure, Y-axis: Enrichment score; X-axis: Position of gene set after ordering; The lines on the top represent genes in the gene set. Green curve represents the enrichment score of each gene set across positions. In the lower figure, X-axis: Position of gene set after ordering. Y-axis: Score. Each line represents a gene in gene set. The length of lines indicates corresponding score. NES represent normalised enrichment score. Figure created by (BMKGENE, 2023).

F20_vs_F5

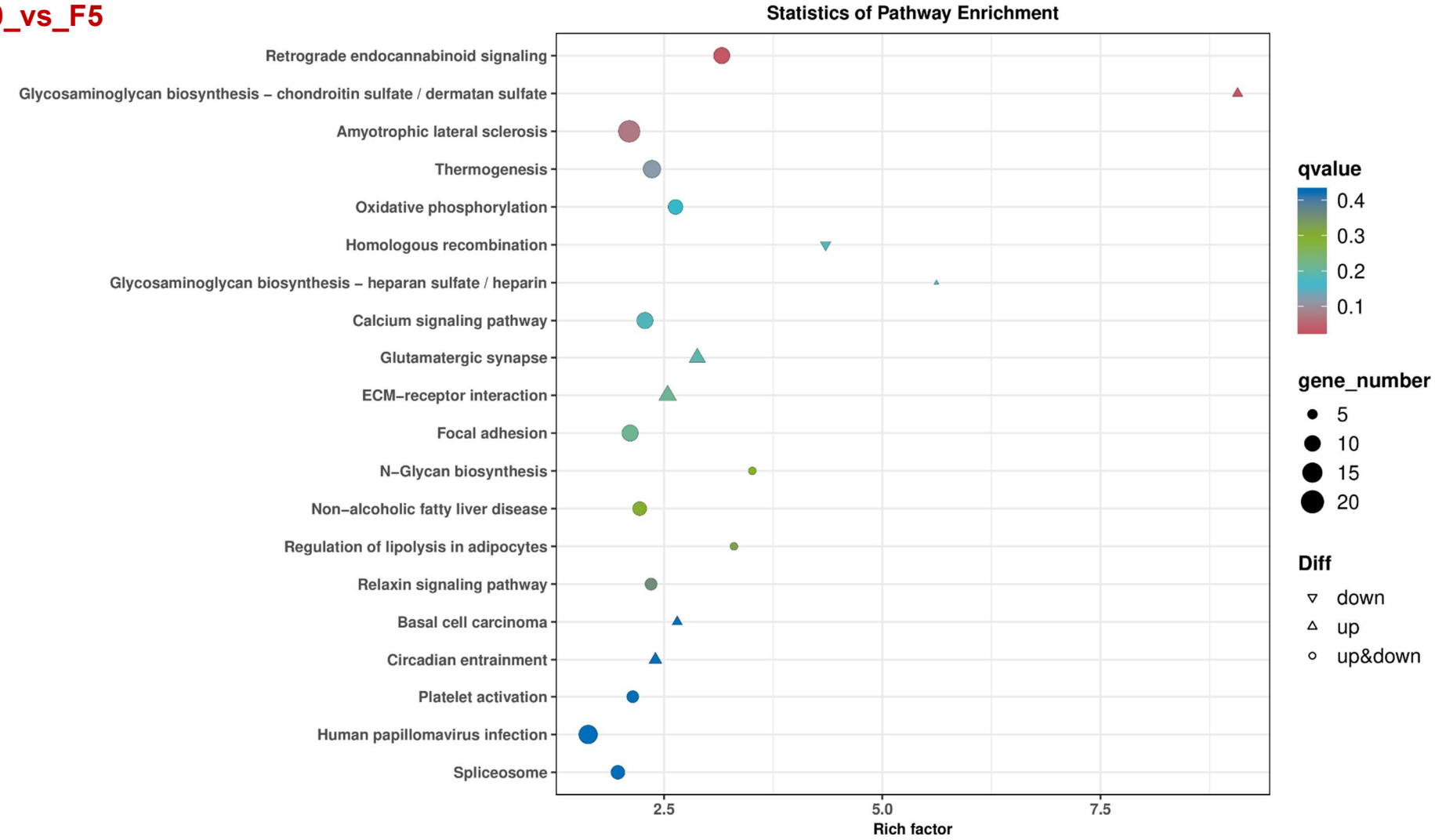

Figure 8.19: Cellular pathways in fibroblasts grown in 20 mM glucose concentration and compared to euglycemic control (5.5 mM) (F20_vs_F5). The Graph shows the top 20 significantly enriched cellular pathway altered in fibroblasts growing in high glucose concentrations (20 mM) compared to fibroblasts growing in euglycemic glucose concentrations (5.5 mM) analysed in KEGG. Each dot represents a cellular pathway. Y-axis: Name of pathway; X-axis: Rich factor represent Enrichment factor that calculated as "Enrichment factor=(Ratio of DEG annotated to the term over all DEG)/(Ratio of genes annotated to the term over all genes)“ A larger enrichment factor represent a more significant enrichment of the pathway. The colour of the dots stands for q-value (adjusted p-value). The smaller the q-value represent the more reliable and significant the enrichment is. The size of the dots represents the number of DEG enriched in this pathway. The larger the dot is, the more genes it contains. Graph created by (BMKGENE, 2023)

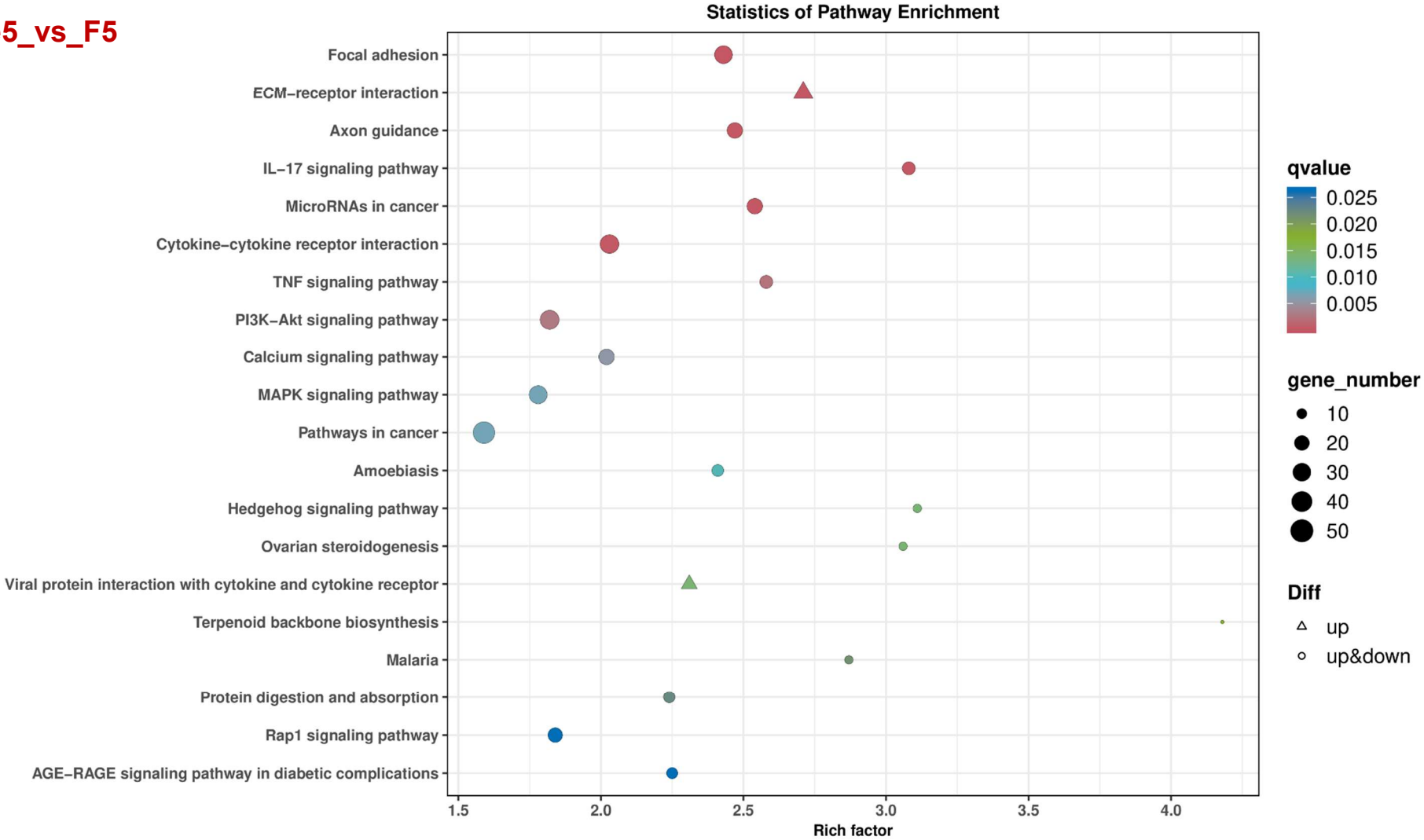

Figure 8.20: Cellular pathway of DEGs in fibroblasts exposed to *S. epidermidis* lysate and compered to no-lysate control in 5.5 mM glucose concentration (FSe5_vs_F5). The Graph shows the top 20 significantly enriched molecular function found in fibroblasts treated with *S. epidermidis* lysate for 12 h in 5.5 mM glucose concentration compared no-lysate control in same glucose concentration analysed by KEGG. Each dot represents a cellular pathway. Y-axis: Name of cellular pathway; X-axis: Rich factor represent Enrichment factor that calculated as "Enrichment factor=(Ratio of DEG annotated to the term over all DEG)/(Ratio of genes annotated to the term over all genes)“ A larger enrichment factor represent a more significant enrichment of the pathway. The colour of the dots stands for q-value (adjusted p-value). The smaller the q-value represent the more reliable and significant the enrichment is. The size of the dots represents the number of DEG enriched in this pathway. The larger the dot is, the more genes it contains. Graph created by (BMKGENE, 2023)

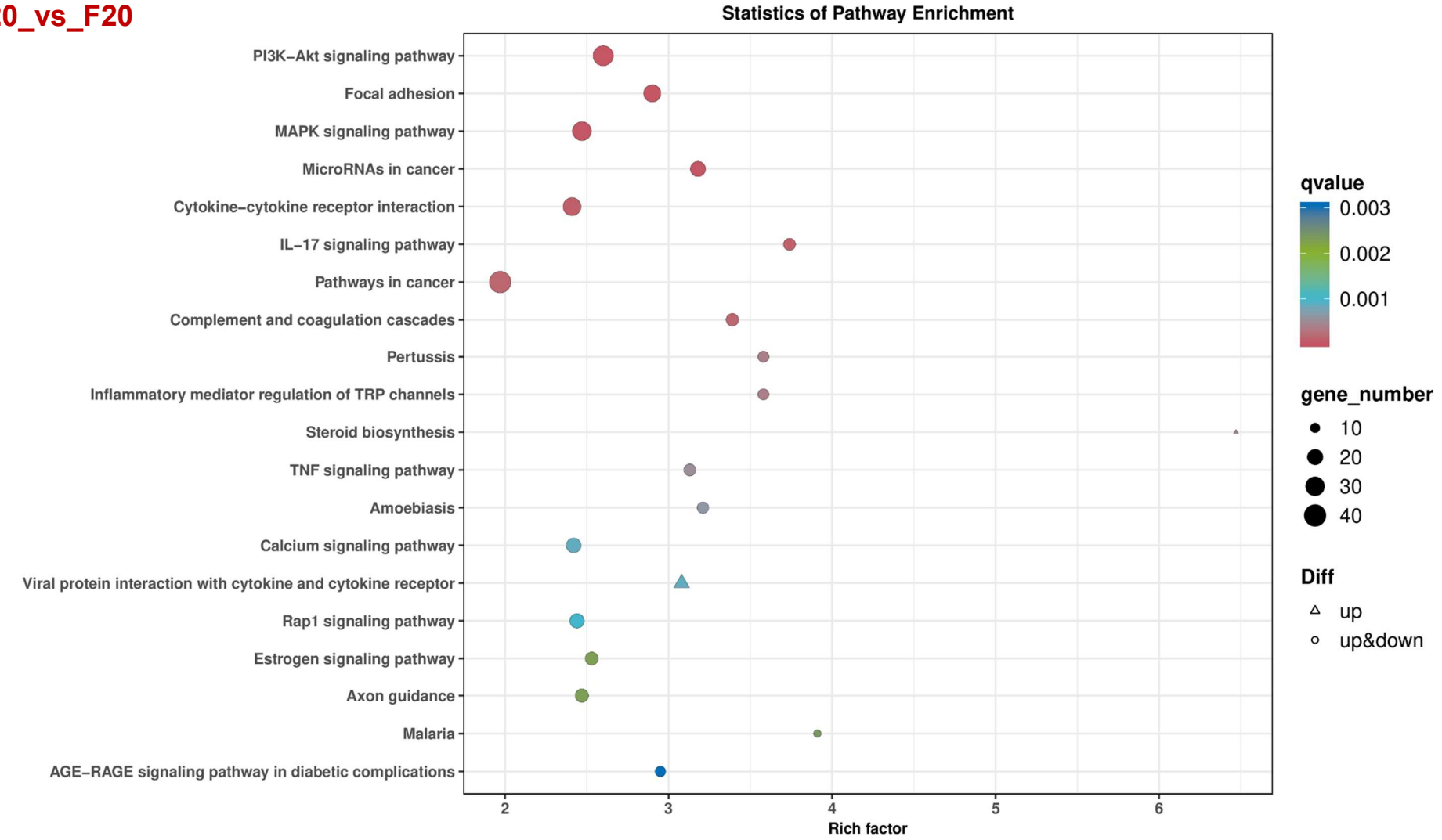

Figure 8.21: Cellular pathway of DEGs in fibroblasts exposed to *S. epidermidis* lysate and compered to no-lysate control in 20 mM glucose concentration (FSe20_vs_F20). The Graph shows the top 20 significantly enriched molecular function found in fibroblasts treated with *S. epidermidis* lysate for 12 h in 5.5 mM glucose concentration compared no-lysate control in same glucose concentration analysed by KEGG. Each dot represents a cellular pathway. Y-axis: Name of cellular pathway; X-axis: Rich factor represent Enrichment factor that calculated as "Enrichment factor=(Ratio of DEG annotated to the term over all DEG)/(Ratio of genes annotated to the term over all genes)“ A larger enrichment factor represent a more significant enrichment of the pathway. The colour of the dots stands for q-value (adjusted p-value). The smaller the q-value represent the more reliable and significant the enrichment is. The size of the dots represents the number of DEG enriched in this pathway. The larger the dot is, the more genes it contains. Graph created by. (BMKGENE, 2023)

Appendix 2

Differentially expressed genes (DEG) in three main groups; Group 1: Fibroblasts grown in high glucose (20 mM) compared to euglycemic control (5.5 mM) (F20_vs_ F5); Group 2: Fibroblasts exposed to *S. epidermidis* lysate compared to no-lysate control in 5.5 mM glucose concentration (FSe5 _vs_F5); Group 3: Fibroblasts exposed to *S. epidermidis* lysate compared to no-lysate control in 20 mM glucose concentration (FSe20 _vs_F20).

Table 8.1: DEG in (F5_vs_F20)

#ID	FDR	log2FC	regulated
gene-TBC1D16-2	8E-13	9.37	up
gene-MAMDC2-2	4E-06	4.68	up
gene-LOC124905366	8E-13	3.58	up
gene-TENM4	4E-18	3.47	up
gene-NRK	5E-04	3.15	up
gene-FAM20C-4	2E-04	2.71	up
gene-PGF	1E-14	2.70	up
gene-DLL4	2E-06	2.65	up
gene-SLC7A8	7E-08	2.55	up
gene-PTGER1	2E-05	2.54	up
gene-FSTL5	5E-05	2.50	up
NewGene_2518	3E-04	2.50	up
gene-INAFM1	3E-06	2.47	up
gene-THBD	2E-05	2.46	up
gene-SLC38A5	2E-09	2.39	up
gene-CPXM2	3E-16	2.37	up
gene-GALNT14	2E-06	2.25	up
gene-EPB41L3	3E-40	2.23	up
gene-HHIP	5E-05	2.22	up
gene-EPHB6	7E-04	2.21	up
gene-TRIM27-6	7E-05	2.21	up
gene-SPTBN5	4E-05	2.16	up
gene-FRAS1	4E-26	2.15	up
gene-DYNLT4	3E-03	2.12	up
gene-FIBCD1	1E-30	2.09	up
NewGene_14	2E-09	2.07	up
gene-SLC15A3	2E-07	2.06	up
gene-LAMA5	2E-18	2.04	up
gene-CNIH3	9E-11	2.03	up
gene-PCDHGB1	1E-04	2.02	up
gene-CLDN4	2E-10	2.01	up
gene-PRELP	1E-06	1.95	up
gene-SCO2	8E-10	1.94	up
gene-PRSS3	2E-11	1.92	up
gene-NPTX2	3E-05	1.92	up
gene-MMP1	8E-35	1.91	up
gene-PCDHGC5	7E-05	1.91	up

gene-PTGER3	6E-03	1.91	up
gene-FOXQ1	3E-05	1.90	up
gene-LRRC4	1E-03	1.90	up
NewGene_2114	3E-04	1.86	up
gene-CITED4	1E-05	1.86	up
gene-CABP1	8E-06	1.86	up
gene-TMEM158	9E-11	1.85	up
gene-EHD3	9E-23	1.83	up
gene-GUCY1A2	5E-05	1.81	up
gene-EPHB6-2	3E-03	1.80	up
gene-IL13RA2	2E-03	1.80	up
gene-DSCAM	1E-04	1.80	up
gene-TRIM27	7E-05	1.79	up
gene-CTU1	1E-17	1.79	up
gene-NCALD	5E-05	1.79	up
gene-KISS1	8E-09	1.78	up
gene-MGAT5B	4E-05	1.77	up
gene-KRTAP1-1-2	2E-04	1.75	up
gene-FOXE1	2E-06	1.75	up
gene-FAM180A	7E-08	1.74	up
gene-CAMK1G	5E-08	1.74	up
gene-MAMDC2	2E-06	1.73	up
gene-SBSPON	7E-04	1.73	up
gene-IER5L	8E-23	1.72	up
NewGene_4495	5E-27	1.70	up
gene-DUSP2	9E-07	1.69	up
gene-C13orf46-2	5E-07	1.69	up
gene-JAM2	4E-05	1.69	up
gene-CSMD2	3E-26	1.68	up
gene-CXCL1	1E-03	1.68	up
gene-SHC3	7E-11	1.68	up
gene-ZFPM1	5E-10	1.68	up
gene-ISLR-2	1E-05	1.67	up
gene-SDK1	3E-05	1.67	up
gene-IGFBP2	1E-17	1.66	up
gene-NAPRT-2	5E-03	1.65	up
gene-ISLR	4E-06	1.64	up
gene-FRMPD3	4E-04	1.64	up
gene-MMP3	7E-34	1.63	up
gene-EDIL3	7E-27	1.63	up
NewGene_6040	9E-03	1.63	up
gene-SOD3	4E-06	1.62	up
gene-TNFRSF6B	4E-03	1.62	up
gene-TINAGL1	2E-15	1.59	up
NewGene_2511	7E-19	1.59	up
gene-TENM3	3E-05	1.58	up
gene-RELN	8E-05	1.57	up

gene-SAMD11	2E-05	1.56	up
gene-MAPK13	7E-10	1.56	up
gene-DCH1	2E-09	1.56	up
gene-CAPN15	2E-32	1.56	up
NewGene_2519	1E-15	1.55	up
gene-FAM222A	2E-03	1.55	up
gene-SOBP	5E-03	1.55	up
gene-KCNQ3	7E-05	1.54	up
gene-ADRA2C	3E-03	1.53	up
gene-PCDHGA9	3E-03	1.53	up
gene-LRRN4CL	6E-08	1.52	up
gene-GRIA1	2E-04	1.51	up
NewGene_2516	6E-05	1.50	up
gene-TAGLN3	1E-03	1.50	up
gene-MALL	2E-08	1.50	up
gene-ADRA1D	4E-35	1.49	up
gene-PSD4	5E-10	1.49	up
gene-FASN	1E-17	1.49	up
gene-SCARA3	8E-28	1.49	up
gene-CXCL14	3E-06	1.48	up
gene-MAML3	9E-05	1.48	up
gene-CEMIP	3E-07	1.48	up
gene-TBX2	2E-17	1.48	up
gene-IL21R	3E-03	1.47	up
gene-PODXL	5E-05	1.47	up
gene-CBARP	5E-19	1.46	up
gene-F8A2	2E-04	1.46	up
gene-SLC2A6	1E-08	1.46	up
gene-CRLF1	8E-03	1.46	up
gene-PLEC	1E-12	1.45	up
gene-ANGPTL4	6E-13	1.45	up
gene-CHPF	1E-34	1.45	up
gene-IVL	2E-03	1.44	up
gene-SCN5A	2E-06	1.44	up
gene-TMEM204	2E-12	1.43	up
gene-HIVEP3	2E-05	1.43	up
gene-FAT3	4E-04	1.43	up
gene-DGAT1	3E-04	1.42	up
gene-CLSTN2	1E-02	1.42	up
gene-ATOH8	4E-05	1.42	up
gene-IFI6	2E-05	1.42	up
gene-PKD1-2	1E-14	1.42	up
gene-LAMA1	7E-07	1.42	up
gene-AMH	3E-03	1.41	up
gene-SLCO4A1	8E-04	1.41	up
gene-ENDOG	7E-14	1.40	up
gene-ZNF469	6E-06	1.40	up

gene-PRRX2	1E-11	1.40	up
gene-CHY3	2E-04	1.40	up
gene-GNB1L	6E-09	1.39	up
gene-SPHK1	2E-18	1.39	up
gene-HAND2	4E-04	1.39	up
gene-DLK2	6E-05	1.38	up
gene-RNF152	2E-12	1.38	up
gene-EVA1B	2E-10	1.37	up
gene-METRN	7E-17	1.37	up
gene-GRIN2D	5E-12	1.37	up
gene-SLC52A2	6E-22	1.37	up
gene-PCDHGA11	8E-05	1.37	up
gene-IGFBP6	2E-14	1.36	up
gene-ZNF219	4E-13	1.35	up
gene-ADAMTSL1	5E-24	1.35	up
gene-ADCY7	6E-17	1.35	up
gene-LRATD1	8E-05	1.35	up
gene-PRRT2	9E-04	1.35	up
gene-NEFM	1E-05	1.34	up
gene-FAM171A2	1E-08	1.34	up
gene-RTN4R	7E-03	1.34	up
gene-ITPR3	4E-20	1.34	up
gene-RGPD1	2E-03	1.34	up
gene-ARHGAP23-2	7E-06	1.34	up
gene-LRP1	1E-07	1.33	up
gene-ZNHIT2	1E-05	1.33	up
gene-SLC2A9	2E-08	1.31	up
gene-TMEM256	3E-03	1.31	up
gene-DOHH	4E-20	1.31	up
gene-GP1BB	5E-05	1.31	up
gene-OPLAH	1E-08	1.30	up
gene-SIPA1L3	5E-10	1.30	up
gene-TMEM121	5E-03	1.30	up
gene-COMTD1	2E-03	1.30	up
gene-ANKRD9	2E-13	1.30	up
gene-TMEM86B	4E-04	1.30	up
gene-CSPG4	3E-28	1.30	up
gene-HPG2	4E-12	1.29	up
gene-FBXL14	1E-05	1.29	up
gene-LRRC32	1E-07	1.29	up
gene-PRR7	3E-14	1.29	up
gene-TNFRSF12A	7E-33	1.28	up
gene-KIAA1549L	9E-22	1.27	up
gene-ABHD17A	2E-28	1.27	up
gene-COL18A1-2	2E-09	1.27	up
gene-RAB11FIP3	2E-11	1.27	up
gene-LOXL1	1E-22	1.27	up

gene-SHANK3	1E-04	1.26	up
gene-CCDC85B	3E-45	1.26	up
gene-DNHD1	5E-05	1.26	up
gene-RGPD2	3E-03	1.26	up
gene-ADGRG1	5E-05	1.26	up
gene-VARS1-2	8E-03	1.25	up
gene-PITX1	1E-22	1.25	up
gene-DNM1	6E-07	1.25	up
gene-PITPNM1	2E-15	1.25	up
gene-SATB2	2E-11	1.25	up
gene-SELENBP1	5E-05	1.24	up
gene-ABCA7	2E-03	1.24	up
gene-ELFN2	8E-07	1.24	up
gene-LOC105373989	1E-04	1.24	up
gene-FZD8	1E-03	1.24	up
gene-PEAR1	6E-24	1.24	up
gene-SYNE1	4E-08	1.23	up
gene-ADAMTS10	6E-03	1.23	up
gene-PKD1	5E-20	1.23	up
gene-SCARF2	4E-30	1.22	up
gene-ISG15	2E-10	1.22	up
gene-CSDC2	5E-06	1.22	up
gene-SHISA4	1E-15	1.22	up
gene-OAF	3E-14	1.22	up
gene-ADAM33	9E-27	1.22	up
gene-GPR153	2E-09	1.22	up
gene-C1orf122	9E-28	1.22	up
gene-ZSWIM5	6E-03	1.21	up
gene-NOG	6E-14	1.21	up
gene-TCF7	9E-04	1.21	up
gene-HECTD4	3E-08	1.21	up
gene-TET1	1E-05	1.21	up
gene-SMAD6	1E-06	1.21	up
gene-AP5Z1	1E-13	1.20	up
gene-KMT2D	8E-11	1.20	up
NewGene_2505	7E-14	1.20	up
gene-TM4SF1	4E-05	1.20	up
gene-OBSCN	2E-06	1.20	up
gene-GLI4	7E-06	1.20	up
gene-PODN	2E-13	1.20	up
gene-FOXC2	3E-15	1.19	up
NewGene_7117	3E-07	1.19	up
gene-EPHB3	1E-03	1.19	up
gene-WDR81-2	4E-11	1.19	up
gene-SELENOO	1E-23	1.19	up
gene-BOP1-2	2E-03	1.19	up
NewGene_6532	1E-03	1.18	up

gene-ADCY4-2	8E-03	1.18	up
gene-NR2F6	2E-24	1.17	up
gene-HGH1	2E-23	1.17	up
gene-ACSS1	4E-03	1.17	up
gene-NOC4L	4E-04	1.17	up
gene-TRAPPC5	1E-13	1.17	up
gene-GPSM1	2E-14	1.17	up
gene-TNFRSF14-2	5E-03	1.17	up
gene-B3GNT9	1E-07	1.17	up
gene-PYCARD	8E-04	1.17	up
NewGene_2512	2E-10	1.17	up
gene-NYNRIN	1E-04	1.16	up
gene-ZNF765-ZNF761	7E-05	1.16	up
gene-CCDC85A	2E-04	1.16	up
gene-KIF26B	7E-06	1.16	up
gene-KIF7	2E-25	1.16	up
gene-DLX2	8E-06	1.16	up
gene-BCAR1	3E-14	1.15	up
gene-GSDMD-2	2E-03	1.15	up
gene-SHC2	4E-03	1.15	up
gene-CHT7	2E-10	1.15	up
gene-CHT2	1E-10	1.15	up
gene-NAV2	2E-14	1.15	up
gene-NAPRT	5E-05	1.15	up
gene-PHLDA2	4E-28	1.15	up
gene-DOT1L	3E-16	1.15	up
gene-CILP2	2E-03	1.15	up
gene-PTGFRN	5E-05	1.14	up
gene-CORO7	1E-04	1.14	up
gene-C8orf82	5E-11	1.14	up
gene-HDAC5	7E-05	1.14	up
gene-ALX3	4E-07	1.14	up
gene-LOC124905135	5E-04	1.14	up
gene-FOXD1	1E-15	1.14	up
gene-PLXNA2	5E-09	1.14	up
gene-CCDC102A	3E-08	1.14	up
gene-TFPI2	4E-04	1.13	up
gene-GLIS2-2	2E-05	1.13	up
gene-MFSD3	7E-06	1.13	up
gene-TNC	4E-12	1.13	up
gene-SYNDIG1	5E-03	1.13	up
gene-TPGS1	9E-07	1.13	up
gene-TIGD5-2	4E-06	1.13	up
gene-ZNF524	3E-05	1.12	up
gene-NCOR2	4E-12	1.12	up
gene-NRN1	5E-05	1.12	up
gene-NBPF1	9E-04	1.12	up

gene-SLC26A1	8E-04	1.12	up
gene-COL18A1	2E-05	1.12	up
gene-PROCR	1E-09	1.11	up
gene-KAZALD1	4E-07	1.11	up
gene-PCDHGB7	4E-08	1.11	up
gene-PARP12	3E-07	1.11	up
gene-RASL10B	3E-03	1.11	up
gene-HCFC1	5E-17	1.11	up
gene-MIB2	3E-07	1.11	up
gene-CEBPD	7E-04	1.10	up
gene-FJX1	2E-10	1.10	up
gene-HELZ2	5E-13	1.10	up
gene-PIEZO1	1E-50	1.10	up
gene-CCDC107	1E-14	1.10	up
gene-ZNF771	1E-08	1.10	up
gene-PHLDA2-2	2E-24	1.10	up
gene-SLIT3	2E-03	1.10	up
gene-TNFRSF1B	3E-04	1.10	up
gene-RAB40C	2E-21	1.09	up
gene-PREX1	3E-07	1.09	up
gene-LTBP4	2E-03	1.09	up
gene-XYLT1	9E-15	1.09	up
gene-SRFBP1	6E-07	1.09	up
gene-SREBF1	4E-35	1.09	up
gene-COL4A5	6E-06	1.09	up
gene-PPP1R35	2E-04	1.09	up
gene-GLI2	8E-05	1.09	up
NewGene_4472	5E-03	1.09	up
gene-IRX1	5E-03	1.09	up
gene-PTGS1	1E-04	1.08	up
gene-LRFN4	2E-13	1.08	up
gene-CLDN11	2E-16	1.08	up
gene-DMWD	2E-09	1.08	up
gene-FAAP100	3E-15	1.08	up
gene-FRMD4A	2E-13	1.08	up
gene-SDF2L1	6E-08	1.08	up
gene-NTNG1	4E-03	1.08	up
gene-LZTS2	1E-19	1.08	up
gene-PTPN23	1E-18	1.07	up
gene-KCNK2	1E-09	1.07	up
gene-ARSI	4E-06	1.07	up
gene-UBTD1	3E-21	1.07	up
gene-SLC6A6	4E-07	1.07	up
gene-VASN	6E-07	1.07	up
gene-KCNMA1	5E-08	1.07	up
gene-KALRN	6E-09	1.07	up
gene-PGAP6	2E-42	1.07	up

gene-UBR4	4E-12	1.06	up
gene-VILL	2E-03	1.06	up
gene-ZNF775	2E-04	1.06	up
gene-ADAMTS14	2E-03	1.06	up
gene-XYLT1-2	8E-15	1.06	up
gene-CIC	3E-18	1.06	up
NewGene_2507	1E-07	1.06	up
gene-CRYZL2P-SEC16B	5E-04	1.06	up
gene-NAGLU	2E-22	1.06	up
gene-BCL7A	8E-05	1.06	up
gene-PLEKHG5	4E-06	1.06	up
gene-EMILIN2	2E-05	1.05	up
gene-ISYNA1	1E-05	1.05	up
gene-XDH	1E-07	1.05	up
gene-JUND	9E-05	1.05	up
gene-ATAD3B	8E-13	1.05	up
gene-FBXL6	3E-03	1.05	up
gene-ZNF668	9E-18	1.05	up
gene-GMIP	4E-06	1.05	up
gene-YDJC	2E-15	1.05	up
gene-VASN-2	8E-07	1.05	up
gene-ZNF837	5E-03	1.04	up
gene-SCN4B	1E-05	1.04	up
gene-TRNP1	2E-28	1.04	up
gene-TRIM46	5E-05	1.04	up
gene-FRMD8	3E-07	1.04	up
gene-NAV1	3E-14	1.04	up
gene-CDC42EP5-3	2E-03	1.04	up
gene-PTX3	6E-06	1.04	up
gene-FOXF2	7E-06	1.04	up
gene-TIGD5	9E-06	1.04	up
gene-C4orf48	1E-04	1.04	up
gene-TNRC18	2E-09	1.04	up
gene-HIC1	3E-15	1.03	up
gene-IER2	9E-15	1.03	up
gene-IFI35	9E-05	1.03	up
gene-ZMIZ1	7E-05	1.03	up
gene-TCIRG1	6E-22	1.03	up
gene-CDCP1	3E-15	1.03	up
gene-TRRAP	1E-17	1.03	up
gene-FBXL15	2E-07	1.03	up
gene-HLA-C-4	1E-07	1.03	up
gene-HYAL3	3E-04	1.02	up
gene-PLXNA1	4E-13	1.02	up
gene-MAP3K11	8E-14	1.02	up
gene-CLEC11A	6E-16	1.02	up
gene-KCNC4	2E-20	1.02	up

gene-FBXW5	1E-18	1.02	up
gene-ZNF444	2E-16	1.02	up
gene-CACNA1A	2E-06	1.02	up
gene-SNED1	2E-03	1.02	up
gene-SHANK1	2E-06	1.02	up
gene-RIN1	2E-16	1.02	up
gene-CDR2L	1E-18	1.02	up
gene-CDC42EP5	2E-03	1.02	up
gene-SLC2A6-2	4E-05	1.02	up
gene-CDYL2	7E-06	1.01	up
gene-ZBTB4-2	2E-05	1.01	up
gene-ZSWIM9	5E-10	1.01	up
gene-SIX5	2E-05	1.01	up
gene-PCDHGA12	6E-06	1.01	up
gene-REPIN1	8E-27	1.01	up
gene-S100A4	3E-05	1.01	up
gene-MX2	8E-03	1.01	up
gene-GRAMD1B	1E-12	1.01	up
gene-MFSD12	3E-24	1.01	up
gene-PCNX3	1E-11	1.01	up
gene-TUSC1	1E-06	1.01	up
gene-WNK4	6E-13	1.01	up
gene-RAI1	8E-11	1.00	up
gene-PYCR3	2E-06	1.00	up
gene-BAHCC1	4E-07	1.00	up
gene-H3ST3A1	2E-18	1.00	up
gene-ZC3H3-2	2E-03	1.00	up
gene-FURIN	1E-11	1.00	up
gene-TYMP	5E-05	1.00	up
gene-FBRSL1	9E-18	1.00	up
gene-PPIH	2E-06	-1.00	down
gene-RPL22	3E-25	-1.00	down
gene-CENPC	1E-07	-1.00	down
gene-SFR1	1E-03	-1.00	down
gene-MGARP	5E-10	-1.00	down
gene-ZNF793	6E-03	-1.00	down
gene-STOX2	7E-04	-1.01	down
gene-TMEM267	6E-09	-1.01	down
gene-CCSAP	2E-03	-1.02	down
gene-MRPL54	8E-09	-1.02	down
gene-POMP	2E-32	-1.02	down
gene-LSM6	9E-11	-1.02	down
gene-SRGN	9E-04	-1.03	down
gene-ROMO1	3E-07	-1.03	down
gene-MRE11	8E-06	-1.03	down
gene-NCOA7	6E-12	-1.03	down
NewGene_3305	7E-03	-1.03	down

gene-ZC2HC1A	5E-08	-1.03	down
gene-KIAA0825	3E-03	-1.03	down
gene-LOC124900217	7E-03	-1.03	down
gene-LURAP1L	2E-03	-1.03	down
gene-DYNLT3	4E-27	-1.04	down
gene-CCDC81	2E-05	-1.04	down
gene-RPL35A	8E-23	-1.04	down
gene-SWT1	6E-03	-1.04	down
gene-ANP32E	5E-04	-1.04	down
gene-PSAT1	9E-15	-1.04	down
gene-KLHL28	1E-14	-1.04	down
gene-INSIG2	9E-09	-1.05	down
gene-DNAI4	3E-03	-1.05	down
gene-SEC61G	2E-13	-1.05	down
gene-SLIRP	2E-07	-1.05	down
gene-LRRC37A2-2	2E-05	-1.05	down
gene-NDUFB3	3E-09	-1.06	down
gene-HYI	2E-03	-1.06	down
gene-GCSH-2	3E-03	-1.06	down
gene-EXOSC8	4E-05	-1.06	down
gene-B3GALT2	4E-03	-1.06	down
gene-HIBCH	8E-06	-1.07	down
gene-ZNF404	7E-07	-1.08	down
gene-COX7C	6E-19	-1.08	down
NewGene_1203	3E-04	-1.08	down
gene-BCL2L2-PABPN1	8E-05	-1.08	down
gene-RBIS	5E-10	-1.08	down
gene-TSPAN2	6E-06	-1.08	down
gene-PFDN4	1E-18	-1.09	down
gene-RGS7	3E-03	-1.09	down
NewGene_2833	4E-03	-1.09	down
gene-MRPL24	2E-12	-1.10	down
gene-ALG10	7E-03	-1.10	down
gene-SNRPG	5E-10	-1.10	down
gene-XRCC4	5E-11	-1.10	down
gene-LSM3	4E-17	-1.11	down
gene-SNRPE	2E-08	-1.11	down
gene-MTRES1	6E-14	-1.11	down
gene-MSANTD3-TMEFF1	1E-04	-1.12	down
gene-TBCA	2E-40	-1.12	down
gene-COX6C	2E-21	-1.13	down
gene-LY96	7E-04	-1.13	down
gene-RPL37	1E-19	-1.13	down
gene-IFT25	1E-05	-1.14	down
gene-CEP57L1	4E-04	-1.14	down
gene-RPS26	9E-09	-1.14	down
gene-NDUFB5	2E-23	-1.14	down

gene-LSM8	7E-16	-1.14	down
NewGene_3261	1E-08	-1.15	down
gene-NDUFA5	2E-37	-1.15	down
gene-CARF	1E-04	-1.15	down
gene-SDHAF4	7E-04	-1.15	down
NewGene_2798	2E-08	-1.16	down
gene-AKAP7	2E-03	-1.16	down
gene-RWDD3	2E-07	-1.16	down
gene-AARD	4E-03	-1.16	down
gene-HPE1	3E-14	-1.16	down
gene-COX16	5E-29	-1.16	down
gene-CCNG2	3E-20	-1.16	down
gene-TMEM144	6E-03	-1.17	down
gene-MAGOH	7E-20	-1.17	down
gene-ADI1-2	3E-04	-1.17	down
gene-MFAP5	1E-05	-1.17	down
gene-ARHGAP28	3E-03	-1.18	down
gene-MZT1	3E-05	-1.19	down
gene-PFDN5-2	2E-03	-1.19	down
gene-SASS6	2E-03	-1.19	down
gene-KCTD16	1E-08	-1.20	down
gene-ZNF493	9E-03	-1.20	down
gene-RPA3	8E-04	-1.21	down
gene-C16orf87	5E-17	-1.21	down
gene-TMEM38B	4E-05	-1.22	down
gene-LCA5L	9E-04	-1.22	down
gene-FGF9	7E-03	-1.23	down
gene-THAP5	1E-22	-1.24	down
gene-SSBP1-2	1E-08	-1.25	down
gene-NME1-NME2	7E-07	-1.25	down
gene-ITGB3BP	2E-08	-1.25	down
gene-EIF1AY	7E-18	-1.27	down
gene-SEM1	1E-21	-1.27	down
gene-PIN4	2E-09	-1.27	down
gene-DMAC1	1E-14	-1.27	down
gene-C5orf34	8E-03	-1.27	down
gene-MCTS1-2	2E-13	-1.27	down
NewGene_2970	4E-05	-1.27	down
gene-MRPL33	8E-07	-1.28	down
gene-RPL41	4E-23	-1.28	down
gene-RPL37A	2E-36	-1.29	down
gene-CD163L1	8E-03	-1.29	down
gene-KIF18A	9E-04	-1.29	down
gene-DNAAF4	5E-03	-1.29	down
NewGene_5070	2E-03	-1.30	down
gene-SERF1B	9E-03	-1.30	down
gene-KBTBD3	3E-03	-1.31	down

gene-ARHGDIB	8E-06	-1.31	down
gene-KLHL24	7E-08	-1.32	down
gene-ND3	4E-07	-1.32	down
gene-NAP1L3	4E-05	-1.33	down
gene-PMAIP1	1E-07	-1.33	down
gene-INHBE	1E-03	-1.33	down
gene-SMN2	6E-10	-1.33	down
gene-LSM5	3E-08	-1.33	down
gene-APBB1IP	2E-10	-1.36	down
gene-UQCC5	9E-03	-1.36	down
gene-TGFB2	1E-12	-1.37	down
gene-COPS9	2E-21	-1.37	down
gene-RAD54B	9E-03	-1.37	down
gene-ZFPM2	3E-05	-1.37	down
gene-POSTN	9E-25	-1.37	down
gene-CMC2	2E-04	-1.38	down
gene-IER3	8E-03	-1.40	down
gene-CCDC126	4E-11	-1.40	down
gene-CCND2	1E-09	-1.40	down
gene-RPL39	1E-29	-1.41	down
gene-IMMP1L	1E-03	-1.41	down
gene-NDUFAF5-2	2E-03	-1.42	down
gene-CHCHD10-2	4E-04	-1.42	down
gene-HLA-A-5	7E-03	-1.43	down
gene-NFIB	5E-04	-1.43	down
gene-TOMM7	3E-17	-1.43	down
gene-EGF	1E-03	-1.45	down
gene-ANKRD1	2E-13	-1.45	down
gene-TPRKB-2	8E-07	-1.46	down
gene-MTCH2-2	1E-19	-1.48	down
gene-CAVIN2	9E-03	-1.50	down
gene-POLR1H-7	6E-04	-1.51	down
gene-CETN3	4E-10	-1.52	down
gene-ENPP4	1E-05	-1.54	down
gene-NDUFB1	3E-10	-1.55	down
gene-CHML	1E-05	-1.55	down
gene-SURF1	4E-03	-1.56	down
gene-CMKLR2-2	2E-04	-1.58	down
gene-RPS29	2E-24	-1.58	down
gene-CMKLR2	1E-04	-1.59	down
gene-NDUFA1	2E-21	-1.61	down
gene-GTF2H2-2	7E-03	-1.63	down
gene-TMA7	3E-45	-1.63	down
gene-PCDHB3	2E-04	-1.64	down
gene-ELAPOR2	1E-09	-1.65	down
gene-ATP5ME	1E-12	-1.67	down
NewGene_3501	3E-04	-1.67	down

gene-TMEM178B	5E-04	-1.70	down
gene-PGAM4	1E-07	-1.70	down
gene-C4orf19	1E-04	-1.72	down
gene-ACYP1	3E-03	-1.73	down
gene-CNTNAP3B	7E-05	-1.76	down
gene-ULBP1	2E-04	-1.81	down
gene-COX7A1	8E-10	-1.81	down
gene-FRG1	4E-04	-1.85	down
gene-FSD2	3E-04	-1.88	down
gene-PAPPA2	2E-07	-1.91	down
gene-PET100	1E-06	-2.01	down
gene-MICOS10-NBL1	3E-04	-2.05	down
NewGene_4872	1E-12	-2.09	down
NewGene_2845	5E-18	-2.14	down
gene-NXF3	3E-06	-2.88	down
gene-SLC7A2	5E-04	-3.57	down
gene-EYA4	9E-06	-3.71	down
NewGene_3714	3E-45	-4.96	down

Table 8.2: DEG in (FSe5_vs_F5)

#ID	FDR	log2FC	regulated
gene-CXCL6	8E-18	9.49	up
gene-RPS10-NUDT3	2E-09	8.24	up
gene-SST	8E-05	7.54	up
gene-CXCL3	7E-39	6.85	up
gene-CSF3	2E-20	6.67	up
gene-CXCL1	6E-226	6.37	up
gene-EGFL6	1E-29	6.33	up
gene-NPTX1	1E-99	5.91	up
gene-CXCL8	3E-174	5.76	up
gene-PCSK9	5E-08	5.44	up
gene-TNXB-3	4E-16	5.39	up
gene-TNXB-6	2E-19	5.38	up
gene-NTN1	7E-28	5.35	up
gene-IL18R1	6E-07	5.21	up
gene-TNXB-4	4E-13	5.18	up
gene-CXCL2	8E-16	5.04	up
gene-GPC3	2E-22	5.02	up
gene-TNXB	4E-15	5.00	up
gene-LAMC3	1E-13	4.86	up
gene-SCARA5	7E-10	4.86	up
gene-CFD-2	1E-33	4.78	up
gene-RIPOR3	3E-12	4.76	up
gene-CFD	3E-33	4.64	up
gene-C11orf96	9E-10	4.60	up
gene-ELOVL7	9E-06	4.59	up

gene-IL33	5E-07	4.54	up
gene-ADAMTS8	2E-23	4.53	up
gene-ABCA9	1E-08	4.51	up
gene-SLC1A3	3E-11	4.44	up
gene-LYPD3	9E-48	4.41	up
gene-CH25H	1E-10	4.40	up
gene-CXCL5	3E-10	4.31	up
gene-IL13RA2	2E-27	4.23	up
gene-IL1B	2E-41	4.23	up
gene-DPT	5E-06	4.18	up
gene-GPM6B	5E-14	4.09	up
gene-PDK4	6E-10	4.09	up
gene-ABCA6	2E-06	4.08	up
gene-PLEKHG1	3E-11	3.91	up
gene-FAM20C-4	7E-13	3.90	up
gene-CDKN1C-2	6E-07	3.90	up
gene-SDK1	5E-38	3.79	up
gene-PRELP	2E-33	3.77	up
gene-BMF	1E-08	3.77	up
gene-CCL11	3E-11	3.65	up
gene-AQP3	2E-08	3.62	up
gene-CYP1B1	7E-296	3.61	up
gene-PGF	4E-35	3.61	up
gene-PTGDS	3E-10	3.56	up
gene-LTBP4	3E-30	3.53	up
gene-CD14	2E-07	3.52	up
gene-TSPAN11	1E-11	3.52	up
gene-CTSS	1E-12	3.46	up
gene-CHDL2	8E-05	3.46	up
gene-SHISAL1	3E-51	3.44	up
gene-IGFBP2	2E-99	3.44	up
gene-FAM43A	2E-77	3.40	up
gene-FSTL5	5E-17	3.34	up
gene-THBD	2E-10	3.33	up
gene-ANXA10	3E-04	3.31	up
gene-BEND5	4E-04	3.30	up
gene-EPHB6	4E-09	3.30	up
NewGene_6371	3E-15	3.29	up
gene-CSF3R	2E-06	3.26	up
gene-TENM4	2E-17	3.25	up
gene-MAP2K6	3E-09	3.25	up
gene-BRINP1	2E-03	3.23	up
gene-TMEM132D	1E-17	3.22	up
gene-CCL7	4E-13	3.21	up
gene-FOXQ1	1E-18	3.21	up
gene-ANGPTL4	6E-56	3.20	up
gene-PTPRE	2E-04	3.15	up

gene-PTGIS	5E-08	3.14	up
gene-HMOX1	9E-106	3.14	up
gene-MMP1	1E-120	3.14	up
gene-GRIA1	8E-20	3.14	up
gene-CACNA1G	6E-05	3.13	up
gene-SECTM1	1E-04	3.13	up
gene-ZNF853	1E-15	3.11	up
gene-HD11B1	5E-27	3.11	up
gene-PCSK6	1E-12	3.09	up
gene-AJAP1	7E-09	3.03	up
gene-ITGB8	2E-25	3.02	up
gene-IGF1	2E-04	3.01	up
gene-CILP	3E-05	2.98	up
gene-HD17B2	3E-04	2.98	up
gene-FOXL2	5E-13	2.98	up
gene-ISM1	1E-08	2.97	up
gene-CLIC6	1E-06	2.96	up
gene-EFNB3	7E-14	2.96	up
gene-KCNJ2	1E-07	2.95	up
gene-ECM2-2	3E-15	2.95	up
gene-HTRA3	1E-05	2.94	up
gene-ECM2	7E-14	2.93	up
NewGene_4499	7E-07	2.92	up
gene-CRLF1	5E-22	2.92	up
gene-EPHB6-2	2E-08	2.90	up
gene-RAB42	2E-10	2.89	up
gene-MEDAG	1E-09	2.89	up
gene-ADAMTS15	1E-45	2.86	up
gene-WNT2	3E-11	2.84	up
gene-ZNF608	3E-18	2.83	up
gene-IL1R1	3E-24	2.83	up
gene-PPL	6E-03	2.80	up
gene-GUCY1A2	2E-16	2.79	up
gene-FOS	2E-08	2.79	up
gene-THB	8E-18	2.79	up
gene-APCDD1	2E-43	2.74	up
gene-TFPI2	8E-23	2.74	up
gene-APLN	1E-12	2.73	up
gene-CGA	1E-06	2.73	up
gene-RGCC	4E-03	2.72	up
gene-TNFAIP6	5E-11	2.72	up
gene-AREG	1E-07	2.70	up
NewGene_6937	8E-07	2.70	up
NewGene_2549	3E-21	2.69	up
NewGene_6246	2E-04	2.68	up
gene-OLFML1	2E-05	2.67	up
gene-TMT1A	4E-08	2.66	up

gene-INSIG1	2E-04	2.66	up
gene-STC1	5E-23	2.65	up
gene-TESK2	8E-11	2.65	up
gene-TMEM132B	3E-11	2.64	up
gene-AKR1C3	8E-05	2.64	up
gene-DTNA	1E-17	2.64	up
gene-HMCN1	1E-15	2.64	up
gene-FMOD	2E-20	2.62	up
gene-SOD3	2E-19	2.62	up
gene-MAN1A1	1E-05	2.62	up
gene-GDF10	3E-07	2.61	up
gene-HGF	3E-12	2.58	up
gene-SOX8	8E-06	2.57	up
gene-SLIT3	2E-07	2.57	up
gene-PKDCC	2E-18	2.56	up
gene-COL26A1	6E-09	2.55	up
gene-SLC38A5	8E-20	2.55	up
gene-NIM1K	1E-13	2.55	up
gene-PHACTR1	8E-11	2.55	up
gene-CABP1	2E-18	2.55	up
gene-XPNPEP2	3E-04	2.54	up
gene-SOD2	9E-82	2.53	up
gene-CYP7B1	1E-08	2.53	up
gene-ZSWIM5	4E-15	2.52	up
gene-C3	1E-13	2.52	up
gene-GDF5	1E-35	2.52	up
gene-ANO7	2E-05	2.51	up
gene-PTGES	5E-51	2.50	up
gene-GPR68	7E-26	2.50	up
gene-TMEM158	6E-23	2.50	up
gene-CCN5	3E-08	2.50	up
gene-PTGER2	8E-35	2.49	up
gene-RARRES1	4E-08	2.48	up
gene-MYLIP	6E-17	2.47	up
gene-ACKR3	4E-03	2.46	up
gene-RAPGEF4	2E-11	2.46	up
gene-EPB41L3	1E-54	2.46	up
gene-CXCL14	6E-21	2.45	up
gene-PDE3B	5E-05	2.44	up
gene-CHI3L1	2E-06	2.44	up
gene-RAB20	6E-14	2.44	up
gene-SYT7	4E-05	2.43	up
gene-FADS2	3E-06	2.43	up
gene-IGF2	1E-13	2.42	up
gene-BMP2	2E-06	2.41	up
gene-MXRA5	2E-04	2.41	up
gene-S1PR3	1E-37	2.40	up

gene-OLFML2A	1E-06	2.40	up
gene-FNDC1	2E-04	2.40	up
gene-FADS1	2E-34	2.39	up
gene-SIPA1L2	2E-22	2.37	up
gene-C1orf115	1E-11	2.37	up
gene-TBC1D8	2E-22	2.36	up
gene-NPTX2	4E-10	2.36	up
gene-PDPN	1E-09	2.35	up
gene-SNED1	1E-14	2.35	up
gene-SOBP	2E-06	2.34	up
gene-ENPEP	4E-17	2.32	up
gene-SHC2	3E-11	2.32	up
gene-HEPH	2E-14	2.30	up
gene-ISLR-2	9E-12	2.30	up
NewGene_2114	8E-07	2.29	up
gene-FRAS1	2E-29	2.26	up
gene-FBXL14	3E-22	2.26	up
gene-SLC39A8	4E-16	2.25	up
gene-ISLR	8E-13	2.25	up
gene-CDON	2E-15	2.25	up
gene-SCD	1E-04	2.24	up
gene-AKR1C1	4E-08	2.24	up
gene-ANGPTL2	7E-04	2.23	up
gene-CPZ	2E-04	2.23	up
gene-ABCA8	7E-22	2.22	up
gene-KIT	7E-49	2.22	up
gene-ATP8B4	4E-04	2.22	up
gene-NFATC2	6E-07	2.21	up
gene-LRRN4CL	2E-25	2.20	up
gene-MMP11	1E-07	2.20	up
gene-DENND2A	4E-07	2.20	up
gene-H	1E-10	2.19	up
gene-ACP3	2E-10	2.19	up
gene-CPXM2	1E-16	2.19	up
gene-SLC15A3	4E-08	2.19	up
gene-JUND	8E-19	2.18	up
gene-DH13	2E-20	2.18	up
gene-PLPPR3	1E-03	2.18	up
gene-N4BP3	9E-12	2.17	up
gene-TNFRSF19	7E-33	2.17	up
gene-EGR1	1E-04	2.16	up
gene-ADAMTS10	6E-10	2.16	up
gene-PLA2G4A	4E-14	2.16	up
gene-FRAT1	7E-07	2.16	up
gene-ARHGAP6	1E-10	2.16	up
gene-CEBPD	2E-12	2.15	up
gene-LDLR	9E-04	2.15	up

gene-FAXDC2	6E-12	2.15	up
gene-CHD7	9E-06	2.14	up
gene-SLCO4A1	2E-09	2.14	up
gene-EBF4	1E-15	2.13	up
gene-BPI	2E-04	2.12	up
gene-SLC14A1	1E-06	2.12	up
gene-OLFML2B	3E-06	2.12	up
gene-ZNF219	6E-35	2.11	up
gene-MINAR1	3E-05	2.11	up
gene-MAML3	9E-10	2.11	up
gene-CCR7	4E-07	2.10	up
gene-CA9	5E-07	2.10	up
gene-PTGS1	3E-15	2.10	up
gene-KIF26B	6E-20	2.10	up
gene-TSPOAP1	5E-05	2.10	up
gene-CA11	5E-06	2.09	up
gene-COL15A1	9E-12	2.09	up
gene-PTX3	4E-20	2.08	up
gene-COLEC12	6E-03	2.08	up
gene-DCH1	2E-18	2.08	up
gene-LOC124902508	1E-08	2.07	up
gene-FBLN1	1E-12	2.06	up
gene-ZNF395	2E-43	2.05	up
gene-STON1	1E-08	2.05	up
gene-PSD	5E-05	2.04	up
gene-PDGFRA	7E-22	2.04	up
gene-LAMA5	5E-18	2.04	up
gene-PITPNC1	2E-32	2.04	up
gene-SLC2A12	3E-16	2.04	up
gene-C2orf72	3E-06	2.04	up
gene-LXN	2E-10	2.04	up
gene-OLFM2	3E-03	2.03	up
gene-XG	4E-09	2.03	up
gene-ABI3BP	8E-18	2.03	up
gene-CHD	2E-05	2.03	up
gene-MMP11-2	5E-05	2.02	up
gene-HOXA3	2E-04	2.01	up
gene-VPS37D	2E-06	2.00	up
gene-MN1	8E-06	1.99	up
gene-PDGFD	8E-05	1.99	up
gene-ICOSLG	2E-06	1.99	up
gene-IER5L	3E-32	1.99	up
gene-CLSTN2	5E-06	1.99	up
gene-RGS17	1E-04	1.98	up
gene-ROR2	1E-28	1.98	up
gene-MGP	2E-08	1.97	up
gene-COLEC10	8E-06	1.97	up

gene-ZFPM1	4E-19	1.97	up
gene-MTSS1	2E-07	1.96	up
gene-VWA1	5E-11	1.96	up
gene-SCO2	1E-07	1.96	up
gene-FAM20C-2	1E-35	1.96	up
gene-PRRX2	4E-27	1.96	up
gene-SRRM3	9E-09	1.96	up
gene-GAS7	1E-10	1.96	up
gene-MAGEL2-2	2E-04	1.96	up
gene-PCDHGB1	2E-08	1.96	up
gene-CHM3	1E-04	1.95	up
gene-ATP2A3	6E-17	1.95	up
gene-BMP6	8E-03	1.95	up
gene-LOC124904077	3E-09	1.94	up
gene-NDUFA4L2	3E-08	1.94	up
gene-PPP1R14C	4E-04	1.94	up
gene-C1QTNF1	2E-09	1.94	up
gene-MAGEL2	2E-04	1.93	up
gene-MTUS1	1E-04	1.93	up
gene-PFKFB4	1E-16	1.93	up
NewGene_2516	4E-09	1.93	up
gene-TMEM121	1E-06	1.93	up
gene-SHC3	3E-14	1.91	up
gene-SELENOP	8E-04	1.91	up
gene-APOD	6E-06	1.90	up
gene-F8A2	1E-09	1.89	up
gene-RCOR2	5E-04	1.89	up
gene-KLHL35	5E-05	1.89	up
gene-GALNT14	2E-06	1.88	up
gene-THBS2	2E-17	1.88	up
gene-NCKAP5	1E-05	1.88	up
gene-SLC29A2	1E-03	1.88	up
gene-RASL11A	3E-11	1.88	up
gene-FZD3	1E-03	1.88	up
gene-KLHL13	3E-09	1.87	up
gene-LRRC32	2E-15	1.87	up
gene-ALPL	1E-05	1.87	up
gene-BDKRB2	1E-10	1.86	up
gene-PRSS3	5E-13	1.86	up
gene-MAF	4E-10	1.85	up
gene-ZNF358	2E-11	1.85	up
gene-ADAMTS14	6E-09	1.84	up
gene-FAM20C	6E-31	1.84	up
gene-PLPP3	3E-10	1.84	up
NewGene_4495	3E-24	1.84	up
gene-NDRG1	4E-12	1.84	up
gene-IL15RA	7E-07	1.84	up

gene-ETV1	2E-05	1.84	up
gene-DNM1	1E-16	1.83	up
gene-CLDN4	3E-16	1.83	up
gene-CASP1	5E-09	1.83	up
gene-LONRF2	2E-06	1.82	up
gene-OAS3	2E-03	1.82	up
gene-CYP2S1	5E-04	1.82	up
gene-PPFIA4	2E-22	1.82	up
gene-ENDOG	1E-18	1.81	up
gene-PTH1R	2E-04	1.81	up
gene-MAP2	4E-03	1.81	up
gene-LRFN1	2E-04	1.81	up
gene-TLE2	2E-08	1.81	up
gene-ZNF469	2E-09	1.81	up
gene-LRIG1	2E-10	1.81	up
gene-SMPDL3A	8E-25	1.81	up
gene-SLC16A6	3E-15	1.81	up
gene-KBTBD11	2E-04	1.81	up
NewGene_4681	6E-04	1.80	up
gene-ACKR4	1E-15	1.80	up
gene-DIRAS3	2E-04	1.80	up
gene-RTN4RL2	9E-04	1.80	up
gene-PRRX1	2E-26	1.80	up
gene-FAM171A2	5E-16	1.80	up
gene-ADORA2B	6E-19	1.79	up
gene-PTGFRN	2E-11	1.79	up
gene-CCDC102A	2E-23	1.79	up
gene-NOS1AP	3E-04	1.79	up
gene-APOL3	3E-05	1.79	up
gene-TLE1	6E-27	1.79	up
gene-HMGCS1	2E-03	1.79	up
gene-FAM20A	2E-03	1.79	up
gene-ADGRA3	6E-37	1.78	up
gene-LRFN1-2	1E-04	1.78	up
gene-FOXF2	2E-20	1.78	up
gene-CERS1	4E-03	1.78	up
gene-SULF2	9E-03	1.78	up
gene-KBTBD11-2	2E-04	1.77	up
gene-PIM1	4E-16	1.77	up
gene-F2RL1	5E-04	1.77	up
gene-SPATA13	2E-44	1.77	up
gene-HES6	3E-04	1.77	up
gene-GRIN3B	1E-03	1.76	up
gene-SHF	1E-13	1.76	up
gene-LRP4	7E-08	1.76	up
gene-AUTS2	4E-07	1.76	up
gene-SLC6A6	4E-21	1.76	up

gene-COL18A1-2	4E-21	1.76	up
gene-SETBP1	4E-21	1.75	up
NewGene_5644	6E-04	1.75	up
gene-RIPOR2	3E-33	1.75	up
gene-SCARA3	8E-38	1.75	up
gene-DHCR7	1E-14	1.74	up
gene-HLA-E-5	1E-03	1.74	up
gene-GPR146	4E-07	1.73	up
gene-TNFRSF14	3E-06	1.73	up
gene-RASL10B	1E-11	1.73	up
gene-FGF11-2	3E-05	1.72	up
gene-C1R	2E-03	1.72	up
gene-ADGRD1	6E-03	1.72	up
NewGene_5986	1E-04	1.72	up
gene-TMEM170B	8E-11	1.71	up
gene-LOC102723996	1E-04	1.71	up
gene-ANKRD9	1E-37	1.71	up
gene-ALX4	2E-05	1.71	up
gene-AH	7E-37	1.70	up
gene-CYP26B1	1E-04	1.70	up
gene-FBXL8	7E-06	1.70	up
gene-IRF2BPL	3E-51	1.70	up
gene-IFIH1	2E-04	1.70	up
gene-CEBPB	7E-14	1.70	up
gene-CLDN11	2E-47	1.70	up
gene-COL14A1	1E-07	1.70	up
gene-FZD9	1E-03	1.70	up
gene-COL4A4	1E-04	1.69	up
gene-GALNT16	8E-09	1.69	up
gene-SATB1	3E-14	1.69	up
gene-IRX1	8E-07	1.69	up
gene-PDE1A	1E-03	1.69	up
gene-ADAMTS3	2E-06	1.69	up
gene-SLC1A2	1E-06	1.69	up
gene-TUSC1	1E-23	1.68	up
gene-PCOLCE2	7E-04	1.68	up
gene-KLF9	4E-15	1.68	up
NewGene_6899	5E-04	1.68	up
gene-TSNARE1	7E-11	1.68	up
gene-TNFRSF1B	1E-12	1.68	up
gene-SESN3	3E-08	1.68	up
gene-ORAI3	2E-21	1.68	up
gene-STAT5A	2E-09	1.68	up
gene-SEMA4D	1E-06	1.68	up
gene-C2orf81	4E-04	1.68	up
gene-GLIS3	6E-17	1.67	up
gene-EPHB4	1E-15	1.67	up

gene-OAF	1E-29	1.67	up
gene-MELTF	5E-05	1.67	up
gene-STRA6-2	5E-05	1.66	up
gene-EBF1	4E-05	1.66	up
gene-OSR2	1E-12	1.65	up
gene-TWIST2-2	5E-08	1.65	up
gene-HLA-C	2E-05	1.65	up
gene-GALNT12	9E-08	1.65	up
gene-GLI3	2E-15	1.65	up
gene-VWF	3E-03	1.65	up
gene-ADRA2C	8E-04	1.64	up
gene-SORCS2	3E-06	1.64	up
gene-SPRY1	3E-05	1.64	up
gene-FBLN7	2E-11	1.64	up
gene-KCNQ3	2E-07	1.63	up
gene-BMERB1	2E-28	1.63	up
gene-SMAD6	3E-11	1.63	up
gene-SERPINF1	1E-07	1.63	up
gene-PRRT2	7E-07	1.63	up
gene-EPHB3	1E-06	1.63	up
gene-NCALD	4E-04	1.63	up
NewGene_2511	1E-19	1.63	up
gene-WLS	5E-08	1.63	up
gene-SDCBP2	4E-05	1.62	up
gene-ZNF521	1E-09	1.62	up
gene-NOP53	4E-10	1.62	up
gene-PLXNC1	2E-03	1.61	up
gene-PITX1	1E-37	1.61	up
gene-LAMA1	9E-12	1.61	up
gene-TBX2	9E-21	1.61	up
gene-PLEKHF1	1E-04	1.60	up
gene-C17orf67	1E-05	1.60	up
gene-GEM	3E-19	1.60	up
gene-TET1	2E-10	1.60	up
gene-GRHL1	2E-05	1.60	up
gene-ZNF775	1E-11	1.59	up
gene-LYNX1	1E-09	1.59	up
gene-NTRK2	6E-04	1.59	up
gene-SOCS1	4E-04	1.59	up
gene-PARP14	1E-15	1.58	up
gene-TRIM47	6E-05	1.58	up
gene-MGAT3	1E-04	1.58	up
gene-C1R-2	5E-03	1.58	up
gene-SELENBP1	8E-09	1.58	up
gene-KCND1	2E-03	1.58	up
gene-HOXC12	5E-03	1.58	up
gene-CDC42EP5-2	1E-07	1.57	up

gene-PCDHGB7	6E-29	1.57	up
gene-PLTP	1E-14	1.57	up
gene-DNHD1	9E-07	1.57	up
gene-GAA	1E-10	1.57	up
gene-ZNF503	7E-16	1.56	up
gene-MVD	2E-10	1.56	up
gene-AMH	4E-04	1.56	up
gene-GP1BB	6E-07	1.56	up
gene-PKD1-2	7E-21	1.56	up
gene-KREMEN1	5E-11	1.56	up
gene-PLCL2-2	3E-08	1.56	up
gene-SCN5A	6E-08	1.56	up
gene-ANK1	6E-06	1.56	up
gene-RORA	7E-34	1.55	up
gene-PIEZO2	4E-06	1.55	up
gene-METRN	7E-24	1.55	up
gene-GATA6	7E-13	1.55	up
gene-MVK	3E-15	1.55	up
gene-GK	7E-03	1.54	up
gene-CITED4	2E-03	1.54	up
gene-ARHGAP45	5E-11	1.54	up
gene-GAS1	4E-07	1.53	up
gene-BAHCC1	4E-15	1.53	up
gene-MYLK4	7E-04	1.53	up
gene-PITPNM1	4E-25	1.53	up
NewGene_2519	1E-14	1.53	up
gene-C15orf61	2E-04	1.53	up
gene-ZC3H12A	4E-11	1.53	up
gene-CYP27A1	1E-06	1.53	up
gene-PODN	2E-25	1.53	up
gene-ABHD14A	6E-10	1.53	up
gene-HLA-A-3	5E-05	1.53	up
gene-RARRES2	5E-05	1.52	up
gene-TENM3	9E-05	1.52	up
gene-SH2B2	7E-06	1.52	up
gene-BOC	1E-11	1.52	up
gene-CDC42EP5-4	3E-07	1.52	up
gene-ATOH8	5E-06	1.52	up
gene-ASPN	2E-04	1.52	up
gene-MARCKSL1	3E-31	1.51	up
gene-HPA6	1E-03	1.51	up
gene-PCDHB9-2	1E-02	1.51	up
gene-MBNL3	3E-03	1.51	up
gene-THD4	2E-13	1.51	up
gene-TMEM38A	2E-04	1.50	up
gene-RNF24	7E-65	1.50	up
gene-SEMA4B	4E-17	1.50	up

gene-DPYSL3	6E-31	1.50	up
gene-SIX5	4E-11	1.49	up
gene-MSC	2E-05	1.49	up
gene-GSDMD-2	2E-07	1.49	up
gene-EPOP-2	3E-04	1.49	up
gene-PTCHD4	1E-03	1.49	up
gene-EMX2	1E-10	1.49	up
gene-CCDC85B	1E-66	1.49	up
gene-CLUL1	8E-03	1.49	up
gene-SNAI1	5E-05	1.48	up
gene-SMO	3E-26	1.48	up
gene-SERPINB2	6E-10	1.48	up
gene-LENG9	1E-03	1.48	up
gene-CDC42EP5	1E-05	1.48	up
gene-PLAC9	1E-13	1.48	up
gene-CRABP2	6E-07	1.48	up
gene-CBARP	1E-19	1.48	up
gene-FAM117B	1E-06	1.47	up
gene-CDC42EP5-3	1E-05	1.47	up
gene-PLCL2	2E-07	1.47	up
gene-KIF26A	8E-04	1.47	up
NewGene_7251	2E-06	1.47	up
gene-BCL3	3E-09	1.47	up
gene-ANO3	2E-04	1.46	up
gene-STAMBPL1	2E-11	1.46	up
gene-EMILIN2	1E-18	1.46	up
gene-ARPIN-AP3S2	1E-06	1.46	up
gene-C8orf82	4E-25	1.46	up
gene-TWIST2	4E-10	1.46	up
gene-SLC7A14	1E-25	1.46	up
gene-CFAP410	8E-22	1.46	up
gene-CFI	1E-03	1.46	up
gene-KCNS2	2E-03	1.45	up
gene-LRP1	4E-09	1.45	up
gene-NDNF	1E-16	1.45	up
gene-LRRC73	5E-05	1.45	up
gene-ADAMTS9	2E-03	1.45	up
gene-CCL2	2E-13	1.45	up
gene-FAM167A-2	8E-06	1.45	up
gene-ISM2	2E-03	1.45	up
gene-TNC	6E-17	1.45	up
gene-DH3	3E-14	1.45	up
gene-GPR153	1E-12	1.45	up
gene-BCL2L11	3E-07	1.44	up
gene-CABLES1	2E-06	1.44	up
gene-LOC124904583	1E-03	1.44	up
gene-RHOU	2E-03	1.44	up

gene-FES	4E-05	1.44	up
NewGene_1869	3E-03	1.44	up
gene-PDLIM4	2E-11	1.44	up
gene-PNPLA3	4E-05	1.44	up
gene-F8A3	3E-03	1.44	up
gene-IER3-4	1E-08	1.43	up
gene-SREBF2	8E-06	1.43	up
gene-MXI1	9E-20	1.43	up
gene-YPEL3	2E-12	1.43	up
gene-LAMA3	1E-06	1.43	up
gene-CYS1	5E-06	1.43	up
gene-NEFM	9E-09	1.43	up
gene-KNDC1	6E-07	1.43	up
gene-CACNA1H	7E-03	1.43	up
gene-FASN	8E-15	1.42	up
gene-SHANK3-2	2E-06	1.42	up
gene-LENG9-2	2E-03	1.42	up
gene-HD17B7	3E-05	1.42	up
gene-NRP2	2E-16	1.42	up
gene-CXCL12	2E-07	1.42	up
gene-ARL10	4E-38	1.42	up
gene-SLC1A7	1E-03	1.42	up
gene-FIBCD1	9E-13	1.41	up
gene-MLLT6-2	1E-21	1.41	up
gene-SPSB3	1E-09	1.41	up
gene-SHANK3	8E-05	1.41	up
gene-RNASE4	1E-04	1.41	up
gene-SAMD11	2E-07	1.41	up
gene-SAP30L	1E-23	1.41	up
gene-GPRC5B	1E-04	1.41	up
gene-COL5A3	2E-05	1.41	up
gene-PIANP	6E-07	1.41	up
gene-TPGS1	9E-17	1.41	up
gene-IRAK3	2E-17	1.41	up
gene-ZBED1-2	1E-06	1.40	up
gene-ELN	2E-15	1.40	up
gene-RHOU-2	2E-03	1.40	up
gene-CROCC-2	8E-06	1.40	up
gene-IER3-3	3E-08	1.40	up
gene-VASH1	6E-22	1.40	up
gene-TMEM198	2E-04	1.40	up
gene-RGS2	2E-03	1.40	up
gene-TNFAIP2	2E-22	1.39	up
gene-G0S2	3E-07	1.39	up
gene-SERPINE2	2E-06	1.39	up
gene-MX2	6E-04	1.39	up
gene-NDRG4	8E-10	1.39	up

gene-THAP11	2E-33	1.38	up
gene-HILPDA	4E-09	1.38	up
gene-KLF4	6E-09	1.38	up
gene-PALM	3E-05	1.38	up
gene-TCAF2	6E-07	1.38	up
gene-GLI4	7E-08	1.38	up
gene-SQOR	9E-58	1.38	up
gene-REV3L	2E-13	1.38	up
gene-MAP3K8	2E-05	1.38	up
gene-HH1	7E-15	1.38	up
gene-PAPPA	2E-07	1.37	up
gene-PID1	4E-10	1.37	up
gene-PYCARD	8E-06	1.37	up
gene-LZTS2	6E-32	1.37	up
gene-IER3-6	1E-08	1.37	up
gene-HIPK2	2E-28	1.37	up
gene-FRAT2	1E-04	1.37	up
gene-EBF3	6E-12	1.37	up
gene-MXD4	5E-10	1.37	up
gene-CASTOR1	6E-11	1.36	up
gene-FOXO4	9E-11	1.36	up
gene-SYNE1	7E-08	1.36	up
gene-HUNK	4E-04	1.36	up
gene-PPARA	5E-18	1.36	up
NewGene_2505	2E-07	1.36	up
gene-ZSWIM4-2	1E-07	1.36	up
gene-PCDHGA9	8E-03	1.35	up
gene-DAPK2	1E-03	1.35	up
gene-PLPP7	7E-09	1.35	up
gene-TMEM171	7E-05	1.35	up
gene-PAQR5	2E-15	1.35	up
gene-ZNF837	3E-04	1.35	up
gene-COL18A1	3E-05	1.35	up
gene-IGFBP4	5E-16	1.35	up
gene-DNMT3A	2E-10	1.34	up
gene-ADGRL1	2E-09	1.34	up
gene-GPC6	2E-06	1.34	up
gene-CCDC69	2E-04	1.34	up
gene-PSD3	6E-19	1.34	up
gene-SLIT2	2E-35	1.34	up
gene-SLC12A7-2	7E-10	1.34	up
NewGene_1618	6E-05	1.33	up
NewGene_1500	6E-08	1.33	up
gene-TMEM140	1E-12	1.33	up
gene-PPP1R16A	4E-26	1.33	up
gene-ITPR1	2E-05	1.33	up
gene-ZFYVE28	6E-08	1.33	up

gene-IER3-2	3E-08	1.33	up
gene-SLC22A23	3E-06	1.33	up
gene-KAZALD1	3E-10	1.33	up
gene-PCDHGB2	2E-06	1.33	up
gene-KCNG1	3E-05	1.32	up
gene-KIAA1755	1E-03	1.32	up
gene-SHOOM2	1E-04	1.32	up
gene-TCF21	3E-06	1.32	up
gene-TMEM129	2E-20	1.32	up
gene-GRK5	4E-14	1.32	up
gene-KIF26B-2	3E-03	1.32	up
gene-C17orf100	2E-04	1.32	up
gene-ARHGAP44	5E-05	1.31	up
gene-DVL2	4E-29	1.31	up
gene-ABTB1	4E-09	1.31	up
gene-ITPKB	3E-07	1.31	up
gene-ACE	1E-03	1.31	up
gene-PRLR	2E-04	1.31	up
gene-CSF1	9E-17	1.31	up
gene-ZDHHC1	3E-06	1.31	up
gene-AMOT	1E-05	1.30	up
gene-COL6A1	9E-09	1.30	up
gene-TMEM35A	6E-03	1.30	up
gene-GJD3	1E-08	1.30	up
gene-PREX1	5E-09	1.30	up
gene-CAMK1D	4E-07	1.30	up
NewGene_6486	3E-04	1.30	up
gene-CXCL16	2E-09	1.30	up
gene-RXFP1	6E-03	1.29	up
gene-SPAG4	2E-05	1.29	up
gene-UST	7E-10	1.29	up
gene-ZNF524	2E-10	1.29	up
gene-NANOS1	9E-03	1.29	up
gene-ITGA8	9E-04	1.28	up
gene-MZF1	6E-11	1.28	up
gene-TMOD1	6E-03	1.28	up
gene-FAM167A	2E-04	1.28	up
gene-CFAP69	5E-04	1.28	up
gene-ADGRB2	2E-14	1.28	up
gene-KCTD12	7E-06	1.28	up
gene-SNTB1	5E-11	1.28	up
gene-GABRE	2E-03	1.28	up
gene-PRR7	4E-10	1.28	up
gene-AKAP12	2E-09	1.28	up
gene-PCDHGA11	2E-04	1.27	up
gene-ADAM33	3E-27	1.27	up
gene-ADAT3	3E-03	1.27	up

gene-EFS	6E-07	1.27	up
gene-MMD	5E-14	1.27	up
gene-STC2	9E-31	1.27	up
gene-LOXL4	3E-20	1.27	up
gene-CARD10	3E-12	1.27	up
gene-SEMA4C	1E-22	1.27	up
gene-SH2B3	3E-36	1.27	up
gene-CCDC102B	6E-03	1.26	up
gene-CILP2	3E-05	1.26	up
gene-DTX4	7E-12	1.26	up
gene-MSX2	5E-06	1.26	up
gene-MIB2	3E-09	1.26	up
gene-PDZRN3	2E-11	1.26	up
gene-SLC5A3	2E-22	1.26	up
gene-LAMA2	8E-05	1.25	up
gene-LOC728743	1E-05	1.25	up
gene-MFHAS1-2	1E-07	1.25	up
gene-CLCN6	6E-11	1.25	up
gene-KCNIP3	1E-05	1.25	up
gene-CAPN15	2E-21	1.25	up
gene-RAB11FIP3	9E-11	1.25	up
gene-RNF152	4E-11	1.25	up
gene-IL21R	1E-03	1.25	up
gene-NYNRIN	1E-05	1.25	up
gene-FZD1	5E-35	1.24	up
gene-GLIS1	1E-09	1.24	up
gene-HEXD	5E-06	1.24	up
gene-CRYBG1	1E-06	1.24	up
gene-HLA-C-4	1E-10	1.24	up
gene-H1-10	8E-09	1.24	up
gene-LIF	2E-06	1.24	up
gene-FBLN2	2E-07	1.24	up
gene-ANKRD29	3E-14	1.23	up
gene-APBA2	6E-03	1.23	up
gene-CHT2	3E-17	1.23	up
gene-FNDC10	5E-14	1.23	up
gene-COL6A2	3E-09	1.23	up
gene-CTU1	6E-07	1.23	up
gene-IFITM1	7E-03	1.23	up
gene-STRA6	1E-03	1.23	up
gene-CTSK	3E-05	1.23	up
gene-EVC2	9E-10	1.23	up
gene-ZMIZ1	8E-07	1.23	up
gene-MAP7	1E-07	1.23	up
NewGene_14	1E-04	1.23	up
gene-TRIB2	7E-09	1.23	up
gene-EVA1B	1E-08	1.22	up

gene-SOX4	3E-05	1.22	up
gene-ARRDC3	2E-22	1.22	up
gene-CIART	3E-04	1.22	up
gene-C1orf122	2E-24	1.22	up
gene-TGFBR3	4E-16	1.22	up
gene-OBSCN	1E-07	1.22	up
gene-TM7SF2	2E-03	1.22	up
gene-DCN	8E-05	1.22	up
gene-LRIG3	2E-10	1.22	up
gene-PLEKHA4	1E-24	1.22	up
gene-WDR90	4E-12	1.22	up
gene-FLT3LG	6E-03	1.22	up
gene-DGAT1	3E-03	1.22	up
gene-C14orf132	5E-25	1.22	up
gene-PTPRU	9E-09	1.22	up
gene-LRP3	6E-26	1.22	up
gene-WHN	2E-04	1.22	up
gene-SLC16A13	9E-03	1.22	up
gene-GYPC	1E-10	1.22	up
NewGene_2801	2E-10	1.21	up
gene-CCDC107	2E-14	1.21	up
gene-TRAPPC5	3E-13	1.21	up
gene-STK26	2E-03	1.21	up
gene-SDHAF1	7E-13	1.21	up
gene-SORL1	1E-03	1.21	up
gene-RASSF4	2E-03	1.21	up
gene-STK32B	1E-23	1.21	up
gene-PARP8	4E-09	1.21	up
gene-MACROD2	1E-05	1.20	up
gene-SREBF1	2E-35	1.20	up
gene-VWA5A	3E-03	1.20	up
gene-MPST	1E-16	1.20	up
gene-SHFL	2E-15	1.20	up
gene-ZNF771	2E-07	1.20	up
gene-ARAP1	8E-13	1.20	up
gene-NAV1	1E-18	1.20	up
gene-EVC	4E-10	1.20	up
gene-ARHGAP26	6E-06	1.20	up
gene-USP28	2E-26	1.20	up
gene-GPR161	7E-18	1.20	up
gene-CTF1	9E-05	1.19	up
gene-VPS13B	2E-13	1.19	up
gene-PRR5	8E-14	1.19	up
gene-CAPN3	1E-03	1.19	up
gene-MLLT6	1E-11	1.19	up
gene-B3GNT9	3E-08	1.19	up
gene-TSHZ1	4E-15	1.19	up

gene-GALNT15	4E-13	1.19	up
gene-SNX9	2E-11	1.19	up
gene-PLK5	5E-03	1.19	up
gene-PKD1	4E-18	1.18	up
gene-PNRC1	8E-18	1.18	up
NewGene_4080	2E-04	1.18	up
gene-TMEM132A	2E-19	1.18	up
gene-ACAN	1E-04	1.18	up
gene-EDNRA	4E-04	1.18	up
gene-PENK	8E-08	1.18	up
gene-SHANK2	1E-11	1.18	up
gene-NUMBL	6E-18	1.18	up
gene-SBNO2-2	2E-07	1.17	up
gene-TLE3	4E-14	1.17	up
gene-TEKTIP1	7E-06	1.17	up
gene-SNX33	6E-21	1.17	up
gene-ABHD8	1E-17	1.17	up
gene-SEMA6C	1E-03	1.17	up
gene-SALL2	6E-08	1.17	up
gene-ST6GALNAC6	2E-06	1.17	up
gene-MMAB	5E-05	1.17	up
gene-IFI6	1E-03	1.17	up
NewGene_1516	3E-03	1.17	up
gene-GNB1L	1E-07	1.17	up
gene-SEMA3B	3E-07	1.16	up
gene-C1orf226	8E-04	1.16	up
gene-MFSD3	8E-07	1.16	up
gene-MFSD12	2E-28	1.16	up
gene-ADSS1	9E-05	1.16	up
gene-LHFPL2	2E-14	1.16	up
gene-CRYZL2P-SEC16B	4E-05	1.16	up
gene-PRDM11	3E-07	1.16	up
gene-CELF2	6E-12	1.16	up
gene-H6PD	8E-08	1.16	up
gene-P4HA3	1E-10	1.16	up
gene-RALGAPA2	1E-09	1.16	up
gene-RGL1	7E-11	1.16	up
gene-CA12	2E-09	1.16	up
gene-SHISA4	2E-09	1.15	up
gene-PCBP3	8E-03	1.15	up
gene-LRRK1	3E-27	1.15	up
gene-MRC2	8E-11	1.15	up
gene-IGFBP6	1E-11	1.15	up
gene-BMP8A	8E-03	1.15	up
gene-GAA-2	5E-08	1.15	up
gene-TRPA1	2E-03	1.15	up
gene-PRICKLE4	5E-05	1.14	up

gene-SYNGR3	3E-03	1.14	up
gene-EGFR	2E-55	1.14	up
gene-CRTC1	3E-16	1.14	up
gene-KLHL26	3E-07	1.14	up
gene-ZNRF1	1E-19	1.14	up
gene-GRIN2D	2E-07	1.14	up
gene-FBXL15	2E-07	1.14	up
gene-ASPHD2	2E-05	1.14	up
gene-SLC37A1	4E-03	1.14	up
gene-EFNA4	3E-04	1.14	up
gene-OPLAH	5E-07	1.14	up
gene-TYMP	4E-06	1.14	up
gene-NR1D1	3E-05	1.14	up
gene-SLC43A1	2E-08	1.14	up
gene-PDK3	4E-11	1.14	up
gene-CCNG2	1E-30	1.14	up
gene-MARCHF9	6E-05	1.14	up
gene-HMGCR	1E-04	1.14	up
gene-NATD1	3E-22	1.14	up
gene-PIM3	4E-16	1.14	up
NewGene_2512	1E-28	1.14	up
gene-PLIN2	4E-22	1.13	up
gene-NUTM2A	2E-03	1.13	up
gene-RNF208	2E-03	1.13	up
gene-HD11B1L	5E-04	1.13	up
gene-DUSP28	2E-03	1.13	up
gene-CCDC74B-2	5E-04	1.13	up
gene-SMIM3	1E-25	1.13	up
gene-BAHCC1-2	4E-09	1.13	up
gene-HELZ2	1E-06	1.13	up
gene-DAAM2	1E-14	1.13	up
gene-LIPE	4E-07	1.13	up
gene-PTOV1	1E-19	1.13	up
gene-MPG	3E-07	1.13	up
gene-SAP30	3E-04	1.13	up
gene-SFRP1	1E-08	1.13	up
gene-IER3-5	2E-09	1.13	up
gene-AKR1C2	4E-03	1.12	up
gene-RAB40C	5E-20	1.12	up
gene-IDUA	2E-09	1.12	up
gene-FBRSL1	6E-12	1.12	up
gene-LTBP3	1E-05	1.12	up
gene-FUT11	3E-11	1.12	up
gene-LOXL1	5E-16	1.12	up
gene-ARRB1	2E-07	1.12	up
gene-TBKBP1	1E-06	1.12	up
gene-KAT6B-2	2E-16	1.12	up

gene-ANKZF1	2E-28	1.12	up
gene-GPANK1-3	2E-03	1.12	up
gene-ANGPTL1	9E-03	1.12	up
gene-SAC3D1	1E-04	1.11	up
gene-HPG2	1E-10	1.11	up
gene-PLA2R1	4E-05	1.11	up
gene-MMP17	4E-15	1.11	up
gene-MEGF8	2E-05	1.11	up
gene-KIFC3	2E-15	1.11	up
gene-TTYH3	4E-35	1.11	up
gene-SLC52A2	4E-12	1.11	up
gene-C15orf48	2E-04	1.11	up
gene-ABHD17A	5E-18	1.11	up
gene-IVL	4E-03	1.11	up
gene-SLC35E2B	3E-26	1.10	up
gene-ADGRL1-2	4E-03	1.10	up
gene-TSKU	2E-05	1.10	up
gene-TRIOBP	4E-17	1.10	up
gene-TRRAP	3E-25	1.10	up
gene-HLA-A	3E-06	1.10	up
gene-A4GALT	5E-05	1.10	up
gene-MAFF	9E-09	1.10	up
gene-IDI1	3E-05	1.10	up
gene-MOB3C	3E-10	1.10	up
gene-ARHGAP35	2E-45	1.10	up
gene-ACAT2	2E-09	1.10	up
gene-NIPAL1	3E-07	1.10	up
gene-COL4A5	2E-07	1.10	up
gene-GFPT2	4E-04	1.10	up
gene-GLIS2	1E-07	1.10	up
gene-ARL4C	2E-09	1.10	up
gene-LLGL1	3E-14	1.09	up
gene-NFATC4-2	6E-05	1.09	up
gene-TNFRSF25	9E-03	1.09	up
gene-RPS6KA2	4E-11	1.09	up
gene-SIK3	2E-15	1.09	up
gene-HDAC4	1E-11	1.09	up
gene-PPP1R35	7E-05	1.09	up
gene-MCRIP2	7E-11	1.09	up
gene-PLSCR4	4E-07	1.09	up
gene-FAT4	9E-19	1.09	up
gene-ASAP3	1E-04	1.09	up
gene-PDXP	3E-06	1.09	up
gene-ITIH5	2E-03	1.08	up
gene-MME	5E-07	1.08	up
gene-TIGD5-2	8E-06	1.08	up
gene-MC1R	2E-04	1.08	up

gene-GTF2IRD2	1E-07	1.08	up
gene-UNC93B1	1E-09	1.08	up
gene-CADM4	2E-05	1.08	up
gene-ZNF765-ZNF761	3E-04	1.08	up
gene-TCP11L2	6E-07	1.08	up
gene-RAI1	6E-12	1.08	up
gene-GPNMB	2E-04	1.08	up
gene-SLC27A3	7E-04	1.08	up
gene-ACVRL1	3E-08	1.08	up
gene-ARHGAP20	3E-07	1.08	up
gene-ZNF385A	3E-07	1.07	up
gene-AP5B1	3E-26	1.07	up
gene-TPRA1	1E-10	1.07	up
gene-FGD1	4E-10	1.07	up
gene-SASH1	2E-17	1.07	up
gene-PARP12	2E-07	1.07	up
gene-REPIN1	1E-25	1.07	up
gene-TTC28	4E-22	1.07	up
gene-IRX5	1E-04	1.07	up
gene-TRNP1	3E-40	1.07	up
gene-CIC	8E-18	1.07	up
gene-CTXN1	9E-05	1.07	up
gene-PTPRS	8E-40	1.06	up
gene-FAM89B	8E-10	1.06	up
gene-LOC122526780	1E-03	1.06	up
gene-IL4R	7E-21	1.06	up
gene-THEM6	2E-03	1.06	up
gene-NPAS2	6E-04	1.06	up
gene-ZNF446	1E-06	1.06	up
gene-PC	7E-04	1.06	up
gene-VASN	3E-07	1.06	up
gene-CEMIP	3E-04	1.06	up
gene-MYCBP2	4E-14	1.06	up
gene-EPDR1	3E-05	1.06	up
gene-AMPD3	4E-08	1.06	up
gene-FGFR1	6E-12	1.06	up
gene-ZSWIM8	7E-12	1.05	up
gene-PHETA1	5E-12	1.05	up
gene-TNFRSF21	3E-05	1.05	up
gene-ADAM12	3E-04	1.05	up
gene-PMEPA1	9E-06	1.05	up
NewGene_6045	7E-04	1.05	up
gene-SLC26A6	2E-05	1.05	up
gene-SH3RF3	6E-15	1.05	up
gene-RAB11FIP3-2	8E-03	1.05	up
gene-PCMTD1	7E-11	1.05	up
gene-SV2A	8E-09	1.05	up

gene-MEX3D	8E-08	1.05	up
gene-ETV4	3E-09	1.05	up
gene-EHD3	1E-08	1.04	up
gene-VASN-2	3E-07	1.04	up
gene-RALGDS	5E-19	1.04	up
gene-IER2	7E-08	1.04	up
gene-SPSB1	5E-10	1.04	up
gene-SYNGAP1-2	4E-04	1.04	up
gene-GDNF	5E-04	1.04	up
gene-PAG1	4E-07	1.04	up
gene-FAM135A	3E-07	1.04	up
gene-RCAN2	6E-03	1.04	up
gene-ZBTB47	3E-13	1.04	up
gene-FDFT1-2	1E-09	1.04	up
gene-ANKRD16	8E-04	1.04	up
gene-ABCC1	6E-07	1.04	up
gene-FGD4	3E-06	1.04	up
gene-SEMA5A	7E-11	1.03	up
gene-SLC12A7	4E-10	1.03	up
gene-FANK1	3E-03	1.03	up
gene-ZFP41	1E-11	1.03	up
gene-SMOX	3E-09	1.03	up
gene-PELI3	8E-08	1.03	up
gene-TMEM243	1E-10	1.03	up
gene-KCNK1	4E-03	1.03	up
gene-PHF21A	8E-25	1.03	up
gene-PORCN	2E-11	1.03	up
gene-RNF213	3E-13	1.03	up
gene-PARD6G	1E-03	1.03	up
gene-TRABD2A	8E-08	1.03	up
gene-YPEL2	5E-10	1.03	up
gene-RFX2	5E-09	1.02	up
gene-DHX58	6E-04	1.02	up
gene-PHETA2	1E-05	1.02	up
gene-CD302	8E-03	1.02	up
gene-PSMB10	1E-04	1.02	up
gene-NUDT18	5E-06	1.02	up
gene-NINL	1E-06	1.02	up
gene-DACT3	3E-05	1.02	up
gene-SELENOO	8E-16	1.02	up
gene-ADORA1	1E-02	1.02	up
gene-CEP250	5E-10	1.02	up
gene-TWIST1	2E-15	1.02	up
gene-TNS2	2E-06	1.02	up
NewGene_6529	6E-03	1.01	up
gene-AKAP17A-2	4E-04	1.01	up
gene-VPS51	2E-32	1.01	up

gene-SYNPO	3E-05	1.01	up
gene-ZNF496	9E-08	1.01	up
gene-HNMT	3E-04	1.01	up
gene-ZNF75D	2E-15	1.01	up
gene-HECTD4	1E-09	1.01	up
gene-LPIN1	2E-14	1.01	up
gene-ZNF628	3E-07	1.01	up
gene-MAF1	3E-11	1.01	up
gene-FAM210B	9E-12	1.01	up
gene-TNRC18	5E-09	1.01	up
gene-ATG2A	3E-16	1.01	up
gene-KDM4B	2E-09	1.01	up
gene-SLC37A2	1E-02	1.00	up
gene-DGKQ	3E-17	1.00	up
gene-DENND2D	3E-03	1.00	up
gene-MPP7	6E-04	-1.00	down
gene-CLIC4	5E-32	-1.00	down
gene-PNN	7E-16	-1.00	down
gene-HNRNPH3	1E-05	-1.00	down
gene-APBB1IP	1E-08	-1.00	down
gene-UAP1	6E-21	-1.00	down
gene-CCND2	2E-12	-1.00	down
gene-UQCC2	2E-04	-1.01	down
gene-IFT25	3E-05	-1.01	down
gene-RCAN1	8E-32	-1.01	down
gene-C2orf74	7E-05	-1.01	down
gene-ANP32E	5E-04	-1.01	down
gene-POSTN	7E-12	-1.01	down
gene-DDAH1	6E-26	-1.01	down
gene-JPT1	2E-06	-1.01	down
gene-PLCXD2	2E-03	-1.01	down
gene-SLC22A15	5E-07	-1.01	down
gene-ATP10D	8E-19	-1.01	down
gene-ADAT2	4E-10	-1.01	down
gene-SLC4A8	7E-06	-1.02	down
gene-CNN1	2E-09	-1.02	down
gene-SMN2	3E-05	-1.02	down
gene-CNTNAP3B	2E-03	-1.02	down
gene-PSG3	1E-04	-1.02	down
gene-MAK16	2E-13	-1.02	down
gene-COBLL1	8E-14	-1.02	down
gene-NIFK	1E-11	-1.02	down
gene-HACD2	3E-36	-1.02	down
gene-EDN1	7E-06	-1.03	down
gene-ATP5MK	3E-07	-1.03	down
gene-TUBE1	1E-09	-1.03	down
gene-SEC11C	8E-04	-1.03	down

gene-SRGN	4E-05	-1.03	down
gene-GTF2F2	7E-21	-1.03	down
gene-RPL37A	7E-10	-1.04	down
gene-ACTG2	1E-17	-1.04	down
gene-DGKA	2E-20	-1.04	down
gene-PIN4	2E-07	-1.04	down
gene-AP2S1	5E-25	-1.04	down
gene-SSBP1	1E-15	-1.04	down
gene-FEZ2	5E-52	-1.04	down
gene-NET1	1E-17	-1.04	down
gene-RNF138	8E-05	-1.04	down
gene-TRMT10A	2E-03	-1.04	down
gene-HNRNPA3	1E-19	-1.04	down
gene-SNAPC1	4E-36	-1.04	down
gene-GRAMD1C	4E-03	-1.04	down
gene-WNK4	2E-14	-1.04	down
gene-TRAF5	5E-19	-1.05	down
gene-MGME1	6E-03	-1.05	down
gene-NOP16	9E-19	-1.05	down
gene-ITGAE	3E-09	-1.05	down
gene-SRSF7	1E-19	-1.05	down
gene-DCUN1D3	4E-20	-1.05	down
gene-CENPN-2	5E-03	-1.05	down
gene-UTP15	5E-15	-1.05	down
gene-ABRACL	7E-06	-1.05	down
gene-MET	1E-06	-1.06	down
gene-SCD5	9E-15	-1.06	down
gene-TIPIN	9E-03	-1.06	down
gene-GTF3C6	1E-09	-1.06	down
gene-NME1-NME2	1E-04	-1.06	down
gene-PCBD2	1E-03	-1.06	down
gene-PHTF2	1E-47	-1.06	down
gene-TSPAN2	6E-06	-1.06	down
gene-MCTS1-2	1E-13	-1.06	down
gene-PDLIM5	1E-21	-1.07	down
gene-PQBP1-2	5E-03	-1.07	down
gene-THD1	4E-03	-1.07	down
gene-PSG5	3E-43	-1.07	down
gene-PTGS2	4E-08	-1.07	down
gene-ZNF365	2E-04	-1.07	down
gene-POLR1F	4E-20	-1.07	down
gene-PSMG1	4E-06	-1.08	down
gene-KRT34-2	1E-13	-1.08	down
gene-ADRA1D	9E-11	-1.08	down
gene-RTCA	8E-26	-1.08	down
gene-TIMM8A	1E-05	-1.08	down
gene-GLS	1E-16	-1.08	down

gene-LOC100653049	5E-08	-1.09	down
gene-PALS1	3E-17	-1.09	down
gene-PINX1-2	3E-04	-1.09	down
gene-SORT1	7E-24	-1.09	down
gene-PSPH	3E-04	-1.09	down
gene-NAP1L5	2E-13	-1.09	down
gene-ATL1	2E-03	-1.09	down
gene-NDUFA12	4E-09	-1.09	down
gene-PRDX6	8E-18	-1.10	down
gene-GIN1	2E-05	-1.10	down
gene-KATNAL1	7E-05	-1.10	down
gene-LOC124900417	4E-03	-1.10	down
gene-TRIM6	1E-03	-1.10	down
gene-SEM1	1E-15	-1.10	down
gene-PDSS1	4E-04	-1.10	down
gene-H2AZ1	2E-03	-1.10	down
gene-FKBP5	4E-03	-1.10	down
gene-MOK	1E-11	-1.10	down
gene-TMEM178B	3E-03	-1.10	down
gene-FAM98B	2E-33	-1.10	down
gene-MYOCD	3E-13	-1.10	down
gene-FGF5	6E-31	-1.11	down
gene-SMAGP	2E-08	-1.11	down
gene-EIF5AL1	7E-10	-1.11	down
gene-OXCT1	4E-03	-1.11	down
gene-STX12	4E-54	-1.11	down
gene-SERPINE1	1E-15	-1.11	down
gene-TMEM255B	3E-11	-1.11	down
gene-CAV2	3E-25	-1.11	down
NewGene_7109	1E-19	-1.11	down
gene-C11orf98	2E-06	-1.12	down
gene-RALA	1E-14	-1.12	down
gene-DNAI3	1E-02	-1.13	down
gene-TAF13	1E-25	-1.13	down
gene-SLC20A1	5E-18	-1.13	down
gene-SLIRP	2E-06	-1.13	down
gene-DCLK2	5E-11	-1.13	down
gene-OPCML	2E-13	-1.13	down
gene-VASP	1E-27	-1.14	down
gene-OTUD6B	3E-17	-1.14	down
gene-S1PR1	9E-10	-1.14	down
gene-RBKS	1E-05	-1.14	down
gene-TPM2	1E-49	-1.14	down
gene-SFR1	6E-04	-1.15	down
gene-EXOSC9	6E-23	-1.15	down
gene-ARK2N	2E-43	-1.15	down
gene-HYPK	3E-10	-1.15	down

gene-NDUFA6-4	5E-03	-1.15	down
gene-BAIAP2L1	2E-19	-1.16	down
gene-MARCHF10	2E-06	-1.16	down
gene-UQCC5	2E-03	-1.16	down
gene-SEL1L3	2E-32	-1.16	down
gene-NLK	5E-14	-1.16	down
gene-SERF1A	8E-03	-1.16	down
gene-MTRES1	1E-14	-1.17	down
NewGene_1533	5E-08	-1.17	down
gene-CALD1	3E-13	-1.17	down
gene-CYB5R1	1E-11	-1.17	down
gene-NMNAT2	2E-04	-1.17	down
gene-RFC4	6E-04	-1.17	down
gene-CETN3	9E-08	-1.18	down
gene-NDUFB3	4E-11	-1.18	down
gene-TBCA	8E-20	-1.18	down
gene-POLR1G	2E-04	-1.18	down
gene-ZNF30	1E-04	-1.19	down
gene-SPAG1	4E-04	-1.19	down
gene-MRPL54	9E-13	-1.19	down
gene-MYEF2	1E-04	-1.19	down
gene-OTUB2	1E-02	-1.20	down
gene-PLEKHF2	3E-18	-1.20	down
gene-FAIM	1E-03	-1.20	down
gene-OLR1	1E-15	-1.20	down
gene-NEK7	4E-63	-1.20	down
gene-IFFO2	2E-31	-1.21	down
gene-SNRPG	2E-11	-1.21	down
gene-ZWILCH	5E-03	-1.21	down
gene-LOC100996709	4E-03	-1.21	down
gene-ENAH	2E-48	-1.21	down
gene-MTHFD2	8E-35	-1.21	down
gene-POMP	5E-49	-1.22	down
gene-ZNF789	3E-05	-1.22	down
gene-ANGPT1	8E-30	-1.22	down
gene-RRP15	3E-28	-1.22	down
gene-NUAK1	4E-10	-1.22	down
gene-ROMO1	7E-12	-1.22	down
gene-GTF2H2-2	4E-03	-1.23	down
gene-NOP56	7E-40	-1.23	down
gene-PTS	5E-22	-1.23	down
gene-EEF1B2-2	1E-04	-1.23	down
gene-TSC22D3	1E-06	-1.23	down
gene-AKAP6	8E-04	-1.23	down
gene-LMOD1	3E-20	-1.23	down
gene-ZNF121	6E-10	-1.23	down
gene-SERPINB7	6E-11	-1.23	down

NewGene_3305	8E-04	-1.24	down
gene-LOC124904228	1E-04	-1.24	down
gene-HHAT-2	2E-03	-1.24	down
gene-GEN1	2E-05	-1.24	down
gene-DIO2	1E-15	-1.25	down
gene-ASTN2	5E-07	-1.25	down
gene-SGIP1	9E-07	-1.25	down
gene-ACTR3	3E-91	-1.25	down
NewGene_6000	1E-05	-1.25	down
gene-SUSD2	5E-04	-1.26	down
gene-STOX2	2E-04	-1.26	down
gene-DAB1	6E-06	-1.26	down
gene-GDAP1	6E-04	-1.26	down
gene-GTF2H2C	5E-06	-1.26	down
gene-HMGN2	3E-08	-1.26	down
NewGene_3261	2E-08	-1.26	down
gene-ULBP2	2E-05	-1.27	down
gene-LZTS1	1E-08	-1.27	down
gene-HACD1	4E-06	-1.27	down
gene-ATP5MF	3E-17	-1.28	down
gene-BPGM	8E-22	-1.28	down
gene-GFOD1	3E-04	-1.28	down
gene-CFAP299	2E-03	-1.28	down
gene-MTCH2-2	9E-10	-1.28	down
gene-COPS9	2E-30	-1.29	down
gene-DCK	3E-06	-1.29	down
gene-STEAP1B	6E-18	-1.29	down
gene-COQ3	4E-06	-1.29	down
gene-COX17	2E-07	-1.30	down
gene-KRT80	2E-11	-1.30	down
gene-TMEM52B	2E-03	-1.31	down
gene-VRK1	4E-04	-1.31	down
gene-NEDD1	2E-34	-1.31	down
gene-NEXN	2E-32	-1.31	down
gene-GLIPR1	9E-20	-1.31	down
gene-F3	4E-14	-1.32	down
gene-RGS7	4E-03	-1.32	down
gene-IFIT2	2E-04	-1.32	down
NewGene_7030	7E-09	-1.32	down
gene-CCDC167	4E-06	-1.32	down
gene-TXNIP	2E-18	-1.32	down
gene-AATF	1E-03	-1.32	down
gene-NES	6E-35	-1.33	down
gene-DPY19L2	4E-03	-1.33	down
gene-MACIR	1E-07	-1.33	down
gene-MLLT11	1E-03	-1.34	down
gene-MYL6	2E-33	-1.34	down

gene-NIPSNAP3A	5E-09	-1.34	down
gene-POLR3G	6E-03	-1.35	down
gene-TRIM34	1E-03	-1.35	down
gene-ENDOD1	2E-12	-1.36	down
gene-HPB8	3E-09	-1.36	down
gene-CMKLR2-2	6E-04	-1.36	down
gene-CALM2	3E-80	-1.36	down
gene-TRMT9B-2	8E-08	-1.36	down
gene-MGARP	3E-14	-1.36	down
NewGene_2833	8E-05	-1.36	down
gene-SSBP1-2	1E-28	-1.37	down
gene-INTU	2E-20	-1.37	down
gene-PRPS1	2E-82	-1.37	down
gene-MRPL33	7E-07	-1.37	down
gene-PAWR	2E-17	-1.37	down
gene-SCUBE3	3E-23	-1.37	down
gene-TMEM184A	8E-05	-1.38	down
gene-ZFPM2	3E-05	-1.38	down
gene-MYL9	2E-35	-1.39	down
gene-LOC128706665	2E-04	-1.40	down
gene-EZR	4E-10	-1.40	down
gene-PDCL3	3E-26	-1.40	down
gene-CMKLR2	3E-04	-1.40	down
gene-MAGOH	1E-18	-1.40	down
gene-SEPTIN6-2	2E-03	-1.41	down
gene-TRIM59	4E-04	-1.41	down
NewGene_1631	2E-14	-1.41	down
gene-TUFT1	6E-15	-1.41	down
gene-PWP2	3E-05	-1.41	down
gene-IMMP1L	2E-04	-1.42	down
gene-ZNF239	8E-10	-1.42	down
gene-SDSL	4E-07	-1.42	down
gene-CAP2	1E-06	-1.42	down
gene-KBTBD8	8E-04	-1.42	down
gene-CFL2	4E-16	-1.42	down
NewGene_5535	8E-06	-1.42	down
NewGene_3156	8E-03	-1.42	down
gene-SSTR1	3E-20	-1.42	down
gene-SUSD5	1E-04	-1.43	down
gene-CHORDC1-2	7E-10	-1.43	down
gene-GBP1	2E-35	-1.43	down
gene-ALDH1B1	2E-13	-1.43	down
gene-EXTL1	1E-14	-1.44	down
gene-MRPL24	1E-21	-1.44	down
gene-TPD52	4E-04	-1.45	down
gene-KRT15	3E-04	-1.45	down
gene-AMD1	3E-30	-1.46	down

gene-TRIM55	2E-06	-1.46	down
gene-SCN9A	2E-18	-1.48	down
gene-ACTA2	2E-13	-1.48	down
gene-LOC107985567	5E-04	-1.48	down
NewGene_3501	3E-06	-1.49	down
gene-ATP5ME	4E-08	-1.49	down
gene-CDH6	1E-77	-1.49	down
gene-CCT8	1E-10	-1.49	down
gene-IGFBPL1	3E-04	-1.49	down
NewGene_1380	1E-03	-1.50	down
gene-REXO5	8E-03	-1.50	down
gene-DNAJB4	2E-94	-1.50	down
gene-C4orf33	2E-03	-1.51	down
gene-FANCB	6E-03	-1.51	down
gene-KCTD16	1E-16	-1.51	down
gene-EPHB1	2E-03	-1.51	down
gene-KCNQ5	6E-08	-1.51	down
gene-SLC28A3	2E-03	-1.52	down
gene-TP53I3	1E-08	-1.52	down
gene-KIAA0040	2E-05	-1.52	down
gene-VSTM2L	3E-03	-1.52	down
gene-HD17B6	9E-07	-1.52	down
gene-CCDC112	2E-14	-1.53	down
gene-LHX9	2E-11	-1.53	down
gene-CENPP-2	5E-03	-1.53	down
gene-MCOLN2	1E-04	-1.53	down
gene-IVNS1ABP	5E-16	-1.54	down
gene-CASP3	8E-16	-1.54	down
gene-ADAM19	7E-33	-1.54	down
gene-UCP2	1E-03	-1.55	down
gene-NIPAL4	2E-03	-1.55	down
gene-MBOAT1	8E-06	-1.55	down
gene-CDH2	4E-79	-1.56	down
gene-KIF18A	9E-05	-1.56	down
gene-SKP2	5E-18	-1.56	down
gene-FSD2	7E-04	-1.57	down
gene-ZNF93	3E-03	-1.58	down
gene-PPM1H	5E-07	-1.59	down
gene-TMA7	8E-28	-1.60	down
gene-C16orf87	1E-32	-1.60	down
gene-WFDC1	7E-16	-1.60	down
gene-B3GALT2	2E-06	-1.62	down
gene-C4orf19	7E-03	-1.63	down
gene-NXF3	4E-03	-1.63	down
gene-TPM1	1E-192	-1.63	down
gene-ENPP4	7E-07	-1.63	down
gene-SEC16B	1E-03	-1.64	down

gene-GIPC2	2E-03	-1.64	down
gene-CHCHD10-2	5E-07	-1.65	down
gene-POLR1H-7	8E-05	-1.66	down
gene-PSAT1	2E-34	-1.66	down
gene-COX7A1	1E-13	-1.66	down
gene-HBEGF	4E-24	-1.68	down
gene-DIAPH3	5E-05	-1.68	down
gene-CHAC2	4E-03	-1.69	down
gene-P2RX5	1E-13	-1.69	down
gene-CTPS1	3E-131	-1.71	down
gene-CAPS2	3E-03	-1.71	down
gene-ANKEF1	1E-04	-1.71	down
gene-LRRN3	3E-05	-1.72	down
gene-LOC112268170	4E-05	-1.73	down
gene-MPZL3	8E-04	-1.73	down
gene-CPA3	2E-03	-1.73	down
gene-NDUFA1	5E-28	-1.75	down
gene-SH3TC2	1E-02	-1.75	down
gene-LYPD6B	4E-06	-1.76	down
gene-NABP1	3E-43	-1.77	down
gene-NDUFB1	2E-08	-1.77	down
gene-ASB5	2E-13	-1.79	down
gene-ENC1	6E-36	-1.79	down
gene-HYI	1E-07	-1.80	down
gene-TLL1	2E-12	-1.80	down
gene-BRIP1	4E-04	-1.81	down
NewGene_2233	2E-06	-1.82	down
gene-KRT34-3	3E-14	-1.82	down
gene-POLE2	8E-03	-1.83	down
gene-OXTR	2E-48	-1.84	down
gene-GADD45B	6E-53	-1.84	down
gene-TRPC4	2E-57	-1.85	down
gene-PGAM4	2E-09	-1.85	down
gene-CD274	1E-18	-1.86	down
NewGene_2845	2E-12	-1.89	down
gene-C3orf52	4E-09	-1.90	down
gene-CLIC3	9E-08	-1.91	down
gene-ARHGDIB	2E-08	-1.92	down
gene-ASNS	1E-45	-1.93	down
gene-NRXN3	5E-06	-1.94	down
gene-CLDN1	9E-22	-1.95	down
gene-MAT2A	3E-25	-1.96	down
NewGene_5875	1E-03	-1.97	down
NewGene_4872	8E-10	-1.97	down
gene-KRT7	6E-58	-1.98	down
gene-RAD54B	5E-05	-1.98	down
gene-MICOS10-NBL1	3E-03	-1.99	down

gene-CCDC15	4E-03	-2.00	down
gene-GALNT3	7E-29	-2.00	down
gene-TSPAN13	8E-21	-2.00	down
gene-NAP1L3	5E-09	-2.01	down
gene-SPDYE3	2E-04	-2.01	down
gene-JPH2	8E-29	-2.03	down
gene-PMAIP1	2E-16	-2.04	down
NewGene_477	2E-12	-2.06	down
gene-RIMS1	2E-07	-2.07	down
gene-DNAAF4	9E-05	-2.07	down
gene-FAM72B	9E-03	-2.08	down
gene-PLCB4	2E-42	-2.09	down
gene-SYT16	1E-39	-2.16	down
gene-CHMP4A-2	1E-03	-2.18	down
gene-NXPH3	7E-07	-2.20	down
gene-KRT18	8E-143	-2.27	down
gene-MYBL1	5E-20	-2.29	down
gene-HELLS	2E-03	-2.31	down
gene-GARRE1-4	2E-04	-2.36	down
gene-PTGES3L-AARSD1	1E-03	-2.39	down
gene-PSME2-2	5E-03	-2.47	down
gene-KRT81	3E-27	-2.51	down
gene-HCT1	1E-03	-2.54	down
gene-PET100	1E-06	-2.56	down
gene-CCDC81	9E-24	-2.63	down
NewGene_1122	3E-06	-2.77	down
gene-TGFB2	2E-40	-2.90	down
gene-STYK1	1E-08	-3.19	down
gene-EGF	6E-13	-3.30	down
gene-SYNPO2L	1E-19	-3.47	down
gene-EFHD1	2E-29	-3.47	down
gene-MYOZ1	2E-10	-3.54	down
gene-ANKRD1	4E-81	-3.87	down
NewGene_3714	3E-35	-4.29	down

Table 8.3: DEG in (FSe20_vs_F20)

#ID	FDR	log2FC	regulated
gene-ADH1B	2E-13	9.56	up
gene-CORO7-PAM16	1E-12	9.32	up
gene-SST	2E-26	8.41	up
gene-RASL12	3E-09	8.23	up
gene-CXCL6	2E-191	7.11	up
gene-PDK4	2E-15	6.75	up
gene-EGFL6	4E-29	6.65	up
gene-CXCL8	6E-56	5.77	up
gene-DPT	7E-17	5.58	up

gene-FGF13	1E-07	5.35	up
gene-IL18R1	6E-10	5.24	up
gene-CXCL1	4E-67	5.22	up
gene-RASL11B	3E-22	5.07	up
gene-CH25H	4E-14	4.95	up
gene-CXCL3	1E-63	4.92	up
gene-NPTX1	9E-131	4.68	up
gene-CXCL2	4E-21	4.59	up
gene-ADAMTS8	8E-18	4.52	up
gene-NTN1	1E-67	4.40	up
gene-ISM1	5E-27	4.38	up
gene-SCARA5	4E-08	4.22	up
gene-IL34	6E-09	4.11	up
gene-CYP1B1	0E+00	4.09	up
gene-BMF	6E-23	4.01	up
gene-CYP19A1	8E-05	3.94	up
gene-SIX2	2E-07	3.92	up
gene-HMOX1	7E-13	3.91	up
gene-TNFAIP6	3E-61	3.88	up
gene-CYP7B1	6E-21	3.79	up
gene-TMT1A	1E-03	3.78	up
gene-CXCL5	1E-38	3.77	up
gene-GDF10	7E-27	3.71	up
gene-LYPD3	3E-53	3.71	up
gene-RIPOR3	6E-21	3.71	up
gene-PLEKHG1	3E-08	3.70	up
gene-SLC39A8	3E-50	3.68	up
gene-GLDN	3E-52	3.60	up
gene-TNXB-3	2E-15	3.60	up
gene-C10orf105	8E-08	3.54	up
gene-TNXB-6	9E-21	3.51	up
gene-ELOVL7	6E-08	3.47	up
gene-CSF3	2E-12	3.47	up
gene-TNXB-4	5E-13	3.43	up
gene-MAP2K6	6E-11	3.39	up
gene-ABCA9	2E-05	3.37	up
gene-CFD-2	7E-25	3.36	up
gene-COL14A1	6E-39	3.33	up
gene-EYA4	7E-06	3.30	up
gene-THB	1E-47	3.30	up
gene-TNXB	1E-16	3.29	up
gene-TNXB-5	2E-05	3.27	up
gene-APOD	3E-75	3.21	up
gene-ZNF608	4E-78	3.20	up
gene-TSPAN11	1E-39	3.20	up
gene-VCAM1	1E-09	3.19	up
gene-OLFML1	8E-32	3.18	up

gene-CFAP298-TCP10L	2E-03	3.16	up
NewGene_6246	2E-20	3.15	up
gene-CGA	7E-08	3.11	up
gene-TMEM132D	7E-15	3.09	up
gene-CCDC102B	1E-07	3.08	up
gene-ITGB8	1E-31	3.02	up
gene-IL1B	7E-07	2.97	up
gene-IL33	4E-08	2.96	up
gene-KCNH5	8E-06	2.95	up
gene-HGF	8E-63	2.91	up
gene-APCDD1	3E-195	2.88	up
gene-SOD2	0E+00	2.86	up
gene-SYTL5	1E-06	2.85	up
gene-SHISAL1	1E-52	2.83	up
gene-ABCA6	2E-08	2.83	up
gene-XPNPEP2	7E-08	2.80	up
gene-AQP3	3E-20	2.80	up
gene-AREG	2E-19	2.79	up
gene-PTPRE	9E-09	2.79	up
gene-CSF3R	9E-04	2.77	up
gene-PTGDS	3E-17	2.76	up
gene-FOS	8E-05	2.76	up
gene-MMP11	7E-15	2.72	up
gene-CFD	1E-15	2.71	up
gene-AKR1C1	3E-91	2.71	up
gene-FAM43A	3E-166	2.71	up
gene-PTGIS	2E-83	2.70	up
gene-HD11B1	7E-25	2.70	up
gene-MMP11-2	3E-23	2.69	up
gene-SMPDL3A	6E-43	2.69	up
gene-CD14	2E-03	2.67	up
gene-HD17B2	2E-10	2.66	up
gene-MEDAG	5E-37	2.66	up
gene-SECTM1	7E-63	2.66	up
gene-SLC1A3	2E-08	2.65	up
gene-MYLIP	2E-34	2.65	up
gene-IL13RA2	5E-34	2.65	up
gene-ECM2-2	4E-14	2.62	up
gene-PDPN	8E-31	2.62	up
gene-ABI3BP	1E-68	2.61	up
gene-IL1R1	9E-263	2.59	up
gene-ARHGAP6	2E-16	2.59	up
gene-C3	1E-17	2.59	up
gene-ECM2	8E-13	2.58	up
gene-CHI3L1	4E-07	2.58	up
gene-LAMC3	1E-07	2.57	up
gene-SESN3	7E-21	2.56	up

gene-RGCC	4E-11	2.54	up
gene-FAXDC2	9E-20	2.54	up
gene-ALX4	3E-06	2.52	up
gene-PLA2G4A	2E-33	2.52	up
gene-LTBP4	8E-179	2.51	up
gene-COL26A1	1E-08	2.51	up
gene-CSNK2A3	3E-09	2.50	up
gene-KIT	6E-44	2.49	up
gene-NOVA1	2E-04	2.48	up
gene-GPC3	5E-11	2.48	up
gene-ANGPTL2	2E-223	2.47	up
gene-RARRES1	2E-15	2.44	up
gene-APOE	2E-10	2.44	up
gene-KLF9	2E-114	2.43	up
NewGene_2549	1E-17	2.42	up
gene-CHM3	1E-06	2.37	up
gene-WNT2	7E-35	2.36	up
gene-FOXP2	6E-05	2.36	up
gene-TNFRSF19	4E-27	2.34	up
gene-PCOLCE2	3E-06	2.33	up
gene-CTSS	9E-11	2.30	up
gene-ENPEP	4E-17	2.30	up
gene-LDB2	1E-59	2.30	up
gene-LXN	8E-65	2.29	up
gene-MAN1A1	7E-190	2.29	up
gene-SIPA1L2	4E-24	2.28	up
gene-ADAMTS15	5E-25	2.28	up
gene-KCNS2	1E-06	2.28	up
gene-GUCY1B1	5E-13	2.28	up
gene-STON1	6E-26	2.27	up
gene-RGS17	3E-06	2.26	up
gene-KCNJ2	3E-45	2.26	up
gene-AKR1C3	1E-10	2.25	up
gene-CPXM1	8E-08	2.25	up
gene-KBTBD11-2	4E-04	2.25	up
gene-ALPL	2E-26	2.24	up
gene-CCL7	9E-06	2.24	up
gene-SNAP25	6E-07	2.23	up
gene-CACNA1G	1E-05	2.22	up
gene-FOXQ1	1E-23	2.21	up
gene-KBTBD11	6E-04	2.21	up
gene-TESK2	8E-09	2.20	up
gene-EREG	5E-06	2.20	up
gene-CCL20	1E-07	2.19	up
gene-BPI	6E-05	2.19	up
gene-APOL3	2E-09	2.15	up
gene-RASL11A	1E-14	2.14	up

gene-FMOD	2E-77	2.14	up
gene-SNED1	7E-173	2.13	up
gene-ZNF853	2E-10	2.13	up
gene-PLEKHF1	3E-10	2.12	up
gene-KLHL24	2E-32	2.12	up
gene-TMEM132B	2E-30	2.11	up
gene-CCNG2	1E-91	2.10	up
gene-PCMTD1	7E-77	2.10	up
gene-PTGES	1E-63	2.10	up
gene-PKDCC	1E-16	2.09	up
gene-GNAO1	5E-04	2.09	up
gene-IGF2	7E-73	2.08	up
gene-SELENOP	3E-29	2.07	up
gene-COLEC10	1E-05	2.07	up
gene-AKR1C2	2E-13	2.07	up
gene-N4BP3	3E-17	2.07	up
gene-OSR2	1E-162	2.05	up
gene-NCKAP5	4E-08	2.04	up
gene-HTRA3	3E-08	2.04	up
gene-ARHGAP28	8E-14	2.04	up
gene-PENK	2E-17	2.03	up
gene-TNFSF13B	6E-05	2.03	up
gene-CFI	6E-12	2.03	up
gene-LPAR6	2E-13	2.01	up
gene-SDK1	5E-33	1.99	up
gene-PHF24	4E-05	1.99	up
gene-S1PR3	1E-143	1.99	up
gene-HMCN1	1E-26	1.97	up
gene-MAF	3E-34	1.97	up
gene-AJAP1	1E-06	1.97	up
gene-SLC2A12	3E-15	1.96	up
gene-MMD	6E-48	1.95	up
gene-ABCA8	2E-12	1.95	up
gene-SFMBT2	2E-03	1.94	up
gene-FOXL2NB	5E-03	1.94	up
gene-HNMT	3E-18	1.94	up
gene-SLC9A9	9E-08	1.93	up
gene-TBC1D8	5E-15	1.92	up
gene-CHDL1	7E-52	1.91	up
gene-SOD3	3E-44	1.90	up
gene-OLFML2B	1E-15	1.89	up
gene-SURF1	2E-04	1.89	up
gene-GATA6	2E-32	1.89	up
gene-FRAT1	2E-06	1.89	up
gene-KLHL13	6E-08	1.88	up
gene-RIPOR2	8E-67	1.88	up
gene-LURAP1L	2E-12	1.88	up

gene-MTUS1	9E-04	1.87	up
gene-GDF5	2E-11	1.87	up
gene-F2RL1	2E-06	1.85	up
gene-PRELP	3E-26	1.85	up
gene-GRHL1	7E-04	1.85	up
gene-C1R	5E-53	1.84	up
gene-INSIG1	6E-45	1.84	up
gene-MFAP4	7E-76	1.84	up
gene-FADS1	1E-68	1.84	up
gene-ZNF521	8E-93	1.83	up
gene-HH1	2E-32	1.83	up
gene-ETV1	4E-13	1.82	up
gene-EGR1	3E-07	1.82	up
gene-PIWIL4	4E-04	1.81	up
gene-SULF2	5E-78	1.81	up
gene-BMP2	2E-10	1.81	up
gene-STAMBPL1	1E-75	1.81	up
gene-BMERB1-2	3E-17	1.80	up
gene-MAPT	7E-04	1.79	up
gene-C1R-2	1E-50	1.78	up
gene-C1S	8E-59	1.78	up
gene-CCR7	1E-03	1.78	up
gene-CILP	4E-05	1.78	up
gene-PPL	2E-03	1.77	up
gene-CYGB	7E-08	1.77	up
gene-IER3	5E-04	1.76	up
gene-ADAMTS19	9E-06	1.76	up
gene-SEMA4D	8E-05	1.75	up
gene-C16orf86	4E-03	1.75	up
gene-ARHGAP20	2E-17	1.74	up
gene-PIM1	6E-28	1.74	up
gene-CYP27A1	5E-13	1.73	up
gene-BDKRB2	4E-34	1.73	up
gene-ATP8B4	8E-05	1.72	up
gene-SERPINF1	6E-64	1.72	up
gene-MSC	1E-16	1.70	up
gene-PTGER2	1E-13	1.69	up
gene-PRKAR2B	8E-19	1.69	up
gene-IL15RA	4E-11	1.69	up
NewGene_6590	3E-07	1.69	up
gene-GPNMB	2E-47	1.69	up
gene-C1orf115	6E-33	1.69	up
gene-MGP	3E-06	1.69	up
gene-SOX8	5E-04	1.69	up
gene-BCL2L11	6E-09	1.67	up
gene-MMP1	6E-31	1.67	up
gene-ARRDC3	1E-38	1.67	up

gene-LOC124902508	1E-06	1.66	up
gene-SNURF	5E-03	1.66	up
gene-FNDC1	1E-04	1.65	up
gene-CREBRF	3E-30	1.65	up
gene-HMGCS1	2E-43	1.65	up
gene-TRABD2A	3E-14	1.65	up
gene-RXFP1	3E-05	1.64	up
gene-CASP1	3E-27	1.64	up
gene-ITGA8	8E-06	1.64	up
gene-CPZ	1E-30	1.63	up
gene-NETO1	2E-03	1.63	up
gene-DCN	2E-54	1.63	up
gene-STAT5A	2E-18	1.62	up
gene-DLG3	7E-11	1.62	up
gene-FOXL2	1E-05	1.61	up
gene-PDGFRL	4E-09	1.61	up
gene-ZNF395	1E-50	1.61	up
gene-PDGFD	6E-20	1.61	up
gene-SLC1A2	8E-08	1.60	up
gene-SCD	2E-13	1.60	up
gene-DTNA	1E-11	1.60	up
gene-CLDN23-2	1E-03	1.60	up
gene-REV3L	4E-92	1.59	up
gene-PELI2	2E-10	1.59	up
gene-ZNF483	6E-03	1.59	up
gene-TRPA1	4E-08	1.58	up
gene-GREM2	4E-53	1.58	up
gene-RGL1	2E-48	1.58	up
gene-CHM2	1E-54	1.58	up
gene-LRIG3	5E-26	1.57	up
gene-HBP1	9E-21	1.57	up
gene-TCP11L2	1E-09	1.57	up
gene-EBF4	4E-09	1.56	up
gene-CRLF1	5E-06	1.56	up
NewGene_6416	9E-03	1.56	up
gene-EBF1	3E-04	1.55	up
gene-THBS2	2E-136	1.55	up
gene-CCN5	1E-03	1.55	up
gene-ADGRA3	9E-56	1.55	up
gene-WLS	9E-39	1.54	up
gene-TMEM119	3E-29	1.54	up
NewGene_6937	1E-05	1.54	up
gene-GTF2IRD2	3E-10	1.54	up
gene-SLC16A6	3E-09	1.53	up
gene-FADS2	1E-43	1.53	up
gene-ENOX1	1E-07	1.53	up
gene-RAPGEF4	1E-04	1.53	up

gene-HBP1-2	1E-16	1.53	up
gene-GAS1	3E-28	1.52	up
gene-SLC14A1	5E-05	1.51	up
gene-MAFB	3E-04	1.51	up
gene-DH3	1E-35	1.50	up
gene-PCSK6	6E-06	1.50	up
gene-PLPPR3	2E-03	1.49	up
gene-LOC112268016	6E-04	1.48	up
gene-BMP4	5E-10	1.48	up
gene-HLA-E-5	7E-03	1.48	up
gene-IGFBP2	9E-51	1.47	up
gene-CDON	8E-09	1.47	up
gene-MAP3K8	1E-08	1.47	up
gene-SQOR	4E-56	1.46	up
gene-FAM20A	8E-12	1.46	up
gene-SRRM3	2E-05	1.45	up
gene-TFPI2	3E-36	1.45	up
gene-MELTF	8E-06	1.45	up
gene-SALL2	3E-11	1.45	up
gene-SPON2	6E-35	1.44	up
gene-ADORA1	7E-04	1.44	up
gene-GLI3	2E-17	1.44	up
gene-SLC12A8	2E-03	1.44	up
gene-FAM117B	3E-06	1.43	up
gene-PARP9	3E-16	1.43	up
gene-KLF4	2E-30	1.43	up
gene-CCDC69	2E-05	1.43	up
gene-PRRX1	2E-54	1.42	up
gene-IER3-6	1E-04	1.42	up
gene-TRIM47	4E-05	1.42	up
gene-IER3-3	1E-04	1.42	up
gene-RASSF9	6E-03	1.42	up
gene-ZBTB44	1E-35	1.42	up
gene-CLUL1	2E-06	1.42	up
gene-SWT1	6E-05	1.41	up
gene-TFPI	3E-74	1.41	up
gene-ACKR3	7E-27	1.41	up
gene-RASGRF2	1E-08	1.41	up
gene-TMEM170B	2E-06	1.40	up
NewGene_370	2E-04	1.40	up
gene-PNRC1	5E-47	1.40	up
gene-SORCS2	2E-06	1.40	up
gene-FBLN1	5E-36	1.39	up
gene-SNCA	2E-03	1.39	up
gene-IER3-4	1E-04	1.39	up
gene-CSRP2	1E-21	1.39	up
gene-A4GALT	1E-14	1.38	up

gene-NFATC2	7E-07	1.38	up
gene-PLA2R1	8E-41	1.38	up
gene-SERPINE2	4E-13	1.38	up
gene-TLE1	5E-24	1.38	up
gene-LDLR	5E-89	1.38	up
gene-ROR2	6E-18	1.38	up
gene-C15orf48	5E-07	1.37	up
gene-PLPP3	2E-35	1.37	up
gene-ANKRD29	1E-22	1.37	up
gene-ACVR2A	4E-20	1.37	up
gene-SOX4	8E-30	1.36	up
gene-GPR68	7E-16	1.35	up
gene-PDGFRA	3E-61	1.34	up
gene-GDF15	5E-04	1.34	up
gene-PIK3IP1	3E-15	1.34	up
gene-PCBP3	1E-13	1.34	up
NewGene_3264	6E-03	1.34	up
gene-PCDHB13	1E-03	1.34	up
gene-KIF26B	4E-15	1.34	up
gene-FBXO32	2E-06	1.34	up
gene-CA11	5E-06	1.34	up
gene-IDI1	4E-38	1.33	up
gene-SPATA13	1E-26	1.33	up
gene-PLSCR4	2E-41	1.33	up
gene-RAB7B	1E-10	1.33	up
gene-NAMPT	8E-54	1.32	up
gene-TTC39C	2E-36	1.32	up
gene-PLEKHA5	9E-31	1.32	up
gene-OTULINL	7E-05	1.32	up
gene-ARHGAP26	9E-08	1.32	up
gene-GRIA1	7E-19	1.32	up
gene-SLC29A2	9E-03	1.32	up
gene-RGS2	9E-08	1.32	up
gene-CD302	4E-20	1.32	up
gene-SLIT3	3E-47	1.31	up
gene-PPIL6	2E-03	1.31	up
gene-MSX2	6E-08	1.31	up
gene-RALGPS2	1E-46	1.31	up
gene-YPEL2	5E-13	1.31	up
gene-LOC102723996	4E-03	1.31	up
gene-TSHZ1	5E-79	1.31	up
gene-P4HA3	1E-10	1.30	up
gene-PLD1	5E-04	1.30	up
NewGene_1663	1E-03	1.30	up
gene-RARRES2	3E-11	1.30	up
gene-AH	2E-56	1.30	up
gene-DACT1	2E-18	1.30	up

NewGene_4989	1E-05	1.30	up
gene-GSTM5	7E-05	1.29	up
gene-CREB5	1E-16	1.29	up
gene-SNAI1	4E-20	1.29	up
gene-BMERB1	2E-17	1.29	up
gene-CEP162	7E-09	1.28	up
gene-OLFML2A	8E-16	1.28	up
gene-PLSCR1	2E-10	1.28	up
gene-SETBP1	7E-18	1.28	up
gene-CCL11	8E-03	1.27	up
gene-CFH-2	2E-27	1.27	up
gene-TSPOAP1	5E-03	1.27	up
gene-CCDC146	3E-03	1.27	up
gene-CXCL14	6E-14	1.27	up
gene-LRP4	1E-06	1.27	up
gene-CRABP2	2E-16	1.27	up
gene-CRYBG1	1E-15	1.27	up
gene-GEM	5E-19	1.26	up
gene-TP53INP1	2E-20	1.26	up
gene-ZNF503	4E-19	1.26	up
gene-ATF3	9E-04	1.26	up
gene-MSMO1	2E-26	1.26	up
gene-CASTOR1	2E-06	1.26	up
gene-STC1	2E-22	1.25	up
gene-MAP7	2E-06	1.25	up
gene-ARMC9	5E-30	1.25	up
gene-PLCL2	1E-08	1.25	up
gene-PXK	2E-20	1.25	up
NewGene_2801	9E-07	1.25	up
gene-PCCA	2E-08	1.24	up
gene-HEPH	3E-19	1.24	up
gene-NOP53	3E-41	1.24	up
gene-IRAK3	3E-09	1.24	up
gene-PLCL2-2	1E-08	1.23	up
gene-CYP51A1	5E-37	1.23	up
gene-THBD	7E-03	1.23	up
gene-EML5	3E-04	1.23	up
gene-ORAI3	5E-20	1.23	up
gene-PPARG	4E-13	1.23	up
gene-APOL1	1E-06	1.23	up
gene-NFIB	2E-04	1.22	up
gene-FBLN7	4E-12	1.22	up
gene-FAM135A	2E-11	1.22	up
NewGene_3586	1E-04	1.22	up
gene-UST	2E-23	1.22	up
gene-CTSK	1E-58	1.22	up
gene-C1QTNF1	3E-32	1.22	up

gene-ANKRD33B	2E-18	1.22	up
gene-LRRC56-2	6E-03	1.21	up
gene-ELF1	8E-35	1.21	up
gene-DENND2A	1E-05	1.21	up
NewGene_6371	2E-03	1.21	up
gene-PSD	1E-04	1.21	up
gene-LRRK2	4E-06	1.21	up
gene-ACAT2	2E-24	1.21	up
NewGene_1942	3E-07	1.21	up
gene-IER3-5	1E-06	1.21	up
gene-NEMP2	2E-05	1.21	up
gene-SC5D	4E-22	1.20	up
gene-GAS7	3E-18	1.20	up
gene-MBNL3	2E-05	1.20	up
gene-DDIT4	8E-30	1.20	up
gene-PLXNC1	5E-12	1.20	up
gene-NCOA7	2E-15	1.20	up
gene-GBP2	7E-06	1.20	up
gene-EGR3	1E-03	1.20	up
gene-BTG1	2E-57	1.19	up
gene-MMAB	9E-13	1.19	up
NewGene_3014	3E-03	1.19	up
NewGene_1363	3E-03	1.19	up
gene-KLF11	2E-11	1.19	up
gene-CFH	3E-18	1.19	up
gene-MINAR1	6E-05	1.19	up
gene-CARF	4E-05	1.19	up
gene-ZFP14	9E-03	1.19	up
gene-HUNK	9E-04	1.19	up
gene-MN1	2E-09	1.18	up
gene-IFITM1	5E-28	1.18	up
gene-APOL6	2E-13	1.18	up
gene-LOC124904077	4E-04	1.18	up
gene-PHF10	6E-15	1.18	up
gene-IRF1	7E-18	1.17	up
gene-PPP1R3C	5E-23	1.17	up
gene-SLC16A7	5E-33	1.17	up
gene-CSGALNACT1	6E-05	1.17	up
gene-NR1H3	6E-05	1.16	up
gene-EMX2	4E-06	1.16	up
gene-WWOX	2E-04	1.16	up
gene-SQLE	2E-26	1.16	up
gene-RMDN2	3E-06	1.16	up
gene-ACKR4	2E-12	1.16	up
gene-GAS2L3	2E-04	1.15	up
gene-NDRG1	1E-27	1.15	up
gene-TNFRSF14	5E-03	1.15	up

gene-KIF26B-2	1E-15	1.15	up
gene-PTCHD4	6E-12	1.15	up
gene-PLPPR4	9E-15	1.15	up
gene-BBS12	2E-06	1.15	up
gene-OTUD1	3E-07	1.15	up
gene-KLHDC1	3E-03	1.15	up
gene-H	9E-05	1.14	up
gene-EYA2	7E-04	1.14	up
gene-SAT1	2E-16	1.14	up
gene-KANSL1L	4E-05	1.14	up
gene-TGFBR3	2E-09	1.14	up
gene-OSGIN1	5E-03	1.13	up
gene-FOXF2	8E-24	1.13	up
gene-TM7SF2	9E-03	1.13	up
gene-PRRG1	3E-27	1.13	up
gene-PRKG2	3E-07	1.13	up
gene-MVK	2E-08	1.13	up
gene-SAP30L	1E-33	1.13	up
gene-CEP19	6E-04	1.13	up
gene-EFCAB7	2E-04	1.12	up
gene-CDC42EP4	2E-39	1.12	up
gene-HD17B7	9E-08	1.12	up
gene-CEP70	2E-07	1.12	up
gene-ITPR1	1E-06	1.12	up
gene-KCNE4	2E-03	1.11	up
gene-BOC	3E-33	1.11	up
gene-GALNT12	4E-05	1.11	up
gene-YPEL3	2E-11	1.11	up
gene-DPYSL2	5E-53	1.11	up
gene-COL15A1	1E-05	1.11	up
gene-PID1	9E-23	1.11	up
gene-FDFT1	6E-04	1.11	up
gene-PLTP	2E-11	1.11	up
gene-PTGS1	3E-25	1.11	up
gene-LHFPL2	2E-22	1.10	up
gene-GTF2IRD2B	5E-15	1.10	up
gene-IRF2BPL	1E-22	1.10	up
gene-CTSL	1E-64	1.10	up
gene-DMKN	2E-05	1.10	up
gene-PGF	3E-08	1.09	up
gene-C5	2E-04	1.09	up
gene-DUS4L-BCAP29-2	7E-13	1.09	up
gene-PDE5A	2E-38	1.09	up
NewGene_3298	9E-03	1.09	up
gene-LRRC2	4E-07	1.09	up
gene-RAB9A	8E-15	1.08	up
gene-TMTC4	2E-06	1.08	up

gene-ELN	1E-22	1.08	up
gene-SLC6A6	3E-23	1.08	up
gene-CTSF	3E-19	1.08	up
gene-EPSTI1	3E-04	1.08	up
gene-PITPNC1	2E-13	1.07	up
gene-DIRAS3	4E-03	1.07	up
gene-MDFIC	3E-48	1.07	up
gene-COLEC12	7E-39	1.07	up
gene-GCH1	5E-03	1.07	up
gene-LACC1	7E-15	1.07	up
gene-PLEKHA4	1E-16	1.07	up
gene-PBX1	1E-49	1.07	up
gene-JUND	2E-26	1.06	up
gene-FOSB	6E-03	1.06	up
gene-PAG1	3E-07	1.06	up
gene-PLAAT4	7E-03	1.06	up
gene-CDC42EP5-2	3E-04	1.06	up
gene-PLAC9	3E-06	1.05	up
gene-PTGFR	3E-09	1.05	up
gene-LCA5	1E-05	1.05	up
gene-PRUNE1	2E-08	1.05	up
gene-RUNX2	3E-07	1.05	up
gene-ZDHHC14	4E-06	1.05	up
gene-DDR1-4	4E-03	1.05	up
NewGene_1500	3E-10	1.05	up
gene-AARD	5E-03	1.05	up
gene-GRK5	4E-23	1.05	up
gene-SMO	8E-14	1.05	up
gene-CFAP69	4E-04	1.04	up
gene-DTX4	1E-05	1.04	up
gene-RB1CC1	1E-45	1.04	up
gene-FDFT1-2	2E-34	1.04	up
gene-LRRN4CL	3E-08	1.04	up
gene-ISLR	9E-12	1.03	up
gene-ATXN1	2E-17	1.03	up
gene-BTN3A3	9E-09	1.03	up
gene-NTRK2	5E-03	1.03	up
gene-FBXO36	3E-03	1.03	up
gene-PRX	4E-06	1.03	up
gene-EFS	2E-04	1.03	up
gene-MEX3A	2E-04	1.03	up
gene-RNASE4	4E-11	1.03	up
gene-LRRC49	1E-08	1.03	up
gene-PARP14	1E-18	1.02	up
gene-SHOX2	6E-13	1.02	up
gene-LOC728743	1E-03	1.02	up
gene-PHF21A	3E-15	1.02	up

gene-DPYSL3	1E-50	1.02	up
gene-ANKRD10	2E-16	1.02	up
gene-HECTD2	7E-10	1.02	up
gene-SHC2	9E-05	1.02	up
gene-NRP2	2E-14	1.01	up
gene-NPTX2	2E-03	1.00	up
gene-URB2	5E-10	-1.00	down
gene-H3ST3A1	6E-23	-1.00	down
gene-ITGA11	7E-18	-1.00	down
gene-VASP	8E-26	-1.00	down
NewGene_17	9E-03	-1.00	down
gene-MARCHF10	3E-03	-1.00	down
gene-ENTPD7	4E-38	-1.00	down
gene-APBA1-2	2E-08	-1.01	down
gene-KHDRBS3	1E-13	-1.01	down
gene-TRAM2	4E-53	-1.01	down
gene-FGF5	2E-21	-1.01	down
gene-CORO2B	4E-12	-1.01	down
gene-NFASC	1E-39	-1.01	down
gene-MMP24	7E-13	-1.01	down
gene-ZNF703	7E-40	-1.01	down
gene-NT5DC3	1E-11	-1.01	down
gene-FLNA	4E-34	-1.01	down
gene-CHT7	4E-13	-1.01	down
gene-AFAP1L1	5E-06	-1.01	down
gene-PPP1R13L	4E-11	-1.02	down
gene-RBM14	2E-26	-1.02	down
gene-ACTN4	6E-03	-1.03	down
gene-EXO1	6E-05	-1.03	down
gene-TENM2	9E-04	-1.03	down
gene-KCTD20	2E-48	-1.03	down
gene-FGF1	1E-27	-1.03	down
gene-XYLT1-2	1E-26	-1.03	down
gene-EHD4	2E-27	-1.03	down
gene-HCLS1	1E-03	-1.03	down
gene-NOP56	9E-60	-1.03	down
gene-FZD8	4E-09	-1.04	down
gene-SGK3	4E-04	-1.04	down
gene-MCM2	1E-18	-1.04	down
gene-MYH9	9E-39	-1.04	down
gene-RTN1	3E-03	-1.04	down
gene-FKBP5	5E-10	-1.04	down
gene-PAWR	2E-33	-1.04	down
gene-PRICKLE1	2E-17	-1.04	down
gene-UBASH3B	2E-37	-1.04	down
gene-GGT5	9E-13	-1.05	down
gene-MYOCD	7E-22	-1.05	down

gene-RELN	6E-03	-1.05	down
gene-GADD45B	1E-14	-1.05	down
gene-PNP	7E-22	-1.05	down
gene-RRS1	6E-13	-1.05	down
gene-GDPD5	6E-05	-1.05	down
gene-SCHIP1	4E-23	-1.05	down
gene-PXN	8E-65	-1.05	down
gene-PHLDA2-2	4E-21	-1.05	down
gene-ANKRD34A	3E-05	-1.06	down
gene-KIF18B	3E-03	-1.06	down
gene-CLDN1	8E-08	-1.06	down
gene-SMTN	3E-49	-1.06	down
gene-TRMT9B-2	6E-07	-1.06	down
gene-KIFC1-3	8E-03	-1.06	down
gene-TUBB6	2E-67	-1.06	down
gene-PVR	3E-64	-1.07	down
NewGene_495	1E-03	-1.07	down
gene-SH3BP5L	1E-51	-1.07	down
gene-CDCP1	1E-20	-1.07	down
gene-PHLDA2	5E-21	-1.07	down
gene-HMGA2	2E-45	-1.07	down
gene-PLEC	2E-40	-1.07	down
gene-COL4A1	1E-61	-1.07	down
gene-SPOCD1	9E-38	-1.07	down
gene-CAP2	6E-30	-1.07	down
gene-TGFA	1E-09	-1.07	down
gene-MCM5	4E-15	-1.08	down
gene-PSG6	6E-03	-1.08	down
gene-PTPRF	3E-70	-1.08	down
gene-CEND1	4E-03	-1.08	down
gene-LMNB1	3E-12	-1.08	down
gene-PRAG1	1E-16	-1.08	down
gene-ADCK5	5E-03	-1.08	down
gene-PPP1R14A	1E-03	-1.08	down
gene-CDK6	7E-34	-1.08	down
gene-PITX2	2E-08	-1.09	down
gene-CORIN	2E-25	-1.09	down
gene-HPB1	2E-38	-1.09	down
gene-ULBP2	2E-08	-1.09	down
gene-KIFC1	5E-03	-1.09	down
gene-DNMT3B	3E-03	-1.09	down
gene-OLR1	5E-11	-1.09	down
gene-MBLAC1	7E-03	-1.09	down
gene-KCTD16	9E-05	-1.10	down
gene-RAP1GAP2	3E-24	-1.10	down
gene-HPB7	5E-26	-1.10	down
gene-DLK2	1E-05	-1.10	down

gene-CSRP1	2E-60	-1.10	down
gene-TMPPE	2E-03	-1.10	down
gene-ALDH4A1	6E-10	-1.10	down
gene-TUFT1	2E-25	-1.11	down
gene-SH3RF1	4E-28	-1.11	down
gene-LHX9	2E-04	-1.11	down
gene-CASP3	8E-23	-1.11	down
gene-PKMYT1	2E-03	-1.11	down
NewGene_4436	1E-09	-1.11	down
gene-KCNH1	2E-09	-1.12	down
gene-SEL1L3	2E-35	-1.12	down
gene-ACTA2	9E-91	-1.12	down
gene-ZNF239	2E-08	-1.12	down
gene-EDN1	4E-26	-1.12	down
gene-SPINT2	4E-06	-1.12	down
gene-XYLT1	5E-33	-1.13	down
gene-SHOOM2	6E-05	-1.14	down
gene-PLEKHN1	7E-09	-1.14	down
gene-F3	6E-31	-1.14	down
gene-ADAMTS12-2	5E-04	-1.14	down
gene-FBXL6-2	2E-10	-1.14	down
gene-DGKA	3E-35	-1.14	down
gene-CDK5R1	5E-04	-1.14	down
gene-TSPAN13	1E-16	-1.14	down
gene-KCTD4	6E-04	-1.14	down
gene-LOC102724428	1E-04	-1.14	down
gene-SORT1	2E-31	-1.14	down
gene-PRAG1-2	1E-20	-1.15	down
gene-NOCT	5E-06	-1.15	down
gene-CCDC28B	3E-03	-1.15	down
gene-TAGLN	1E-83	-1.15	down
gene-ITPRIP	5E-16	-1.15	down
gene-SLC20A1	5E-36	-1.15	down
gene-EME1	2E-03	-1.15	down
gene-CDK18	9E-03	-1.16	down
gene-BRIP1	2E-07	-1.16	down
gene-CCBE1	4E-58	-1.16	down
gene-SELPLG	2E-14	-1.16	down
gene-DPF1	1E-03	-1.16	down
gene-EZR	1E-26	-1.16	down
gene-TBC1D2	6E-38	-1.16	down
gene-PDCD2L	5E-03	-1.16	down
gene-EPHA2	2E-20	-1.16	down
gene-ACTN1	1E-62	-1.16	down
gene-ATP2B4	2E-39	-1.17	down
gene-MPP4	1E-04	-1.17	down
gene-COL11A1	3E-75	-1.17	down

gene-ORC1	1E-04	-1.17	down
gene-MET	6E-25	-1.17	down
gene-WWC1	1E-08	-1.17	down
gene-SCN9A	3E-30	-1.18	down
gene-AMZ1	3E-21	-1.18	down
gene-ITGA6	4E-16	-1.18	down
gene-SUSD2	4E-06	-1.19	down
gene-RAD54L	5E-03	-1.20	down
gene-MLPH	1E-24	-1.20	down
gene-FERMT1	2E-04	-1.20	down
gene-LOXL2	4E-86	-1.20	down
gene-LOC124902313	6E-04	-1.21	down
gene-UHF1	6E-30	-1.21	down
gene-PRPS1	7E-88	-1.21	down
gene-TRPV2	6E-12	-1.22	down
gene-HASPIN	4E-04	-1.23	down
gene-PLEKHA2	5E-56	-1.23	down
gene-CLIC3	5E-05	-1.23	down
gene-ALS2CL	4E-09	-1.25	down
gene-AHNAK2	2E-19	-1.25	down
gene-NUAK1	3E-28	-1.25	down
gene-FHOD3	2E-28	-1.25	down
gene-LOC102723750	7E-04	-1.25	down
gene-ADCY7	2E-33	-1.26	down
gene-CDT1	6E-08	-1.27	down
gene-DNAJB4	2E-73	-1.27	down
gene-TPM1	4E-56	-1.27	down
NewGene_1380	5E-03	-1.27	down
gene-CNN1	9E-70	-1.27	down
gene-DBNDD2	1E-09	-1.27	down
gene-OTUB2-2	1E-02	-1.27	down
gene-TNS1	1E-46	-1.27	down
gene-TICRR	9E-10	-1.28	down
gene-GINS2	9E-05	-1.28	down
gene-KRT19	4E-54	-1.28	down
gene-S1PR1	1E-37	-1.28	down
gene-NES	2E-51	-1.29	down
gene-ARFGEF3	3E-07	-1.29	down
gene-HYI	5E-04	-1.29	down
gene-CDH2	5E-49	-1.29	down
gene-RHBDF2	9E-24	-1.29	down
gene-PSG2	5E-05	-1.29	down
gene-MARCHF4	2E-95	-1.30	down
gene-SAPCD2	2E-05	-1.30	down
gene-MYO10	1E-135	-1.30	down
gene-CTPS1	3E-44	-1.30	down
gene-SLCO2A1	6E-07	-1.30	down

gene-NPAS4	9E-03	-1.30	down
gene-WNT5B	3E-79	-1.31	down
gene-ALDH1B1	5E-48	-1.31	down
gene-GALNT3	1E-05	-1.31	down
gene-SIPA1L3	8E-74	-1.31	down
gene-NET1	1E-56	-1.31	down
gene-FSCN1	2E-148	-1.32	down
gene-RGS4	4E-32	-1.32	down
gene-KIAA0040	2E-04	-1.32	down
gene-PLCXD1-2	4E-20	-1.32	down
gene-ADGRE5	3E-30	-1.32	down
gene-DOK5	4E-22	-1.33	down
gene-DTL	7E-12	-1.33	down
gene-MAGI1	1E-58	-1.34	down
gene-PLEK2	3E-03	-1.35	down
gene-KIF17	1E-06	-1.36	down
gene-PDE1C	2E-45	-1.36	down
gene-CDA	6E-05	-1.36	down
gene-SH2D5	3E-20	-1.37	down
gene-GNAZ	5E-46	-1.37	down
gene-ARHGAP22	4E-64	-1.37	down
gene-CLSPN	1E-06	-1.37	down
gene-MBOAT1	2E-06	-1.38	down
NewGene_5609	3E-03	-1.38	down
gene-MAP2K3	1E-40	-1.38	down
gene-PLXNB3	1E-13	-1.39	down
gene-XRCC2	1E-04	-1.39	down
gene-HD17B6	1E-09	-1.40	down
gene-MAP3K9	6E-03	-1.40	down
gene-JAM2	3E-10	-1.40	down
gene-CELSR1	2E-11	-1.40	down
gene-TENT5B	1E-05	-1.40	down
gene-RASGRP1	2E-22	-1.40	down
gene-MT1E	8E-25	-1.40	down
gene-ATP10A	4E-45	-1.42	down
gene-CCDC85A	4E-10	-1.42	down
gene-GRAMD1B	3E-31	-1.43	down
gene-CDC25A	5E-10	-1.44	down
gene-ADTRP	2E-03	-1.44	down
gene-LRRC4	4E-03	-1.45	down
gene-PLCXD1	6E-20	-1.45	down
gene-MACIR	1E-48	-1.45	down
gene-HPB8	1E-20	-1.46	down
gene-L1CAM	2E-44	-1.46	down
NewGene_1631	7E-10	-1.46	down
NewGene_265	1E-05	-1.49	down
gene-KRT7	9E-59	-1.49	down

gene-SEMA7A	6E-05	-1.49	down
gene-ITGA3	3E-66	-1.50	down
gene-ANKHD1	1E-03	-1.50	down
gene-TPD52	3E-04	-1.50	down
gene-OPCML	5E-15	-1.50	down
gene-LZTS1	2E-17	-1.51	down
gene-SPTBN5	6E-04	-1.51	down
gene-PODXL	9E-16	-1.51	down
gene-ZFHX2	2E-15	-1.51	down
gene-TRIM55	6E-18	-1.53	down
gene-IFFO2	5E-76	-1.54	down
gene-TPD52L1	4E-16	-1.54	down
gene-HAS2	2E-40	-1.54	down
gene-CDC6	2E-16	-1.54	down
gene-JPH2	9E-11	-1.54	down
gene-TMEM255B	1E-19	-1.55	down
gene-SCUBE3	1E-47	-1.57	down
gene-SPON1	2E-05	-1.57	down
gene-SH3TC2	1E-03	-1.57	down
gene-MICAL2	1E-82	-1.58	down
gene-PLD5	2E-12	-1.58	down
gene-XDH	5E-11	-1.59	down
gene-CPA4	5E-45	-1.59	down
NewGene_477	2E-05	-1.60	down
gene-FLNC	2E-101	-1.60	down
gene-FAT3	5E-06	-1.60	down
gene-C13orf46-2	1E-04	-1.61	down
NewGene_6040	1E-03	-1.62	down
gene-LOC124904228	1E-08	-1.62	down
gene-ACOT11	1E-09	-1.62	down
gene-NXPH3	1E-03	-1.63	down
gene-ABCA3	8E-12	-1.64	down
gene-MPZL3	5E-04	-1.64	down
gene-FRMPD3	6E-04	-1.65	down
gene-KIAA1549L	1E-152	-1.66	down
gene-GABBR2	8E-44	-1.66	down
gene-CSPG4	3E-11	-1.67	down
gene-SSTR1	3E-38	-1.67	down
gene-EPHB1	6E-04	-1.68	down
gene-PPM1H	7E-04	-1.68	down
gene-FSTL3	1E-106	-1.69	down
gene-CDCA7	5E-14	-1.69	down
gene-KRT80	3E-08	-1.70	down
gene-FAM180A	6E-14	-1.73	down
NewGene_975	3E-04	-1.73	down
gene-DSP	1E-31	-1.73	down
gene-C11orf91	2E-03	-1.75	down

gene-DYNLT4	2E-04	-1.75	down
gene-HBEGF	1E-43	-1.76	down
gene-PTPRB	9E-20	-1.79	down
gene-PLCB4	4E-37	-1.80	down
gene-CD274	7E-21	-1.80	down
gene-TLL1	1E-08	-1.80	down
gene-POLR1G	7E-11	-1.81	down
gene-TM4SF20	3E-14	-1.81	down
gene-TRPC4	1E-78	-1.82	down
gene-ZNF367	8E-17	-1.82	down
gene-SERPINE1	3E-251	-1.84	down
gene-MYBL1	1E-52	-1.87	down
NewGene_4949	9E-04	-1.87	down
gene-SEMA7A-2	5E-57	-1.88	down
gene-EGF	3E-04	-1.88	down
gene-PLXNA2	2E-31	-1.90	down
gene-MAT2A	1E-88	-1.91	down
gene-CCNE2	5E-11	-1.91	down
gene-ENC1	2E-66	-1.92	down
gene-INHBB	3E-11	-1.93	down
gene-MCM10	3E-14	-1.93	down
gene-UCP2	6E-07	-1.95	down
gene-NRN1	4E-13	-1.97	down
gene-LOC105373989	1E-24	-2.01	down
gene-MALL	3E-21	-2.02	down
gene-LYPD6B	1E-08	-2.03	down
gene-KCNQ5	1E-82	-2.03	down
gene-LOC100653049	1E-49	-2.03	down
gene-ASB5	5E-20	-2.04	down
gene-WNK4	2E-73	-2.06	down
gene-GJA5	6E-05	-2.07	down
gene-KRT15	6E-05	-2.07	down
NewGene_5875	5E-08	-2.07	down
gene-ADAM19	4E-196	-2.07	down
gene-PCDHGC5	3E-06	-2.09	down
gene-EDIL3	2E-34	-2.09	down
gene-FOXE1	4E-24	-2.09	down
gene-KRTAP1-1-2	4E-06	-2.13	down
gene-TSPAN10	3E-04	-2.15	down
gene-TATDN1-2	3E-03	-2.18	down
gene-ERBB3	9E-03	-2.20	down
gene-STYK1	9E-04	-2.21	down
gene-P2RX5	5E-25	-2.24	down
gene-KRT18	2E-281	-2.24	down
gene-EXTL1	4E-49	-2.25	down
gene-KRT34-2	1E-29	-2.27	down
gene-BCAP29-2	6E-19	-2.27	down

gene-CCDC81	8E-13	-2.30	down
gene-IGFBPL1	2E-08	-2.30	down
gene-OXTR	0E+00	-2.31	down
gene-ADRA1D	4E-11	-2.32	down
gene-KRT34-3	8E-25	-2.32	down
gene-SYT16	2E-33	-2.33	down
gene-FAM111B	2E-15	-2.35	down
gene-LOC124905366	2E-13	-2.37	down
gene-FAM184B	4E-10	-2.39	down
gene-RIMS1	4E-14	-2.40	down
gene-KRT33B-3	4E-03	-2.41	down
gene-TMEM184A	1E-11	-2.45	down
gene-E2F2-2	9E-05	-2.48	down
gene-TGFB2	1E-28	-2.50	down
gene-SYNPO2L	1E-08	-2.70	down
gene-NRXN3	2E-11	-2.76	down
gene-KISS1	4E-32	-2.78	down
gene-NRK	9E-08	-2.82	down
gene-ANKRD1	2E-09	-2.83	down
gene-EPPK1	9E-06	-2.89	down
gene-EFHD1	7E-35	-3.00	down
gene-KRT81	2E-51	-3.02	down
NewGene_1203	1E-19	-3.04	down
gene-SLFNL1	2E-07	-3.20	down
gene-DSCAM	3E-10	-3.58	down

Appendix 3

Table 8.4: DEG linked to each significantly enriched term in biological process in GO. Results are shown for DEG in fibroblasts grown in high glucose (20 mM) compared to euglycemic control (5.5 mM) (F20_vs_F5). (BMKGENE, 2023)

Description	geneID
Kidney development	NewGene_2505;NewGene_2507;NewGene_2511;NewGene_2512;NewGene_2516;NewGene_2519;NewGene_4495;gene-CRLF1;gene-DCH1;gene-FOXC2;gene-GLIS2-2;gene-LAMA5;gene-PKD1;gene-PKD1-2
Lymph vessel morphogenesis	NewGene_2505;NewGene_2511;NewGene_2516;NewGene_2519;NewGene_4495;gene-FOXC2
Branching morphogenesis of an epithelial tube	NewGene_2505;NewGene_2511;NewGene_2516;NewGene_2519;NewGene_4495;gene-DCH1;gene-FOXC2;gene-LAMA1;gene-LAMA5
Regulation of mitotic spindle organization	NewGene_2505;NewGene_2511;NewGene_2516;NewGene_2519;NewGene_4495;gene-CCSAP
Cartilage condensation	NewGene_2505;NewGene_2511;NewGene_2516;NewGene_2519;NewGene_4495
Response to fluid shear stress	NewGene_2505;NewGene_2511;NewGene_2516;NewGene_2519;NewGene_4495
Establishment of cell polarity	NewGene_2505;NewGene_2511;NewGene_2516;NewGene_2519;NewGene_4495;gene-LAMA1;gene-TCIRG1
Mesonephric epithelium development	NewGene_2511;gene-CRLF1;gene-DCH1;gene-FOXC2;gene-LAMA5
Cytoplasmic sequestering of transcription factor	NewGene_2505;NewGene_2511;NewGene_2516;NewGene_2519;NewGene_4495
Cellular response to redox state	gene-ARHGDIB;gene-VASN;gene-VASN-2
Mesonephric tubule development	NewGene_2511;gene-CRLF1;gene-DCH1;gene-FOXC2;gene-LAMA5
Placenta blood vessel development	NewGene_2505;NewGene_2511;NewGene_2516;NewGene_2519;NewGene_4495
Mesonephros development	NewGene_2511;gene-CRLF1;gene-DCH1;gene-FOXC2;gene-LAMA5
Detection of mechanical stimulus	NewGene_2505;NewGene_2511;NewGene_2516;NewGene_2519;NewGene_4495
Regulation of cellular response to growth factor stimulus	gene-FAM20C-4;gene-FBXL15;gene-MICOS10-NBL1;gene-TMEM204;gene-VASN;gene-VASN-2;gene-XDH
Protein export from nucleus	NewGene_2505;NewGene_2511;NewGene_2516;NewGene_2519;NewGene_4495;gene-ZC3H3-2
Kidney epithelium development	NewGene_2511;gene-CRLF1;gene-DCH1;gene-FOXC2;gene-LAMA5
Embryonic placenta development	NewGene_2505;NewGene_2511;NewGene_2516;NewGene_2519;NewGene_4495
Lymph vessel development	NewGene_2511;gene-FOXC2;gene-FOXF2;gene-TMEM204
Positive regulation of protein binding	NewGene_2505;NewGene_2511;NewGene_2516;NewGene_2519;NewGene_4495;gene-EPHB6

Table 8.5: DEG linked to each significantly enriched term in biological process in GO. Results are shown for DEG in fibroblasts grown exposed to *S. epidermidis* lysate compared to no-lysate control in 5.5 mM glucose concentration (FSe5_vs_F5). (BMKGENE, 2023)

Description	geneID liked to the enriched term
Extracellular matrix organisation	gene-BCL3;gene-DPT;gene-ECM2;gene-ECM2-2;gene-FBLN1;gene-FBLN2;gene-ITGAE;gene-LAMA1;gene-LAMA5;gene-LAMC3;gene-MPZL3;gene-NDNF;gene-OLFML2A;gene-OLFML2B;gene-POSTN;gene-SCUBE3;gene-SLC39A8;gene-VWA1;gene-VWF
Branching morphogenesis of an epithelial tube	NewGene_2505;NewGene_2511;NewGene_2516;NewGene_2519;NewGene_4495;NewGene_4499;gene-CLIC4;gene-CLIC6;gene-CXCL12;gene-DCH1;gene-LAMA1;gene-LAMA5
Kidney development	NewGene_2505;NewGene_2511;NewGene_2512;NewGene_2516;NewGene_2519;NewGene_4495;gene-BCL2L11;gene-CRLF1;gene-CYS1;gene-DCH1;gene-DCN;gene-GLIS2;gene-LAMA5;gene-OSR2;gene-PCSK9;gene-PKD1;gene-PKD1-2;gene-SERPINF1
Response to fluid shear stress	NewGene_2505;NewGene_2511;NewGene_2516;NewGene_2519;NewGene_4495;NewGene_4499;gene-KLF4
Regulation of cell adhesion	NewGene_2505;NewGene_2511;NewGene_2516;NewGene_2519;NewGene_4495;NewGene_4499;gene-AJAP1;gene-CD274;gene-COL26A1;gene-CXCL12;gene-DAB1;gene-ECM2;gene-ECM2-2;gene-EFNB3;gene-KLF4;gene-LAMA1;gene-LAMA2;gene-LAMA3;gene-LAMA5;gene-NDNF;gene-PAG1;gene-RGCC;gene-TRIOBP;gene-ZC3H12A;gene-ZNF608
Cartilage condensation	NewGene_2505;NewGene_2511;NewGene_2516;NewGene_2519;NewGene_4495;NewGene_4499
Lymph vessel morphogenesis	NewGene_2505;NewGene_2511;NewGene_2516;NewGene_2519;NewGene_4495;NewGene_4499
Cellular response to hypoxia	NewGene_1516;gene-ANKRD1;gene-EDN1;gene-ENDOG;gene-HILPDA;gene-MGARP;gene-NDNF;gene-RGCC;gene-STC2;gene-VASN;gene-VASN-2
Enamel mineralisation	gene-FAM20A;gene-FAM20C;gene-FAM20C-2;gene-FAM20C-4;gene-PPARA
Detection of mechanical stimulus	NewGene_2505;NewGene_2511;NewGene_2516;NewGene_2519;NewGene_4495;NewGene_4499;gene-CXCL12
Embryonic placenta development	NewGene_2505;NewGene_2511;NewGene_2516;NewGene_2519;NewGene_4495;NewGene_4499;gene-LIF;gene-SNAI1
Cell volume homeostasis	gene-SHANK3;gene-SHANK3-2;gene-SLC12A7;gene-SLC12A7-2
Extracellular structure organisation	gene-BCL3;gene-DPT;gene-ECM2;gene-ECM2-2;gene-ITGAE;gene-LAMA1;gene-LAMA5;gene-LAMC3;gene-MPZL3;gene-NDNF;gene-OLFML2A;gene-SCUBE3;gene-VWA1;gene-VWF
Establishment of cell polarity	NewGene_2505;NewGene_2511;NewGene_2516;NewGene_2519;NewGene_4495;NewGene_4499;gene-FAM89B;gene-LAMA1;gene-MPP7
Regulation of cell migration	NewGene_4681;gene-CD274;gene-CEMIP;gene-CXCL12;gene-CXCL16;gene-FAM89B;gene-KLF4;gene-LAMA1;gene-LAMA2;gene-LAMA3;gene-LAMA5;gene-MACIR;gene-MICOS10-

	NBL1;gene-MTUS1;gene-NDRG4;gene-NTN1;gene-PODN;gene-PRR5;gene-RGCC;gene-SASH1;gene-SNAI1;gene-SST;gene-ZC3H12A
Response to mechanical stimulus	NewGene_2511;gene-CXCL12;gene-DCN;gene-ENDOG;gene-GDF5;gene-POSTN;gene-RCAN1;gene-SHANK3;gene-SHANK3-2;gene-TXNIP
Cytoplasmic sequestering of transcription factor	NewGene_2505;NewGene_2511;NewGene_2516;NewGene_2519;NewGene_4495;NewGene_4499
Biomineral tissue development	gene-FAM20C;gene-FAM20C-2;gene-FAM20C-4;gene-FBXL15;gene-SLC20A1;gene-TUFT1
Angiogenesis	gene-ACKR3;gene-ANGPT1;gene-ANGPTL4;gene-CLIC4;gene-CLIC6;gene-CXCL12;gene-HMOX1;gene-LAMA5;gene-NDNF;gene-NRP2;gene-RNF213;gene-SHC2
Receptor signalling pathway via JAK-STAT	NewGene_2505;NewGene_2511;NewGene_2516;NewGene_2519;NewGene_4495;NewGene_4499;gene-LIF;gene-SOCS1

Table 8.6: DEG linked to each significantly enriched term in biological process in GO. Results are shown for DEG in fibroblasts grown exposed to *S. epidermidis* lysate compared to no-lysate control in 20 mM glucose concentration (F20_vs_FSe20). (BMKGENE, 2023)

Description	geneID
Collagen fibril organisation	gene-DPT;gene-FMOD;gene-FOXF2;gene-TNXB;gene-TNXB-3;gene-TNXB-4;gene-TNXB-5;gene-TNXB-6
Extracellular matrix organisation	gene-COL4A1;gene-DPT;gene-ECM2;gene-ECM2-2;gene-FBLN1;gene-ITGA6;gene-LAMC3;gene-MFAP4;gene-MPZL3;gene-OLFML2A;gene-OLFML2B;gene-SCUBE3;gene-SLC39A8
Positive regulation of epithelial to mesenchymal transition	gene-BMP2;gene-BMP4;gene-RGCC;gene-SNAI1;gene-ZNF703
Positive regulation of cell-substrate adhesion	gene-COL26A1;gene-ECM2;gene-ECM2-2;gene-EDIL3;gene-EGFL6;gene-ITGA3;gene-ITGA6
Positive regulation of cell division	gene-EREG;gene-FGF1;gene-IL1B;gene-RGCC;gene-TGFB2
Hair cycle	gene-APCDD1;gene-CELSR1;gene-MPZL3;gene-PPP1R13L;gene-SNAI1
Negative regulation of angiogenesis	gene-EPHA2;gene-FOXF2;gene-ISM1;gene-KLF4;gene-RGCC;gene-SERPINF1;gene-THBS2
Regulation of cell-substrate adhesion	gene-AJAP1;gene-COL26A1;gene-ECM2;gene-ECM2-2;gene-EDIL3;gene-ITGA6
Phospholipid dephosphorylation	gene-PLPP3;gene-PLPPR3;gene-PLPPR4
Artery morphogenesis	gene-APOE;gene-FOXF2;gene-GJA5;gene-LDLR
Regulation of cellular component movement	gene-CCL20;gene-CD274;gene-CFAP298-TCP10L;gene-EREG;gene-ITGA6;gene-KLF4;gene-MACIR;gene-MTUS1;gene-NTN1;gene-PHLDA2;gene-PHLDA2-2;gene-

	PRAG1;gene-PRAG1-2;gene-RGCC;gene-SNAI1;gene-SST;gene-ZNF703
Regulation of cell motility	gene-CCL20;gene-CD274;gene-EREG;gene-ITGA6;gene-KLF4;gene-MACIR;gene-MTUS1;gene-NTN1;gene-PHLDA2;gene-PHLDA2-2;gene-PRAG1;gene-PRAG1-2;gene-RGCC;gene-SNAI1;gene-SST;gene-ZNF703
Intermediate filament cytoskeleton organisation	gene-DSP;gene-EPPK1;gene-KLHL24;gene-PLEC;gene-PPL
Ovulation cycle process	gene-EREG;gene-KISS1;gene-MAP2K6;gene-SCHIP1
Negative regulation of cell adhesion	gene-AJAP1;gene-CD274;gene-KLF4;gene-PAG1;gene-PODXL;gene-RGCC;gene-RIPOR2;gene-UBASH3B;gene-ZNF608;gene-ZNF703
Mammary gland development	gene-BCL2L11;gene-CYP19A1;gene-NTN1;gene-XDH;gene-ZNF703
Transmembrane receptor protein tyrosine kinase signalling pathway	gene-COL4A1;gene-DOK5;gene-ERBB3;gene-EREG;gene-GDF15;gene-LRIG3;gene-MET;gene-PAG1;gene-PDGFRA;gene-PDGFRL;gene-ROR2;gene-SCHIP1;gene-UBASH3B
Extracellular structure organisation	gene-COL4A1;gene-DPT;gene-ECM2;gene-ECM2-2;gene-ITGA6;gene-LAMC3;gene-MFAP4;gene-MPZL3;gene-OLFML2A;gene-SCUBE3
DNA replication initiation	gene-CCNE2;gene-CDC6;gene-MCM10;gene-MCM2;gene-MCM5
Cellular response to transforming growth factor beta stimulus	gene-CILP;gene-CLDN1;gene-EDN1;gene-GDF15;gene-PENK;gene-WWOX

Table 8.7: DEG linked to significantly enriched terms of biological process in GSEA. Results are shown for DEG in fibroblasts grown in high glucose (20 mM) compared to euglycemic control (5.5 mM) (F20_vs_F5) (BMKGENE, 2023).

Description	core enrichment
System development	gene-FAM20C-4;gene-FAM20C-3;gene-SPTBN5;gene-LAMA5;gene-SCO2;gene-ZFPM1;NewGene_2511;gene-DCH1;gene-SOBP;gene-TAGLN3;gene-CRLF1;gene-TMEM204;gene-HIVEP3;gene-LAMA1;gene-RTN4R;gene-IGSF3;gene-SHANK3;gene-FZD8;gene-AUTS2;gene-ARMCX5-GPRASP2;gene-FOXC2;gene-PHLDA2;gene-GLIS2-2;gene-FJX1;gene-PHLDA2-2;gene-NTNG1;gene-HOXD9;gene-XDH;gene-FBXL15;gene-ZSWIM9;gene-KLHL17;gene-NDNF;gene-NPAS1;gene-TRIOBP;gene-IRX5;gene-NOTCH1;gene-EP300;gene-GLIS2;gene-KLHL26;gene-SCRIB;gene-KLF2;gene-PTGER2;gene-EPN1;gene-LLGL1;gene-FSCN2;gene-ZNF358;NewGene_5086;gene-TTC7A;gene-ZNF335;gene-COL27A1;gene-PRAG1-2;gene-CTF1;gene-SHANK2;gene-SHANK3-2;gene-BCL3;gene-CELSR1;gene-HPS1;gene-NCDN;gene-MYCBP2;gene-FAM20C;gene-CXCL12;gene-FOXO3B;gene-MAML1-2;gene-SCRIB-2;gene-FAM20C-2;gene-PLXNB1;gene-CPNE5;gene-LLGL1-2;gene-PRAG1;gene-KMT2B;gene-COL12A1;gene-TMEM132A;gene-SNAI1;gene-SPEN;gene-ZNF513;gene-BTBD2;gene-MFHAS1-2;gene-BLOC1S4;gene-ANKRD11;gene-CYS1;gene-GAB2;gene-ATN1;gene-LAMB2;gene-MFHAS1;gene-IRX3;gene-SLC38A10;gene-GRN;gene-AMER1;gene-ID4;gene-APCDD1;gene-FUZ;gene-MAML1;gene-HTT;gene-MICALL2;gene-LY6E-2;gene-ZNF609;gene-LRCH4;gene-NBEAL2;gene-TRAK1;gene-IRS1;gene-ZBTB42;gene-LY6E;gene-SMTN;gene-MAMLD1;gene-SELENOM;gene-OBSL1;gene-SALL1;gene-ASH1L;gene-IGHMBP2;gene-ZBTB7B;gene-CC2D2A;gene-DLG5;gene-ZFAT;gene-PPP1R9B;gene-UTRN;gene-GREB1L;gene-SPR;gene-COL13A1;gene-KANK1;gene-ZNF516
Signalling	gene-SPTBN5;gene-LAMA5;gene-NPTX2;gene-TMEM158;gene-GUCY1A2;gene-KISS1;gene-TNFRSF6B;NewGene_2511;gene-DCH1;gene-MAML3;gene-CRLF1;gene-HIVEP3;gene-LAMA1;gene-GNB1L;gene-RTN4R;gene-IGSF3;gene-SHANK3;gene-FZD8;gene-PEAR1;gene-ISG15;gene-PODN;gene-FOXC2;gene-TPGS1;gene-COLEC12;gene-CEBPD;gene-FJX1;gene-DISP2;gene-VASN;gene-PTPRH;gene-VASN-2;gene-IFI35;gene-PODNL1-2;gene-NDNF;gene-G0S2;gene-MRC2;gene-PHLDA3;gene-COL16A1;gene-NOTCH1;gene-EP300;gene-FAM83G;gene-SCRIB;gene-PTGER2;gene-ACOT11;gene-EPN1;gene-CREBBP;gene-CTF1;gene-SHANK3-2;gene-BCL3;gene-CELSR1;gene-EPS8L2;gene-CXCL12;gene-FOXO3B;gene-MAML1-2;gene-HOMER3;gene-ZC3H12A;gene-SCRIB-2;gene-TRIM8;gene-RGS19;gene-PLXNB1;gene-MAP3K6;gene-SNAI1;gene-CDC42EP1;gene-CFAP410;gene-MFHAS1-2;gene-ADGRD1;gene-CORO1B;gene-STK10;gene-GAB2;gene-MFHAS1;gene-NFKBIB-2;gene-GRN;gene-AMER1;gene-MAML1;gene-LYNX1;gene-HIVEP2;gene-LY6E-2;gene-LRCH4;gene-SHF;gene-FCHD1;gene-IRS1;gene-LRRC3;gene-PRR5;gene-PODNL1;gene-AMOTL2;gene-LY6E;gene-SELENOM;gene-AMPH;gene-WDR83;gene-ERC1;gene-ASH1L;gene-PPFIA1;gene-WWC1;gene-MAST4;gene-CC2D2A;gene-DLG5;gene-PPP1R9B;gene-CXXC1;gene-VAV2;gene-DOK3;gene-GPR176;gene-ZNF516;gene-RIPOR1;gene-TRIM62;gene-NPAS4;gene-ZBTB17;gene-FRS3;gene-UTS2B;gene-KLF16;gene-CSRNP1;gene-MAML2;gene-CLEC16A;gene-

	SHARPIN;gene-RTKN;gene-LMTK2;gene-TICAM2;gene-RIC8A;gene-SHB;gene-MICB-5;gene-FOXO3;gene-CUL7;gene-NDRG4;gene-DLGAP4;gene-EFS

Table 8.8: DEG linked to significantly enriched terms of biological process in GSEA. Results are shown for DEG in fibroblasts grown exposed to *S. epidermidis* lysate compared to no-lysate control in 5.5 mM (FSe5_vs_F5). (BMKGENE, 2023)

Description	core enrichment
Regulation of response to stimulus	gene-SST;gene-PCSK9;gene-FAM20C-3;gene-FAM20C-4;gene-CHDL2;gene-CCL20;gene-AJAP1;gene-CILP;gene-CRLF1;gene-APCDD1;gene-APLN;gene-RGCC;gene-CCN5;gene-PTGER2;gene-ACP3;gene-MAML3;gene-COLEC12;gene-FAM20C-2;gene-MTUS1;gene-FAM20C;gene-RTN4RL2;gene-NOS1AP;gene-SHF;gene-AUTS2;gene-LYNX1;gene-GAS1;gene-SPON2;gene-ZC3H12A;gene-PODN;gene-SNAI1;gene-BCL3;gene-BCL2L11;gene-SHANK3-2;gene-CXCL12;gene-SHANK3;gene-G0S2;gene-NDRG4;gene-KLF4;gene-MFHAS1;gene-CXCL16;gene-MFHAS1-2;gene-LIF;gene-CTF1;gene-PRR5;gene-FBXL15;gene-GLIS2;gene-SASH1;gene-FAM89B;gene-VASN;gene-MYCBP2;gene-SH3RF3;gene-VASN-2;gene-RTN4R;gene-PAG1;gene-TRABD2A;gene-DACT3;gene-NBL1;gene-EP300;gene-SRPX;gene-TMEM204;gene-MAML1-2;gene-ANKRD10;gene-CHDL1;gene-MOAP1-2;gene-PLXNB1;gene-GLIS2-2;gene-RGS19;gene-FOXO3B;gene-PHLDA3;gene-MAML1;gene-THEMIS2;gene-DENND4B;gene-JMY;gene-TRAF3IP2;gene-EREG;gene-CREBBP;gene-DENND2B;gene-IL17D;gene-FUZ;gene-JCAD;gene-GRN;gene-FRRS1L;gene-MCC;gene-CFH;gene-SALL1;gene-LY6E-2;gene-ZBTB7B;gene-GAB1;gene-KANK2;gene-AMER1;gene-LY6E;gene-TRIM62;gene-RDH11;gene-CFH-2;gene-FOXC2;gene-GPS2;gene-EPN1
System development	gene-PCSK9;gene-NTN1;gene-LAMC3;gene-FAM20C-3;gene-FAM20C-4;gene-EFNB3;gene-CRLF1;gene-APCDD1;gene-APLN;gene-PTGER2;gene-SOBP;gene-DCH1;gene-LAMA5;gene-ZFPM1;gene-SCO2;gene-FAM20C-2;gene-ZNF358;gene-FAM20C;gene-RTN4RL2;gene-NOS1AP;gene-AUTS2;gene-OSR2;NewGene_2511;gene-ZNF521;gene-LAMA1;gene-SPON2;gene-EPOP-2;gene-SNAI1;gene-BCL3;gene-NDNF;gene-BCL2L11;gene-CYS1;gene-SHANK3-2;gene-CXCL12;gene-SHANK3;gene-NDRG4;gene-EPOP;gene-KLF4;gene-MFHAS1;gene-MFHAS1-2;gene-LIF;gene-MACROD2;gene-CTF1;gene-TMEM132A;gene-SHANK2;gene-SALL2;gene-KLHL26;gene-FBXL15;gene-SMIM3;gene-SAP30;gene-CCDC40-2;gene-TRIOBP;gene-GLIS2;gene-LLGL1;gene-IRX5;gene-CTXN1;gene-MYCBP2;gene-RTN4R;gene-NBL1;gene-EP300;gene-BTBD2;gene-TMEM204;gene-ZSWIM9;gene-ZBTB42;gene-MAML1-2;gene-CHDL1;gene-UTRN;gene-PLXNB1;gene-GLIS2-2;gene-LAMB1;gene-FOXO3B;gene-MAML1;gene-MTURN;gene-BLOC1S4;gene-EREG;gene-COL12A1;gene-MRTFB;gene-HPS1;gene-FUZ;gene-GRN;gene-MICALL2;gene-ZFP36L2;gene-COL27A1;gene-EML1;gene-HOXD9;gene-PHF2;gene-SALL1;gene-LY6E-2;gene-ZBTB7B;gene-IRX3;gene-GAB1;gene-SVIL;gene-AMER1;gene-NTNG2;gene-SLC38A10;gene-BLTP1;gene-LY6E;gene-LAMB2;gene-FOXC2;gene-GPS2;gene-EPN1

Table 8.9: DEG linked to significantly enriched terms of biological process in GSEA. Results are shown for DEG in fibroblasts grown exposed to *S. epidermidis* lysate compared to no-lysate control in 20 mM (FSe20_vs_F20). (BMKGENE, 2023)

Description	core enrichment
Immune response	gene-CXCL6;gene-CXCL8;gene-CXCL1;gene-CXCL3;gene-CXCL2;gene-CXCL5;gene-CSF3;gene-IL1B;gene-SECTM1;gene-RGCC;gene-CCL7;gene-CCL20;gene-BPI;gene-TNFSF13B;gene-CCR7;gene-HLA-E-5;gene-SPON2;gene-HLA-A-5;gene-CCL11;gene-CFH-2;gene-CXCL14;gene-ULBP1;gene-HLA-B-6;gene-CFH;gene-HLA-C-2;gene-MFHAS1;gene-COLEC12;gene-HLA-C;gene-CXCL12;gene-TCIM;gene-RNF135-2;gene-TNFRSF11B;gene-NFIL3;gene-HLA-A-8;gene-HLA-A-4;gene-PTX3;NewGene_6631;gene-SWAP70;gene-EMP2;gene-HLA-A-2;gene-SDHAF4;gene-HLA-A;gene-CCL2;gene-CXCL16;gene-CLU;gene-BCL3;gene-LIF;gene-HLA-A-3
Chemotaxis	gene-CH25H;gene-NTN1;gene-CCL20;gene-IL16;gene-CCR7;gene-SPON2;gene-DOK6;gene-ACKR3;gene-ACKR4;gene-EFNB3;gene-GAB1;gene-CXCL12

Table 8.10: DEG linked to each significantly enriched term in cellular component in GO. Results are shown for DEG in fibroblasts grown in high glucose (20 mM) compared to euglycemic control (5.5 mM) (F20_vs_F5). (BMKGENE, 2023)

Description	geneID
Polycystic complex	NewGene_2505;NewGene_2511;NewGene_2516;NewGene_2519;NewGene_4495
Platelet alpha granule lumen	gene-ISLR;gene-ISLR-2;gene-SRGN
U6 snRNP	gene-LSM3;gene-LSM6;gene-LSM8
Mitotic spindle astral microtubule	gene-CCSAP;gene-DYNLT3
Aster	gene-CCSAP;gene-DYNLT3
Astral microtubule	gene-CCSAP;gene-DYNLT3
Platelet alpha granule	gene-ISLR;gene-ISLR-2;gene-SRGN
U4/U6 x U5 tri-snrnp complex	gene-LSM3;gene-LSM6;gene-LSM8;gene-SNRPE
Anchored component of plasma membrane	gene-NRN1;gene-NTNG1;gene-RTN4R;gene-ULBP1
Spliceosome complex	gene-FRG1;gene-LSM3;gene-LSM5;gene-LSM8;gene-SNRPE;gene-SNRPG
Collagen-containing extracellular matrix	gene-ADAMTS14;gene-LAMA1;gene-LAMA5;gene-POSTN;gene-PRELP;gene-SOD3;gene-TNC
Mitochondrial membrane	gene-ATP5ME;gene-COX16;gene-DMAC1;gene-MGARP;gene-MRPL33;gene-MRPL54;gene-ND3;gene-SCO2;gene-SDHAF4
Membrane	NewGene_2505;NewGene_2511;NewGene_2516;NewGene_2519;NewGene_4495;NewGene_6040;NewGene_7117;gene-ABHD17A;gene-AKAP7;gene-ARHGDIB;gene-ATP5ME;gene-B3GALT2;gene-B3GNT9;gene-CEMIP;gene-CHT7;gene-CLSTN2;gene-DCH1;gene-DMAC1;gene-DUSP2;gene-ENPP4;gene-FZD8;gene-GNB1L;gene-GUCY1A2;gene-HHIP;gene-IL13RA2;gene-IL21R;gene-KISS1;gene-LAMA1;gene-MAMDC2;gene-MAMDC2-2;gene-MFSD3;gene-MGARP;gene-MRPL33;gene-MRPL54;gene-NTNG1;gene-PEAR1;gene-PGF;gene-PRRT2;gene-RASL10B;gene-RTN4R;gene-SCO2;gene-SDF2L1;gene-SDHAF4;gene-SHANK3;gene-SLC26A1;gene-SPTBN5;gene-TMEM204;gene-TMEM86B;gene-TNFRSF6B;gene-TPGS1;gene-UBR4;gene-ULBP1;gene-VASN;gene-VASN-2;gene-XYLT1;gene-XYLT1-2
Laminin complex	gene-LAMA1;gene-LAMA5
Cytoplasmic vesicle lumen	gene-ISLR;gene-ISLR-2;gene-NPTX2;gene-PTX3;gene-SRGN
Secretory granule lumen	gene-ISLR;gene-ISLR-2;gene-NPTX2;gene-PTX3;gene-SRGN
Vesicle lumen	gene-ISLR;gene-ISLR-2;gene-NPTX2;gene-PTX3;gene-SRGN
Organelle inner membrane	gene-ATP5ME;gene-DMAC1;gene-MRPL33;gene-MRPL54;gene-SCO2;gene-SDHAF4

Basement membrane	gene-LAMA1;gene-LAMA5
Ribosome	gene-MRPL24;gene-MRPL33;gene-MRPL54;gene-RPL22;gene-RPL35A;gene-RPL37;gene-RPL37A;gene-RPL39;gene-RPL41;gene-RPS26

Table 8.11: DEG linked to each significantly enriched cellular component terms in GO. Results are shown for DEG in fibroblasts exposed to *S. epidermidis* lysate compared to no-lysate control in 5.5 mM (FSe5_vs_F5) (BMKGENE, 2023).

Description	geneID
Collagen-containing extracellular matrix	gene-ADAMTS14;gene-ADAMTS3;gene-ADAMTS8;gene-CILP;gene-ECM2;gene-ECM2-2;gene-ELN;gene-FBLN2;gene-FMOD;gene-GPC3;gene-GPC6;gene-LAMA1;gene-LAMA5;gene-LAMC3;gene-MGP;gene-NTN1;gene-POSTN;gene-PRELP;gene-SOD3;gene-TNC;gene-TNXB;gene-TNXB-3;gene-TNXB-4;gene-TNXB-6;gene-VWA1
Polycystic complex	NewGene_2505;NewGene_2511;NewGene_2516;NewGene_2519;NewGene_4495;NewGene_4499
Extracellular matrix	gene-ADAMTS15;gene-CILP;gene-COL26A1;gene-COL6A1;gene-COL6A2;gene-DCN;gene-DPT;gene-ECM2;gene-ECM2-2;gene-LAMA1;gene-LAMA5;gene-LAMC3;gene-MMP1;gene-MMP11;gene-MMP11-2;gene-MMP17;gene-NDNF;gene-NTN1;gene-OLFML2A;gene-OLFML2B;gene-VWA1;gene-VWF
Extracellular space	NewGene_2511;gene-ACP3;gene-ADAMTS15;gene-ANGPTL1;gene-ANGPTL2;gene-ANGPTL4;gene-APLN;gene-BMP2;gene-C3;gene-CCL11;gene-CCL2;gene-CCL7;gene-CCN5;gene-CD274;gene-CFD;gene-CFD-2;gene-CHI3L1;gene-CILP;gene-CRLF1;gene-CSF1;gene-CXCL1;gene-CXCL12;gene-CXCL16;gene-CXCL2;gene-CXCL3;gene-CXCL5;gene-CXCL6;gene-CXCL8;gene-DPT;gene-DPYSL3;gene-ECM2;gene-ECM2-2;gene-EDN1;gene-FAM20C;gene-FAM20C-2;gene-FAM20C-4;gene-HILPDA;gene-IGF1;gene-IGF2;gene-IGFBP4;gene-IL1B;gene-LAMA1;gene-LAMA5;gene-LIF;gene-LOXL1;gene-LOXL4;gene-MICOS10-NBL1;gene-PCSK9;gene-PLTP;gene-PODN;gene-POSTN;gene-PTX3;gene-SCUBE3;gene-SERPINB2;gene-SERPINB7;gene-SERPINE1;gene-SERPINE2;gene-SERPINF1;gene-SMPDL3A;gene-SOD3;gene-SRGN;gene-SST;gene-SULF2;gene-TGFB2;gene-TSKU;gene-VASN;gene-VASN-2;gene-WFDC1
NMDA selective glutamate receptor complex	gene-SHANK2;gene-SHANK3;gene-SHANK3-2
Membrane	NewGene_2505;NewGene_2511;NewGene_2516;NewGene_2519;NewGene_2801;NewGene_4495;NewGene_4681;gene-ABHD17A;gene-ACE;gene-ACP3;gene-ADGRD1;gene-ADGRL1;gene-ADGRL1-2;gene-AJAP1;gene-ANKZF1;gene-ANO7;gene-AP5B1;gene-APCDD1;gene-ARHGDIB;gene-ATP5ME;gene-ATP5MK;gene-B3GALT2;gene-B3GNT9;gene-BAIAP2L1;gene-BCL2L11;gene-BCL3;gene-BRIP1;gene-CADM4;gene-CCN5;gene-CD274;gene-CEMIP;gene-CFAP410;gene-CFI;gene-CH25H;gene-CHMP4A-2;gene-CLSTN2;gene-COL26A1;gene-COLEC12;gene-CXCL12;gene-CXCL16;gene-CYP2S1;gene-CYS1;gene-DAB1;gene-DCH1;gene-DCUN1D3;gene-DIRAS3;gene-EFNB3;gene-EGFL6;gene-ENPP4;gene-FAM210B;gene-FOS;gene-GAS1;gene-GEM;gene-GLIPR1;gene-GNB1L;gene-GPR146;gene-GUCY1A2;gene-GYPC;gene-IL13RA2;gene-IL21R;gene-ITGAE;gene-JPT1;gene-KCNS2;gene-LAMA1;gene-LAMC3;gene-LLGL1;gene-LOXL4;gene-LYNX1;gene-LZTS1;gene-MAN1A1;gene-MARCKSL1;gene-

	MFSD3;gene-MGARP;gene-MGAT3;gene-MPP7;gene-MRC2;gene-MRPL33;gene-MRPL54;gene-MTUS1;gene-NDRG4;gene-NDUFA6-4;gene-NOS1AP;gene-PAG1;gene-PCSK9;gene-PGF;gene-PLEKHA4;gene-PLPPR3;gene-PNN;gene-PNPLA3;gene-PRLR;gene-PRRT2;gene-PSG3;gene-PTGER2;gene-RAB20;gene-RARRES1;gene-RASL10B;gene-RASL11A;gene-RGS17;gene-RIMS1;gene-RTN4RL2;gene-SASH1;gene-SCARA5;gene-SCO2;gene-SCUBE3;gene-SGIP1;gene-SH3TC2;gene-SHANK2;gene-SHANK3;gene-SHANK3-2;gene-SLC16A13;gene-SLC28A3;gene-SLC2A12;gene-SLC7A14;gene-SREBF2;gene-SYT7;gene-TBC1D8;gene-TMEM132A;gene-TPGS1;gene-TRABD2A;gene-TSNARE1;gene-VASN;gene-VASN-2;gene-VPS51;gene-ZC3H12A;gene-ZNRF1
Obsolete extracellular region part	NewGene_2511;gene-ACP3;gene-ADAMTS15;gene-ANGPTL1;gene-ANGPTL2;gene-APLN;gene-CCN5;gene-CD274;gene-CILP;gene-COL26A1;gene-CRLF1;gene-CXCL12;gene-CXCL16;gene-DPT;gene-ECM2;gene-ECM2-2;gene-FAM20C;gene-FAM20C-2;gene-FAM20C-4;gene-HILPDA;gene-LAMA1;gene-LAMA5;gene-LAMC3;gene-LIF;gene-MICOS10-NBL1;gene-NDNF;gene-NINL;gene-NTN1;gene-OLFML2A;gene-PCSK9;gene-PODN;gene-PTX3;gene-SCUBE3;gene-SMPDL3A;gene-SRGN;gene-SST;gene-THAP11;gene-VASN;gene-VASN-2;gene-VWA1;gene-VWF;gene-WFDC1
Platelet alpha granule lumen	gene-ISLR;gene-ISLR-2;gene-SRGN;gene-VWF
Extracellular region	NewGene_2511;gene-ACP3;gene-ADAMTS15;gene-AMH;gene-ANGPTL1;gene-ANGPTL2;gene-APLN;gene-APOL3;gene-BMP6;gene-BMP8A;gene-C1QTNF1;gene-CCN5;gene-CD274;gene-CEMIP;gene-CGA;gene-CILP;gene-COL26A1;gene-CRLF1;gene-CSF3;gene-CTF1;gene-CXCL12;gene-CXCL14;gene-CXCL16;gene-DPT;gene-ECM2;gene-ECM2-2;gene-EMILIN2;gene-ENDOD1;gene-EPDR1;gene-FAM20C;gene-FAM20C-2;gene-FAM20C-4;gene-FBLN1;gene-FGF11-2;gene-FGF5;gene-GDF10;gene-GDF5;gene-GDNF;gene-HILPDA;gene-IGFBP2;gene-IGFBP6;gene-IGFBPL1;gene-ISLR;gene-ISLR-2;gene-KAZALD1;gene-LAMA1;gene-LAMA5;gene-LAMC3;gene-LIF;gene-MELTF;gene-MICOS10-NBL1;gene-NDNF;gene-NINL;gene-NPTX1;gene-NPTX2;gene-NTN1;gene-OLFML2A;gene-PCOLCE2;gene-PCSK9;gene-PENK;gene-PODN;gene-PSG3;gene-PTX3;gene-RTN4RL2;gene-SCUBE3;gene-SFRP1;gene-SLIT2;gene-SLIT3;gene-SMPDL3A;gene-SRGN;gene-SST;gene-STC1;gene-STC2;gene-TFPI2;gene-TGFBR3;gene-THAP11;gene-THBS2;gene-TUFT1;gene-VASN;gene-VASN-2;gene-VSTM2L;gene-VWA1;gene-VWF;gene-WFDC1;gene-WNT2
Integral component of plasma membrane	NewGene_2511;NewGene_4499;gene-AJAP1;gene-APCDD1;gene-BOC;gene-CADM4;gene-CDH2;gene-CDON;gene-CHM3;gene-CLDN1;gene-EFNB3;gene-EPHB1;gene-EPHB3;gene-EPHB4;gene-EPHB6;gene-EPHB6-2;gene-GYPC;gene-ITGAE;gene-MFSD3;gene-MPZL3;gene-MRC2;gene-NTRK2;gene-P2RX5;gene-PAG1;gene-PDGFRA;gene-PLPP3;gene-PLPPR3;gene-PSG3;gene-PTGER2;gene-SHANK2;gene-SHANK3;gene-SHANK3-2;gene-SLC12A7;gene-SLC12A7-2;gene-SLC16A13;gene-SLC1A3;gene-SLC26A6;gene-SLC28A3;gene-SLC29A2;gene-SLC52A2;gene-TENM3;gene-TENM4;gene-THBD;gene-TRABD2A

Cell surface	NewGene_2505;NewGene_2511;NewGene_2516;NewGene_2519;NewGene_4495;NewGene_4499;gene-ADAMTS15;gene-AJAP1;gene-C3;gene-CCN5;gene-CD274;gene-CDH2;gene-CXCL12;gene-EPHB6;gene-HILPDA;gene-ITGAE;gene-LDLR;gene-LYNX1;gene-MRC2;gene-PCSK9;gene-PSG3;gene-RTN4RL2;gene-SCUBE3;gene-SLC1A3;gene-SULF2;gene-VASN;gene-VASN-2
Histone deacetylase complex	gene-HDAC4;gene-H;gene-PHF21A;gene-SAP30;gene-SAP30L
Platelet alpha granule	gene-ISLR;gene-ISLR-2;gene-SRGN;gene-VWF
Lipid droplet	gene-EHD3;gene-G0S2;gene-HILPDA;gene-PLIN2;gene-PNPLA3;gene-RAB20;gene-TMT1A
Basement membrane	gene-COL15A1;gene-LAMA1;gene-LAMA5;gene-LAMC3;gene-NTN1;gene-SERPINF1;gene-VWA1
Proton-transporting ATP synthase complex	gene-ATP5ME;gene-ATP5MK
Proton-transporting two-sector atpase complex	gene-ATP5ME;gene-ATP5MK
Mitochondrial proton-transporting ATP synthase complex	gene-ATP5ME;gene-ATP5MK
Ionotropic glutamate receptor complex	gene-SHANK2;gene-SHANK3;gene-SHANK3-2
Endoplasmic reticulum	NewGene_2505;NewGene_2516;NewGene_2519;NewGene_4495;NewGene_4499;gene-ADAMTS9;gene-ANO7;gene-CEMIP;gene-CH25H;gene-CHI3L1;gene-COL26A1;gene-CRYZL2P-SEC16B;gene-CYP2S1;gene-DHCR7;gene-ELOVL7;gene-FAM20A;gene-FAM20C;gene-FAM20C-2;gene-FAM20C-4;gene-FDFT1-2;gene-FOS;gene-H6PD;gene-HMOX1;gene-HD17B7;gene-ITPR1;gene-NDRG4;gene-NOS1AP;gene-P4HA3;gene-PCSK9;gene-PNPLA3;gene-PSMG1;gene-SCARA3;gene-SEC16B;gene-SLC27A3;gene-SLC28A3;gene-SREBF2;gene-STC2;gene-SULF2;gene-TM7SF2;gene-TMEM132A;gene-TPD52;gene-UTP15;gene-VWA1;gene-VWF;gene-ZC3H12A

Table 8.12: DEG linked to each significantly enriched cellular component terms in GO. Results are shown for DEG in fibroblasts exposed to *S. epidermidis* lysate compared to no-lysate control in 20 mM (FSe20_vs_F20). (BMKGENE, 2023)

Description	geneID
collagen-containing extracellular matrix	gene-ADAMTS12-2;gene-ADAMTS8;gene-CILP;gene-COL4A1;gene-ECM2;gene-ECM2-2;gene-ELN;gene-FMOD;gene-GPC3;gene-ITGA6;gene-LAMC3;gene-MGP;gene-NTN1;gene-PRELP;gene-SOD3;gene-TNXB;gene-TNXB-3;gene-TNXB-4;gene-TNXB-5;gene-TNXB-6
extracellular matrix	gene-ADAMTS12-2;gene-ADAMTS15;gene-CILP;gene-COL26A1;gene-COL4A1;gene-DCN;gene-DPT;gene-ECM2;gene-ECM2-2;gene-ITGA6;gene-LAMC3;gene-MFAP4;gene-MMP1;gene-MMP11;gene-MMP11-2;gene-MMP24;gene-NTN1;gene-OLFML2A;gene-OLFML2B;gene-SPON2
extracellular space	gene-ADAMTS15;gene-ANGPTL2;gene-BMP2;gene-BMP4;gene-C3;gene-CCL11;gene-CCL20;gene-CCL7;gene-CCN5;gene-CD274;gene-CFD;gene-CFD-2;gene-CFH;gene-CFH-2;gene-CHI3L1;gene-CILP;gene-CRLF1;gene-CXCL1;gene-CXCL2;gene-CXCL3;gene-CXCL5;gene-CXCL6;gene-CXCL8;gene-DPT;gene-DPYSL3;gene-ECM2;gene-ECM2-2;gene-EDN1;gene-EREG;gene-FSTL3;gene-GDF15;gene-GREM2;gene-IGF2;gene-IL1B;gene-IL34;gene-INHBB;gene-KISS1;gene-LOXL2;gene-NAMPT;gene-NRN1;gene-PLTP;gene-SCUBE3;gene-SERPINE1;gene-SERPINE2;gene-SERPINF1;gene-SMPDL3A;gene-SOD3;gene-SPON2;gene-SST;gene-SULF2;gene-TGFA;gene-TGFB2;gene-XDH
extracellular region	gene-ADAMTS12-2;gene-ADAMTS15;gene-ANGPTL2;gene-APOL1;gene-APOL3;gene-APOL6;gene-C1QTNF1;gene-C5;gene-CCL20;gene-CCN5;gene-CD274;gene-CFH;gene-CFH-2;gene-CGA;gene-CHDL1;gene-CILP;gene-COL26A1;gene-COL4A1;gene-CRLF1;gene-CSF3;gene-CXCL14;gene-DPT;gene-ECM2;gene-ECM2-2;gene-EDIL3;gene-EREG;gene-FBLN1;gene-FGF1;gene-FGF13;gene-FGF5;gene-FZD8;gene-GDF10;gene-GDF15;gene-GDF5;gene-IGFBP2;gene-IGFBPL1;gene-INHBB;gene-ISLR;gene-ITGA6;gene-KISS1;gene-LAMC3;gene-MELTF;gene-MFAP4;gene-NPTX1;gene-NPTX2;gene-NTN1;gene-OLFML2A;gene-PCOLCE2;gene-PENK;gene-PNP;gene-PRRG1;gene-PSG6;gene-SCUBE3;gene-SLIT3;gene-SMPDL3A;gene-SPON2;gene-SST;gene-STC1;gene-TFPI;gene-TFPI2;gene-TGFBR3;gene-THBS2;gene-TUFT1;gene-WNT2;gene-WNT5B;gene-XDH
adherents junction	NewGene_495;gene-AJAP1;gene-CDH2;gene-ITGA6;gene-KLHL24;gene-KRT19;gene-MYH9;gene-PRAG1;gene-PRAG1-2;gene-TM4SF20
integral component of plasma membrane	gene-AJAP1;gene-APCDD1;gene-BOC;gene-CDH2;gene-CDON;gene-CELSR1;gene-CHM3;gene-CLDN1;gene-DDR1-4;gene-DLG3;gene-DSCAM;gene-EPHA2;gene-

	EPHB1;gene-EREG;gene-ITGA6;gene-KCNH1;gene-KCNH5;gene-MMP24;gene-MPZL3;gene-NTRK2;gene-P2RX5;gene-PAG1;gene-PDGFRA;gene-PLPP3;gene-PLPPR3;gene-PLPPR4;gene-PSG6;gene-PTGER2;gene-SLC16A7;gene-SLC1A3;gene-SLC29A2;gene-TENM2;gene-THBD;gene-TRABD2A
intermediate filament	gene-IFFO2;gene-KRT15;gene-KRT19;gene-KRT33B-3;gene-KRT34-2;gene-KRT34-3;gene-KRT80;gene-LMNB1;gene-LOC100653049;gene-NES
obsolete extracellular region part	gene-ADAMTS12-2;gene-ADAMTS15;gene-ANGPTL2;gene-CCL20;gene-CCN5;gene-CD274;gene-CFH;gene-CFH-2;gene-CILP;gene-COL26A1;gene-COL4A1;gene-CRLF1;gene-DPT;gene-ECM2;gene-ECM2-2;gene-EREG;gene-GDF15;gene-INHBB;gene-ITGA6;gene-KISS1;gene-LAMC3;gene-MFAP4;gene-NTN1;gene-OLFML2A;gene-SCUBE3;gene-SMPDL3A;gene-SPON2;gene-SST;gene-XDH
cell-substrate junction	NewGene_495;gene-ITGA6;gene-PRAG1;gene-PRAG1-2;gene-TM4SF20
symmetric synapse	gene-CHM2;gene-PENK
basement membrane	gene-COL15A1;gene-COL4A1;gene-ITGA6;gene-LAMC3;gene-NTN1;gene-SERPINF1
anchoring junction	gene-AJAP1;gene-ITGA6;gene-KLHL24;gene-PRAG1;gene-PRAG1-2;gene-TM4SF20
actin cytoskeleton	gene-ACTA2;gene-CDC42EP4;gene-CDC42EP5-2;gene-CORIN;gene-DENND2A;gene-FLNA;gene-FLNC;gene-HPB7;gene-MLPH;gene-MPP4;gene-SMTN;gene-SPTBN5;gene-TPM1
filopodium	gene-ACTA2;gene-FSCN1;gene-ITGA6;gene-VASP
lamellipodium	gene-ACTA2;gene-CDH2;gene-DPYSL3;gene-FSCN1;gene-PODXL;gene-VASP
dendritic shaft	gene-DLG3;gene-LZTS1;gene-PRKAR2B
MCM complex	gene-MCM2;gene-MCM5
cortical cytoskeleton	gene-ACTN4;gene-MLPH;gene-MYH9;gene-SPTBN5
apical plasma membrane	gene-AJAP1;gene-CDH2;gene-CLDN1;gene-KISS1;gene-LZTS1;gene-OXTR;gene-PODXL;gene-PSG6;gene-RIPOR2;gene-SLC39A8
integrin complex	gene-ITGA11;gene-ITGA6;gene-ITGA8;gene-ITGB8

Table 8.13: DEG linked to significantly enriched terms of cellular component in GSEA. Results are shown for genes differentially expressed in fibroblasts grown in high glucose (20 mM) compared to fibroblasts grown in low glucose (5.5 mM) (F20_vs_F5). (BMKGENE, 2023)

Description	core enrichment
Endomembrane system	gene-TBC1D16-2;gene-FAM20C-4;gene-FAM20C-3;gene-NPTX2;gene-DUSP2;gene-ISLR-2;gene-ISLR;NewGene_2511;gene-SCARA3;gene-CEMIP;gene-ADAMTSL1;gene-RTN4R;gene-TMEM86B;gene-ABHD17A;gene-ACP3;gene-FZD8;NewGene_7117;gene-B3GNT9;gene-CHST7;gene-CCDC78;gene-CLCA2;gene-UBR4;gene-XDH;gene-PTX3;gene-DENND4B;gene-CLIP2;gene-ANO7;gene-TOR4A;gene-COL16A1;gene-NOTCH1;gene-PHETA1;gene-ADORA2A;gene-EPN1;gene-LLGL1;NewGene_5086;gene-COL27A1;gene-PNPLA3;gene-NHERF1;gene-ADPRHL1;gene-ZDHHC8;gene-FAM20C;NewGene_4805;gene-SLC16A13;gene-ZC3H12A;gene-FAM20C-2;gene-LMF2;gene-RGS19;gene-GBF1;gene-MOXD1;gene-LLGL1-2;gene-CD320;gene-COL12A1;gene-RAB20;gene-TMEM132A;gene-TMEM214;gene-SLC35A4;gene-PLEKHM2;gene-STK10;gene-MGAT4B-2;gene-PHETA2;gene-LAMB2;gene-SLC38A10;gene-GRN;gene-TBC1D10B;gene-COL7A1;gene-HTT;gene-ZNRF1;gene-POM121;gene-P3H4;gene-MICALL2;gene-RBM15B;gene-ANKRD13D;gene-C2CD2L;gene-EMC10;gene-NBEAL2;gene-TRAK1;gene-FCHSD1;gene-NECAB3;NewGene_1042;gene-MAMLD1;gene-TBC1D8;gene-SELENOM;gene-VWA1;gene-AMPH;gene-OBSL1;gene-THAP7;gene-FICD;gene-WDR83;gene-TBC1D16;gene-MARCHF9;gene-TONSL;gene-ASH1L;gene-SPON1;gene-POM121C;gene-SRPX;gene-MARCHF4;gene-VPS51;gene-TXNDC11;gene-DOK3;gene-FUT4;gene-COL13A1;gene-TBC1D2;gene-EMC6;gene-RIPOR1;gene-ATP10A;gene-PIGO;gene-CRELD2;gene-TANGO2;gene-CLEC16A;gene-H6PD;NewGene_5702;gene-DHRS1;gene-ATF6B-2;gene-LMTK2;gene-TICAM2;gene-TBC1D17;gene-COLGALT2;gene-CPED1;gene-RUSC1;gene-CRAT;gene-CDAN1;gene-ATF6B-4;gene-CUL7;gene-NDRG4;gene-B3GLCT;gene-CHST3;gene-LAMB1;gene-SPESP1
cell periphery	gene-SPTBN5;gene-GUCY1A2;gene-KISS1;NewGene_6040;gene-TNFRSF6B;NewGene_2511;gene-CEMIP;gene-TMEM204;gene-GNB1L;gene-RTN4R;gene-IGSF3;gene-ABHD17A;gene-SHANK3;gene-ACP3;gene-FZD8;gene-PEAR1;gene-MFSD3;gene-SLC26A1;gene-COLEC12;gene-CCDC78;gene-CLCA2;gene-DISP2;gene-NTNG1;gene-VASN;gene-UBR4;gene-PTPRH;gene-VASN-2;gene-MRC2;gene-PHLDA3;gene-ANO7;gene-TRIOBP;gene-NOTCH1;gene-SCRIB;gene-PTGER2;gene-ARRDC1;gene-EPN1;gene-LLGL1;NewGene_5086;NewGene_4681;gene-SHANK2;gene-SHANK3-2;gene-BCL3;gene-CELSR1;gene-KIAA1549;gene-EPS8L2;gene-CXCL12;gene-MARCKSL1;gene-SLC16A13;gene-SCRIB-2;gene-LRRC45;gene-PSG6;gene-SRPX2;gene-RGS19;gene-

	PLXNB1;gene-LLGL1-2;gene-CD320;gene-FSD1;gene-RAB20;gene-CDC42EP1;gene-CFAP410;gene-ADGRD1;gene-SH3D21;gene-MLPH;gene-ANKRD11;gene-CORO1B;gene-STK10;gene-CYS1;gene-GAB2;gene-CPNE2;NewGene_4812;gene-PSG1;gene-AMER1;gene-TBC1D10B;gene-AHNAK2;gene-APCDD1;gene-TMEM150A;gene-PHLDB1;gene-LYNX1;gene-MICALL2;gene-LY6E-2;gene-ANKRD13D;gene-LRCH4;gene-WDR13;gene-C2CD2L;gene-NBEAL2;gene-IRS1;gene-ARRDC2;gene-S100A16;gene-PRRC2A-3;gene-ZBTB42;gene-AMOTL2;gene-LY6E;gene-AMPH;gene-CERCAM;gene-AHNAK;gene-ERC1;gene-TONSL;gene-WWC1;gene-CCDC8;gene-DLG5;gene-PPP1R9B;gene-DOK3;gene-FUT4;gene-UTRN;gene-COL13A1;gene-GPR176;gene-KANK1;gene-ATP10A;gene-TRAPPC14;gene-FRS3;gene-CALHM2;gene-LRATD2;gene-TICAM2;gene-RIC8A;gene-NLRP10;gene-FILIP1;gene-SHB;gene-CDAN1;gene-MICB-5;gene-MTCL1;gene-NDRG4;gene-DLGAP4

Table 8.14: DEG linked to significantly enriched terms of cellular component in GSEA. Results are shown for DEG in fibroblasts exposed to *S. epidermidis* lysate compared to no-lysate control in (5.5 mM) (FSe5_vs_F5).

Description	core enrichment
cell periphery	gene-PCSK9;gene-NTN1;gene-AJAP1;gene-EFNB3;gene-GUCY1A2;gene-APCDD1;gene-COL26A1;gene-ANO7;gene-CCN5;gene-PTGER2;gene-RAB20;gene-ACP3;gene-PLPPR3;gene-COLEC12;gene-SLC2A12;gene-RGS17;gene-MTUS1;NewGene_4681;gene-RTN4RL2;gene-GPR146;gene-ADGRD1;NewGene_2511;gene-LYNX1;gene-GAS1;gene-MARCKSL1;gene-BCL3;gene-CFAP410;gene-KCNS2;gene-CYS1;gene-SHANK3-2;gene-CXCL12;gene-SHANK3;gene-NDRG4;gene-PLEKHA4;gene-SLC16A13;gene-GYPC;NewGene_2801;gene-SHANK2;gene-GNB1L;gene-MFSD3;gene-MRC2;gene-ABHD17A;gene-TRIOBP;gene-LLGL1;gene-CADM4;gene-VASN;gene-CEMIP;gene-VASN-2;gene-RTN4R;gene-PAG1;gene-TRABD2A;NewGene_20;gene-LRRC45;gene-CCDC78;gene-TMEM204;gene-ZBTB42;gene-UTRN;gene-TNFRSF6B;gene-UBR4;gene-PLXNB1;gene-SLC26A1;gene-RGS19;gene-VSTM4;gene-PHLDA3;gene-EREG;gene-ARRDC2;gene-JCAD;gene-MICALL2;gene-TRO;gene-TPBG-2;gene-MCC;gene-CFH;gene-LY6E-2;gene-ANKRD13D;gene-SRPX2;gene-SVIL;gene-AMER1;gene-NTNG2;gene-LY6E;gene-CFH-2;gene-KIAA1549;gene-EPN1;gene-TAMALIN;gene-SH3D21;gene-DOK3;gene-MPP2;gene-ZNRF2;gene-TMEM150A;gene-CD320;gene-DLG3;gene-SLCO3A1;gene-IQCE;gene-CLCA2;gene-LRCH2;gene-NTM;gene-IGDCC4;gene-CCDC8;gene-PEAR1;gene-LAMC2;gene-WDR13;NewGene_5841;gene-TNFRSF11B;gene-MPDZ;gene-ITM2C;gene-TPBG;gene-PDE4B;gene-IRS1;gene-CPNE2;gene-PPP1R9B;gene-GAB2;gene-TUB;gene-FZD8;gene-TTC7B;gene-CORO1B;gene-TBC1D10B;gene-FRS3;gene-NLRX1;gene-

	NBEA;gene-ATP23;gene-CALHM2;gene-FUT4;gene-ATP23-2;gene-DENND4C;gene-CERCAM;gene-ARRDC1;gene-RFFL;gene-RGS12;gene-PLEKHO1;gene-DLG5;gene-PLEKHM3;NewGene_4812
endoplasmic reticulum	gene-PCSK9;gene-ELOVL7;gene-CH25H;gene-FAM20C-3;gene-FAM20C-4;gene-HMOX1;NewGene_4499;gene-FOS;gene-COL26A1;gene-ANO7;gene-CHI3L1;gene-VWA1;gene-FAM20C-2;NewGene_2516;gene-FAM20C;NewGene_4495;gene-CYP2S1;gene-NOS1AP;gene-FAM20A;gene-SULF2;gene-SCARA3;gene-DHCR7;gene-VWF;NewGene_2519;gene-ZC3H12A;gene-ADAMTS9;gene-PNPLA3;gene-SREBF2;gene-HD17B7;gene-NDRG4;NewGene_2505;gene-ITPR1;gene-STC2;gene-TM7SF2;gene-TMEM132A;gene-CRYZL2P-SEC16B;gene-H6PD;gene-P4HA3;gene-SLC27A3;gene-CEMIP;gene-RTN4R;gene-FDFT1-2;gene-CCR10;gene-CCDC78;gene-SRPX;gene-GHDC;gene-FDFT1;gene-COL16A1;gene-CHDL1;gene-ITPR3;gene-LAMB1;gene-COL12A1;gene-RPL13;gene-FNDC4;gene-WFS1;gene-CYP51A1;gene-GRN;gene-COL27A1;gene-MOXD1;gene-TPBG-2

Table 8.15: DEG linked to significantly enriched terms of cellular component in GSEA. Results are shown for DEG in fibroblasts exposed to *S. epidermidis* lysate compared to no-lysate control in 20 mM (FSe20_vs_F20). (BMKGENE, 2023)

Description	core enrichment
Extracellular region	gene-SST;gene-DPT;gene-FGF13;gene-NPTX1;gene-NTN1;gene-GDF10;gene-CSF3;gene-CGA;gene-SMPDL3A;gene-ECM2-2;gene-ECM2;gene-LAMC3;gene-COL26A1;gene-ANGPTL2;gene-WNT2;gene-PCOLCE2;gene-ADAMTS15;gene-EREG;gene-CCL20;gene-APOL3;gene-PENK;gene-CHDL1;gene-GDF5;gene-MFAP4;gene-CILP;gene-FAM20C-3;gene-CRLF1;gene-THBS2;gene-CCN5;gene-IGFBP2;gene-TFPI2;gene-MELTF;gene-SPON2;gene-TFPI;gene-FBLN1;gene-GDF15;gene-SLIT3;gene-OLFML2A;gene-CFH-2;gene-CXCL14;gene-STC1;gene-ULBP1;gene-APOL1;gene-C1QTNF1;gene-CFH;gene-APOL6;gene-BMP8A;gene-TGFBR3;gene-PRRG1;gene-C5;gene-FAM20C-4;gene-ISLR;gene-NPTX2;gene-ISLR-2;gene-EMILIN2;gene-PROS1;gene-FAM20C-2;gene-CXCL12;gene-CLCA2;gene-FGF7;gene-BMP6;gene-WNT9A;gene-DNAJC8-2;gene-WNT3-2;gene-STC2;gene-TNFRSF11B;gene-IL17D;gene-KAZALD1;gene-EPDR1;gene-PLAU;gene-COL8A1;gene-FAM20C;gene-MEGF9;gene-VWA1;gene-RSPO3;gene-PTX3;gene-HILPDA;gene-NINL;gene-FGF9;gene-THAP11;gene-NBL1;gene-SIAE;gene-VIT;gene-LAMB1;gene-SFRP1;gene-CYB5D2;gene-APOLD1;gene-CXCL16;gene-CLU
Extracellular space	gene-SST;gene-CXCL6;gene-CXCL8;gene-DPT;gene-CXCL1;gene-CXCL3;gene-CXCL2;gene-IL34;gene-CXCL5;gene-CFD-2;gene-IL1B;gene-CFD;gene-SMPDL3A;gene-ECM2-2;gene-C3;gene-ECM2;gene-CHI3L1;gene-ANGPTL2;gene-ADAMTS15;gene-CCL7;gene-EREG;gene-CCL20;gene-IGF2;gene-IL16;gene-SOD3;gene-SULF2;gene-BMP2;gene-CILP;gene-SERPINF1;gene-FAM20C-3;gene-GREM2;gene-CRLF1;gene-CCN5;gene-BMP4;gene-SPON2;gene-SERPINE2;gene-GDF15;gene-NAMPT;gene-CCL11;gene-CFH-2;gene-ULBP1;gene-CFH;gene-PLTP;gene-FAM20C-4;gene-DPYSL3;gene-SERPINB2;gene-FAM20C-2;gene-CXCL12;gene-TNFRSF11B;gene-IL17D;gene-SERPING1;gene-FAM20C;gene-A2M;gene-PTX3;gene-HILPDA;gene-CSF1;gene-NBL1;gene-AKR1B1;gene-CAT;gene-FABP3;gene-LAMB1;gene-IL6;gene-ANGPTL4;gene-TGFB3;gene-CCL2;gene-CXCL16;gene-CLU

Table 8.16: DEG linked to each significantly enriched term in molecular function in GO. Results are shown for DEG in fibroblasts grown in high glucose (20 mM) euglycemic control (5.5 mM) (F20_vs_F5). (BMKGENE, 2023)

Description	geneID
Transforming Growth Factor Beta Binding	gene-LRRC32;gene-VASN;gene-VASN-2
Cytokine Binding	gene-CRLF1;gene-MICOS10-NBL1;gene-VASN;gene-VASN-2
Nicotinate Phosphoribosyl transferase Activity	gene-NAPRT;gene-NAPRT-2
Calcium Channel Activity	NewGene_2505;NewGene_2511;NewGene_2516;NewGene_2519;NewGene_4495
Alpha-1,6-Mannosylglycoprotein 6-Beta-N-Acetylglucosaminyltransferase Activity	gene-CCDC126;gene-MGAT5B
Cargo Receptor Activity	gene-SCARA3;gene-SCARF2
Acetylgalactosaminyltransferase Activity	gene-CHPF;gene-CHY3
Tumour Necrosis Factor-Activated Receptor Activity	gene-TNFRSF1B;gene-TNFRSF6B
Insulin-Like Growth Factor Binding	gene-IGFBP2;gene-IGFBP6;gene-KAZALD1
Adenylate Cyclase Activity	gene-ADCY4-2;gene-ADCY7
Hyaluronoglucosaminidase Activity	gene-CEMIP;gene-HYAL3
Transition Metal Ion Binding	gene-DOHH;gene-FAM20C-4;gene-S100A4;gene-SCO2;gene-SHANK3;gene-XDH;gene-ZNF493
Sphingolipid Binding	gene-LAMA1;gene-RTN4R
Glycosphingolipid Binding	gene-LAMA1;gene-RTN4R
Nuclear Receptor Transcription Coactivator Activity	gene-HELZ2;gene-NCOA7;gene-SFR1
Calcium Ion Binding	gene-CABP1;gene-CETN3;gene-CLSTN2;gene-DCH1;gene-DLK2;gene-DLL4;gene-EGF;gene-EHD3;gene-FAM20C-4;gene-FAT3;gene-HPG2;gene-LRP1;gene-LTBP4;gene-NCALD;gene-PCDHB3;gene-PCDHGA11;gene-PCDHGA12;gene-PCDHGA9;gene-PCDHGB1;gene-PCDHGB7;gene-PCDHGC5;gene-PTX3;gene-RAB11FIP3;gene-S100A4;gene-SLIT3;gene-SNED1;gene-THBD
Ephrin Receptor Activity	gene-EPHB3;gene-EPHB6;gene-EPHB6-2
Prostaglandin E Receptor Activity	gene-PTGER1;gene-PTGER3
Nicotinate-Nucleotide Diphosphorylase (Carboxylation) Activity	gene-NAPRT;gene-NAPRT-2

Table 8.17: DEG linked to each significantly enriched molecular function terms in GO. Results are shown for DEG in fibroblasts exposed to *S. epidermidis* lysate compared to no-lysate control in 5.5 mM (FSe5_vs_F5). (BMKGENE, 2023)

Description	geneID
Calcium ion binding	gene-ACAN;gene-ANKEF1;gene-ANXA10;gene-ASPN;gene-C1R;gene-C1R-2;gene-CABP1;gene-CALM2;gene-CAPN3;gene-CAPS2;gene-CDH2;gene-CDH6;gene-CETN3;gene-CLSTN2;gene-COLEC12;gene-DCH1;gene-DGKA;gene-EFHD1;gene-EGF;gene-EGFL6;gene-EHD3;gene-EPDR1;gene-FAM20C;gene-FAM20C-2;gene-FAM20C-4;gene-FAT4;gene-FBLN1;gene-FBLN2;gene-FBLN7;gene-H1-10;gene-HMCN1;gene-HPG2;gene-KCNIP3;gene-LDLR;gene-LRP1;gene-LRP4;gene-LTBP3;gene-LTBP4;gene-MAN1A1;gene-MGP;gene-MYL6;gene-MYL9;gene-NCALD;gene-NINL;gene-PCDHB9-2;gene-PCDHGA11;gene-PCDHGA9;gene-PCDHGB1;gene-PCDHGB2;gene-PCDHGB7;gene-PLA2G4A;gene-PLCB4;gene-PTX3;gene-RAB11FIP3;gene-RAB11FIP3-2;gene-SCUBE3;gene-SLIT2;gene-SLIT3;gene-SNED1;gene-SULF2;gene-THBD;gene-THBS2;gene-TLL1;gene-TNFAIP6;gene-TPD52
Ephrin receptor activity	gene-EFNB3;gene-EPHB1;gene-EPHB3;gene-EPHB4;gene-EPHB6;gene-EPHB6-2
Oxidoreductase activity, acting on paired donors, with oxidation of a pair of donors resulting in the reduction of molecular oxygen to two molecules of water	gene-FADS1;gene-SCD;gene-SCD5
Structural constituent of postsynapse	gene-SHANK2;gene-SHANK3;gene-SHANK3-2
Structural constituent of postsynaptic density	gene-SHANK2;gene-SHANK3;gene-SHANK3-2
Structural constituent of synapse	gene-SHANK2;gene-SHANK3;gene-SHANK3-2
Synaptic receptor adaptor activity	gene-SHANK2;gene-SHANK3;gene-SHANK3-2
Growth factor activity	gene-AMH;gene-BMP2;gene-BMP6;gene-BMP8A;gene-CCN5;gene-CSF1;gene-FGF11-2;gene-FGF5;gene-GDF10;gene-GDF5;gene-GDNF;gene-HGF;gene-IGF1;gene-IGF2;gene-LIF;gene-PGF;gene-TGFB2
Chemokine activity	gene-CCL11;gene-CCL2;gene-CCL7;gene-CXCL1;gene-CXCL12;gene-CXCL14;gene-CXCL16;gene-CXCL2;gene-CXCL3;gene-CXCL5;gene-CXCL6;gene-CXCL8
SH3 domain binding	gene-ADAM19;gene-DPYSL3;gene-EFS;gene-SHANK2;gene-SHANK3;gene-SHANK3-2;gene-VASP
Integrin binding	NewGene_7251;gene-CCN5;gene-CXCL12;gene-ECM2;gene-ECM2-2;gene-EGFL6;gene-FBLN1;gene-LAMA5;gene-VWF

Semaphorin receptor binding	gene-SEMA3B;gene-SEMA4B;gene-SEMA4C;gene-SEMA4D;gene-SEMA5A;gene-SEMA6C
Low-density lipoprotein particle binding	gene-COLEC12;gene-LDLR;gene-PCSK9
Insulin-like growth factor binding	gene-CCN5;gene-IGFBP2;gene-IGFBP4;gene-IGFBP6;gene-IGFBPL1;gene-KAZALD1
Solute: proton symporter activity	gene-MFSD3;gene-SLC2A12
Prostaglandin-endoperoxide synthase activity	gene-PTGS1;gene-PTGS2
Inositol 1,4,5 trisphosphate binding	gene-ITPR1;gene-PLCL2;gene-PLCL2-2

Table 8.18: DEG linked to each significantly enriched molecular function terms in GO. Results are shown for DEG in fibroblasts exposed to *S. epidermidis* lysate compared to no-lysate control in 20 mM (FSe20_vs_F20). (BMKGENE, 2023)

Description	geneID
Growth factor activity	gene-BMP2;gene-BMP4;gene-CCN5;gene-EREG;gene-FGF1;gene-FGF13;gene-FGF5;gene-GDF10;gene-GDF15;gene-GDF5;gene-HGF;gene-IGF2;gene-INHBB;gene-OSGIN1;gene-PGF;gene-TGFB2
Semaphorin receptor activity	gene-MET;gene-NRP2;gene-PLXNA2;gene-PLXNB3;gene-PLXNC1
Lipid phosphatase activity	gene-PLPP3;gene-PLPPR3;gene-PLPPR4
Chemokine activity	gene-CCL11;gene-CCL20;gene-CCL7;gene-CXCL1;gene-CXCL14;gene-CXCL2;gene-CXCL3;gene-CXCL5;gene-CXCL6;gene-CXCL8
Heparan sulphate proteoglycan binding	gene-APOE;gene-CFH;gene-CFH-2
Integrin binding	gene-CCN5;gene-ECM2;gene-ECM2-2;gene-EDIL3;gene-EGFL6;gene-FBLN1;gene-ITGA3;gene-ITGA6
Glycosaminoglycan binding	gene-ADAMTS15;gene-CCN5;gene-CFH;gene-CFH-2;gene-DCN;gene-ECM2;gene-ECM2-2
Squalene synthase activity	gene-FDFT1;gene-FDFT1-2
Farnesyl-diphosphate farnesyltransferase activity	gene-FDFT1;gene-FDFT1-2
Complement component C3b binding	gene-CFH;gene-CFH-2
Heparin binding	gene-ADAMTS15;gene-BMP4;gene-CCN5;gene-CFH;gene-CFH-2;gene-ECM2;gene-ECM2-2;gene-FGF1
Phosphoric diester hydrolase activity	gene-GDPD5;gene-PLCB4;gene-PLCXD1;gene-PLCXD1-2;gene-SMPDL3A
Inositol 1,4,5 trisphosphate binding	gene-ITPR1;gene-PLCL2;gene-PLCL2-2
Calcium ion binding	gene-ACTN1;gene-ACTN4;gene-ADGRE5;gene-C1R;gene-C1R-2;gene-C1S;gene-CCBE1;gene-CDH2;gene-CELSR1;gene-COLEC12;gene-DGKA;gene-DLK2;gene-EFCAB7;gene-EFHD1;gene-EGF;gene-EGFL6;gene-EHD4;gene-FAT3;gene-FBLN1;gene-FBLN7;gene-HMCN1;gene-LDLR;gene-LOC124902313;gene-LRP4;gene-LTBP4;gene-MAN1A1;gene-MGP;gene-PCDHB13;gene-PCDHGC5;gene-PHF24;gene-PLA2G4A;gene-PLCB4;gene-PRRG1;gene-RASGRP1;gene-SCUBE3;gene-SLIT3;gene-SNED1;gene-SULF2;gene-SYTL5;gene-TENM2;gene-THBD;gene-THBS2;gene-TLL1;gene-TNFAIP6;gene-TPD52
Metalloendopeptidase activity	gene-ADAM19;gene-ADAMTS12-2;gene-ADAMTS15;gene-ADAMTS19;gene-ADAMTS8;gene-MMP1;gene-MMP11;gene-MMP11-2;gene-MMP24;gene-TLL1;gene-TNFAIP6;gene-TRABD2A

Transmembrane receptor protein tyrosine kinase activity	gene-ERBB3;gene-KIT;gene-LRIG3;gene-MET;gene-PDGFRA;gene-PDGFRL
Wnt-protein binding	gene-APCDD1;gene-FZD8;gene-TRABD2A;gene-WLS
Protein kinase C inhibitor activity	gene-HPB1;gene-HPB8
Iron ion binding	gene-CH25H;gene-CYGB;gene-CYP19A1;gene-CYP1B1;gene-CYP27A1;gene-CYP51A1;gene-CYP7B1;gene-MSMO1;gene-P4HA3;gene-PTGIS;gene-SC5D;gene-TRMT9B-2;gene-XDH
Extracellular matrix binding	gene-ADAMTS15;gene-DCN;gene-ITGA6;gene-OLFML2A;gene-OLFML2B

Table 8.19: DEG linked to significantly enriched terms of molecular function in GSEA. Results are shown for DEG in fibroblasts grown in high glucose 20 mM compared to euglycemic control (5.5 mM) (F20_vs_F5). (BMKGENE, 2023)

Description	Core Enrichment
DNA-Binding Transcription Factor Activity, RNA Polymerase II-Specific	gene-ZFPM1;gene-HIVEP3;gene-ZNF469;gene-GLI4;gene-FOXC2;gene-GLIS2-2;gene-ZNF524;gene-CEBPD;gene-ZNF771;gene-HOXD9;gene-ZNF775;gene-ZNF668;gene-ZNF837;gene-FOXF2;gene-ZBTB4-2;gene-ZC3H3-2;gene-NPAS1;gene-IRX5;gene-EP300;gene-ZNF408;gene-GLIS2;gene-KLF2;gene-ZNF574;gene-MLXIP-2;gene-ZFP41;gene-CREBBP;gene-ZNF358;gene-ZNF316;gene-ZNF335;gene-HIC2;gene-ZNF623-2;gene-KIAA1549;gene-ZNF628;gene-ZNF526;gene-FOXO3B;gene-ZNF319;gene-ZNF618;gene-MLXIP;gene-ZNF142;gene-MIER2;gene-ZNF414;gene-ZC3H3;gene-KMT2B;gene-WIZ;gene-ZNF462;gene-SNAI1;gene-ZNF513;gene-ZNF579;gene-CYS1;gene-ELF4;gene-IRX3;gene-ZBTB47;gene-ID4;gene-ZNF275;gene-HIVEP2;gene-THAP11;gene-DLX1;gene-TSC22D1;gene-ZBTB39;gene-ZNF646;gene-ZBTB42;gene-SALL1;gene-THAP7;gene-ZNF407;gene-ZNF692;gene-ZSCAN22;gene-CRAMP1;gene-ASH1L;gene-ZNF710;gene-IGHMBP2;gene-ZNF787;gene-ZBTB7B;gene-ZFAT;gene-ZXDC;gene-CXXC1;gene-ZNF575;gene-ZNF497;gene-ZNF516;gene-DLX1-2;gene-ZNF687;gene-ZBED4;gene-TSC22D4;gene-PRDM8;gene-NPAS4;gene-ZBTB17;gene-ZNF341;gene-KLF16;gene-CSRNP1;gene-ZNF512B;gene-ZNF76;gene-ZNF696;gene-ZNF697;gene-MAZ;gene-PLAGL2;gene-FOXO3;gene-FIZ1
Calcium Ion Binding	gene-FAM20C-4;gene-DLL4;gene-FAM20C-3;gene-THBD;gene-PCDHGB1;gene-PLA2G4B;gene-PCDHGC5;gene-CABP1;gene-EHD3;gene-NCALD;gene-DCH1;gene-PCDHGA9;gene-FAT3;gene-CLSTN2;gene-DLK2;gene-PCDHGA11;gene-LRP1;gene-HPG2;gene-RAB11FIP3;gene-COLEC12;gene-PCDHGB7;gene-SLIT3;gene-LTBP4;gene-PTX3;gene-LOC124902313;gene-FBLN1;gene-SNED1;gene-PCDHGA12;gene-LRP4;gene-S100A4;gene-NOTCH3;gene-KCNIP3-2;gene-SLIT2;gene-MASP1;gene-NOTCH1;gene-PCDHGB2;gene-PCDH10;gene-KCNIP3;gene-CDH24;gene-PCDH8;gene-LDLR;gene-RHOT2;gene-NID2;gene-EPDR1;gene-AGRN;gene-FAT1;gene-LTBP3;gene-PCDHGC3;gene-DST;gene-LTBP2;gene-HMCN1;gene-CELSR1;gene-FAM20C;gene-MEGF6;gene-FAT4;gene-MACF1;gene-FAM20C-2;gene-MAN1A1;gene-CD320;gene-CDH4;gene-H1-10;gene-FBN2;gene-EFEMP2;gene-ADGRE2;gene-MASP1-2;gene-EHD2;gene-CELSR2;gene-CAPN3;gene-LPCAT1;gene-ANXA3;gene-EHD1;gene-EGFL7;gene-RCN3;gene-S100A16;gene-CD248;gene-PCDHGB4;gene-ADGRE5;gene-PCDHGA6;gene-CBL;gene-PCDHGA10;gene-CAPN1;gene-LRP8;gene-SLC25A12;gene-PCDH7;gene-FBLN2;gene-ACTN4;gene-TBC1D9B;gene-CRELD2;gene-SELENON;gene-FBN1;gene-ACAN;gene-F10;gene-EHD4;gene-THBS3;gene-PLCB3;gene-EFHD2

Table 8.20: DEG linked to significantly enriched terms of molecular function in GSEA. Results are shown for DEG in fibroblasts exposed to *S. epidermidis* Lysate compared to no-lysate control at 5.5 mM (FSe5_vs_F5). (BMKGENE, 2023)

Description	Core Enrichment
Calcium Ion Binding	Gene-EGFL6;Gene-FAM20C-3;Gene-FAM20C-4;Gene-LTBP4;Gene-THBD;Gene-ANXA10;Gene-TNFAIP6;Gene-HMCN1;Gene-MAN1A1;Gene-SLIT3;Gene-CABP1;Gene-SNED1;Gene-PLA2G4A;Gene-LDLR;Gene-PTX3;Gene-COLEC12;Gene-DCH1;Gene-FBLN1;Gene-CLSTN2;Gene-MGP;Gene-FAM20C-2;Gene-PCDHGB1;Gene-THBS2;Gene-FAM20C;Gene-SULF2;Gene-LRP4;Gene-C1R;Gene-FBLN7;Gene-PCDHB7-2;Gene-NCALD;Gene-C1R-2;Gene-PCDHGB7;Gene-ASPN;Gene-PCDHB9-2;Gene-LRP1;Gene-PCDHGA9;Gene-SLIT2;Gene-PCDHGB2;Gene-PPP2R3B-3;Gene-PCDHGA11;Gene-KCNIP3;Gene-RAB11FIP3;Gene-C1S;Gene-H1-10;Gene-FBLN2;Gene-CAPN3;Gene-ACAN;Gene-MASP1;Gene-LTBP3;Gene-HPG2;Gene-GUCA1B;Gene-FAT4;Gene-MASP1-2;Gene-PCDHGB6;Gene-EPDR1;Gene-RAB11FIP3-2;Gene-EHD3;Gene-NINL;Gene-ASPN-2;Gene-KCNIP3-2;Gene-PCDHB9;Gene-CELSR3;Gene-PCDHGA10;Gene-PCDHB16-2;Gene-SVEP1;Gene-PCDHB14-2;Gene-S100A4;Gene-DST;Gene-PCDHGA3;Gene-TBC1D9B;Gene-FBN2;Gene-CELSR2;Gene-PCDHB10-2;Gene-DLK2;Gene-PCDHB7;Gene-MCC;Gene-EML1;Gene-PCDHB13-2;Gene-F10;Gene-EGFL7;Gene-LRP8;Gene-PCDH8;Gene-PROS1;Gene-NOTCH3
Sequence-Specific DNA Binding	Gene-FOXQ1;Gene-THB;Gene-H;Gene-CEBPD;Gene-HOXA3;Gene-ZFPM1;Gene-PRRX2;Gene-ETV1;Gene-PRRX1;Gene-FOXF2;Gene-ALX4;Gene-OSR2;Gene-HOXC12;Gene-RORA;Gene-GATA6;Gene-SIX5;Gene-SNAI1;Gene-CYS1;Gene-NR4A3;Gene-THAP11;Gene-KLF4;Gene-FOXO4;Gene-SALL2;Gene-GLIS2;Gene-ETV4;Gene-PHF21A;Gene-EP300;Gene-MSX1;Gene-FOXD1;Gene-PBX1;Gene-GLIS2-2;Gene-NR1H3;Gene-PPARG;Gene-FOXO3B;Gene-ZBTB4-2;Gene-IRF1;Gene-SIX4;Gene-CREBBP;Gene-AR;Newgene_6969;Gene-MBD3;Gene-FOXO1;Gene-BEND3;Gene-HOXD9;Gene-SALL1;Gene-ZBTB7B;Gene-POU2F2;Gene-ISL2;Gene-HF1;Gene-AP5Z1;Gene-HOXA11;Gene-TRPS1;Gene-MYPOP;Gene-FOXC2;Gene-CXXC1;Gene-ZFHX4;Gene-NR2F1;Gene-VDR;Gene-FOXC1;Gene-HF4;Gene-CUX1;Gene-HOXC10;Gene-ISL1;Gene-RFX7;Gene-SHOX2;Gene-SMG5;Gene-TSC22D1;Gene-ELF4;Gene-KDM3A;Gene-H1-0;Gene-PAX3;Gene-RARG;Gene-MAZ;Gene-FOXN3;Gene-SETX;Gene-BMAL1;Gene-PRDM5;Gene-ZBTB10;Gene-ZNF76;Gene-ELK3;Gene-RERE;Gene-HOXD11;Gene-ELF2;Gene-ZBTB17;Gene-HIVEP3;Gene-ZFHX3;Gene-HIVEP2;Gene-ZNF516;Gene-FOXP4;Gene-ZNF668;Gene-ZBED6;Gene-LONP1

Table 8.21: DEG linked to significantly enriched terms of molecular function in GSEA. Results are shown for DEG in fibroblasts exposed to *S. epidermidis* Lysate compared to no-lysate control at 20 mM (FSe20_vs_F20). (BMKGENE, 2023)

Description	Core Enrichment
Signalling Receptor Binding	Gene-SST;Gene-ECM2-2;Gene-ECM2;Gene-ANGPTL2;Gene-WNT2;Gene-EREG;Gene-CCL20;Gene-DLG3;Gene-CCN5;Gene-SPON2;Gene-GDF15;Gene-RARRES2;Gene-TSPOAP1;Gene-ULBP1;Gene-NCOA7;Gene-H;Gene-OSGIN1;Gene-EFNB3;Gene-PAG1;Gene-GPRASP2;Gene-CXCL12;Gene-WNT9A;Gene-TCIM;Gene-LYNX1;Gene-LAMA3;Gene-WNT3-2;Gene-TRAF1;Gene-TNFRSF11B;Gene-IL17D;Gene-MEGF9;Gene-RSPO3;Gene-HILPDA;Gene-GYPC;Gene-NBL1;Gene-BMAL1;Gene-EMP2;Gene-LAMB1;Gene-MED30;Gene-OSGIN2;Gene-CXCL16;Gene-CLU;Gene-LIF;Gene-LAMA2;Gene-KDM3A
Metalloendopeptidase Activity	Gene-ADAMTS8;Gene-TNFAIP6;Gene-MMP11;Gene-MMP11-2;Gene-ADAMTS15;Gene-ADAMTS19;Gene-MMP1;Gene-TRABD2A;Gene-MMP12;Gene-ADAMTS3;Gene-PAPPA;Gene-CLCA2;Gene-ADAMTS9;Gene-ATP23;Gene-ADAMTS10

Table 8.22: DEG linked to each significantly enriched pathway in KEGG. Results are shown for DEG in fibroblasts grown in high glucose (20 mM) euglycemic control (5.5 mM) (F20_vs_F5). (BMKGENE, 2023)

Pathway	geneID
Retrograde endocannabinoid signalling	NewGene_3714;gene-ADCY4-2;gene-ADCY7;gene-CACNA1A;gene-GRIA1;gene-ITPR3;gene-MAPK13;gene-ND3;gene-NDUFA1;gene-NDUFA5;gene-NDUFB1;gene-NDUFB3;gene-NDUFB5
Glycosaminoglycan biosynthesis - chondroitin sulphate / dermatan sulphate	gene-CHPF;gene-CHT7;gene-CHY3;gene-XYLT1;gene-XYLT1-2
Amyotrophic lateral sclerosis	NewGene_3261;NewGene_7117;gene-CHCHD10-2;gene-COX6C;gene-COX7A1;gene-COX7C;gene-GRIA1;gene-GRIN2D;gene-ITPR3;gene-MAPK13;gene-ND3;gene-NDUFA1;gene-NDUFA5;gene-NDUFB1;gene-NDUFB3;gene-NDUFB5;gene-NEFM;gene-NXF3;gene-RGPD1;gene-RGPD2;gene-SEM1;gene-TNFRSF1B
Thermogenesis	gene-ADCY4-2;gene-ADCY7;gene-ATP5ME;gene-COX16;gene-COX6C;gene-COX7A1;gene-COX7C;gene-MAPK13;gene-ND3;gene-NDUFA1;gene-NDUFA5;gene-NDUFAF5-2;gene-NDUFB1;gene-NDUFB3;gene-NDUFB5
Oxidative phosphorylation	gene-ATP5ME;gene-COX6C;gene-COX7A1;gene-COX7C;gene-ND3;gene-NDUFA1;gene-NDUFA5;gene-NDUFB1;gene-NDUFB3;gene-NDUFB5;gene-TCIRG1
Homologous recombination	gene-MRE11;gene-RAD54B;gene-RPA3;gene-SEM1;gene-SSBP1-2
Glycosaminoglycan biosynthesis - heparan sulphate / heparin	gene-H3ST3A1;gene-SOBP;gene-XYLT1;gene-XYLT1-2
Calcium signalling pathway	NewGene_14;gene-ADCY4-2;gene-ADCY7;gene-ADRA1D;gene-CACNA1A;gene-CAMK1G;gene-EGF;gene-GRIN2D;gene-ITPR3;gene-KIAA1549L;gene-PTGER1;gene-PTGER3;gene-SPHK1
Glutamatergic synapse	gene-ADCY4-2;gene-ADCY7;gene-CACNA1A;gene-GRIA1;gene-GRIN2D;gene-ITPR3;gene-SHANK1;gene-SHANK3
ECM-receptor interaction	gene-COL4A5;gene-FAM171A2;gene-FRAS1;gene-GP1BB;gene-HPG2;gene-LAMA1;gene-LAMA5;gene-RELN;gene-TNC
Focal adhesion	gene-BCAR1;gene-CCND2;gene-COL4A5;gene-EGF;gene-FAM171A2;gene-LAMA1;gene-LAMA5;gene-NRN1;gene-PGF;gene-RELN;gene-SHC2;gene-SHC3;gene-TNC

N-Glycan biosynthesis	gene-ALG10;gene-C16orf87;gene-CCDC126;gene-MGAT5B;gene-ZSWIM5
Non-alcoholic fatty liver disease	gene-COX6C;gene-COX7A1;gene-COX7C;gene-MAP3K11;gene-NDUFA1;gene-NDUFA5;gene-NDUFB1;gene-NDUFB3;gene-NDUFB5;gene-SREBF1
Regulation of lipolysis in adipocytes	NewGene_3714;gene-ADCY4-2;gene-ADCY7;gene-PTGER3;gene-PTGS1
Relaxin signalling pathway	gene-ADCY4-2;gene-ADCY7;gene-COL4A5;gene-DNAI4;gene-MAPK13;gene-MMP1;gene-SHC2;gene-SHC3
Basal cell carcinoma	gene-FZD8;gene-GLI2;gene-HHIP;gene-KIF7;gene-TCF7
Circadian entrainment	gene-ADCY4-2;gene-ADCY7;gene-GRIA1;gene-GRIN2D;gene-GUCY1A2;gene-ITPR3
Platelet activation	gene-ADCY4-2;gene-ADCY7;gene-APBB1IP;gene-GP1BB;gene-GUCY1A2;gene-ITPR3;gene-MAPK13;gene-PTGS1
Human papillomavirus infection	NewGene_3714;gene-CCND2;gene-COL4A5;gene-EGF;gene-FZD8;gene-HLA-A-5;gene-HLA-C-4;gene-ISG15;gene-LAMA1;gene-LAMA5;gene-MAML3;gene-MX2;gene-RELN;gene-TCF7;gene-TCIRG1;gene-TNC;gene-UBR4
Spliceosome	NewGene_3261;gene-LSM3;gene-LSM5;gene-LSM6;gene-LSM8;gene-MAGOH;gene-PPIH;gene-SNRPE;gene-SNRPG;gene-ZNHIT2

Table 8.23: DEG linked to each significantly enriched pathway in KEGG. Results are shown for DEG in fibroblasts exposed to *S. epidermidis* lysate compared to no-lysate control in 5.5 mM (FSe5_vs_F5). (BMKGENE, 2023)

Pathway	geneID
Focal adhesion	gene-ARHGAP35;gene-CAV2;gene-CCND2;gene-COL4A4;gene-COL4A5;gene-COL6A1;gene-COL6A2;gene-EFS;gene-EGF;gene-EGFR;gene-FAM171A2;gene-HGF;gene-IGF1;gene-ITGA8;gene-ITGB8;gene-LAMA1;gene-LAMA2;gene-LAMA3;gene-LAMA5;gene-LAMC3;gene-LENG9;gene-LENG9-2;gene-LOC122526780;gene-MET;gene-MYL9;gene-MYLK4;gene-PDGFD;gene-PDGFRA;gene-PGF;gene-SHC2;gene-SHC3;gene-THBS2;gene-TNC;gene-TNXB;gene-TNXB-3;gene-TNXB-4;gene-TNXB-6;gene-VASP;gene-VWF
ECM-receptor interaction	gene-COL4A4;gene-COL4A5;gene-COL6A1;gene-COL6A2;gene-EGFL6;gene-FAM171A2;gene-FRAS1;gene-GP1BB;gene-HPG2;gene-ITGA8;gene-ITGB8;gene-LAMA1;gene-LAMA2;gene-LAMA3;gene-LAMA5;gene-LAMC3;gene-LOC122526780;gene-SV2A;gene-THBS2;gene-TNC;gene-TNXB;gene-TNXB-3;gene-TNXB-4;gene-TNXB-6;gene-VWF
Axon guidance	gene-BOC;gene-CFL2;gene-CXCL12;gene-DPYSL3;gene-EFNA4;gene-EFNB3;gene-ENAH;gene-EPHB1;gene-EPHB3;gene-EPHB4;gene-EPHB6;gene-EPHB6-2;gene-FES;gene-FZD3;gene-MET;gene-NFATC2;gene-NFATC4-2;gene-NTN1;gene-PARD6G;gene-PLXNC1;gene-SEMA3B;gene-SEMA4B;gene-SEMA4C;gene-SEMA4D;gene-SEMA5A;gene-SEMA6C;gene-SLIT2;gene-SLIT3;gene-SMO;gene-TRPC4
IL-17 signalling pathway	NewGene_3714;NewGene_6000;gene-CASP3;gene-CCL11;gene-CCL2;gene-CCL7;gene-CEBPB;gene-CILP;gene-CSF3;gene-CXCL1;gene-CXCL2;gene-CXCL3;gene-CXCL5;gene-CXCL6;gene-CXCL8;gene-FOS;gene-IL1B;gene-JUND;gene-MMP1;gene-PTGS2;gene-TRAF5
MicroRNAs in cancer	NewGene_3714;gene-ABCC1;gene-BCL2L11;gene-BMF;gene-CASP3;gene-CCND2;gene-CYP1B1;gene-DNMT3A;gene-EFNA4;gene-EGFR;gene-EZR;gene-FZD3;gene-GLS;gene-HDAC4;gene-HMOX1;gene-MET;gene-PAQR5;gene-PDGFRA;gene-PIM1;gene-PTGS2;gene-SOCS1;gene-SOX4;gene-TGFB2;gene-TNC;gene-TNXB;gene-TNXB-3;gene-TNXB-4;gene-TNXB-6;gene-TPM1;gene-ZFPM2
Cytokine-cytokine receptor interaction	gene-ACKR3;gene-ACKR4;gene-ACVRL1;gene-AMH;gene-BMP2;gene-BMP6;gene-BMP8A;gene-CCL11;gene-CCL2;gene-CCL7;gene-CCR7;gene-CRLF1;gene-CSF1;gene-CSF3;gene-CSF3R;gene-CTF1;gene-CXCL1;gene-CXCL12;gene-CXCL14;gene-CXCL16;gene-CXCL2;gene-CXCL3;gene-CXCL5;gene-CXCL6;gene-CXCL8;gene-GDF10;gene-GDF5;gene-

	IL13RA2;gene-IL15RA;gene-IL18R1;gene-IL1B;gene-IL1R1;gene-IL21R;gene-IL33;gene-IL4R;gene-LIF;gene-PRLR;gene-TGFB2;gene-TNFRSF14;gene-TNFRSF19;gene-TNFRSF1B;gene-TNFRSF21;gene-TNFRSF25
TNF signalling pathway	NewGene_3714;gene-BCL3;gene-CASP3;gene-CCL2;gene-CEBPB;gene-CSF1;gene-CXCL1;gene-CXCL2;gene-CXCL3;gene-CXCL5;gene-CXCL6;gene-EDN1;gene-FOS;gene-IL18R1;gene-IL1B;gene-LIF;gene-MAP2K6;gene-MAP3K8;gene-PTGS2;gene-TNFRSF1B;gene-TRAF5
PI3K-Akt signalling pathway	NewGene_6000;gene-ANGPT1;gene-AREG;gene-BCL2L11;gene-CCND2;gene-COL4A4;gene-COL4A5;gene-COL6A1;gene-COL6A2;gene-CSF1;gene-CSF3;gene-CSF3R;gene-EFNA4;gene-EGF;gene-EGFR;gene-FGF5;gene-FGFR1;gene-FLT3LG;gene-HGF;gene-IGF1;gene-IGF2;gene-IL4R;gene-ITGA8;gene-ITGB8;gene-KIT;gene-LAMA1;gene-LAMA2;gene-LAMA3;gene-LAMA5;gene-LAMC3;gene-LOC122526780;gene-MET;gene-NTRK2;gene-PDGFD;gene-PDGFRA;gene-PGF;gene-PRLR;gene-THBS2;gene-TNC;gene-TNXB;gene-TNXB-3;gene-TNXB-4;gene-TNXB-6;gene-VWF
Calcium signalling pathway	NewGene_14;gene-ADORA2B;gene-ADRA1D;gene-ASPHD2;gene-ATP2A3;gene-BDKRB2;gene-CACNA1G;gene-CACNA1H;gene-CALM2;gene-CAMK1D;gene-CHM3;gene-EDNRA;gene-EGF;gene-EGFR;gene-GRIN2D;gene-HH1;gene-ITPKB;gene-ITPR1;gene-LENG9;gene-LENG9-2;gene-MCOLN2;gene-MYLK4;gene-ORAI3;gene-OXTR;gene-P2RX5;gene-PDE1A;gene-PDGFD;gene-PDGFRA;gene-PLCB4;gene-SHF
MAPK signalling pathway	gene-ANGPT1;gene-AREG;gene-ARRB1;gene-CACNA1G;gene-CACNA1H;gene-CASP3;gene-CD14;gene-CSF1;gene-EFNA4;gene-EGF;gene-EGFR;gene-FGF5;gene-FGFR1;gene-FLT3LG;gene-FOS;gene-GADD45B;gene-HGF;gene-HPA6;gene-IGF1;gene-IGF2;gene-IL1B;gene-IL1R1;gene-JUND;gene-KIT;gene-KNDC1;gene-LENG9;gene-LENG9-2;gene-MAP2K6;gene-MAP3K8;gene-MET;gene-NLK;gene-NTRK2;gene-PDGFD;gene-PDGFRA;gene-PGF;gene-PLA2G4A;gene-RPS6KA2;gene-SASH1;gene-SBNO2-2;gene-TGFB2
Pathways in cancer	NewGene_2233;NewGene_3714;NewGene_6000;gene-BCL2L11;gene-BDKRB2;gene-BMP2;gene-CASP3;gene-CCND2;gene-COL4A4;gene-COL4A5;gene-CSF3R;gene-CXCL12;gene-CXCL8;gene-DAPK2;gene-DVL2;gene-EDN1;gene-EDNRA;gene-EGF;gene-EGFR;gene-FGF5;gene-FGFR1;gene-FLT3LG;gene-FOS;gene-FRAT1;gene-FRAT2;gene-FZD1;gene-FZD3;gene-FZD9;gene-GADD45B;gene-GLI3;gene-HGF;gene-HMOX1;gene-IGF1;gene-IGF2;gene-IL15RA;gene-IL4R;gene-KIT;gene-LAMA1;gene-LAMA2;gene-LAMA3;gene-

	LAMA5;gene-LAMC3;gene-MET;gene-MMP1;gene-PDGFRA;gene-PGF;gene-PIM1;gene-PLCB4;gene-PTGER2;gene-PTGS2;gene-RALA;gene-RALGDS;gene-SKP2;gene-SMO;gene-STAT5A;gene-TGFB2;gene-TRAF5;gene-WNT2
Amoebiasis	gene-CASP3;gene-CD14;gene-COL4A4;gene-COL4A5;gene-CXCL1;gene-CXCL2;gene-CXCL3;gene-CXCL8;gene-IL1B;gene-IL1R1;gene-LAMA1;gene-LAMA2;gene-LAMA3;gene-LAMA5;gene-LAMC3;gene-LOC122526780;gene-PLCB4;gene-TGFB2
Hedgehog signalling pathway	gene-ARRB1;gene-BOC;gene-CCND2;gene-CDON;gene-EVC;gene-EVC2;gene-GAS1;gene-GLI3;gene-GPR161;gene-MEGF8;gene-SMO
Ovarian steroidogenesis	NewGene_3714;gene-AKR1C3;gene-BMP6;gene-CGA;gene-CYP1B1;gene-HD17B2;gene-HD17B7;gene-IGF1;gene-LDLR;gene-PLA2G4A;gene-PTGS2
Viral protein interaction with cytokine and cytokine receptor	gene-ACKR3;gene-ACKR4;gene-CCL11;gene-CCL2;gene-CCL7;gene-CCR7;gene-CSF1;gene-CXCL1;gene-CXCL12;gene-CXCL14;gene-CXCL2;gene-CXCL3;gene-CXCL5;gene-CXCL6;gene-CXCL8;gene-IL18R1;gene-TNFRSF14;gene-TNFRSF1B
Terpenoid backbone biosynthesis	gene-ACAT2;gene-HMGCR;gene-HMGCS1;gene-IDI1;gene-MVD;gene-MVK;gene-PDSS1
Malaria	NewGene_14;gene-CCL2;gene-CSF3;gene-CXCL8;gene-GYPC;gene-HGF;gene-IL1B;gene-LRP1;gene-MET;gene-TGFB2;gene-THBS2
Protein digestion and absorption	gene-COL14A1;gene-COL15A1;gene-COL18A1;gene-COL18A1-2;gene-COL26A1;gene-COL4A4;gene-COL4A5;gene-COL5A3;gene-COL6A1;gene-COL6A2;gene-CPA3;gene-ELN;gene-EMILIN2;gene-LOC122526780;gene-MME;gene-PRSS3;gene-XPNPEP2
Rap1 signalling pathway	NewGene_14;gene-ADORA2B;gene-ANGPT1;gene-APBB1IP;gene-CSF1;gene-EFNA4;gene-EGF;gene-EGFR;gene-ENAH;gene-FGF5;gene-FGFR1;gene-HGF;gene-IGF1;gene-KIT;gene-MAP2K6;gene-MET;gene-PARD6G;gene-PDGFD;gene-PDGFRA;gene-PGF;gene-PLCB4;gene-RALA;gene-RALGDS;gene-RAPGEF4;gene-SIPA1L2;gene-VASP
AGE-RAGE signalling pathway in diabetic complications	gene-CASP3;gene-CCL2;gene-COL4A4;gene-COL4A5;gene-CXCL8;gene-EDN1;gene-EGR1;gene-F3;gene-IL1B;gene-LOC122526780;gene-PIM1;gene-PLCB4;gene-SERPINE1;gene-STAT5A;gene-TGFB2;gene-THBD

rt

Table 8.24: DEG linked to each significantly enriched pathway in KEGG. Results are shown for DEG in fibroblasts exposed to *S. epidermidis* lysate compared to no-lysate control in 20 mM (FSe20_vs_F20). (BMKGENE, 2023)

Pathway	geneID
PI3K-Akt signalling pathway	gene-AREG;gene-BCL2L11;gene-CCDC28B;gene-CCNE2;gene-CDK6;gene-CHM2;gene-COL4A1;gene-CREB5;gene-CSF3;gene-CSF3R;gene-DDIT4;gene-EGF;gene-EPHA2;gene-ERBB3;gene-EREG;gene-FGF1;gene-FGF5;gene-HGF;gene-IGF2;gene-ITGA11;gene-ITGA3;gene-ITGA6;gene-ITGA8;gene-ITGB8;gene-KIT;gene-LAMC3;gene-LPAR6;gene-MAGI1;gene-MET;gene-NTRK2;gene-PDGFD;gene-PDGFRA;gene-PGF;gene-RELN;gene-SGK3;gene-TGFA;gene-THBS2;gene-TNXB;gene-TNXB-3;gene-TNXB-4;gene-TNXB-5;gene-TNXB-6
Focal adhesion	gene-ACTN1;gene-ACTN4;gene-COL4A1;gene-EFS;gene-EGF;gene-FLNA;gene-FLNC;gene-HGF;gene-ITGA11;gene-ITGA3;gene-ITGA6;gene-ITGA8;gene-ITGB8;gene-LAMC3;gene-MET;gene-NRN1;gene-PDGFD;gene-PDGFRA;gene-PDGFRL;gene-PGF;gene-PXN;gene-RALGPS2;gene-RELN;gene-SHC2;gene-THBS2;gene-TNXB;gene-TNXB-3;gene-TNXB-4;gene-TNXB-5;gene-TNXB-6;gene-VASP
MAPK signalling pathway	gene-AREG;gene-CACNA1G;gene-CASP3;gene-CD14;gene-EGF;gene-EPHA2;gene-ERBB3;gene-EREG;gene-FGF1;gene-FGF5;gene-FLNA;gene-FLNC;gene-FOS;gene-GADD45B;gene-HGF;gene-HPB1;gene-IGF2;gene-IL1B;gene-IL1R1;gene-JUND;gene-KIT;gene-MAP2K3;gene-MAP2K6;gene-MAP3K8;gene-MAPT;gene-MET;gene-NTRK2;gene-PDGFD;gene-PDGFRA;gene-PDGFRL;gene-PGF;gene-PLA2G4A;gene-RALGPS2;gene-RASGRF2;gene-RASGRP1;gene-TGFA;gene-TGFB2
MicroRNAs in cancer	gene-BCL2L11;gene-BMF;gene-CASP3;gene-CCNE2;gene-CDC25A;gene-CDK6;gene-CYP1B1;gene-DDIT4;gene-DNMT3B;gene-E2F2-2;gene-ERBB3;gene-EZR;gene-FSCN1;gene-HMOX1;gene-MET;gene-PDGFRA;gene-PIM1;gene-SOX4;gene-TGFB2;gene-TNXB;gene-TNXB-3;gene-TNXB-4;gene-TNXB-5;gene-TNXB-6;gene-TPM1
Cytokine-cytokine receptor interaction	gene-ACKR3;gene-ACKR4;gene-ACVR2A;gene-BMP2;gene-BMP4;gene-CCL11;gene-CCL20;gene-CCL7;gene-CCR7;gene-CRLF1;gene-CSF3;gene-CSF3R;gene-CXCL1;gene-CXCL14;gene-CXCL2;gene-CXCL3;gene-CXCL5;gene-CXCL6;gene-CXCL8;gene-GDF10;gene-GDF15;gene-GDF5;gene-IL13RA2;gene-IL15RA;gene-IL18R1;gene-IL1B;gene-IL1R1;gene-IL33;gene-IL34;gene-INHBB;gene-TGFB2;gene-TNFRSF14;gene-TNFRSF19;gene-TNFSF13B

IL-17 signalling pathway	gene-CASP3;gene-CCL11;gene-CCL20;gene-CCL7;gene-CILP;gene-CSF3;gene-CXCL1;gene-CXCL2;gene-CXCL3;gene-CXCL5;gene-CXCL6;gene-CXCL8;gene-FOS;gene-FOSB;gene-IL1B;gene-JUND;gene-MMP1
Pathways in cancer	gene-ADCY7;gene-BCL2L11;gene-BDKRB2;gene-BMP2;gene-BMP4;gene-CASP3;gene-CCNE2;gene-CDK6;gene-COL4A1;gene-CSF3R;gene-CXCL8;gene-E2F2-2;gene-EDN1;gene-EFCAB7;gene-EGF;gene-FGF1;gene-FGF5;gene-FOS;gene-FRAT1;gene-FZD8;gene-GADD45B;gene-GLI3;gene-GSTM5;gene-HGF;gene-HMOX1;gene-IGF2;gene-IL15RA;gene-ITGA3;gene-ITGA6;gene-KIT;gene-LAMC3;gene-LPAR6;gene-MET;gene-MMP1;gene-PDGFRA;gene-PGF;gene-PIM1;gene-PLCB4;gene-PLD1;gene-PPARG;gene-PTGER2;gene-RASGRP1;gene-SMO;gene-STAT5A;gene-TGFA;gene-TGFB2;gene-WNT2;gene-WNT5B
Complement and coagulation cascades	gene-BDKRB2;gene-C1R;gene-C1R-2;gene-C1S;gene-C3;gene-C5;gene-CFD;gene-CFD-2;gene-CFH;gene-CFH-2;gene-CFI;gene-F3;gene-LYPD3;gene-PIK3IP1;gene-PRRG1;gene-SERPINE1;gene-TFPI;gene-THBD
Pertussis	gene-C1R;gene-C1R-2;gene-C1S;gene-C3;gene-C5;gene-CASP1;gene-CASP3;gene-CD14;gene-CXCL5;gene-CXCL6;gene-CXCL8;gene-EFCAB7;gene-FOS;gene-IL1B;gene-IRF1
Inflammatory mediator regulation of TRP channels	gene-ADCY7;gene-BDKRB2;gene-EFCAB7;gene-F2RL1;gene-HH1;gene-IL1B;gene-IL1R1;gene-ITPR1;gene-MAP2K3;gene-MAP2K6;gene-PLA2G4A;gene-PLCB4;gene-PTGER2;gene-TRPA1;gene-TRPV2
Steroid biosynthesis	gene-CYP51A1;gene-FDFT1;gene-FDFT1-2;gene-HD17B7;gene-MSMO1;gene-SC5D;gene-SQLE;gene-TM7SF2
TNF signalling pathway	gene-CASP3;gene-CCL20;gene-CREB5;gene-CXCL1;gene-CXCL2;gene-CXCL3;gene-CXCL5;gene-CXCL6;gene-EDN1;gene-FOS;gene-IL18R1;gene-IL1B;gene-IRF1;gene-MAP2K3;gene-MAP2K6;gene-MAP3K8;gene-VCAM1
Amoebiasis	gene-ACTN1;gene-ACTN4;gene-CASP3;gene-CD14;gene-COL4A1;gene-CXCL1;gene-CXCL2;gene-CXCL3;gene-CXCL8;gene-HPB1;gene-IL1B;gene-IL1R1;gene-LAMC3;gene-PLCB4;gene-RAB7B;gene-TGFB2
Calcium signalling pathway	NewGene_17;NewGene_4436;gene-ADCY7;gene-ADRA1D;gene-ATP2B4;gene-BDKRB2;gene-CACNA1G;gene-CCDC28B;gene-CHM2;gene-CHM3;gene-EFCAB7;gene-EGF;gene-ERBB3;gene-HH1;gene-ITPR1;gene-KIAA1549L;gene-ORAI3;gene-OXTR;gene-P2RX5;gene-PDE1C;gene-PDGFD;gene-PDGFRA;gene-PLCB4;gene-PTGFR

Viral protein interaction with cytokine and cytokine receptor	gene-ACKR3;gene-ACKR4;gene-CCL11;gene-CCL20;gene-CCL7;gene-CCR7;gene-CXCL1;gene-CXCL14;gene-CXCL2;gene-CXCL3;gene-CXCL5;gene-CXCL6;gene-CXCL8;gene-IL18R1;gene-IL34;gene-TNFRSF14
Rap1 signalling pathway	NewGene_17;NewGene_4436;gene-ADCY7;gene-EFCAB7;gene-EGF;gene-EPHA2;gene-FGF1;gene-FGF5;gene-GNAO1;gene-HGF;gene-KIT;gene-MAGI1;gene-MAP2K3;gene-MAP2K6;gene-MET;gene-PDGFD;gene-PDGFRA;gene-PGF;gene-PLCB4;gene-RAPGEF4;gene-SIPA1L2;gene-SIPA1L3;gene-VASP
Oestrogen signalling pathway	gene-ADCY7;gene-CREB5;gene-EFCAB7;gene-FKBP5;gene-FOS;gene-GABBR2;gene-GNAO1;gene-HBEGF;gene-ITPR1;gene-KRT15;gene-KRT18;gene-KRT19;gene-KRT33B-3;gene-KRT34-2;gene-KRT34-3;gene-LOC100653049;gene-PLCB4;gene-SHC2;gene-TGFA
Axon guidance	gene-BOC;gene-DPYSL2;gene-DPYSL3;gene-EPHA2;gene-EPHB1;gene-L1CAM;gene-LRRC4;gene-MET;gene-NFATC2;gene-NTN1;gene-PLXNA2;gene-PLXNB3;gene-PLXNC1;gene-SEMA4D;gene-SEMA7A;gene-SEMA7A-2;gene-SLIT3;gene-SMO;gene-TRPC4;gene-WNT5B
Malaria	NewGene_17;NewGene_4436;gene-CSF3;gene-CXCL8;gene-HGF;gene-IL1B;gene-MET;gene-TGFB2;gene-THBS2;gene-VCAM1
AGE-RAGE signalling pathway in diabetic complications	gene-CASP3;gene-COL4A1;gene-CXCL8;gene-EDN1;gene-EGR1;gene-F3;gene-IL1B;gene-PIM1;gene-PLCB4;gene-SERPINE1;gene-STAT5A;gene-TGFB2;gene-THBD;gene-VCAM1